UNIVERSIDAD COMPLUTENSE DE MADRID

FACULTAD DE CIENCIAS FÍSICAS

DEPARTAMENTO DE FÍSICA DE LA TIERRA, ASTRONOMÍA Y ASTROFÍSICA I (GEOFÍSICA Y METEOROLOGÍA)

TESIS DOCTORAL

SEISMIC STRUCTURE OF THE CRUST ACROSS NE CARIBBEAN PLATE (DOMINICAN REPUBLIC)
ESTRUCTURA SÍSMICA DE LA CORTEZA EN EL NE DE LA PLACA CARIBE (REPÚBLICA DOMINICANA)

MEMORIA PARA OPTAR AL GRADO DE DOCTORA

PRESENTADA POR

Diana Núñez Escribano

Director

Diego Córdoba Barba

Madrid, 2014

PhD Thesis

SEISMIC STRUCTURE OF THE CRUST ACROSS NE CARIBBEAN PLATE (DOMINICAN REPUBLIC)

Diana Núñez Escribano

Departamento de Física de la Tierra, Astronomía y Astrofísica I
(Geofísica y Meteorología)

Facultad de Ciencias Físicas, Universidad Complutense de Madrid

Madrid, 2014

UNIVERSIDAD COMPLUTENSE DE MADRID

Facultad de Ciencias Físicas

Departamento de Física de la Tierra, Astronomía y Astrofísica I (Geofísica y Meteorología)

SEISMIC STRUCTURE OF THE CRUST ACROSS NE CARIBBEAN PLATE (DOMINICAN REPUBLIC)

Estructura sísmica de la corteza en el NE de la Placa Caribe (República Dominicana)

Memoria para optar al Grado de Doctor en Física que presenta

Dña. Diana Núñez Escribano

Realizada en el *Departamento de Física de la Tierra, Astronomía y Astrofísica I (Geofísica y Meteorología)* de la Universidad Complutense de Madrid, bajo la dirección del Dr. Diego Córdoba Barba.

Madrid, 2014

ISBN 978-84-697-0331-1

UNIVERSIDAD COMPLUTENSE DE MADRID

Facultad de Ciencias Físicas

Departamento de Física de la Tierra, Astronomía y Astrofísica I (Geofísica y Meteorología)

SEISMIC STRUCTURE OF THE CRUST ACROSS NE CARIBBEAN PLATE (DOMINICAN REPUBLIC)

Estructura sísmica de la corteza en el NE de la Placa Caribe (República Dominicana)

Memoria para optar al Grado de Doctor en Física que presenta

Dña. Diana Núñez Escribano

Realizada en el *Departamento de Física de la Tierra, Astronomía y Astrofísica I (Geofísica y Meteorología)* de la Universidad Complutense de Madrid, bajo la dirección del Dr. Diego Córdoba Barba.

Vº. Bº. del Director de Tesis

Dr. D. Diego Córdoba Barba

La interesada,

Dña. Diana Núñez Escribano

Madrid, 2014

Este trabajo ha sido financiado por el actual Ministerio de Economía y Competitividad mediante el programa de ayudas FPI BES-2008-01997 asociado al proyecto de investigación CTM2006-13666-C02-02. Además, este trabajo ha sido financiado por los proyectos de investigación REN2003-08520-C02 y CGL2011-29474-C02-01, las acciones complementarias REN2002-12494-E/RIES y CTM2008-02955-E/MAR, y por las ayudas a los grupos de investigación de la Universidad Complutense de Madrid. Finalmente, el programa de ayudas complementarias para Estancias Breves en el extranjero ha permitido la realización de dos estancias en el Institute for Geophysics (Department of Earth Sciences, Swiss Federal Institute of Technology) en Zurich (Suiza) y una en Boone Pickens School of Geology (Oklahoma State University) en Stillwater (OK, Estados Unidos de América).

This work was supported by the FPI fellowship program BES-2008-01997, associated to investigation project CTM2006-13666-C02-02. Moreover, this work was supported by investigation projects REN2003-08520-C02 and CGL2011-29474-C02-01, complementary actions REN2002-12494-E/RIES and CTM2008-02955-E/MAR, and investigation groups funds of Universidad Complutense de Madrid. Finally, the complementary fellowship program of abroad Short Stays has allowed two investigation stays in Institute for Geophysics (Department of Earth Sciences, Swiss Federal Institute of Technology) in Zurich (Switzerland) and one in Boone Pickens School of Geology (Oklahoma State University) in Stillwater (OK, United States of America).

Acknowledgements

Me gustaría comenzar agradeciendo a mi director, D. Diego Córdoba Barba, todos los conocimientos tanto científicos como personales que me ha aportado en este inicio en la investigación y que ha hecho que esta tesis haya podido salir adelante. Además, me gustaría agradecerte que me hayas llevado a conocer medio mundo con las campañas de tierra y mar, congresos y estancias. En todos ellos, he aprendido pero, sobre todo, he disfrutado mucho.

I am especially grateful with Prof. Edi Kissling. Thank you very much for being always available to host me at ETHZ and teaching me the principles of Local Earthquake Tomography but, also, the principles of Refraction Seismology. Thanks to Stephan Husen for his constructive comments about LET and all the officemates that I had during my stays in Zurich, but specially to Matteo Spada for helping me a lot with everything there.

Gracias a todos los miembros del Departamento de Física de la Tierra, Astronomía y Astrofísica I por las facilidades prestadas durante estos años, pero en especial a los que considero como sus pilares fundamentales, Salvador y Lucía. Sin ellos, ¿qué sería de este departamento?

Cuando acabé mi licenciatura no tenía muy claro qué dirección tomar, pero gracias a la profesora Elisa Buforn terminé haciendo el Máster de Geofísica y Meteorología. Y fue en esa primera clase con la profesora Ana Negredo cuando se me abrió un mundo nuevo. Gracias a esos consejos he hecho este doctorado en esto tan bonito que es la Fisica de la Tierra.

No me gustaría olvidarme de todas las personas que estuvieron en la campaña CARIBE NORTE en Abril del 2009, tanto en tierra como en mar. Quizás no lo sepan, pero han sido la parte más importante de este trabajo. Sin ellos no habría datos. También querría agradecer a las instituciones que participaron y apoyaron este proyecto, tanto en España como en la República Dominicana (Dirección General de Minería, UASD, Instituto Sismológico Universitario (ISU) y Marina de Guerra Dominicana, quienes proporcionaron los barcos guardacostas 106-BELLATRIX y 109-ORION). También quisiera agradecer el apoyo prestado por la Red Sísmica de Puerto Rico. Thanks to IRIS-PASSCAL Consortium for logistical support providing 300 land seismic stations.

También me gustaría dar las gracias a todos mis compañeros del departamento, los que están y los que se han marchado, esos buenos ratos de cafés, comidas y sobremesas que hacían tan llevadero pasar tanto tiempo en la facultad. Comenzaré por los que estaban cuando llegué: Ana, Javi M., Juan Luis, Tatiana, Javi P., Blanca,

Álvaro, Javi B., Esther… y los que llegaron un poco después pero que siguen ahí: María y Sergio, Bea, Mariano Marta R., Izarra... La lista es larga y no quiero dejarme a nadie, así que si es así, no era mi intención. Gracias a David (Termi) por esos programitas tan estupendos que me facilitaron tanto la descarga de los datos de sismicidad, qué grande! Pero, sobre todo, gracias a mis brujitas, por esos aquelarres tan revitalizantes, y a Yasmina, por las charlas interminables de gmail que tenemos, estemos en la parte del mundo que estemos.

Pero el gran artífice de que haya conseguido acabar todo lo que me he propuesto en mi vida, no es otro que mi marido. Aunque todavía me sigue sonando raro llamarle marido! Gracias por toda tu inmensa comprensión, apoyo, ayuda y por cuidar siempre de mis pequeños, pasado y presentes. Sé que he tenido muchos momentos malos, pero tú siempre has estado conmigo. Rubén, sin ti no habría podido hacer nada de esto.

A Rubén

INDEX

Acronyms and Abbreviations

Tectonic Structures

AR	*Aruba Rise*
BR	*Beata Ridge*
CB	*Colombia Basin*
CDB	*Colombian Deformed Belt*
CP	*Caribbean Plate*
GB	*Grenada Basin*
HE	*Hess Escarpment*
MT	*Muertos Trough*
MTDB	*Muertos Thust Deformed Belt*
NAP	*North American Plate*
SAP	*South American Plate*
VB	*Venezuela Basin*
VDB	*Venezuelan Deformed Belt*

Geological Formations and Fractures Zones

AB	*Azúa Basin*
BGFZ	*Bonao – La Guácara*
CV	*Cibao Valley*
EB	*Enriquillo Basin*
EPGFZ	*Enriquillo – Plantain Garden Fault Zone*
HAFZ	*Hatillo Fault Zone*
HFZ	*Hispaniola Fault Zone*
PPBC	*Puerto Plata Basement Complex*
SFZ	*Septentrional Fault Zone*
SJB	*San Juan Basin*
SJRFZ	*San José – Restauración Fault Zone*
SJLPFZ	*San Juan – Los Pozos Fault Zone*
TFm	*Tireo Formation*
WP	*Windward Passage*

Seismic Catalogs, Networks, Stations and data

CN	*Canadian National Seismograph Networks*
CSS	*Controlled-Source Seismology*
CU	*Caribbean Network*
DR	*Instituto Sismológico Universitario (Universidad Autónoma de Santo Domingo) (ISU-UASD)*
GS	*Geological Survey*

IRIS	*Incorporated Research Institutions for Seismology*
ISC	*International Seismological Center*
JSN	*Jamaica Seismic Network*
LET	*Local Earthquake Tomography*
MCS	*Multichannel Seismic data*
OBS	*Ocean Bottom Seismometer*
PRSN	*Puerto Rico Seismic Network*
USGS	*U.S Geological Survey*

Extended Abstract

The North America-Caribbean plate boundary is a complex area of mainly left-lateral strike-slip deformation. In our study area, the Hispaniola Island is being impacted by collision with the Bahamas Platform in the north and in the south, Beata Ridge is penetrating into the island and hitting with Muertos Trough. These processes alter the central and eastern parts of Hispaniola Island dividing it into different tectonostratigraphic terrains characterized by folds, thrust and left-lateral faults and shear zones.

1. Introduction

The Caribbean Plate (CP) consists of a nearly undeformed central portion (Colombia and Venezuela Basins) bounded by active margins. The active northern and southern margins (from Guatemala to Greater Antilles and northern Venezuela, respectively) mainly consist of shear zones bounded by E-W trending strike-slip faults. The western and eastern margins are represented by convergent systems related with magmatic arcs (Middle America Trench and Lesser Antilles). Its interior is characterized by different basins and ridges. In the NW extreme of the plate, the Yucatan Basin and Caiman Trough are located and separated by Caiman Ridge. Central sector is represented by Colombia and Venezuela Basins (CB and VB) separated by the Beata Ridge (BR). Southern BR and VB, Curaçao Ridge delimits CP and northern margin of South American continent. Eastern CP is characterized by Grenada Basin separated by Aves and Barbados Ridges and bathymetric rises. Towards SW, the large extension area coincides with Nicaragua Rise.

The area of Hispaniola and Puerto Rico Islands is limited by subduction zone with oblique convergence in the north and incipient subduction zone associated to Muertos Trough in the south. The CP is moving to E-NE direction with rate of 18-20 mm/yr, relative to North American Plate (NAP), and azimuth of 70^{o}, from GPS measurements [Mann et al., 2002]. This direction implies maximum oblique convergence between the CP and NAP centered on Hispaniola Island. In the south, deformation is accommodated along the left-lateral Enriquillo-Plantain Garden Fault (EPGFZ) and north-dipping thrust faults of the Los Muertos deformed belt. The left-lateral Septentrional strike-slip fault (SFZ) and the south-dipping thrust faults of the North Hispaniola deformed belt accommodate deformation in the north.

In northern Caribbean, southern and western Cuba (active zones and faults [Cotilla et al., 2013 *a* and *b*]) and northern Hispaniola register the most intense seismicity. In particular, the seismicity of Hispaniola is plainly justified by its geodynamic position with respect to the frequency of occurrence and to the magnitude of seismic events

[Cotilla & Cordoba, 2011]. The seismic activity near Puerto Rico and Hispaniola defines the eastward continuation of the northern boundary of the CP where the earthquake depth increases both from N to S and from E to W.

Despite the large number of studies conducted in the northern CP, there are certain areas where no agreement exists on geodynamic models that govern the structure and tectonic development of the area concerned due to the absence mainly deep geophysical research. To resolve this anomalous distribution of geophysical studies in the NE Caribbean Plate, have been carried out two ambitious projects called GEOPRICO-DO [Carbó et al., 2005; Córdoba et al., 2009] and CARIBE NORTE [Carbó et al., 2010; Córdoba et al., 2010] in recent years.

2. Objective

The main objective of this thesis is to constrain the lithospheric structure in NE Caribbean Plate, specifically, beneath Dominican Republic and their adjacent areas. To achieve this objective, we can establish some specific aims depending of the area to study.

In the northern offshore area of Dominican Republic, the aim is determine how the contact is between North American Plate, Bahamas Platform and Hispaniola. Moreover, it is important to study the geometry of this structure along the northern coast.

The main target to solve in the island is obtaining a complete view about Moho discontinuity and upper mantle and studying the possible differences between the north and south and, also between east and west. In the eastern part of the island, the aim is the determination of geological structures that indicate high seismicity in that zone and could be associated to the subduction in the northern zone.

Another specific target is to characterize the contact between Muertos Thrust with north Beata Ridge and Hispaniola Island and the possible influence in onshore structures as Enriquillo Plantain Garden Fault Zone or Septentrional Fault Zone. Therefore, Beata Ridge has been densely studied in the south but there is no agreement about how the structure in the north is and if it penetrates into the island.

3. Data and Methodology

The study area was registered during GEOPRICO-DO project (2005) by eight seismic portable stations along Profile F which extends from Bahía de Neiba to Azúa and Enriquillo Basins crossing western area of Muertos Trough recording L6 marine shooting line; ten land seismic portable stations along NE – SW Profile G, which record the marine shooting line L7, from Ocoa Bay to Bonao region and ten seismic

stations along Profile H from San Pedro de Macorís to Sabana de la Mar recording the marine line L8 in with an orientation N – S.

During CARIBE NORTE project (2009) four profiles (A, B, C and D) were deployed in N-S and E-W Dominican Republic directions to complete the seismic information on land and at sea and one (Profile E) exclusively in the south coast of Dominican Republic. Profile A is located from Bahamas Bank (N) to BR (S) crossing western area of Dominican Republic. The Profile A was recorded by 97 land portable stations deployed from Pedernales (S) to Puerto Plata (N) and three OBS (OBS 10, OBS 11 and OBS 12) situated in the Caribbean Sea. Profile B is made of 58 land seismic stations from Ocoa Bay to Nagua and four OBS (OBS 1, OBS 2, OBS 3 and OBS 4) located in the northern part of the study area. Profile C consists of 39 one component land seismic portable stations from San Pedro de Macorís to north area of Samaná Peninsula, two three components seismic stations in Hato Mayor and Samaná, and five OBS (OBS 5, OBS 6, OBS 7, OBS 8 and OBS 9) anchored in San Pedro basin and northern slope of Muertos Trough. Profile D is W – E oriented in a length of 450 km. The deployment was made of 140 land seismic stations of one vertical component and one land station of three components located near Hato Mayor. Profile E is WNW-ESE trending line in the south coast of Dominican Republic crossing the northern flank of Beata Ridge with a total length of 220 km recorded by five OBS (OBS 11, OBS 13, OBS 14, OBS 15 and OBS 16) and one three components land station deployed at Beata Island.

The seismic sources used in CARIBE NORTE experiment correspond to six marine shooting lines in the north, south and east extremes (LM1N, LM1S, LM3N, LM3S, LM2 and LM4, respectively) and three land borehole explosions 1 Ton (S1, S2 and S3). Besides these data, seismicity data have been used to complete the crustal velocity models and to get Minimum 1D velocity model.

After data processing, new methodology developed for seismograms applied to seismic record sections obtained in our experiment will be explained in this thesis [Núñez et al., 2011]. The used criterion is according Diehl et al., (2009) but modified considering that our data correspond to refraction data, so the main feature is possible establish phase correlations. This fact means that every pick can be determined with its appropriated uncertainty relating trace-to-trace and obtaining correlations.

In short, for controlled source seismology (CSS) refraction it is necessary to pick correlatable phases, i.e. same phase onset in different traces. Hence our methodology consists of:

1) Pick each wavelet separately using the principles for single signal picking.

2) Define correlation of phases.
3) Repick earliest phase onset times for each trace.

This new methodology allows us obtaining uncertainties of velocity and depth of our crustal velocity models due to the travel time uncertainty. Moreover, it has been consider the relative position between the instrument and the seismic line that implies when the instrument is offset the seismic transect, an error has to be quantified.

4. Results

North American – Caribbean Plates boundary (Northern Dominican Republic)

In NW Dominican Republic, the southern Bahamas Platform (Mouchoir Bank) is characterized by shallow water depth with thin sedimentary cover (less than 1 km) and basement increasing through the coast where reaches 6 km in the area of Puerto Plata Basement Complex. In the area of Samaná Complex this depth is 8 km with P-wave velocities of 3.3 ± 0.1 km/s for sediments and basement ranges between 5.2 km/s and 5.8 km/s, with 0.1 km/s of uncertainty. The presence of the Silver and Navidad Banks is reflected in the sedimentary layer with an increase respect to the west, reaching 2 km deep. These areas also are characterized by shallow Moho discontinuity that it has been possible to determine at 10 ± 1 km in the west and 10-15 ± 1 km in the eastern study area.

The deep structure of the crust and upper mantle presents dipping layers penetrating into the island with different dip angles reducing its value towards to the east. From W to E, these angles are 12^{o}, 9^{o} and 6^{o} but it is noteworthy that profiles orientation, where these angles have been obtained, is not parallel between them. Then, the NAP is subducting beneath CP with NNE-SSW direction in our study area and the subducting angle corresponds to 12^{o}. Also, in this thesis it has been possible to determine V_P of the first seismic layers in the upper mantle with maximum values of 8.6 ± 0.3 km/s reaching depths up to 85 ± 4 km.

Hispaniola Island

The basins and mountain ranges crustal structure, present in Hispaniola Island, have been described in our study area. The results have corroborated previous data and have provided slight changes respect to the previous studies in the area. Thus, we have obtained the following characterization of the main sedimentary basins: 1) *Cibao Valley* consists in different stratigraphic sequences that reach a maximum thickness of 4 km; 2) *San Juan Basin* is not as deep as previous studies indicated in this area (7 km), reaching a sedimentary depth of 5 km, while in the southeastern area of this basin is 3 km; 3) *Enriquillo Basin* (Angostura and Mella blocks), defined

by being under sea level and filled by alluvium deposits, is 6 km of basin thickness; 4) *Llanura Costera del Caribe* defined by thin sedimentary layer with V_P of 2.3-3.4 ± 0.1 km/s and 1.2 km deep and a basement of 5.5 km. Main effects observed in the crustal velocity model of the mountain range areas are the absence of sedimentary cover and the rise of basement to the subsurface. These effects appear in Cordillera Central and its southern flank with Peralta Belt, Cordillera Oriental and Sierra de Bahoruco excepting Sierra de Neiba, whose basement is deeper than other mountain ranges, providing better knowledge about the volcano-sedimentary rocks velocities that are made of. Moreover, the stage of the seismic profiles through the western flank of Cordillera Septentrional does not provide enough information to define its structure.

Deep structure in the area of Dominican Republic is featured by a crustal thickening that in this study has been obtained from three seismic transect with N-S direction and one oriented from W to E. Through these data, it has been possible to establish the marked differences between N and S and from W to E. Specifically, Moho discontinuity increases towards the interior of the island from Bahamas Platform but gets different maximum depth values being roughly 30 ± 2 km deep in the western and central, while rises up to 24 ± 2 km deep, in the eastern area. Moreover, in the Peralta Belt vicinity appears laminated and showing a velocity lateral contrast due to the presence of the San José - Restauración and Bonao – La Guácara Fault Zones. Going toward southern coast, Moho depth decreases being shallower in the west (19 ± 2 km) and east (16 ± 2 km), and deeper in Bahía de Ocoa area (21 ± 2 km). In this area, Beata Ridge is colliding and penetrating into the island [Cotilla et al., 2007], whose effect is reflected in the P-wave velocity model as the existence of thickening of the crust.

It is noteworthy that the comparison between P-wave velocity and layer depths obtained from two different data and methodologies (refraction seismology data and seismicity applied to LET), provides similar values of these magnitudes. Being 7.6 ± 0.2 km/s from refraction data and 7.5 km/s from LET, average values of P-wave velocity. While average values of Moho depth under Hispaniola Island are close to 30 ± 2 km.

Eastern offshore Hispaniola

The different crustal structure, topography and deep seismicity in the eastern offshore and onshore area of Hispaniola make more pronounced the difference between W and E. Previous studies attribute this fact to the oblique subduction of NAP, establishing this process as dominant [Ladd et al., 1991; McCann and Sykes, 1984]. In the present study, a structure dipping towards eastern interior of the island has been obtained with a dip angle of 18^o reaching depths of 120 ± 5 km. The relocation and analysis of one earthquake registered by CARIBE NORTE land seismic

deployment have allowed obtaining these values. This structure could explain deep seismicity in the area. Furthermore, it has been shown that the earthquake relocation based on 1D models obtained from the wide-angle and local earthquake tomography data, greatly improve the derived event parameters from those used by the seismic networks operating in the region.

Beata Ridge and Muertos Trough Contact (Southern Dominican Republic)

The study carried out in this thesis provides values of the crust beneath the BR that are not as deep as expected being thickened beneath Beata Island whose differences could be due to the existence of contemporary set of active faults [Núñez et al., 2010; Núñez et al., (submitted)]. Moreover, some tectonic differences between west and east zones separated by Beata Island in the shallow structure show that Haiti Basin is characterized by two sedimentary layers with V_P of 3.3 ± 0.1 km/s and 4.5-4.8 ± 0.1 km/s, respectively, and a maximum total thickness of 4.4 km. While eastward, these layers remain constant at 8 km depth due to the presence of Venezuela Basin. In the area of southern Hispaniola where BR collides with the island and Muertos Trough, the sedimentary cover and basement close to the coast appear thickened and then, disappear in the junction with Muertos Trough.

Under Beata Island, Moho depth is thickened (24 ± 2 km) confirming the crust of Caribbean Plateau is unusually thick. Then, it rises up to 13 ± 2 km in the area of seamount located further east and is constant at 15 ± 2 km in VB area. Deeper layers follow the topography established by Moho with increasing V_P in depth reaching values of 8.5 ± 0.3 km/s. Eastward, the area is characterized by the deformation of the crust and the upper mantle due to the presence of Muertos Thrust Belt and Muertos Trough producing a thickening of the first layers of upper mantle and subsequent a thinning further to the south. Moho discontinuity and upper mantle in the southernmost area of the study model are relatively shallow (10-12 ± 1 km deep) presenting a dip angle of 7^o-8^o northwards. Gravity studies in this area report similar dip angle values [Granja Bruña et al., 2009; 2010].

The extension towards Hispaniola of NE direction of the Beata Ridge structure, as morphotectonic alignment, is articulated transversely with EPGFZ and SFZ active faults. This alignment has been identified as a first-order limit between mountain and plain morphostructures [Cotilla et al., 2007] explaining the divergence of rivers and basins in opposite directions. Deep structure along this lineament have been determined in this study, obtaining a thickening in the upper mantle dipping 12^o-18^o that penetrates into the island in a SN direction and reaching depths of up to 80 ± 4 km.

Septentrional and Enriquillo – Plantain Garden Fault Zones

The main two faults that accommodate deformation in N and S of Hispaniola have been studied. Along northern Dominican Republic, SFZ is responsible for the uplift of the Cordillera Septentrional and faulting in Cibao Valley area. Our study reveals that the presence of Septentrional Fault in the westernmost area appears as loss of seismic energy in seismic record sections, while in central and eastern parts, it is possible to establish an effect of this structure in the velocity models. In the area of Río San Juan Complex, this effect is observed as a lateral variation in V_P from offshore to onshore regions, increasing its value towards the island and reaching first layers of upper mantle. In the area of Samaná Bay, SFZ indicates a thinning of the uppermost layers and a lateral velocity variation. The seismicity in the region shows a concentration of events north of Cordillera Septentrional whose shallow seismicity could be associated SFZ but the deepest is tied to Hispaniola Trench.

The region of Enriquillo Basin is mainly traversed by EPGFZ that is formed as response to oblique subduction of the Bahamas Platform due to the thicker-than-average crust subduction of the Bahamas Platform resisted the eastward motion of the central and northern parts of Hispaniola. Our study has obtained an anomalous zone with lateral velocity variation observed in two consecutive layers, which decrease from 7.6 ± 0.2 km/s to 7.0 ± 0.2 km/s for the shallowest one, and 8.0 ± 0.2 km/s to 7.5 ± 0.2 km/s for the deepest, both from west to east. The structure reaches the first layers of upper mantle up to 60 ± 3 km deep. This structure could be interpreted as EPGFZ and also, Mann et al., (2002) show a possible detached oceanic slab from NAP that could produce reflections. Comparing with the P-wave velocity model of Profile A, it is possible to extract similarities with the anomalous area obtained, whose reflections are located up to 70 km depth. Moreover, the seismicity of this zone has been checked in ISC catalog from 1950 at present, revealing that earthquakes are grouped mainly in the northern and southern flanks. Events in eastern part are deeper than those of the west and some of them reach depths of 90-100 km. The seismicity associated to this region reveals that events in the southeastern part are deeper than those of the southwest and some of them reach depths of 90-100 km indicating that this structure reaches large depths.

5. Conclusions and Main Contributions of this Thesis

After the study that is carried out during the elaboration of this thesis, it is possible to emphasize in the following aspects:

i. This study combines seismic wide-angle data from two geophysical experiments where eight seismic transects have been processed and interpreted. Moreover, controlled-source seismology and seismicity data complete the data set.

ii. It is the first time that a method for uncertainty estimation developed for earthquake phase picking has been applied to wide-angle seismic data, allowing to obtaining phase correlation uncertainties used to determine error estimations in layer depth and seismic velocities.

iii. All data from GEOPRICO-DO and CARIBE NORTE seismic experiments have been processed and more than 120 seismic record sections have been interpreted to obtain six P-wave velocity models with more than 7800 rays traced, providing information onshore and offshore Dominican Republic in NS and EW directions checked by ray tracing and synthetic seismogram calculations.

iv. Lithosphere structure under Dominican Republic has been obtained, showing for first time a perspective more elaborated, characterizing shallow and deep parts including Moho and upper mantle. The results show differences between northern and southern and also, western and eastern parts of the Dominican Republic and adjacent marine regions.

v. The contact between Bahamas Platform – North American Plate and Hispaniola Island in northern and eastern areas has been determined. This contact corresponds to an oblique subduction in a NNE-SSW direction with dip angles of 12^{o} to the north and 12^{o}-18^{o} to the east.

vi. Beata Ridge, Muertos Trough and Muertos Thrust Belt have been described seismically, as well as the contact between these structures with southern coast of the island.

vii. Main active fault zones (Septentrional and Enriquillo-Plantain Garden Fault Zones) in the island have been seismically defined obtaining P-wave velocities and depths.

viii. It has been obtained a minimum 1D velocity model computed by simultaneous inversion of arrival time data for seismic velocities and hypocenter locations (Local Earthquake Tomography technique), which improves the 1D velocity models used in regional seismic networks and it is the starting point to generate a 3D structure model. Also, obtained P-wave velocities below Moho and upper mantle from this technique corroborate that values obtained with refraction seismology and observed in the literature.

Resumen Extendido

El límite entre las placas de Norte América y Caribe (NAP y CP) es una extensión compleja con deformación principalmente de strike-slip lateral-izquierda. En nuestra área de estudio, la isla de la Española está siendo impactada mediante colisión con la Plataforma de las Bahamas por el norte y en el sur, la Cresta de Beata (BR) está penetrando en la isla y colisionando con el Surco de los Muertos. Estos procesos alteran las partes centrales y orientales de la Española, dividiendo así la isla en diferentes terrenos tectonoestratigráficos caracterizados por pliegues, cabalgamientos, fallas de componente lateral izquierda y zonas de cizalla.

1. Introducción

La CP consiste en una porción central sin deformar (Cuencas de Colombia y Venezuela (CB y VB)) limitadas por márgenes activos. Los márgenes norte y sur (desde Guatemala a las Antillas Mayores y el norte de Venezuela, respectivamente) consisten principalmente en zonas de cizalla limitadas por fallas de strike-slip con componente E-W. Los márgenes occidentales y orientales están representados por sistemas convergentes relacionados con arcos magmáticos (Fosa Mesoamericana y Antillas Menores). Su interior está caracterizado por diferentes cuencas y dorsales. En el extremo NW de la placa, la Cuenca del Yucatán y el Surco de las Caimán están separados por la Dorsal de las Caimán. Mientras que el sector central está constituido por las CB y VB, a su vez separados por BR. Al sur de BR y VB, la Dorsal de Curaçao delimita la CP y el margen septentrional de Sudamérica. El este de CP está caracterizado por la Cuenca de Grenada separada por las Dorsales de Aves y Barbados y altos batimétricos. Hacia el SW, el Alto de Nicaragua coincide con una zona de gran extensión.

El área de La Española y Puerto Rico está limitada por una zona de subducción con convergencia oblicua en el norte y una incipiente zona de subducción asociada al Surco de los Muertos en el sur. La CP se está moviendo en dirección E-NE con una tasa de 10-20 mm/a, relativo a NAP, y con un azimut de 70^{o}, a partir de medidas de GPS [Mann et al., 2002]. Esta dirección implica máxima convergencia oblicua entre CP y NAP centrada en La Española. En el sur, la deformación está acomodada a lo largo de la zona de Falla de Enriquillo-Plantain Garden (EPGFZ) y el cabalgamiento con buzamiento norte del Cinturón Deformado de Los Muertos. La Falla Septentrional (SFZ) y el cabalgamiento con buzamiento sur del Cinturón Deformado de Norte de La Española acomodan la deformación en el norte.

La sismicidad de la zona norte del Caribe está registrada con mayor intensidad al sur y oeste de Cuba (fallas y zonas activas [Cotilla et al., 2013 a and b]). En concreto, la

sismicidad de La Española justificada por su posición geodinámica respecto a la frecuencia de ocurrencia y a la magnitud de los eventos sísmicos [Cotilla & Córdoba, 2011]. La actividad sísmica cerca de Puerto Rico y La Española define la continuación hacia el este del límite norte de CP, donde la profundidad de los terremotos aumenta tanto de N a S como de E a W.

A pesar del gran número de estudios llevados a cabo en la zona norte de la CP, existen ciertas áreas donde no hay acuerdo en cuanto a los modelos geodinámicos que gobiernan la estructura y el desarrollo tectónico, debido a la ausencia principalmente de investigaciones geofísicas profundas. Para resolver la anómala distribución de estudios geofísicos en la zona NE de la CP, se han realizado dos ambiciosos proyectos denominados GEOPRICO-DO [Carbó et al., 2005; Córdoba et al., 2009] y CARIBE NORTE [Carbó et al., 2010; Córdoba et al., 2010] en la última década.

2. Objetivos

El principal objetivo de esta tesis es conocer la estructura litosférica en el NE de la Placa del Caribe, en concreto, bajo la República Dominicana y sus áreas adyacentes. Para alcanzar este conocimiento, estableceremos algunos objetivos específicos en las diferentes zonas del área de estudio.

En la zona norte del litoral de la isla, el objetivo se centrará en determinar como es el contacto de la Placa de Norte América, la Plataforma de las Bahamas y La Española. Además, es importante conocer la geometría de esta estructura a lo largo de la costa septentrional.

Obtener una completa visión acerca de la Moho y el manto superior en la isla será el principal objetivo, además de estudiar las posibles diferencias entre el N y el S, y también, entre el E y el W. En la parte este de la isla, el objetivo consistirá en determinar las posibles estructuras geológicas que provocan una alta sismicidad.

Otro objetivo específico es caracterizar el contacto entre el Surco de los Muertos con la parte norte de la Cresta de Beata y la isla de La Española y su posible influencia en estructuras como la zona de falla de Enriquillo o Septentrional. Además, se estudiará cómo es la zona norte de la Cresta de Beata y si penetra en el interior de la isla, ya que ha sido densamente estudiada en el sur pero no existe un acuerdo sobre la zona norte.

Estos objetivos específicos permitirán establecer la topografía de la Moho bajo la República Dominicana y sus alrededores.

3. Datos Sísmicos y Metodología

Los proyectos GEOPRICO-DO y CARIBE NORTE, en 2005 y 2009, respectivamente, cubrieron nuestra área de estudio. Durante el proyecto GEOPRICO-DO, se realizaron tres perfiles sísmicos en tres áreas seleccionadas de la isla. El perfil F se extiende desde la Bahía de Neiba hasta las Cuencas de Enriquillo y Azúa cruzando el área del Surco de los Muertos, donde se instalaron ocho estaciones sísmicas portátiles que registraron la línea sísmica marina L6. Diez estaciones sísmicas se desplegaron a lo largo del Perfil G con dirección NE-SW, registrando la línea en mar L7, desde la Bahía de Ocoa a la región de Bonao. Por último, en el Perfil H, desde San Pedro de Macorís hasta Sabana de la Mar, se instalaron diez estaciones que registraron la línea L8 en dirección NS.

El proyecto CARIBE NORTE fue realizado íntegramente en la región de la República Dominicana y sus costas. Durante este proyecto fueron desplegadas 340 estaciones sísmicas a lo largo de tres perfiles NS (A, B y C), uno EW (D) y uno exclusivamente en la costa sur (E). El Perfil A estuvo localizado desde la Plataforma de las Bahamas (N) a la Cresta de Beata (S) cruzando la zona oeste de la República Dominicana. Este perfil fue registrado por 97 estaciones sísmicas situadas entre Pedernales (S) y Puerto Plata (N) y tres estaciones de fondo oceánico (OBS) fondeadas en el Mar Caribe (OBS 10, OBS 11 y OBS 12). El Perfil B fue realizado con 58 estaciones sísmicas desde la Bahía de Ocoa (S) a Nagua (N) y cuatro OBS en la zona norte del área de estudio (OBS 1, OBS 2, OBS 3 y OBS 4). El Perfil C consistió en 39 estaciones sísmicas de una componente desde San Pedro de Macorís hasta la zona norte de la Península de Samaná, dos estaciones de tres componentes situadas en Hato Mayor y Samaná, y cinco OBS (OBS 5, OBS 6, OBS 7, OBS 8 y OBS 9) fondeados en la cuenca de San Pedro y la pendiente norte del Surco de los Muertos. El Perfil D con orientación EW tuvo una longitud total de 450 km con un despliegue de 140 estaciones sísmicas de una componente y una estación de tres componentes en el área de Hato Mayor. El Perfil E cruza el flanco norte de la Cresta de Beata a lo largo de una transecta WNW-ESE en la costa sur de la República Dominicana con una extensión de 220 km y fue registrado por cinco OBS (OBS 11, OBS 13, OBS 14, OBS 15 y OBS 16) y una estación de tres componentes instalada en la isla de Beata.

Las fuentes sísmicas que se utilizaron durante dicho experimento corresponden a seis líneas de disparo marinas en el norte, sur y este (LM1N, LM1S, LM3N, LM3S, LM2 y LM4, respectivamente) y tres explosiones controladas de 1 Tonelada en tres puntos seleccionados de la isla (S1, S2 y S3). Además de estos datos, se han utilizado datos de sismicidad para completar los modelos de velocidad cortical y obtener un modelo de velocidad de 1D, que mejore los utilizados por las redes sísmicas que operan en la zona.

Después del procesamiento de los datos, una nueva metodología desarrollada para la determinación de los tiempos de llegada de ondas sísmicas en sismogramas ha sido aplicada por primera vez a los ensamblajes sísmicos de nuestro experimento y que se muestra en esta tesis. El criterio usado está de acuerdo con la técnica desarrollada por Diehl et al., (2009) pero ha sido modificada considerando que nuestros datos corresponden a datos de sísmica de refracciónc uya principal característica consiste en establecer correlaciones de fase. Esto significa que cada punto (tiempo de llegada) seleccionado puede estar determinado con su apropiada incertidumbre relacionando traza a traza y obteniendo correlaciones.

En concreto, para sísmica de refracción activa es necesario determinar fases que se puedan correlacionar, por ejemplo, la misma llegada de la misma fase en diferentes trazas. Por tanto, nuestra metodología consiste en:

1) Picar cada forma de onda separadamente usando los principios para el picado de señales individuales.
2) Definir la correlación de fases.
3) Repicar los tiempos llegadas de fase preliminares para cada traza.

Esta nueva metodología permite obtener incertidumbres de la velocidad y profundidad de nuestros modelos corticales de velocidad debido a la incertidumbre asociada a los tiempos de llegada. Además, se ha considerado la posición relativa entre el instrumento y la línea sísmica, lo que implica que cuando el instrumento se encuentra fuera de dicha línea, un error debe ser cuantificado.

4. Resultados

Límite de las Placas Norte Americana – Caribe (Norte de República Dominicana)

En la zona noroeste de la República Dominicana, el sur de la Plataforma de las Bahamas (Banco de Mouchoir) está caracterizado por profundidades someras de la capa de agua con una cobertura sedimentaria y basamento cristalino que aumentan hacia la costa donde alcanzan profundidades de 6.1 km en el área del Complejo de Basamento de Puerto Plata, mientras que en el área del Complejo de Samaná alcanza profundidades de 8 km con velocidades de ondas P de 3.3 ± 0.1 km/s para sedimentos y para el basamento oscila entre 5.2 km/s y 5.8 km/s, con incertidumbres de 0.1 km/s. La presencia de los Bancos de Silver y Navidad en esta área está reflejada en un aumento de la capa de sedimentos con respecto al oeste. Estas zonas también están caracterizadas por tener una Moho superficial localizada a 10 ± 1 km en el oeste y a 10-15 ± 1 km en la parte oriental de la zona norte de estudio.

La estructura profunda de la corteza y el manto superior presenta capas con buzamiento penetrando en la isla con diferentes ángulos cuyo valor disminuye hacia el este. De W a E, estos ángulos son 12º, 9º y 6º, pero es importante recalcar que la orientación de los perfiles donde estos ángulos han sido obtenidos no es paralela entre ellos. Con lo cual, como NAP tiene una dirección NNE-SSW como la orientación del Perfil A de nuestro estudio, es posible establecer que la subducción de la NAP bajo CP se produce con un ángulo de 12º. Además, en esta tesis ha sido posible determinar que la V_P de las primeras capas del manto superior alcanza valores máximos de 8.6 ± 0.3 km/s a unas profundidades de 85 ± 4 km.

La Española

En el interior de La Española, en concreto, en la República Dominicana, nuestro estudio ha permitido determinar sísmicamente las cuencas sedimentarias y los sistemas montañosos en la parte más superficial de la corteza. Los resultados corroboran datos previos y proporcionan ligeras diferencias respecto a estudios anteriores en la zona. De esta manera, las cuencias sedimentarias muestran las siguientes características: 1) El Valle de Cibao consiste en diferentes secuencias estratigráficas que alcanzan espesores máximos de 4 km; 2) La Cuenca de San Juan no es tan profunda como estudios anteriores estimaban (7 km), alcanzando un profundidad de 5 km, mientras que en la parte sureste es 3 km; 3) La Cuenca de Enriquillo, en concreto los bloques de Angostura y Mella definidos por estar bajo el nivel del mar y rellenos de depósitos aluviales, tiene un espesor de 6 km; y, por último, 4) La Llanura Costera del Caribe está definida por una delgada capa de sedimentos con velocidades de onda P de 2.3-3.4 ± 0.1 km/s y 1 km de profundidad y un basamento cristalino de 5.5 km. Los principales efectos observados en el modelo de velocidades, en cuando a los sistemas montañosos presentes en la isla, son la ausencia de la cobertura sedimentaria y el ascenso del basamento hacia la superficie. Estos efectos son apreciables en la Cordillera Central y en su flanco meridional denominado Cinturón de Pliegues y Cabalgamientos de Peralta, Cordillera Oriental y Sierra de Bahoruco, exceptuando la Sierra de Neiba cuyo basamento se encuentra más profundo que en otros sistemas montañosos, proporcionando un mejor conocimiento de las velocidades correspondientes a ondas P de las rocas volcano-sedimentarias de las que está formado. En cuanto a la Cordillera Septentrional, los perfiles sísmicos que cruzan su parte occidental no proporcionan información suficiente para definir su estructura.

La estructura profunda del área de la República Dominicana está caracterizada por un engrosamiento cortical determinado a través de tres perfiles sísmicos con dirección NS y uno orientado WE. Estos datos muestran marcadas diferencias entre el norte y el sur de la región, así como las zonas orientales y occidentales. En concreto, la discontinuidad de la Moho aumenta hacia el interior de la isla desde la

Plataforma de las Bahamas, obteniendo diferentes valores de profundidades máximas siendo próxima a 30 ± 2 km en las zonas centrales y occidentales, mientras que asciende a 24 ± 2 km en la zona más oriental. Además, en los alrededores del Cinturón de Peralta aparece laminado y mostrando cambios laterales en la velocidad que puede ser debido a las zonas de falla de San José – Restauración y Bonao – La Guácara. Hacia la costa sur, la profundidad de la Moho disminuye siendo más superficial hacia el oeste (19 ± 2 km) y el este (16 ± 2 km), y más profunda en la zona de la Bahía de Ocoa (21 ± 2 km) donde la Cresta de Beata está colisionando y penetrando en la isla [Cotilla et al., 2007], cuyo efecto se reflecta en el modelo obtenido en esta tesis como la existencia de un engrosamiento de la corteza.

La comparación de velocidad de ondas P y profundidades obtenidas a partir de dos tipos de datos y metodologías diferentes (datos de sísmica de gran ángulo y de sismicidad aplicados a Tomografía Sísmica), proporcionan valores similares entre dichas magnitudes. En concreto, se han obtenido 7.6 ± 0.2 km/s a partir de datos de refracción y 7.5 km/s a partir de datos de sismicidad. Además, valores promedios de la Moho bajo la isla están próximos a 30 ± 2 km.

Zona de Costa Oriental de La Española

La diferente estructura cortical, topografía y sismicidad profunda de la zona oriental de La Española y su costa hacen más pronunciada la diferencia con la zona occidental. Nuestro estudio ha obtenido que una estructura está buzando hacia la zona este del interior de la isla con un ángulo de 17º alcanzando profundidades de 120 ± 5 km. La relocalización y posterior análisis de un terremoto registrado por las estaciones sísmicas desplegadas durante el proyecto CARIBE NORTE ha permitido obtener estos valores. Estudios anteriores dicha diferencia a la subducción oblicua de la NAP, estableciendo este proceso como dominante [Ladd et al., 1991; McCann and Sykes, 1984]. Esta estructura podría explicar la sismicidad profunda de la zona. Además, se ha demostrado que la relocalización basada en modelos de 1D a partir de datos de sísmica de gran ángulo y tomografía sísmica local mejora los parámetros del terremoto de aquellos obtenidos a partir de las redes sísmicas que operan en la región.

El contacto entre Cresta de Beata y el Surco de los Muertos (Sur de la República Dominicana)

Parte del estudio llevado a cabo en esta tesis ha estado centrado en determinar la estructura cortical del flanco norte de BR. Este estudio ha proporcionado valores corticales bajo no tan profundos como eran de esperar, estando engrosado bajo la isla de Beata, y cuyas diferencias pueden deberse a la existencia de fallas contemporáneas activas. Además, existen claras diferencias tectónicas entre la zona oriental y occidental del perfil separadas por la isla de Beata en superficie. En el

estudio se muestra que la Cuenca de Haití está caracterizada por dos capas de sedimentos con velocidades de 3.3 ± 0.1 km/s y 4.5-4.8 ± 0.1 km/s, respectivamente, y un espesor total de 4.4 km. En la zona este, estas capas permanecen constantes a 8 km de profundidad debido a la presencia de VB. En el área del sur de La Española, donde BR colisiona con la isla y el Surco de Los Muertos, las capas sedimentarias y el basamento cristalino aparecen engrosados cerca de la costa para luego desaparecer en el punto de unión con el Surco de Los Muertos.

Bajo la isla de Beata, la Moho se encuentra engrosada (24 ± 2 km) confirmando así que la corteza del Plateau Caribeño es inusualmente gruesa, para luego ascender hasta los 13 ± 2 km en el área de la montaña submarina situada más al este y siendo constante en 15 ± 2 km bajo VB. Las capas más profundas muestran la misma topografía determinada por la Moho con aumento en V_P con la profundidad alcanzando valores de 8.5 ± 0.3 km/s. Hacia el este, el área está caracterizada por la deformación de la corteza y el manto superior debido a la presencia del Cinturón Deformado de Los Muertos y el Surco de Los Muertos, produciendo un engrosamiento en las primeras capas del manto superior y posteriormente un adelgazamiento más hacia el sur. La discontinuidad de la Moho y el manto superior en el área más meridional es relativamente superficial (10-12 ± 1) presentando un ángulo de buzamiento de entre 7º y 8º hacia el norte. Estudios de gravimetría muestran valores similares [Granja Bruña et al., 2007; 2010].

La extensión de BR hacia el NE de La Española, como un alineamiento morfotectónico, está articulada transversalmente con las fallas activas de EPGFZ y SFZ. Este alineamiento ha sido identificado como un límite de primer orden entre morfoestructuras montañosas y planas [Cotilla et al., 2007] explicando la divergencia de ríos y cuencas en direcciones opuestas cuya estructura profunda a lo largo de este alineamiento ha sido determinado en este estudio, obteniendo un engrosamiento en el manto superior que buza entre 12º y 18º penetrando hacia la isla en una dirección S-N y alcanzando profundidades de hasta 80 ± 4 km.

Zonas de Falla Septentrional y de Enriquillo – Plantain Garden

En este estudio, se han estudiado sísmicamente las dos principales fallas que acomodan la deformación en el norte y el sur de la isla. A lo largo del norte de la República Dominicana, SFZ es la responsable del ascenso de la Cordillera Septentrional y el fallamiento del Valle de Cibao. Nuestro estudio revela que la presencia de esta falla en la zona más occidental produce una disminución en la energía sísmica tal y como aparece en los ensamblajes. Mientras, en las partes centrales y orientales, es posible establecer un efecto de esta estructura en los modelos de velocidad. En el área del Complejo Río San Juan, se ha obtenido una variación lateral en el odelo desde la región costera hacia el interior, alcanzando las primeras capas del manto superior. En el área de la Bahía de Samaná, SFZ se observa

como un adelgazamiento en las capas más superficiales y un cambio lateral en la velocidad. La sismicidad en la región muestra una concentración de eventos en el norte de la Cordillera Septentrional cuya sismicidad superficial podría estar asociada a la SFZ mientras que la más profunda correspondería con la zona de subducción.

La región de la Cuenca de Enriquillo está atravesada por la EPGFZ, formada como respuesta a la subducción oblicua de la Plataforma de las Bahamas. Nuestro estudio ha obtenido una zona anómala con una variación lateral en la velocidad observada en dos capas consecutivas, cuyo valor disminuye de 7.6 ± 0.2 km/s a 7.0 ± 0.2 km/s para la más superficial y de 8.0 ± 0.2 km/s a 7.5 ± 0.2 km/s para la más profunda, de oeste a este. La estructura se interpreta como la EPGFZ en profundidad, pero también podría estar relacionado con un posible slab oceánico descolgado de NAP que podría producir reflexiones [Mann et al., (2002)]. Comparando estos resultados con los obtenidos en el modelo de velocidad del Perfil A, se pueden extraer similitudes con la zona anómala obtenida. Ambas situaciones podrían ser perfectamente compatibles, sin embargo, según los datos mostrados en dicho perfil, este slab habría pertenecido a CP y no a NAP. Además, la sismicidad asociada a esta región revela que los terremotos en la parte sureste son profundos de aquellos situados al suroeste. Algunos de ellos muestran profundidades de 90-100 km, lo que indica que esta estructura alcanza grandes profundidades como demuestra nuestro estudio.

5. Conclusiones and Principales Contribuciones de esta Tesis Doctoral

Después del estudio llevado a cabo durante la elaboración de esta tesis, es posible enfatizar en los siguientes aspectos:

i. Este estudio combina datos de sísmica de gran ángulo de dos experimentos geofísicos en el área NE de la Placa del Caribe, donde ocho perfiles sísmicos han sido procesados e interpretados completamente. Además, datos de sismología activa y sismicidad completan los datos usados.
ii. Es la primera vez que un método para la estimación de la incertidumbre desarrollado para la determinación de tiempos de llegada de fases sísmicas en terremotos ha sido aplicado a datos de sísmica de gran ángulo, permitiendo obtener incertidumbres en los tiempos de recorrido que a su vez han sido usados para la estimación del error en la velocidad y profundidad de los modelos corticales de velocidad presentados en esta tesis doctoral.
iii. Todos los datos de los experimentos sísmicos GEOPRICO-DO y CARIBE NORTE han sido procesados y más de 120 ensamblajes sísmicos han sido interpretados para obtener seis modelos de velocidad de ondas P con más de 7800 rayos trazados, proporcionando información tanto en la República

Dominicana como en su mar territorial adyacente. Dichos modelos han sido comprobados a partir de trazados de rayos y sismogramas sintéticos.

iv. Se ha obtenido la estructura litosférica bajo la República Dominicana, mostrando por primera vez una perspectiva prácticamente completa, caracterizando las partes superficiales y profundas incluyendo la Moho y el manto superior. Los resultados revelan diferencias entre las zonas norte y sur y, también este y oeste de la República Dominicana y sus alrededores.

v. En este estudio se ha determinado el contacto entre la Plataforma de las Bahamas – Placa de Norte América – Española en el norte y este. Este contacto corresponde a una subducción oblicua en dirección NNE-SSW con ángulos de buzamiento de 12^{o} en el norte y entre 12^{o} y 18^{o} en el este.

vi. La Cresta de Beata, el Surco de Los Muertos y el Cinturón Deformado de Los Muertos han sido estudiados desde un punto de vista sísmico, así como el contacto entre ellos y la costa sur de la isla.

vii. Se han caracterizado sísmicamente las principales zonas de fallas activas: las Fallas Septentrional y de Enriquillo-Plantain Garden.

viii. Se han obtenido modelos de velocidad 1D a partir de la aplicación de las técnicas de Tomografía Sísmica Local, los cuales mejoran los modelos usados en las redes sísmicas locales y que son el punto de partida para la generación de un modelo estructural tridimensional. Además, las velocidades obtenidas bajo la Moho y el manto superior a partir de esta técnica corroboran aquellos valores determinados a partir de sísmica de refracción y los observados en literatura previa.

CHAPTER 1

INTRODUCTION

The area of Hispaniola Island is immersed in an ongoing debate about the tectonic processes in the area of NE Caribbean Plate. This chapter introduces the tectonic frame of the Caribbean Plate and the problem in the study area, explaining the previous and recent works and defining the objectives that this study is intended to resolve.

1.1 GEOLOGICAL AND TECTONIC SETTING

The region of the Caribbean Plate (CP) is characterized by a very complex plate-tectonic configuration. In this frame, the Hispaniola Island represents the second extensional island inside the Greater Antilles in the northeastern border region of CP. In this section, the main tectonic, geological and structural features of CP and, pointedly, Hispaniola Island are presented.

1.1.1 Caribbean Plate

The CP consists of a nearly undeformed central portion (Colombia and Venezuela Basins) bounded by active margins (Fig. 1.1.1.1). The active northern (from Guatemala to Greater Antilles) and southern (northern Venezuela) margins mainly consist of shear zones within Jurassic/Cretaceous deformed terranes, bounded by E-W trending sinistral and dextral strike-slip faults, respectively. The western and eastern margins are represented by convergent systems and related magmatic arcs (Middle America Trench and Lesser Antilles). Deformed and dismembered Jurassic/Cretaceous ophiolitic terranes crop out along suture zones and strike-slip faults at the northern, southern and western edges of the CP [Giunta et al., 2006].

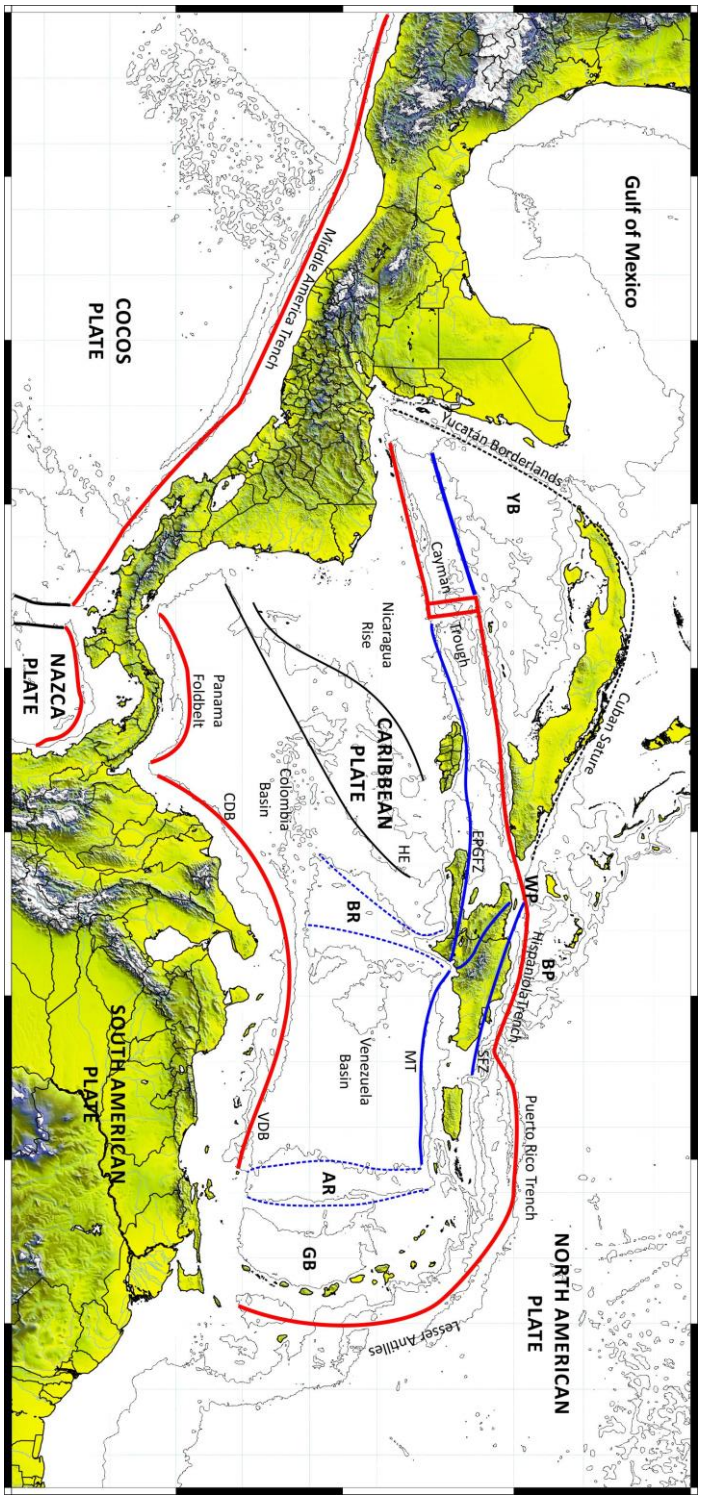

Fig. 1.1.1.1 Present day tectonic map of the Caribbean region. AR = Aves Ridge; BP = Bahamas Platform; BR = Beata Ridge; CDB = Colombia Deformed Belt; EPGFZ = Enriquillo-Plantain Garden Fault Zone; GB = Grenada Basin; HE = Hess Escarpment; MT = Muertos Trough; SFZ = Septentrional Fault Zone; VDB = Venezuela Deformed Belt; YB = Yucatán Basin; WP = Windward Passage (after Pindell and Barrett, 1990).

The interior of the CP is characterized by different basins and ridges. In the NW extreme of the plate, the Yucatan Basin and Caiman Trough are located and separated by Caiman Ridge. While central sector is represented by Colombia and Venezuela Basins (CB and VC) that are separated by the Beata Ridge (BR). Southern BR and VB, Curaçao Ridge delimits CP and northern margin of South American continent. Eastern CP is characterized by Grenada Basin separated by Aves and Barbados Ridges and bathymetric rises. Towards SW, the large extension area coincides with Nicaragua Rise. This rise is subdivided between northern and southern, which are higher and deeper, respectively.

The present-day CP interacts with North and South American plates (NAP and SAP) to the north, south and east and with Nazca and Cocos plates to the west (Fig. 1.1.1.1). The border region between NAP and CP is a transform fault system that continues to the west, as a transcurrent fault system in Guatemala, whose extension and interaction with Middle American Trench is not well defined. To the east, NAP is subducting beneath CP along Puerto Rico Trench and continues in Lesser Antilles. The wide earthquake distribution indicates that the boundary NAP-SAP and PC-SAP are diffused [Dolan and Mann, 1998].

The Caribbean island arc lies between the continents of North and South America and comprises the Greater Antillean islands on the west and the Lesser Antillean islands on the east. The Greater Antilles are larger and consists of the islands of Cuba, Jamaica, Hispaniola and Puerto Rico. These islands have virtually no recent volcanic activity. The Lesser Antilles, on the other hand, are smaller and many of them have present volcanic activity. The Dominican Republic and the Republic of Haiti share the Hispaniola Island, the second largest of the Greater Antilles. Hispaniola is especially intriguing because four structural trends converge upon it: the main axis of the island arc, the southeastern part of the Bahamas, the swell (Nicaragua Rise) extending from Central America to southwestern Hispaniola, and the Beata Ridge [Bowin, 1975].

1.1.2 Caribbean Plateau

The oceanic plateaus (Fig. 1.1.2.1) are vast areas of elevated topography, generally 2-3 km above the abyssal ocean floor [Kerr & Mahoney, 2007]. The principal reason for the elevated nature of oceanic plateaus is their crustal thickness, which is generally much greater than the 6-7 km thickness of normal oceanic crust generated at spreading centers. For instance, the Ontong Java Plateau has a crustal thickness of at least 30 km over much of its area whereas the Caribbean Plateau varies from 8-15 km thick [Case et al., 1990; Mauffret and Leroy, 1997].

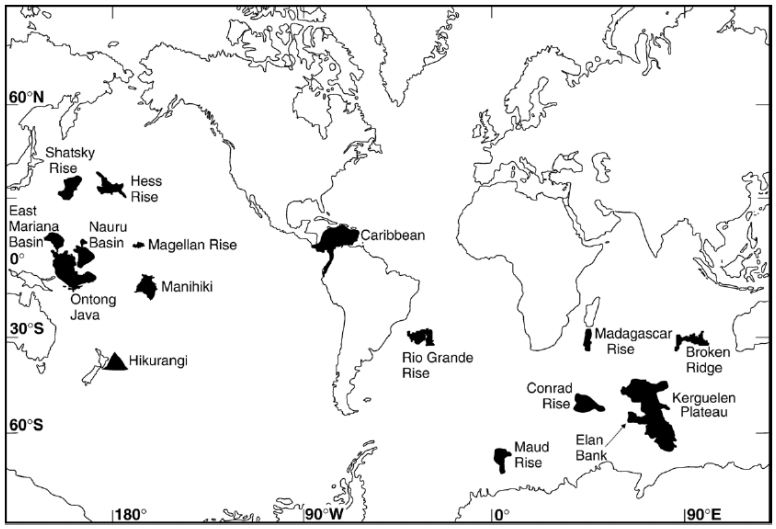

Fig. 1.1.2.1 Map showing the locations of Cretaceous oceanic plateaus (after Kerr, 2003) [From Kerr & Mahoney, 2007].

One of the first areas of such over-thickened crust to be identified was the CP, which Donnelly (1973) proposed to be an "oceanic flood basalt province". The term oceanic plateau was coined by Kroenke (1974). Eldholm and Coffin (2000) introduced the term "large igneous provinces" (LIPs) as a generic term encompassing oceanic plateaus continental, flood basalt provinces and those provinces, which form at the continental-oceanic boundary (volcanic rifted margins). LIPs are generally believed to be formed by decompression melting of upwelling hotter mantle, known as mantle plumes. LIPs erupted over a relatively short time, often less than 2-3 Ma, with important implications for mantle processes and source regions. Oceanic plateaus can also become accreted to continental, being significant contributors to the growth continental crust [Kerr et al., 2003].

The Caribbean-Colombian Oceanic Plateau (CCOP) (Fig. 1.1.2.1) is believed that was formed in the Pacific at 90 Ma [Sinton et al., 1998; Hauff et al., 2000]. Within 10 Ma the eastward-moving Farallon plate had brought the southern portion of the plateau into collision with continental northwestern South America, resulting in the accretion of slices of the plateau on to the continental margin [Kerr et al., 1997b]. This accretion was accompanied by back-stepping of the subduction zone west of the accreted plateau slices. Shortly after its formation the northern portion of the plateau began to move into the proto-Caribbean seaway between North and South America [Burke, 1988; Kerr et al., 1999; White et al., 1995]. In doing so the plateau encountered the eastward-dipping "Great Arc of the Caribbean". Unable to subduct, the thick plateau clogged the subduction zone, resulting in a reversal in the polarity of subduction from east to west. This reversal in subduction polarity in conjunction with a back-stepping of subduction behind the advancing plateau [Burke, 1988],

effectively isolated the Caribbean as a separate plate. Over the past 80 Ma the northern portion of the Caribbean plateau has moved into the gap between North and South America and has been uplifted and sub-aerially exposed around its margins, thus making it available for detailed study. It is in ways such as these that remnants of these thick, buoyant oceanic plateaus can be preserved and incorporated into the continental crust.

The CCOP is exposed around the margins of the Caribbean and along the northwestern continental margin of South America. The thickened nature of the bulk of the Caribbean plate (8-20 km) [Edgar et al., 1971; Mauffret and Leroy, 1997] testifies to its origin as an oceanic plateau. The accreted plateau material in Colombia, Ecuador, Costa Rica and Hispaniola consists of fault-bounded slices of basaltic, and occasionally lavas and sills with relatively few intercalated sediments and ash layers [Kerr et al., 1997a].

1.1.3 Crustal structure of the Caribbean large igneous province

Mauffret and Leroy (1997) establishes the deep crust by refraction data (Fig. 1.1.3.1), whereas information on the upper crust comes mainly from sonobuoys, although Moho is sometimes reached with this method. In deep parts of the Caribbean Sea, Haiti and Puerto Rico sub-basins, and the eastern Colombia and Venezuela basins, the crust is less than 10 km thick. In contrast, shallow parts such as the Nicaragua Rise, Beata Ridge and the western Colombia basin have thick crusts. The crust of Beata ridge is particularly thick (20 km). The Puerto Rico basin has a thin crust although the acoustic basement is smooth.

In the Haiti sub-basin, the 5 km contour (Fig. 1.1.3.1) is based on just one sonobuoy results which gives an apparent velocity of 9.2 km/s for Moho refracted arrival (P_n). A dipping Moho would be able to explain this high value, but two-ship refraction data indicate the crust is less than 10 km thick and the seismic reflection profiles show a 5 km thick crust in this basin.

From these authors, the crust can be divided into two parts: an upper part with compressional velocities between 4.5 and 6.0 km/s, and a lower part with velocities from 6.0 to 8.0 km/s. Some techniques give velocities of 2.5-6.6 km/s and 6.6-7.6 km/s for layers 2 and 3, respectively, and mean thicknesses of 2.1 km for layer 2 and 5.0 km for layer 3 [White et al., 1995]. However, layer 2 is characterized by high velocity (6.6 km/s), whereas the mean velocities obtained during the older refraction studies are lower. This suggests that if the mean velocity is 6.0 km/s, the layer must have an interval of high velocity at its base. MCS profiles in Venezuela basin confirm that the crust can be divided into two parts: layer 2V (V for volcanic plateau) with velocities ranging from 5.0 to 6.0 km/s, and layer 3V with velocities higher than 6.0 km /s. Moho interface is interpreted at 15.5 km deep.

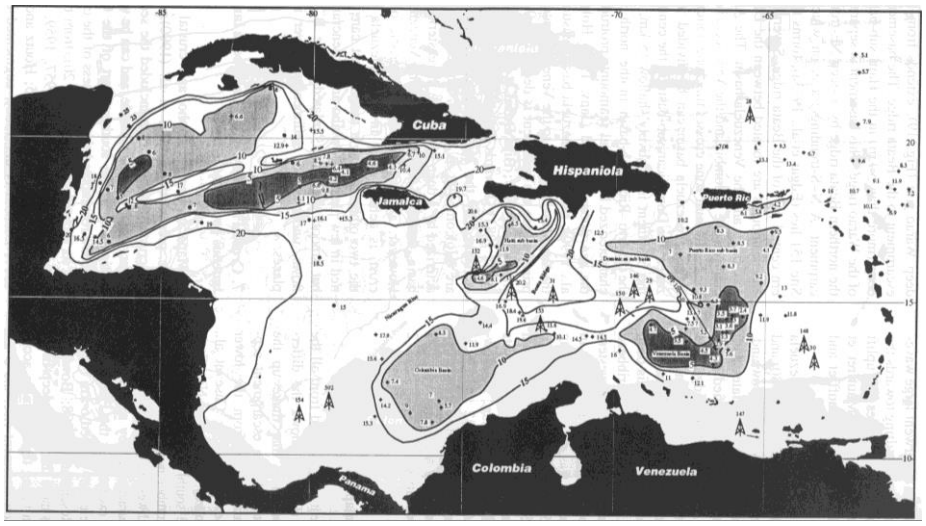

Fig. 1.1.3.1. Crustal thickness from refraction data [Officer et al., 1957; Ewing et al., 1960; Ludwig et al., 1975; Houtz and Ludwig, 1977; Talwani et al., 1977; Diebold et al., 1981]. Contour interval 5 km. Three areas have a thin crust (less than 10 km). The crust of the Venezuela basin is particularly thin (less than 5 km) and corresponds to a deep rough basement (from Mauffret and Leroy, 1997)

Although layer 2V has a mean thickness of 2.2 km, the total thickness varies from low values in the basins to 4 km on the Beata ridge and Nicaragua rise (Fig. 1.1.3.2.a). Layer 3 is thin beneath the deep Haiti sub-basin, Colombia and Venezuela basins, and thick beneath the lower Nicaragua rise and Beata Ridge.

In the Caribbean, the thickness of layer 3V controls the structure of oceanic crust with velocities ranging from 6.0 km/s to 8.0 km/s and variable thicknesses: thin beneath the basins (beneath Venezuela basin is 2 km) but very thick below Beata Ridge (13 km) and Nicaragua Rise (14 km). Layer 2 has velocities between 4.5 km/s and 6.0 km/s and is normally thin (around 2.2 km) and only in places reaches 4 km (Fig. 1.1.3.2.b).

In an igneous province, intrusion and extrusion of volcanic material might be expected to disturb the oceanic crustal structure to the extent that the original structure could no longer be identified. This fact is probably true for layer 3V, which appears to have been thickened by deep magmatic processes and has a velocity structure very different from normal oceanic crust. However, layer 2V of the igneous provinces is not very different from layer 2 of normal oceanic crust. In the Caribbean igneous province, layer 2 is composed by a thin volcanic layer (1 to 2.5 km and maximum 4 km) overlying the preserved layer 2 of the original oceanic crust (Fig. 1.1.3.2).

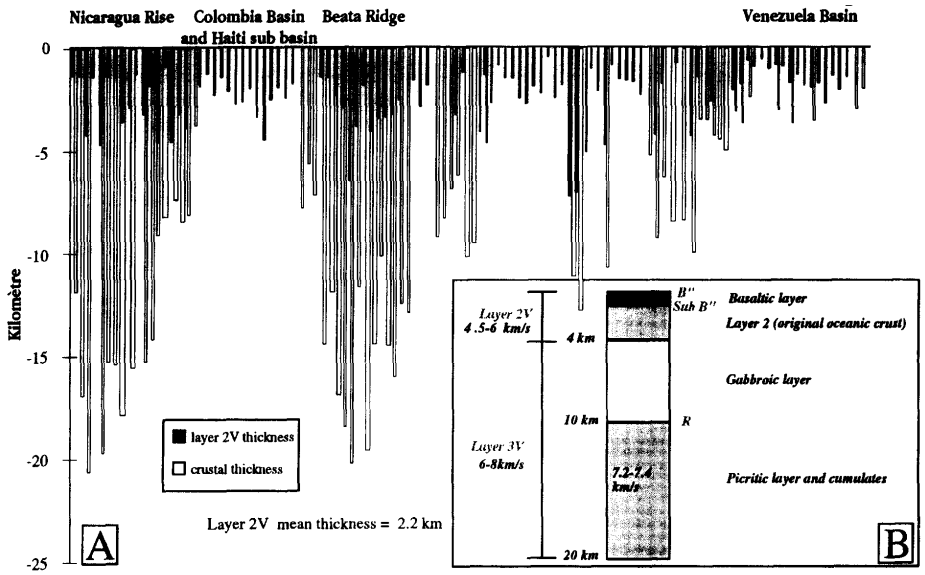

Fig. 1.1.3.2. a) Compilation of total crustal thickness and layer 2V thickness. b) Comparison between layer 2 of the original oceanic crust, sandwiched between an upper basaltic layer and layer 3V, and layer 2V. (From Mauffret and Leroy, 1997).

1.1.4 Seismicity in the Caribbean Plate

Caribbean region is known by high seismic and tsunamigenic activity (Fig. 1.1.4.1). This seismicity is important in border regions and characterized by very low intraplate events. Epicenters define the widest and most dense belts along the Middle America and Lesser Antilles subduction zones as well as transform-subduction zone regions of Puerto Rico and eastern Hispaniola in the northeastern Caribbean and Trinidad in the southeastern Caribbean [Mann and Burke, 1984]. Both subduction zones differ from each other in transverse profile, depth, frequency and magnitude of events but both are able to generate tsunamis. In this sense, Middle American subduction zone is the most active with volcanoes and significant tsunamigenic activity [Cotilla, 2011]. The density of earthquakes droops dramatically along the northern and southern strike-slip boundaries.

In northern Caribbean, southern and western Cuba (active zones and faults [Cotilla et al., 2013 *a* and *b*]) and northern Hispaniola register the most intense seismicity. In particular, the seismicity of Hispaniola is plainly justified by its geodynamic position with respect to the frequency of occurrence and to the magnitude of seismic events [Cotilla & Cordoba, 2011]. The seismic activity near Puerto Rico and Hispaniola defines the eastward continuation of the northern boundary of the Caribbean plate where the earthquake depth increases both from N to S and from E to W; the deepest shocks occur west of Puerto Rico beneath the eastern end of Hispaniola southwest of the Puerto Rico trench [Molnar & Sykes, 1969]. The seismicity associated to strike-slip fault zones in northern (Septentrional fault zone, SFZ) and

southern (Enriquillo-Plantain Garden fault zone, EPGFZ) is, in general, shallow (less than 70 km) but there are some evidences that indicate the existence of hypocenters at 100 km and reports events with large magnitudes (January 12, 2010 (M_w 7.0 Haiti Earthquake) or May 7 1842 that probably occurred along the section of SFZ offshore north Haiti [Prentice et al., 2010]). Nevertheless, those events associated with subducted slab at arcs or hinge areas are intermediate to deep (from 70 to 200 km) [Sykes et al., 1982].

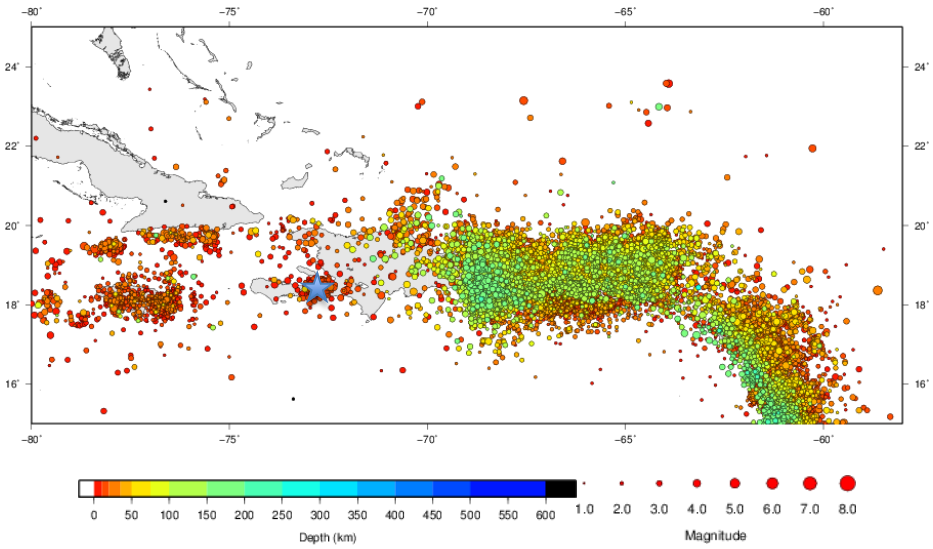

Fig. 1.1.4.1. Seismicity map in the area of study from 2000 to 2012. Blue star denotes the M7 2010 Haiti Earthquake. Data extracted from International Seismological Centre, On-line Bulletin, http://www.isc.ac.uk, Internatl. Seis. Cent., Thatcham, United Kingdom, 2010).

Throughout the history, the record of the northeast Caribbean islands offers a unique opportunity to study the long-term seismic activity of a plate boundary due to the existence of more than 500 years of historical written reports [Cotilla and Núñez, 2013]. There are large earthquakes occurred in northern Hispaniola and Mona Passage from 16th to 20th centuries such as 1562 in Santiago de los Caballeros, or the events occurred along 17th century (1615, 1665, 1673, 1684 and 1691) with M_I 6.5-7.5 near the south coast of Dominican Republic. During 19th century, several significant earthquakes occurred along the north coast of Hispaniola and Mona Passage like 1842 with M_I 7.6 or September 1887 near Septentrional fault with M_I 6.7. At the end of this century, some events were registered with similar size and location to the September 12, 2003 M_w 6.4 Puerto Plata shallow trust earthquake [Dolan & Bowman, 2004]. In 20th century, M > 6.5 earthquakes continued in these zones. It is important to note, the six large earthquakes occurred in 1946 (M_S 7.0-8.1) in Septentrional fault [ten Brink et al., 2011]. The main quake occurred in August 4, 1946, M 7.8-8.1, accompanied by a tsunami. Ali et al., (2008) studied at least eleven

large events (M ≥ 7.0) occurred over the past 250 yr. that shows how active faults in the northeastern Caribbean communicate and influence each other through Coulomb stress changes. All of the faults systems are interseismically loaded by the regional tectonics associated with the oblique subduction and associated strain partitioning between the Caribbean and North American plates. For instance, the observed westward propagation of earthquakes on the Septentrional Fault (1842, 1887), the Enriquillo Fault (1751, 1770) and along the megathrust (1787, 1943, 1946, 1953, 2003) (Fig. 1.1.4.2).

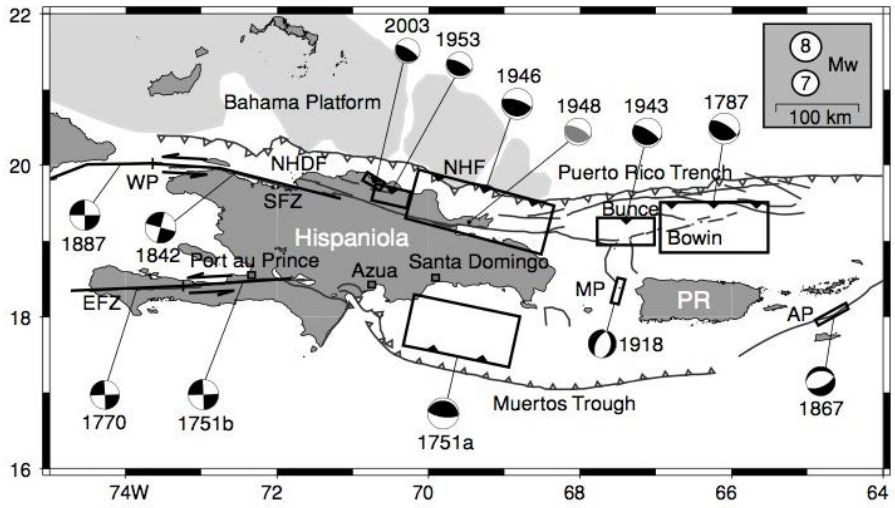

Fig. 1.1.4.2. Map showing the focal mechanism and surface projection of estimated rupture planes/geometry for large (M ≥ 7.0) historic and a recent M6.5 earthquake in the region since 1751. NHDF, North Hispaniola Deformation Front; NHF, North Hispaniola Fault; WP, Windward Passage; EFZ, Enriquillo Fault Zone; SFZ, Septentrional Fault Zone; MP, Mona Passage; PR, Puerto Rico (extracted from Ali et al., 2008).

Only moderate-size earthquakes have occurred in the 20th century north of Puerto Rico and the Virgin Islands but only two large shocks are known in this area in 1785 and 1787 (M 8-8.25 estimated by McCann [2007]). It is noteworthy that the most devastating earthquake occurred in the last few years corresponds to the 12th January 2010 in Haiti. The magnitude was 7.0 and it was located at 10 km depth near Puerto Principe, which was the deadliest earthquake in this century killing more people than the great earthquakes in Sumatra (2004) and Tohuko (Japan, 2011).

1.1.5 Potential Fields in the Caribbean Plate

- Gravity Field

Free-air gravity anomalies in the Caribbean region are among the largest in the world, ranging from −355 mgal north of Puerto Rico over the Puerto Rico Trench to greater than +200 mgal on the adjacent Greater Antilles (Fig. 1.1.5.1). Although large positive and negative free-air anomalies are associated with portions of the margins of the Caribbean lithospheric plate, the interior regions of the Caribbean and Atlantic plates generally have anomalies within ±50 mgal of zero and hence are close to being in isostatic equilibrium [Bowin, 1976].

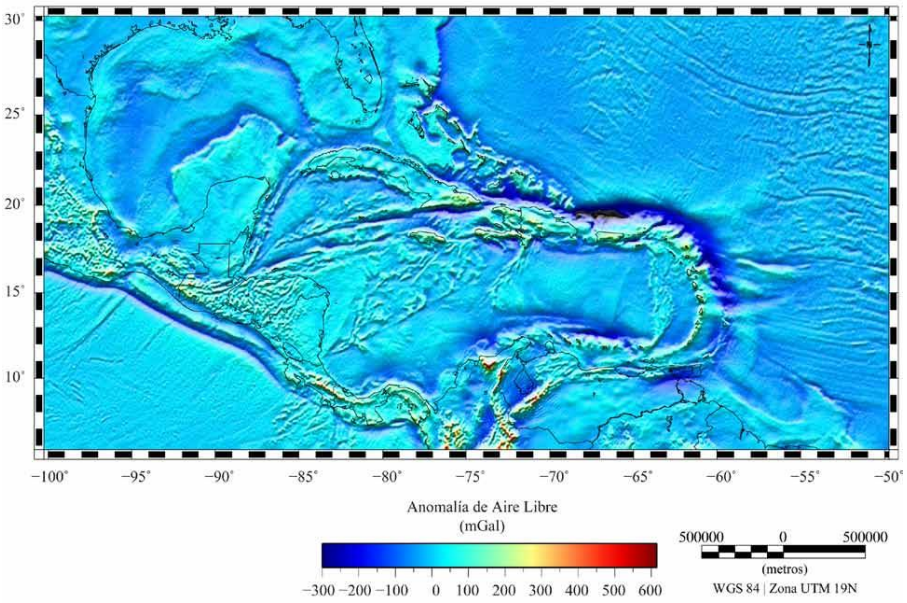

Fig. 1.1.5.1 Free-air anomaly map in the Caribbean Plate and surrounding areas (from Arnaiz Rodríguez and Garzón, 2012).

The Cayman Trough also is in nearly isostatic equilibrium, which is compatible with its origin by sea-floor spreading. Variations of the gravity field are interpreted to indicate that the easternmost end of Cuba, Jamaica, parts of Hispaniola, Puerto Rico, the Lesser Antilles, the Sierra Nevada de Santa Marta, the Eastern, Central, and Western Cordillera of the Colombian Andes, the Coast Range of Colombia, central Panama, and the Nicoya Peninsula of Costa Rica are sites of mass excess and are probably being uplifted. Mass deficiency in the eastern Caribbean is associated with the negative anomaly belt east of the Lesser Antilles, and the east-trending zones along the Puerto Rico Trench north of Puerto Rico and in eastern Venezuela and Trinidad [Bowin, 1976].

Venezuela Basin shows maximum values of +350 mGal less than NAP in the region of Puerto Rico Trench (> +400 mGal [Granja et al., 2009]). This fact is due to Venezuela Basin is part of Caribbean plateau. Beata Ridge is characterized by strong gradients aligned in a NE-SW direction as the structure is identified in the bathymetry. The values are between oceanic plateau and island arc values.

In the Hispaniola Island, there are positive Bouguer anomalies over almost the entire surface in a quiet regional field. Three zones stand out, of successively parallel tendencies, with gravitational minimums oriented in an E-W to N-W direction. The first one corresponds with the area of Cibao and Vega Central Valleys whose values are between -20 mGal and -40 mGal with a NW-SE direction bounded in the north and south by deep faults [Cotilla et al., 1997]. Second area corresponds to the central part of Hispaniola with (-30, -40) mGal interval. The Bouguer anomaly value for the last area is -20 mGal and has a predominantly WNW-ESE direction and corresponds to the Enriquillo depression [Cotilla et al. 2007]. On the other hand, the maximum positive gravity values are situated in the southeastern part of the Enriquillo depression (260 mGal). These values of 100-160 mGal appear in the north and central parts of Hispaniola and are associated with mountain ranges of a NW direction [Cotilla and Córdoba, 2010].

- Magnetic Field

In the Eastern Caribbean, the vertical component of the magnetic field ranges from -200 to 200 nT. The Greater Antilles Arc shows a continuous positive anomaly over Puerto Rico and the Dominican Republic, but loses lateral continuity over the Anegada Passage to the east. North of the arc, over Puerto Rico Trench, there is an extensive negative anomaly from the Anegada Passage to the east front of the Lesser Antilles [Orihuela et al., 2012].

The Lesser Antilles Arc features positive anomalies and a significant lateral rupture with a magnetic low that extends between Guadalupe and Martinique. The Leeward Antilles are associated with a magnetic high. At the western edge (Aruba-Curaçao), this high connects with NE–SW-oriented positive anomalies from the inner Venezuelan Basin. North of these islands, the Los Roques Basin is associated with a negative anomaly that connects at the northeast with the anomaly of the Venezuelan Basin triangular zone [Ghosh et al. 1984].

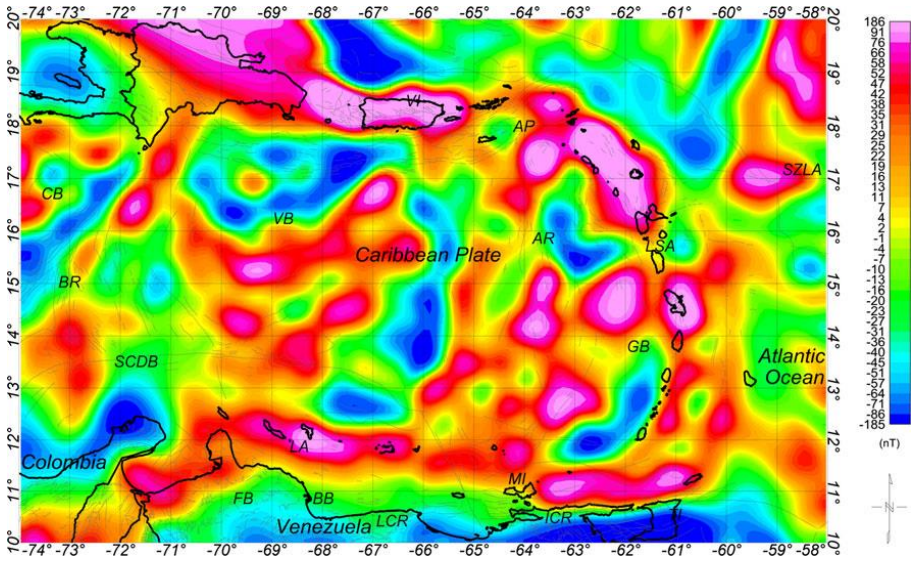

Fig. 1.1.5.2 Vertical component of the Eastern Caribbean magnetic field NGDC-720 [Maus, 2010] where SCDB = Southern Caribbean Deformed Belt; FB = Falcón Basin; BB = Bonaire Basin; BR = Beata Ridge; LCR = Littoral Coastal Range; LA = Leeward Antilles; AR = Aves Ridge, VB = Venezuelan Basin; CB = Colombian Basin; GB = Grenada Basin, ICR = Interior Coastal Range; LSA = Lesser Antilles; AP = Anegada Passage; SZLA = Subduction Zone of the Lesser Antilles [from Orihuela, et al., 2012].

The Beata Ridge shows a negative anomaly, while its flanks have positive anomalies. The Venezuelan Basin basically features NE–SW-oriented positive and negative anomalies, subparallel to the Beata Ridge. The Aves Ridge is expressed as a north–south alignment of discrete magnetic highs. NE–SW-trending magnetic highs and lows occur between the ridge and the Lesser Antilles.

In the area of Hispaniola Island, it is possible to recognize three different domains from a magnetic anomaly point of view. These domains are: i) the North Atlantic Plate; ii) a high amplitude narrow zone, that extends from the Dominican Republic to Puerto Rico-Virgin Islands; and iii) the Caribbean Plate. Particularly, the figure 1.1.5.3 presents a clear dichotomy between the Dominican Republic and Puerto Rico-Virgin Islands, delineating two different blocks. They appear to be fractured in the Mona Channel as well as at San Pedro Basin suggesting a left-lateral strike slip between them. This dichotomy suggests the separation of the Dominican Republic and Puerto Rico-Virgin Islands into different tectonic blocks [Catalán and Martín-Dávila, 2013].

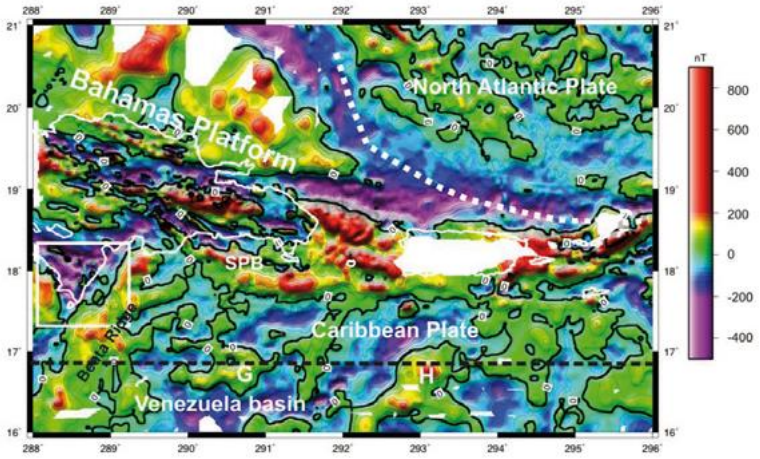

Fig.1.1.5.3. Final gridded magnetic anomaly map. G and H mark the magnetic maxima in the North Caribbean Plate. The inserted white square limits the negative magnetic anomaly area. The white dotted line delineates the southern boundary of a slightly positive magnetic anomaly plateau. SPB: San Pedro Basin (From Catalán and Martín-Dávila, 2013).

1.2 THE NORTHEASTERN CARIBBEAN PLATE TECTONIC PROBLEM. STATE OF THE ART

The development of knowledge in NE of the CP started at beginning of twentieth century due mainly to geological exploration of hydrocarbons. The early modern studies carried out dating where surface geology and big earthquakes associated to tsunamis as the Virgin Islands earthquake on 1867 with Ms 7.3 [Taber, 1922].

From the 50's to 70's, many geological and geophysical fieldtrips were carried out due to the exploration of hydrocarbons as Ewing et al., (1957), Bunce and Fahlquist (1962) or Ladd et al., (1977). But in the eighties besides the hydrocarbon exploration, seismological studies were conducted and early tectonic models appeared with new ideas about microplates that form the CP [Mann et al., (1984) or Byrne et al., (1985)].

Nowadays, it is possible to find studies especially about seismicity related with active faults present in Hispaniola Island (EPGFZ and SFZ) whose main peak took place with the devastating earthquake in Haiti (2010) [Calais et al., 2010; or Prentice et al., 2010; among others]. Geological investigations in the Dominican Republic have been carried out in the last years by both state institutions and Spanish agencies, which highlights the Geothematic Mapping Program of the Dominican Republic [Hernáiz-Huerta and Pérez-Estaún, 2002; Lewis et al., 2002; Escuder-Viruete et al., 2010; or Hernáiz-Huerta et al. 2011]. Also, studies in the area of gravity and magnetic field

such as Granja et al., (2009, 2010) or Catalán and Martín-Dávila (2013) have been developed.

In summary, the region of Dominican Republic has been studied in the N, S and E but different tectonic hypothesis about the processes that happens in Hispaniola Island have been developed by different authors but two of them are stronger that the others. In this section both hypothesis are described.

1.2.1 Tectonic hypothesis 1: No active subduction

The Caribbean domain and Central America form a small lithospheric plate inserted between North and South America that is moving eastward relative to North America (Fig. 1.2.1.1). Its northern boundary is a left-lateral transcurrent fault system connected around its eastern end to the subduction of the Atlantic oceanic lithosphere under the Lesser Antilles [Calais et al., 1992].

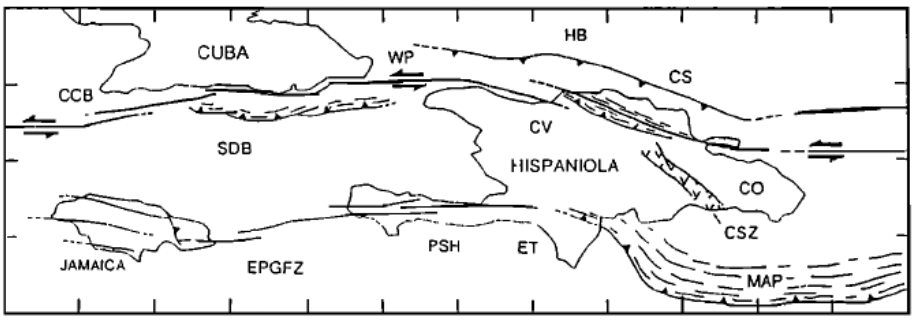

Fig. 1.2.1.1. Structural sketch map. Abbreviations are CCB, Cabo Cruz basin,; SDB, Santiago Deformed Belt; CS, Cordillera Septentrional of Dominican Republic; CV, Cibao Valley; CO, Cordillera Oriental of Dominican Republic; CSZ, Cretaceous suture zone; ET, Enriquillo trough; PSH, Presq'île du Sud of Haiti; EPGFZ, Enriquillo-Plantain Garden fault zone; MAP, Muertos acretionary prism; WP, Windward Passage, and HB, Hispaniola Basin (from Calais et al., 1992).

The distribution of shallow earthquakes (0 < depth < 50 km) in the NE Caribbean domain establishes four main regions: south of Cuba, east of Jamaica, north of Hispaniola and southeast of the Dominican Republic (Fig. 1.2.1.2 a). There is a good correlation between distribution of shallow earthquakes, their focal mechanism and active transcurrent faults, along this plate boundary. This combination between seismicity and kinematic data documents that the strain and stress distributions are the result of strike-slip motion combined with a minor convergence component. Thus it is possible to conclude that the northern Caribbean plate boundary is a transcurrent fault system, not a subduction zone, from Cuba to western Hispaniola at least.

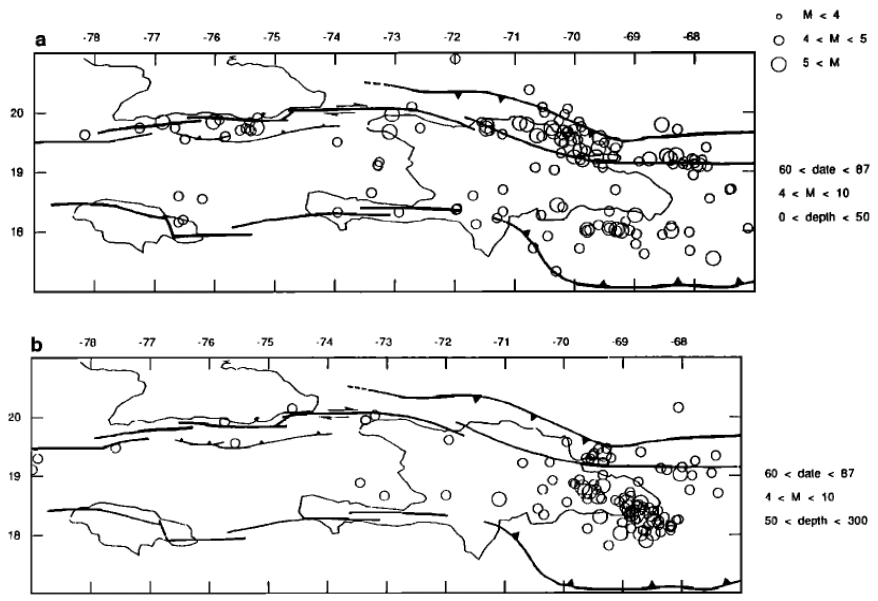

Fig. 1.2.1.2. a) Map of shallow seismic events. b) Map of intermediate to deep seismic events (from Calais et al., 1992).

The deep events (depth > 50 km) are mainly located in the eastern part of Hispaniola (onshore and offshore) (Fig. 1.2.1.2 b). Obviously, if there is no subduction, the question is how to explain this intermediate and deep seismicity. Some studies [Sykes et al, 1982; Calais et al., 1992] propose the existence of a lithospheric slab under the northeastern corner of the Caribbean plate, inherited from the frontal subduction of the Atlantic oceanic lithosphere under the Lesser Antilles. This slab has been disconnected from the Atlantic oceanic lithosphere by transcurrent faulting along the plate boundary (Fig. 1.2.1.3).

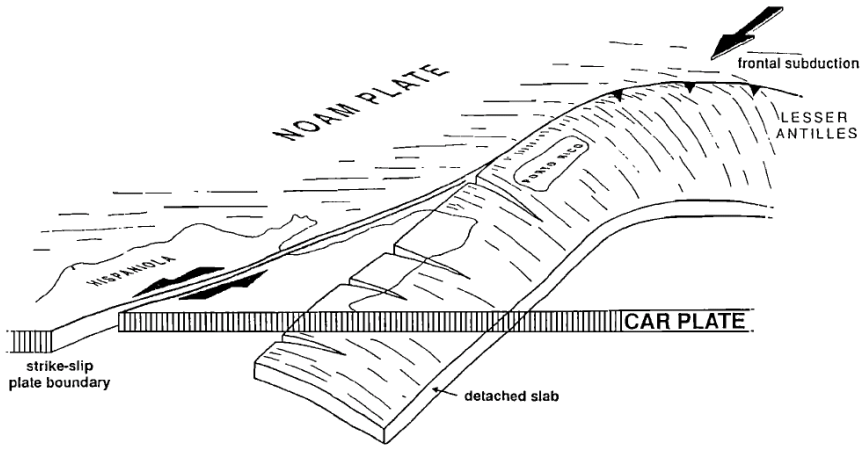

Fig. 1.2.1.3. Three dimensional interpretation of the transition from frontal subduction to transcurrent faulting along the northern Caribbean (CAR) plate boundary (from Calais et al., 1992).

1.2.2 Tectonic hypothesis 2: Dual Subduction

The North America-Caribbean plate boundary zone consists of a 100-250 km wide seismogenic zone of mainly left-lateral strike-slip deformation extending over 2000 km along the northern edge of the Caribbean Sea [Mann et al, 1995] (Fig. 1.2.2.1 a).

To the east of the Cayman Trough in Jamaica, Hispaniola, and Puerto Rico (Fig. 1.1.1.1), the plate boundary is especially wide with a seismogenic zone up to 250 km wide at the longitude of the island of Hispaniola. The width of the plate boundary is reflected in:

- A multi-branched, active, left-lateral strike-slip and convergent fault zone. Strike-slip faults occupy an inboard position on the higher-standing, land and shallow marine areas. Convergent faults and acretionary prisms form the break between abyssal depths of the Caribbean Sea and Atlantic Ocean [Dillon et al., 1992] (Fig. 1.2.2.1 a).
- A dual zone of shallow active seismicity west of 71°W [Sykes et al., 1982, Calais et al., 1992] (Fig. 1.2.2.1 a).
- Dual rupture zones of large, historical earthquakes. A northern zone of historical seismicity passes through northern Hispaniola and southern Cuba and a southern zone passes through southern Hispaniola and Jamaica (Fig. 1.2.2.1 b).

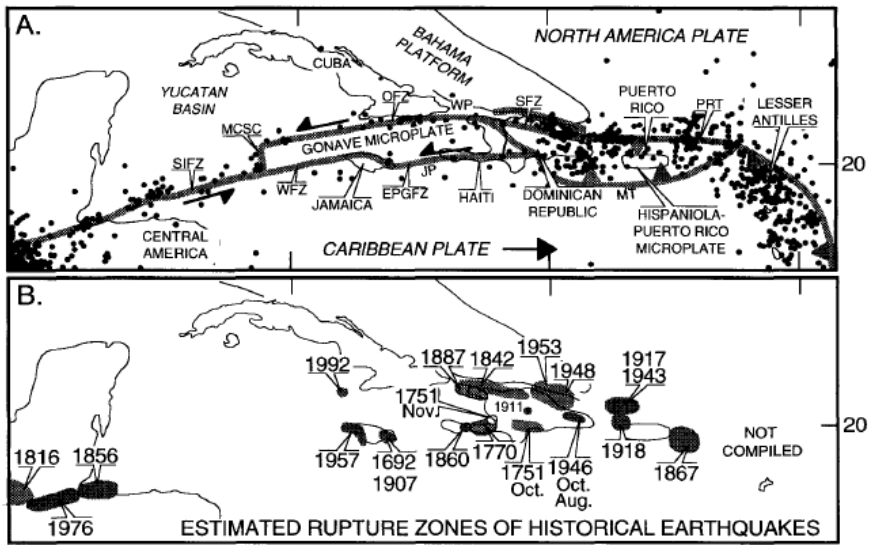

Fig. 1.2.2.1. (a) Tectonic setting and seismicity (1963-1992, M > 4.5, source: ISC) of the North America-Caribbean plate boundary zone. Heavy gray lines indicate major plate boundary faults. Key to abbreviations: SIFZ = Swan Islands fault zone; WFZ = Walton fault zone; MCSC = Mid-Cayman spreading center; OFZ = Oriente fault zone; EPGFZ = Enriquillo-Plantain Garden fault zone; SFZ = Septentrional fault zone; JP= Jamaica Passage; WP= Windward Passage; MT= Muertos trench; PRT= Puerto Rico trench. (b) Estimated rupture zones of northern Caribbean historical earthquakes (From Mann et al., 1995).

From seismicity data of the region with reliable focal mechanisms (Fig. 1.2.2.2), Dolan et al., (1998) construct a structure-contour map on the top of the south- to south-southwest-dipping, underthrust Atlantic (North America) slab (Fig. 1.2.2.3).

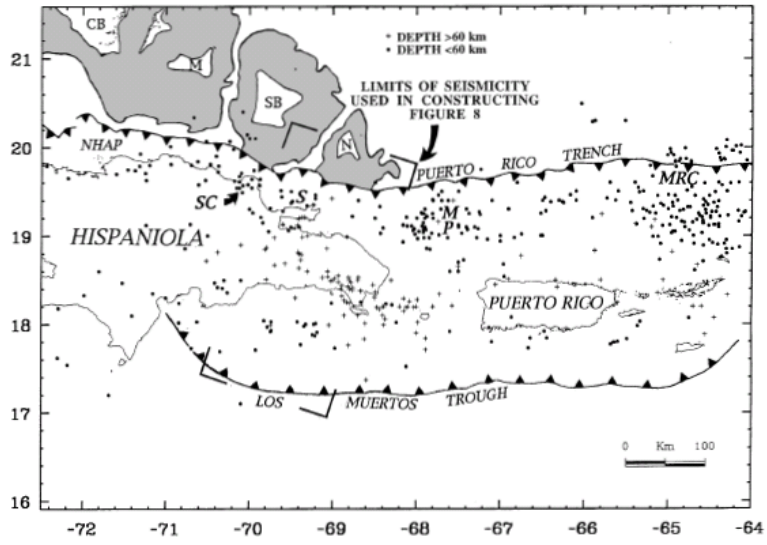

Fig. 1.2.2.2. Map of seismicity (1962–1992) from ISC catalog. Gray shading denotes limits of southeastern Bahamas carbonate province. Rectangular box shown in Fig. 1.2.2.4. CB = Caicos bank; M = Mouchoir bank; MP = Mona Passage seismicity cluster; MRC = Main Ridge seismicity cluster; N = Navidad bank; NHAP = northern Hispaniola acretionary prism; S = Samana seismicity cluster; SB = Silver bank; SC = Sosua seismicity cluster (from Dolan et al., 1998).

The figure 1.2.2.4 shows a summary of seismicity in a cross section in north-northeastern to south-southwest direction where the Atlantic oceanic slab dips southward between 20º and 45º and from 100 km the slab has a strong vertical component due to the presence of the Caribbean slab which dips northward 15º [Dolan et al., 1998]. Although this profile is oriented approximately perpendicular to regional strike, the profile is oblique to some tectonic and topographic features.

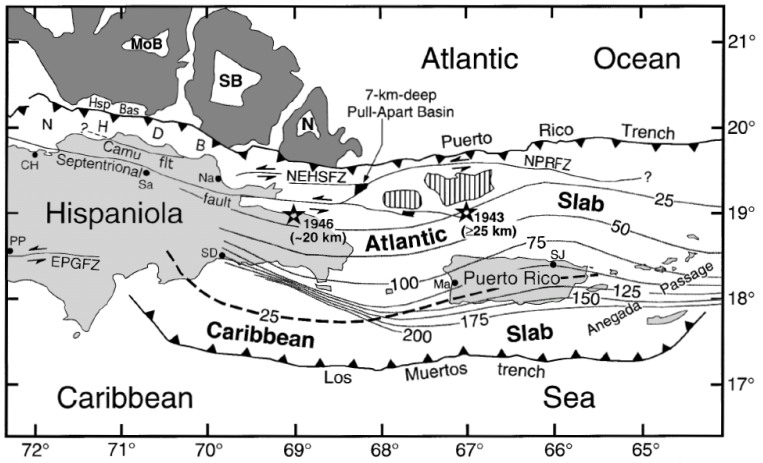

Fig. 1.2.2.3. Structure contour map of underthrust Atlantic and Caribbean slabs in north-central Caribbean region. Depth contour interval is 25 km. Slab contours shown as solid gray lines are constructed along the top of a south-dipping zone of seismicity interpreted to represent the top of the underthrust slab of Atlantic oceanic lithosphere of the North America plate. Slab contour shown by black dashed line is constructed along top of north-dipping upper limit of a north-dipping zone of seismicity thought to represent the top of underthrust Caribbean lithosphere. Dark shading denotes limits of Bahamas carbonate province. Black circles show locations of major cities. Irregular black areas northeast of Hispaniola denote pull-apart basins at left-steps along the Septentrional fault system (from Dolan et al., 1998).

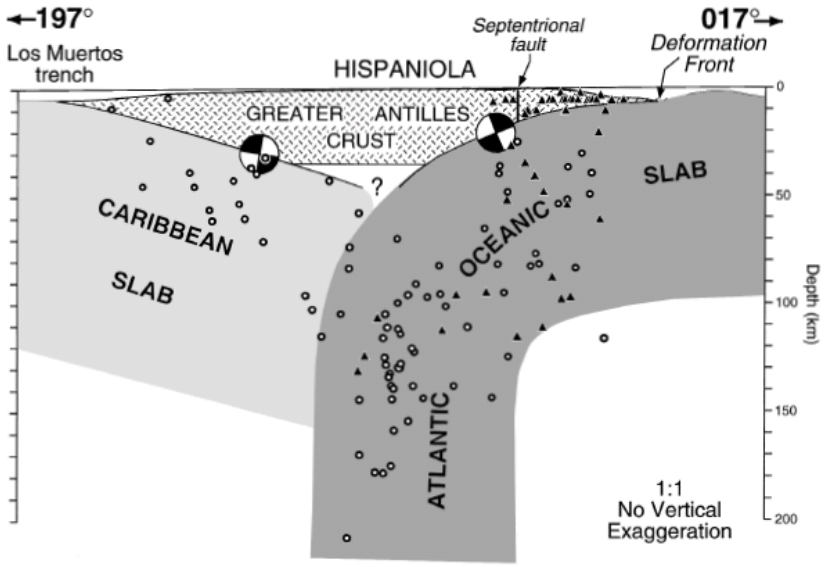

Fig. 1.2.2.4. Cross section oriented 17° showing recent seismicity in the region of the 1946 northern Hispaniola earthquake. Heavy line at top of figure represents bathymetry-topography along center line of cross section. No vertical exaggeration. Triangles denote 1946 aftershocks relocated by Russo and Villaseñor (1995). (From Dolan et al., 1998)

In accordance with these hypotheses, some aspects are remarked. These are:

- Bahamas platform makes the oceanic lithosphere of NA plate locally buoyant, hence, the possibility of a tear in the subducting slab (tectonic hypothesis 1).
- According to the tectonic hypothesis 1, the northern part of Hispaniola would still belong to the NA plate while de southern parts denote the northern edge of the overriding Caribbean plate (Fig. 1.2.1.3).
- If one speculates that Hispaniola and Puerto Rico were once buoyant parts of the NAP analog to Bahamas, their detachment from the subducting slab could have led to the formation of a microplate (tectonic hypothesis 2).

With the advent of the nineties, geodetic investigations with GPS clarify the kinematics of the diffuse boundary between NAP and CP, setting rates and directions of relative movement between such plates. Some the authors responsible for these investigations are: Jansma et a., (2000), Mann et al., (2002) or Calais et al., (2002).

1.3 CARIBE NORTE AND GEOPRICO-DO PROJECTS

Despite the large number of studies conducted in the northern Caribbean plate, there are certain areas where no agreement exists on geodynamic models that govern the structure and tectonic development of the area concerned due to the absence mainly deep geophysical research. To resolve this anomalous distribution of geophysical studies in the NE Caribbean Plate, have been carried out two ambitious projects called GEOPRICO-DO and CARIBE NORTE in recent years.

In the following sections, both projects will be explained. Technical characteristics about instrumentation used during both projects will be described precisely in the Chapter 2.

1.3.1 GEOPRICO-DO Project (2005)

The GEOPRICO-DO project (*Estructura y geodinámica del borde noreste de la Placa Caribe: Microplaca de Puerto Rico*) (REN2003-08520-C02-01/02) was an offshore-onshore geophysical study carried out between 28th March and 17th April 2005 [Carbó et al., 2005; Córdoba et al., 2009]. This project was coordinated by Universidad Complutense de Madrid (UCM) and different Spanish and international institutions collaborated: Real Instituto y Observatorio de la Armada (ROA); Instituto Geográfico Nacional (IGN); Instituto Español de Oceanografía (IEO); Universidad Autónoma de Santo Domingo (UASD); Dirección General de Minería de la República Dominicana (DGM); Universidad de Mayagüez and Puerto Rico Seismic Network (PRSN). The experiment collected the following data:

- Multibeam bathymetry in a total area of 2.868 miles using Simrad EM-120/EM-1002 Multibeam.

- Gravity using Bell Aerospace Textron BMG-3 Marine Gravimeter in the same area.

- Magnetic data collected in all surveyed area with SeaSPY Marine Magnetometer.

- High-resolution seismic using Topographic Parametric Seismic System (TOPAS) recorded in all study area.

- Refraction/wide-angle data were recorded onshore along three profiles to the south of Dominican Republic (276 miles) and five seismic transects to northeast of Puerto Rico and Virgin Islands (281 miles). There was used an air gun array with 3680 c.i. (cubic inch) every 90 second (shot interval) recorded by 28 land seismometers deployed on land and 10 short-period ocean bottom seismometers (OBS), which were left on the seafloor to record local seismicity and retrieved in November 2005.

- Multichannel seismic reflection data along four profiles northeast of Puerto Rico and Virgin Islands (252 miles) with a 2700 c.i. airgun array in a shot interval of 50 meters and using a hydrophone streamer of 2.4 km and 96 channels.

During the experiment, two different areas were studied (Fig. 1.3.1.1). The first area is the triple junction of the Muertos Trough subduction/thrust zone, the Enriquillo strike-slip fault zone and the aseismic Beata Ridge [Mauffret and Leroy, 1999] where the deformation regime changes from underthrusting in the Muertos Trough to convergence and left-lateral strike-slip in the Enriquillo fault zone with an abrupt bathymetry. The second area is the northeastern zone of Puerto Rico and Virgin Islands where the Puerto Rico Trench is the main tectonic and bathymetric feature (8340 m in depth and -350 mGal free-air gravity anomaly).

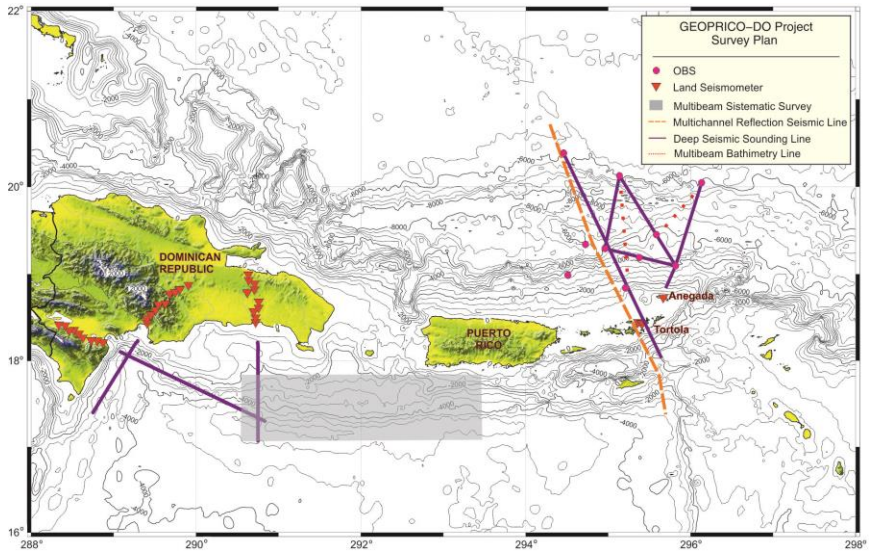

Figure 1.3.1.1. Location and track lines on a map of the GEOPRICO-DO Project surveyed area. Orange line represents a series of Line-seismic-Reflection surveys. Purple lines are Line-seismic-Refraction surveys. All tracks lines included combine multibeam, potential fields, and sub-bottom profiling data. The magenta points indicate the deployed OBS and red inverted triangles represent land seismic portable stations. Bathymetry is shown and given in meters below sea level.

According to these areas, the project aims for the first zone is to understand why the change in the deformation regime occurs in the south of Dominican Republic, the possibility of obtaining correlations between the onshore and offshore structures in Hispaniola and the Muertos zone and analyzing the role of Beata Ridge in this system. Regarding the second area, the main aim is to understand the tectonic regime in the northeastern part of Puerto Rico and Virgin Islands and explain the reason for high seismic activity and its potential hazard in the closest areas and densely populated [Carbó et al., 2005].

The data was collected aboard the Spanish research vessel *Hespérides* (Fig. 1.3.1.2) and the Puerto Rican commercial tugboat *Kruger B* was used to deploy the OBS.

Fig. 1.3.1.2 Spanish Research Vessel Hespérides.

The seismic data acquisition system and seismic recording system configuration onboard R/V Hespérides are shown in Table 1.3.1.I and Table 1.3.1.II, respectively.

Seismic Data Acquisition System (R/V Hespérides)	
Seismic Source	13 airguns Bolt Technology models 1900 and 1500LL
Configuration	7 airguns (2 groups)
Main group capacity	22.45 liters
Secondary group capacity	12.37 liters
Volume	34.04 liters
Nominal pressure	136 atm
Depth	10±1 m
Shooting interval	90 s
Distance between shots	75-150 m

Table 1.3.1.I. Seismic Data Acquisition System onboard R/V Hespérides during GEOPRICO-DO Project.

The R/V Hespérides has a large number of scientific and technical equipment. The equipment used to carry out seismic studies consists of energy sources, acquisition equipment and processing systems.

The recording system features used in this project are reflected in the following table.

Seismic Recording System Configuration (R/V Hespérides)	
Streamer length	2500 m
No. of channels	96 channels
No. of hydrophones/channels	24 hydrophones
Streamer depth	9±1 m

Table 1.3.1.II. Seismic recording system configuration onboard R/V Hespérides during GEOPRICO-DO project.

The onshore experiment was developed in two areas: Dominican Republic and British Virgin Islands (Fig. 1.3.1.1). In the south of Dominican Republic, 28 seismic stations were deployed along 3 profiles from 30th March to 1st April. For the purpose of this work, just this area will be analyzed. Table 1.3.1.III shows a summary of seismic lines (in the taken order) in Dominican Republic during GEOPRICO-DO project.

Line ID	AZ (º)	Vm (knots)	GFH ini	GFH fin	Time (hours)	Miles	# Shots
L8	180.0	5.00	301528Z MAR 05	310454Z MAR 05	13.42	73.14	538
L6	296.5	5.09	310855Z MAR 05	010800Z ABR 05	23.07	118.80	924
L7	206.5	5.17	011119Z ABR 05	012321Z ABR 05	12.03	62.05	482
TOTAL					48.52	253.99	1944

Table 1.3.1.III. Dominican Republic seismic profiles summary in GEOPRICO-DO project.

The technical specifications of digital stations are observed in Table 1.3.1.IV.

Model	Brand	No. Deployed stations	No. Registering components	Sample Rate	Geophones
TEXAN 125A	REFTEK (USA)	16	1	50 sps	1C geophones of 4.5 Hz
TAURUS	NANOMETRICS (CANADA)	10	3	100 sps	Seismometers LE-3D 1 Hz
HATHOR3	LEAS (FRANCE)	2	3	100 sps	Seismometers LE-3D 1 Hz

Table 1.3.1.IV. Seismic stations deployed in Dominican Republic (GEOPRICO-DO Project).

In the British Virgin Island, four seismic stations were deployed on Tortola Island and 2 digital stations on Anegada Island from 8th to 15th of April 2005. Table 1.3.1.V shows the technical specifications of these seismic stations used for this project.

	Model	Brand	No. Deployed stations	No. Registering components	Sample Rate	Geophones
TORTOLA	TAURUS	NANOMETRICS (Canada)	3	3	100 sps	Seismometer LE-3D 1 Hz
	HATHOR3	LEAS (France)	1	3	100 sps	Seismometer LE-3D 1 Hz
ANEGADA	TAURUS	NANOMETRICS (Canada)	1	3	100 sps	Seismometer LE-3D 1 Hz
	MARS LITE	LENNARTZ ELECTRONICS GmbH (Germany)	1	3	100 sps	Seismometer LE-3D 1 Hz

Table 1.3.1.V. Seismic stations deployed on the British Virgin Islands (GEOPRICO-DO Project).

1.3.2 CARIBE NORTE Project (2009)

The CARIBE NORTE Project (Caribbean-North American Plate Boundary Analysis: From Beata Ridge (Dominican Republic) to Anegada Passage (Lesser Antilles)) (CTM2006-13666-C02-01/02) was carried out onshore and offshore surveys in the Dominican Republic region from 25th March to 25th April [Carbó et al., 2010; Córdoba et al., 2010]. This project complements the study started on 2005 with GEOPRICO-DO project. This project was coordinated by UCM. Some associated Spanish institutions collaborated during the project as ROA, IGN and IEO. In addition, Dominican Republic and Puerto Rico institutions participated actively in diverse tasks (UASD and DGM).

The main goals of CARIBE NORTE project complements the study started on 2005 with GEOPRICO-DO project. They are:

- Checking the existence of subduction in the Muertos Trough.
- Determining the deep structure across and along Hispaniola and Beata Ridge (general mapping of subsurface structures).
- Studying the existence of a possible tear fault in Beata Ridge that sharply changes the tectonic regime from frontal thrusting in the Muertos Trough to strike-slip in the Enriquillo-Plantain Garden Fault Zone (EPGFZ).
- Exploring the possible correlations between the onshore structures on Hispaniola Island and the offshore structures in the Muertos margin.
- Evaluating the active deformation and submarine landslides to assess seismic and tsumani hazards.

To achieve these targets, work on land and sea were made. The marine geophysical cruise, aboard the Spanish R/V Hespérides, collected multibeam bathymetry, gravity and magnetic, high-resolution seismic and seismic wide-angle reflection/refraction data. The marine experiment took place in 20 days. During this period, four wide-angle seismic lines were made, two of them divided in the northern and southern parts (LM1N, LM1S, LM3N and LM3S), one across Beata Ridge (LM2) and the last one in front of east coast of Dominican Republic (LM4). These lines were made combining multibeam bathymetry, gravity and magnetic studies.

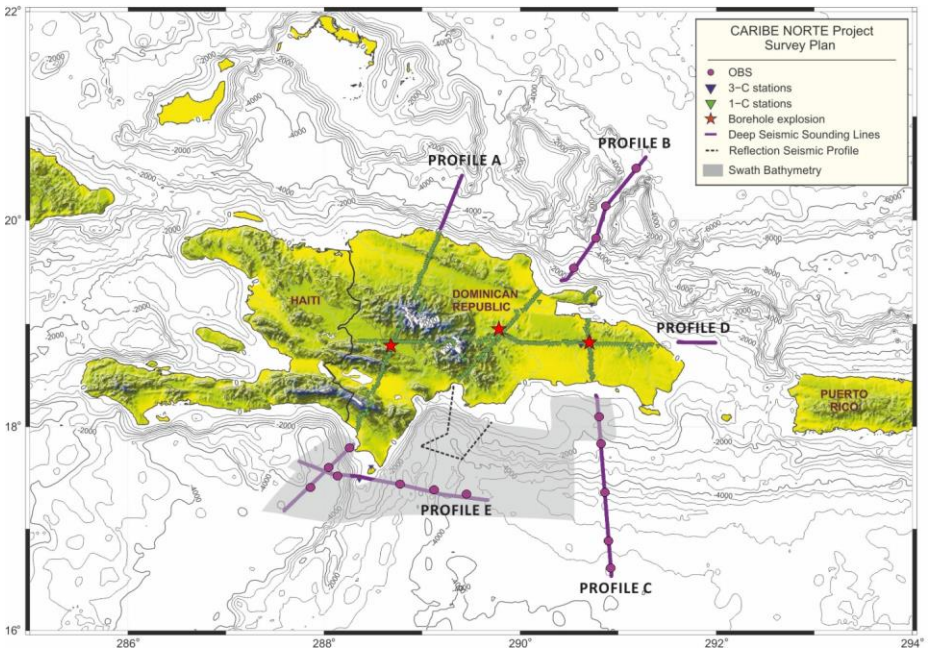

Fig. 1.3.2.1. Map of the area surveyed by the CARIBE NORTE project. Along the onshore deep seismic sounding profiles, 340 land seismometers were deployed. Bathymetry is shown and given in meters below sea level.

In the frame of the land seismic experiment, a set of 340 portable seismic stations were deployed along four main onshore profiles of 200-300 km length, with a ratio of 1 station/3 km (Fig. 1.3.2.1). In addition to the onshore deployment, a network of 16 OBS were anchored in the territorial sea of the Dominican Republic to extend the wide angle seismic profiles deployed on land to the sea. Furthermore, the fifth profile was only deployed at sea with 5 OBS crossing Beata Ridge. This was the first time in which OBS have been used to acquire seismic data in the exclusive economic zone of the Dominican Republic. Both OBS and land stations recorded air gun shots (3850 inches) provided each 90 seconds by the R/V Hespérides and three land shots of 1000 kg explosive (80 m depth and a diameter of 12-14 cm wide) detonated in three points selected at the Central and Oriental Cordilleras whose exact locations were Hato Mayor (S1, east), Cotui (S2, central) and San Juan de la Maguana (S3, west) (Fig. 1.3.2.2). Control of shooting times at each borehole was carried out by two seismic stations model TAURUS.

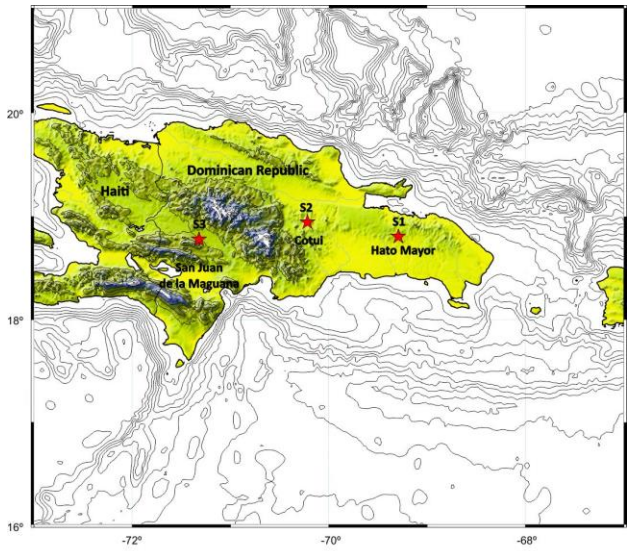

Fig. 1.3.2.2. Land shots localization map in CARIBE NORTE project.

The charges were detonated at local time showed in the following table (Table 1.3.2.I).

	Latitude	Longitude	Altitude	Date	Local Time
Hato Mayor (S1)					
Test drilling	18 48.4	69 17.5	234	16/04/2009	14:30:47
Geophone 1 (1-C)	18 48.4	69 17.5	234		
Geophone 2 (1-C)	18 48.4	69 17.4	229		
Equipment-1 (T?)	18 48.4	69 17.4	229		
Equipment-2 (T161)	18 48.4	69 17.5	235		
Cotui (S2)					
Test drilling	18 56.7	70 13.0	228	16/04/2009	21:09:10
Geophone 1 (1-C)	18 56.7	70 13.0	228		
Geophone 2 (1-C)	18 56.6	70 13.0	228		
Equipment-1 (T?)	18 56.6	70 13.0	228		
Equipment-2 (T161)	18 56.7	70 13.0	228		
San Juan de la Maguana (S3)					
Test drilling	18 46.7	71 19.1	590	17/04/2009	16:06:13
Geophone 1 (1-C)	18 46.7	71 19.1	590		
Geophone 2 (1-C)	18 46.7	71 19.1	590		
Equipment-1 (T?)	18 46.7	71 19.1	590		
Equipment-2 (T161)	18 46.6	71 19.1	590		

Table 1.3.2.I. Localization and time for the boreholes S1, S2 and S3 carried out during CARIBE NORTE experiment.

From 3rd to 6th April were deployed 340 land stations of which 8 correspond to the model TAURUS (3 component seismometers LE-3D/lite 1 Hz, *3C*) and 332 to TEXAN 125A (vertical component 4.5 Hz, *1C*). The 332 TEXAN 125A were installed along four seismic profiles (Fig. 1.3.2.1), three of them in NS direction (Profiles A, B and C) and another one in EW (Profile D). Profile A had 101 seismic stations situated from Pedernales (south DR) to Puerto Plata (north DR) crossing San Juan de la Maguana (S3 shot). Profile B consisted of 58 stations located from Azúa (south) to Nagua (north) crossing the land shot named S2 in Cotui. The last NS profile is Profile C deployed from San Pedro de Macorís (south) to Playa El Valle (north Samaná Peninsula) through Hato Mayor (S1) with 39 seismic stations. Profile D was deployed from western San Juan de la Maguana, near the Haitian border, to Bavaro Beach with a total of 140 seismic stations; three of them were in common with profiles A, B and C. These stations were working continuously for 6 days. For this purpose, we designed an adapter for increasing the station autonomy with 6 batteries instead of two. During the fieldwork, less than a 10% of TEXAN stations did not work properly nor had any problem.

The 3C seismic stations were used close to land shots and in some strategic places where were working for registering the marine shots provided by R/V Hespérides and land shots. These stations where located in Hato Mayor, Samaná, Beata and Alto Velo Islands. Marina de Guerra Dominicana provided BELLATRIX patrol vessel (GC-106) to reach both islands and install these two stations.

Deployment of OBS began on 5th to 9th April by CSIC-UTM (Unidad de Tecnología Marina) and ROA technicians aboard patrol vessel ORION (GC-109) provided by Marina de Guerra Dominicana. CSIC-UTM staff was responsible for synchronization, calibration and programming of the OBS (see Chapter 2 section 2.2.3). The order in the deployment of OBS during this project (Fig. 1.3.2.3) was carried out according to a plan, being first installed OBS of seismic line LM2 (OBS 16, 15, 14, 13, 11) followed by the line LM1S (OBS 10, 11 and 12). The last line deployed in the south of the Dominican Republic was the LM3S (OBS 9, 8, 7, 6 and 5) passing then to the north of the island for the deployment of the OBS 1, 2, 3 and 4 corresponding to the LM3N seismic line. This deployment was made in 3 days, 7 hours and 30 minutes in a total distance of 839 miles.

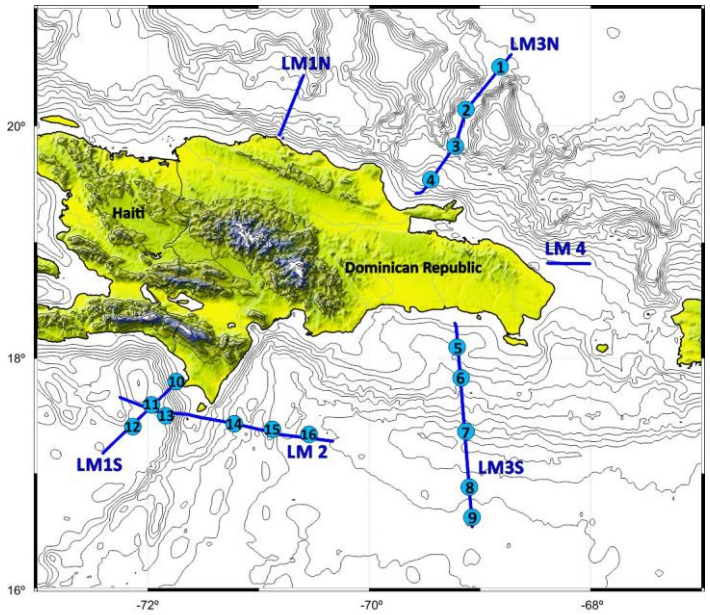

Fig. 1.3.2.3. OBS deployment map in CARIBE NORTE project. Blue dots with a number inside are the OBS with its corresponding number. Dark blue lines are the marine seismic lines.

The collecting process of the OBS was conducted between 18th and 22nd April 2009 aboard ORION patrol vessel, starting with the OBS located in seismic line LM3N, followed by lines LM3N, LM2 and finishing with line LM1S.

The recovery process was completed in 4 days, 2 hours and 40 minutes with a total distance of 939 miles.

Table 1.3.2.II indicates total effective time length, number of shots and miles for each seismic profiles made in the Exclusive Economic Zone of Dominican Republic.

PROFILE	Total time length	# Shots	Nautic Miles
LM1N	6h 39m 18s	269	27.8
LM3N	17h 03m 36s	683	91.1
LM4	4h 03m 39s	165	24.6
LM3S	20h 53m 07s	832	105.8
LM2	21h 22m 21s	854	125.3
LM1S	10h 34m 30s	423	59.2
TOTAL	**3d 8h 36m 31s**	**3226**	**433.8**

Table 1.3.2.II. Summary of time length, number of shots and distances for each seismic profile in CARIBE NORTE project.

Table 1.3.2.III summarized the most relevant data of the profiles made.

PROFILE	Beginning of the line				Ending of the line			
	Date	**Time**	**Latitude**	**Longitude**	**Date**	**Time**	**Latitude**	**Longitude**
LM1N	**11/04/09**	06:14:35	19º 56′ N	70º 48′ W	**11/04/09**	12:35:00	20º 25′ N	70º 35′ W
LM3N	**11/04/09**	22:05:00	19º 25′ N	69º 33′ W	**11/04/09**	22:30:30	19º 25′ N	69º 31′ W
		22:30:30	19º 25′ N	69º 31′ W	**12/04/09**	04:15:30	19º 49′ N	69º 13′ W
	12/04/09	04:15:30	19º 49′ N	69ºº 13′ W		07:59:00	20º 08′ N	69º 07′ W
		07:59:00	20º 08′ N	69º 07′ W		14:59:00	20º 36′ N	68º 43′ W
LM4	**13/04/09**	02:49:21	18º 49′ N	68º 00′ W	**13/04/09**	06:53:00	18º 49′ N	68º 23′ W
LM3S	**13/04/09**	21:58:23	18º 18′ N	69º 13′ W	**13/04/09**	22:44:00	18º 15′ N	69º 12′ W
		22:44:00	18º 15′ N	69º 12′ W	**14/04/09**	18:51:30	16º 32′ N	69º 04′ W
LM2	**15/04/09**	20:29:00	17º 16′ N	70º 19′ W	**16/04/09**	09:59:00	17º 29′ N	71º 31′ W
	16/04/09	09:59:00	17º 29′ N	71º 31′ W		10:45:30	17º 30′ N	71º 35′ W
		10:45:30	17º 30′ N	71º 35′ W		11:21:30	17º 30′ N	71º 38′ W
		11:21:30	17º 30′ N	71º 38′ W		14:11:00	17º 32′ N	71º 54′ W
		14:11:00	17º 32′ N	71º 54′ W		15:45:30	17º 32′ N	71º 55′ W
		15:45:30	17º 32′ N	71º 55′ W		19:25:51	17º 39′ N	72º 15′ W
LM1S	**17/04/09**	02:02:00	17º 10′ N	72º 24′ W	**17/04/07**	12:36:30	17º 49′ N	71º 41′ W

Table 1.3.2.III. Summary of seismic lines carried out in Dominican Republic.

1.4 AIMS OF THIS WORK

According to tectonic hypothesis exposed in previous sections, the state of the art, and considering that Hispaniola has been the locus of moderate to large earthquakes along the Septentrional Fault in the north and the Enriquillo Fault zone in the south, the main objective of this thesis is to constrain the lithospheric structure in NE Caribbean Plate, specifically, beneath Dominican Republic and their adjacent areas. This aim will let to obtain a better understanding of the tectonic boundary conditions that lead to those earthquakes. To fulfill this objective, we can establish some specific aims depending of the region to study.

In the northern offshore area of Dominican Republic, the aim is determine how the contact is between North American Plate, Bahamas Platform and Hispaniola. Moreover, it is important to study the geometry of this structure along the northern coast.

The main target to solve in the island is obtaining a complete view about Moho discontinuity and upper mantle and studying the possible differences between the north and south and, also between east and west. In the eastern part of the island, the aim is the determination of geological structures that indicate high seismicity in that zone and could be associated to the subduction in the northern zone.

Another specific target is to characterize the contact between Muertos Thrust with north Beata Ridge and Hispaniola Island and the possible influence in onshore structures as Enriquillo Plantain Garden Fault Zone or Septentrional Fault Zone. Therefore, Beata Ridge has been densely studied in the south but there is no agreement about how the structure in the north is and if it penetrates into the island.

1.5 THESIS OUTLINE

This thesis is organized in eight chapters grouped in four main blocks. First block corresponds with the present chapter concerning some geological and tectonic aspects of the Caribbean Plate and the background of both projects whose data have been analyzed in this study. Following block is the bulk of this thesis dedicated to Controlled Source Seismology (CSS) and its application to Dominican Republic wide-angle seismic data. Third block deals with Local Earthquake Tomography applied to Hispaniola Island and the last block summarizes the conclusions obtained from the study carried out in this thesis. The abbreviated content of each block is as follows:

- *Block I (Chapter 1)*: The introductory block is structured in five main points where the geological problem and previous studies are analyzed, followed by the description of the CARIBE NORTE and GEOPRICO-DO projects and, finally, the main goals to be achieved in this thesis.

- *Block II*: This block includes the Chapters 2, 3, 4, 5 and 6 dedicated to Controlled-Source Seismology (CSS) using seismic waves produced by land and marine explosions as data to our study. Chapter 2 describes the methodology, instrumentation and data used in the following chapters. Chapter 3 is dedicated to the study of northern Beata Ridge while Chapters 4, 5 and 6 are entirely dedicated to the study of Dominican Republic crustal structure and adjacent offshore areas. Chapter 4 studies the westernmost area of Dominican Republic from north to south. The study carried out in the Chapter 5 is centered in the east and central island from a north-south point of view, while Chapter 6 analyzes the crustal structure from west to east.

- *Block III (Chapter 7)*: This block describes the methodology applied for Local Earthquake Tomography using local and regional seismicity data. In this block, we explain the seismicity data collection and the programs used to obtain the Minimum 1D model and its extension to 3D, which will be obtained in the future.

- *Block IV (Chapter 8 and 9)*: In this block, we will analyze the results of the previous sections and develop the main conclusions obtained in this thesis and show the references used in the manuscript.

CHAPTER 2

METHODOLOGY AND INSTRUMENTATION IN REFRACTION SEISMOLOGY

2.1 INTRODUCTION

Controlled-source seismic methods are used widely at small, medium, and large scales for investigating the Earth from shallow subsurface (upper tens of meters) to structures in and below the continental lithosphere (a few meters to a few hundred kilometers depth). Marine investigations of the crust and top of the mantle commonly utilize the release of pressurized air, whereas on land oscillating masses and borehole explosions at the surface are used. Generally the seismic data are recorded on fairly dense arrays of portable seismic instruments.

Wide-angle seismic data have been used to constrain the lithospheric structure of continents, oceans, and their margins for over 40 years. For land experiments the critical issue is usually the source, in terms of the type, cost, number and location. The interpretation of crustal seismic refraction data is generally carried out using a trial-and-error forward-modeling approach base on 2-D ray tracing [e.g. Spence et al., 1985; Mereu et al., 1986; Meltzer et al., 1987]. The theoretical travel time and amplitude response of a laterally inhomogeneous medium are repeatedly compare with observed seismic record sections until a model is constructed which provides a satisfactory match between calculation and observation [Zelt and Ellis, 1988]. These iterative and forward modeling approaches need a lot of trial and error to get a starting model and evaluate model parameterization.

A number of algorithms base on asymptotic ray theory [Cerveny et al., 1977] have been developed and widely used. In practice, the analytic and numeric techniques are often about equally efficient if the analytic method uses a fine mesh of nodes to represent a sufficiently smooth velocity field as dictated by ray theory, and if the numeric scheme adjusts the step length according to the velocity gradients [Zelt and Ellis, 1988].

The main steps to follow when modeling wide-angle travel time data are the following [Zelt, 1999]:

1. Arrival picking
2. Reciprocity check
3. Straight-line projection
4. Development of a starting model
5. Inversion of data
6. Using predicted travel times to identify additional picks
7. More inversions if necessary, and
8. May be appropriate to provide additional constraint on particular model features such as velocity gradients, discontinuities and amplitude modeling.

The presentation of wide-angle modeling and assessment results should be at least final model, ray tracing diagram, comparison of observed and predicted travel times, amplitude studies, between others.

The instrumentation used for wide-angle experiment, processing of obtained data, how first arrivals have been determined, data picking procedure modeling methodology and error estimation used to elaborate this manuscript are going to be described in this chapter.

2.2 INSTRUMENTATION IN REFRACTION SEISMOLOGY (CARIBE NORTE AND GEOPRICO-DO PROJECTS)

In this section, it is going to be described the different instruments used for wide-angle refraction seismology during GEOPRICO-DO and CARIBE NORTE projects aboard R/V Hespérides and seismic stations and OBS deployment on land and at sea, respectively.

Nowadays, seismic studies are the most used method to image geological structures in the marine and land subsurface. The main aim is to obtain a representation of the structures below the sea floor continuing onshore or onshore structures by analyzing the characteristics of seismic wave propagation through them. The equipment used in this kind of studies is divided in three groups depending of its function:

- Energy sources provide a pulse of seismic energy.
- Acquisition equipment is responsible for capturing and recording the signals reflected and/or refracted by the sea floor and land structures.
- Processing systems use to analyze and represent the seismic signals.

In the following sections, it will be explained the different equipment that were used onshore and offshore Dominican Republic in GEOPRICO-DO and CARIBE NORTE projects differentiating between marine and land instrumentation.

2.2.1 Seismic Instrumentation aboard R/V Hespérides

The seismic equipment aboard Spanish R/V Hespérides comprises Bolt air gun arrays, Sleeve Gun air guns, compressors and umbilicals, acquisition equipment, control air gun equipment and processing systems.

- BOLT air gun array

Generally, air gun arrays developed by Bolt Technology Corporation are the most used as acoustic energy source for shallow water and deep basin hydrocarbon explorations and deep-crustal seismology studies. The array used in R/V Hespérides consists of 13 Long Life Air Guns, four belonging to 1900LL model and 9 corresponding to 1500LL model, with different capacities that ensure the generation of signals with broad frequency spectrum. Due to the vessel and equipment features, it is possible use a maximum of 7 Bolt air guns at the same time. These air guns are arranged in two strings, main and secondary strings. The main string consists of five air guns deployed by the port side of the vessel, while the secondary are two air guns deployed using the vessel's stern gantry.

Fig. 2.2.1.1. a) Air gun shooting aboard R/V Hespérides. b) Shot at sea.

- Compressors and umbilicals

To generate compress air, which air guns store and release after receiving an electric signal, are arranged four compressors model 4TH 190 W 70 from Hamworthy. These compressors supply from 304 to 314 m^3/h of air 140 bars pressure. Two of these compressors are permanently in R/V Hespérides and the other two can be easily installed in vessel deck. Different umbilicals are used to conduct the air from

compressors to guns and electric signals to the shot. The umbilical of 120 m length and 8 channels is used with the Bolt air gun main string, an umbilical of 60 m and three channels for secondary string and, the last umbilical used in operations with Sleeve Guns with 70 m and 6 channels.

- Acquisition equipment

Aboard R/V Hespérides, the signals from different reflectors are captured by an array of sensors called hydrophones used for seismic reflection. This array is known as streamer. The streamer converts acoustic signals into voltage differences to be digitized, visualized and recorded in the laboratory. During GEOPRICO-DO project was used Teledyne Streamer model 40508 (Teledyne Brown Engineering) with distance between hydrophones groups of 6.25, 12.5 or 25 m, with maximum number 96 channels in distances between hydrophones of 25 m. Different depth controllers, known as birds, are placed along the equipment to visualize and control the streamer depth during the line. These birds are controlled from a computer and modem in the laboratory. With Strata Visor Tm NX Seismic Recorder (Geometrics) is possible registering seismic signals captured by the streamer and it has the capacity of digitizing and registering up to 96 channels.

Note: This streamer was not used during CARIBE NORTE experiment and MCS data were not acquired in the seismic lines of GEOPRICO-DO project used in this work.

Fig. 2.2.1.2. Streamer

Signal acquisition may be carried out in different sample intervals from 0.25 to 16 ms. This system allows registering different lines in SEG-D 8048, 8508, SEG-Y and SEG-2 formats.

- Air Gun Control Equipment

Different electronic devices are used to fire air guns in a precise, synchronized and secure way. These devices are: KonMAP HYDAQ Mk4 navigation system, LRS-100 controller responsible for correcting the time differences that may exist in the

explosions of the different air guns used during a seismic line, synchronizing a maximum of 8 air guns and Air Gun Solenoid Power Supply that provides the necessary voltage and current to activate the solenoids of the guns. This equipment generates pulses of up to 80 volts and 10 amps that drive violently to the solenoids installed in the canyons, causing suddenly liberation of stored air.

- Processing systems

The digital processing system PROMAX version 6.0 (Landmark Graphics) allows carrying out the first quality control of the signals acquired during different seismic lines aboard R/V Hespérides.

2.2.2 Seismic Energy Sources used in GEOPRICO-DO and CARIBE NORTE projects

The marine seismic source instrumentation during marine experiment in GEOPRICO-DO project consisted in two air gun arrays (main string with 6 air guns and secondary string with one string) submerged 90 m deep with total shot power of 3850 ci and cadence of 90 s.

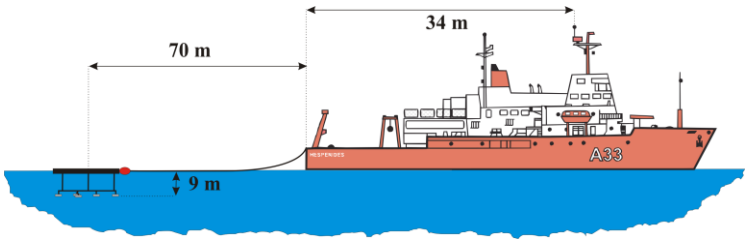

Fig. 2.2.2.1. Air gun array layout scheme and distances during GEOPRICO-DO experiment (from GEOPRICO-DO scientific report).

Below is a diagram of primary and secondary air gun arrays deployment used during GEOPRICO-DO experiment.

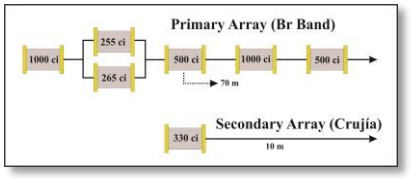

Fig. 2.2.2.2. Main and secondary strings layout scheme in GEOPRICO-DO experiment (from GEOPRICO-DO scientific report).

The file registered by the system when triggered by time interval consists of operational functioning of air guns and GPS message where GCA code provides the information about location and time of the message. This code is transmitted in a

time interval around pulse per second (pps) and variable shape. This time is used to fix the exact second when is produced the trigger. The vessel location and depth is provided by navigation file.

Trigger is produced from a second counter generating the pulse from pps taking place the shot with 160 ms of delay (Fig. 2.2.2.3).

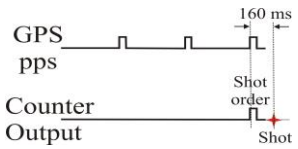

Fig. 2.2.2.3. Scheme of shot times (from GEOPRICO-DO scientific report).

During CARIBE NORTE project, the marine instrumentation for Refraction Seismology experiment used aboard R/V Hespérides consisted in an air gun array distributed in two subarrays with a total capacity of 3850 ci, shooting every 90 s.

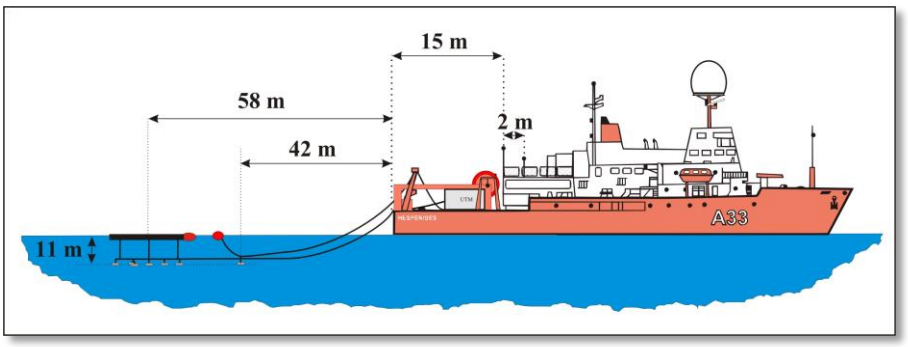

Fig. 2.2.2.4. Air gun array layout scheme and distances respect to the GPS antenna that controls the trigger system in CARIBE NORTE experiment. Furthermore, the distance to the secondary antenna is shown although it was not used (from CARIBE NORTE scientific report).

In figure 2.2.2.5 is shown the layout corresponding to both subarrays and their distances to the transom.

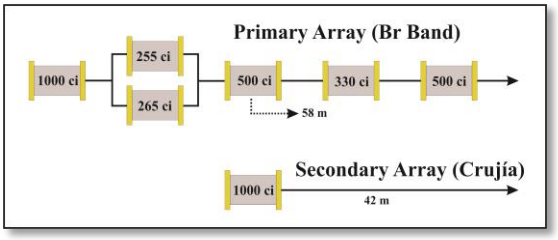

Fig. 2.2.2.5. Layout scheme of two subarrays showing the distances to the transom in CARIBE NORTE experiment (from scientific report of this project).

Shot generation system used in this project is controlled by a GPS pulse generator, which sends a pulse every 90 s to the gun controller. After receiving this order, gun generator creates a pulse to the solenoids and produces the shot with a total delay of 60 ms.

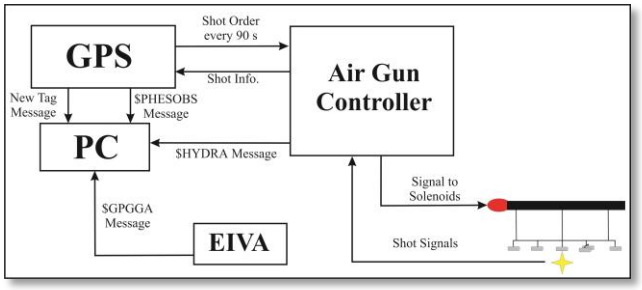

Fig. 2.2.2.6. Shot generation scheme and relation between vessel systems, where is indicated the messages sent for every subsystem to generate information files (from CARIBE NORTE scientific report).

Controller receives the signals of every gun and sends a pulse to the GPS to establish precisely the time at which takes place each shot.

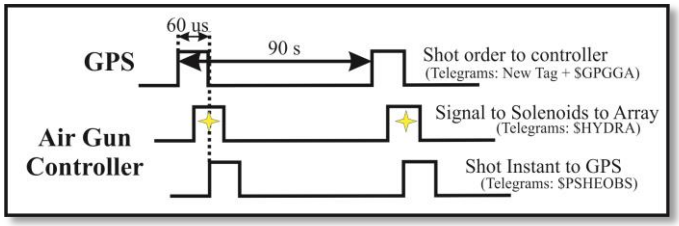

Fig. 2.2.2.7. Control pulse scheme for shot generation and telegrams associated to each signals (from CARIBE NORTE scientific report).

This system generates diverse text files from telegrams indicated in figures 2.2.2.6 and 2.2.2.7. In this way, it is obtained four files for each seismic line.

For air gun array described previously is not available a simulation for shot wave form but it was installed an hydrophone over central air gun in main string connected to the acquisition system to record the wave generated in near-field for each shot. These data were recorded in SEGY format (Fig. 2.2.11).

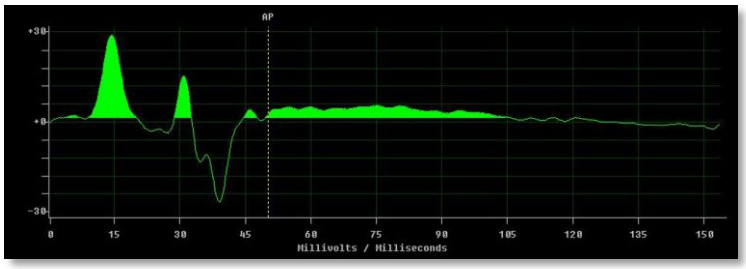

Fig. 2.2.2.8. Example of shot wave form registered by hydrophone (from CARIBE NORTE scientific report).

The different systems aboard R/V Hespérides worked correctly without any damage during the cruise, both the trigger system and air guns.

In CARIBE NORTE experiment, Dirección General de Minería was responsible for drilling the boreholes with explosive charges. In figure 2.2.2.9, it is observed a scheme of one borehole.

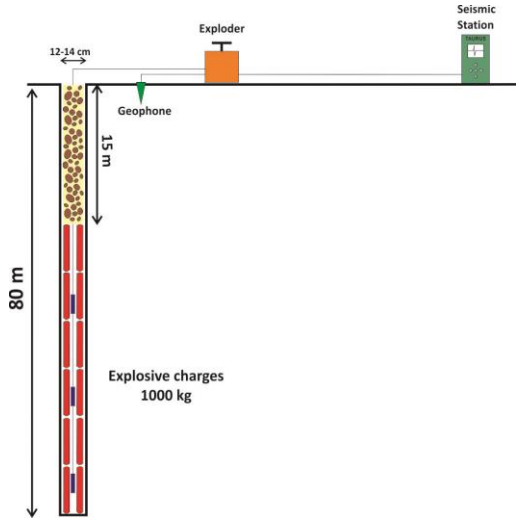

Fig. 2.2.2.9. Scheme of a borehole carried out during CARIBE NORTE experiment. Explosive charges are represented by red cylinders situated at bottom of 80 m deep hole with some detonators in the middle represented in blue and connected to the exploder. The borehole is filled with 15 m deep of gravel. The shot is recorded by seismic station with a geophone near hole.

In this experiment, a drill truck (Fig. 2.2.2.10 a) was used for making the hole, in which a PVC tube was introduced. Inside this tube, it was placed 1000 kg explosive charges in the bottom (Fig. 2.2.2.10 b) with several detonator connected to the exploder. Later, hole was filled with gravel (Fig. 2.2.2.10 d). In the explosion process, the detonator receives a small electrical current generating the appropriated frequency to enter into resonance with explosive charges. The shot is recorded by seismic station with a geophone near the borehole (Fig. 2.2.2.10 e).

a) b)

Fig. 2.2.2.10 a) Drill truck prepared to make the borehole in Hato Mayor (shot S1). b) Moment when the explosive charges are introduced in PVC white tube.

c) d)

Fig. 2.2.2.10 c) Borehole with detonator wires after the insertion of detonators in the borehole. d) Operators filling the borehole with gravel.

e) f)

Fig. 2.2.2.10 e) Situation of one seismic station with respect to the borehole where the operators are. f) Moment when the shot occurs in San Juan de la Maguana (shot S3).

2.2.3 Seismic Data Acquisition Systems

In this section, seismic data acquisition systems used in GEOPRICO-DO and CARIBE NORTE projects and applied to our study are exposed.

- Ocean Bottom Seismometers (OBS)

The ocean bottom seismometers (OBS) are designed to record the earth motion under oceans from marine, land shots or earthquakes. In GEOPRICO-DO project, these OBS were installed in the territorial waters of British Virgin Islands while in CARIBE NORTE project were installed 16 OBS around Dominican Republic. In the study that concerns us, it will be used only the OBS deployed in the Exclusive Economic Zone of Dominican Republic from 5th to 22nd April 2009.

The OBS used were short period model LC2000SP designed in Scripps and bought in 2007 by the Spanish institution CSIC-UTM. The main technical specifications are:

- Sensors: Mark Products L28 three components geophone with natural frequency of 4.5 Hz and one Hitech HYI-90-U hydrophone.
- Acquisition system with storing capacity of 9 GB, 24 bits Crystal A/D converter, Seascan MCXO SISMTB4SC clock card with precision of $5 \cdot 10^{-8}$ s.
- Liberation by acoustic signal by electrolysis.
- Weight in air of 72 kg without anchor and 110 kg with anchor. Dimensions of 1x1x1 m without external elements as flag and radio beacon.
- Buoyancy through glass floats.
- Maximum anchoring time is 6 month with lithium batteries and 60 days with alkaline batteries.

The first step in the preparation of one OBS is programming and synchronizing the acquisition system or data logger where there is a precision clock to maintain internally the time, being synchronized before and after anchoring. Then, OBS assembly begins placing an anchor (metal grid with weight needed to sink the equipment to the bottom leaving there when the equipment is released) on the assembling table and the structure that houses the various systems (white part in figure 2.2.3.1 c) and fixed anchor delivery system. When the acquisition system is programmed, it is placed in the appropriate site and connected the sensors (Fig. 2.2.3.1 d). Then, the acoustic release is situated on its site (site to the right in Figure 2.2.3.1 e) and checked for operation and release system. Finally, it is placed the float (yellow cover) and additional floats (lateral white pieces in Figure 2.2.3.1 f). So it is verified and installed the flash and the radio beacon with the flag.

a) b)

Fig. 2.2.3.1 a) ORION patrol used in OBS deployment in CARIBE NORTE experiment. Behind R/V Hespérides. b) Picking acquisition system for transportation to laboratory.

c) d)

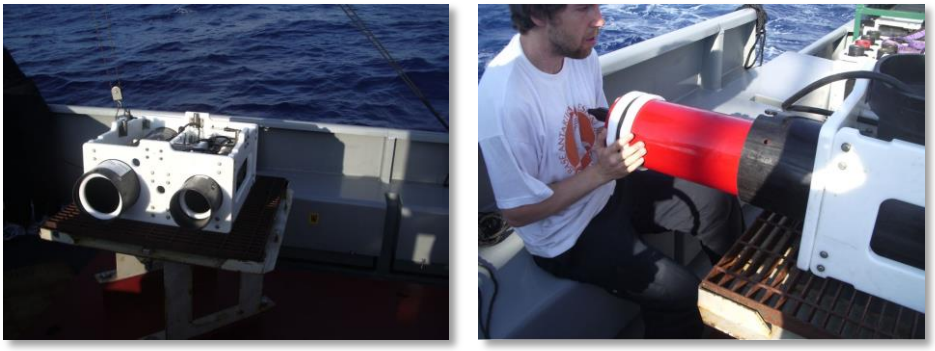

Fig. 2.2.3.1 c) Structure that hosts electronic systems, batteries and acoustic release inside two tubes. d) Maneuver of acquisition system placing.

e) f)

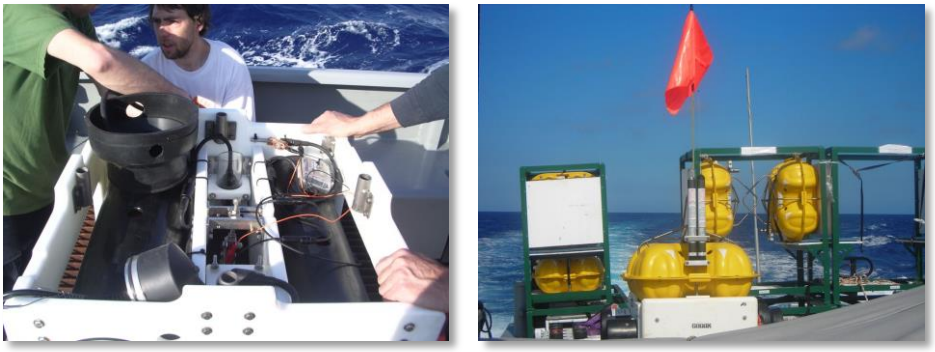

Fig. 2.2.3.1 e) Maneuver of acoustic release placing. f) Float, flash and beacon with the flag for its subsequent recovery.

This process is carried out while the position for the OBS deployment is reached. In the following figures, it is possible to observe the anchoring maneuver of an OBS.

a) b)

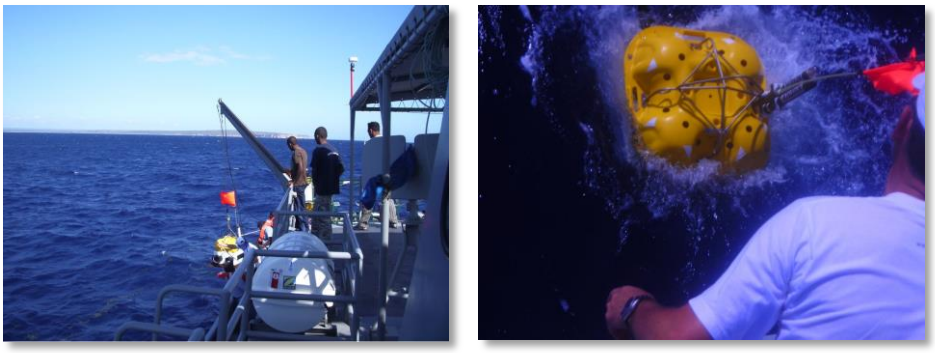

Fig. 2.2.3.2 a) Anchoring position of OBS 10. b) Moment at which the OBS is liberated into the water.

After reaching the position where the OBS was anchored, the collecting begins sending the release order to the OBS. Subsequently, it is used a manual goniometer (Fig. 2.2.3.3 a) to locate the direction in which the OBS comes to the surface to collect it and upload it to the ORION patrol (Fig. 2.2.3.3 b).

a) b)

Fig. 2.2.3.3 a) Manual goniometer used to locate the OBS position after raising the sea surface. b) Recovery maneuver of an OBS.

- Land Seismic Stations

An individual station can provide interesting information on the occurrence of seismic events but multiple stations are require locating events accurately, determining their nature or can be used in active seismic studies to determine lithospheric structures. The characteristics of multiple stations vary depending on their application, but can be grouped in regional networks, global networks and seismic arrays. The land seismic stations used during GEOPRICO-DO and CARIBE NORTE projects are described below.

The HATHOR3 is an acquisition station, which allows data storage on three channels. This station consists in a metal casing made of aluminum or stainless with all connections located on the front panel (Fig. 2.2.3.4).

a) b)

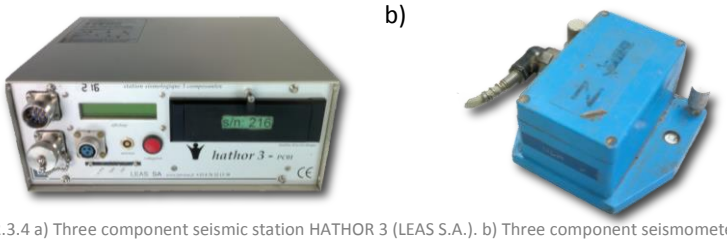

Fig. 2.2.3.4 a) Three component seismic station HATHOR 3 (LEAS S.A.). b) Three component seismometer Le-3D 1Hz used with HATHOR 3 station during GEOPRICO-DO experiment.

HATHOR 3 is featured by three acquisition channels plus one for the battery voltage and the temperature. The acquisition principle is based upon a 24 bits Delta Sigma converter, which inserts an electronics noise in the low-order bits. This tends to make the dynamic range decay each time the acquisition frequency increases. Each channel has an instrumentation preamplifier associated to a selectable gain

electronic switch by software (gain values are 1, 4, 16, 64, 128) and a programmable amplifier inside the converter from 1 to 128 also selectable by software.

The seismometer used in GEOPRICO-DO project with these stations was three components seismometer LE-3D 1Hz (Lennarth Electronic, Germany) (Fig. 2.2.3.4 b). All sensors are calibrated to identical output voltages and no need to keep records of which sensor has been connected to which data logger. Also, these seismometers have low noise, low power (typically 3 mA per component at 12 V DC) and dynamic range higher than 120 dB.

Taurus Digital Seismograph (Fig. 2.2.3.5) can be used either as a stand-alone seismic data logger or as a component in a data acquisition network. Taurus incorporates a three-channel 24 bits ADC, GPS receiver and Time Server, removable data storage, and remote communications options. This seismograph is a hand-held instrument that can record continuous data for over 800 days operating at a mere 750 mw while acquiring 3 channels at 100 sps. User interface is simplified through an integrated color graphics display and a five-button keypad providing instant access to real-time or recorded data. Data output provided in standard format includes: MiniSEED, sorted MiniSEED, ASCII, SEISAN and SEG-Y. These files are recorded directly to FAT32 formatted removable media (Compact Flash), allowing users to seamlessly transfer files to a PC or laptop for immediate analysis.

Fig. 2.2.3.5. Three component seismic portable station TAURUS (Nanometrics, Canada).

The 125A Miniature Seismic Recorder (TEXAN) is shown in Figure 2.2.3.6 a. In CARIBE NORTE project, the IRIS Consortium provided 300 units of these stations. The Texan's self-contained, compact design allows greater flexibility and the ability to easily integrate into system operations. The main features of this seismic station are small, lightweight and low power 24-bit ADC powered from two "D" cell batteries. The Texan uses solid-state data storage.

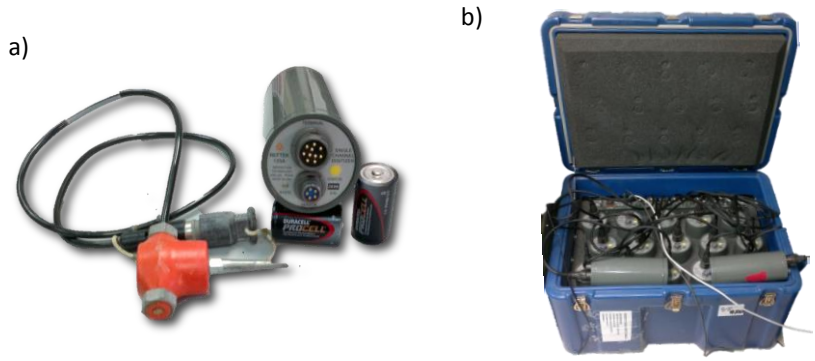

Fig. 2.2.3.6 a). Seismic station TEXAN 125A (REFTEK, USA) with vertical component geophone and two batteries. b). The hub

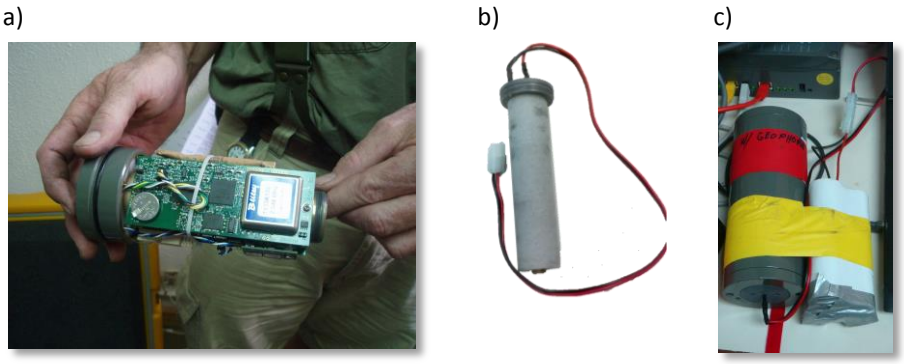

Fig. 2.2.3.7 a). Interior part of TEXAN 125A. b) Adapter developed for CARIBE NORTE project to extend up to 20 days of recording time. c) Texan 125A with dispositive in its interior connected to batteries in parallel configuration (white block).

Fig. 2.2.3.7 d) Technicians placing the batteries in the stations. e) Hubs connected in parallel for programming Texan seismic stations.

For set up, the Texans are connected to a hub that provides power, connection to the host computer via Hi-Speed USB2.0, and timekeeping signals from a GPS receiver. The hub (Fig. 2.2.3.6 b) provides 15 Texan connections, a connection to the USB host, and one port for daisy-chaining addition hubs. Also, several hubs can be operated in parallel allowing simultaneous connection between a single host computer and numerous Texans. Another function provided by hub is routes the 130-GPS Receiver/Clock signals to each Texan for synchronizing internal time to UTC and precisely setting the internal oscillator frequency.

For CARIBE NORTE experiment, it was developed a dispositive (Fig. 2.2.3.7 b) with three blocks connected in parallel configuration of two 1.5 V batteries connected in series providing total power supply of 3 V (Fig. 2.2.3.7 c) and extend recording time up to more than 20 days in continuous mode.

A state LED displays the operating condition of the TEXAN. This feature informs the user that the battery voltage is sufficient, time is set, the acquisition program loaded, and the unit is either ready to acquire or is acquiring data. During the recording session, the Texan can be retimed or data may be downloaded to a laptop or PC.

2.3 DATA PROCESSING

In this section, we describe the Texan data processing, wherein for the remaining seismic stations the procedure is similar.

After data have been downloaded to the workstation, many files are obtained as stations we have, with a name indicating it is raw data and station number with an extension .TRD. The processing begins converting .TRD files into .RSY files with the program 125_SEGY.exe (provided by REFTEK, USA) (Fig. 2.3.1).

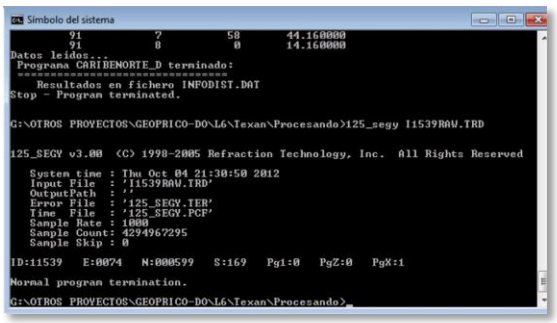

Fig. 2.3.1. Conversion program for Texan raw data (TRD files) named 125_SEGY.exe

This program extracts from raw file one .RSY file of every hour recorded by the station ordered into folders showing the year and Julian Day that were recorded, one .TSH file where it is shown the values of battery level before and during record, and two files for timing and errors (125_SEGY.PCF and 125_SEGY.TER, respectively).

The following step in the processing is converting RSY files into files with PCM5800 format with TEXAN_PCM.exe program. Previously, it is necessary to select the RSY files depending of the profile or land shot studied and create a file with a generic name where these files are (Fig. 2.3.2). All programs used from this point are built in-house.

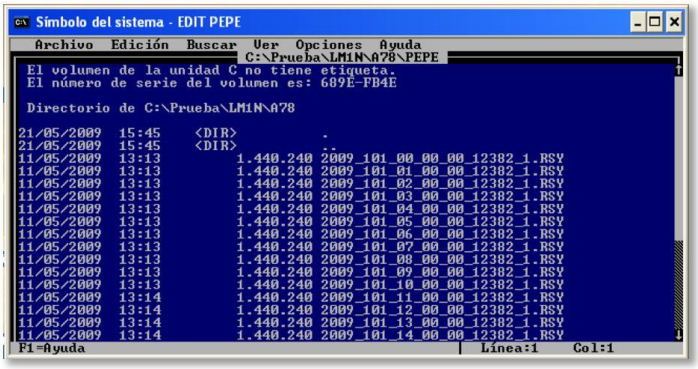

Fig. 2.3.2. Example of generic file called PEPE where all RSY files necessary for the study are.

Now, it is run TEXAN_PCM.exe program (Fig. 2.3.3).

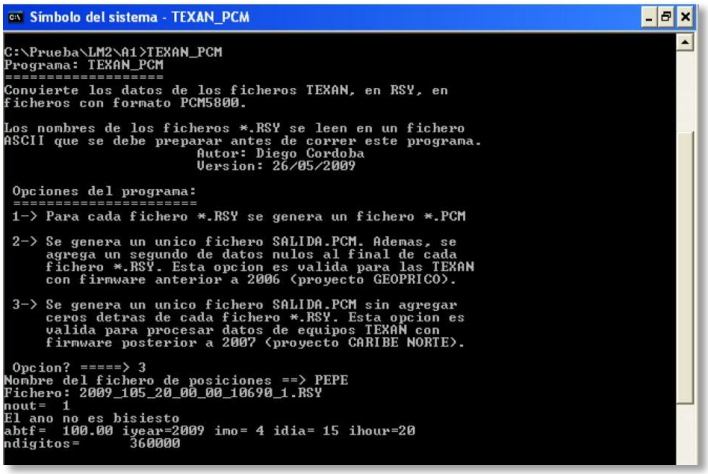

Fig. 2.3.3. TEXAN_PCM.exe program screen shot

The output file gotten after running this program is named SALIDA.pcm. This file cannot be used directly but must have the following format (Fig. 2.3.4) using POS.exe program, which result is POSFI.dat output file.

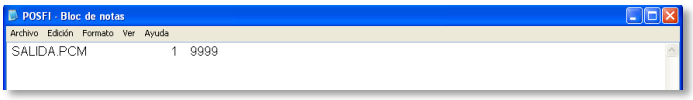

Fig. 2.3.4. Example of POSFI.dat file that results of running POS.exe and is used as input file for ADS_SGY.exe program.

The next step requires implementing ADS_SGY.exe. This program converts PCM into SEG-Y format and requires two input files more. One file is the shooting positions according to the station distance corrected by instrument drift (CORRECCIONES.dat) and the second is the header, which shows the date and time of start and end of the navigation line and the coordinates of the seismic station (CABECERA.dat).

To obtain the CORRECCIONES.dat file, it is necessary to know station coordinates and navigation line data in TXT format. These data are entered into the program CARIBENORTE.EXE (Fig. 2.3.5). This program calculates the distance between epicenters and stations over an ellipsoidal Earth.

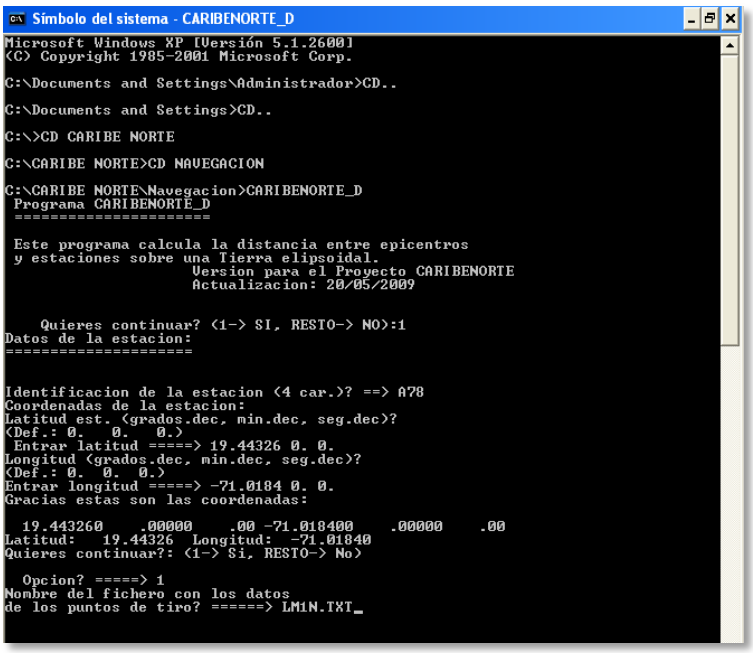

Fig. 2.3.5. Example CARIBENORTE_D.exe

As output file, INFODIST.dat is got (Fig. 2.3.6) whose columns correspond to

- Station name
- Navigation line name
- Shooting number
- Latitude in degrees, minutes and seconds
- Longitude in degrees, minutes and seconds
- Depth in meters
- Julian day
- Shooting time in hours, minutes and seconds
- Epicentral distance
- Azimuth

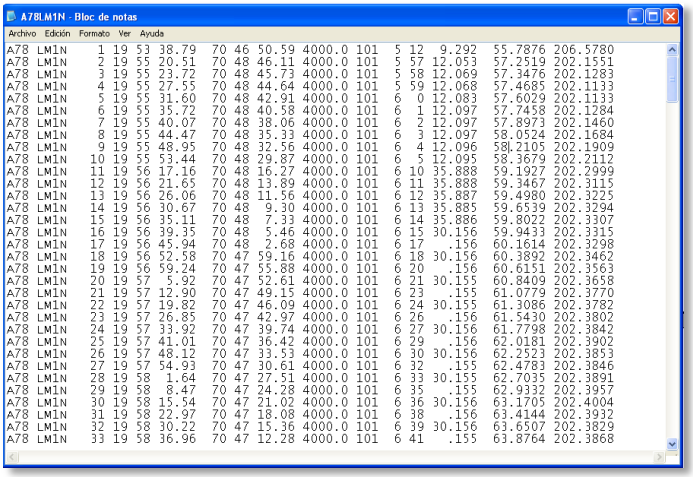

Fig. 2.3.6. Example of INFODIST.dat

INFODIST.dat acts as input file in DERIVA_NAV.exe joined to another file with all station drift of one profile. DERIVA_NAV.exe (Fig. 2.3.7) calculates the time corrections that should be applied to TEXAN data from drift obtained comparing GPS time before and after registering window.

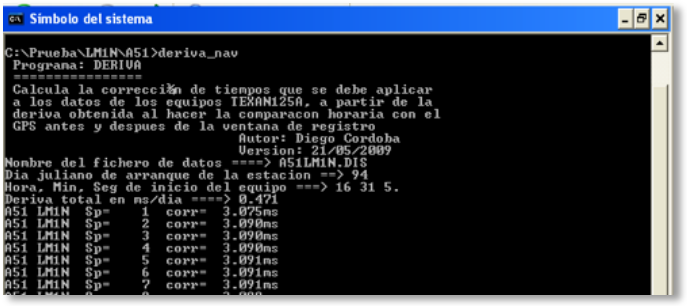

Fig. 2.3.7. DERIVA_NAV.exe screen shot showing an example.

Finally, ADS_SGY.exe is run including the output file CORRECCIONES.dat (Fig. 2.3.8). This program converts data from PCM into SEG-Y format including corrections by station drift. The result is ENSAM.sgy

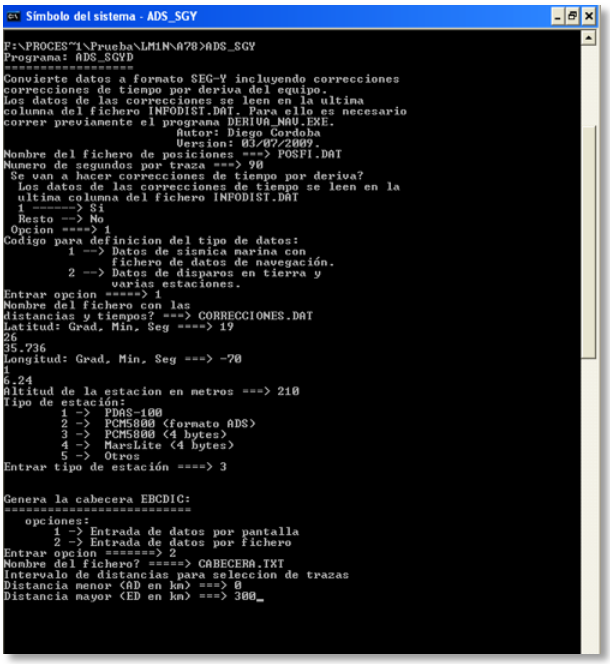

Fig. 2.3.8. ADS_SGY.exe program with an example of input parameters introduced.

Last step of processing is achieving a seismic record section. For this purpose, it is used SGY_PS.exe (Fig. 2.3.9) that draws a seismic record section from a SEG-Y file in PostScript or TGA formats. As input files are used ENSAM.sgy and INDATA.dat where this file represents the necessary parameters for drawing the section. Some of these parameters are:

- Position of drawing (x, y)
- Selected traces to draw
- Axes parameters (initial and final epicentral distance and reduced time axes, parameters for bathymetry)
- Axes names size
- Parameters of band pass filter

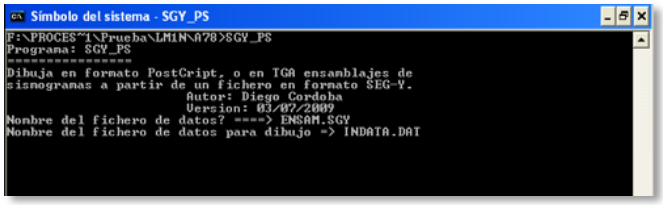

Fig. 2.3.9. SGY_PS.exe screen shot.

Following figure shows an example of seismic record section after following this process.

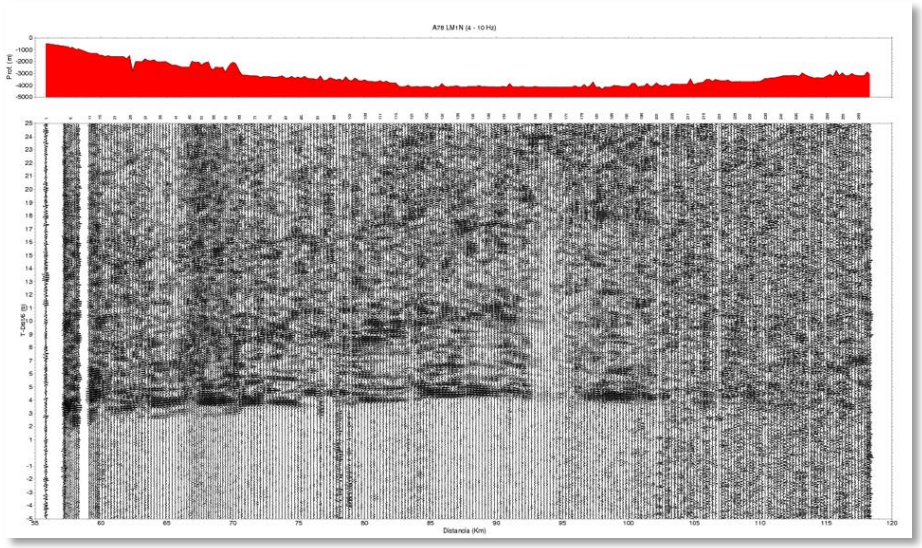

Fig. 2.3.10. Seismic record section corresponds to A78 station recording LM1N profile with a band pass filter of 4-10 Hz, reduction velocity of 6 km/s and distance axis represents the shot-trace offset in km. Top: Bathymetry along this line.

A summary of processing method used in this study is showed a scheme (Fig. 2.3.11) where purple rectangular boxes are main program used while light blue rectangular boxes are auxiliary programs to obtain one input file. Elliptical boxes refer to input or output files.

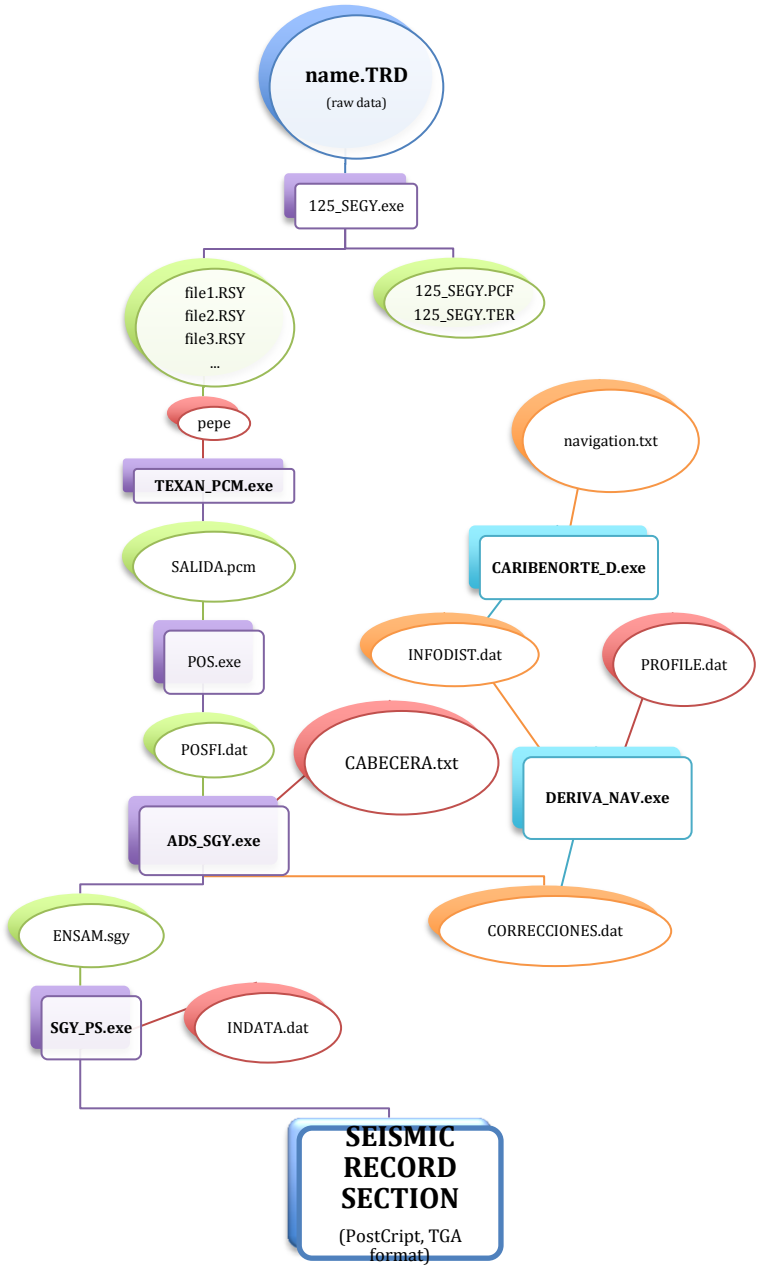

Fig. 2.3.11. Flowchart summarizing Texan data processing

2.4 DATA PICKING

2.4.1 Introduction

In a seismogram, a seismic phase is defined by two visual observations: change of wave field in amplitude and change in frequency content. The change in amplitude is observed when the amplitude based signal-to-noise ratio (ASNR) exceeds the background noise at least by a certain factor. The change in frequency is determined when the frequency based signal-to-noise ratio (FSNR) changes related to dominant frequency of noise. Sometimes is difficult to quantify visually because the dominant frequency of noise and signal can be very similar [Diehl & Kissling, 2008]. In this section, it will be explained new methodology developed for seismograms applied to seismic record sections obtained in our experiment. Also, it will be showed three applications of this methodology: one study for one land shot [Núñez et al., 2011 a], one seismic record section corresponding to one land station and one OBS seismic record section registering marine shots.

- Principle phases refraction. Examples of singles traces

In this section, a description about the principles applied to seismic record section used in this study and some examples extracted of them will be done. The main principles are:

- First arrival of seismic energy is always a direct ray or a refracted ray. The direct ray is overtaken by a refracted ray at a crossover distance, x_{cross} (Fig. 2.4.1.1 a). Beyond this offset distance, the first arrival is always a refracted ray. Since critically refracted rays travel down to the interface at the critical angle, there is a certain distance, known as the critical distance, x_{crit}. At this distance, the travel time of reflected and refracted rays coincide because they follow effectively the same path. Reflected rays are never first arrivals; they are always preceded by direct rays and, beyond critical distance, by refracted rays also. In a seismic record section, sometimes, it is not possible to distinguish between both phases beyond this distance, mainly due to the amplitude of reflected phase is higher than refracted one and, also, noise-level ratio may distinguish the refracted phase signal.

- The phase amplitude decreases with the distance. Usually, the phase signal amplitude in a trace closest to the source is high than another one more distant for a refracted phase. If this does not happen, it is likely it will be another phase (Fig. 2.4.2.4). However, when critical distance is reached, reflected phase amplitude increases respect to the amplitude of refracted wave. An example is the increase of P_MP phase amplitude (Fig. 2.4.1.1 b).

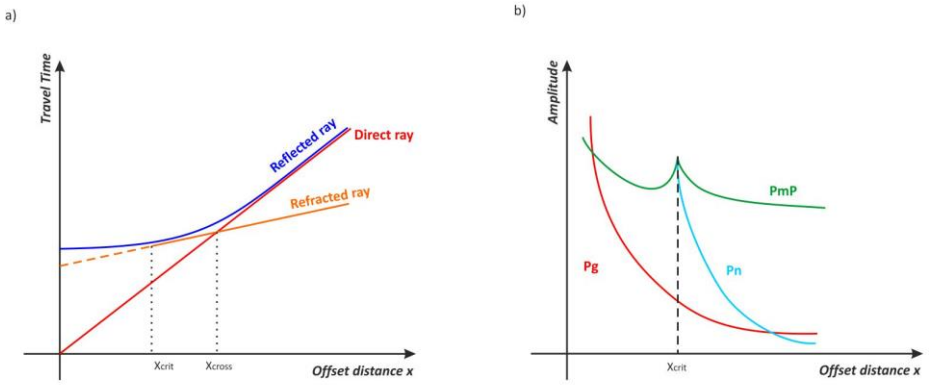

Fig. 2.4.1.1. Demonstration of a) travel time and b) amplitude variations with offset distance for separate phases.

- The wavelet shape will be similar for the same phase over some distances. There are some typical forms for the most prominent phases P_g, P_MP and P_n characteristics [Diehl & Kissling, 2008] (Fig. 2.4.1.1).

    - P_g: Impulsive high-frequency onset, first arrival close to epicenter (Fig. 2.4.1.2) often followed by reflecting intracrustal phases (Fig. 2.4.1.4 d, e, and f).

    - P_n: Usually small amplitude impulse or emergent onset, lower frequency content (absorption leads to smoothed wavelet front), first arrival for larger epicentral distance. Usually followed by strong P_g and P_MP phase (delay up to several seconds).

    - P_MP: Usually strong amplitude due to high reflectivity of Moho, wavelet with high-frequency reverberations. Never first arrival.

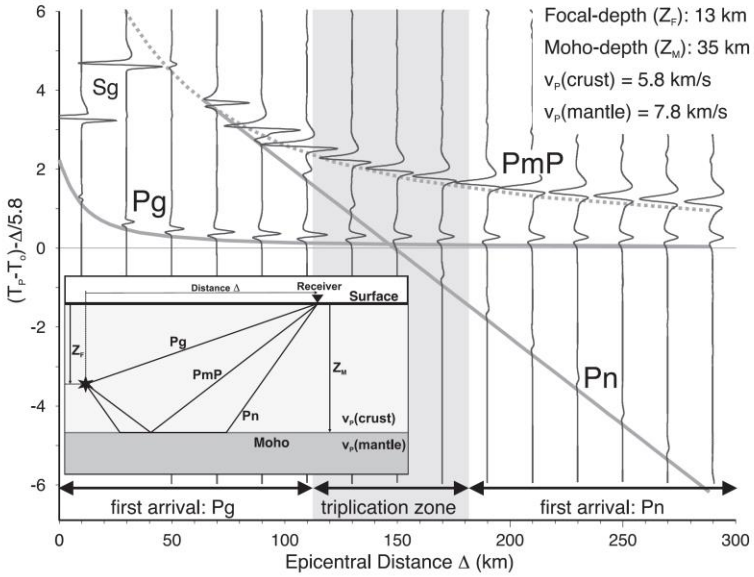

Fig. 2.4.1.2. Reflectivity seismograms (vertical components) and synthetic travel time curves (solid and dashed lines) for main phases observed in local and regional earthquakes (one layer over half space). Focal depth is set to 13 km and time axis is reduced by 5.8 km/s. Phase identification is expected to be difficult in the distance range of phase triplication. The position and width of this zone mainly depends on focal depth and Moho topography [from Diehl & Kissling, 2008].

- The picks of the same phase must be picked in the same way. If some traces are in a very good quality class, the onsets can be picked very precise so the uncertainties will be small. But if there are some traces in lower quality class, we may not pick the very first small amplitude wavelet onset. Consequently, we must pick all onsets according to lower quality class onsets keeping the same feature for all (Fig. 2.4.2.2).

The following figures show some examples of traces taken from seismic record sections corresponding to shots S1, S2 and S3, located in Hato Mayor, Cotui and San Juan (Dominican Republic), respectively, and registered by seismic portable stations of Profile A, B, C and D.

In seismic record sections used in this work, it is possible to observe different sort of traces. Some of them contain one or more onsets that can be identified as P_g, P, S or S to P conversion phases. The figure 2.4.1.3 shows three examples of first arrivals at different distances. Figure 2.4.1.3 a) and b) are characterized by change in amplitude while figure 2.4.1.3 c) is characterized by change in amplitude and frequency. Both onsets, a) and b), are interpreted as P_g phase according to their amplitude and frequency features explained before and c) is not clear yet.

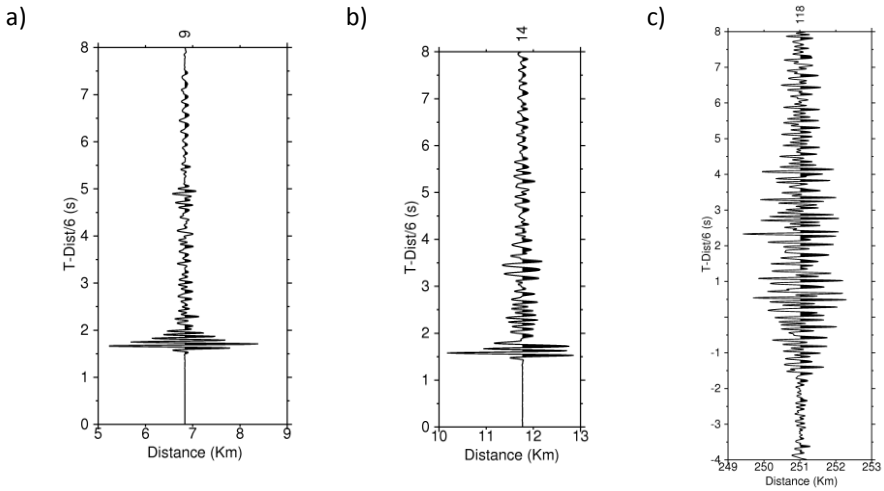

Fig. 2.4.1.3. Traces showing first arrivals characterized by change in amplitude. a) Trace 9 extracted from shot S3 – Profile D seismic record section (WS3). b) Trace 14 taken from shot S3 – Profile D seismic record section (ES3). c) Trace 118 extracted from shot S3 – Profile D seismic record section (ES3). The onset is determined by change in frequency and amplitude.

Figure 2.4.1.4 points to traces with first and consecutive arrivals. Most of the first arrivals are considered like P_g phase whereas the successive arrivals are interpreted as P, S or S to P conversion phases.

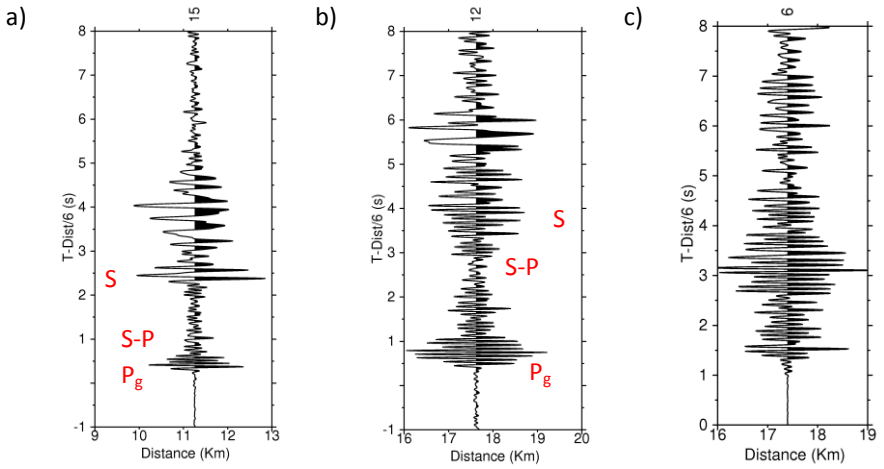

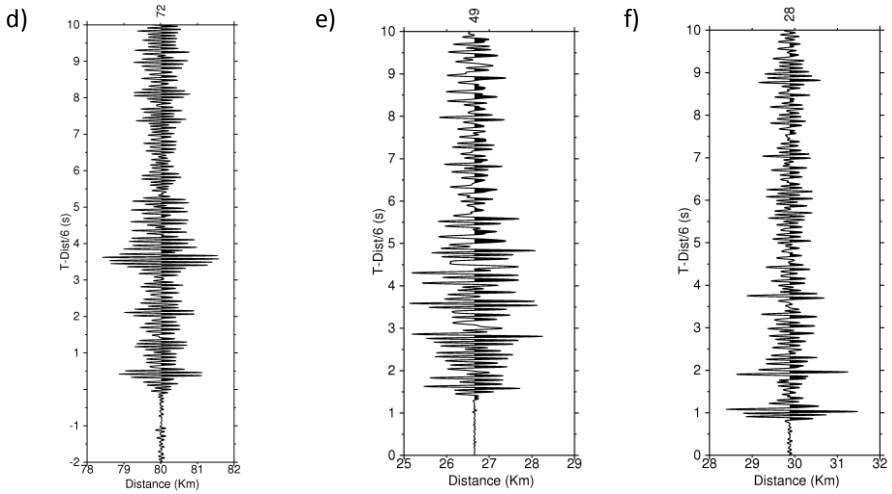

Fig. 2.4.1.4. Traces showing first and consecutive arrivals. a) Trace 15 extracted from shot S1 – Profile C seismic record section (SS1). b) Trace 12 taken from shot S1 – Profile C seismic record section (SS1). In both traces it is observed a first arrival identify as Pg, second arrival as possible S to P conversion and third arrival as S phase. c) Trace 6 taken from shot S3 – Profile D seismic record section (WS3) where is shown a secondary phase without changing in frequency. d) Trace 72 extracted from shot S1 – Profile D seismic record section (WS1) where is shown successive P wave arrivals. e) Trace 49 taken from shot S3 – Profile A seismic record section (NS3). f) Trace 28 extracted from shot S3 – Profile A seismic record section (SS3). In d, e and f traces are shown successive P wave arrivals.

Analyzing single seismograms is very important but, in refraction seismology, it is more important combine single seismograms in seismic record sections to determine phase correlations. Seismic record sections are a powerful tool for both natural and active seismology. The main point is that for active seismology, since the source is quite simple and less energetic, compared to an earthquake, it is almost impossible to properly identify phases in a single seismogram. In the following sections, the methodology applied in this work will be exposed.

- Determination of wavelet onsets (phase arrivals) in single signal traces

Considering the onset of a seismic phase as a probabilistic function $P_a(t)$, the arrival time is expressed as the "most likely" time t_A, with $P_a(t_A)=\text{Max}(P_a)$. The "earliest" possible time for the phase onset is defined as t_E. Similarly, t_L is defined as the "latest" possible time for the phase onset [Diehl et al, 2009].

In practice, it has been determined t_L as the interception between signal amplitude and the a priori noise threshold (Fig. 2.4.1.5). While, t_E is defined as the first zero slope of *a* tangent from t_L (Fig. 2.4.1.5). Subsequently, the arrival of the phase is picked at the most likely position t_A, between the error interval of t_E and t_L.

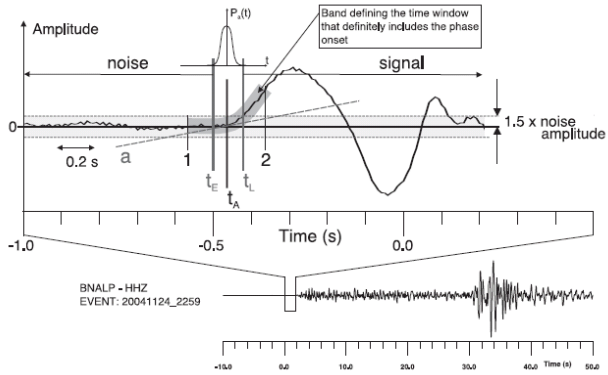

Fig. 2.4.1.5. Probabilistic phase picking approach: the "earliest" possible pick correspond to t_E, the "latest" possible pick corresponds to t_L. The most likely arrival time t_A is located within this interval [Diehl et al, 2009].

In the case of change in frequency (Fig. 2.4.1.6), t_L is defined as a quarter signal wavelength after position *b* and t_E as half a signal wavelength before position *a*.

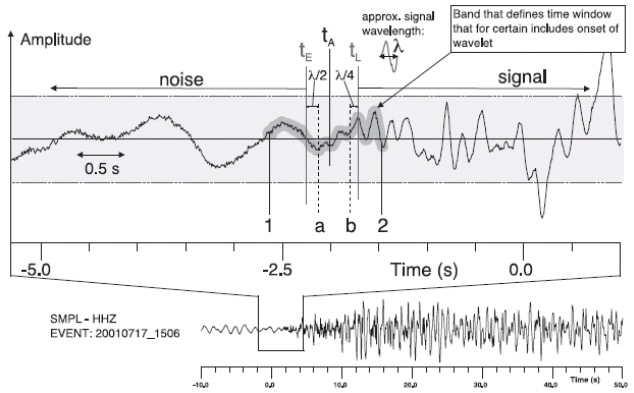

Fig. 2.4.1.6. Probabilistic phase picking approach based on change of FSNR: the "earliest" possible pick correspond to t_E, the "latest" possible pick corresponds to t_L. The most likely arrival time t_A is located within this interval. Primarily frequency is used for determination of t_E and t_L. [Diehl et al, 2009].

- Application to control source refraction seismology CARIBE NORTE data

The criterion used in this study modifies the technique developed by Diehl et al., (2009) considering that our data correspond to refraction data, so the main feature is possible establish phase correlations. This fact means that every pick can be determined with its appropriated uncertainty relating trace to trace and obtaining correlations, according to the principles exposed in the first point (Fig. 2.4.1.1 and Fig. 2.4.1.2). During this work, GET DATA program has been used as hand picker.

The figure 2.4.1.7 shows a fragment of the seismic record section SS1. In this example, three principal phases are observed clearly, being the P_g, S to P conversion and S phases, respectively. These phases can be picked in single trace picking. If we concentrate on the trace number 14 (red box) it is observed that immediately after the arrival of the P_g phase, an intracrustal phase appears (blue arrow). This phase only can be picked when the seismic record is seen in comparison with the surrounding stations.

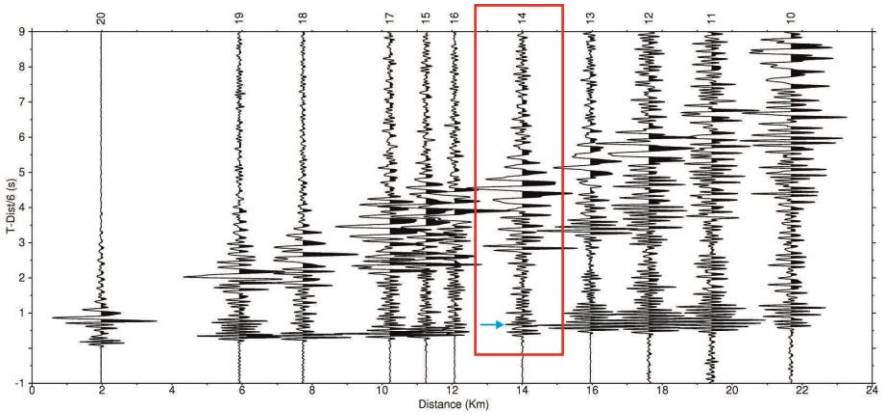

Fig. 2.4.1.7. Demonstration of the importance of phase correlation to determine intracrustal phases. Fragment taken from shot S1 – Profile C seismic record section (SS1).

Now, the principles developed in the second section for single trace picking in an illustrative example will be applied. The figure 2.4.1.8 shows the determination of the most likely arrival time (t_{traces}), the earliest arrival time (t_E) and the latest arrival time (t_L) for every trace considering every trace as an independent single trace. All traces show P_g phase. Wavelets are very similar but due to site effects that indicate variable local noise levels and the fact of signal amplitude decay with distance, wavelet onset is seen slightly different in all traces. Obviously, waveform of trace 114 should be similar as 113 and 115. First arrival in 114 is up like 113, but they do not have the same wavelet onset. Furthermore, 114 is up unlike 115 that is down. So, if we pick consistently, we must pick all first arrivals in the same way showing the same characteristics and according to phase correlation.

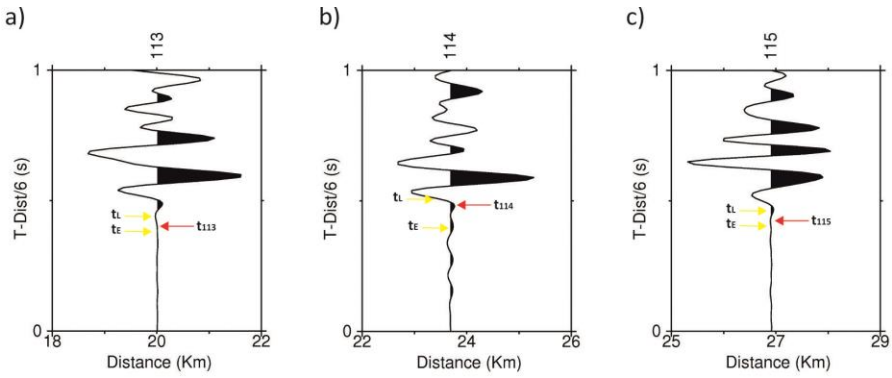

Fig. 2.4.1.8. Demonstration of the methodology applied for single seismograms where most likely arrival time (t_{traces}), earliest arrival time (t_E) and latest arrival time (t_L) are defined. Traces 113 (a), 114 (b) and 115 (c) taken from shot S1 – Profile D seismic record section (ES1).

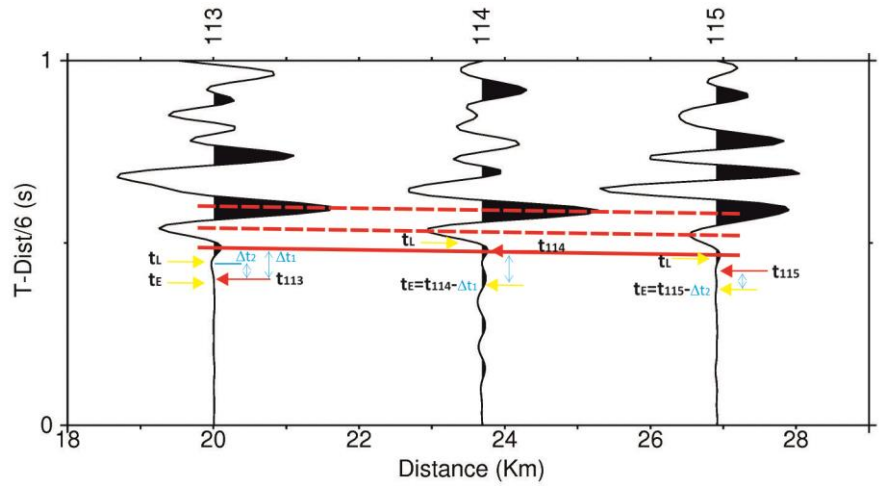

Fig. 2.4.1.9. Demonstration of the methodology applied in this study. Traces taken from seismic record section shot S1 – Profile D where is shown P_g phase correlation (red line) and repicked earliest times (t_E) of traces 114 and 115. Dash red lines show that the phase correlation remains constant after the first one.

For traces presented in figure 2.4.1.8, it is possible to establish that absolute first arrival of correlated wavelet 113 is well known, 114 is poorly known and 115 is fairly well known. So, all of them belong to different quality classes.

Taking into account these principles, phase correlation of traces 113, 114 and 115 (Fig. 2.4.1.9 red line) relating it to the times obtained in single signal picking of that traces are determined. As it was explained before, the only possible onset of the trace 114 is t_{114} because of the noise level. Then, comparing traces 113 and 114 it is observed that the onsets are not possible to find in the same way, so it is possible to define the difference between phase correlation time and most likely arrival time

(t_{113}) as Δt_1. This quantity is subtracted from the probably time t_{114} to obtain the new earliest time (t_E) of trace 114. Finally, the new earliest time of trace 115 in relation to trace 113 is calculating as Δt_2 subtracted from the probably time t_{115}. Both of them are similar in wavelet onset but different polarity because the arrival in trace 113 is up and the arrival in trace 115 is down. Then, Δt_2 is calculated as the difference between t_{113} and next down in the signal of trace 113. The figure 2.4.1.9 shows graphically these concepts.

The analysis of figure 2.4.1.9 provided the uncertainties for single seismograms and phase correlation. These data are shown in Table 2.4.1.I.

TRACE	t_L (s)	t_E (s)	Individual error estimation (t_L-t_E) (s)	Δt (s)	New t_E (s)	Phase correlation uncertainty (s)
113	0.44	0.37	**0.07**	0.00	0.37	**0.07**
114	0.51	0.37	**0.13**	0.12	0.37	**0.14**
115	0.47	0.36	**0.11**	0.06	0.36	**0.11**

Table 2.4.1.I. Uncertainties for single seismograms and phase correlation.

In short, for controlled source seismology (CSS) refraction it is necessary to pick correlatable phases, i.e. same phase onset in different traces. Hence our methodology consists of:

1) Pick each wavelet separately using the principles for single signal picking (Fig. 2.4.1.8).
2) Define correlation of phases (Fig. 2.4.1.9, red line).
3) Repick earliest phase onset times for each trace (Fig. 2.4.1.9).

In this work, various types of seismic record section have been obtained according to stations and seismic sources distribution. These are:

- One land shot registered by all land stations deployed along one profile (Fig. 2.4.1.10 a).
- One land station recording one complete marine line (Fig. 2.4.1.10 b).
- One shot extracted from one marine line registered by all land stations of one profile (Fig. 2.4.1.10 c).
- One OBS registering one complete marine line (Fig. 2.4.1.10 d).

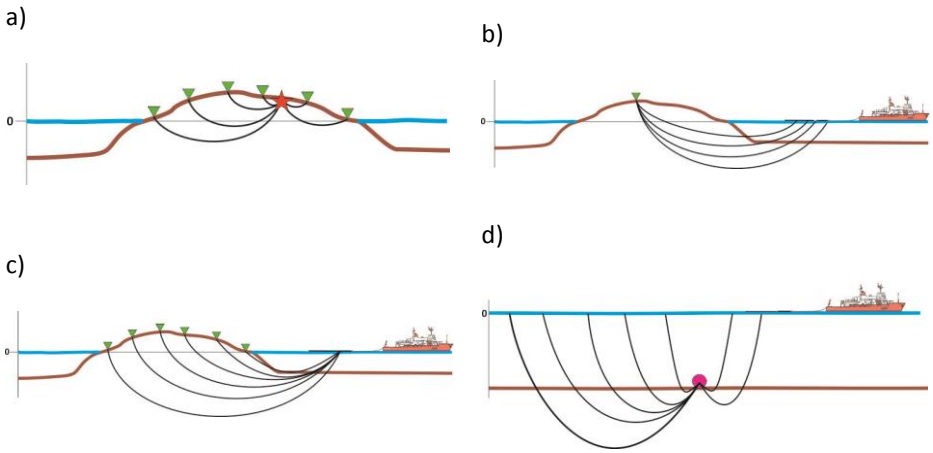

Fig. 2.4.1.10 Different seismic record sections analyzed in this manuscript. a) Land shot registered by all land stations; b) Land station registering marine shooting line; c) One shot at sea registered by all land stations; and d) OBS recording marine shooting line. Inverted green triangles are land stations, red star is land shot and pink circle is OBS.

The following points show how the picked data have been obtained from different seismic record sections used in the subsequent chapters. The determination of onsets corresponding to one shot registered by all land stations of one profile (Fig. 2.4.1.10 a and c) is shown in section 2.4.2, while marine shooting line registered by one station (Fig. 2.4.1.10 b and d) is shown in section 2.4.3.

2.4.2 Application to one land shot registered by land stations: Shot S1 (Hato Mayor, Dominican Republic)

Seismic record section WS1

In this section, it is going to be described the phases identified and how they were picked. As example, it will be analyzed seismic record section WS1 (shot S1 in Fig. 1.3.2.1). The remaining seismic record sections have been analyzed with the same procedure. Seismic record section WS1 (Fig. 2.4.2.1) corresponds to shot S1 recorded by seismic stations of Profile D from Hato Mayor to San Juan de Managua in the West. In this section (Fig. 2.4.2.2), it is observed four first arrival phases named P1, P2, P3 and P4. Therefore, it is identified secondary arrivals, S and a possible S to P conversion phases, although they have not been used in our study. An extraction of seismic record section showed in figure 2.4.2.1 is showed in figure 2.4.2.2 to clarify first arrivals and the methodology applied.

In the purple box (Fig. 2.4.2.3), it is possible to observe the phase identify as P1. This phase shows decay in the amplitude with the distance. The traces 105, 106 and 107 have the same quality class while trace 102 has better quality class than traces 103 and 104, where the uncertainty is higher due to the increasing level of noise.

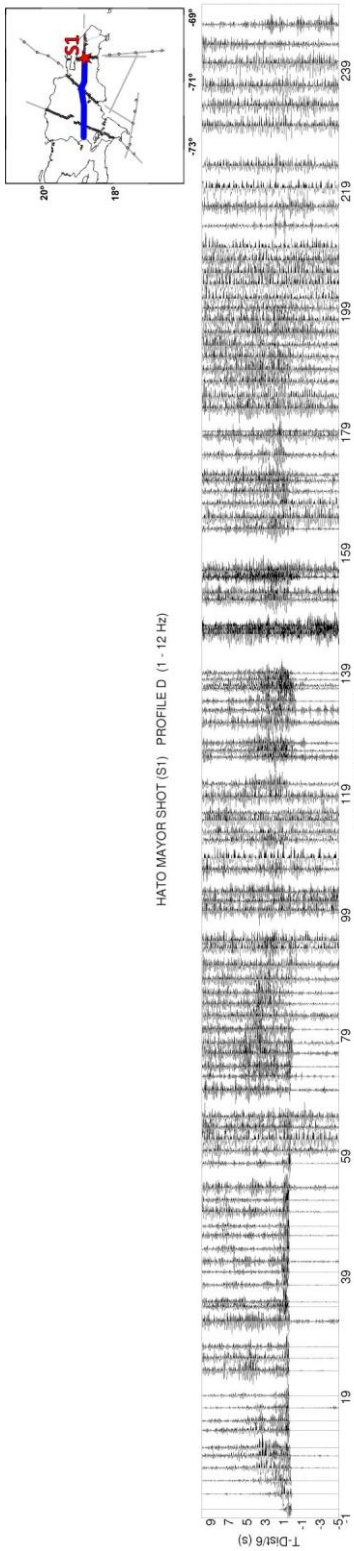

Fig. 2.4.2.1. Complete seismic record section of shot S1 – Profile D (WS1). This section shows first arrivals clearly identifiable at first 100 km and after that it is observed a dispersion of arrivals where the phase onsets are practically unidentifiable.

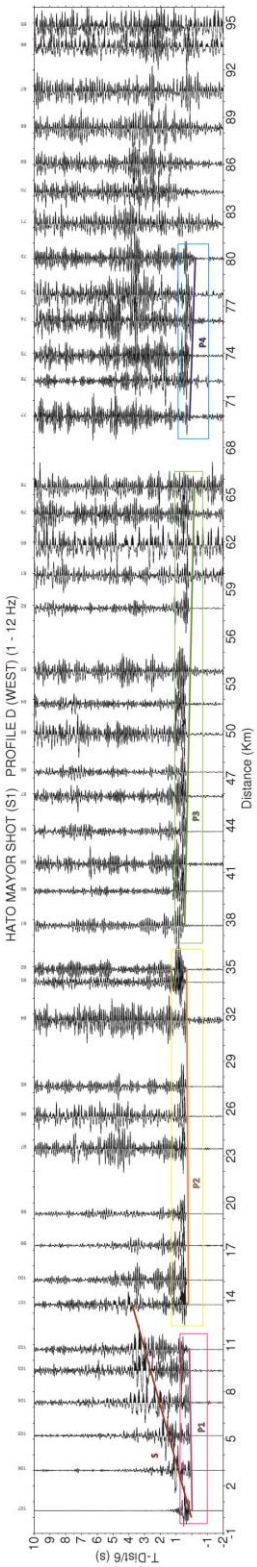

Fig. 2.4.2.2. Enlargement of seismic record section of shot S1 – Profile D (WS1) (Fig. 2.4.2.1) with first arrivals identified (P1, P2, P3 and P4 phases) and characterized by change in amplitude and frequency. Purple, orange, green and blue boxes indicate enlargements of the same ones (Fig. 2.4.2.3, 5, 7 and 9, respectively). In this seismic record section is shown S phase and S to P conversion phase is not clearly identifiable.

Calculating the slope of this phase from most likely arrival time data, we obtain that the apparent velocity is 5.1 km/s whereas the apparent velocity calculated from phase correlated data is 5.4 km/s. Apparently, there is no velocity gradient from this phase.

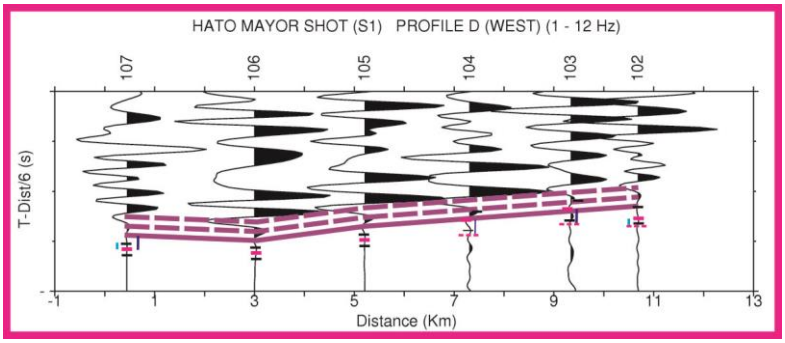

Fig. 2.4.2.3. Enlargement (purple box in Fig. 2.4.2.2) corresponds to P1 phase of seismic record section of shot S1 – Profile D (WS1) where most likely arrival time in purple (t_A), earliest arrival time in black (t_E), new earliest time in dash purple line and latest arrival time in black (t_L) are shown for every pick. Dark red line shows the phase correlation, dark blue line shows Δt_1 and light blue line shows Δt_2.

Next table (Table 2.4.2.I) shows the data used to calculate single trace and phase correlation uncertainties for P1 phase of WS1 seismic record section. As the sample rate of seismic stations used for this study is 100 Hz, individual error estimation and phase correlation uncertainty are rounded to the second decimal place.

TRACE	t_L (s)	t_E (s)	Individual error estimation (t_L-t_E) (s)	Δt (s)	New t_E (s)	Phase correlation uncertainty (s)
107	0.02	-0.04	**0.06**	0.00	-0.04	**0.06**
106	0.02	-0.04	**0.07**	0.00	-0.04	**0.07**
105	0.08	0.04	**0.05**	0.00	0.04	**0.05**
104	0.18	0.02	**0.16**	0.05	0.09	**0.09**
103	0.23	0.04	**0.19**	0.10	0.10	**0.13**
102	0.26	0.16	**0.10**	0.10	0.14	**0.12**

Table 2.4.2.I. Uncertainties calculated for single trace and phase correlation of P1 phase correspond to WS1 seismic record section.

The change between P1 and P2 phases is observed by increasing amplitude in trace 101 respect to trace 102 and a clear change in the shape of these trace wavelets (Fig. 2.4.2.4).

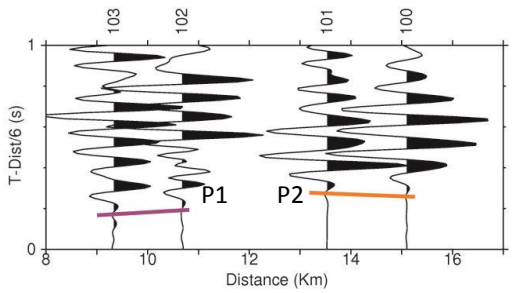

Fig. 2.4.2.4. Extract of shot S1 - Profile D seismic record section (WS1) showing first arrivals characterized by change in amplitude where the wavelets in traces 102 and 103 are similar and the amplitude decreases with distance. However, there is an increase in the amplitude and a difference on the shape of wavelets between trace 101 and 102. This fact indicates different phases arrive in this point.

In the following orange box (Fig. 2.4.2.5), it is possible to observe an enlargement of WS1 seismic record section showing the phase identified as P2. This phase are composed by traces with different quality classes. In particular, four different quality classes that affect the calculation of single trace and phase correlation uncertainties are established. Checking individual times, it is calculated the apparent velocity from most likely arrival time data obtaining 5.8 km/s and from phase correlation data 6.1 km/s without a gradient velocity detected. The Table 2.4.2.II summarizes the uncertainties obtained from single trace and phase correlation studies.

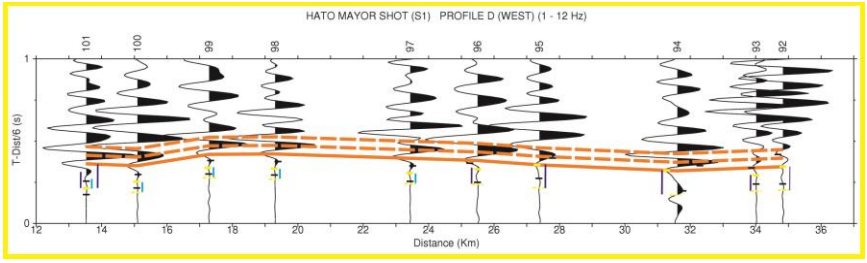

Fig. 2.4.2.5. Enlargement (orange box of Fig. 2.4.2.2) corresponding to P2 phase of seismic record section of shot S1 – Profile D (WS1) where most likely arrival time in orange (t_A), earliest arrival time in black (t_E), new earliest time in dash orange line and latest arrival time in black (t_L) are shown for every pick. Brown solid and dash lines show phase correlation, dark blue line shows Δt_1, blue line shows Δt_2 and light blue line shows Δt_3.

The figure 2.4.2.6 shows the change between P2 and P3 phases. This change is produced due to a change in the amplitude, frequency and an obvious change in the wavelet shape of both phases.

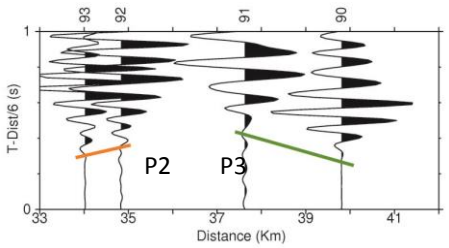

Fig. 2.4.2.6. Extract of shot S1 - Profile D seismic record section (WS1) showing first arrivals characterized by change in amplitude and frequency where the wavelets in traces from 92 and 93 are similar and the amplitude decreases with distance. However, there is an increase in the amplitude and a difference on the shape of wavelets between trace 92 and 91. This fact indicates different phases arrive in this point.

TRACE	t_L (s)	t_E (s)	Individual error estimation (t_L-t_E) (s)	Δt (s)	New t_E (s)	Phase correlation uncertainty (s)
101	0.27	0.20	**0.07**	0.00	0.20	**0.07**
100	0.32	0.19	**0.13**	0.05	0.22	**0.10**
99	0.38	0.29	**0.10**	0.05	0.29	**0.09**
98	0.35	0.26	**0.09**	0.05	0.27	**0.08**
97	0.37	0.23	**0.14**	0.05	0.27	**0.10**
96	0.35	0.18	**0.18**	0.10	0.23	**0.12**
95	0.41	0.18	**0.24**	0.16	0.21	**0.20**
94	0.37	0.01	**0.36**	0.16	0.24	**0.14**
93	0.34	0.25	**0.09**	0.10	0.21	**0.12**
92	0.43	0.23	**0.20**	0.16	0.19	**0.24**

Table 2.4.2.II. Uncertainties calculated for single trace and phase correlation of P2 phase correspond to WS1 seismic record section.

The figure 2.4.2.6 shows the change between P2 and P3 phases. This change is produced due to a change in the amplitude, frequency and an obvious change in the wavelet shape of both phases.

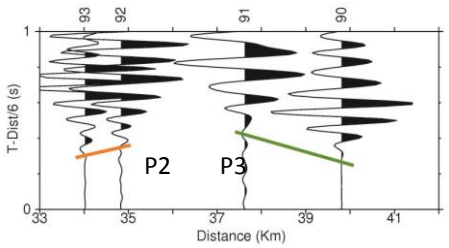

Fig. 2.4.2.6. Extract of shot S1 - Profile D seismic record section (WS1) showing first arrivals characterized by change in amplitude and frequency where the wavelets in traces from 92 and 93 are similar and the amplitude decreases with distance. However, there is an increase in the amplitude and a difference on the shape of wavelets between trace 92 and 91. This fact indicates different phases arrive in this point.

In figure 2.4.2.7, it is observe the phase identify as P3 (Fig. 2.4.2.2). Checking individual times, it is possible to indicate that this phase shows a small velocity gradient with values between 6.3 km/s and 6.6 km/s due to beginning and end of the correlated phase show different slopes. The calculation of average apparent velocity from phase correlation data gives us a value of 6.4 km/s and 6.3 km/s from most likely arrival time data. The obtained uncertainties are summarized in the Table 2.4.2.III.

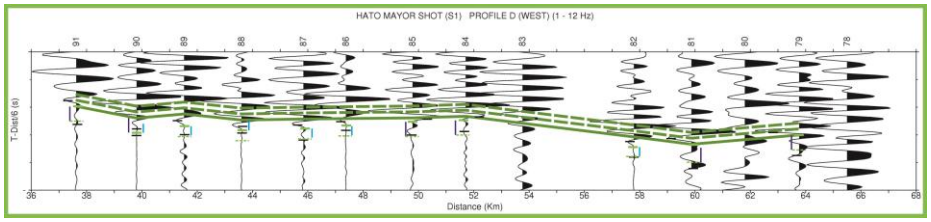

Fig. 2.4.2.7. Enlargement (green box in Fig. 2.4.2.2) corresponds to P3 phase of seismic record section of shot S1 – Profile D (WS1) where most likely arrival time in green (t_A), earliest arrival time in black (t_E), new earliest time in dash green line and latest arrival time in black (t_L) are shown for every pick. Dark green solid and dash lines show the phase correlations. Dark blue line shows Δt_1 and blue line shows Δt_2.

The change between P3 and P4 is not obvious as the previous ones but it is characterized by change in amplitude in the same way. In figure 2.4.2.8, it is possible to observe an increase in the amplitude of trace 77 respects to trace 79 (trace 78 is not possible to define the onset due to the high noise level). As well, P3 and P4 tendency clearly different between them are defined.

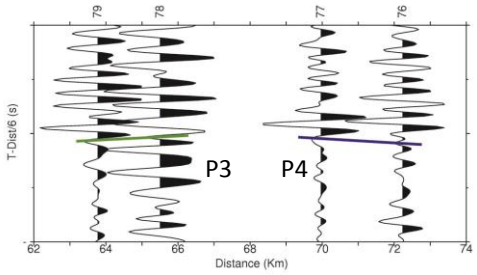

Fig. 2.4.2.8. Extract of shot S1 - Profile D seismic record section (WS1) showing first arrivals characterized by change in amplitude where the wavelets in traces from 82 to 79 are similar and the amplitude decreases with distance. However, there is an increase in the amplitude and a difference on the shape of wavelets between trace 77 and 79. This fact indicates different phases arrive in this point.

TRACE	t_L (s)	t_E (s)	Individual error estimation (t_L-t_E) (s)	Δt (s)	New t_E (s)	Phase correlation uncertainty (s)
91	0.52	0.24	**0.28**	0.05	0.44	**0.08**
90	0.32	0.25	**0.07**	0.00	0.25	**0.07**
89	0.37	0.12	**0.25**	0.05	0.28	**0.09**
88	0.32	0.21	**0.11**	0.05	0.25	**0.07**
87	0.34	0.06	**0.28**	0.05	0.26	**0.08**
86	0.34	0.23	**0.11**	0.05	0.22	**0.12**
85	0.39	-0.10	**0.49**	0.10	0.27	**0.12**
84	0.39	0.09	**0.30**	0.10	0.27	**0.12**
82	0.15	0.07	**0.08**	0.10	0.08	**0.08**
81	0.23	-0.43	**0.65**	0.10	0.12	**0.10**
79	0.23	-0.34	**0.58**	0.10	0.09	**0.15**

Table 2.4.2.III. Uncertainties calculated for single trace and phase correlation of P3 phase correspond to WS1 seismic record section.

The change between P3 and P4 is not obvious as the previous ones but it is characterized by change in amplitude in the same way. In figure 2.4.2.8, it is possible to observe an increase in the amplitude of trace 77 respects to trace 79 (trace 78 is not possible to define the onset due to the high noise level). As well, P3 and P4 tendency clearly different between them are defined.

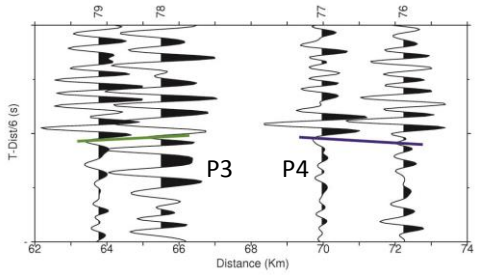

Fig. 2.4.2.8. Extract of shot S1 - Profile D seismic record section (WS1) showing first arrivals characterized by change in amplitude where the wavelets in traces from 82 to 79 are similar and the amplitude decreases with distance. However, there is an increase in the amplitude and a difference on the shape of wavelets between trace 77 and 79. This fact indicates different phases arrive in this point.

The blue box (Fig. 2.4.2.2) shows the phase P4 whose enlargement is seen in Fig. 2.4.2.8. In this phase is possible to observe that the onsets are not as good as the onsets of previous phases due to the high noise level. For this reason, the onsets have to be picked in the same place as phase correlation onsets. This fact produces that the uncertainty of each pick matches up with the uncertainty of phase correlation. The average apparent velocity of P4 phase is 8.2 km/s but considering that the traces 75 and 76 are delayed respect to the others; apparent velocity in this phase is 7.6 km/s.

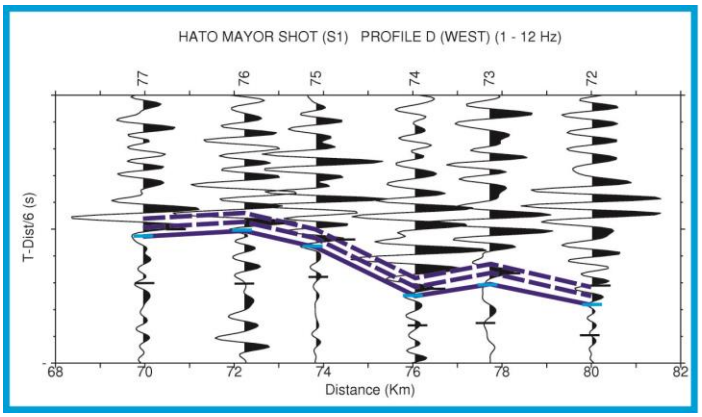

Fig. 2.4.2.9. Enlargement (blue box of Fig. 2.4.2.2) corresponds to P4 phase of seismic record section of shot S1 – Profile D (WS1) where most likely arrival time in blue (t_A), earliest arrival time in black (t_E) and latest arrival time in black (t_L) are shown for every pick. Dark blue and dash lines show phase correlation.

Once timing data are obtained, it is calculated the corresponding uncertainties. As it was said previously, in this phase the uncertainties for individual traces and phase correlation are coincident. The results are shown in the Table 2.4.2.IV.

TRACE	t_L (s)	t_E (s)	Individual error estimation (t_L-t_E) (s)	Phase correlation uncertainty (s)
77	0.25	-0.30	**0.55**	**0.55**
76	0.29	-0.37	**0.66**	**0.66**
75	0.20	-0.20	**0.40**	**0.40**
74	-0.01	-0.65	**0.64**	**0.64**
73	0.01	-0.78	**0.78**	**0.78**
72	-0.05	-0.43	**0.38**	**0.38**

Table 2.4.2.IV. Uncertainties calculated for single trace and phase correlation of P4 phase correspond to WS1 seismic record section.

Finally, it has been determined different seismic phases from seismic record sections of shot S1 (Fig. 2.4.2.1 a), whose seismic record sections are not shown in this section, applying the principles of seismic refraction exposed at the beginning of this chapter. As result, it has been calculated the individual error estimation of every trace and the uncertainty of phase correlation of every phase applying the principles developed previously. Moreover, all phase apparent velocities obtaining in some cases velocity gradients have been determined. Analyzing these values (Table 2.4.2.V), it is possible to observe some important results that must be verified in the corresponding velocity models. These are:

i. Starting with profile C (Fig. 1.3.2.1), the average velocity of first identified phase named P1 in NS1* section is less than the same phase apparent velocity in SS1* for single trace and phase correlation data. However, the end of the velocity gradient interval, in the case of P1 phase (NS1), is much higher than the same one of the P1 phase (SS1), while the initial ends are very similar in both sections. *Figures corresponding to NS1 and SS1 are not shown in this manuscript to simplify the methodology application.

ii. In the second phase identified in NS1 and SS1 seismic record sections, the situation is opposite to the previous point. In NS1 section, P2 is faster than P2 in SS1 where the velocity gradient decreases at the end. These facts must be related with the geology in the study area and must be reflected in the velocity model.

Shot	Profile	Seismic record section	Phase	Velocity gradient	Top and Bottom Velocities (km/s)			Average apparent velocity (km/s)	
								Single trace	Phase correlation
S1	C	NS1	P1	✓	4.6		5.8	4.8	5.0
			P2	✓	6.4	6.6	6.9	5.9	6.1
			P3	✗				7.1	7.0
		SS1	P1	✓	4.6		5.2	5.2	5.4
			P2	✓	5.6		4.9	5.0	5.2
			P3	✗				8.5	8.5
	D	ES1	P1	✗				5.3	5.3
			P2	✗				5.9	6.0
			P3	✗				6.3	6.2
		WS1	P1	✗				5.1	5.4
			P2	✗				5.9	6.1
			P3	✓ almost ✗	6.3		6.6	6.3	6.4
			P4	✓	6.2		8.3	7.6	7.6

Table 2.4.2.V. Summary of apparent velocities calculated for every phase in every seismic record section of shoot S1.

iii. The third phase in NS1 and SS1 seismic record sections is practically constant being P3 (NS1) slower than P3 (SS1) phase. But it is important emphasize that both sections show similar characteristics with different apparent velocities due to the differences in the geology between north and south parts of this profile.

iv. In the profile D (Fig. 2.4.2.2), both seismic record sections have similar features because it is not seen velocity gradients for the first observed phases. As well, there are similarities in the values of apparent velocities comparing phase to phase except for P4 phase, which is not seen in ES1 seismic record section.

2.4.3 Application to marine shooting line registered by one OBS

The seismic record sections correspond to one seismic station recording a line of shots shows a dense number of traces whose phases can be followed in a distance interval. These kinds of seismic record sections are slightly different to seismic record sections corresponding to one land shot registered by land stations of a seismic profile, as it has showed in the previous section, and it is not possible to extract single trace travel times, just phase correlation arrivals.

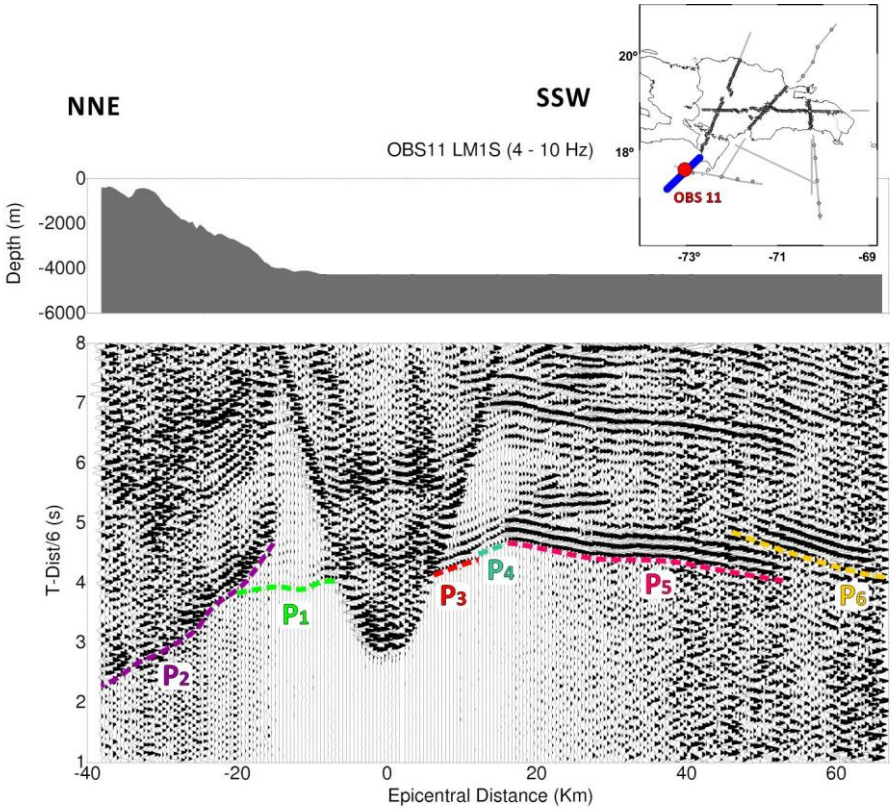

Fig. 2.4.3.1 Seismic record section corresponding to OBS 11 recording marine seismic line LM1S (Fig. 1.3.2.3). Top: Bathymetry along this line.

The example showed in this section corresponds to marine shooting line LM1S recording by OBS 11 (Fig. 1.3.2.3) and the procedure for determining the phases coincide both in the case of a land seismic station as a marine seismic station recording one marine line of shots (Fig. 2.4.1.10 b and d). This OBS is located 45 km south from Dominican Republic in the Caribbean Sea.

The figure 2.4.3.1 shows the seismic record section corresponding to this OBS with P-wave phases interpreted. From the OBS to the NNE and SSW directions, it has been

determined two and four phases, respectively, represented by lines with different colors. In the following figure, it has been represented the determination of onsets and latest and earliest times obtained following the methodology developed in the previous sections (Fig. 2.4.3.2).

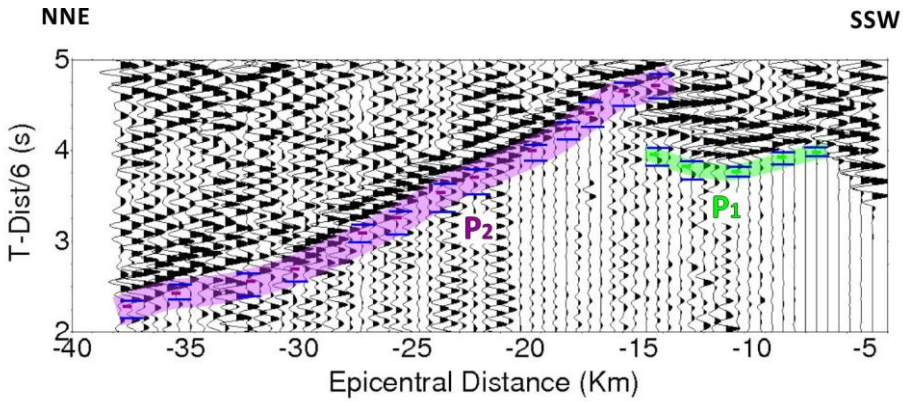

Fig. 2.4.3.2. Extract of OBS 11 seismic record section.

The error estimation has been calculated for every phase as an average of individual error estimations due to the large number of data contained in the phase. Table 2.4.3.I summarizes the calculations for P_1 and P_2 phases in NNE direction.

The P-wave phases determined in the SSW part of the seismic record section have been four (Fig. 2.4.3.3). As previous phases, the error estimation has been calculated from an average of individual error whose data are shown in the Tables 2.4.3.II and 2.4.3.III.

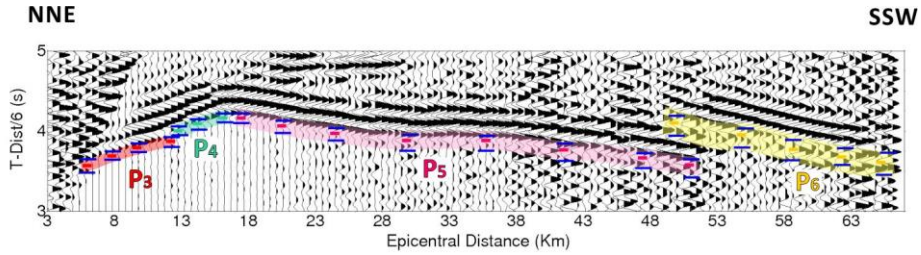

Fig. 2.4.3.3. Extract of OBS11 seismic record section.

P_1	t_L (s)	t_E (s)	Individual error	P_2	t_L (s)	t_E (s)	Individual error
1	4.02	3.93	0.09	1	4.78	4.65	0.14
2	3.99	3.88	0.11	2	4.74	4.51	0.23
3	4.02	3.92	0.10	3	4.63	4.37	0.26
4	3.87	3.75	0.12	4	4.33	4.18	0.15
5	3.94	3.79	0.15	5	4.11	3.93	0.18
6	4.10	3.88	0.22	6	3.77	3.32	0.45
				7	3.48	3.12	0.35
				8	3.19	2.89	0.30
				9	2.99	2.56	0.43
				10	2.52	2.04	0.49
				11	2.54	2.23	0.31
				12	2.45	1.97	0.48
				13	2.49	2.05	0.44
Average Handpicking			**0.13**	Average Handpicking Error			**0.32**

Table 2.4.3.I Average handpicking error for phases P_1 and P_2 of OBS 11 seismic record section.

P_3	t_L (s)	t_E (s)	Individual error estimation (t_L-t_E) (s)	P_4	t_L (s)	t_E (s)	Individual error estimation (t_L-t_E) (s)
1	4.13	3.95	0.18	1	4.56	4.30	0.27
2	4.18	3.96	0.22	2	4.55	4.43	0.12
3	4.23	4.05	0.18	3	4.56	4.41	0.15
4	4.27	4.04	0.23	4	4.57	4.44	0.13
5	4.31	4.14	0.17	5	4.65	4.50	0.15
6	4.37	4.167	0.20	6	4.62	4.46	0.16
7	4.37	4.07	0.30	7	4.62	4.47	0.15
8	4.46	4.19	0.27	8	4.66	4.38	0.28
Average Handpicking Error			**0.22**	Average Handpicking Error			**0.18**

Table 2.4.3.II Average handpicking error for phases P_3 and P_4 of OBS 11 seismic record section.

P_5	t_L (s)	t_E (s)	Individual error estimation (t_L-t_E) (s)	P_6	t_L (s)	t_E (s)	Individual error estimation (t_L-t_E) (s)
1	4.65	4.43	0.22	1	4.66	3.99	0.66
2	4.62	4.44	0.18	2	4.63	4.05	0.58
3	4.59	4.34	0.25	3	4.57	4.11	0.46
4	4.56	4.03	0.53	4	4.50	3.96	0.54
5	4.59	4.11	0.49	5	4.52	4.00	0.52
6	4.56	4.27	0.29	6	4.51	3.99	0.5
7	4.52	4.13	0.39	7	4.46	4.00	0.46
8	4.49	4.11	0.37	8	4.48	3.99	0.50
9	4.50	4.00	0.50	9	4.38	3.94	0.44
10	4.47	4.02	0.46				
11	4.46	3.97	0.50				
12	4.47	3.97	0.50				
13	4.44	3.91	0.53				
14	4.44	3.85	0.60				
15	4.30	3.74	0.56				
16	4.26	3.56	0.70				
17	4.18	3.60	0.58				
Average Handpicking Error			**0.45**	Average Handpicking Error			**0.53**

Table 2.4.3.I Average handpicking error for phases P_5 and P_6 of OBS 11 seismic record section.

2.5 P-WAVE PHASE INTERPRETATION

In the seismic record sections obtained for profiles presented in this work, it was possible to identify time correlations corresponding to P-wave refractions and reflections in the crustal and upper mantle discontinuities. Each phase is assigned a color and a code with subscripts, which represent the layer relative position respects to the subsurface (Table 2.5.I), where P_x represents the refracted wave in layer x, P_xP is the reflected wave in discontinuity separating layer x and x+1, and, finally, P_x' is the wave that travels across the discontinuity between layers.

Color	Phase	Interpretation
	P_2P	Reflected in discontinuity between layers 2 and 3
	P_2'	Head wave travelling across discontinuity between layers 2 and 3
	P_3P	Reflected wave at the bottom of layer 3
	P_3'	Head wave travelling through discontinuity between layers 3 and 4
	P_4P	Reflected in discontinuity between layers 4 and 5
	P_4'	Head wave travelling across discontinuity between layers 4 and 5
	P_5P	Reflected wave at the bottom of layer 5
	P_MP	Reflected in Mohorovicic
	P_6P	Reflected wave at the bottom of layer 6
	P_7P	Reflected in discontinuity between layers 7 and 8
	P_8P	Reflected wave at the bottom of layer 8
	P_9P	Reflected wave at the bottom of layer 9
	$P_{10}P$	Reflected wave at the bottom of layer 10
	$P_{11}P$	Reflected wave at the bottom of layer 11
	$P_{12}P$	Reflected wave at the bottom of layer 12

Table 2.5.I Different phases identified in the seismic refraction profiles analyzed in this chapter.

A scheme of phase interpretation is shown in the following figure:

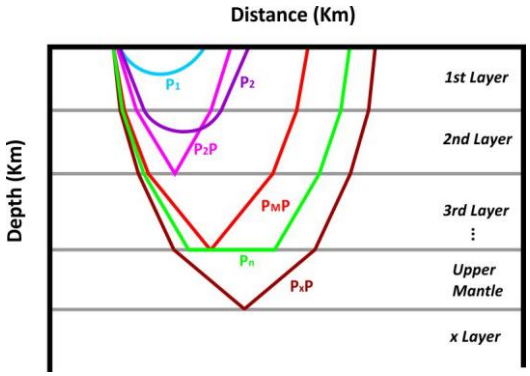

Fig. 2.5.1 Phases interpretation scheme followed in this work.

2.6 MODELING

The interpretation of crustal refraction data for 2D velocity structure often involves laborious trial-and-error ray-trace forward modeling. During this study, it has been used forward and inverting travel times to obtain 2D velocity and interface structure simultaneously developed by Zelt and Smith (1992) in LINUX environment and adapted to WINDOWS environment by Dr. L. Matias.

This method is applicable to any set of travel times for which forward modeling is possible, regardless of the shot-receiver geometry or data quality, since the forward step is equivalent to trial-and-error forward modelling [Zelt & Smith (1992)]. This methodology requires specifying the number and position of velocity and boundary nodes for each layer. The method of ray tracing is by an efficient numerical solution of the 2-D ray tracing equations coupled with an automatic determination of ray take-off angles.

$$\frac{dz}{dx} = \cot\theta \qquad \frac{dx}{dz} = \tan\theta$$

or

$$\frac{d\theta}{dx} = \frac{v_z - v_x \cot\theta}{v} \qquad \frac{d\theta}{dz} = \frac{v_z \tan\theta - v_x}{v}$$

With initial conditions: $x = x_0,\ z = z_0,\ \theta = \theta_0$ [Cerveny et al., 1977]. To complete the basic ray tracing algorithm, Snell's law is applied at the intersection of a ray with a layer boundary.

The effectiveness of this inverse technique is due to a model parameterization that is suited to the requirements of an inverse approach where the number and position of velocity and boundary nodes can be suited to the data's subsurface ray coverage. The forward step (TRAMP) uses a robust method of ray tracing and as such the inversion algorithm benefits from the advantages of ray methods (RAYINVR) (Fig. 2.6 a and b). A simulation of smooth layer boundaries increases the stability of the inversion.

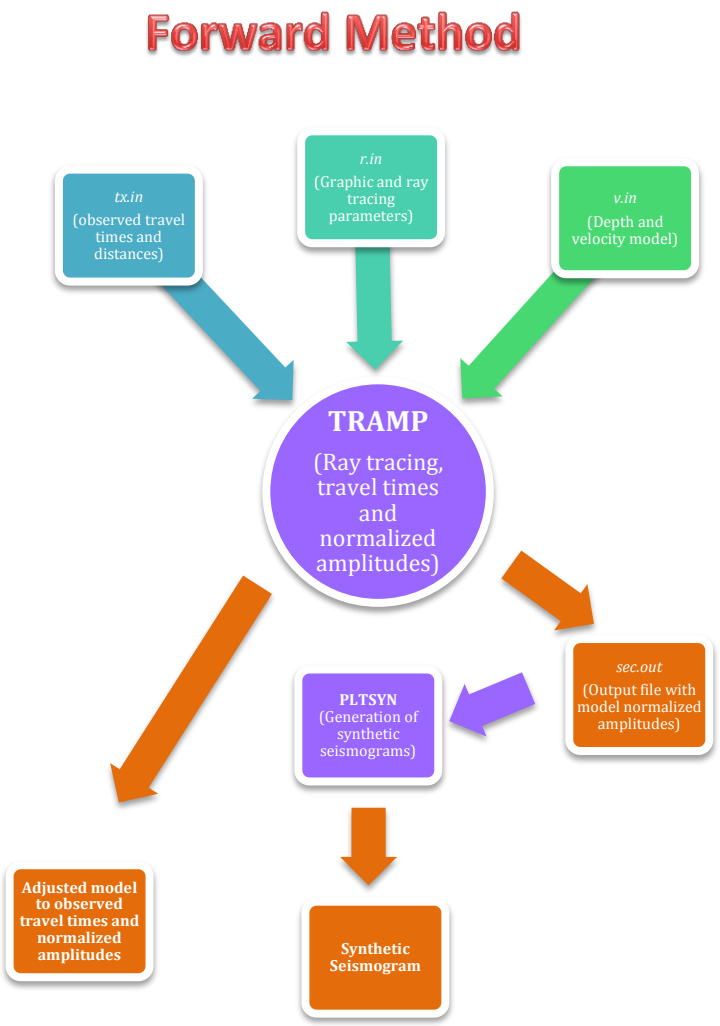

Fig. 2.6 a) Methodology flowchart used for interpretation of wide-angle seismic data corresponding to forward method. Words in capital letters represent used programs, italic word represents input and output files and bold words represent the resulting files.

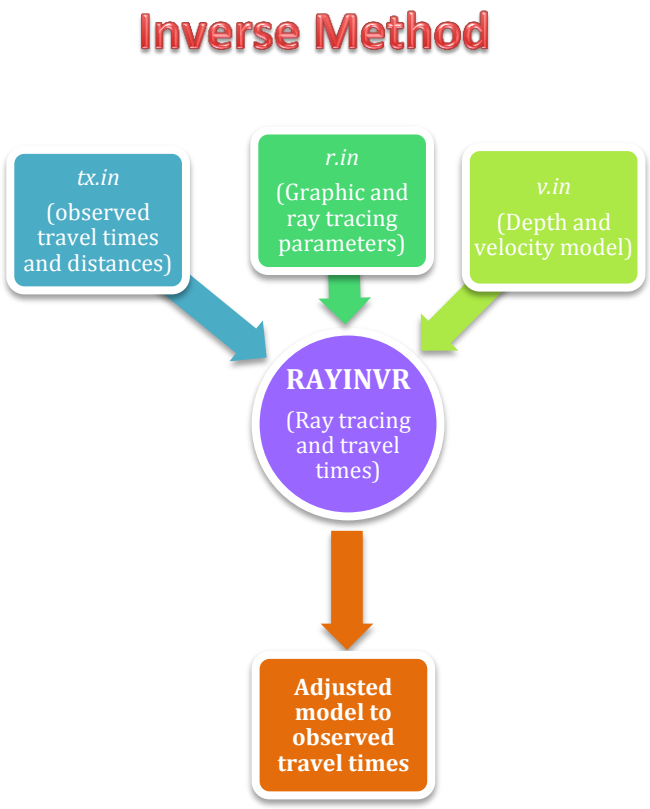

Fig. 2.6 b) Methodology flowchart used for interpretation of wide-angle seismic data corresponding to inverse method. Words in capital letters represent used programs, italic word represents input and output files and bold words represent the resulting files.

A complementary program, SEIS WIDE is used as graph visualizer and interactive manual modifier of velocity and boundary nodes.

2.7 ERROR ASSESSMENT

This work has considered two main sources of error of those that could exist. The first concerns the relative position between the instrument and the seismic line. This fact implies when the instrument is out of the seismic transect, an error has to be quantified and calculated. Furthermore, in the previous section, it has been estimated the error due to the picking process. This travel time uncertainty affects to the determination of velocity and depth.

The methodology for determining the first error leaves from the most common situation, i.e., when the station is below shooting line. In this case, it will determine the travel time for a reflected ray. Then, it is assumed that the station is offset from the vertical position and is calculated the delay travel time, which is considered as the uncertainty. To check that, travel times from a ray tracing program with a realistic velocity model are obtained.

For second source of error, it will be obtained a first approximation of the depth and velocity uncertainty from a general formula of error propagation, fixing a distance and assuming some approximations. Calculations for these errors are:

Travel time uncertainty due to the position between source and instrument

1. Station placed below seismic line

The simplest case is the two-dimensional reflection at a horizontal boundary (Fig. 2.7.1). In this case, the ray that strikes the boundary at R is reflected to the surface and recorded by a geophone at the point G.

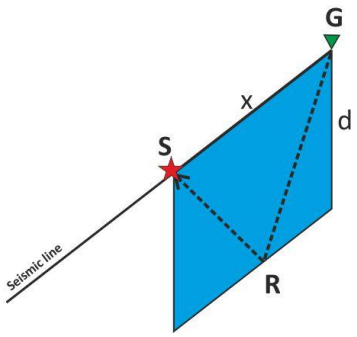

Fig. 2.7.1. Two-dimensional reflection scheme where S represents the shot point, G the receiver point (geophone) and R the point where reflection occurs. The distance between G and S is x while the depth of the layer is d.

If the P-wave velocity is V, the travel time t of the reflected ray SRG is:

$$t = \frac{(SR+RG)}{V} = \frac{\sqrt{x^2+(2d)^2}}{V} \qquad [2.1]$$

2. Offset between seismometer position and seismic profile

Following the previous case, when G is out of the line (Fig. 2.7.2) with an offset x_S, the new travel time corresponding to the reflected ray SR'G is t':

$$t' = \frac{(SR' + R'G)}{V} = \frac{\sqrt{x'^2 + (2d)^2}}{V} \quad [2.2]$$

where $x' = \sqrt{x^2 + x_S^2}$ [2.3]

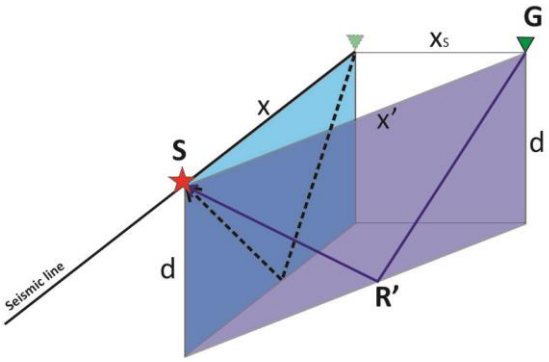

Fig. 2.7.2 Two-dimensional reflection scheme with G out of the seismic line. S represents the shot point, G the receiver point (geophone) and R' the point where reflection occurs. The distance between G and S is x' and separation distance is x_S, while depth of the layer is d.

The delay in the travel time, which is considerate as uncertainty, is calculated as follow:

$$\Delta t = t' - t = \frac{1}{V}\left(\sqrt{x'^2 + (2d)^2} - \sqrt{x^2 + (2d)^2}\right) \quad [2.4]$$

3. Realistic model

In this section, a realistic model is understood as a velocity model characterized by bathymetry and successive layers may have dips. To determine the uncertainty associated with a realistic model, we begin with a model of flat constant velocity layers with increasing velocity (Fig. 2.7.3) in depth using TRAMP program [Zelt and Smith, 1992] (Fig. 2.7.4 and 2.7.5).

Theoretical travel times and positions have been calculated using a defined velocity model (Fig. 2.7.3) and the following expressions:

$$T_{H_n} = \frac{x}{v_n} + \tau_n \quad [2.5]$$

being $\tau_n = 2\sum_{j=0}^{n-1} h_j \left(\frac{1}{v_j^2} - \frac{1}{v_n^2}\right)^{1/2}$ [2.6]

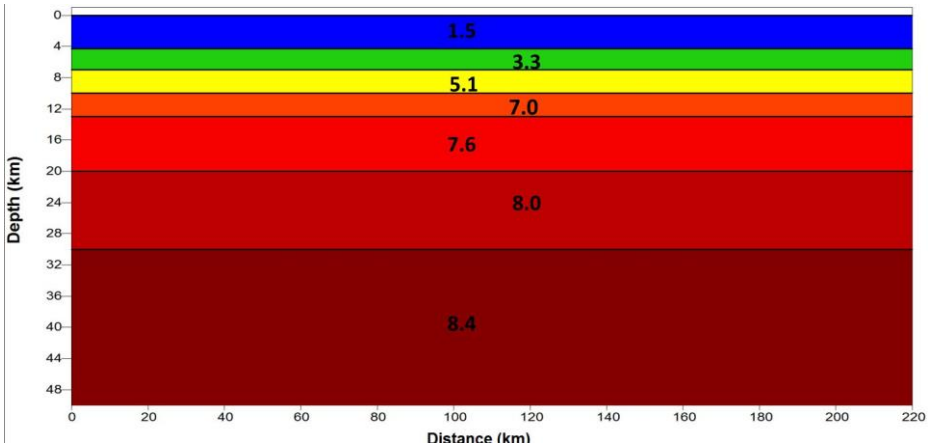

Fig. 2.7.3 P-wave velocity model with flat layers

After that, it has been taking into account that as the absolute travel time is the same for one station in or out of the seismic line, being the reduced travel time, which will provide the uncertainty for every P-wave phase. Figure 2.7.4 shows flat layer model with theoretical travel times and positions compared with calculated data with station over seismic line, while figure 2.7.5 shows the same calculation but a fixed separation distance of 2.5 km. In last figure, it is possible to observe that the most superficial layers are affected by this separation but the deepest layer not.

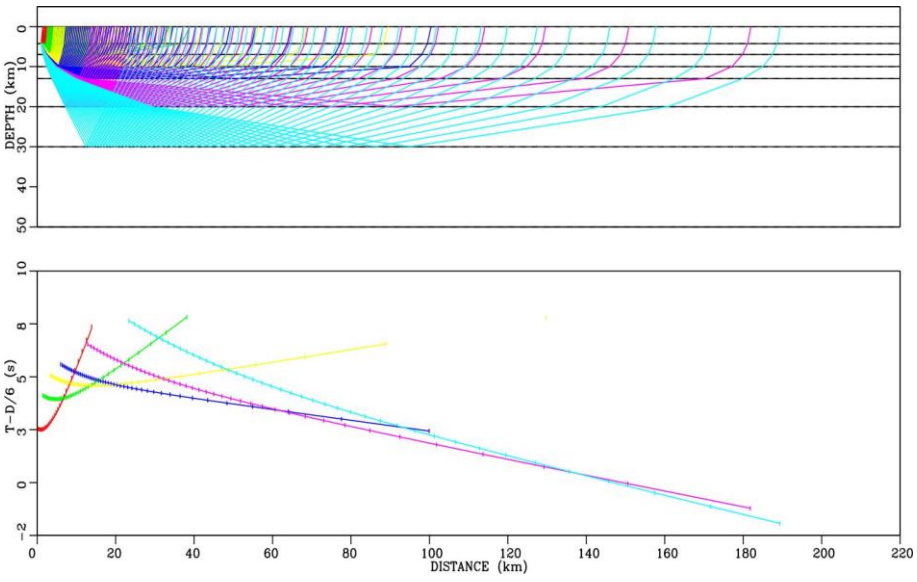

Fig. 2.7.4 Ray tracing showing theoretical travel times and positions.

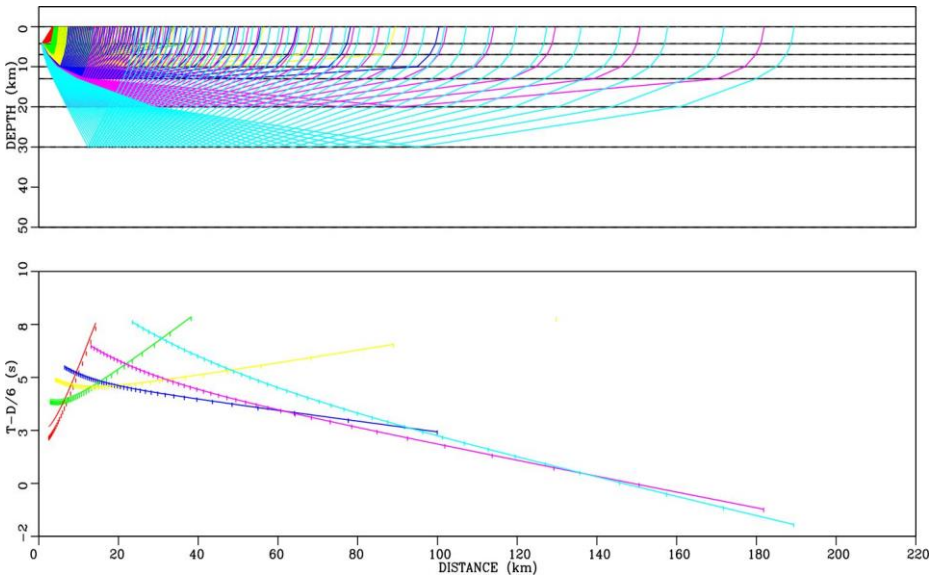

Fig. 2.7.5. Ray tracing showing theoretical travel times and positions with an offset geophone distance of 2.5 km compared with calculated travel times.

Next step consists of introducing a bathymetry and layers with dips (Fig. 2.7.6). The results show that for separations less than 1.5 km, the error is within the uncertainty estimated for every phase in the picking phase (Fig. 2.7.7). Practically most of the stations are in this case. However, there are some OBS separated distances longer than 1.5 km. In these cases, the error estimation has been added to the uncertainty due to the hand picking showed in the previous section.

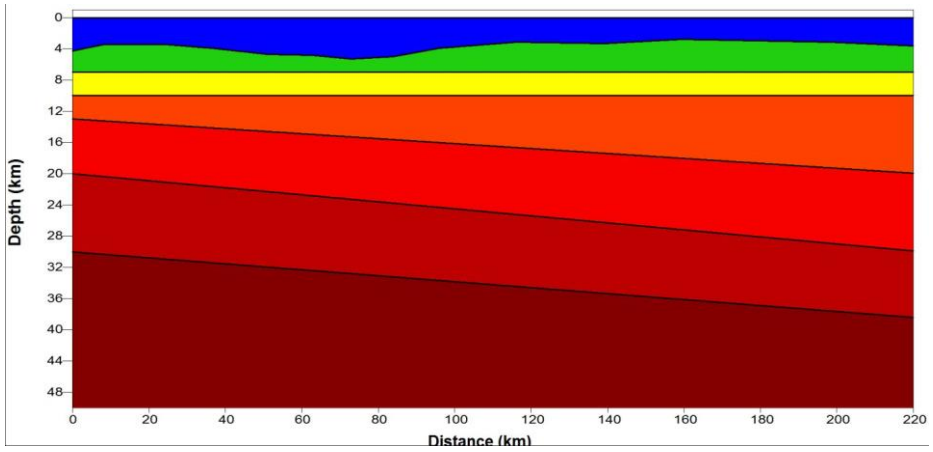

Fig. 2.7.6. P-wave velocity model with bathymetry and dip layers.

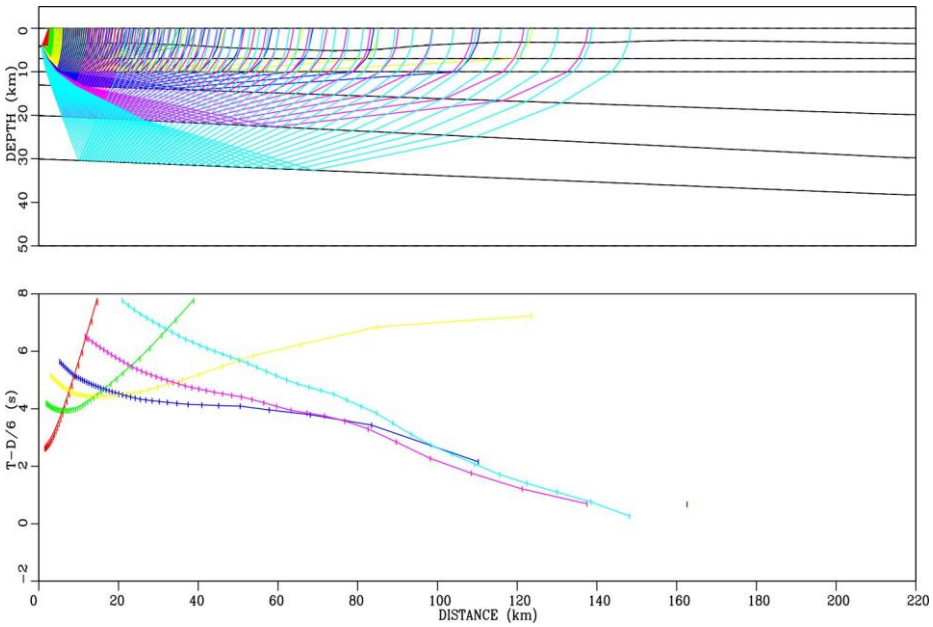

Fig. 2.7.7 Ray tracing showing theoretical travel times and positions with an offset geophone distance of 1.5 km compared with calculated travel times.

Depth and velocity error estimation

Considering that the possible error sources are travel time (*T*), distance (*x*), depth (*h*) and velocity (*v*), and using as example the flat layer velocity model of previous point, it is going to be estimated the uncertainty for depth and velocity from general formula of error propagation and assuming some approximations.

$$\Delta T_H = \frac{\partial T_H}{\partial x}\Delta x + \frac{\partial T_H}{\partial h}\Delta h + \frac{\partial T_H}{\partial v}\Delta v \quad [2.7]$$

Depth: To determine Δh, we assume that $\Delta x = \Delta v = 0$ and the uncertainty depends just of absolute travel time, whose value has been determined in the previous sections. In this case

$$\Delta h = \frac{\Delta T_H}{\frac{\partial T_H}{\partial h}} \quad [2.8]$$

Using the data of velocity model (Fig. 2.7.3), it is possible to observe that depth uncertainty increases as absolute travel time uncertainty, obtained in picking phase, increases. This depth uncertainty varies from 0.03 to 0.38 km for deepest layer in the model. Calculations for models with layers at 100 km deep have provided maximum values of 1.3 km.

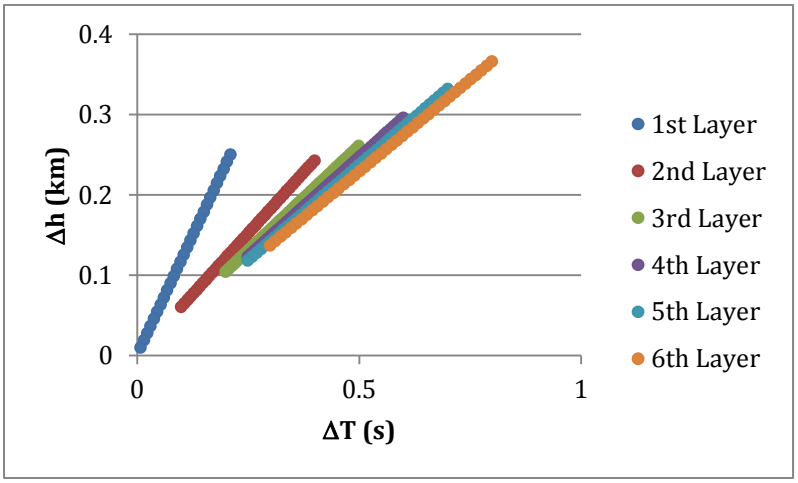

Fig. 2.7.8 Graphic representation Δh vs. ΔT

Velocity: To calculate Δv, we assume that $\Delta x = \Delta h = 0$ and the uncertainty depends just of absolute travel time, whose value has been determined in the previous sections. In this case

$$\Delta v = \frac{\Delta T_H}{\frac{\partial T_H}{\partial v}} \quad [2.9]$$

Using the same data, uncertainty corresponding to velocity of the layer increases in distance and depth obtaining maximum values between 0.05 km/s and 0.11 km/s for model showed in Fig. 2.7.3. Calculations for models with layers at 100 km show uncertainty values of 0.3 km/s.

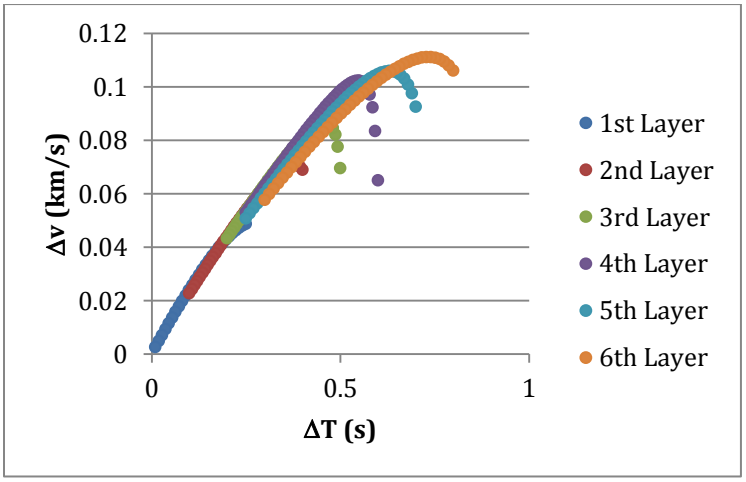

Fig. 2.7.8 Graphic representation Δv vs. ΔT

Travel time fit and model evaluation

A final velocity model should adequately fir the data predicting arrival times within the data error bounds, ideally with $\chi^2 = 1$. If $\chi^2 < 1$ the data is over-fit and if $\chi^2 > 1$ the data is under-fit [Zelt and Smith, 1992]. However, in practive final χ^2 values significantly different from 1 are often obtained in travel time inversion [Zelt and Forsyth, 1994]. In the following chapters, estimates of arrival-time fit quality for each phase and for all phases are presented in different tables.

CHAPTER 3

MODELING THE CRUST AND UPPER MANTLE IN NORTHERN BEATA RIDGE (Caribe Norte Project)

A synthesis of the most relevant results of this chapter has been submitted in ***PAGEOPH*** *[Núñez et al., *](PAAG-1394)*

ABSTRACT

The complex tectonic region of NE Caribbean, where Hispaniola and Puerto Rico are located, is bordered in the north by subduction zone with oblique convergence and, in the south, by incipient subduction zone associated to Muertos Trough. Central Caribbean basin is characterized by the presence of a prominent topographic structure known as Beata Ridge whose oceanic crustal thickness is unusual. The northern part of Beata Ridge is colliding with the central part of Hispaniola along a transverse NE alignment constituting a morphostructural limit producing the interruption of the Cibao Valley and the divergence of the rivers and basins in opposite directions. The direction of this alignment coincides with the discontinuity that could explain the extreme difference between west and east seismicity of the island. Different studies have provided information about Beata Ridge, mainly about the shallow structure from MCS data. In this work, CARIBE NORTE (2009) wide-angle seismic data, along WNW-ESE trending line in the northern flank of Beata Ridge, are analyzed providing a complete tectonic view about shallow and deep structures. The results show some tectonic differences between west and east separated by Beata Island. In the area of Haiti Basin, sedimentary cover is strongly influenced by the bathymetry and its thickness decreases toward to the island. In this area, the Upper Mantle reaches 20 km deep increasing up to 24 km below the island where the sedimentary cover disappears. Eastern, the three seamounts of Beata Ridge indicate the appearance of a structure completely different where sedimentary cover reaches thicknesses of 4 km between seamounts and Moho rises up to 13 km deep. This study has allowed determining Moho topography and characterizing seismically

the first Upper Mantle layers along northern Beata Ridge, which is not possible from previous MCS data.

KEYWORDS: Beata Ridge, Caribbean Plate, Hispaniola, shallow and deep structures, wide-angle seismic

3.1 INTRODUCTION

It is well known that the Caribbean-North America plate boundary zone is a complex region where different tectonic processes occur (Fig. 3.1.1). This plate boundary zone (PBZ) consists of a 100-250 km wide seismogenic zone of mainly left-lateral strike-slip deformation extending over 2000 km along the northern edge of the Caribbean plate (CP) [Mann et al, 1995]. The relative movement is wards to North America plate in the E-NE direction with a rate of 20±0.4 mm/yr. and an azimuth of $74^{o}\pm1^{o}$, from GPS measurements [Mann et al., 2002; DeMets et al., 2010]. These results explain the geodynamic for the Caribbean – North America plate boundary, implying a maximum oblique convergence between both plates centered on Hispaniola Island. The area of Hispaniola and Puerto Rico Islands is limited by a subduction zone with oblique convergence in the North and an incipient subduction zone associated to Muertos Trough in the South. The left-lateral Septentrional strike-slip fault (SFZ) and the south-dipping thrust faults of the North Hispaniola deformed belt accommodate deformation in the North while, in the South, the deformation is accommodated along the left-lateral Enriquillo-Plantain Garden Fault (EPGFZ) and north-dipping thrust faults of the Los Muertos deformed belt separated by the Beata Ridge. The Beata Ridge is a prominent NE – SW trending topographic structure in the central Caribbean basin characterized by unusually thick oceanic crust (up to 20 km). It is believed to form a part of the ancient Caribbean oceanic plateau [Révillon et al., 2000]. It extends 400 km south from Cape Beata, Hispaniola, dividing the Caribbean into the Colombia and Venezuela basins (Fig. 3.1.1), that are subducting in a normal way below the South American deformed belt.

Despite the large number of studies conducted in the northern Caribbean plate ([Ewing et al, 1960 a], [Fox, et al, 1970], [Talwani et al, 1977], [Moore and Fahlquist, 1976], among others), there are certain areas where no agreement exists on geodynamic models that govern the structure and tectonic development of the area due to the absence of deep geophysical research.

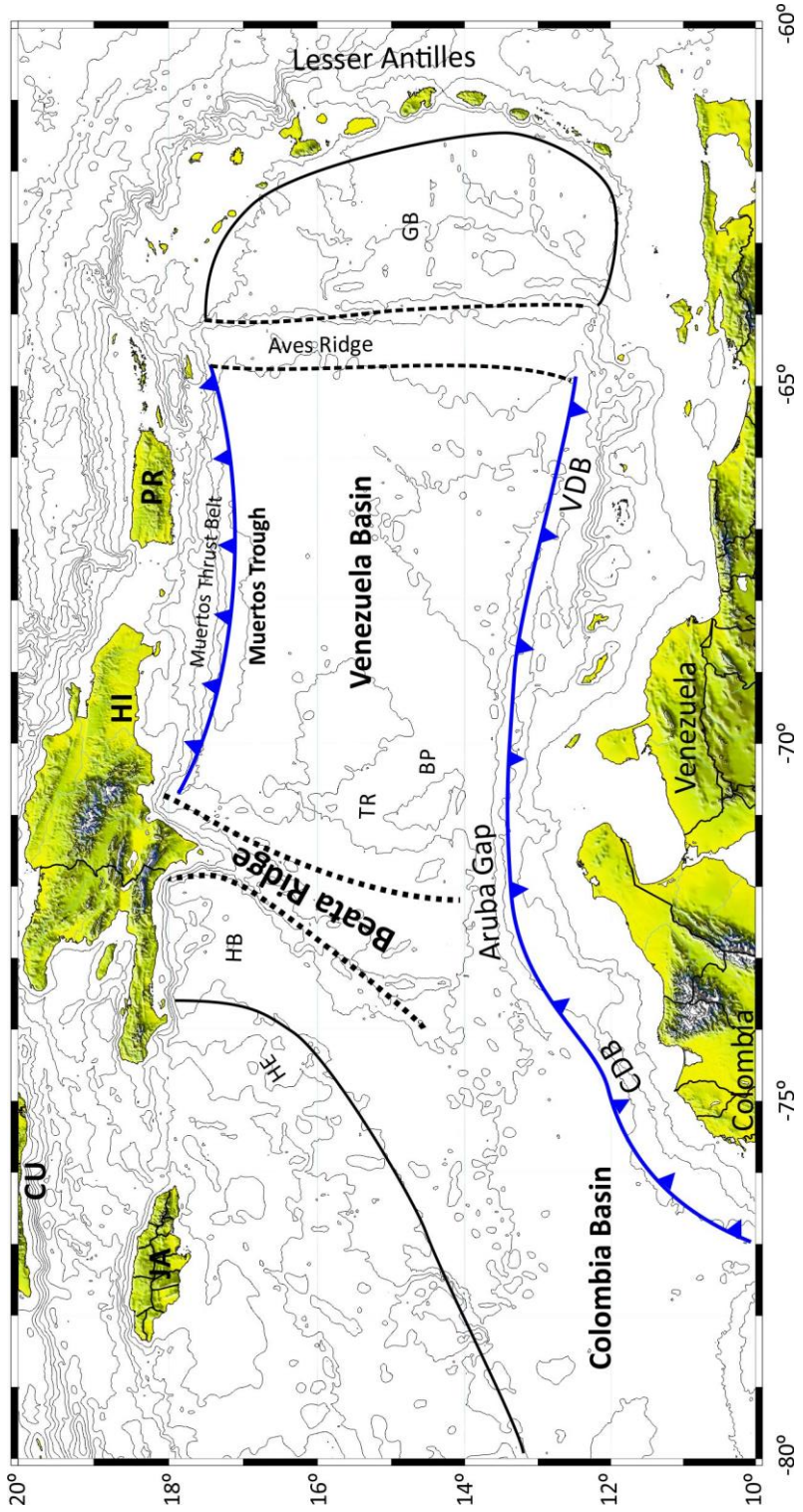

Fig. 3.1.1. Tectonic frame of Caribbean region where red star represents the position of the earthquake occurred on 1673 with Ms = 7.5 [from Cotilla et al., 2007]. The Greater Antilles islands are represented by CU (Cuba), JA (Jamaica), HI (Hispaniola) and PR (Puerto Rico). HE = Hess Escarpment; HB = Haiti Basin; TR = Taino Ridge; BP = Beata Plateau; GB = Grenada Basin; CDB = Colombia Deformed Belt; VDB = Venezuela Deformed Belt; EPGFZ = Enriquillo – Plantain Garden Fault Zone; SFZ = Septentrional Fault Zone; SJB = San Juan Basin; EB = Enriquillo Basin; AB = Azúa Basin.

In particular, Beata Ridge has been analyzed from North to South with different studies [Mauffret and Leroy, 1999; Driscoll and Diebold, 1999] from Multi-channel Seismic (MCS) data obtaining the shallow structure along several transversal lines (Fig. 3.1.2).

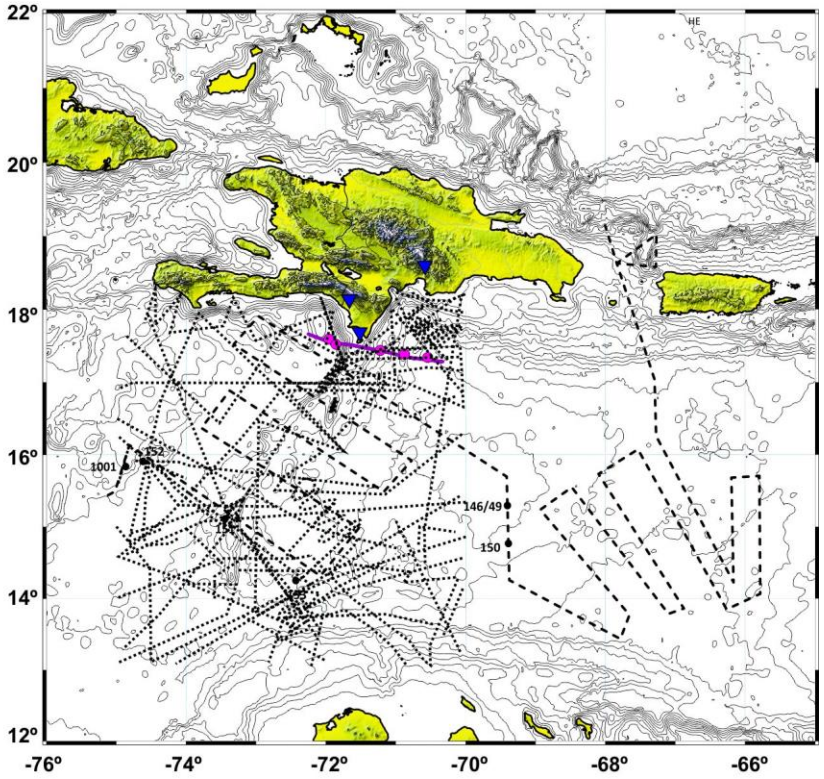

Fig. 3.1.2 Previous MCS and DSDP studies in the area where thick dashed lines represent the MCS data from Mauffret and Leroy (1999), while thin dashed lines represent other studies from different data sources.

3.2 GEOLOGY AND TECTONIC SETTING

As mentioned before, the Beata Ridge is a NE-SW trending structure located in the interior of the CP, between the extended Colombian and Venezuelan basins. The Aruba Gap, a narrow connection between these two basins, truncates the Beata Ridge structure before it reaches the continental slope of South America. In contrast, the northern part of the Beata Ridge collides with the central part of Hispaniola in relation with the eastwards drift of the CP relative to Hispaniola. This collision results from the buoyancy of thick volcanic crust that resists subduction beneath Hispaniola [Burke et al., 1978; Mercier de Lepinay et al., 1988]. The Beata Ridge and the central Caribbean were dredged [Fox et al., 1970] and drilled during the Deep Sea Drilling

Program (DSDP) (Fig. 3.1.2) recovering samples that were mainly basalts and sediments with dolerites at certain sites [Donnelly et al., 1973, Donnelly et al., 1990].

The northern part of the ridge is ~100 km-wide and emerged (Sierra de Bahoruco in the southern Hispaniola Island) and the southern part is approximately 350 km wide and more than 4000 m below sea level suggesting that northern part of the ridge is colliding with the E-W trending of the Caribbean island arc. This structure brings Caribbean crust up to shallower depths and it appears to be underlain by somewhat thicker crust than that of the adjacent Venezuelan Basin to the east, and it appears to be bounded on its southeastern edge by faults [Driscoll and Diebold, 1998; Mauffret and Leroy, 1999]. In the north, the contact of Beata Ridge with Hispaniola Island is observed along a transverse NE alignment that constitutes a morphostructural limit producing the interruption of the Cibao Valley and the divergence of the rivers and basins in opposite directions [Cotilla et al., 2007].

The Beata Ridge is composed mainly of intrusive rocks (gabbros and dolerites) emplaced in a subsurface, hypabyssal environment. The bulk of the ridge probably represents an imbricated sill/dike complex [Révillon, et al., 2000].

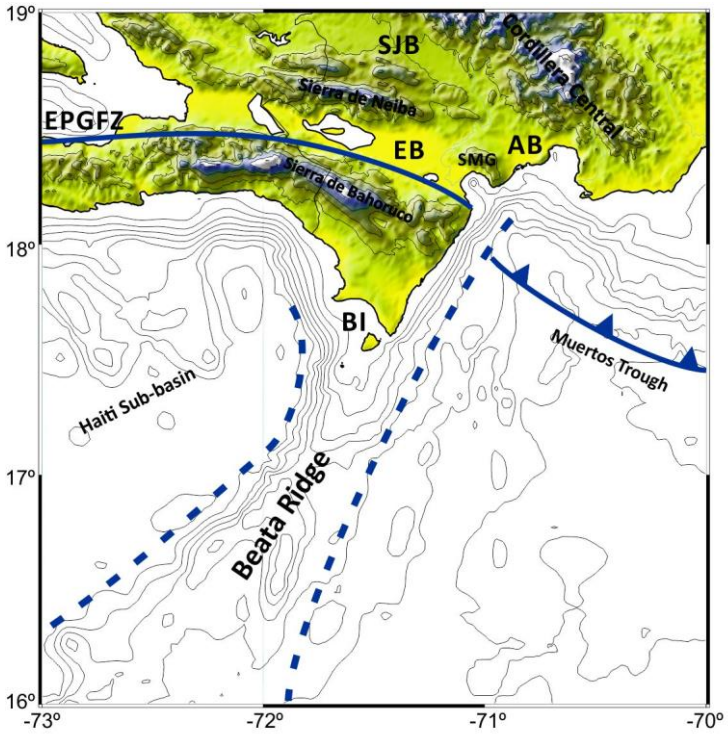

Fig. 3.2.1. Schematic tectonic frame of Hispaniola Island with main tectonic and geologic features in studied area. SJB = San Juan Basin; SN = Sierra de Neiba; EB = Enriquillo Basin; SMG = Sierra de Martín García; AB = Azúa Basin; BI = Beata Island; EPGFZ = Enriquillo-Plantain Garden Fault Zone.

The seismicity in the area of Hispaniola Island is mainly distributed on the eastern side of Dominican Republic and along main strike-slip faults (SFZ and EPGFZ), marked by a clear discontinuity with the western part, which coincides with the direction of Beata Ridge indentation. In the northern part of this structure, few shallow earthquakes have been located recently (see International Seismological Centre, on-line bulletin) but in the past, there have been some large earthquakes such as the event occurred in 1673 with magnitude Ms = 7.5. The event was located at the junction of Beata Ridge, Muertos Trough and EPGFZ [Cotilla et al., 2007] (Fig. 3.1.1).

Seismic refraction studies [Ewing et al., 1960; Edgar et al., 1970] show that the crustal structure of the ridge consists of a 5.4 km/s layer overlying a 6.7 km/s layer. The velocity structure is similar to ocean basin velocity structure but the total thickness of the Beata Ridge crust is twice as thick as that of normal oceanic basin [Fox et al., 1970]. This structure is characterized by unusually thick oceanic crust (up to 20 km) and is believed to form part of the ancient Caribbean oceanic plateau. This thickness is mainly caused by a volcanic underplating that initiated the uplift and rifting of the Beata Ridge [Mauffret and Leroy, 1999].

The CARIBE NORTE project [Carbó et al., 2010] was carried out during spring of 2009 using Spanish Navy research ship R/V Hespérides. As a part of this marine experiment, a 220 km wide-angle seismic profile (LM2 line) was carried out to determine mainly the deep structure across Beata Ridge between Beata and Alto Velo Islands from wide angle seismic data.

3.3 SEISMIC DATA

The seismic wide-angle measurements analyzed in this work were made along a WNW-ESE trending line (LM2) in the south coast of Dominican Republic crossing the northern flank of Beata Ridge with a total length of 220 km (Fig. 3.3.1) (CARIBE NORTE Project). The seismic source used aboard R/V Hespérides consisted of two airgun subarrays with a total capacity of 3850 ci, shooting every 90 s. The cruise velocity was 5 knots. These shots were registered by five OBS deployed, using the Dominican Navy patrol boat “Orion”, along the LM2 line and also by one three components seismic land station at Beata Island. The OBS 11 and 13 were in the western side of the transect (Haiti Basin) and OBS 14, 15 and 16 to the east crossing the Beata Ridge. OBS 14 was just below the shooting line but the others were 1.3 km to 4.0 km offline. The station placed in Beata Island is 13.5 km from the LM2 line. For this reason, it has been necessary to apply a correction in travel times (*see Chapter 2, Section 2.7, Case 1*).

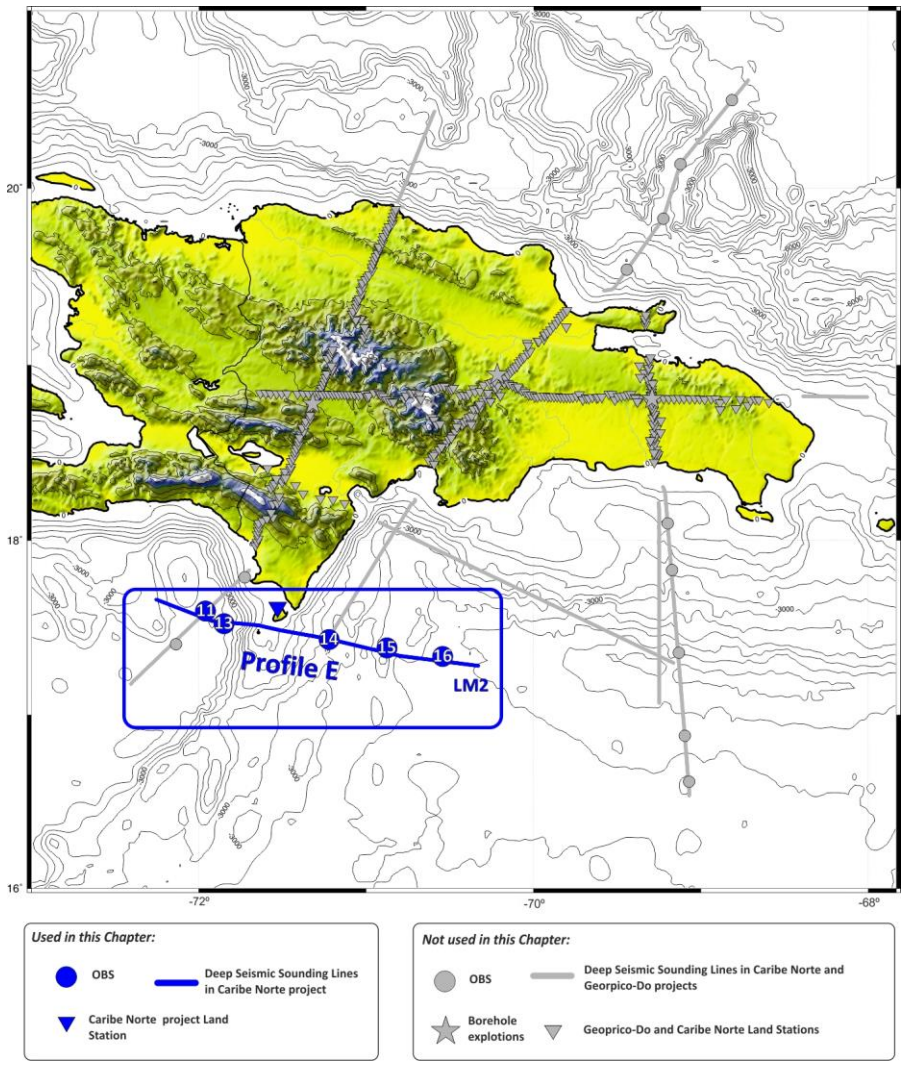

Fig. 3.3.1 Deployment map with stations and seismic sources used in this chapter and all stations deployed during Caribe Norte and Geoprico-Do projects (grey symbols). Blue rectangle represents the study area.

The seismic energy was sufficient to trace signals on the OBS seismic record sections to distances up to 220 km. Processing included navigation data, band-pass filtering and corrections due to instrument drift, and the mentioned travel time correction except for OBS 14 (*see Section 2.7, Chapter 2*).

Moreover, it has been used MCS seismic record sections from Mauffret and Leroy (1999) to compare basin geometry obtained from wide-angle and near vertical seismic reflection data.

3.4 INTERPRETATION

Data processing allowed obtaining seismic record sections whose interpretation has provided the travel times and distances necessary to elaborate the northern Beata velocity model. This interpretation consisted of determining the P-wave phases observed in each seismic record and their corresponding apparent velocities. Subsequently, ray tracing models and synthetic seismograms have been made to finally obtain the velocity models corresponding to this profile.

3.4.1 Seismic record sections and Correlation Data

In the seismic record sections obtained for Profile E, it was possible to identify time correlations corresponding to P-wave refractions and reflections in the crustal and upper mantle discontinuities. Each phase is assigned a color and a code with subscripts, which represent the layer relative position respects to the subsurface (see Table 2.5.I, Section 2.5, Chapter 2).

Profile E

Profile E is 220 km length with WNW – ESE direction starting at Haiti Basin and finishing in the northern part of Beata Ridge. The LM2 marine shooting line crosses between Beata and Alto Velo Islands (DR) and it was recorded for five OBS, two of which were placed west of the Beata Island and three located east over the Beata Ridge.

In this section, three of the six seismic records are going to be shown as an example of the work that has been carried out. The first seismic record section analyzed is OBS 11. This station is located at 4.17 km over sea floor and 32.164 km from the origin of the model and it is 4.0 km far from the seismic line. This fact implies the introduction of an error term in the determination of uncertainty, which mainly affects the upper layers of the crust.

Figure 3.4.1.1 shows the seismic record section corresponding to OBS 11. In this figure, it has been represented the P-wave phases determined in the interpretation. First phase interpreted is P_2' that is observed on both sides of the OBS from 3 to 20 km to the west (4.6 km/s average apparent velocity (a.a.v)) and 5 to 22 km to the east (5.7 km/s a.a.v). On the west, between 17 km to 32 km source-receiver offset, P_4P is interpreted with a.a.v of 9.7 km/s indicating layer 4 is dipping.

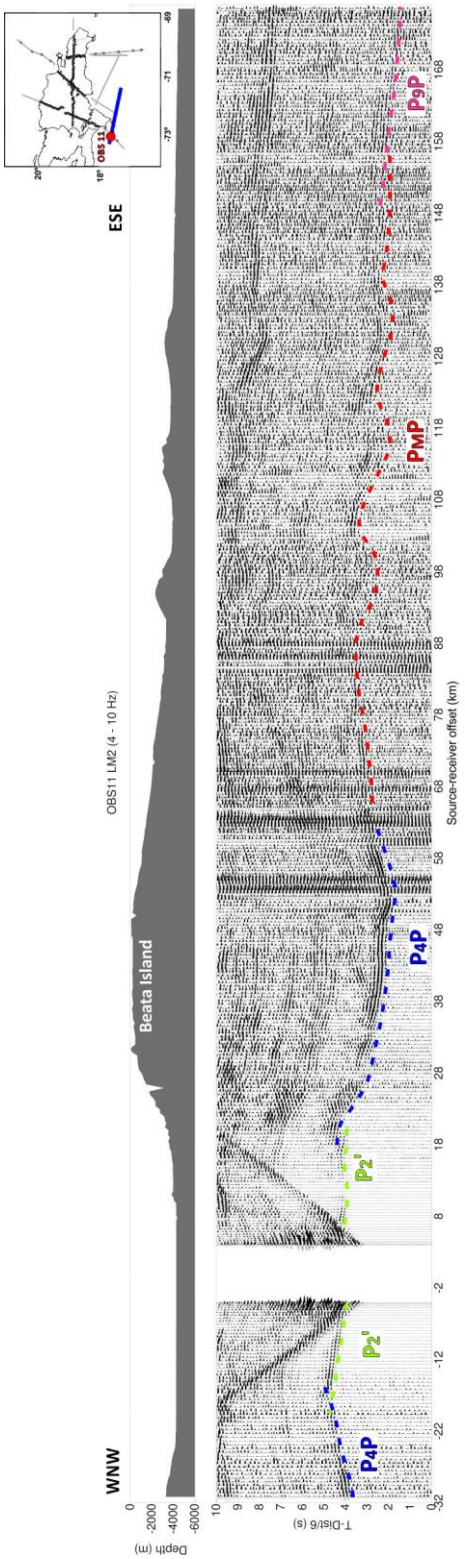

Fig. 3.4.1.1 OBS 11 seismic record section registering seismic line LM2. Colored lines point out reflected/refracted P-wave trains. In this figure vertical component and bathymetry along this line are shown. In the upper right corner, red circle shows location of registration point and marine shooting line in blue. Reduction velocity is 6 km/s, band-pass filtering of 4 – 10 Hz and amplitudes-trace normalized

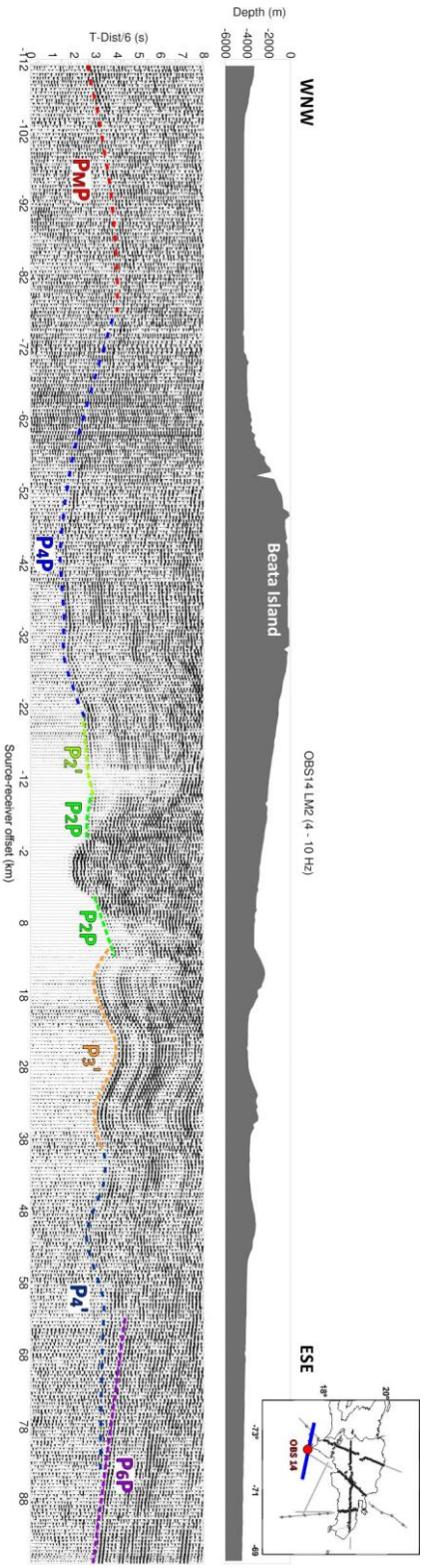

Fig. 3.4.1.2. OBS 14 seismic record section registering seismic line LM2. Colored lines point out reflected/refracted P-wave trains. In this figure vertical component and bathymetry along this line are shown. In the upper right corner, red circle shows location of registration point and marine shooting line in blue. Reduction velocity is 6 km/s, band-pass filtering of 4 – 10 Hz and amplitudes-trace normalized.

On the east side, also it is possible to observe this phase from 18 to 53 km offset showing correspondence with the bathymetry in the area. Following, phase observed is P_MP phase that can be correlated from 66 km to 156 km across Beata Ridge. Behind this phase, P_9P is observed from 148 km to the end of the seismic record section with an a.a.v of 8.5 km/s.

Eastern to Beata Island, OBS 14 is found at 112 km distance from the beginning of seismic line LM2 and 2.8 km below sea level. This OBS is located in the marine shooting line, so, it is not necessary add any additional error term. The P-wave phases identified on the western side of this seismic record section (Fig. 3.4.1.2) correspond to P_2P, P_2', P_4P and P_MP. The first one is a reflected phase on the discontinuity between layer 2 and 3 and can be followed from 3 to 10 km offset range with an a.a.v of 4.9 km/s. The head wave that travels through this discontinuity (P_2') is correlated between 10 and 22 km offset and 7.6 km/s of a.a.v. The phase interpreted in surrounding area of Beata Island is P_4P and observed from 20 to 75 km followed by P_MP correlated up to the end of the seismic record section (112 km offset).

The eastern side of OBS 14 seismic record section registers the phases through the three seamounts that characterize this area. Between 5 and 15 km, it is correlated P_2P phase with an a.a.v of 3.9 km/s, followed by P_3' and P_4' from 10 to 40 and 40 to 85 km offset ranges, respectively. Last phase identifies in this seismic record section is the reflected phase in the sixtieth layer P_6P, between 60 km to 97 km showing an a.a.v of 8.5 km/s.

Figure 3.4.1.3 shows the seismic record section corresponding to OBS 16. This OBS is the last station located in the profile at 185 km and 4.17 km below sea level. This station is 3.5 km out of the seismic line and an error term is added to the uncertainty for upper layers. In the study to estimate this error, it has been obtained that the separation between the station and the line affects more to the first three layers and phases closest to the station.

The analysis of this seismic record section has provided the following P-wave phases. In this case, the eastern part is shorter than previous and two phases have been interpreted, P_2P and P_3'. The first one is followed from 5 km to 12 km and the second one from 12 to 24 km offset. The average apparent velocities obtained for this phase is 3.7 km/s. On the other side, P_2' is found from 5 to 17 km distance with 7.3 km/s of a.a.v indicating a certain dip due to the presence of third seamount of Beata Ridge. After this phase, P_4P is correlated between 17 km to 35 km and then, P_MP phase from 35 km to 65 km offset ranges. The diving wave that travels through Moho discontinuity, P_n, is followed from 65 km to 148 km source-receiver offset in the area of Beata Island. In this profile, P_6P is interpreted from 148 to 185 km offset range in the area of Haiti Basin.

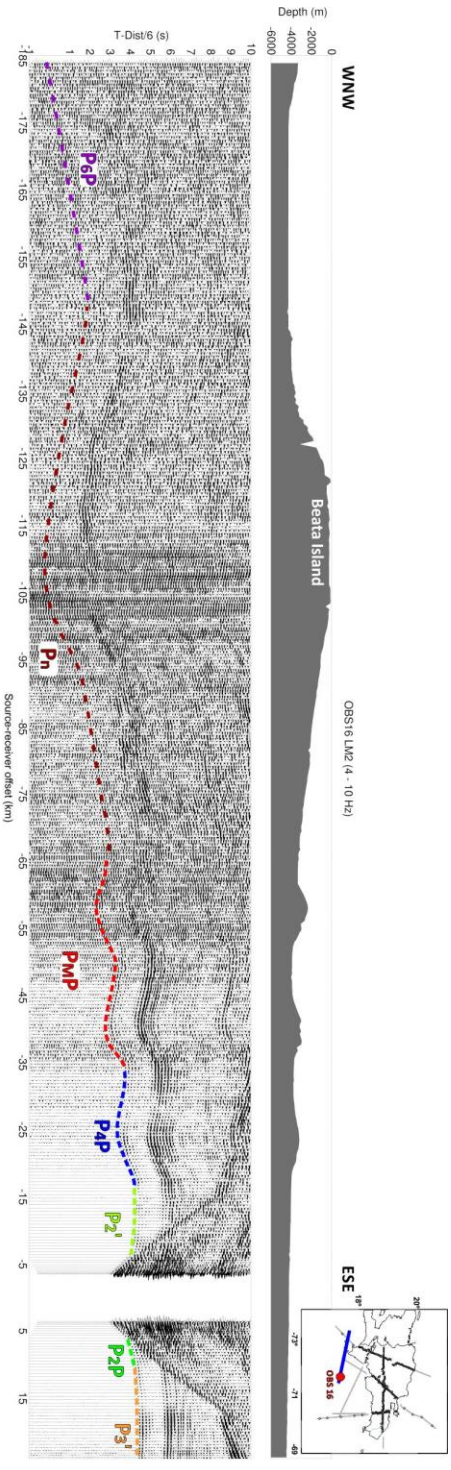

Fig. 3.4.1.3 OBS 16 seismic record section registering seismic line LM2. Colored lines point out reflected/refracted P-wave trains. In this figure vertical component and bathymetry along this line are shown. In the upper right corner, red circle shows location of registration point and marine shooting line in blue. Reduction velocity is 6 km/s, band-pass filtering of 4 – 10 Hz and amplitudes-trace normalized.

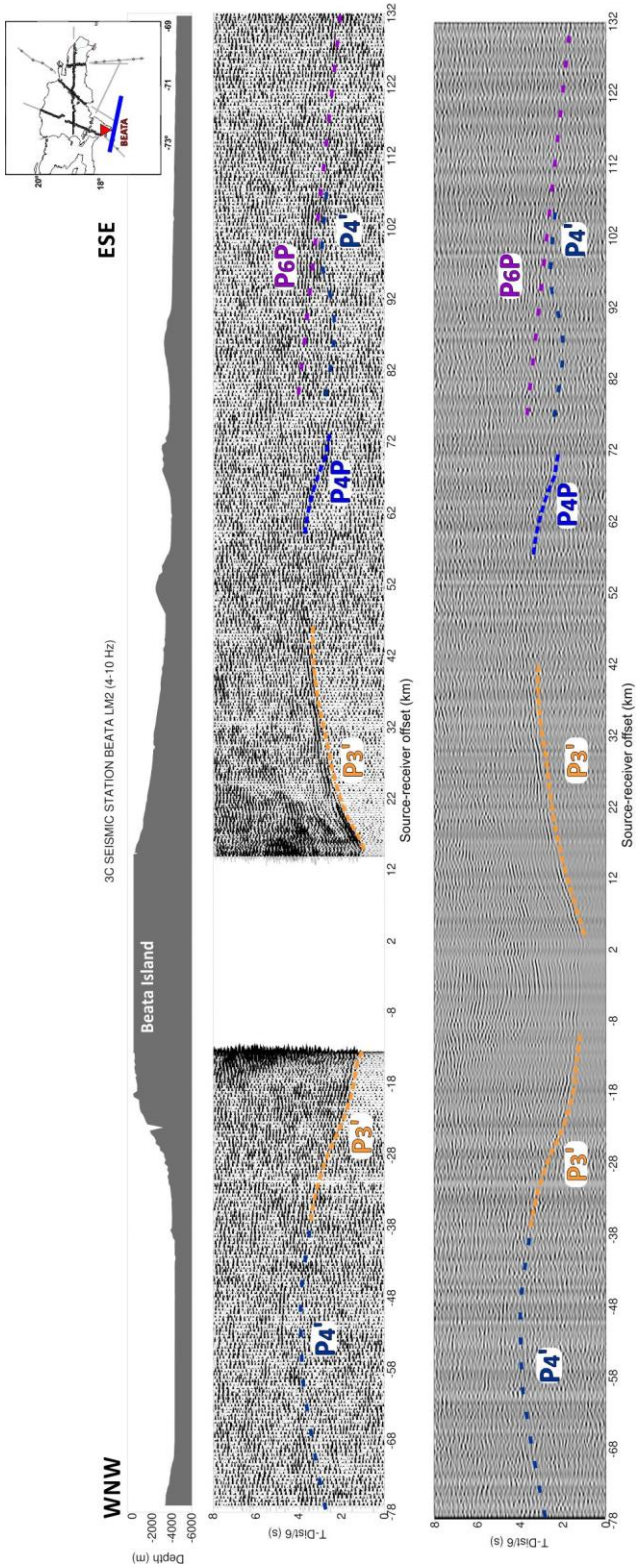

Fig. 3.4.1.4. Seismic record section corresponding to BEATA station registering seismic line LM2. Colored lines point out reflected/refracted P-wave trains. In this figure vertical component and bathymetry along this line are shown. In the upper right corner, red triangle shows location of registration point. Reduction velocity is 6 km/s, band-pass filtering of 4 – 10 Hz and amplitudes-trace normalized.

Moreover, it is possible to observe in OBS 16 seismic record section that the amplitudes of multiple waves are higher than the other seismic record sections of this profile.

The portable seismic station BEATA is located in Beata Island, 6 km south from Beata Cape (DR). This station is 13.5 km separated from the seismic line, then, the estimated error is much higher than the others station reaching values larger than 1 second for the first layers.

In the seismic record section corresponding to BEATA seismic station, high absorption in the seismic signal in the western and eastern flanks has been observed. Towards Haiti Basin, it is found P_3' from 14 km to 38 km offset (Fig. 3.4.1.4) followed by the head wave that travels through fourth layer discontinuity, P_4', between 38 to 78 km. The eastern part shows the correlation of P_3', P_4P, P_4' and P_6P. The first one has been interpreted from 14 to 48 km whose shape is in correspondence with the bathymetry while the second one is followed from 60 to 73 km source-receiver offset. The last P-wave phases interpreted are less precise due to existing noise. These phases are P_4', from 78 km to 108 km, and P_6P between 78 to 132 km offset range, and an average apparent velocity of 9.2 km/s.

3.4.2 Modeling

Data processing allowed obtaining seismic record sections whose interpretation has provided the travel times and distances necessary to elaborate the northern Beata velocity model (Fig. 3.4.2.1) [Núñez et al., 2010]. This interpretation consisted of determining the P-wave phases observed in each seismic record and their corresponding apparent velocities. Subsequently, ray tracing models and synthetic seismograms have been made to finally obtain the velocity model corresponding to this profile. The seismic wide-angle data have been interpreted using forward modeling techniques [Zelt and Smith, 1992], and we have divided in shallow and middle-deep crustal structures in order to analyze as in detail as possible both structures. Water-depth/elevation from the airgun-shots/land stations was taken from the navigation data provided by R/V Hespérides.

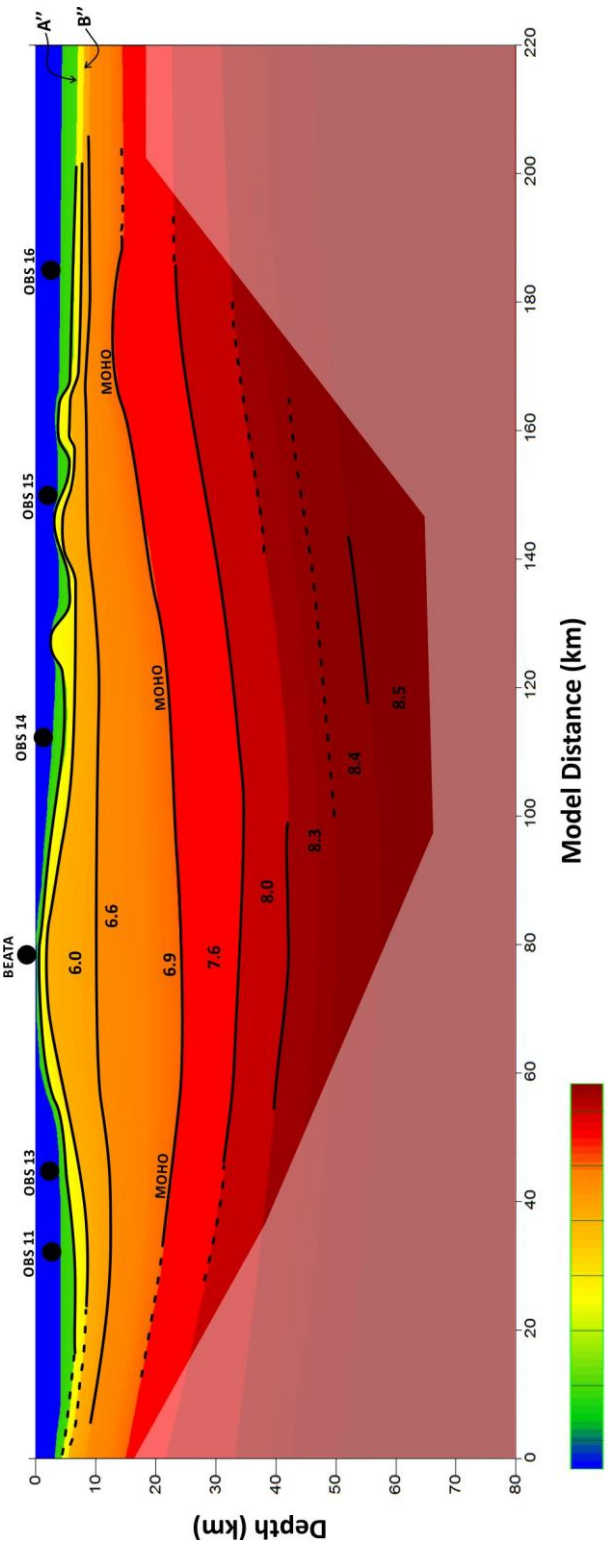

Fig. 3.4.2.1. P-Wave velocity model of CARIBE NORTE seismic profile across northern flank of Beata Ridge. Shadow zone denotes the areas not illuminated by ray beams. Black circles show the stations used in this study. The black lines show where reflected or diving waves phases are. Dash black line denotes where ray beams Figure is scaled according depth and distance. Color scale denotes P-wave velocity in km/s.

Shallow crustal structure

In the western part of Beata Island (Haiti Basin), the sedimentary cover has two layers, whose depth has been defined from OBS 11 (Fig. 3.4.1.1) and OBS 13 data. Thickness of first sedimentary layer is 2.3 km decreasing towards Beata Island to 1.2 km with an uncertainty less than 1 km. In this layer the P-wave velocity is 3.3 ± 0.1 km/s. The layer immediately below it reaches 4.6 km depth with velocity gradient of 4.5-4.8 ± 0.1 km/s. This layer, like previous, raises up nearby the island (Fig. 3.4.2.2). The uncertainty in depth is less than 1 km for shallow part of the model.

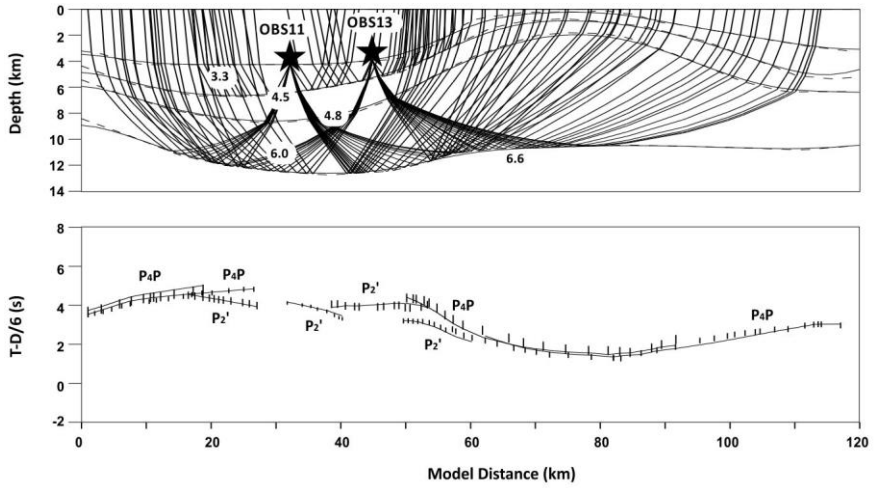

Fig. 3.4.2.2 *Top*: Ray tracing corresponding to shallow structure in Haiti Basin and Beata Island with OBS 11 and OBS 13 marine stations and velocity model with velocities in km/s. *Bottom*: Comparison between calculated (lines) and observed (vertical bars) travel times whose height is the uncertainty estimated for every phase. Distances refer to the origin of the velocity model. Stars represent the location of the stations in the model.

East of Beata Island, the area is characterized by the influence of Beata Ridge shown as three seamounts in the model. The structure cannot be associated with geodynamic blocks in the eastern Hispaniola proposed by Cotilla et al., (2007). The shallow structure (Fig. 3.4.2.3) is determined by wide-angle seismic data of OBS 14, OBS 15 and OBS 16. At model distance of 90-120 km, the sedimentary cover thickens reaching a maximum value of 2.2 km for the first layer and 2.1 km for the second one. These layers are strongly influenced by the bathymetry of the area. The first layer disappears near the top of seamounts and the vicinity of the island. The second layer is practically constant in thickness up to reaching 6.4 km below westernmost seamount. Between the western and middle seamounts, the first sedimentary layer is 2.0 km thick and the second one is 1.2 km thick. The thicknesses between middle and eastern seamounts are 1.8 km and 1.5 km, respectively, remaining practically constant in the area of Venezuela Basin.

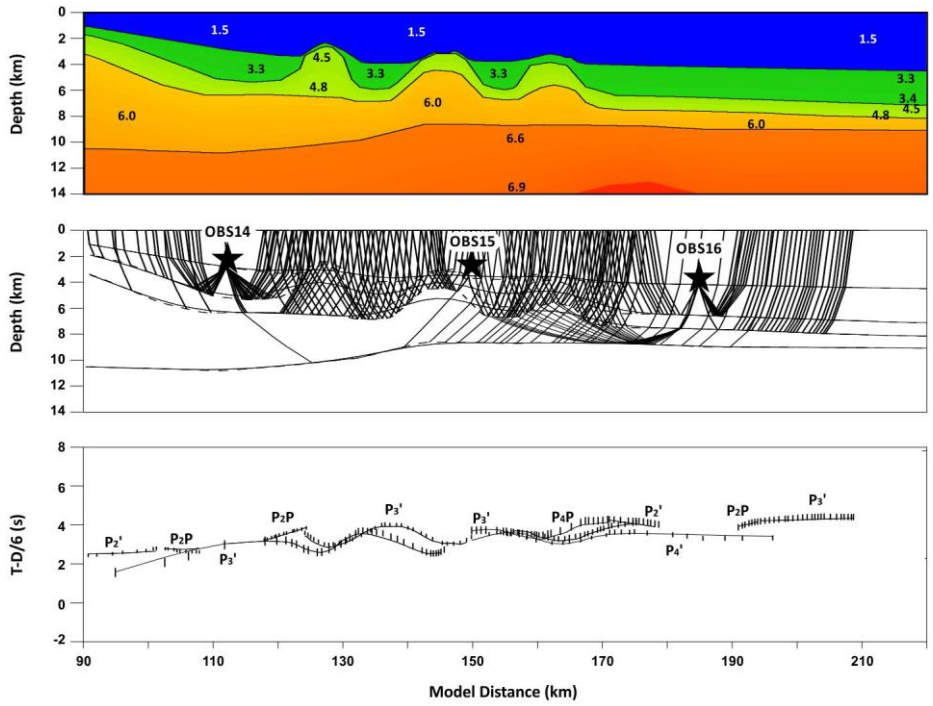

Fig. 3.4.2.3 *Top*: P-wave velocity model with velocities in km/s in the area of Beata Ridge. Middle: Ray tracing corresponding to shallow structure in Beata Ridge with OBS 14, OBS 15 and OBS 16 marked. *Bottom*: Comparison between calculated (lines) and observed (vertical bars) travel times whose height is the uncertainty estimated for every phase. Distances refer to the origin of the velocity model. Stars represent the location of the stations in the model.

Comparing the structure determined by this paper with a previous MCS study [Mauffret and Leroy, 1999], it is possible to establish a correlation between first sedimentary layer and Horizon A'' while second sedimentary layer corresponds to Horizon B''. Mauffret and Leroy (1999) define Horizon A'' and B'' as reflectors that form the base of Middle to Early Miocene chalks and Santonian to Conician basalts intervals, respectively. Both reflectors characterize the seismic stratigraphy of Venezuela Basin. These correlations allow us determining the composition of the sedimentary cover. As we mentioned previously, first layer of this study corresponds to Middle Eocene to Early Miocene chalks while the second one is Santonian to Coniacian basalts. In this way, the thinning of the A'' – B'' layer (Fig. 3.4.2.1), old sedimentary fill, in the study area, suggests that these features are contemporaneous related to volcanic plateau formation [Mauffret and Leroy, 1999]. The estimation of depth uncertainty provides values of less than 1 km.

Middle and deep crustal structure

The middle crust is 4 km thick west of Beata Island and decreases in depth but not in thickness between 30 and 100 km distance where it reaches a maximum thickness of 9 km with a V_P value of 5.9-6.1 ± 0.1 km/s. Below the island, thickness of the middle crust remains practically constant at 9-10 km up to Venezuela Basin area.

Moho depth is 20 ± 2 km deep in the west and increases to 24 ± 2 km below the island. The P wave velocity is 6.9 ± 0.1 km/s in lower crust and 7.6 ± 0.2 km/s below Moho (Fig. 3.4.2.4). In this part of the model, some phases determine two deeper layers with V_P of 8.0 km/s and 8.3 km/s with uncertainty of 0.2 km/s, respectively, reaching a maximum depth of 42 ± 3 km. Below Beata Island (Fig. 3.4.2.5), Moho depth reaches 24 ± 2 km and P wave velocity contrast at Moho boundary is 6.9 to 7.6 km/s ($\Delta v = 0.2\ km/s$).

Figure 3.4.2.6 shows ray tracing diagram, observed and computed travel times and uncertainty for BEATA land station. The uncertainty stems mainly from handpicking error of the onsets [Núñez, et al., 2011] and offset between seismometer position and seismic profile due to that station is 13.5 km away from the seismic line. Uncertainty for the other stations has been defined similarly.

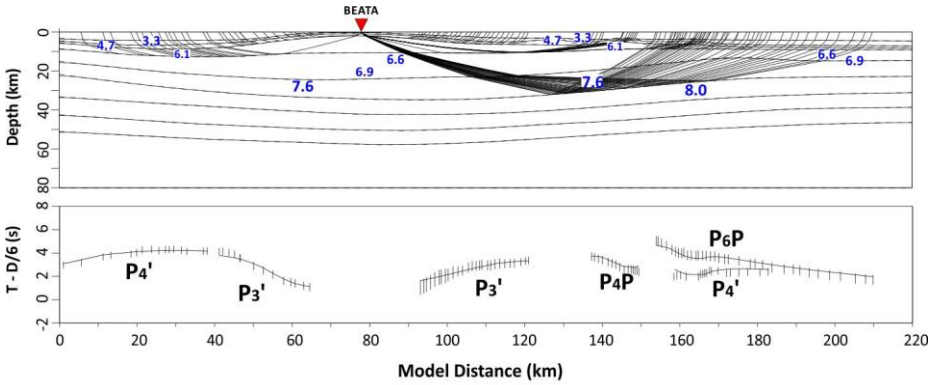

Fig. 3.4.2.6 *Top*: Ray tracing corresponding to BEATA land station and velocity model with velocities in km/s. *Bottom*: Comparison between calculated (lines) and observed (vertical bars) travel times whose height is the uncertainty estimated for every phase. Distances refer to the origin of the velocity model. Red triangle represents the location of the station in the model.

In the eastern Beata Island region (Fig. 3.4.2.7), it is possible to find Moho discontinuity at 24 km depth rising up to 13 km depth at model distance of 170 km (Fig. 3.4.2.1). Next layer is located at 34 ± 2 km depth and rises, following Moho discontinuity, up to 23 km with a V_P contrast of 7.6 ± 0.2 and 8.0 ± 0.2 km/s determined by several rays reflecting in this layer (Fig. 3.4.2.4). The study of relative amplitudes reveals observed and theoretical data are comparable being within

uncertainty interval (Figs. 3.4.2.5 and 3.4.2.7). The deepest layer interpreted from wide-angle seismic data of this line is found from 125 to 150 km with a depth between 50 and 55 ± 3 km. Below this layer, P-wave velocity is 8.5 ± 0.2 km/s.

East of Beata Island, it is possible to observe variation of seismic energy, especially in Beata Island seismic record section (Fig. 3.4.2.5) that could be associated to more complicated structure. OBS seismic record sections located west of the island do not show similar variation of energy. OBS located in east of the island show less energy. This effect is more pronounced in easternmost seamount. According Mauffret and Leroy (1999), two of these seamounts have conical symmetry and another one is asymmetrical. Checking this phenomenon, from a qualitative point of view, we have plotted azimuthal seismic record sections from Profile A (station A1 western Beata Ridge) and Profile B (station B1 eastern Beata Ridge). Figure 3.4.2.8 shows that in A1 seismic record section is not observed any loss of seismic energy while B1 section does. This fact, also, could be due to the interaction between Beata Ridge and Muertos Trough and its effect into the eastern area of southern Hispaniola Island.

Estimates of arrival-time fit quality for each phase and for all phases are given in Table 3.4.I. Our final model produces a normalized χ^2 of 0.7 with individual phase under-fit ($\chi^2 < 1$ for all phases).

Phase	NC	SIGMA (s)	NR	Trms (s)	χ^2
P_2P/P_2'	95	0.138	89	0.104	0.678
P_3'	158	0.221	156	0.147	0.510
P_4P/P_4'	201	0.203	195	0.230	0.871
P_MP	130	0.184	124	0.167	0.810
P_n	25	0.210	25	0.102	0.245
P_6P	114	0.244	113	0.180	0.669
P_7P	10	0.170	10	0.079	0.243
P_9P	13	0.195	13	0.165	0.750
FIT	756	0.198	725	0.176	0.690

Table 3.4.I Travel-time fit for each phase: NC = number of picks; SIGMA = mean pick uncertainty; NR = number of traced rays; Trms = travel time root mean square misfit; χ^2 = normalized chi square.

3.5 DISCUSSION AND CONCLUSIONS

The analysis of wide-angle seismic data for LM2 profile obtained in CARIBE NORTE project (2009) reveals new features about the northern part of Beata Ridge, which collides with the central part of the Hispaniola. In this section, a summary of the velocity model is presented and compared with all other studies carried out in the study area.

The proposed model presents tectonic differences between west and east zones separated by the Beata Island. In the western area, Haiti sub-basin, two sedimentary layers are found. The top of this layer presents V_P of 3.3 ± 0.1 km/s and the second

one shows a velocity range of 4.5 – 4.8 ± 0.1 km/s, characterizing the sequence continuous highly-reflective reflectors that correspond with ponded sediments present in Haiti sub-basin [Granja Bruña, et al., 2014]. The maximum total thickness is 4.4 km, observed below OBS 11. These layers practically disappear in the vicinity of Beata Island, which could indicate the presence of a compressive deformed belt. Eastern Beata Island, shallow structure shows an alternation of seamounts and basins. These hills are uplift as result of transpressional tectonics, which would be active, and bounded by strike-slip structures [Mauffret and Leroy, 1999]. Crossing this structure, they remain constant at 8 km depth due to this seismic profile crosses the northern Venezuela Basin, which is characterized by two reflection horizons, A'' and B'' (Fig. 3.1.1). Next layer is located at 10 km depth with a P-wave velocity of 6.0 ± 0.1 km/s and thickness of this layer beneath Beata Island is 6 km. The depth uncertainty calculations for shallow part of the model reveal values less than 1 km.

Our velocity model is in agreement with previous wide-angle seismic studies of this area that provided information in the south of this area. Fox et al., (1970) collated some previous studies in Beata Ridge area. Some of them used refraction data and they estimated the sedimentary cover to be 2 km thick with P-wave velocities in the range 1.9-4.2 km/s characterized by two prominent horizons. Moreover, the upper crustal layer over Beata Ridge is 3-5 km thick with a compressional wave velocity of 5.4-5.9 km/s and the lower crustal layer has a velocity of 6.7 km/s and a thickness of 7-10 km. The values obtained in this paper are close to those, even though this study crosses area north of areas of those studies. The values of the crust beneath northern Beata Ridge provided by CARIBE NORTE seismic profile LM2 are not as deep as expected in western and eastern flanks but crustal thickness is thickened beneath Beata Island. The differences in the eastern part model could be due to the existence of contemporary set of active faults.

Moho discontinuity is found to be deeper under Beata Island with a maximum value of 24 ± 2 km confirming that the crust of Caribbean Plateau is unusually thick. Moho depth rises up to 13 km in the area of seamount located further east and then is constant at 15 km in Venezuela Basin area. These values are according to Diebold et al., (1999) or Leroy (1995) that establishing the crustal thickening under Beata Ridge is at least 20 km, while in Venezuela and Colombia basins are 10-15 km and 5 km, respectively. Apparently, previous studies do not show thickness and P-wave velocity values for layers under Moho. In this work, deeper layers follow the topography of Moho have been established, obtaining increasing V_P in depth up to 8.5 ± 0.2 km/s.

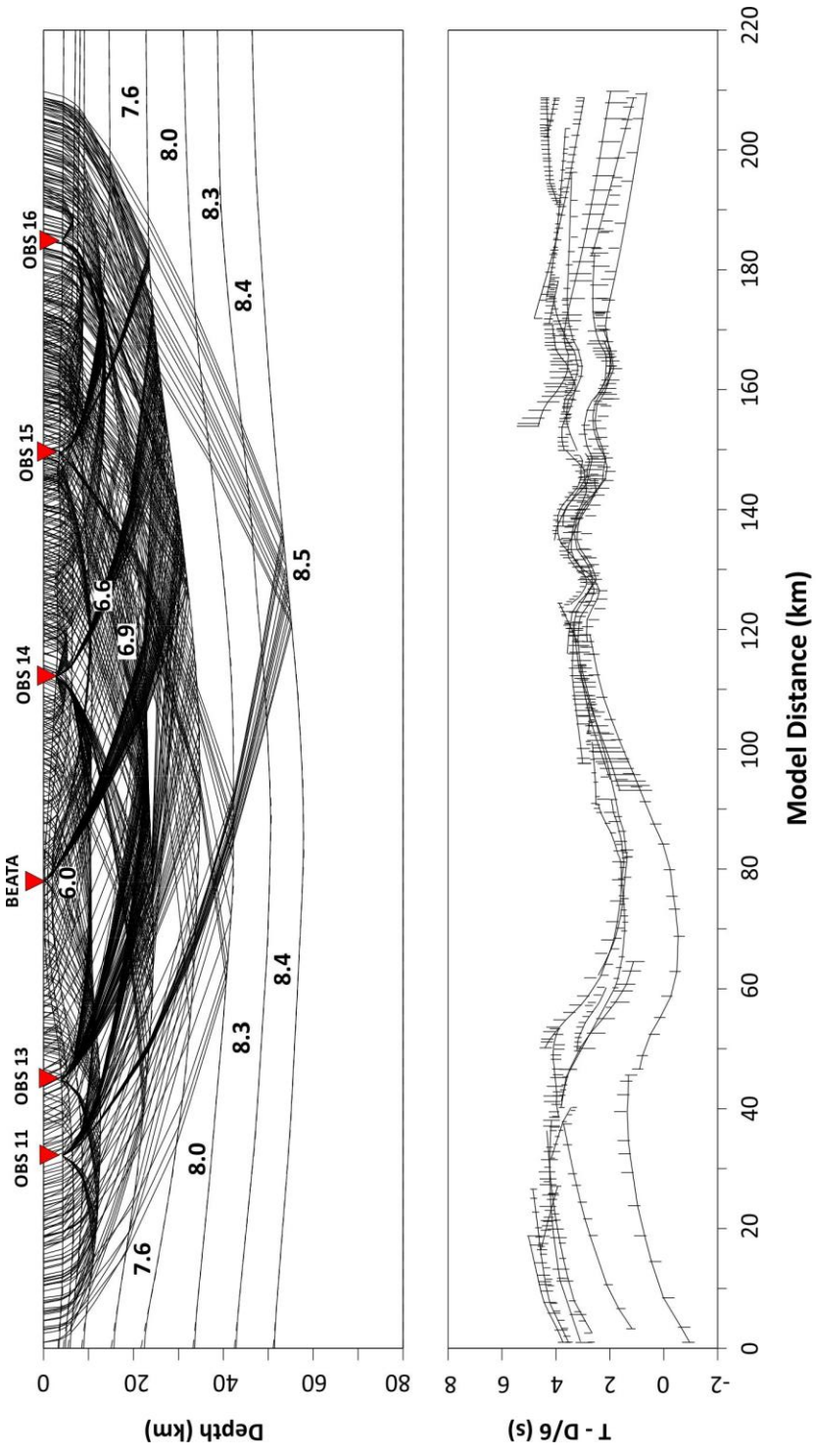

Fig. 3.4.2.4 *Top*: Ray tracing corresponding to Profile E and velocity model with velocities in km/s. *Bottom*: Comparison between calculated (lines) and observed (vertical bars) travel times whose height is the uncertainty estimated for every phase represented in different colours. Distances refer to the origin of the velocity model. Red triangles represent the location of every station in the model.

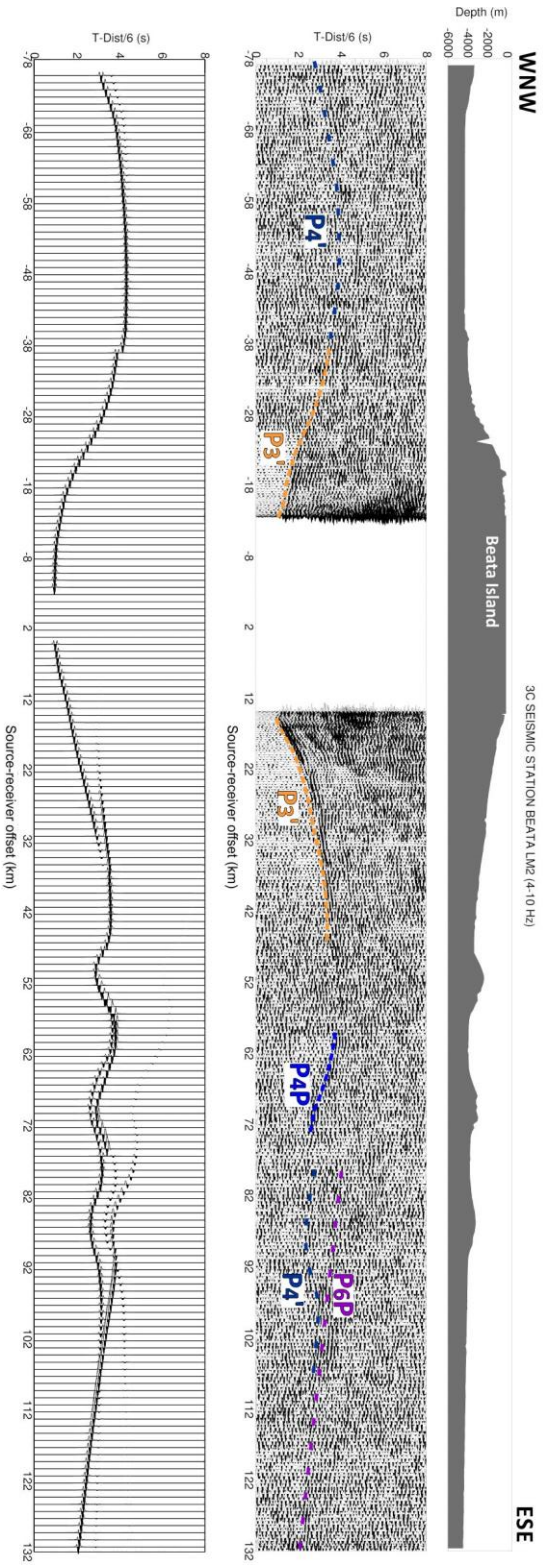

Fig. 3.4.2.5 *Top*: Seismic record section with bathymetric profile and correlated phases. Vertical component and Amplitude-trace normalized. *Bottom*: Synthetic seismogram corresponding to land station BEATA recording marine line LM2. Amplitude-trace normalized.

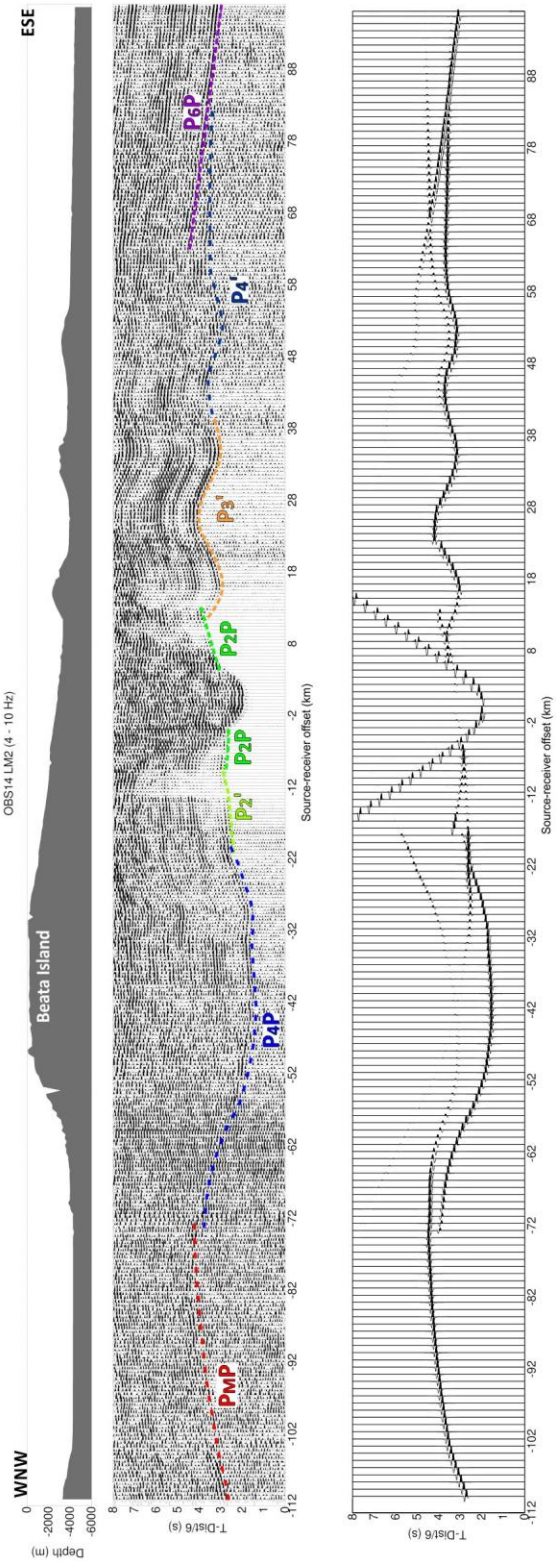

Fig. 3.4.2.7 *Top*: Seismic record section with bathymetric profile and correlated phases. Vertical component and Amplitude-trace normalized. *Bottom*: Synthetic seismogram corresponding to OBS 14 recording marine line LM2. Amplitude-trace normalized.

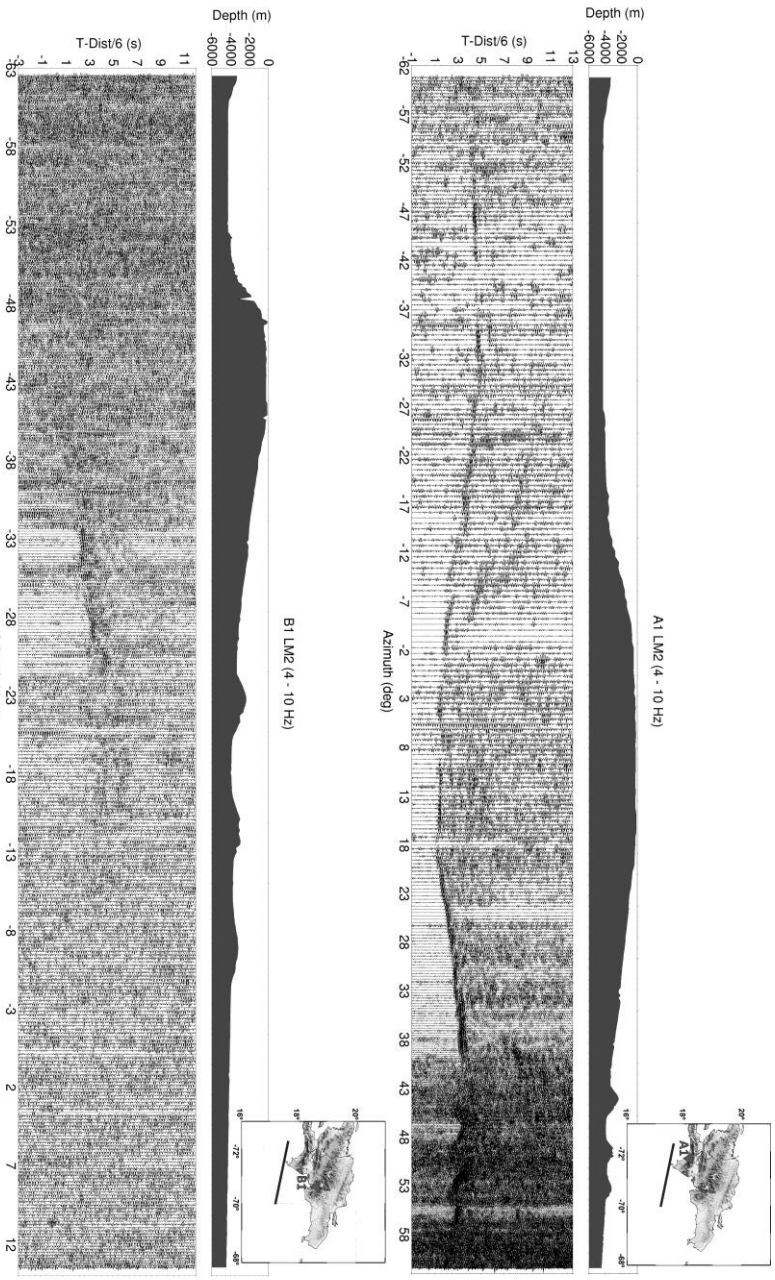

Fig. 3.4.2.8 *Top*: Azimuthal seismic record section of A1 station registering seismic line LM2; *Bottom*: Azimuthal seismic record section of B1 station registering seismic line LM2. In this figure vertical component and bathymetry along this line are shown. In the upper right corner, triangle shows location of registration point and marine shooting line in thick line. Reduction velocity is 6 km/s, band-pass filtering of 4 – 10 Hz and amplitudes-trace normalized

The extension of the Beata Ridge structure towards NE direction is identifies as a first-order limit between mountain and plain morphostructures present in Hispaniola Island [Cotilla et al., 2007]. This morphotectonic alignment is transversely articulated with EPGFZ and SFZ active faults.

Conclusions

The complexity of northern Beata Ridge has provided new constrains about the shallowest part but, also, under Moho discontinuity. Comparisons between previous studies and this work allow obtaining a better knowledge about this domain:

- Sedimentary cover has been determined from wide-angle seismic data being a thicker sequence of layers in the Haiti Basin area, disappearing in Beata Island and reappearing between seamounts of Beata Ridge, where active faults bounded these structures. In Venezuela Basin area, it is practically flat. These seismic layers can be correlated with Horizons A'' and B'', characteristic reflectors of Venezuela Basin related to Middle to Early Miocene chalks and Santonian to Conician basalts intervals, respectively.
- The topography of Mohorovicic discontinuity has been characterized for the first time in this area. It has a pronounced thickening under Beata Island and thinning in Beata Ridge region. Previous MCS data had not been able to establish these depths.
- This study has allowed obtaining the first two seismic layers of Upper Mantle, whose maximum depth 50-55 ± 3 km and P-wave velocities increasing up to 8.5 ± 0.2 km.
- The analysis of CARIBE NORTE seismic record sections reveals a decreasing in the seismic energy of Beata Ridge region. Azimuthal seismic record sections of two land seismic stations located on the both sides of Beata Island corroborate that this loss of seismic energy appears just to the east. The explanation could be the interaction between Beata Ridge, Muertos Trough and eastern Hispaniola.
- Comparisons with previous refraction and MCS studies establish a correspondence with shallow crustal structure results but not for the deep structure in the northern flank of Beata Ridge.

CHAPTER 4

SEISMIC IMAGES OF THE CRUST IN WESTERN DOMINICAN REPUBLIC FROM WIDE ANGLE DATA (CARIBE NORTE & GEOPRICO-DO PROJECTS)

*A synthesis of the most relevant results is in preparation to be submitted to **GRL***

4.1 INTRODUCTION

The North America-Caribbean plate boundary zone consists of a 100-250 km wide seismogenic zone of mainly left-lateral strike-slip deformation extending over 2000 km along the northern edge of the Caribbean Sea [Mann et al, 1995]. Puerto Rico Trench and Virgin Islands are well studied but the tectonic processes in the area of Hispaniola Island are not well defined (Fig. 4.1.1).

Different studies have tried to answer how the border region between North American Plate (NAP) and Caribbean Plate (CP) is, from a tectonically point of view. Some of them suggest that the northern Caribbean plate boundary is a transcurrent fault system, not a subduction zone, from Cuba to western Hispaniola using shallow seismicity data [Calais et al, 1992]. This proposal would explain the intermediate and deep seismicity of the zone through the existence of a lithospheric slab disconnected from the Atlantic oceanic lithosphere by transcurrent faulting along plate boundary. Other studies suppose a dual subduction where the Atlantic oceanic slab dips southward and from 100 km the slab has a strong vertical component due to the presence of the Caribbean slab which dips northward 15^{o} [Dolan et al., 1991]. The knowledge of crustal thicknesses and subMoho velocities will provide the systematic differences in crustal structure between N and S parts of the Hispaniola Island, resolving the tectonic behavior in the western part of NAP-CP interaction zone.

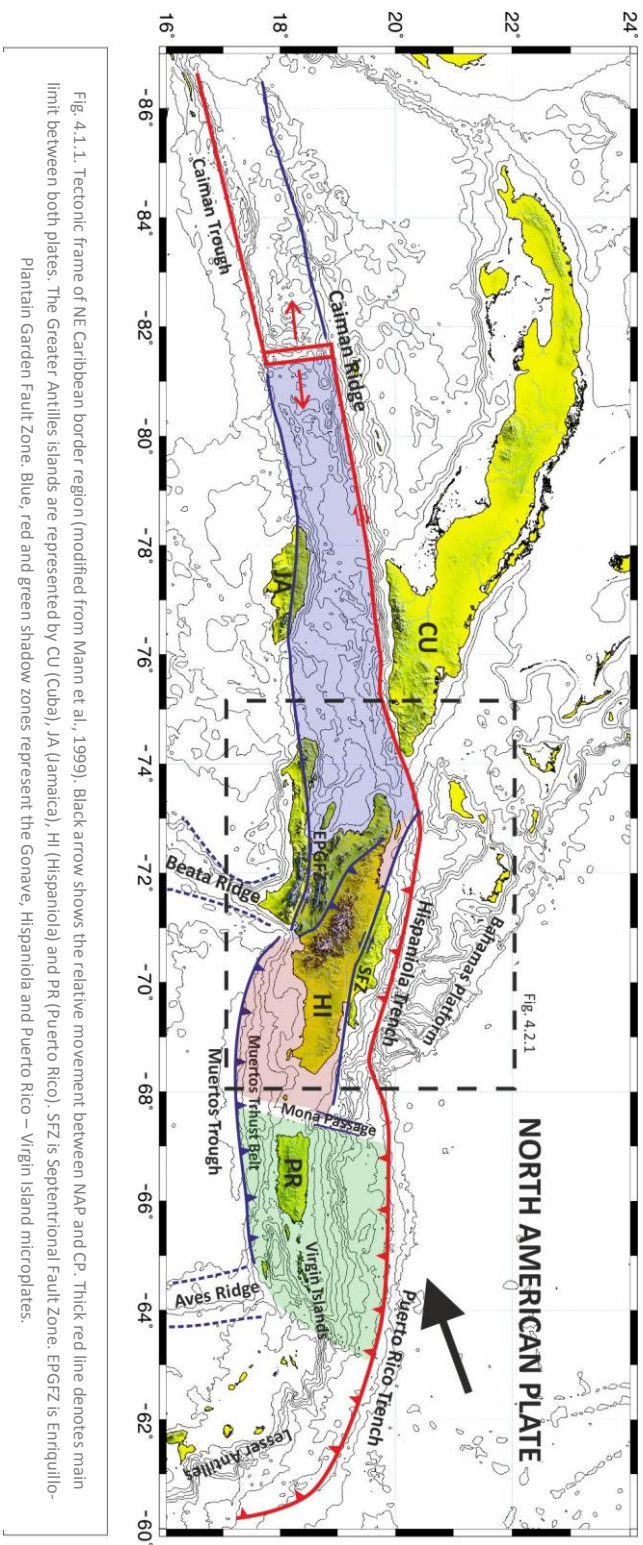

Fig. 4.1.1. Tectonic frame of NE Caribbean border region (modified from Mann et al., 1999). Black arrow shows the relative movement between NAP and CP. Thick red line denotes main limit between both plates. The Greater Antilles islands are represented by CU (Cuba), JA (Jamaica), HI (Hispaniola) and PR (Puerto Rico). SFZ is Septentrional Fault Zone. EPGFZ is Enriquillo-Plantain Garden Fault Zone. Blue, red and green shadow zones represent the Gonave, Hispaniola and Puerto Rico – Virgin Island microplates.

Despite the numerous studies conducted in NE Caribbean Plate, there is not agreement in the geodynamical models that govern the structure and tectonic development of the area due to the absence of deep geophysical research. For solving this anomalous distribution, two multidisplinary investigations had been carried out in recent years, GEOPRICO-DO and CARIBE NORTE projects (2005 and 2009, respectively, *See Chapter 1, Section 1.4*). In this chapter, the results of deep seismic investigations from Bahamas Banks crossing western Dominican Republic are presented.

4.2 GEOLOGY AND TECTONIC SETTING

Within the northeastern Caribbean plate boundary zone, three microplates (Gonave microplate [Mann et al., 1995], Puerto Rico – Virgin Islands block [Jansma et al., 2000] and Hispaniola microplate [Byrne et al, 1985]) are located (Fig. 4.1.1). The area of Hispaniola and Puerto Rico Islands (Fig. 4.1.1) is limited by subduction zone with oblique convergence in the north and incipient subduction zone associated to Muertos Trough in the south. The Caribbean plate is moving to east-northeast direction with rate of 18-20 mm/yr., relative to North American plate, and azimuth of 70^{o}, from GPS measurements [Mann et al., 2002]. This direction implies maximum oblique convergence between the Caribbean and North American plates centered on Hispaniola Island. The collision of Caribbean Plate with Bahamas Platform began in Cuba in the Middle Eocene and ended in Puerto Rico in Lower Oligocene (Fig. 4.1.1). Between these islands, in the Hispaniola segment, the collision happened in the period Middle-Upper Eocene. In the south, deformation is accommodated along the left-lateral Enriquillo-Plantain Garden Fault and north-dipping thrust faults of the Los Muertos deformed belt. The left-lateral Septentrional strike-slip fault and the south-dipping thrust faults of the North Hispaniola deformed belt accommodate deformation in the north (Fig. 4.2.1).

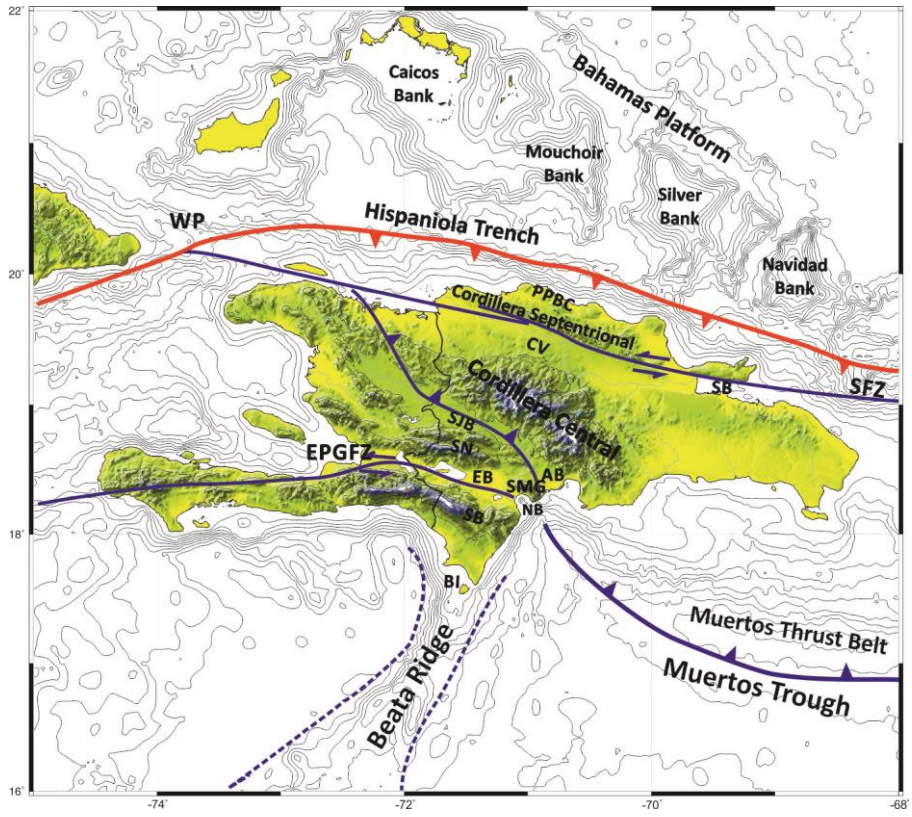

Fig. 4.2.1. Schematic tectonic frame of Hispaniola Island with main tectonic and geologic features in studied area. PPBC = Puerto Plata Basement Complex; CV = Cibao Valley; SJB = San Juan Basin; SN = Sierra de Neiba; EB = Enriquillo Basin; SMG = Sierra de Martín García; AB = Azúa Basin; BN = Bahía de Neiba; BI = Beata Island; SB = Sierra de Bahoruco; SFZ = Septentrional Fault Zone and EPGFZ = Enriquillo-Plantain Garden Fault Zone; SB = Samaná Bay; WP = Windward Passage.

- Regional Setting

The Hispaniola Island is formed by island-arc and oceanic plateau terrains alternating valleys and mountain ranges defined by active reverse, left-lateral strike-slip or oblique-slip faults (Fig. 4.2.1). In the northern part, Bahamas Banks (Bahamas Platform) are located offshore the island. Onshore, Cordillera Septentrional is separated from Cibao Valley by the Septentrional fault followed by Cordillera Central. San Juan Basin is found between Sierra de Neiba and Cordillera Central. Continuing to the south, left-lateral Enriquillo Plantain Garden Fault Zone is sitting as major element of Enriquillo Basin followed by Sierra de Bahoruco and Sierra de Martín García. Offshore southern Dominican Republic coast, the northern Beata Ridge is located.

Bahamas Banks

The southeast Bahamas have been colliding with the island of Hispaniola along a restraining bend within the northern Caribbean plate boundary zone [Mann et al., 1984] since late Miocene [Sykes et al., 1982]. High seismicity along the northeast margin of Hispaniola (*see Chapter 1, section 1.2*) evidences this collision continues offshore where Silver Bank and Navidad Bank (Fig. 4.2.1) indent the northern margin of Hispaniola [Bracey and Vogt, 1970]. This oblique collision accommodates about half of the Caribbean-North America relative motion on a relatively shallow dipping thrust fault at the interface between the two plates [Mann et al., 2002].

Mouchoir Bank (Fig. 4.2.1) is a relatively small, irregular carbonate platform built on top of a regional deep-water plateau, at a depth of about 1 km, which in turn rises from a depth of about 4 km. South of Mouchoir Bank, and separating it from the northern insular slope of Hispaniola, is the flat-floored Hispaniola basin filled with up to 3 km of mixed terrigeneous-cabonate turbidites. Oblique convergence of Mouchoir Bank along the Bahamas-Hispaniola collision zone has generated an active fold and thrust belt along the acretionary prism north of Hispaniola [Mullins et al, 1992]. The southern margin of Mouchoir Bank (Fig. 4.2.1) has also been drowned during the Late Tertiary prior to the mid-Pliocene and is attributed to tectonic tilting and subsidence resulting from oblique underthrusting of the southeast Bahamas beneath Hispaniola.

Onshore western DR

The Puerto Plata Basement Complex (PPBC) (Fig. 4.2.1) consists of highly faulted and dismembered blocks formed by discontinuous but sometimes coherent outcrops of serpentinized or massive peridotite, massive or banded gabbroid cumulates. The PPBC has been identified as an ophiolitic fragment accreted from the North-America subducting slab, based on these rock associations and the relationship with nearby mélange-type formations [Hernaiz-Huerta et al., 2011]. The contact between PPBC and Cordillera Septentrional is resolved by subvertical normal faults.

Running parallel to the northern coast of Dominican Republic, a mountain range named the Cordillera Septentrional is found (Fig. 4.2.1). This cordillera is 15 to 40 km wide oriented WNW-ESE, transversal to NE-SW PPBC orientation. Neogene to present transpressive deformation is partitioned into several main strike-slip faults or fault zones (Septentrional, Camú, Río Grande, among others) and coeval related folding [Hernáiz-Huerta et al., 2011]. In the north of Camú (PPBC) and Septentrional faults (Río San Juan basement complex) (Fig. 4.2.2), several basement complexes are made up metamorphic rocks with plutonic and volcanic rocks. Other complexes consist of igneous, volcanic and plutonic rocks, deriving from volcano-sedimentary island arc magmatic processes.

The Septentrional fault (Fig. 4.2.1) extends onshore for 320 km across northern Hispaniola through the Cibao Valley [Mann et al., 1998] continuing westward across the Windward Passage and the southern coast of Cuba [Calais et al., 1992]. To the east, this fault extends offshore and bifurcates into two major strands north of the Mona Passage [Dolan et al., 1998]. This left-lateral strike-slip fault is responsible for the uplift of the Cordillera Septentrional and for faulting in Cibao Valley area. In the central Cibao Valley, this fault experienced at least 4.6 m of oblique normal and left-lateral displacement during a large earthquake 800 years ago [Prentice et al., 2003]. The mainly onshore strike-slip faults of the SFZ accommodate the purely strike-slip component of deformation while offshore faults accommodate the convergent part of the transpressional NAP-CP. Both zones are active, subparallel and separated by less than 100 km [Mann et al, 1998]. Marine geophysical surveys indicate that Septentrional fault zone extends eastward as far as the Mona rift with earthquake evidence for strike-slip motion [McCann and Sykes, 1984; Calais et al., 1992].

The Cibao Valley extends north of the Hispaniola with NW-SE direction and bounds with Atlantic Ocean in the west and Samana Bay in the east (Fig. 4.2.1). This valley is 230 km long and approximately 30 km width flanked on the south by a moderate slope to the Cordillera Central and bordered on the north by marked relief of the Cordillera Septentrional [Erikson et al., 1998]. The Cibao valley is an asymmetric basin, thickening northward, bound on the north by the SFZ. In the central part, it is 5000 m thick [Mann et al., 1990].

In N and NE directions stands the Cordillera Central (Fig. 4.2.1). In the south-central segment, two domains are found: the Tireo Fm and Peralta Belt. Tireo Fm. (light green color in Fig. 4.2.2) consists of volcanoclastic rocks belonging to Circum-Caribbean Island-Arc. The Rois Rivieres-Peralta terrain in Dominican Republic is called the Peralta Belt (white and yellow color in Fig. 4.2.2). This belt is a sequence of sedimentary rocks with NW-SE direction running along southern flank of the Cordillera Central. The contact between these units is a thrust of the basement over the Peralta Belt modified by faults like San José-Restauración [Mann et al., 1991].

Between the Cordillera Central and Sierra de Neiba is located the San Juan Basin (Fig. 4.2.1) filled by more than 7000 m of sediments. The northern boundary with the Cordillera Central is the main thrust front of the Peralta Belt (series of highly-deformed acretionary sedimentary rocks fringing the SW margin of the island-arc core [Dolan et al., 1991]). The southern border with Sierra de Neiba is a high angle imbricate fault. In the extreme southeast, San Juan Basin connects with the Enriquillo, and changes name to Azúa Basin (Fig. 4.2.1). Azúa Basin is less than 3000 m depth of sediments with a structure more complex than San Juan Basin due to change in the basin geometry produced by Beata Ridge and, possibly, Enriquillo Fault.

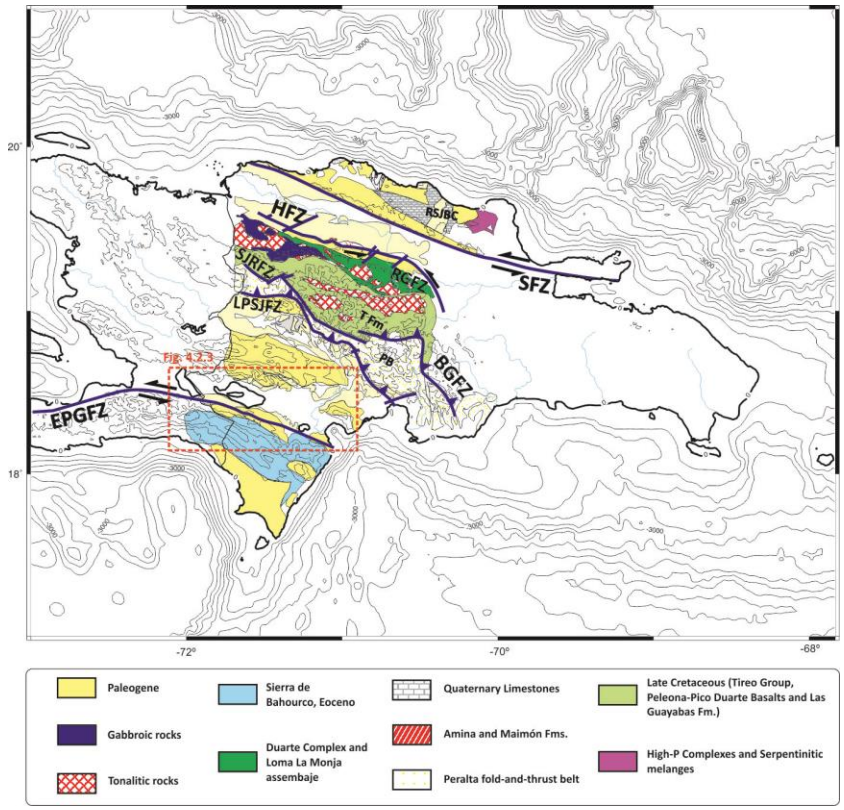

Fig. 4.2.2 Schematic geological map of the studied area in Central Hispaniola (based on Escuder-Viruete et al., 2011). RGFZ = Río Grande Fault Zone; HFZ = Hispaniola Fault Zone; BGFZ = Bonao-La Guácara Fault Zone; SJRFZ = San José-Restauración Fault Zone; LPSJFZ = Los Pozos-San Juan Fault Zone; SFZ = Septentrional Fault Zone; EPGFZ = Enriquillo-Plantain Garden Fault Zone; RSJBC = Río San Juan Basement Complex; PB = Peralta Belt; TFm = Tireo Formation. Red rectangle shows the location of figure 4.2.3.

Sierra de Neiba (Fig. 4.2.1) is defined as part of Pesqu'ile du Nord-Ouest-Neiba terrain and Enriquillo basin. This sierra is formed by calcareous lithologies with folds and relatively discontinuous directions in WNW-ESE to WN-SE [Caribe Norte project scientific report]. This implies an unknowledge of the basement in this sierra. The contact zone between Sierra de Neiba and Enriquillo basin is a sequence of folds with high angles associated to tears.

The Enriquillo basin (Fig. 4.2.1) is a thick basin (5 km) [Mann et al., 1999] that forms an elongate valley bounded by active strike-slip and reverse faults. This basin is rounded for Sierra de Neiba in the north, Sierra de Bahoruco in the south and Sierra de Martín García in the east. Enriquillo Basin is the eastward continuation of the Cul-de-Sac region of Haiti and together form a valley extending from Bahia de Neiba,

Dominican Republic, to Port-au-Prince, in Haiti. In Dominican Republic, the northern side of the trough shows that shortening is accommodated by reverse faults of Peralta Fold and Thrust Belt and Sierra de Neiba (Fig. 4.2.2). While, in the southern side, Beata Ridge is sliced off by curved faults with important vertical offset [Pubellier et al., 2000]. Due to the structure of this basin and the surrounding geological features, it is possible distinguish different blocks: Enriquillo Lake, Angostura, Mella, Vicente Noble and Bahía de Neiba blocks [Mann et al., 1999] (Fig. 4.2.3). This valley was uplifted and modified by erosion with some depressions remain below the sea level like Lake Enriquillo. This lake is 42 m below sea level and is gradually being lowered by evaporation. A sill about 4 m above sea level separates this lake from the Caribbean Sea at Bahía de Neiba [Mann et al., 1999].

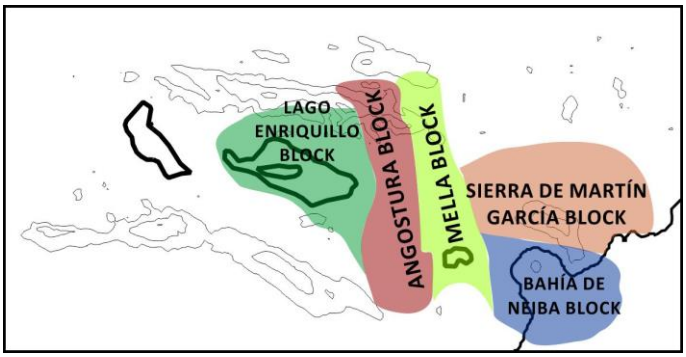

Fig. 4.2.3. Schematic map where is shown different blocks in Enriquillo basin and surrounding geological features (Based on Mann et al., 1999.

The Enriquillo Plantain Garden Fault Zone (EPGFZ) (Fig. 4.2.1, 4.2.2) is a major structural feature traversing the Enriquillo Basin and partly interfering with the northern basin edge faulting. Mann et al. (1995) propose EPGFZ formed in late Neogene time as response to oblique subduction of the Bahamas Platform due to the thicker-than-average crust subduction of the Bahamas Platform resisted the eastward motion of the central and northern parts of Hispaniola. Recently studies indicates EPGFZ extends from south-central Hispaniola to Jamaica and defines the southern edge of the Gonave microplate forming a continuous and prominent lineament from Enriquillo Valley (DR), through the southern peninsula of Haiti, across the Jamaica Passage and along the Plantain Garden fault zone bounding the southern edge of the Blue Mountains of eastern Jamaica [Mann et al., 2008]. Some evidences shows that the motion is left-lateral as the linearity of the fault and its association with folds, pull-apart basins and bends.

Sierra de Bahoruco (*light blue color in Fig. 4.2.2*) is part of Hotte-Selle-Bahoruco terrain [Mann et al., 1991] extended from southern sector of Dominican Republic with WNW-WAW direction. Different studies indicate this terrain is an emerged

fragment of Caribbean oceanic plateau [Maurrase et al. 1979, Sen et al., 1998, Girard et al. 1982] with important discordancy in basaltic volcanism and sedimentary regimen. The contact between Sierra de Bahoruco and Enriquillo basin is a system of strike-slip faults with NW-SE to WNW-ESE direction with high angle thrust faulting to N.

The Sierra de Martín García is a large fault-bounded anticlinal range which partially separates the Azúa and Enriquillo Basins (Fig. 4.2.1) [Mann et al., 1991]. In the northern flank of Sierra Martín García appears an outcrop area as main depocenter of the siliciclastic wedges as thicknesses drop off to the west in the Enriquillo Valley and to the east in the Azúa basin [Mann et al., 1999].

4.3 SEISMIC DATA

4.3.1 Introduction

Different studies have been carried out in CP region ([Ewing et al, 1960], [Officer et al., 1957]; Talwani et al, 1977; among others) but few of them have integrated the wealth of onshore and offshore data to establish an internally consistent model for the development of the Caribbean [Driscoll and Diebold, 1998]. The GEOPRICO-DO and CARIBE NORTE projects (*See Chapter 1, Section 1.4*) (Fig. 4.3.1) encompass multi-disciplinary data collected onshore and offshore of Dominican Republic. During the cruises were recovered multibeam bathymetry, gravity, magnetic, high-resolution seismic, seismic reflection and wide-angle seismic data. The seismic refraction experiment in GEOPRICO-DO project had a set of 30 seismic portable stations (Profiles F, G and H) were deployed in different positions in Dominican Republic to recover three seismic lines (marine shooting lines L6, L7 and L8). During this project, any OBS were installed in the study area. The seismic refraction experiment in CARIBE NORTE project had a set of 340 land seismic portable stations deployed in four land profiles of which three are N-S (Profile A, B and C) and one E-W (profile D), and 16 OBS. All stations recorded 5 marine shooting lines and 3 land shots of 1000 Kg explosives.

4.3.2 Profiles A and F Data

In this chapter, wide-angle seismic data registered by land and marine equipment deployed along two profiles A and F have been analyzed (Fig. 4.3.1).

Profile A is located from Bahamas Bank (N) to Beata Ridge (S) crossing western area of Dominican Republic. The seismic sources used in this profile correspond to two marine shooting lines in the north and south extremes (LM1N and LM1S) and one

land shot (S3). The Profile A was recorded by 97 land portable stations deployed from Pedernales (S) to Puerto Plata (N) and three OBS situated in the Caribbean Sea.

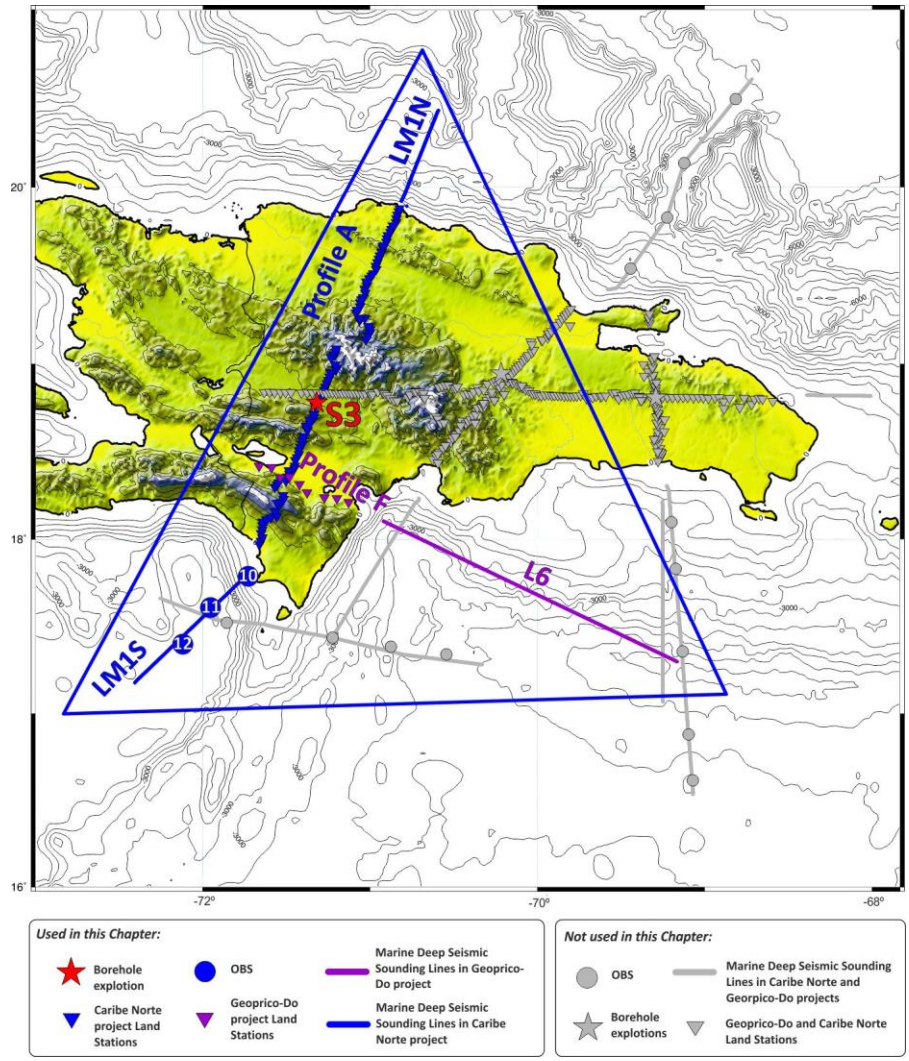

Fig. 4.3.1 Deployment map with stations and seismic sources used in this chapter and all stations deployed during Caribe Norte and Geoprico-Do projects (grey symbols). Blue triangle represents the study area.

Eight seismic portable stations where deployed along Profile F which extends from Bahía de Neiba to Azúa and Enriquillo Basins crossing western area of Muertos Trough recording L6 marine shooting line.

Both profiles register the seismic signals generated by the airguns installed in R/V Hespérides. The airguns were arranged in two strings with total capacity of 3850 ci

and shot every 90 s. Table 4.3.I summarizes the main features of marine lines showing total time length, shots and miles used in this study.

	Total time length	# Shots	Distance (km)
LM1N	6h 39m 18s	269	44.7
LM1S	10h 34m 30s	423	95.3
L6	23h 04m 12s	924	191.2
TOTAL	40h 17m 0s	1616	331.2

Table 4.3.I. Dominican Republic seismic profiles summary in GEOPRICO-DO and CARIBE NORTE projects used in this chapter.

The seismic energy, generated by airguns aboard R/V Hespérides, has been observed on the OBS seismic record sections to distances between 0-100 km (LM1S) and up to 200-300 km on the land stations records. Processing included navigation data, band-pass filtering and time corrections due to instrument drift.

4.4 INTERPRETATION

After data processing, seismic record sections have been obtained whose interpretation has provided the necessary information to elaborate Profile A and Profile F velocity models. This interpretation consisted of determining the P-wave phases observed in each seismic record and their corresponding apparent velocities. Subsequently, ray tracing models and synthetic seismograms have been made to finally obtain the velocity models corresponding to the Profiles A and F.

4.4.1 Seismic record sections and Correlation Data

In the seismic record sections obtained for these profiles, it was possible to identify time correlations corresponding to P-wave refractions and reflections in the crustal and upper mantle discontinuities. Each phase is assigned a color and a code with subscripts, which represent the layer relative position respects to the subsurface (*see Table 2.5.I, Section 2.5, Chapter 2*).

Profile A

Profile A (Fig. 4.3.1) comprises 425 km from south Bahamas Bank to north Beata Ridge. The northern and southern parts of the profile, characterized by significant tectonic features described in the Geology and Tectonic Setting (*Section 4.2*) of this chapter, record the marine shots lines LM1N and LM1S and one land shot. This chapter presents the different types of seismic record sections defined in figure 2.4.1.10.

After interpretation, the most representative seismic record sections have been selected, according to tectonic features crossed by this profile.

In Figure 4.4.1.1, it is possible to observe the seismic record section corresponding to the A98 land station situated at 100 km from the beginning of the seismic line LM1N, in PPBC (Fig. 4.2.1). This seismic record section represents the main features found in PPBC. Between 11 to 28 km epicenter distance, it is observed P_2', head wave travelling through the discontinuity between layer number 2 and 3, with an average apparent velocity (a.a.v) of 2.8 km/s. Second phase interpreted is P_3P, reflected phase in third layer, observed between 28 and 43 km. P_MP is followed from 35 km to 72 km marked in the Fig. 4.4.1.1 as red line.

The seismic records of Septentrional Fault do not show changes in the velocity or discontinuities in phase correlations that indicate the presence of this fault. The stations installed from Septentrional Fault to the coast show an increase in the noise level ratio that could indicate its presence. The figure below (Fig. 4.4.1.2) shows the phases arrival up to 98 km distance. This area corresponds to the arrival of Mouchoir Bank (Fig. 4.2.1). From this offset, increased noise level is observed. This evidence is shown in Fig. 4.4.1.1 from 35 km. Stations located south to A80 do not show this feature.

When Cibao Valley is reached (Fig. 4.2.1), the seismic record sections reveal information about deep structure of the area, with P-wave arrivals deeper than P_MP. A73 station section shows these phases (Fig. 4.4.1.3). From 96 to 126 km offset range, P_MP is observed and also phases reflected in layers 7 and 8 with an approximation in apparent velocities of 7.8 km/s, 15.8 km/s and 25.3 km/s, respectively. These high velocities could suggest a dip to the N.

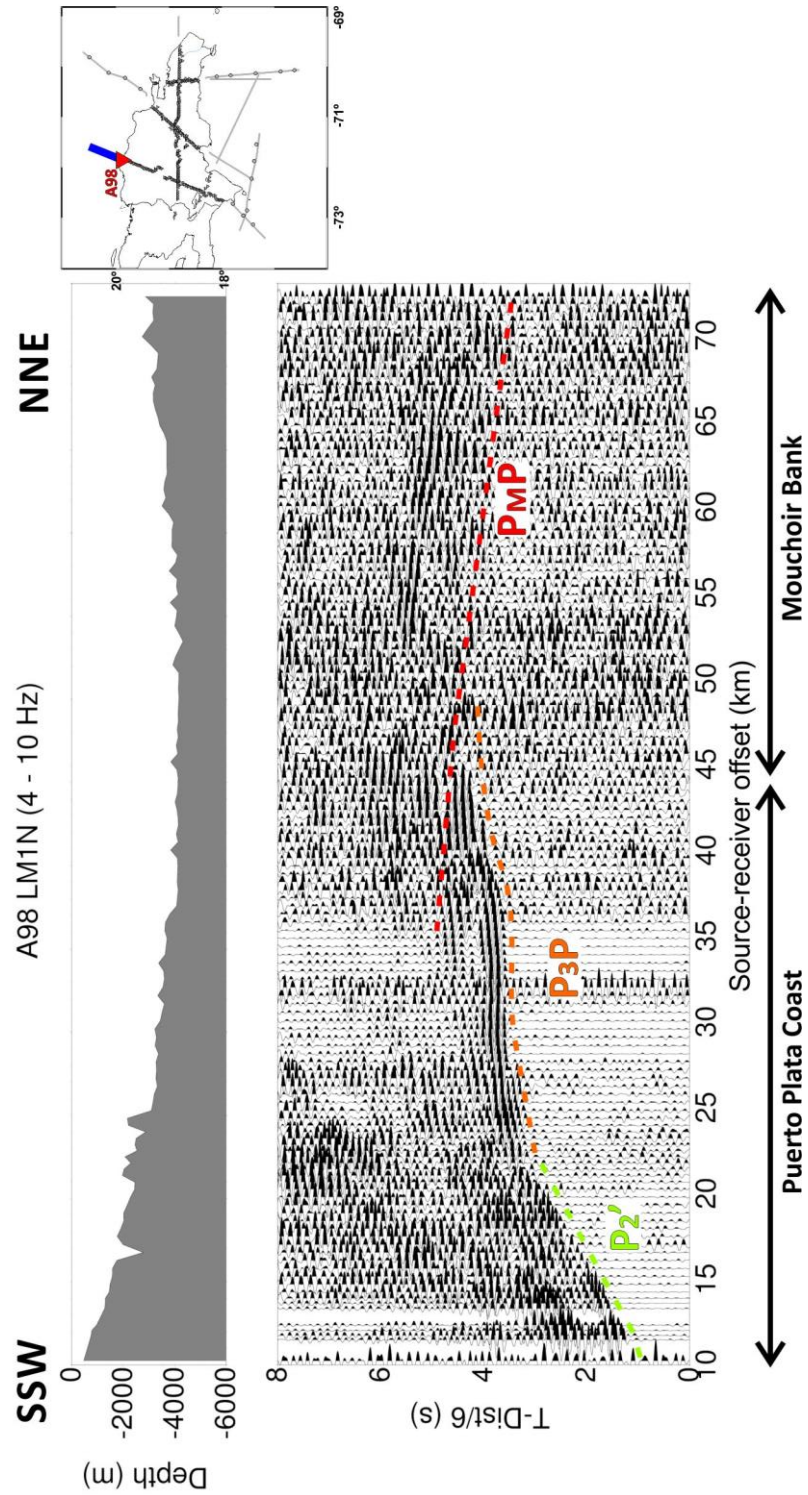

Fig. 4.4.1.1. Seismic record section corresponding to A98 station registering seismic line LM1N. Colored lines point out reflected/refracted P-wave trains. In this figure vertical component and bathymetry along this lines over this section are shown. In the upper right corner, red triangle shows location of registration point and blue line the marine seismic line. Reduction velocity is 6 km/s, band-pass filtering of 4 – 10 Hz and amplitudes-trace normalized.

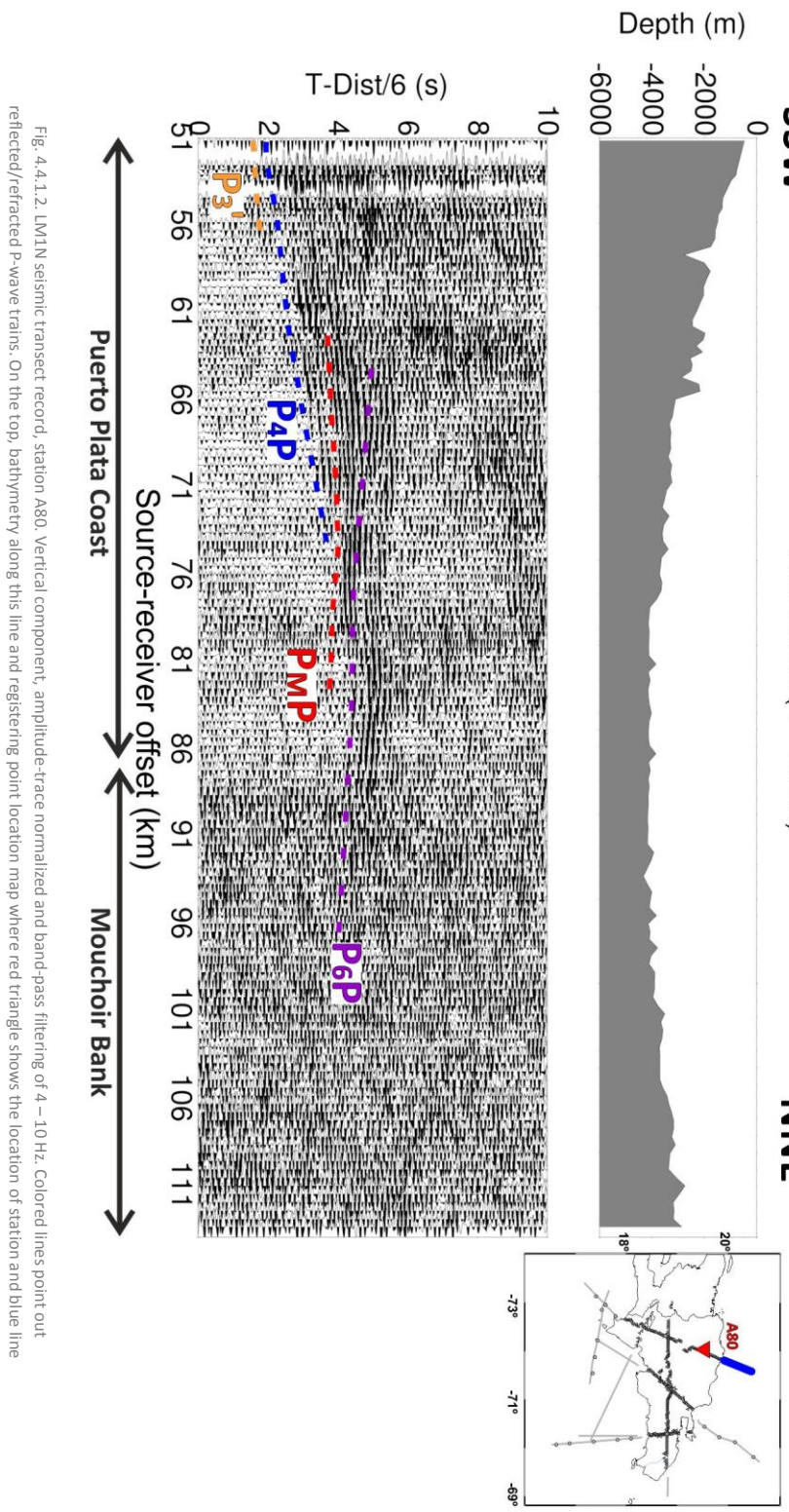

Fig. 4.4.1.2. LM1N seismic transect record, station A80. Vertical component, amplitude-trace normalized and band-pass filtering of 4 – 10 Hz. Colored lines point out reflected/refracted P-wave trains. On the top, bathymetry along this line and registering point location map where red triangle shows the location of station and blue line the shooting line.

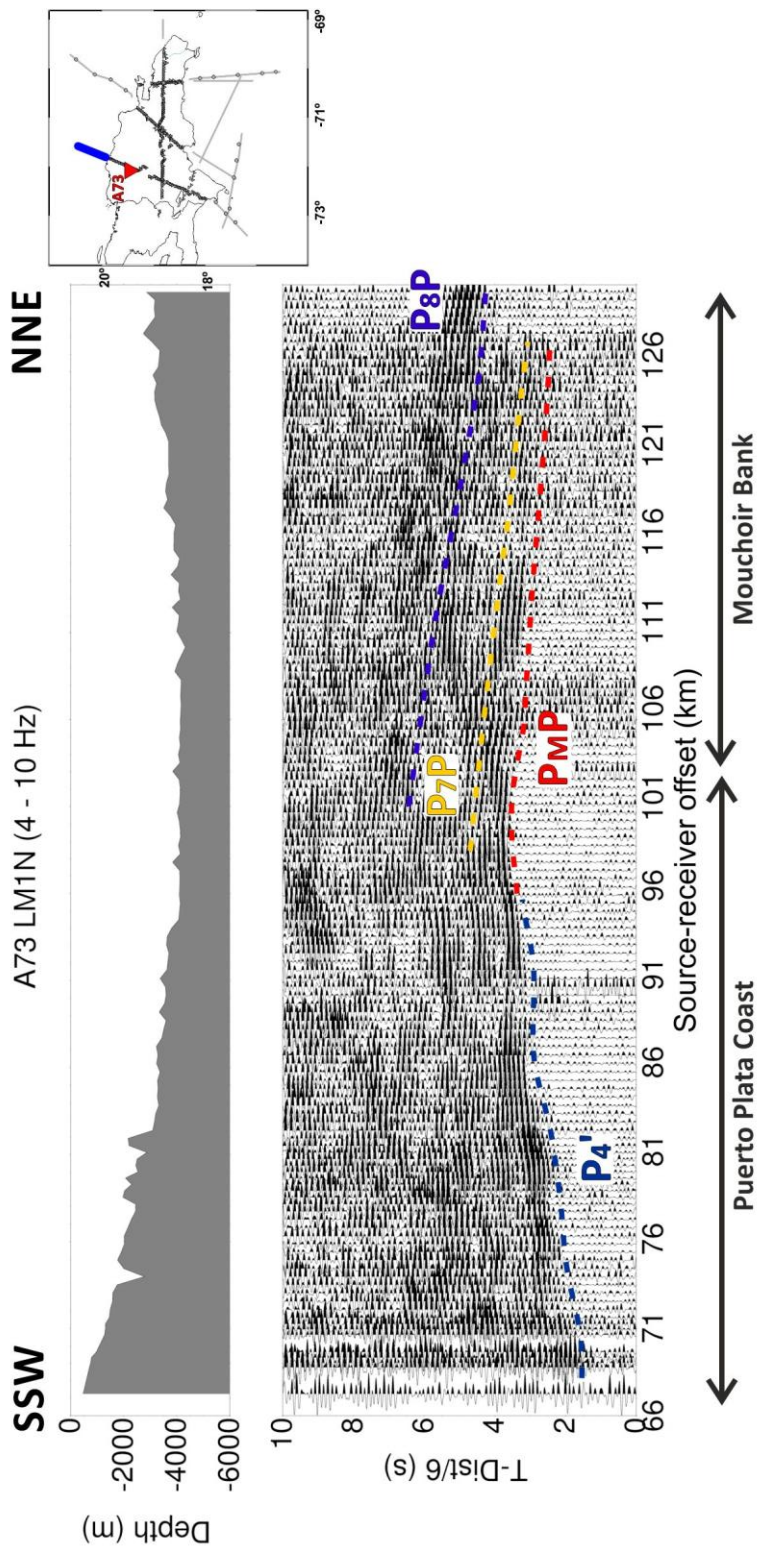

Fig. 4.4.1.3. Seismic record section corresponding to A73 station registering seismic line LM1N. Colored lines point out reflected/refracted P-wave trains. In this figure vertical component and bathymetry along this lines over this section are shown. In the upper right corner, red triangle shows location of registration point and blue line the marine seismic line. Reduction velocity is 6 km/s, band-pass filtering of 4 – 10 Hz and amplitudes-trace normalized.

Figures 4.4.1.4 and 4.4.1.5 show seismic record sections corresponding to station A58 that records marine lines LM1N and LM1S, respectively. This station is located at 192 km from the beginning of the LM1N line, in Cordillera Central area. In the first figure, it is possible to observe a head wave travelling through discontinuity between layer 4 and 5 followed by P_MP from 113 km to 165 km offset.

Figure 4.4.1.5 provides more information about deep structure to the south. This figure shows P_MP phase from 146 to 180 km distance with less amplitude than the deepest phase indicating a strong velocity contrast and the absence of any other phase between them. From 180 km, P_6P and P_7P are found. These phases have small amplitudes but P_7P amplitude is higher than the previous, pointing out velocity contrast between layers 7 and 8 is less than between Moho and layer number 8.

Seismic stations from A29 to A20 are located in EPGFZ and Enriquillo Basin areas. All seismic record sections show very high level of noise and in very few of them it is possible to identify some phases due to the structure features and presence of sediments in this area that indicate the seismic signal is very attenuated. An example is the A25 seismic record section (Fig. 4.4.1.6). Phases identified are P_6P and P_7P that can be followed from 100 to 130 km and 103 to 172 km source-receiver offset.

The southern offshore part of this work (Caribbean Sea) has been monitoring by three OBS (Fig. 4.3.1). Those marine stations provide information about crustal and Upper Mantle structure of this area. OBS 10 is located close to the coast (2.0 km out of the line), followed by OBS 11 (situated over the marine line) and OBS 12 (Fig. 4.4.1.7) is the most distant of the line with an offset of 2.4 km and placed at 4273 m below sea level, determined from Caribe Norte navigation data.

Different phases have been identified in the OBS 12 seismic record section (Fig. 4.4.1.7). Analysis of correlations indicate that the phases located to the north are deeper and have high velocities than the phases localized to the south. First arrivals of this section are refracted and reflected in the second layer and can be correlated from 4 to 20 km to the south and from 11 to 25 to the north. P_MP phase is followed from 19 to 39 km (south) and 20 to 40 km (north) from OBS position with approximated a.a.v of 8.7 km/s and 6.4 km/s, respectively. In the northern part of the record, P_6P is correlated with an approximated a.a.v of 13.9 km/s.

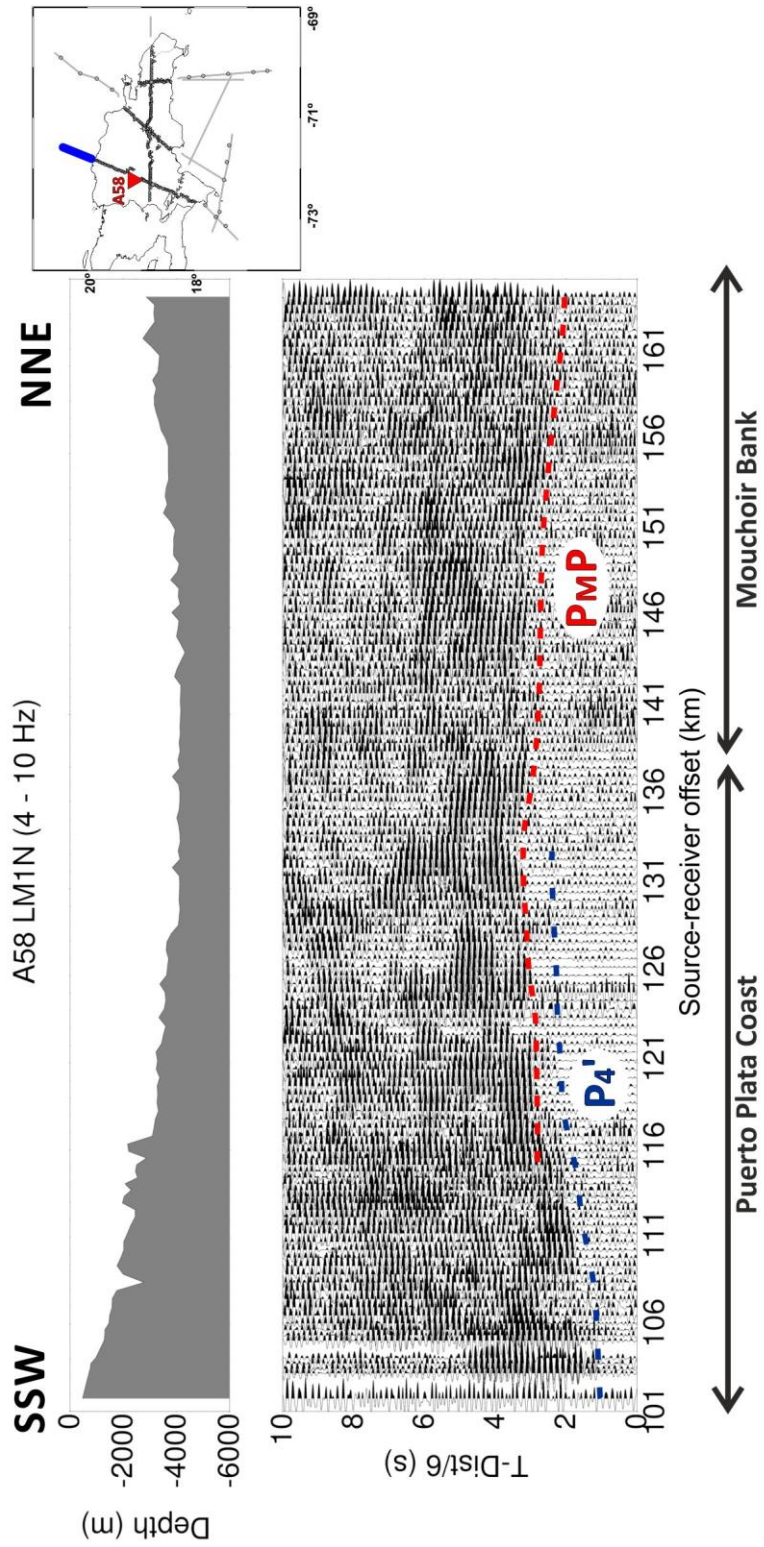

Fig. 4.4.1.4 LM1N seismic transect record, station A58. Vertical component, amplitude-trace normalized and band-pass filtering of 4 – 10 Hz. Colored lines point out reflected/refracted P-wave trains. On the top, bathymetry along this line. In the upper right corner, red triangle shows location of registration point and blue line the marine seismic line.

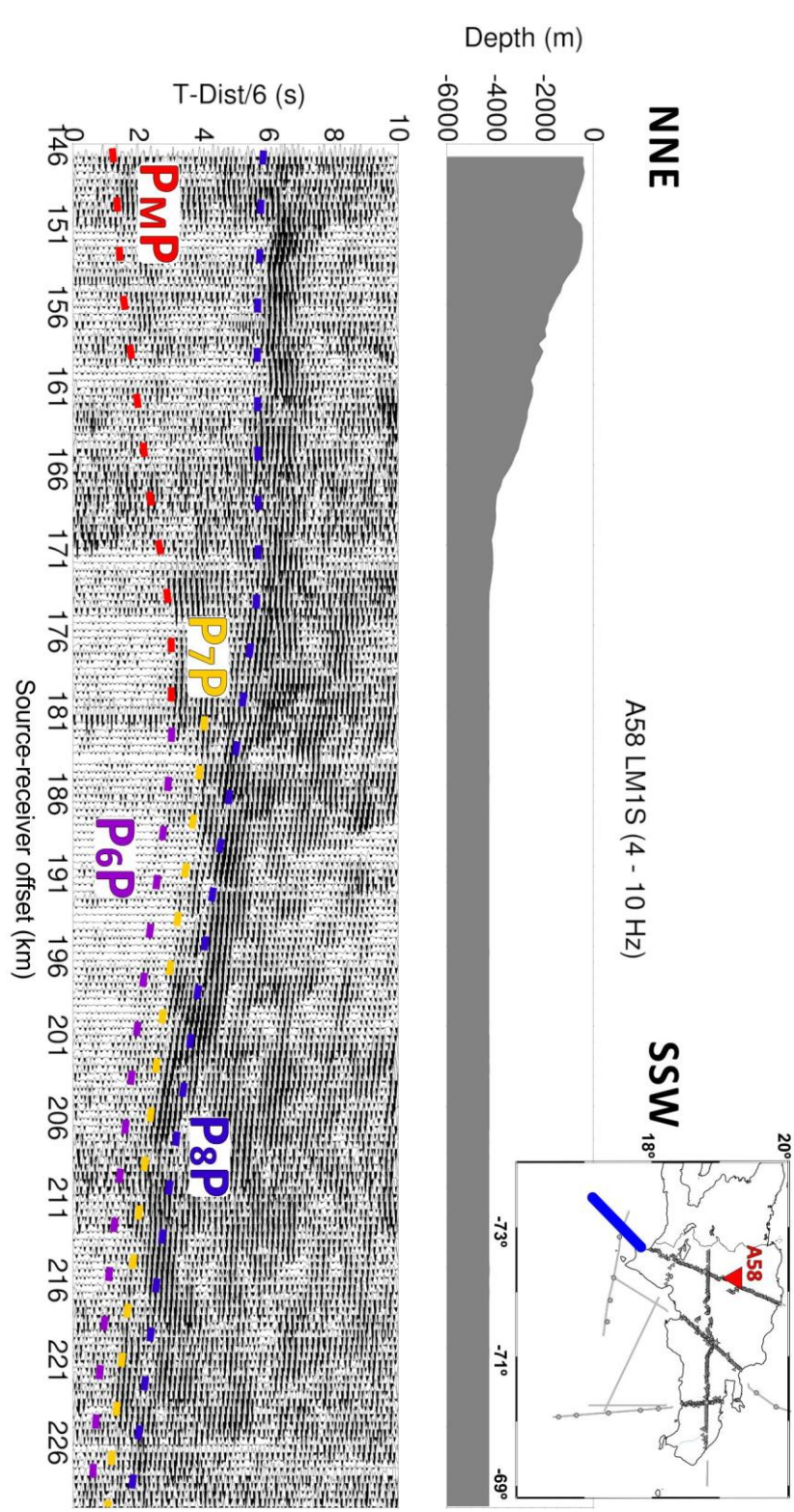

Fig. 4.4.1.5 LM1S seismic transect record, station A58. Vertical component, amplitude-trace normalized and band-pass filtering of 4 – 10 Hz. Colored lines point out reflected/refracted P-wave trains. On the top, bathymetry along this line. In the upper right corner, red triangle shows location of registration point and blue line the marine seismic line.

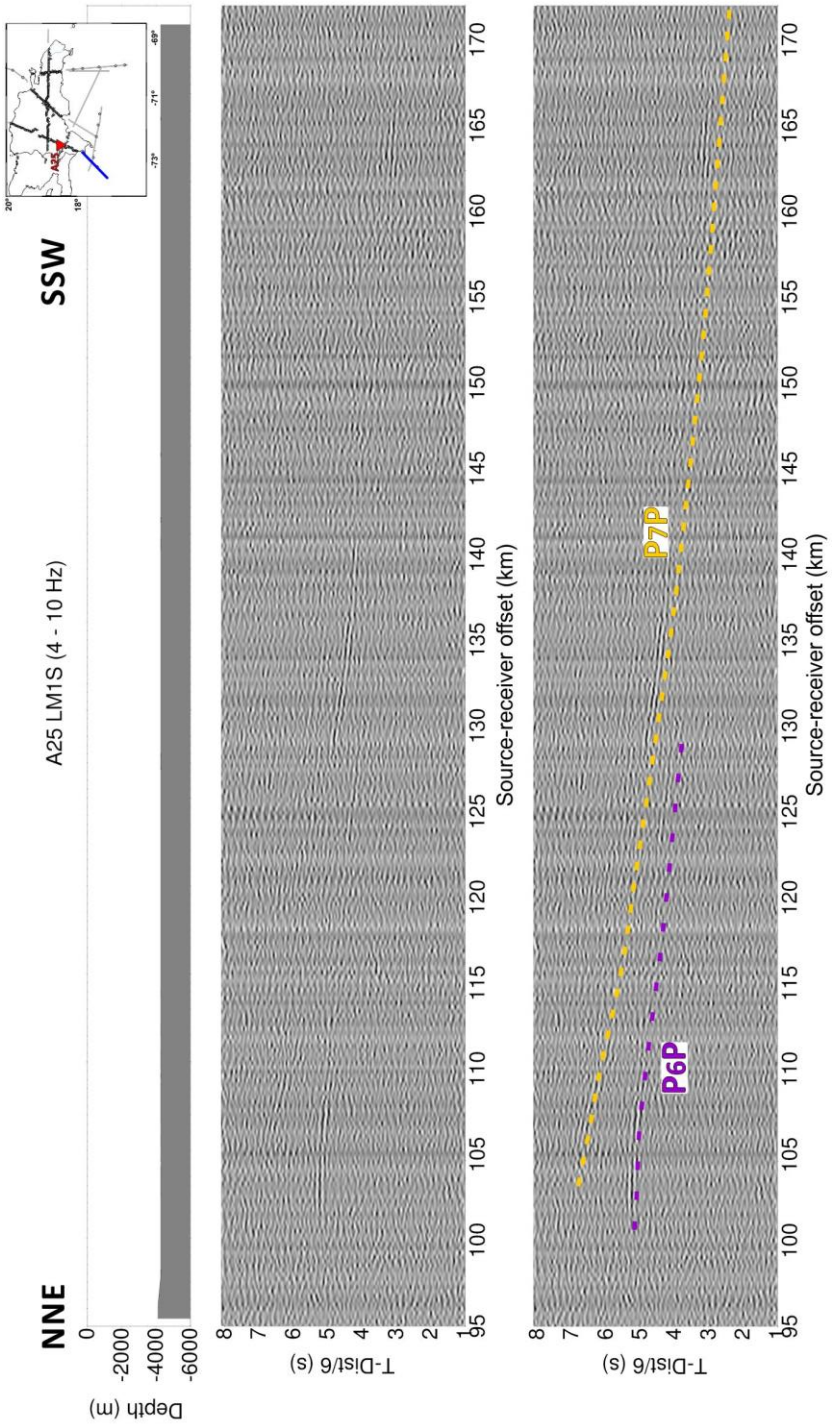

Fig. 4.4.1.6 LM1S seismic transect record, station A25. Vertical component, amplitude-trace normalized and band-pass filtering of 4 – 10 Hz. Colored lines point out reflected/refracted P-wave trains. On the top, bathymetry along this line. In the upper right corner, red triangle shows location of registration point and blue line the marine seismic

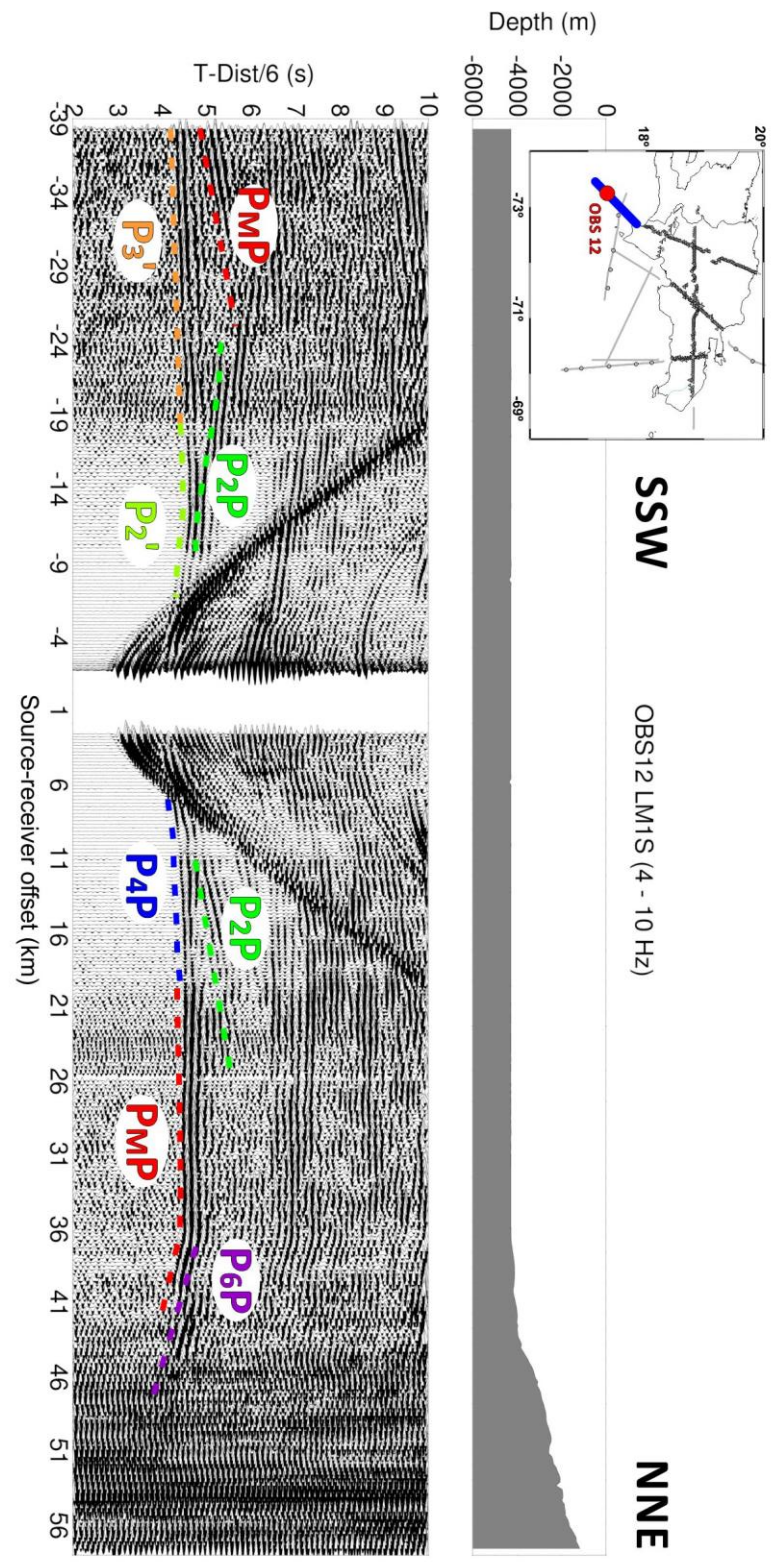

Fig. 4.4.1.7. Seismic record section corresponding to OBS 12 registering seismic line LM1S. Colored lines point out reflected/refracted P-wave trains. In this figure vertical component and bathymetry along this lines over this section are shown. In the upper left corner red circle shows location of registration point and blue line the marine seismic line. Reduction velocity is 6 km/s, band-pass filtering of 4 – 10 Hz and amplitudes-trace normalized.

Single shot registered by land station profile

Land shot S3 is located near San Juan de la Maguana in San Juan Basin (Fig. 4.2.1 and 4.3.1). The figure 4.4.1.8 shows the seismic record section obtained from the shot to the NNE where first arrivals corresponds to sedimentary layer in this basin, P_2P, followed up to 12 km. P_3P is interpreted as reflected phase in discontinuity between layers 3 and 4 correlated from 7 to 27 km offset followed by P_4' in the area of Cordillera Central from a distance of 49 km to 90 km. Between 105 km and 135 km offset range, it is possible identify P_MP with an approximated a.a.v of 7.5 km/s. In the seismic record section, it is observed that between P_4' and P_MP exists a loss in the seismic energy. This feature could be indicated by the presence of Septentrional Fault.

Figure 4.4.1.9 is the seismic record section from the shot to the SSW direction where it has been interpreted P_2' and P_3' (head waves travelling in discontinuity between layers 2 and 3, and 3 and 4, respectively) and one P-wave reflected at the bottom of layer number 4 that can be correlated in 30-98 km. In the bottom of the figure, it has been represented the main structural features that this profile crosses.

Marine shot number 135 (Fig. 4.4.1.10) is located at 60 km from first shot of line LM1S and its seismic record section illustrates the deep structure across the study line showed at the bottom of the figure. In this seismic record section, different reflected phases are correlated. The deepest phases are identified between 130 and 230 km and 225-265 km from the shot to the SSW. These phases correspond to the reflections in the bottom of layer 7 and 8 discontinuities with approximated P-wave velocities of 7.6 km/s and 8.3 km/s, respectively.

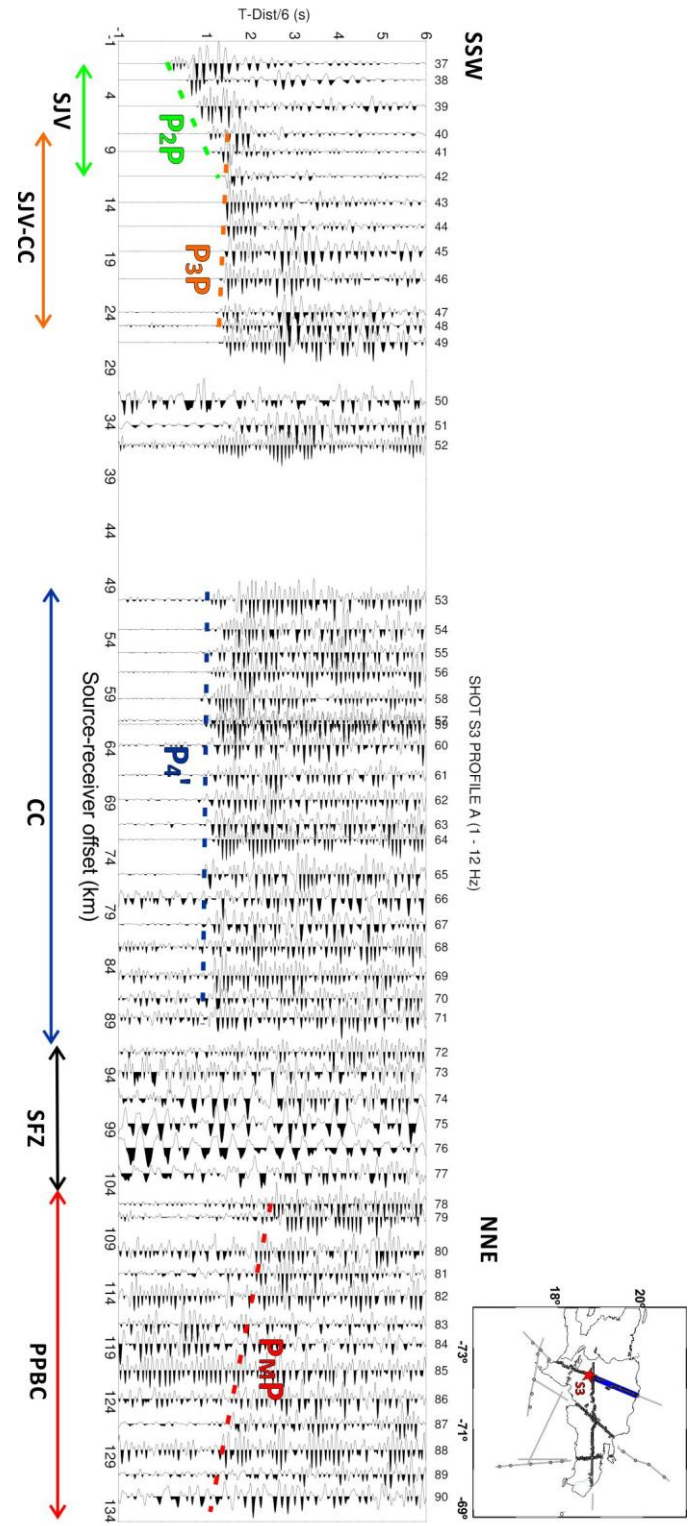

Fig. 4.4.1.8. Seismic record section of Shot 3 (San Juan de la Maguana, DR) registered by land seismic portable stations of Profile A installed from S3 to north. Vertical component, amplitude-trace normalized and band-pass filtering of 1 – 12 Hz. Colored lines point out reflected/refracted P-wave trains. On the top, shot point in red and blue line shows the stations that record this shot. SJB = San Juan Basin; SFZ = Septentrional Fault Zone; CC = Cordillera Central; PPBC = Puerto Plata Basement Complex.

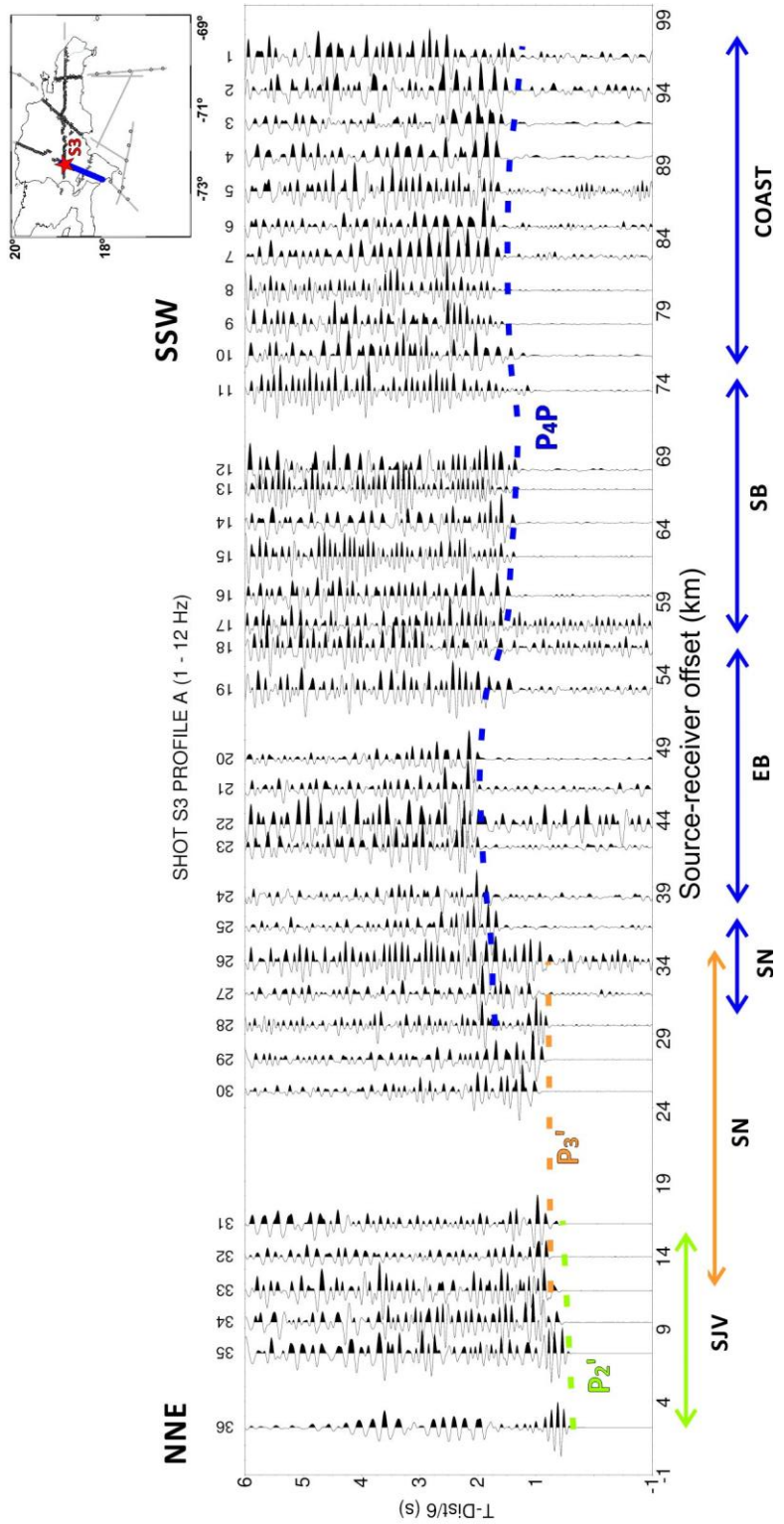

Fig. 4.4.1.9. Seismic record section of Shot 3 (San Juan de la Maguana, DR) registered by land seismic portable stations of Profile A installed from S3 to south. Vertical component, amplitude-trace normalized and band-pass filtering of 1 – 12 Hz. Colored lines point out reflected/refracted P-wave trains. On the top, shot point in red and blue line shows the stations that record this shot. Arrows show the tectonic areas located at that distances where SJB = San Juan Basin; SN = Sierra de Neiba; EB = Enriquillo Basin; SB = Sierra de Bahoruco; COAST = Pedernales Coast.

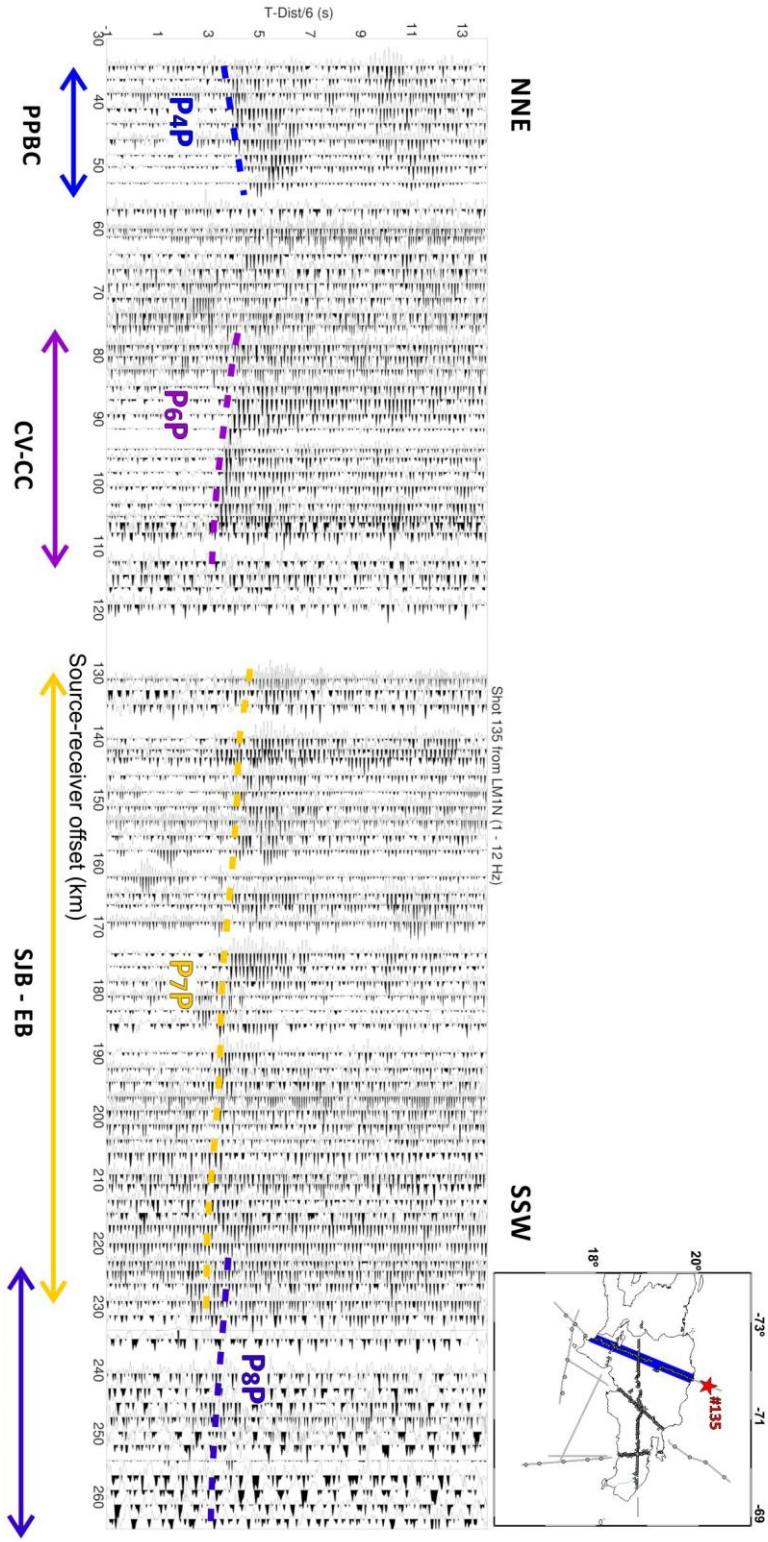

Fig. 4.4.1.10. Seismic record section corresponding to marine shot number 135 recorded by Profile A stations with correlated phases. Vertical component, amplitude-trace normalized and band-pass filtering of 1 – 12 Hz. Colored lines point out reflected/refracted P-wave trains. On the top, shot point in red and blue line shows the stations that record this shot. Arrows show the tectonic areas located at that distances where PPBC = Puerto Plata Basement Complex; CV = Cibao Valley; CC = Cordillera Central; SJB = San Juan Basin; EB = Enriquillo Basin; SB = Sierra de Bahoruco; COAST = Pedernales Coast.

Profile F

In this section, some seismic record section of Profile F (Fig. 4.3.1) will be shown. This profile is 295 km length with marine line L6 and WNW – ESE direction. The main tectonic features, which Profile F crosses, are Enriquillo Basin, Sierra de Martín García, Bahía de Neiba and Muertos Thrust Belt.

Seismic record section of station D (Fig. 4.4.1.11) shows an increasing noise level at the beginning of Muertos Thrust Belt. First showed arrivals correspond to sedimentary layer in the Enriquillo Basin and Bahía de Neiba where this station is installed. After that, a reflected wave in the upper layers of the crust is interpreted between 50 and 80 km offset, P_4', as a diving wave travelling through the bottom of layer 4 with an a.a.v of 5.6 km/s. From 80 km, it is observed the increasing noise level. In this zone, P_MP phase can be followed between 80 and 95 km source-receiver offset range with a velocity of 10.9 km/s that indicates the presence of a dip in Moho discontinuity. P_6P and P_7P are correlated from 95 km to 120 km and 120 to 150 km offset with 8.8 km/s and 7.9 km/s approximated a.a.v, respectively. These data suggest layer 6 could have a dip while layer 7 not.

The farthest station that recovered useful information about this profile is station F. This station is located at 20 km from westernmost one in the line and crosses with Profile A between A20 and A22 stations.

The seismic record section (Fig. 4.4.1.12) shows high noise level due to sediments accumulated in Enriquillo Basin, but it is possible to identify P_4' and P_MP phases in first kilometers of the seismic record section. P_4' is correlated from 65 to 93 km and P_MP from 93 to 124 km offset ranges. The a.a.v are 5.3 km/s and approximately 7.4 km/s, respectively. The slope of P_MP is lower than P_MP phases of different seismic record sections of this profile indicating a different dip of this layer.

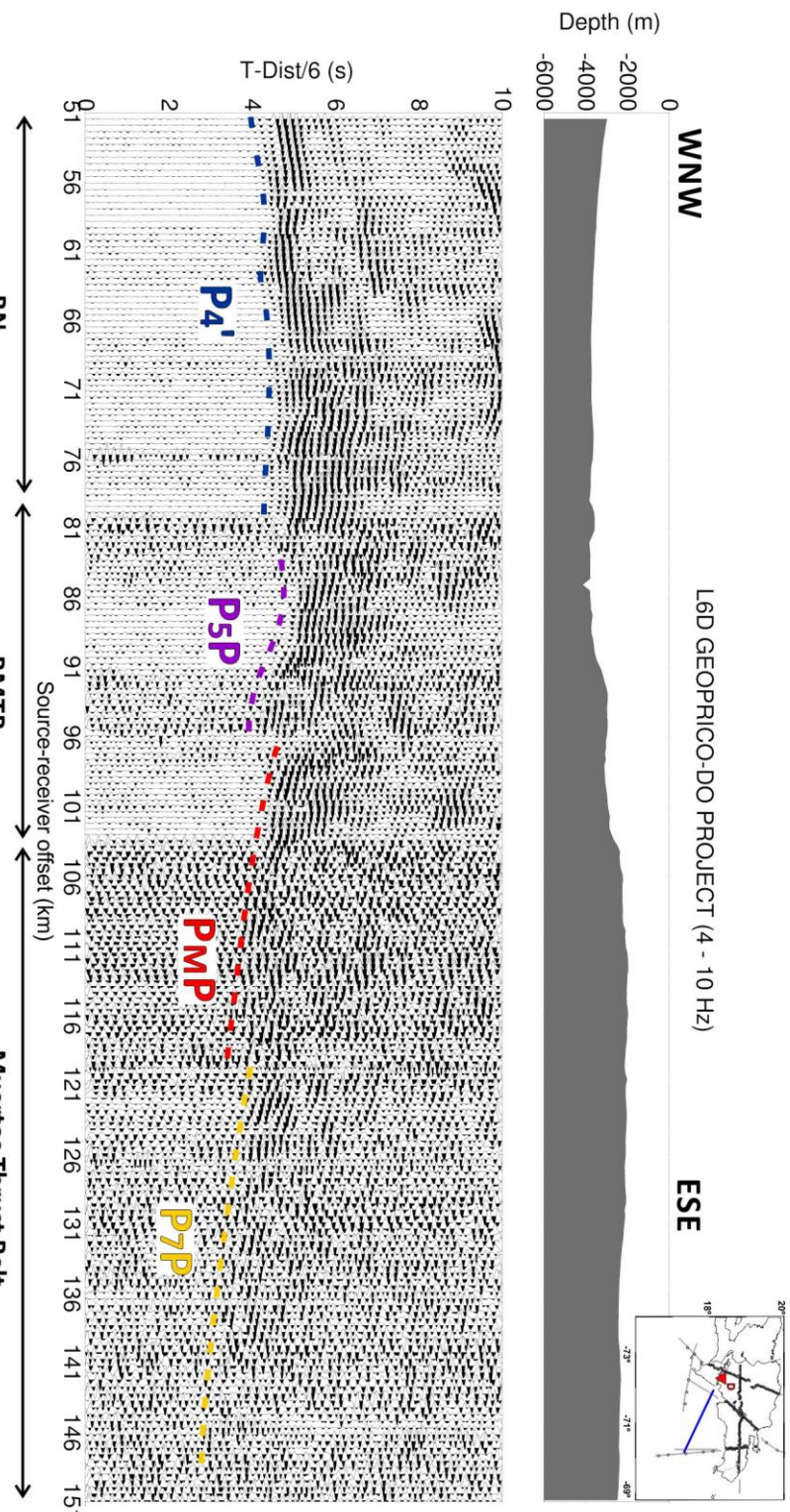

Fig. 4.4.1.11. L6 seismic transect record, station D. Vertical component, amplitude-trace normalized and band-pass filtering of 4 – 10 Hz. Colored lines point out reflected/refracted P-wave trains. On the top, bathrimetry along this line and registering point location map where red triangle shows the station situation and blue line the marine shooting line. Arrows show the tectonic areas located at that epicentral distances where NB = Neiba Bay and BMTB = Beginning of Muertos Thrust Belt.

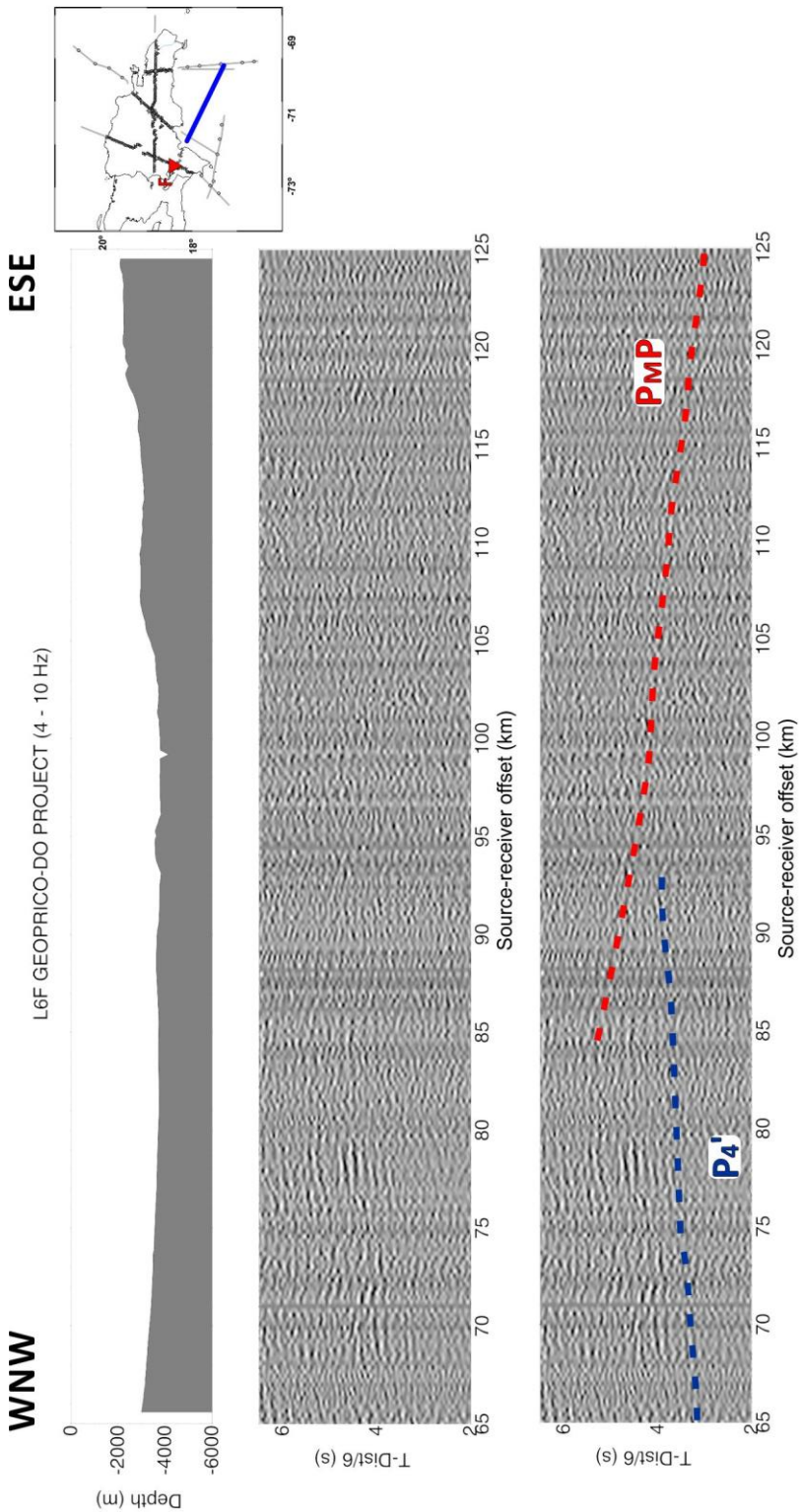

Fig. 4.4.1.12. Seismic record section corresponding to land station F recording marine shooting line L6. Vertical component, amplitude-trace normalized and band-pass filtering of 4 – 10 Hz. Colored lines point out reflected/refracted P-wave trains. On the top, bathymetry along this line registering point location map where red triangle shows the station situation and blue line the marine shooting line. Below, seismic record section in greyscale with correlated phases.

4.4.2 Modeling

Seismic wide-angle data have been interpreted using forward modeling techniques [Zelt & Smith, 1992] (Fig. 4.4.2.1). Water-depth/elevation from the airgun-shots/land stations was taken from the navigation data.

The joint modeling of deployed stations along profiles A and F allows to obtain a global velocity model for both profiles which represents the data features and its interpretation to the western Dominican Republic from the Bahamas Platform to the north of the Beata Ridge.

Profile A

The study of Profile A (Fig. 4.3.1) seismic record sections (Figs. 4.4.1.1 - 4.4.1.10) reveals some features about tectonic and geological structures as it has been discussed in Section 4.4.1. In the northern, water layer is 3.1-4.1 km thick with a P-wave velocity of 1.5 km/s. In this part of the model, a normal oceanic crust is found showing a thin sedimentary layer (<1 km thick) with a V_P increasing from 3.3 to 5.2 km/s (Fig. 4.4.2.1), with 0.1 km/s of uncertainty. Basement is situated at 5 km deep while Mohorovicic discontinuity is reached at 10 ± 1 km (Fig. 4.4.2.2). Depth uncertainty for layers on the top of the model presents values less than 1 km.

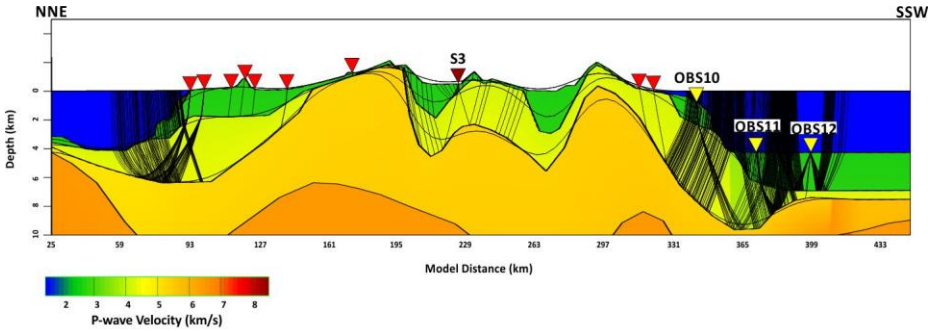

Fig. 4.4.2.1. Ray tracing corresponding to shallow structure across Profile A with land stations and OBS represented by red and yellow inverted triangles, respectively. P-wave velocity model is under ray tracing.

At 90 km from model origin, northern part of Hispaniola Island is reached and sedimentary layer increases in thickness up to 2 km depth (Fig. 4.4.2.1). Moreover, basement is located at 6.4 km, with depth uncertainty less than 1 km. This zone corresponds to PPBC (Fig. 4.2.1). Then, there is the western flank of Cordillera Septentrional whose effect is not very pronounced in the seismic record sections. Following, Cibao Valley (Fig. 4.2.1) is situated where sedimentary thickness is 4 km according to southern flank that is constituted by different stratigraphic sequences. South of Cibao Valley, it is observed that basement rises to subsurface due to

Cordillera Central presence. In this area, Moho discontinuity is 27 ± 2 km deep (Fig. 4.4.2.2).

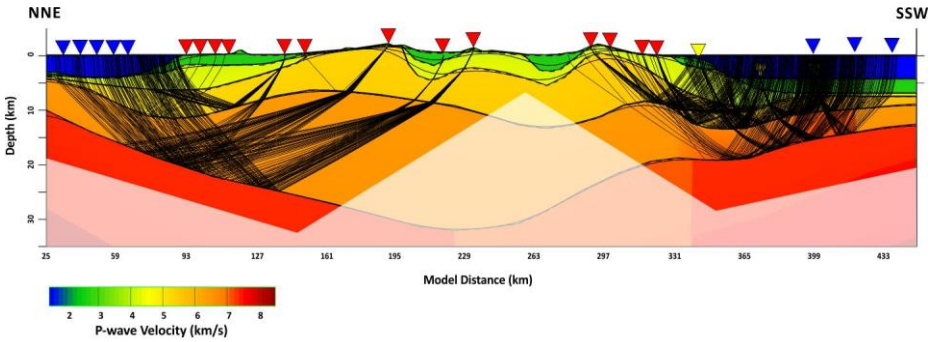

Fig. 4.4.2.2. Ray tracing and P-wave velocity model in the area of Profile A (Fig. 4.3.1) showing middle structure. Shadow zone represents the area not covered by ray beams in this case. Red, blue and yellow inverted triangles represent land stations, marine shots and OBS included in this profile, respectively.

Ray tracing of shot S3 shows these features (Fig. 4.4.2.3). In this figure, the adjustment between calculated and observed travel times is observed.

Velocities obtained in central island region are corroborated by synthetic seismograms (Fig. 4.4.2.4 and 4.4.2.5). The model reveals San Juan Basin is not as deep as previous studies indicated in this area, reaching a sedimentary depth of 5 km (Fig. 4.4.2.1). Sierra de Neiba basement is deeper than other mountain ranges in the study area, providing better knowledge of this structure in volcano-sedimentary rocks velocities that is made of. The uncertainty in depth for shallow part of the model is less than 1 km.

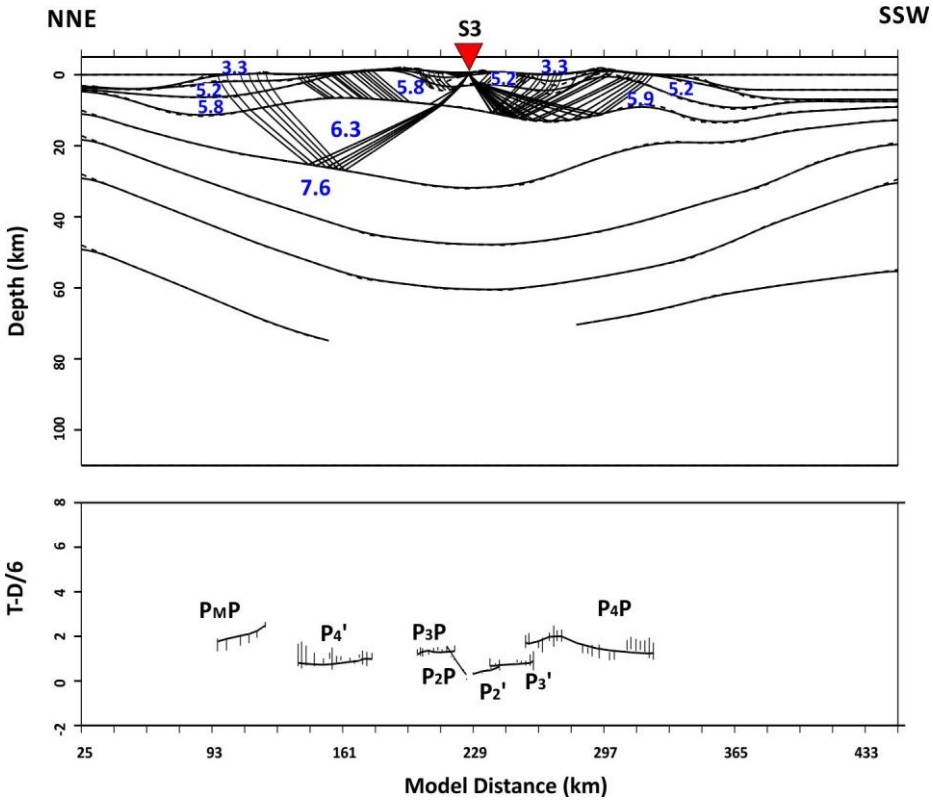

Fig. 4.4.2.3 *Top*: Ray tracing corresponding to shot S3 and velocity model (km/s). *Bottom*: Comparison between calculated (lines) and observed (vertical bars) travel times. Distances refer to the origin of the velocity model.

In Enriquillo basin area (Fig. 4.3.1), maximum sedimentary depth is 5.7 km. Sierra de Bahoruco basement rises again reaching almost subsurface. Then, basement is thickened up to 6.5 km south of the island where appears a thin sedimentary layer disappearing in the location area of OBS 10. The P-wave velocity goes down 4.5-4.8 ± 0.1 km/s up to reaching the basement with V_P 5.8-6.0 ± 0.2 km/s. In Caribbean Sea part of this profile, water depth is 4.7 km and sedimentary layer is 2.5 km thick (Fig. 4.4.2.1).

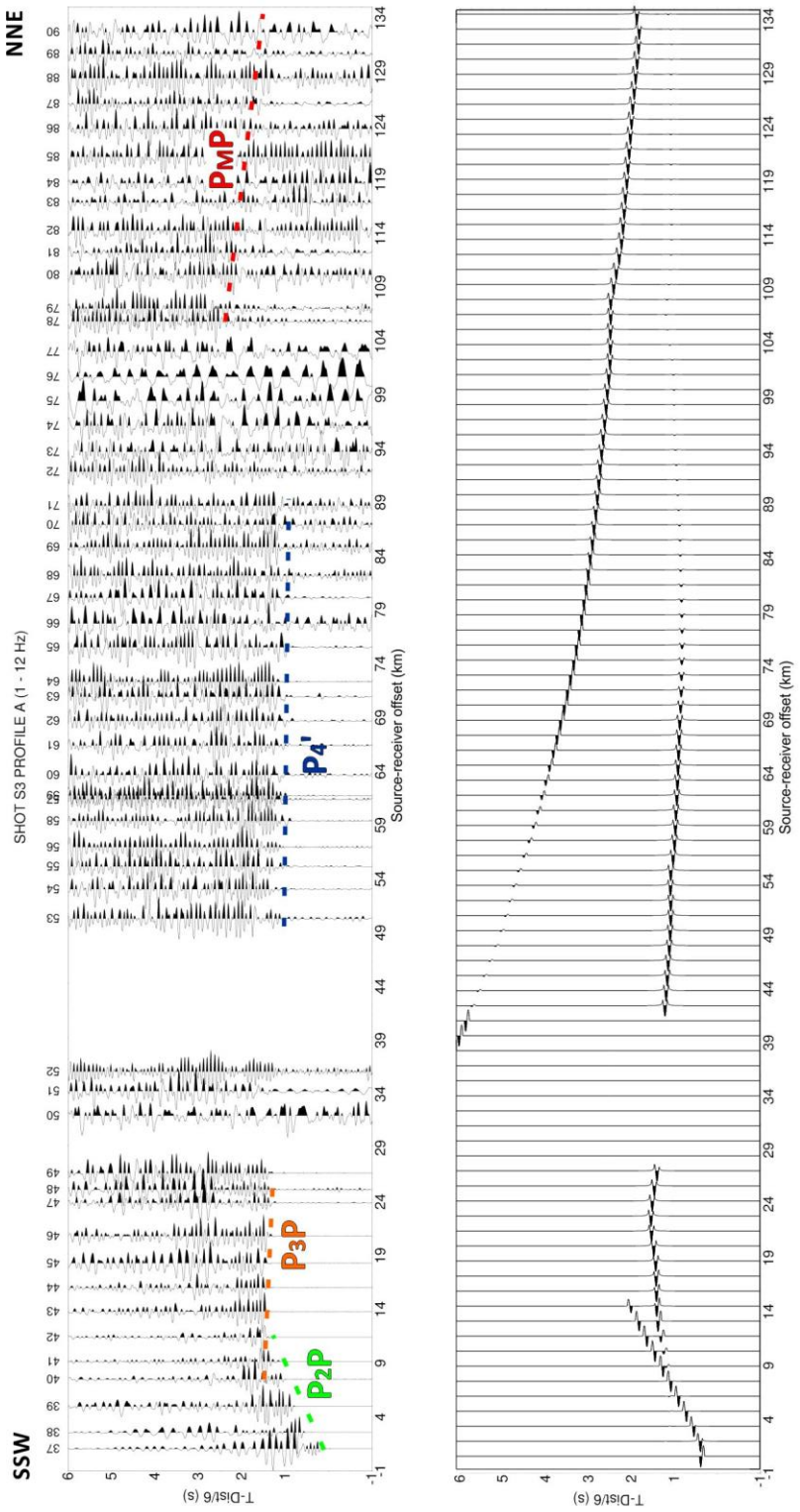

Fig. 4.4.2.4 *Top*: Seismic record section with correlated phases. Vertical component and Amplitude-trace normalized. *Bottom*: Synthetic seismogram corresponding to land shot S3 recorded by stations deployed northward. Amplitude-trace normalized.

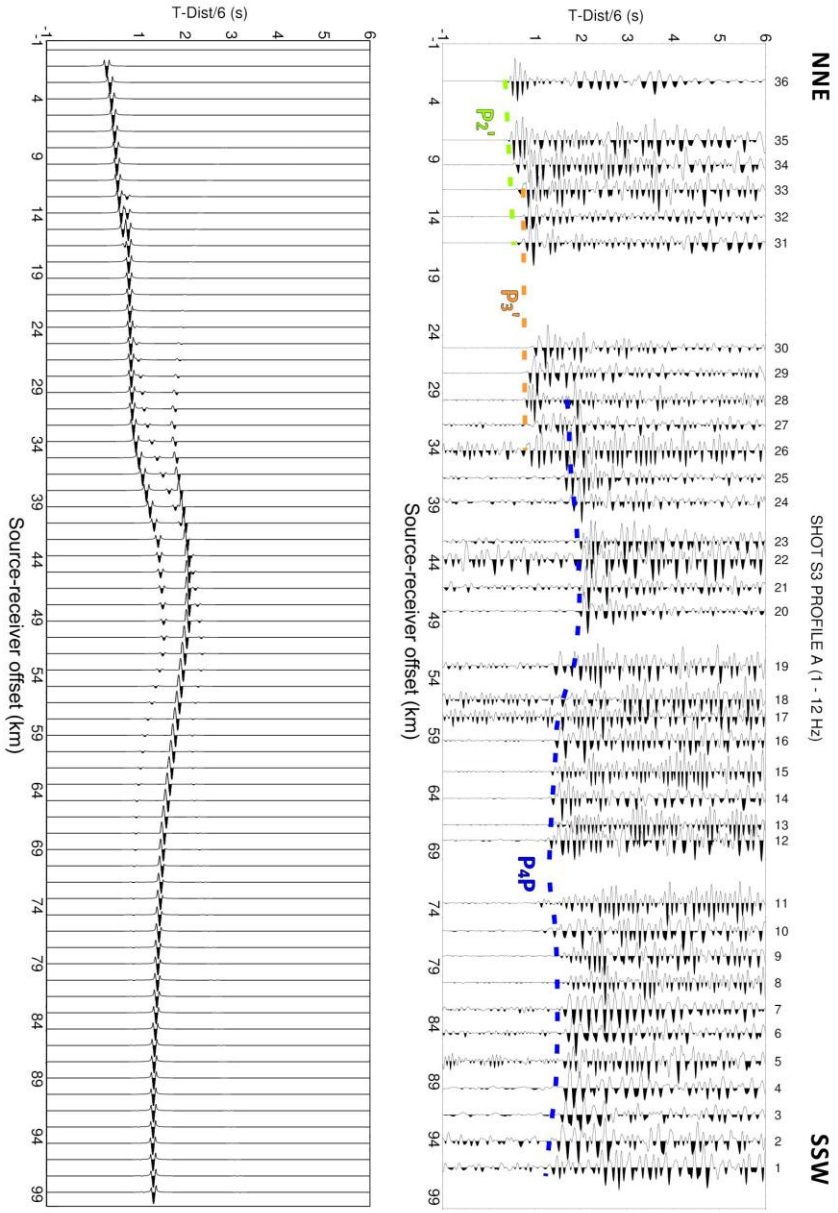

Fig. 4.4.2.5 *Top*: Seismic record section with bathymetric profile and correlated phases. Vertical component and Amplitude-trace normalized. *Bottom*: Synthetic seismogram corresponding to land shot S3 recorded by station deployed southward. Amplitude-trace normalized.

Under OBS 12 (Fig. 4.4.2.6), Moho discontinuity rising up to 10 ± 1 km depth with an increasing velocity respect to northern part of profile. An example of that corresponds to OBS 12 synthetic seismogram displayed in figure 4.4.2.7.

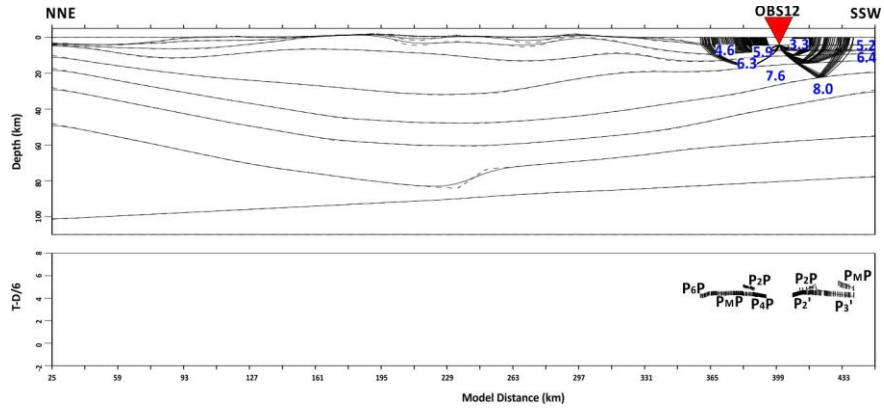

Fig. 4.4.2.6 *Top*: Ray tracing corresponding to OBS 12 and velocity model (km/s). *Bottom*: Comparison between calculated (lines) and observed (vertical bars) travel times. Distances refer to the origin of the velocity model.

Deep structure indicates some differences between north and south, shown in A58 land station ray tracings (Fig. 4.4.2.8 and 4.4.2.9) and theoretical velocities obtained from synthetic seismogram (Fig. 4.4.2.10). In the northern part, NAP penetrates into the island with an angle of 12º. This feature is widely observed on the seismic record section of marine shot 135 (Fig. 4.4.1.11). Nevertheless, in southern part, the structure is different showing higher velocities in deeper layers. Ray tracing of shot 135 (LM1N) displays inclined layers that could indicate the presence of NAP penetrating into the island (Fig. 4.4.2.8).

Between northern and southern parts of the model, an anomalous zone with velocity lateral variation is determined with decreasing velocity from 7.6 ± 0.2 km/s to 7.0 ± 0.2 km/s from W to E (Fig. 4.4.2.12). This change reaches 60 ± 3 km deep and no reflections are seen from the top of this zone. Immediately below that, another anomalous zone can be determined with a slightly higher velocity but lower than the surrounding area (7.5 to 8.0 km/s, with error estimation of 0.2 km/s). The observed phases are characterized by having higher amplitudes in the deepest layers (Fig. 4.4.1.5). Moreover, comparison between figures 4.4.1.4 and 4.4.1.5 indicates that this area is situated just southward.

The deepest phases observed in seismic station seismograms (Fig. 4.4.1.8) reaching up to 70 ± 4 km in the south and 82 ± 4 km in the north with average V_P of 8.4 ± 0.3 km/s (Fig. 4.4.2.12).

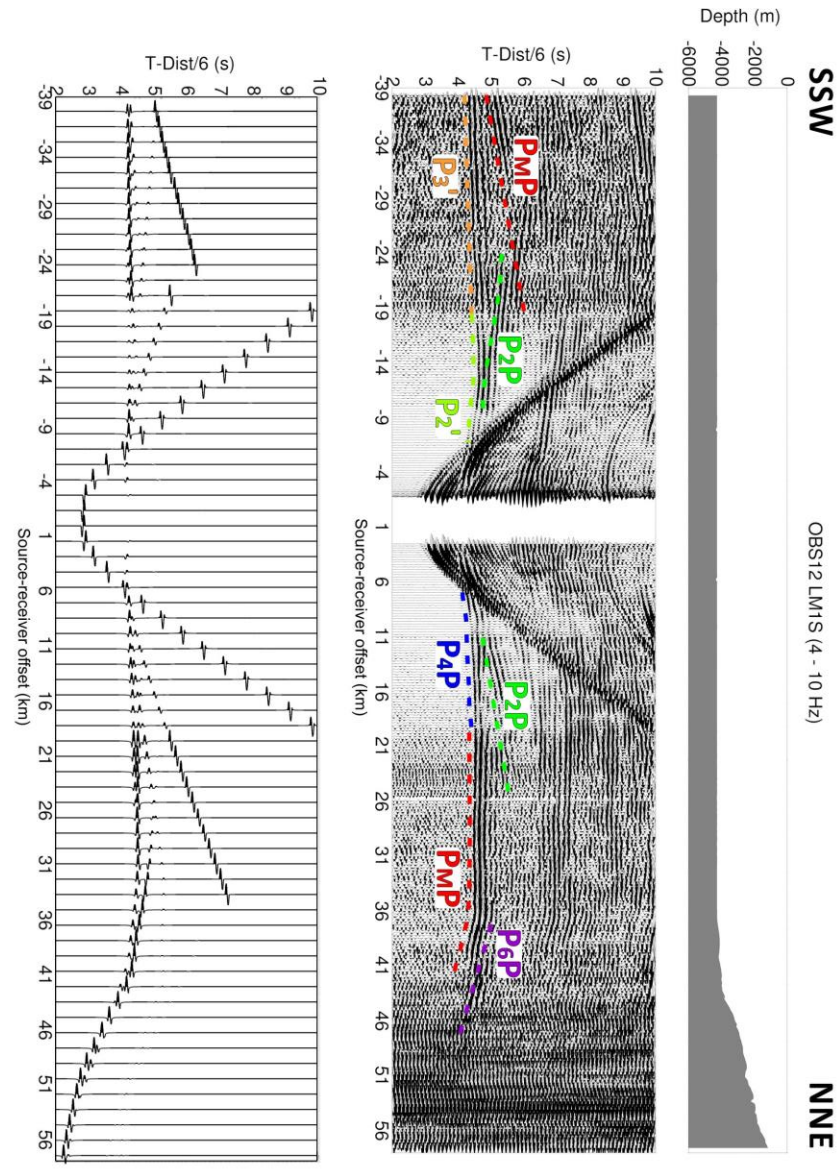

Fig. 4.4.2.7 *Top*: Seismic record section with bathymetric profile and correlated phases. Vertical component and Amplitude-trace normalized. *Bottom*: Synthetic seismogram corresponding to OBS 12 recording marine line LM1S. Amplitud normalized.

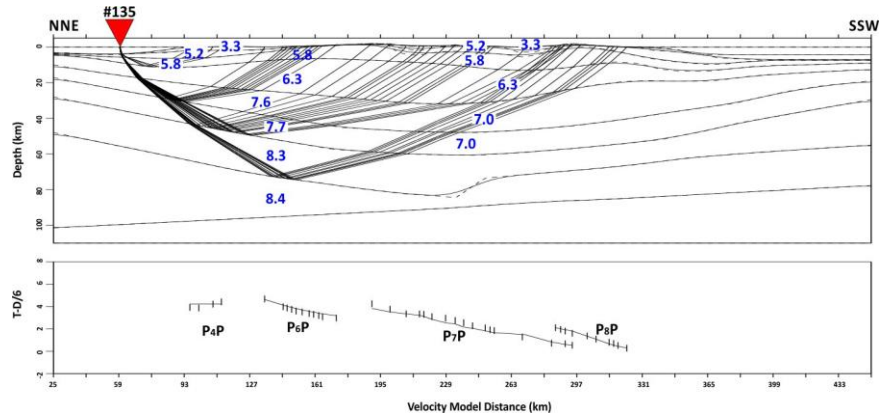

Fig. 4.4.2.8 Top: Ray tracing corresponding to marine shot 135 (LM1N) and velocity model (km/s). Bottom: Comparison between calculated (lines) and observed (vertical bars) travel times. Distances refer to the origin of the velocity model.

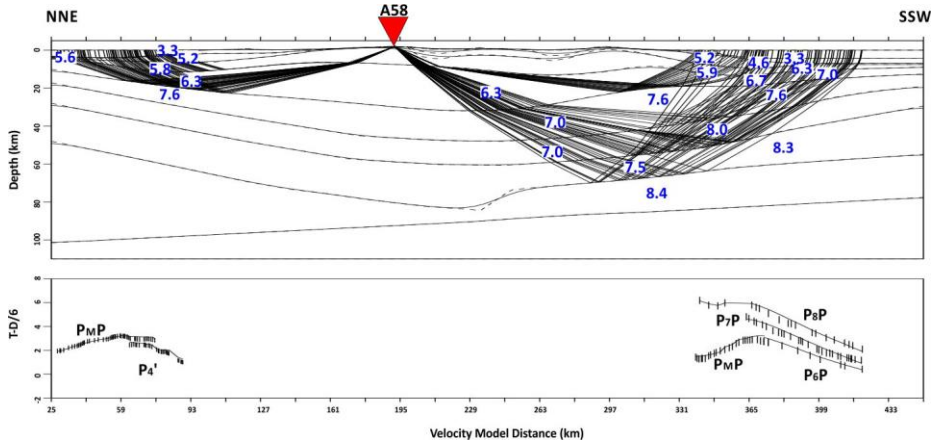

Fig. 4.4.2.9 *Top*: Ray tracing corresponding to station A58 and velocity model (km/s). *Bottom*: Comparison between calculated (lines) and observed (vertical bars) travel times. Distances refer to the origin of the velocity model.

Ray tracing and crustal P-wave velocity model obtained for this profile from NNE to SSW are shown in figures 4.4.2.11 and 4.4.2.12, where all analyzed data have been included. First figure shows ray coverage along Profile A, which is high in SSW direction. In the second one, it is possible to observe Moho discontinuity in northern and southern flanks as a black solid line. Between that, it is not possible to define it (black dash line) and could be located at 70 ± 4 km depth, approximately. The average fit is better than 0.2 s, the maximum misfit is 0.6 s. V_P uncertainty for Moho discontinuity is 0.2 km/s in upper mantle, while depth uncertainty reaches 2 km, obtained from explanation in Section 2.7 of Chapter 2.

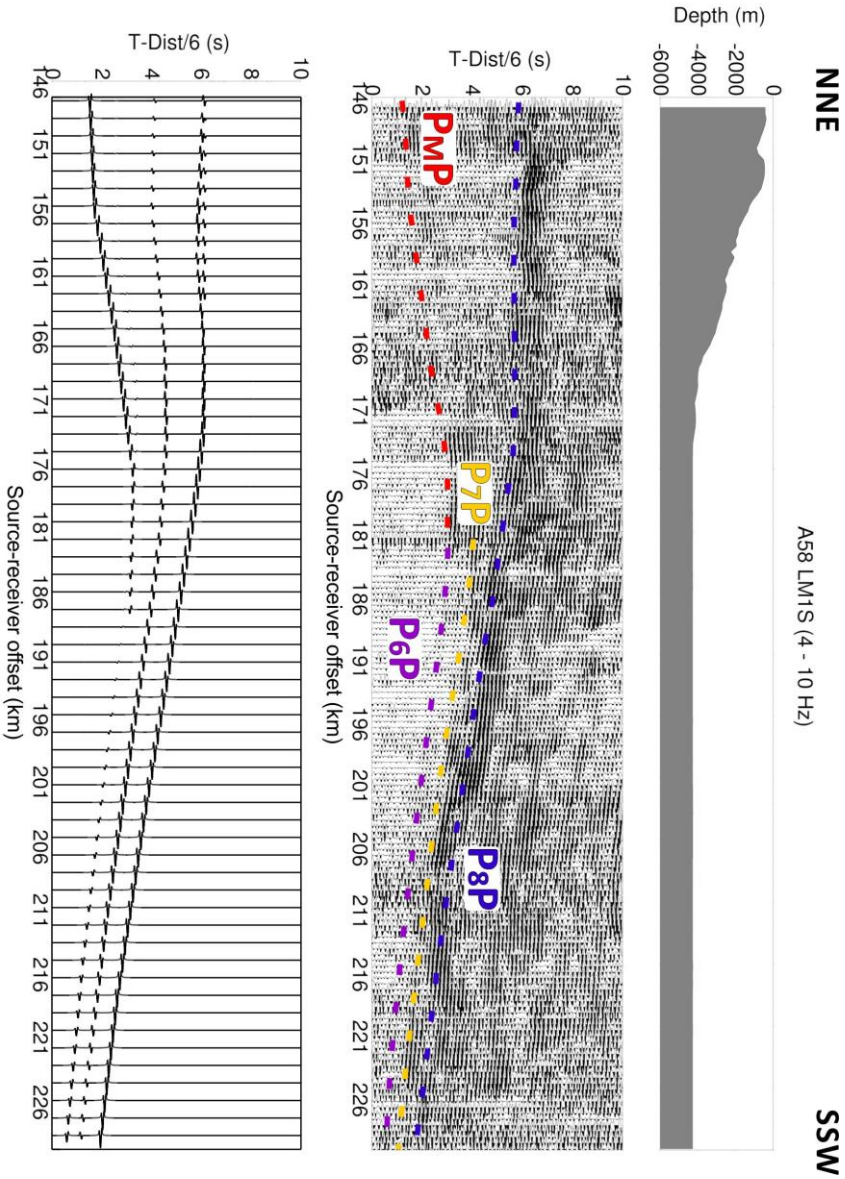

Fig. 4.4.2.10 *Top*: Seismic record section with bathymetric profile and correlated phases. Vertical component and amplitude-trace normalized. *Bottom*: Synthetic seismogram corresponding to land station A58 recording marine line LM1S.

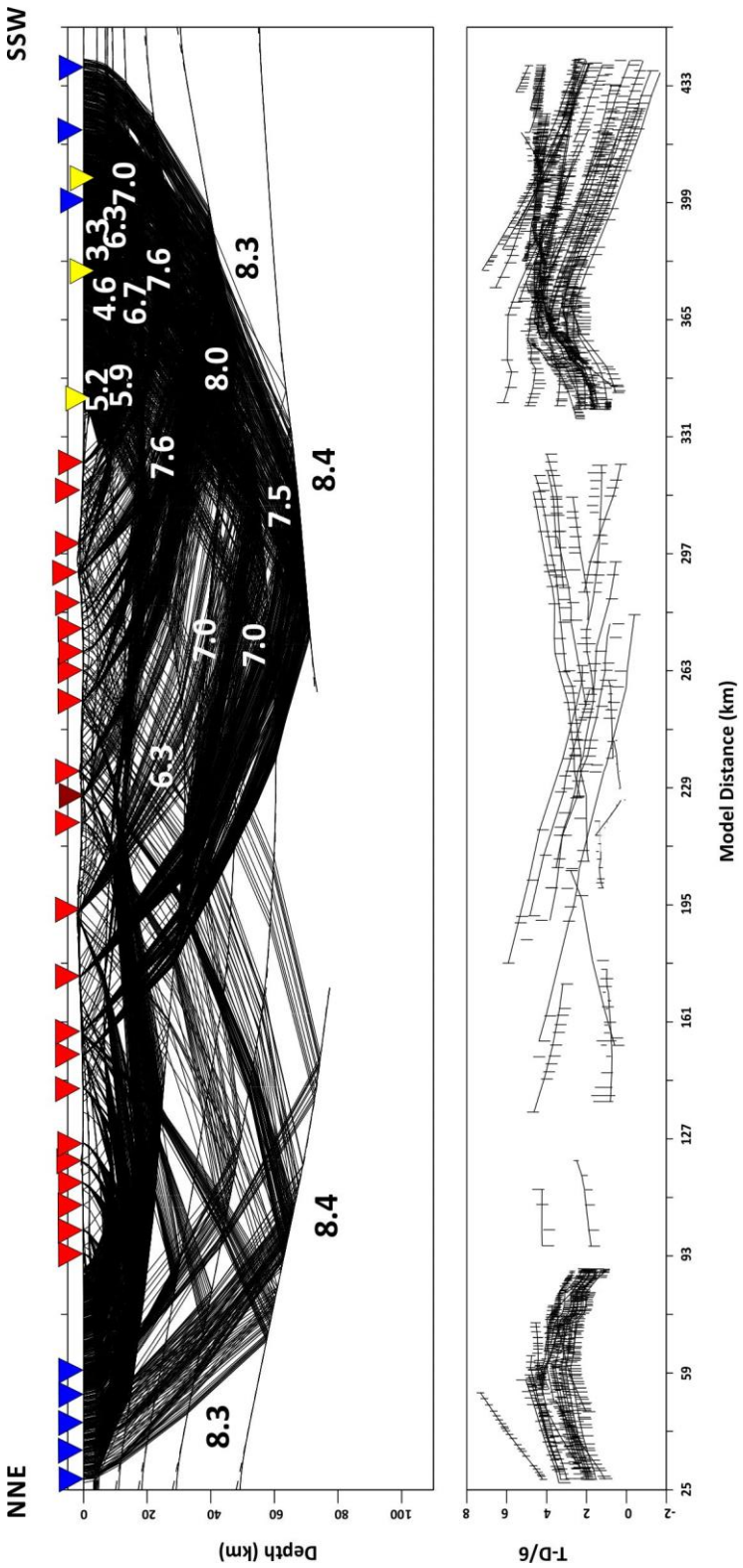

Fig. 4.4.2.11 *Top:* Ray tracing corresponding to all land stations and OBS of Profile A to obtain velocity model. *Bottom:* Comparison between calculated (lines) and observed (vertical bars) travel times. Distances refer to the origin of the velocity model. Blue triangles represent marine shots that are registered by all land stations. Red triangles show land stations used for this study and dark red is shot S3 while yellow triangles represent the location of OBS at the Caribbean Sea.

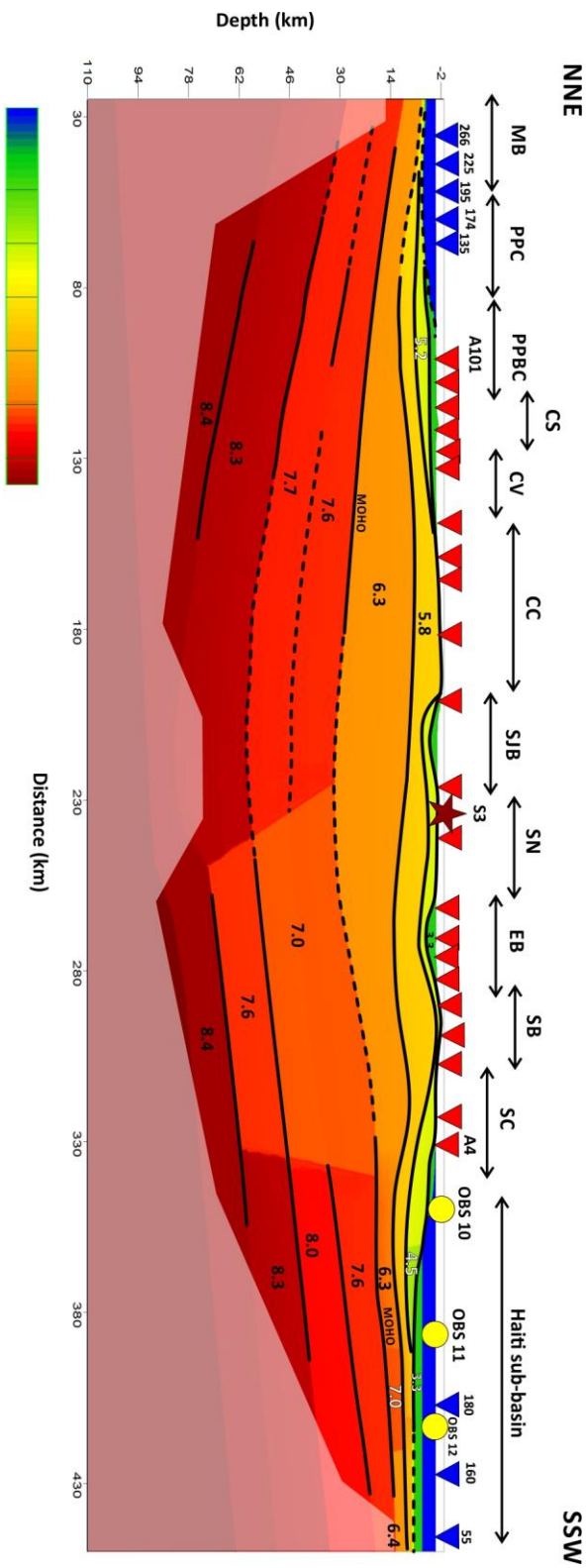

Fig. 4.4.2.12. P-wave velocity model corresponding to Profile A studied in this work where inverted red triangles denote land stations, yellow circles OBS instruments, dark red star corresponds to land shot S3 and inverted blue triangles denotes the marine shots studied. The black lines represent where reflected or diving waves phases are. Dash black line denotes where ray beams travel through. The shaded regions show areas not illuminated by the ray beams. All figures are scaled according depth and distance. MB = Mouchoir Bank; PPC = Puerto Plata Coast; PPBC = Puerto Plata Basement Complex; CS = Cordillera Septentrional; CV = Cibao Valley; CC = Cordillera Central; SJB = San Juan Basin; SN = Sierra de Neiba; EB = Enriquillo Basin; SB = Sierra de Bahoruco; SC = Southern Coast. Color scale denotes P-wave velocity in km/s.

Estimates of arrival-time fit quality for each phase and for all phases are given in Table 4.4.I. Our final model produces a normalized χ^2 of 1.1 with most of individual phase over-fit ($\chi^2 > 1$). These values are close the ideal case, indicating the observed arrival-times are adequately fit by the predicted ones. Our model is able to predict most of the observed arrival-times (NC and NR are similar) with travel-time misfits similar to the pick uncertainty (SIGMA and Trms are similar).

Phase	NC	SIGMA (s)	NR	Trms (s)	χ^2
P_1'	14	0.165	14	0.091	0.313
$P_2/P_2P/P_2'$	241	0.107	241	0.145	3.409
P_3P/P_3'	289	0.161	280	0.156	1.279
P_4P/P_4'	652	0.191	652	0.168	0.786
P_MP	588	0.260	570	0.150	0.336
P_n	120	0.207	120	0.284	2.091
P_6P	299	0.252	299	0.209	0.806
P_7P	490	0.279	488	0.291	1.105
P_8P	437	0.284	432	0.300	1.185
FIT	3130	0.228	3096	0.208	1.108

Table 4.4.I Travel-time fit for each phase: NC = number of picks; SIGMA = mean pick uncertainty; NR = number of traced rays; Trms = travel time root mean square misfit; χ^2 = normalized chi square.

Profile F

Profile F study (Fig. 4.3.1) has been carried out through L6 marine line recorded by eight land seismic portable stations deployed in Enriquillo basin and Sierra de Martín García area. Five seismic station were selected (B, C, D, E, F) for modeling from the eight that were installed. Calculated seismic record sections show a high signal-noise ratio (Fig. 4.4.1.11), which could reveal some features about tectonics.

On land part of velocity model (Fig. 4.4.2.13) is characterized by two thin sedimentary layers with an increasing P-wave velocity from 3.3 km/s to 5.8 km/s where basement is located, with velocity uncertainty of 0.1 km/s. The first sedimentary layer is 1 km thick disappearing at model distance of 60-80 km and being slightly thicker offshore Hispaniola. Second layer is 1 km thick. Basement is located at 4 km depth reducing significantly its thickness in the marine part. Middle and lower crust are characterized for reaching 13 ± 2 km and 26 ± 2 km depth, respectively, with V_P values of 5.8 ± 0.2 and 6.5 ± 0.2 km/s. Middle crust rises to subsurface between 115 km and 145 km distance that could be due to the presence of Muertos Trough and Beata Ridge.

The analysis of P_MP phases in the seismic record sections (Fig. 4.4.1.11 and 4.4.1.12) reveals that Moho is 26 ± 2 km deep, increasing up to 28 ± 2 km and immediately rises up to 18 ± 2 km where Muertos Trough is located. The velocity changes from

6.5 to 7.6 ± 0.2 km/s in this discontinuity. The deepest phase found corresponds to one layer with 8.0 ± 0.3 km/s and located 43 ± 3 km depth (Fig. 4.4.2.13).

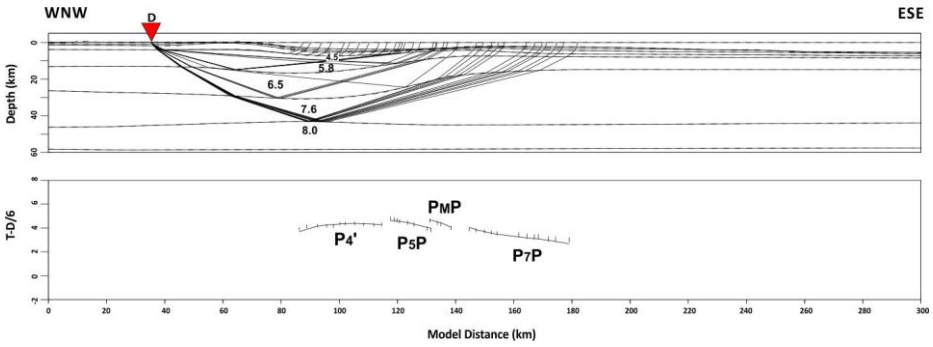

Fig. 4.4.2.13 *Top*: Ray tracing corresponding to station D and velocity model (km/s). *Bottom*: Comparison between calculated (lines) and observed (vertical bars) travel times. Distances refer to the origin of the velocity model.

Figure 4.4.2.14 displays Profile F ray tracing studied in this chapter, showing the comparison between calculated and observed travel times. Figure 4.4.2.15 shows the P-wave velocity model with velocities values indicated in km/s and a shaded zone where we have not any information.

Estimates of arrival-time fit quality for each phase and for all phases are given in Table 4.4.II. Our final model produces a normalized χ^2 of 1.2 with most of individual phase over-fit ($\chi^2 > 1$). These values are close the ideal case, indicating the observed arrival-times are adequately fit by the predicted ones. Our model is able to predict most of the observed arrival-times (NC and NR are similar) with travel-time misfits similar to the pick uncertainty (SIGMA and Trms are similar).

Phase	NC	SIGMA (s)	NR	Trms (s)	χ^2
P_4'	59	0.149	58	0.144	0.924
P_5P/P_5'	52	0.160	52	0.178	1.017
P_MP	25	0.158	23	0.176	1.252
P_7P	36	0.182	36	0.259	2.119
FIT	172	0.161	169	0.188	1.228

Table 4.4.II Travel-time fit for each phase: NC = number of picks; SIGMA = mean pick uncertainty; NR = number of traced rays; Trms = travel time root mean square misfit; χ^2 = normalized chi square.

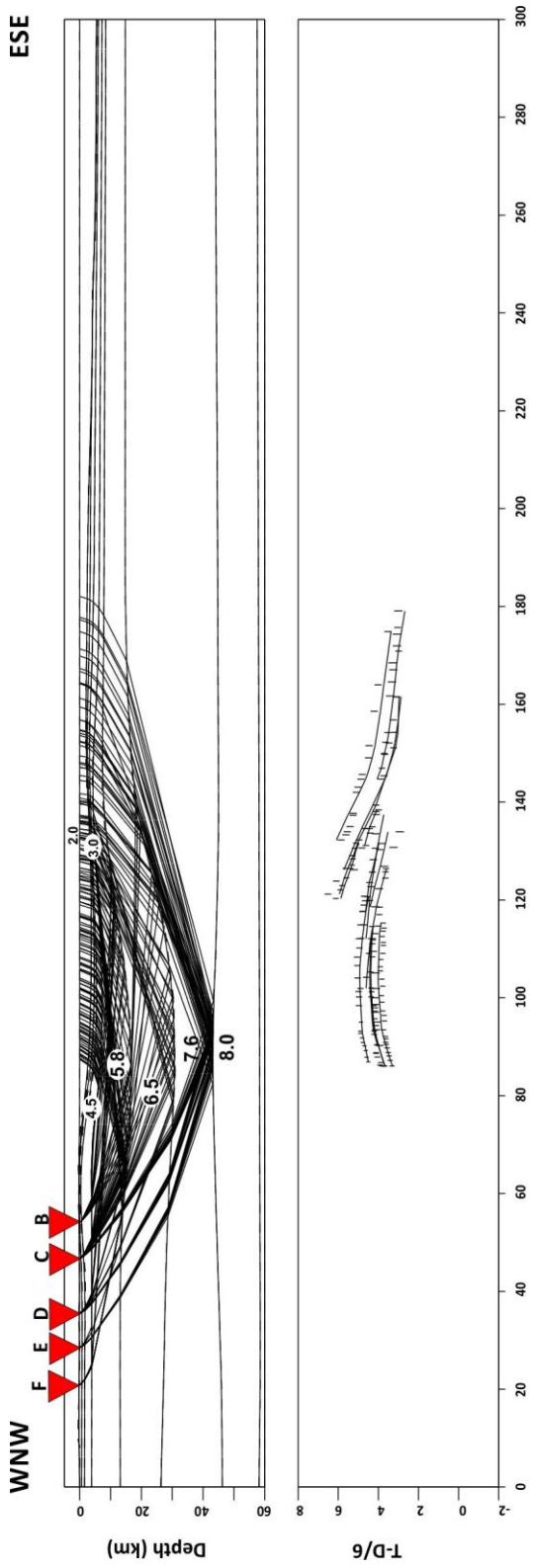

Fig. 4.4.2.14 *Top:* Ray tracing corresponding to all land stations of Profile F to obtain velocity model (km/s). *Bottom:* Comparison between calculated (lines) and observed (vertical bars) travel times. Distances refer to the origin of the velocity model.

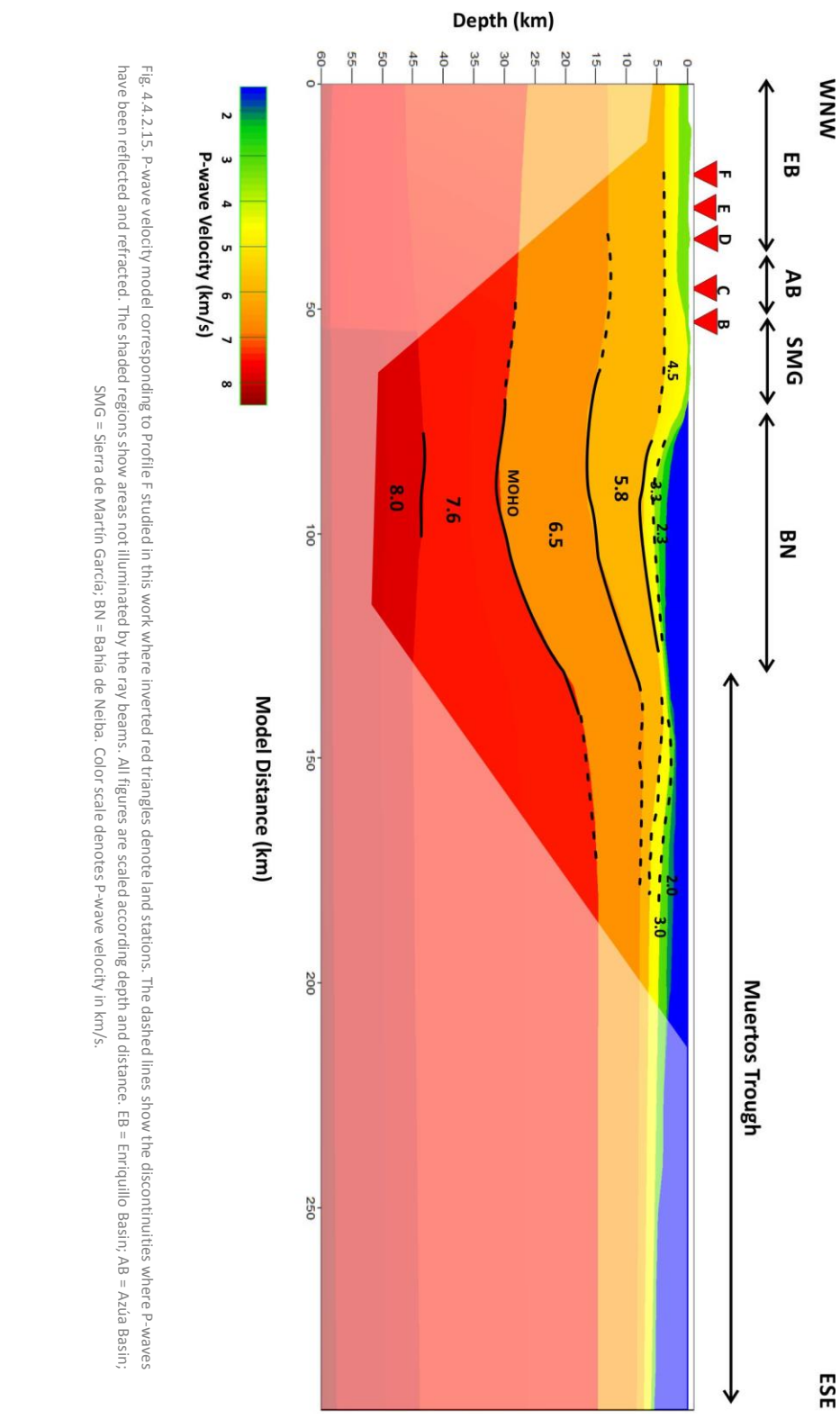

Fig. 4.4.2.15. P-wave velocity model corresponding to Profile F studied in this work where inverted red triangles denote land stations. The dashed lines show the discontinuities where P-waves have been reflected and refracted. The shaded regions show areas not illuminated by the ray beams. All figures are scaled according depth and distance. EB = Enriquillo Basin; AB = Azúa Basin; SMG = Sierra de Martín García; BN = Bahía de Neiba. Color scale denotes P-wave velocity in km/s.

4.5 DISCUSSION AND CONCLUSIONS

In summary, Hispaniola island arc is being impacted by collision with the Bahamas Bank in the north and by collision with the Beata Ridge in the south. This collision processes jointly with the main E-W component of left-lateral strike-slip have yielded the basin and range physiography observed in the Hispaniola Island. The seismic investigation of the western Dominican Republic within GEOPRICO-DO and CARIBE NORTE projects revealed new constraints in this area.

Main features of the Profile A model

The crustal velocity model of Profile A is made up eight seismic layers where crust is divided into upper, middle and lower crust and reaches thicknesses of 10 and 12 km under extremes of the profile (NNE and SSW) and 32 km below the island (Fig. 4.4.2.12), with uncertainty of 2 km.

Upper crust thickness is variable along velocity model and consists of sedimentary layer and basement. In the northern offshore part, this thickness is 1 km increasing through the coast where reaches 6 km (PPBC area). In the area of the Cordillera Central practically disappears and, then, thickens in San Juan Basin (4 km depth). Basement in Sierra de Neiba is 2 km depth. Under Enriquillo basin, it reaches 6 km depth to decrease in Sierra de Bahoruco and increase again towards the southern coast. In the southern offshore part (Caribbean Sea), the thickness is 4 km. Velocities in the sedimentary layer are 3.3-3.4 ± 0.1 km/s while basement velocity is 5.1-5.3 ± 0.1 km/s and decreases 4.5-4.8 ± 0.1 km/s in the southern coast, according to the values obtained in the area of Beata Ridge (*see Chapter 3*). It is noteworthy that wide-angle seismic data do not provide a pronounced effect in western flank of Cordillera Septentrional and SFZ.

Studying the seismicity map (Fig. 4.5.1) of this fault zone shows a concentration of events north Cordillera Septentrional from 1950 to the present. The 36% of events are located above 20 km but 51% of them have an estimated depth between 30 and 70 km. Shallow seismicity could be associated Septentrional Fault but the deepest seismicity is associated to Hispaniola Trench. Principally, a 62% of the events have magnitudes between 4.0 and 4.5.

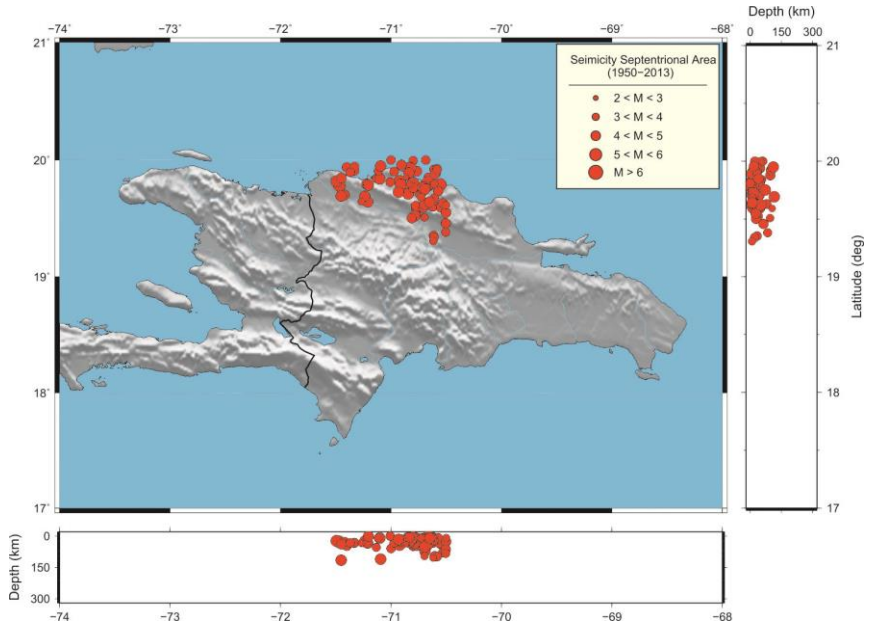

Fig. 4.5.1. Seismicity in the area of Septentrional Fault Zone from 1950 to the present from *ISC catalog online*. Selected area is (19º, 20º) N and (72º, 70.5º) W

Main features of the middle crust (Fig. 4.4.2.12) reside in a thinning both in the Cordillera Central, Sierra de Bahoruco and southern coast where they reach values of 6, 8 and approximately 9 km depth, respectively, with thickening in the northern coast and the Enriquillo basin (11 and 13 km). Lower crust is characterized by thickening through the island interior from NNW to SSE with dips of 12º and 6º (Fig. 4.4.2.12). In the northern part, Moho depth is 10 km increasing up to 32 km and decreasing again up to 12 km in the southern part ($\Delta h = 2$ km). P-wave velocity under Moho discontinuity is anomalous respect to the previous studies south of Sierra de Neiba, Enriquillo Basin and north Sierra de Bahoruco where EPGFZ is located. This feature implies this structure is deep and reaches the first layers of upper Mantle. The velocity value in this anomalous zone is 7.0-7.5 ± 0.2 km/s while in the adjacent areas is 7.6-8.0 ± 0.2 km/s. The maximum depths reached are 85 ± 3 km and correspond to the NAP while the southern part is 71 ± 3 km.

This area is strongly influenced by sub-crustal tectonic features of Hispaniola-Bahamas collision zone, as our velocity model presents and is in agreement with cross section and seismic lines shown in Figure 8a from Mann et al., (2002) (Fig. 4.5.2) revealing thinner crust in the Haiti sub-basin (5-10 km) according the results presented in this chapter. Thrusts in Enriquillo basin dip northeastward and affect clastic sedimentary. Its thickness shown in that cross section is 5 km and Moho depth is 26 km while in this study is 6 ± 1 km and 26 ± 2 km, respectively. The sedimentary units in the San Juan-Azúa ramp basin show no thinning to the north or

south and being 2.4 and 4.9 km depth the sedimentary layers found in this area. From Mann et al., (2002) reverse and oblique-slip faulting is responsible for the present pattern of morphotectonic units in central Hispaniola, including thrust-bound basins the Enriquillo, San Juan-Azúa and the Cibao, associated to the basement thickening in that areas shown in figure 4.4.2.12. The steeper dipping flank of the San Juan-Azúa basin is its northern flank in accordance with southwestward fault movement.

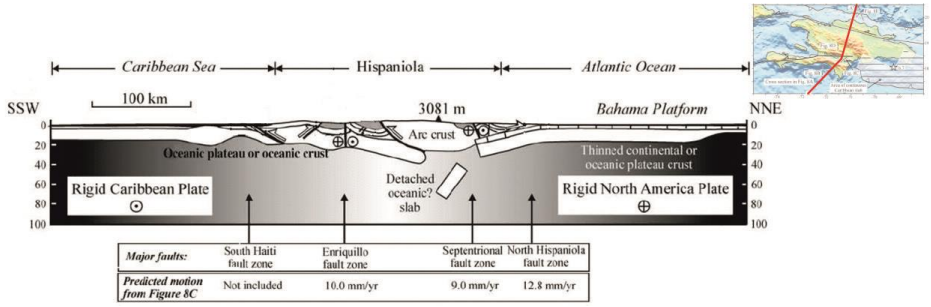

Fig. 4.5.2 Regional schematic cross section extending from the Caribbean Sea across the North America-Caribbean Plate boundary zone in Hispaniola to the Atlantic Ocean (red solid line shown in figure above) (from Mann et al. [2002]).

In this schematic cross section, a possible detached oceanic slab from NAP that could produce reflections is shown. Comparing with Profile A P-wave velocity model, it is possible to extract similarities with the anomalous area obtained, whose reflections are located up to 70 ± 3 km depth, but our ray tracing and velocity model show that this detached oceanic slab would be associated to CP instead of NAP. Also, the seismicity of this zone has been checked in ISC catalog from 1950 at present, revealing that earthquakes are grouped mainly in the northern and southern flanks (Fig. 4.5.3). Events in eastern part are deeper than those of the west and some of them reach depths of 90-100 km. These data agree with results obtained from Profile A velocity model.

Enriquillo basin area crossed by Profile A (Fig. 4.3.1) corresponds mainly to Mella and Angostura blocks (Fig. 4.2.3). Both blocks are characterized by being under sea level and filled by alluvium deposits. These features are correlated with seismic signal increasing the noise level in seismic record sections of this area. The Caribbean Sea part of profile is characterized by lateral variation in the velocity of the layer immediately below sedimentary layer due to indentation of Beata Ridge. The western flank of the Beata ridge is a huge slope that rises from the flat abyssal plain. Specifically, there is a deep terrace at the base of western Bahoruco slope covered products of erosional processes that could alter the region.

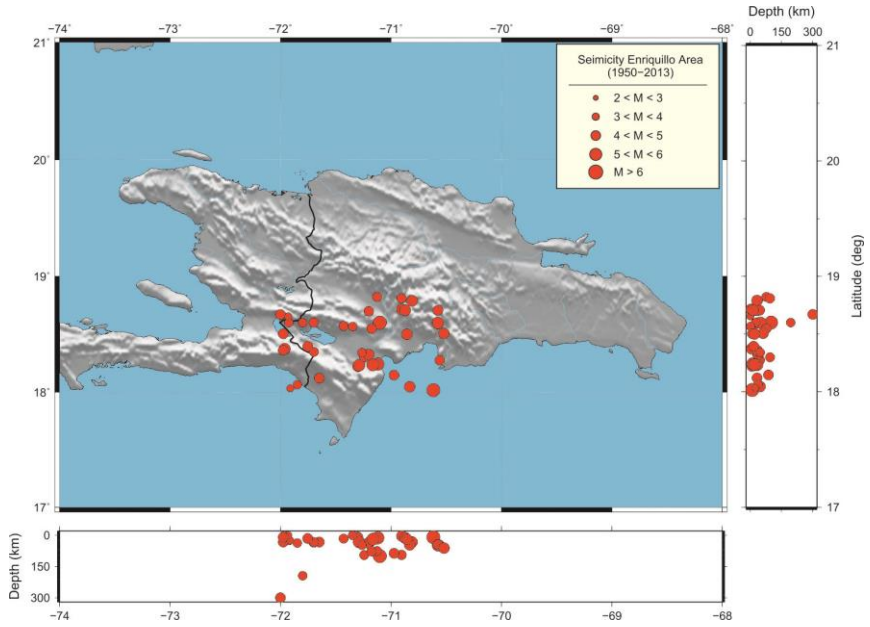

Fig. 4.5.3. Seismicity in the area of Enriquillo-Plantain Garden Fault Zone from 1950 to the present from *ISC catalog online*. Selected area is (18º, 19º) N and (72º, 70.5º) W.

Main features of the Profile F velocity model

The V_P model corresponding to Profile F (Fig. 4.4.2.15) is made of seven seismic layers with increasing velocity in depth. The total length, where seismic information is extracted, is 185 km from the origin of the model.

The crustal velocity model reveals that upper crust consists of two thin sedimentary layers with 1 km thick each, disappearing in Sierra de Martín García area. Basement is located at 4 km depth in the onshore region. The P-wave velocities have been obtained from 3.3 ± 0.1 km/s to 4.5 ± 0.1 km/s.

Middle crust is thicker than previous one and rises to subsurface at 115 km of model distance where Muertos Trough is placed. The velocity changes from 6.5 to 7.6 ± 0.2 km/s in this area. Moho depth is determined at 26 ± 2 km depth in onshore part of the model and increasing towards Bahía de Neiba up to 28 ± 2 km. Then, Moho rises again at 18 ± 1 km due to the presence of Muertos Trough and Beata Ridge, obtaining comparable values with the obtained in the Caribbean Plate. In upper mantle, it is possible to define the deepest layer of the model obtained from wide-angle data that is located at 43 ± 3 km with an average velocity of 8.0 ± 0.3 km/s (Fig. 4.4.2.14).

It is noteworthy that the P-wave velocities obtained in this region are in agreement with those proposed by Driscoll and Diebold (1999). They establish that upper

crustal velocities are commonly around 5.5 km/s, though occasionally, a thin upper layer is detected with velocities from 4.2 to 4.9 km/s. Mid-crustal velocities of 6.6 km/s are typical, and often velocities around 7.1-7.2 km are seen below these. 'Normal' Moho velocities are never seen, but instead, critically refracted energy with velocities between 7.4 and 7.8 km/s appears, corresponding to rays turning at depths below reflection Moho. From James (2007), the Caribbean has 4 km sediment underlain by thicker crust with velocity 6.1 - 6.5 km/s and a major discontinuity below which velocity is 7.4 km/s.

Conclusions

As a synthesis, final conclusions of the study on the crustal structure in the western part of the Dominican Republic set out in this work are enumerated.

- It has established a crustal model for the study area through wide-angle seismic data of LM1N, LM1S and L6 seismic lines and one land shot obtained during the GEOPRICO-DO and CARIBE NORTE projects.
- The cortical models for Profile A and F with NNE-SSW and WNW-ESE directions consists of 8 layers from a seismic point of view grouped in Upper, Middle and Lower Crust and Upper Mantle.
    - Upper Crust is characterized by being the most inhomogeneous part of the model due to the succession of sedimentary basins and mountain ranges crossed by the Profile A. The southern part is characterized by having lateral velocity variations due to the indentation of Beata Ridge whose effect is observable in Middle Crust, while southeastern part is characterized by Upper Crust disappearance in the beginning of Muertos Trough.
    - Middle Crust is thinned in the areas of Cordillera Central, Sierra de Bahoruco and Muertos Trough in the southeast and slightly thickened in the Puerto Plata Basement Complex, Enriquillo-Plantain Garden Fault Zone, and coast of Pedernales in the south.
    - Lower Crust is a homogeneous layer from north part of the model to south coast of Dominican Republic but in the area of Caribbean Sea it is found a lateral velocity variation due to the presence of Beata Ridge.
- The depth of Mohorovicic discontinuity has been determined obtaining that Enriquillo-Plantain Garden Fault Zone reaches depths up to 85 ± 3 km corroborated by seismicity data. In Bahía de Neiba area, Moho rises due to the presence of Muertos Trough.
- In NNE area, Moho and next lower layers have a dip of about 12° thickening towards the interior of the island while this dip is about 6º in the SSW area.

The area where these layers converge is the seismically anomalous zone of Enriquillo-Plantain Garden Fault Zone and could be associated with a detached oceanic slab.

- In the wide-angle seismic data used in this study is not observed structural changes in the area of Septentrional Fault Zone and western flank of Cordillera Septentrional. This fact is confirmed by the seismicity data since the shallower seismicity is associated with the Septentrional Fault while the deepest is associated with the Hispaniola Trench.
- Comparisons with other studies and seismicity data show similarities with the velocity models obtained in this study and show the existence of a possible detached oceanic slab associated to Caribbean Plate.

CHAPTER 5

SEISMIC TRANSECT ACROSS BAHAMAS CARBONATE PLATFORM-DOMINICAN REPUBLIC-MUERTOS THRUST (NE CARIBBEAN PLATE)

Manuscript in preparation (to be submitted)

5.1 INTRODUCTION

The NE Caribbean region marks the tectonic transition between frontal subduction of the NAP beneath the CP in the Lesser Antilles and roughly east-west strike-slip motion along the Cayman Trough [Ali et al, 2008] (Fig. 5.1.1).

The oblique subduction in this area shows a rare example of along-strike transition from a fully partitioned (Hispaniola) to non-partitioned (Puerto Rico) plate motion, in spite of a similar convergence obliquity [Mann et al., 2002; ten Brink and Lin, 2004]. This transition (Fig. 5.1.1) coincides with the subduction of the buoyant Bahamas platform under Hispaniola being the rupture area of the 1946 – 1953 sequence of M7.0 to M8.1 earthquakes [Dolan and Wald, 1998], whereas normal oceanic lithosphere descends beneath Puerto Rico.

South of the eastern Hispaniola and Puerto Rico, Muertos Trough marks the trace of a low-angle thrust fault bounding an acretionary wedge [Byrne et al., 1985]. Studies of seismicity based on the distribution of hypocenter locations in cross-sections, some seismic profiles, reflection profiles and swath bathymetry affirm an active subduction is taking place along the Muertos Trough [Masson and Scanlon, 1991; Dillon et al., 1996; Dolan et al., 1998; Mann et al., 2002; McCann, 2007].

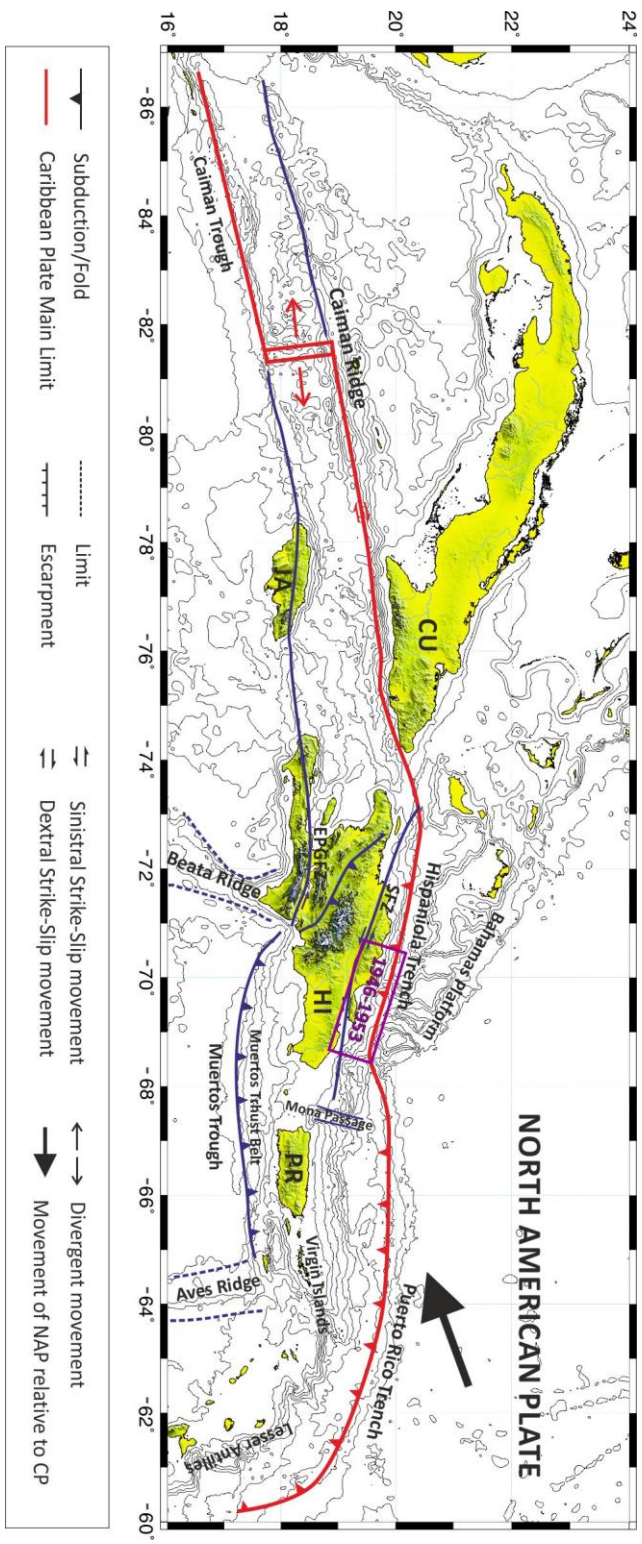

Fig. 5.1.1. Tectonic frame of NE Caribbean border region (modified from Mann et al., 1999). Black arrow shows the relative movement between NAP and CP. Thick red line denotes main limit between both plates. The Greater Antilles islands are represented by CU (Cuba), JA (Jamaica), HI (Hispaniola) and PR (Puerto Rico). SFZ is Septentrional Fault Zone. EPGFZ is Enriquillo-Plantain Garden Fault Zone. Purple rectangle denotes the rupture area of earthquake series of 1946-1953.

Other studies suggest the Muertos thrust belt south of Puerto Rico and eastern Hispaniola is a retrowedge, formed by cross-arc transmission of stress generated by the subduction of the NA plate and by the collision of the Bahamas Platform with Hispaniola [ten Brink et al., 2009; Granja-Bruña et al., 2010].

To study the crustal structure in central Hispaniola, two long seismic profiles from Bahamas Platform to Muertos Trough crossing Hispaniola Island have been studied in this chapter (Profiles B and C) (Fig 5.3.1), using seismic data provided by GEOPRICO-DO and CARIBE NORTE projects.

5.2 GEOLOGY AND TECTONIC SETTING

The WSW to SW oblique collision between the continental margin of NAP and Greater Antilles island-arc system of CP determines the NE Caribbean plate boundary where Hispaniola and Puerto Rico Islands area is limited by active subduction in the north and a probable subduction zone associated to Muertos Trough in the south. Today, this oblique convergence is partitioned between plate-boundary-parallel motion on the Septentrional and Enriquillo strike-slip faults in the overriding plate, and normal motion at the plate interface in the offshore low-angle subduction thrusts of the northern Hispaniola fault and Los Muertos trench [Mann et al., 2002; Manaker et al., 2008].

The on-land geology of Hispaniola in the eastern Greater Antilles is complex (Fig. 5.2.1). A Cretaceous to early Eocene arc assemblage consisting of acretionary prism sediments, volcanic arcs and intrusive, and ophiolites forms the basement of Hispaniola. Eocene and younger clastics and carbonates have accumulated over this arc-assemblage basement. Central Hispaniola is a composite of oceanic derived units bound by the left-lateral strike-slip Hispaniola (HFZ) and San José-Restauración (SJRFZ) fault zones [ten Brink et al., 2009].

In this section, geological and tectonic areas that are crossed by Profile B and C (Fig. 5.3.1) are described.

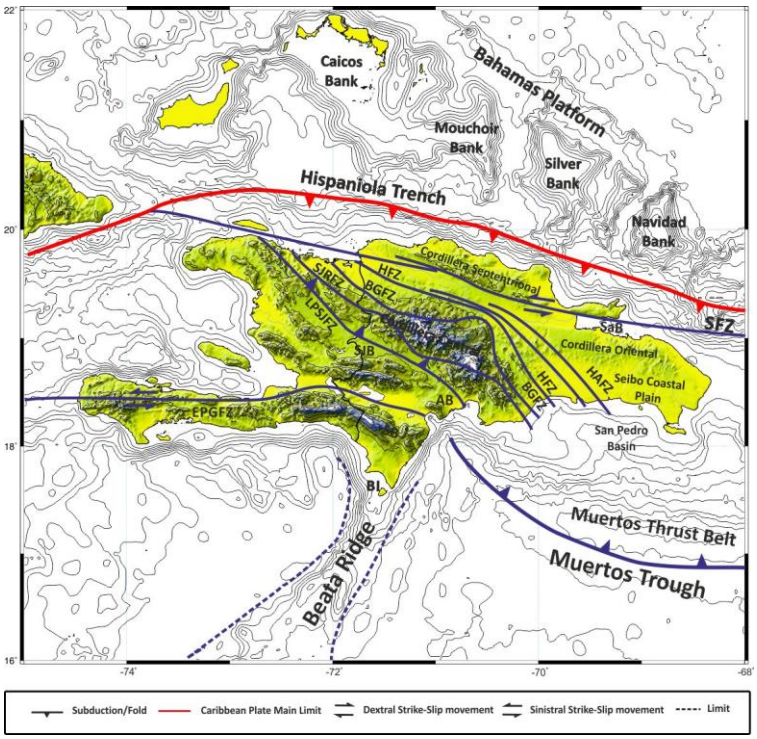

Fig. 5.2.1 Schematic tectonic frame of Hispaniola Island with main tectonic and geologic features in studied area (modified of Mann et al., 1991). BI = Beata Island; SB = Sierra de Bahoruco; SaB = Samaná Bay; SJB = San Juan Basin; AB = Azúa Basin; SFZ = Septentrional Fault Zone; EPGFZ = Enriquillo-Plantain Garden Fault Zone; LPSJFZ = Los Pozos – San Juan Fault Zone; SJRFZ = San José – Restauración Fault Zone; BGFZ = Bonao – La Guacara Fault Zone; HFZ = Hispaniola Fault Zone; HAFZ = Hatillo Fault Zone.

- Regional Setting

The area that concerns the study presented in this chapter occupies central and eastern onshore part of Dominican Republic and offshore surrounding areas located at north and south. In this spacious area, it is possible to identify different tectonic and geological structures. The northern offshore area corresponds to Bahamas Platform, specifically with Silver and Navidad Banks (Fig. 5.2.1). Onshore, eastern Cordillera Septentrional and Samana Peninsula are separated from eastern Cibao Basin and Samana Bay by the Septentrional Fault Zone (SFZ) followed by Los Haitises Fm (Fig. 5.2.2). The central Hispaniola is a complex region whose main tectonic structure is Cordillera Central. In this area also appear different formations and geological zones as Maimón Fm., Loma Caribe Peridotite, Duarte Complex, Tireo Group or Peralta fold and thrust belt separated by Hatillo (HAFZ), Hispaniola (HFZ), Bonao – La Guácara (BGFZ) and San José – Restauración (SJRFZ) Fault Zones (Fig. 5.2.1, 5.2.2). Nevertheless, the eastern Hispaniola is characterized by simpler structures (Cordillera Oriental and Seibo coastal plain) without significant faults. The

southern offshore area corresponds to San Pedro Basin and the north slope of Muertos Through and thrust belt.

Silver and Navidad Banks

North of Silver Bank (Fig. 5.2.1) there is a large (~ 5000 km^2), deep-water (3000-4000 m) plateau that records the drowning and step-back (~ 50 km) of an Early Cretaceous carbonate platform margin. South of Navidad and Silver banks result in part from the accretion of a portion of the Bahamas onto Hispaniola. Extensional stress along the normal faults, which caused the platform margin to retreat, along this transpressive plate boundary may be a consequence of rotation of the nearby Puerto Rico block or lithospheric bending during oblique subduction.

Navidad Bank (Fig. 5.2.1) is the southeastern-most carbonate platform in the Bahamas located at the western end of the Puerto Rico Trench (Fig. 5.2.1). Bathymetry data reveal a very complex seafloor morphology that shoals to the west. The collision of Navidad and Silver banks with Hispaniola has segregated the Hispaniola Basin to the west from the Navidad Basin and Puerto Rico Trench. Cluster of earthquake epicenters occur offshore Hispaniola where Silver Bank and Navidad Bank indent the northern margin of Hispaniola [Mullins et al., 1992].

Central Hispaniola and Samaná Complex

In northern Hispaniola, the Cordillera Septentrional-Samaná Peninsula domain is composed of arc, oceanic and continental margin derived units assembled during arc-continent convergence. The Río San Juan complex contains a segment of the Caribbean subduction-acretionary complex [Escuder-Viruete et al., 2013] and marks the position of the exhumed subduction channel [Krebs et al., 2008].

The geology of Samaná complex (Fig. 5.2.2) consists of mainly stratiphicated metamorphic complex [Escuder-Viruete et al., 2011]. The whole Samaná Peninsula is deformed by a system of sinistral strike-slip and reverse faults associated with the earliest Miocene to Present movement along the SFZ [Mann et al., 2002].

Central Hispaniola is a composite of oceanic derived units bound by the left-lateral strike-slip Hispaniola and San José – Restauración Fault Zones (Fig. 5.2.1). To the north of HFZ, the Maimón Fm forms a NW – trending belt of schists separating the Los Ranchos Fm, the Hatillo Limestones, the Late Cretaceous Las Lagunas Fm and, part of the Loma Caribe Peridotite (Fig. 5.2.2). To the south of HFZ, Central Hispaniola domain is also bounded by the Hato Mayor Fault Zone, and comprises the Loma Caribe Peridotite, the Río Verde Complex, and the Peralvillo Sur Formation [Escuder-Viruete et al., 2010].

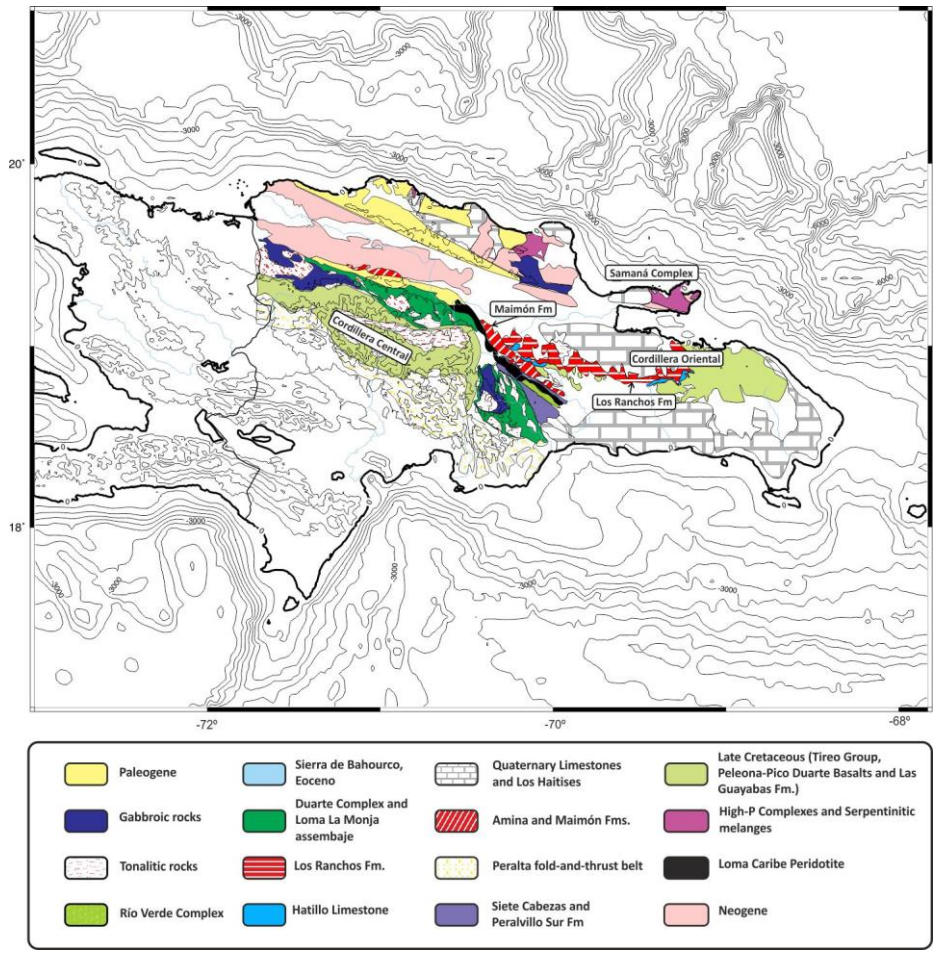

Fig. 5.2.2 Schematic geological map of the studied area in Central and Eastern Hispaniola (based on Escuder-Viruete et al., 2006; Escuder-Viruete et al., 2011 and Braga et al., 2012).

The Peralvillo Sur Fm (Fig. 5.2.2) forms a narrow belt immediately northeast of the Loma Caribe Peridotite. It is composed of a 1500-2300 m thick basaltic sequence of lavas and is overlain by 1000 m of sediments [Lewis et al., 2002].

The Río Verde Complex (Fig. 5.2.2) forms a NW-trending belt of 4-5 km width and 25 km length, with a strongly deformed contact against the Loma Caribe Peridotite. In the lower structural levels and to the SW, it is composed of a 1500-2500 m thick basaltic sequence of massive flows and is overlain by 1000 m of sedimentary rocks [Escuder-Viruete et a., 2010].

To the south, Duarte Complex (Fig. 5.2.2) comprises a 3 km thick sequence of heterogeneously deformed igneous rocks and represents the remnants of the proto-Caribbean plateau generated around 150 Ma by a Galápagos-type hot spot. This

complex consists of several WNW-trending blocks bounded by strike-slip faults [Escuder-Viruete et al., 2007].

Finally, the Peralta Belt is a thick pile of Paleogene deposits that define the southern flank of the Cordillera Central. This domain developed as a NW-SE fold and thrust belt which progressed to the SW until overthrusting the San Juan basin by means of the SJLPFZ (Fig. 5.2.1), producing at the same time the general folding of this basing [Hernáiz-Huerta et al., 2002]. Tireo Fm is turn overthrusts the Peralta Belt by means of the SJRFZ. The structure of the Peralta belt was modified by the effect of the NE directed impingement of the Beata Ridge, that produced the present pattern of the belt, and the E-W strike-slip faults related to the evolution of the Enriquillo-Plantain Garden fault zone [Dolan et al, 1991].

Eastern Hispaniola

The northern zone is a karstic region, largely covered by Los Haitises National Park (Fig. 5.2.2), limited to the north by the Yuna River valley and Samaná Bay (Fig. 5.2.1). The area east and south of the Cordillera Oriental is mainly occupied by the generally flat region called the Llanura Costera del Caribe, extending to the southeastern end of the Cordillera Central near Santo Domingo [Braga et al., 2012].

The Cordillera Oriental is an antiformal structure with igneous rocks in its core. The Cordillera Central basement is separated from the Cordillera Oriental by the Hatillo Thrust [Mann et al., 1991, Escuder Viruete et al., 2002]. Located in the Cordillera Oriental, Los Ranchos Fm (LRF) is part of the oldest and chemically most primitive island arc in the Caribbean Basin [Lewis et al., 2002] and comprises a >3 km thick sequence of volcanic and volcaniclastic rocks [Escuder-Viruete et al., 2006].

The eastern area of Hispaniola consists of Seibo and Oro terrain according to Mann et al., (1991). The Oro terrain consists of a highly folded 1500 m thick section of volcaniclastic sedimentary rocks with minor limestones.

San Pedro Basin and Muertos Trough

The San Juan-Azúa-San Pedro Basin (Fig. 5.2.1) can be considered as an acretionary belt between the island's northern arc-complex and its southern oceanic terrain, which became merged by sinistral transpression during the Eocene to Early Miocene interval. The Muertos Trough acretionary prism bounds the southern San Pedro Basin [Pindell, 1991].

Southern to San Pedro Basin, the boundary between the thrust system and the exposed floor of the Caribbean plate is a linear depression known as the Muertos Trough [ten Brink et al., 2009]. The Muertos thrust belt forms the southern margin of Hispaniola and Puerto Rico. This EW-trending trough is a depression of 650 km long

slightly concave to the north and runs from The Beata Ridge in the west to the insular slope of the Aves Ridge in the east [Case and Holcombe, 1980] (Fig. 5.1.1)

5.3 DATA

In this chapter, seismic data acquires north and south of eastern Dominican Republic as a part of the Geoprico-DO and Caribe Norte cruises are presented [Carbó et al., 2005; Carbó et al., 2010].

The study area (blue triangle in Fig. 5.3.1) was registered during GEOPRICO-DO project (2005) by ten land seismic portable stations along NE – SW Profile G, which record marine shooting line L7, from Ocoa Bay to Bonao region and ten seismic stations along Profile H from San Pedro de Macorís to Sabana de la Mar recording marine line L8 in with an orientation N – S. During CARIBE NORTE project (2009) two profiles (B and C) were deployed in same directions of previous profiles to complete the seismic information on land and at sea. Profile B is made of 58 land seismic stations from Ocoa Bay to Nagua and 4 OBS (OBS 1, OBS 2, OBS 3 and OBS 4) located in the study area northern part. Profile C consists of 39 one component land seismic portable stations from San Pedro de Macorís to north area of Samaná Peninsula, two three-components seismic stations in Hato Mayor and Samaná, and five OBS (OBS 5, OBS 6, OBS 7, OBS 8 and OBS 9) anchored in San Pedro basin and north slope of Muertos Trough. The seismic data along these four profiles have been combined to obtain two crustal velocity models along NE – SW and N-S directions named as Profile B and C.

The seismic sources used in Profile B have been one land borehole explosion (S2) and two marine deep seismic sounding lines (L7 and LM3N) while in Profile C have been one borehole explosion (S1) and three marine lines (L8, LM3N and LM3S). Table 5.3.I summarized the main features of these lines.

	Total time length	# Shots	Distance (km)
LM3N	17.1 h	683	146.6
LM3S	20.9 h	832	170.3
L7	12.0 h	482	99.9
L8	13.4 h	538	117.7
TOTAL	63.4 h	2535	534.5

Table 5.3.I. Dominican Republic seismic profiles summary in GEOPRICO-DO and CARIBE NORTE projects used in this chapter.

Seismic energy propagation across the crust and Upper Mantle was registered for a maximum distance of 270 km.

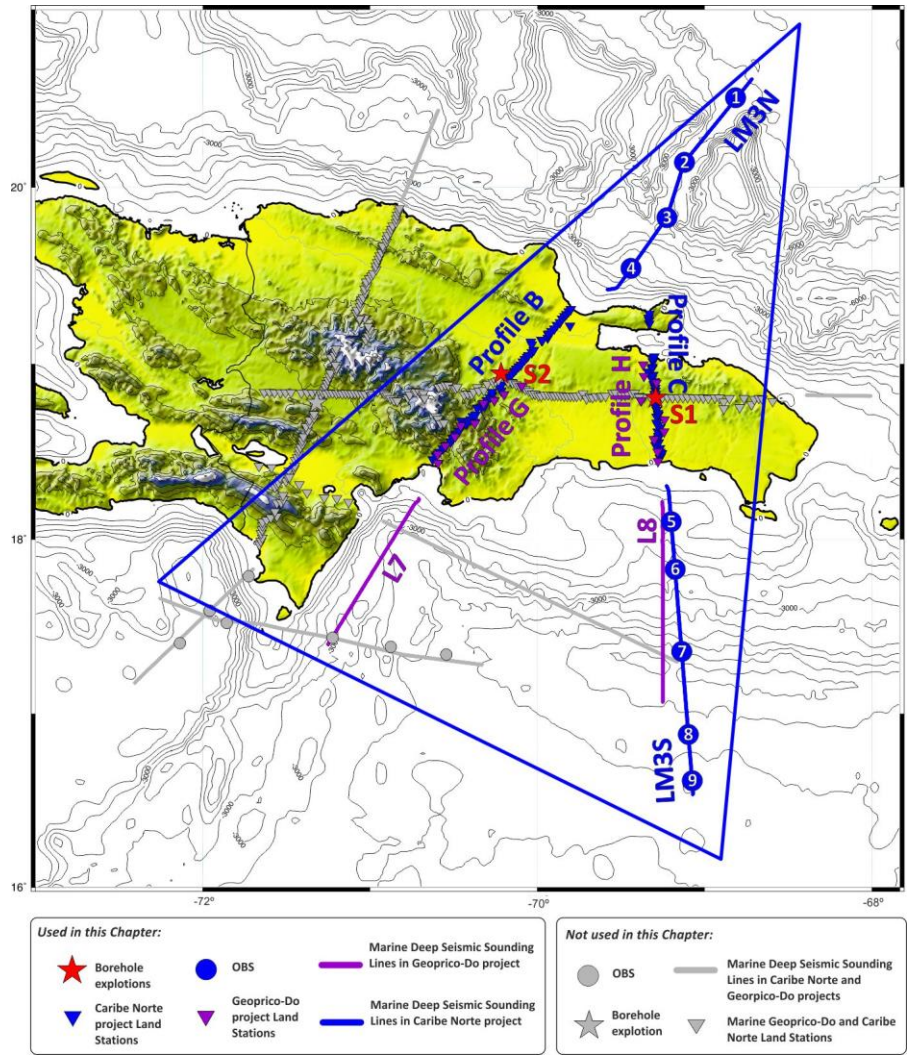

Fig. 5.3.1 Deployment map with stations and seismic sources used in this chapter and all stations deployed during Caribe Norte and GEOPRICO-DO projects (grey symbols). Blue triangle represents the study area.

5.4 INTERPRETATION

Data processing allowed obtaining seismic record sections whose interpretation has provided the travel times and distances to elaborate Profile B and C velocity models. This interpretation consisted of determining the P-wave phases observed in each

seismic record section and their corresponding apparent velocities. Subsequently, ray tracing models and synthetic seismograms have been made to finally obtain the velocity models corresponding to these profiles.

5.4.1 Seismic record sections and Correlation Data

In the seismic record sections obtained from Profiles B and C seismic data, it was possible to identify time correlations corresponding to P-wave refractions and reflections in crust and upper mantle discontinuities. Each phase is assigned a color and a code with subscripts, which represent the layer relative position respects to subsurface (*See Table 2.5.I, Section 2.5, Chapter 2*).

- Profile B

Profile B (Fig. 5.3.1) is 450 km length from Navidad and Silver banks (Fig. 5.2.1) region to offshore southern area of Dominican Republic. Main tectonic features of this profile have been expounded on section 5.2 of this chapter, while its interpretation has been carried out using different seismic sources (marine and land sources). Marine sources correspond to two marine shooting lines, LM3N and L7, obtained during Caribe Norte and GEOPRICO-DO projects, respectively. Land source used in this profile is a borehole explosion situated in the central part of the island (S2).

Marine Sources

The region between Navidad and Silver banks (Fig. 5.2.1) has been studied by four OBS deployed along seismic line LM3N (Fig.5.3.1). OBS1 is the farthest marine station located at 16 km from origin of marine line LM3N. P-wave phases observed in seismic record section corresponding are shown in Fig. 5.4.1.1 and Fig. 5.4.1.2, where a detail of the NE part of that record is shown. Southwestern to the position of the OBS, a reflected phase, P_3P, on the third discontinuity is found. This phase is observed between an offset of 6 and 31 km and followed by P_MP up to 65 km. The deepest phase observed for this seismic record section corresponds to $P_{10}P$ and is interpreted from 71 to 97 km offset. To the NE, the first phase observed in the Fig. 5.4.1.2 is P_3P and it is possible to correlate it from 5 to 12 km. This phase is followed by the reflected phase in Moho (P_MP) from 9 to 16 km.

In the northern area of Profile B (Fig. 5.3.1), B55 land station is located at 31 km from the beginning of seismic line LM3N (Fig. 5.4.1.3). First P-wave train identified is P_4'. This phase travels through the discontinuity below layer 4 from 35 km to 39 km with an a.a.v of 4 km/s. Next phase is a reflected phase over layer 8 discontinuity, P_8P, observed from 48-64 km. In the figure 5.4.1.3, P_9P is correlated between 105 to 137 km and $P_{10}P$ from 98 to 145 km. The deepest phase identified in this seismic record section corresponds to $P_{11}P$ followed between 133 km and 189 km.

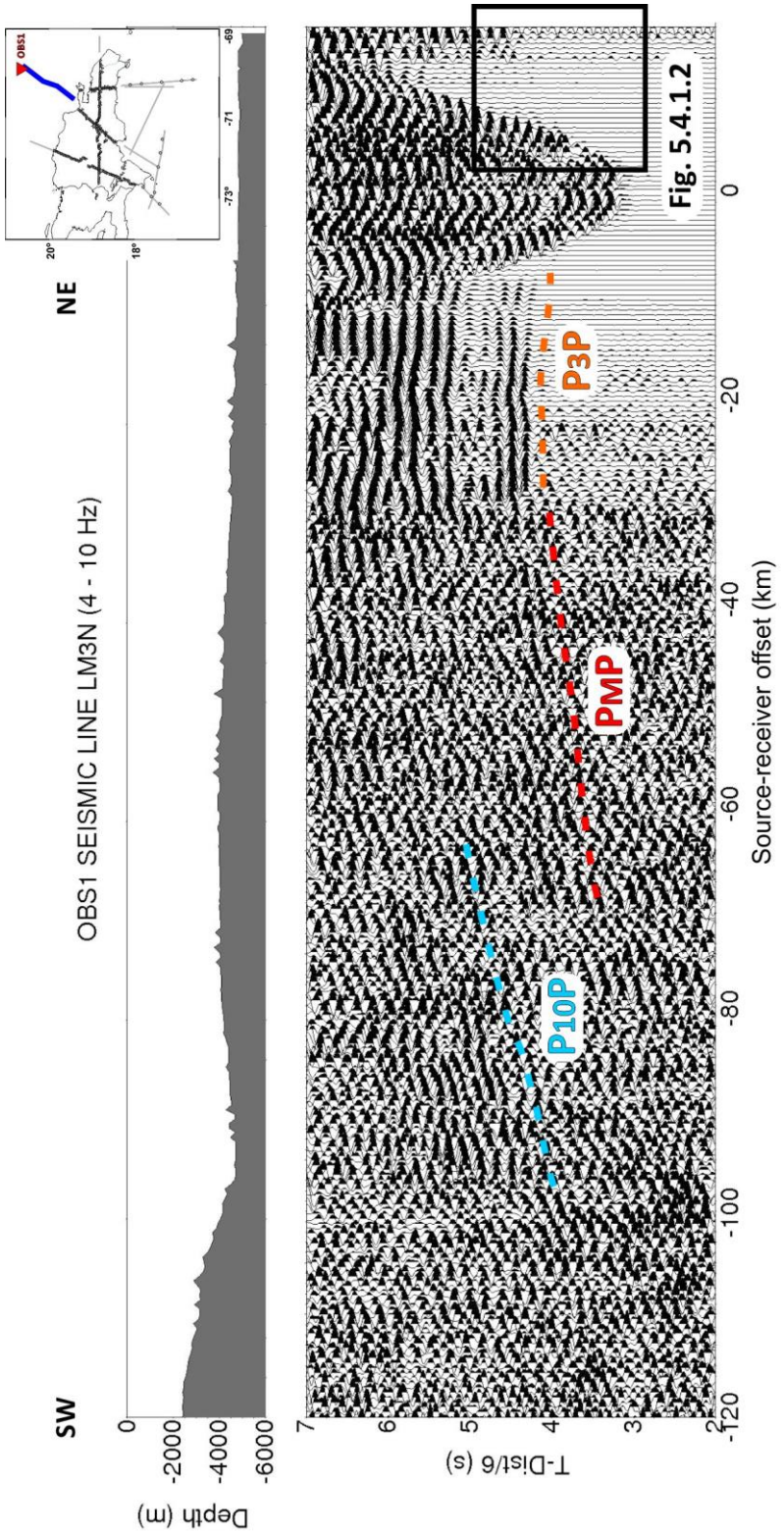

Fig. 5.4.1.1 Seismic record section corresponding to OBS 12 registering seismic line LM3N. Colored lines point out reflected/refracted P-wave trains. In this figure vertical component and bathymetry along this lines over this section are shown. In the upper right corner red triangle shows location of registration point and blue line the marine seismic line. Reduction velocity is 6 km/s, band-pass filtering of 4 – 10 Hz and amplitudes-trace normalized.

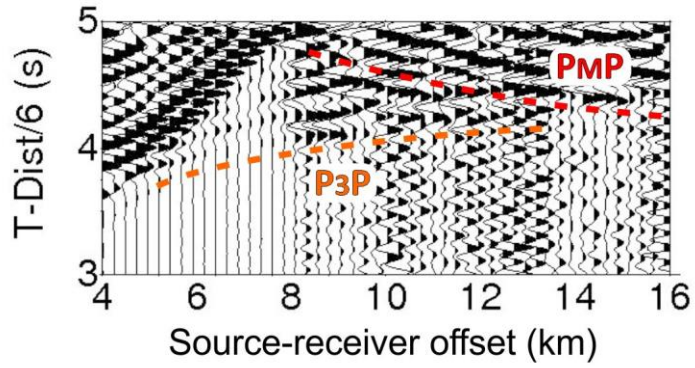

Fig. 5.4.1.2 Enlargement of NE part seismic record section of OBS 1.

Marine seismic line located south of the island was recorded by land stations deployed during GEOPRICO project (*Section 1.4.1, Chapter 1*). Figure 5.4.1.4 shows the seismic record section of the farthest stations that records line L7, land station L7H. The most superficial phase observed in this figure corresponds to P_3' and is followed from 78 to 95 km with an a.a.v of 3.3 km/s. Next phase is a head wave that travels through discontinuity between fourth and fifth layer, P_4', with 4.5 km/s of a.a.v between 83 km and 115 km. This phase is in a forward position from 80 km and 83 km that could be related with any fault of the upper front of Muertos Trough. Last P-wave phase is P_7P correlated from 115 to 185 km.

In southern onshore region of the Profile B (Fig. 5.3.1), L7D is situated at 45 km from the beginning of the seismic line L7 (Fig. 5.4.1.5). The seismic record section corresponding to this station also shows that phase P_3' is ahead from 47 to 73 km with 3.9 km/s of a.a.v. This phase is followed by P_4' determined between 73 to 107 km of source-receiver offset with an a.a.v. of 7.7 km/s. The deepest P-wave phases observed in figure 5.4.1.5 correspond to reflected phases in layers 8, 9 and 11. P_8P and P_9P are followed between 107 km to 147 km and 124 to 148 km while $P_{11}P$ is found from 138 to 153 km with similar amplitudes as P_9P or P_8P.

At 129 km to first trace of seismic line LM3N (Fig. 5.3.1), B9 is situated in the region of Peralta fold-and-thrust belt (Figs. 5.2.2 and 5.3.1). The B9 seismic record section is shown in figure 5.4.1.6 where the most superficial phase correlated from 134 km to 146 km corresponds to P_4' with 4.0 km/s of a.a.v. This phase is followed by a reflected phase over discontinuity of layer 8, P_8P, between 146 km and 173 km offset. After, it is possible to identify P_9P phase that is correlated from 170 km to 204 km. The deepest phases observed in the seismic record section correspond to $P_{10}P$ and $P_{11}P$ phases, interpreted in an offset interval of 179-235 km and 179-253 km, respectively.

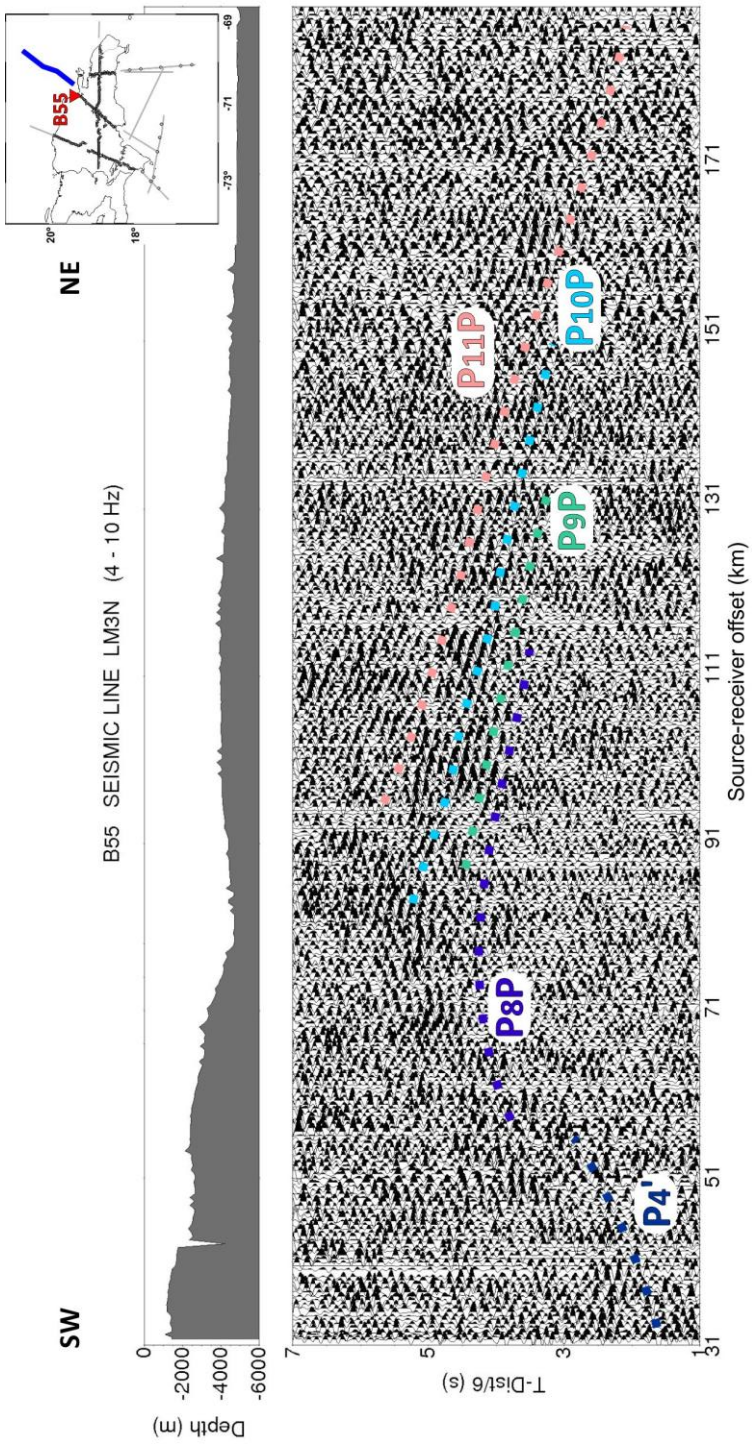

Fig. 5.4.1.3 LM3N seismic transect record, station B55. Vertical component, velocity reduction is 6 km/s, amplitude-trace normalized and band-pass filtering of 4 – 10 Hz. Colored lines point out reflected/refracted P-wave trains. On the top, bathymetry along this line. In the upper right corner, red triangle shows location of registration point and blue line the marine seismic line.

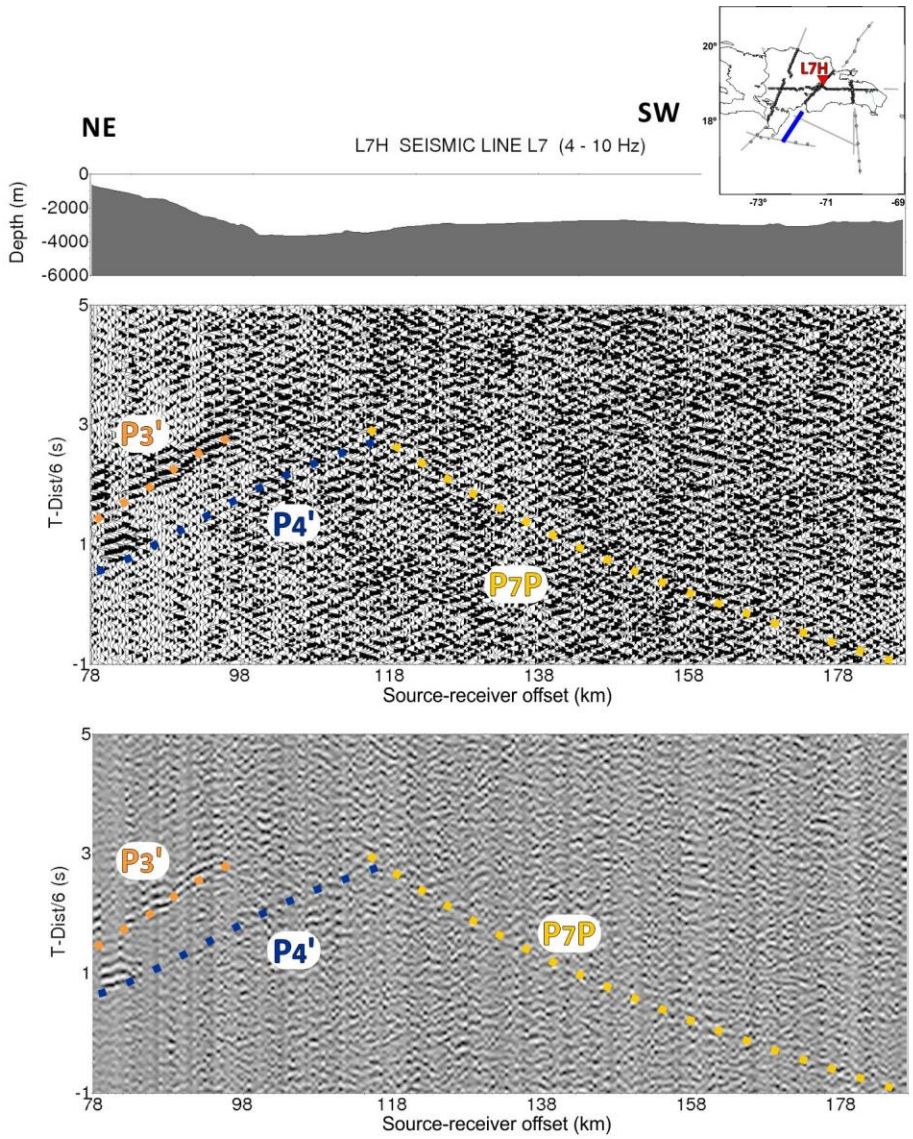

Fig. 5.4.1.4. L7 seismic transect record, station H. Vertical component, velocity reduction is 6 km/s, amplitude-trace normalized and band-pass filtering of 4 – 10 Hz. Colored lines point out reflected/refracted P-wave trains. On the top bathymetry along this line and registering point location map where red triangle shows the station situation and blue line the marine shooting line. Below, seismic record section in greyscale with correlated phases.

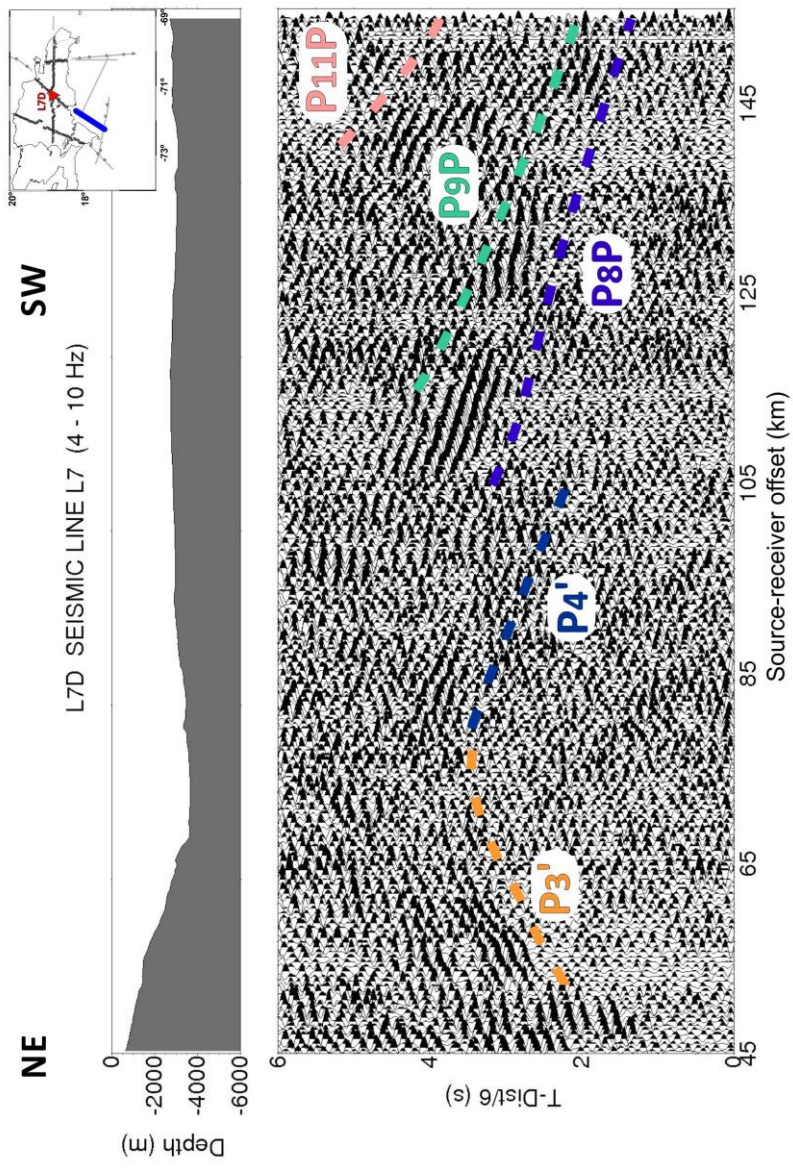

Fig. 5.4.1.5. L7 seismic transect record, station D. Vertical component, velocity reduction is 6 km/s, amplitude-trace normalized and band-pass filtering of 4 – 10 Hz. Colored lines point out reflected/refracted P-wave trains. On the top, bathymetry along this line and registering point location map where red triangle shows the station situation and blue line the marine shooting line.

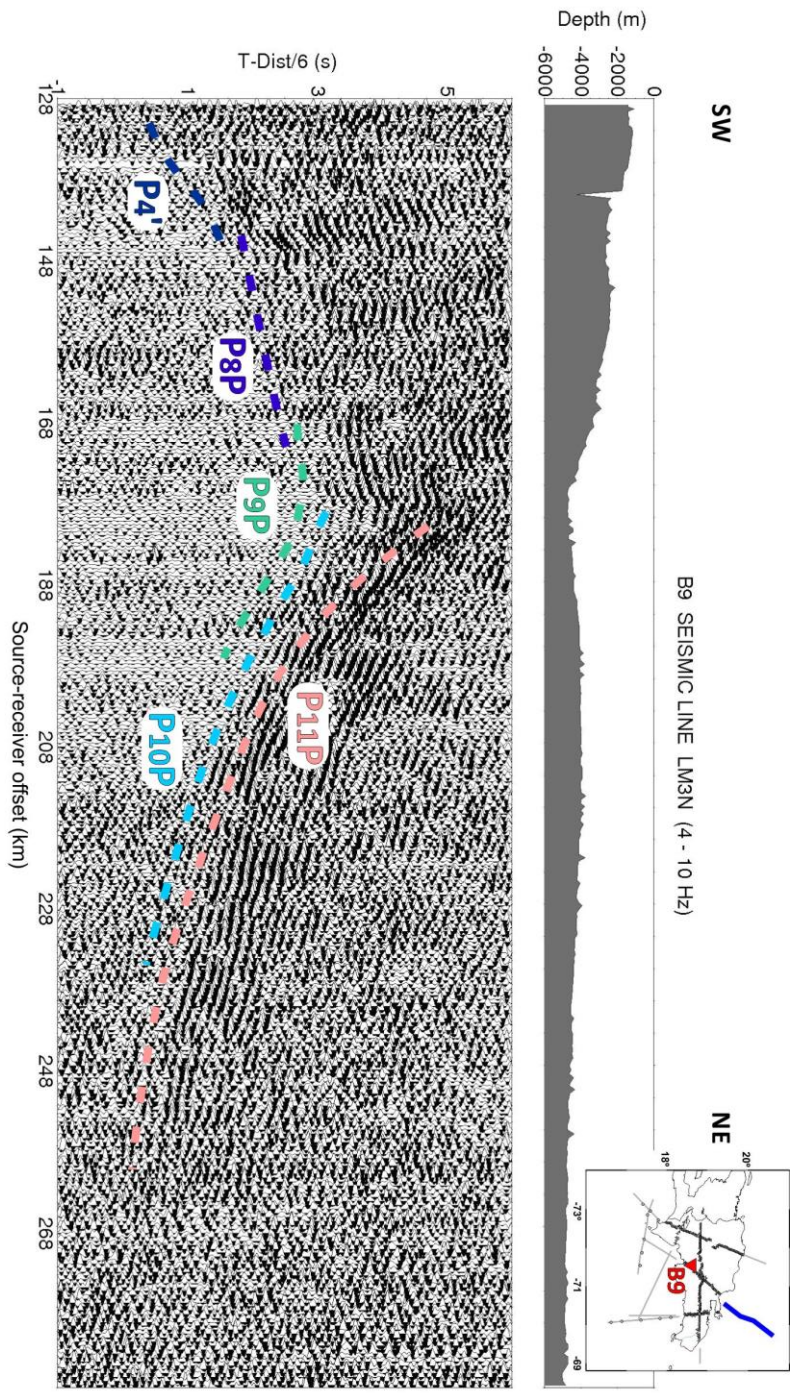

Fig. 5.4.1.6. Seismic record section corresponding to station B9 registering seismic line LM3N. Colored lines point out reflected/refracted P-wave trains. In this figure vertical component and bathymetry along this lines over this section are shown. In the upper left corner red triangle shows location of registration point and blue line the marine seismic line. Reduction velocity is 6 km/s, band-pass filtering of 4 – 10 Hz and amplitudes-trace normalized.

Land Source

One of the seismic sources used in Profile B has been land shot S2 located near Cotui (Fig. 5.3.1) and registered by land stations deployed along Profile B. Due to the shot point is located between Hatillo limestones, Los Ranchos and Maimón Fms. areas (Fig 5.2.1), the seismic signal was not registered far from the borehole and the signal – noise ratio is higher than other seismic record sections corresponding to shot S1 and S3. Figure 5.4.1.7 shows the seismic record section obtained from shot point to NE where a head wave travelling through discontinuity between second and third layers, P_2', has been interpreted in an offset range of 7 to 28 km whose a.a.v is 5.5 km/s. In the figure 5.4.1.8, seismic record section from shot to SW is shown where a P_4' is correlated between 7 and 56 km offset with 6.2 km/s of a.a.v.

- Profile C

The seismic data of Profile C come from Caribe Norte and GEOPRICO-DO projects (*see Sections 1.4.1 and 1.4.2, Chapter 1*). Total length of this N – S profile is 350 km between Navidad and Silver Banks (Bahamas Platform) and northern flank of Muertos Trough (Fig. 5.3.1). Main tectonic elements crossed by this transect are presented in section 5.2 of this chapter. Different seismic sources have been used for the interpretation of this profile being mainly marine shooting lines LM3S and L8. Due to the oblique direction of marine seismic line LM3N respect to the profile, this seismic lines has not been used for determining crustal velocity model of Profile C, but there are some shots that are aligned with the profile. These shots provide information on the northern part of the profile, and land stations along Profile C register them. These stations also recorded one land shot, S1.

Seismic shooting lines

The area of Muertos Trough and San Pedro Basin has been studied with five OBS anchored in this area. One of these marine stations is OBS 9 located at 188 km from first shot of line LM3S being the station farthest from the southern coast of Dominican Republic. The seismic record section corresponding to this station is shown in figure 5.4.1.9. First arrivals of this section are head waves that travel through discontinuity between third and fourth layers on both sides of the OBS position. To the south, this phase is correlated between 7 km and 9 km of short offset with an a.a.v of 5.2 km/s while to the north, it is found between 8 and 25 km with a slightly lower a.a.v whose value is 4.6 km/s. The following P-wave phase interpreted in this seismic record section is P_7P and is followed from 11 to 35 km offset. Deepest phase observed corresponds to P_9P. The offset interval for this phase is 29 km to 76 km.

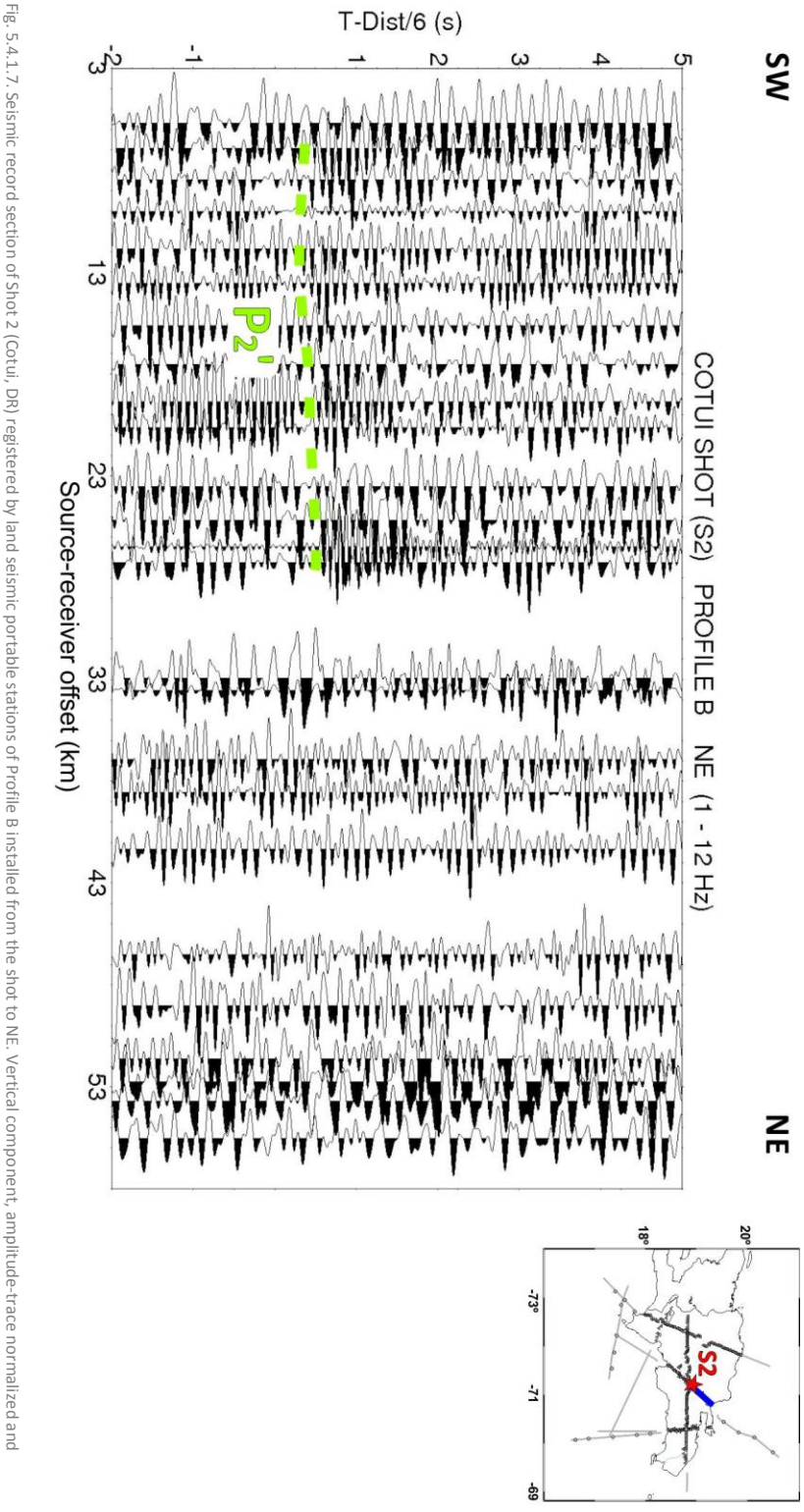

Fig. 5.4.1.7. Seismic record section of Shot 2 (Cotui, DR) registered by land seismic portable stations of Profile B installed from the shot to NE. Vertical component, amplitude-trace normalized and band-pass filtering of 1 – 12 Hz. Colored lines point out reflected/refracted P-wave trains. On the top, shot point in red and blue line shows the stations that record this shot.

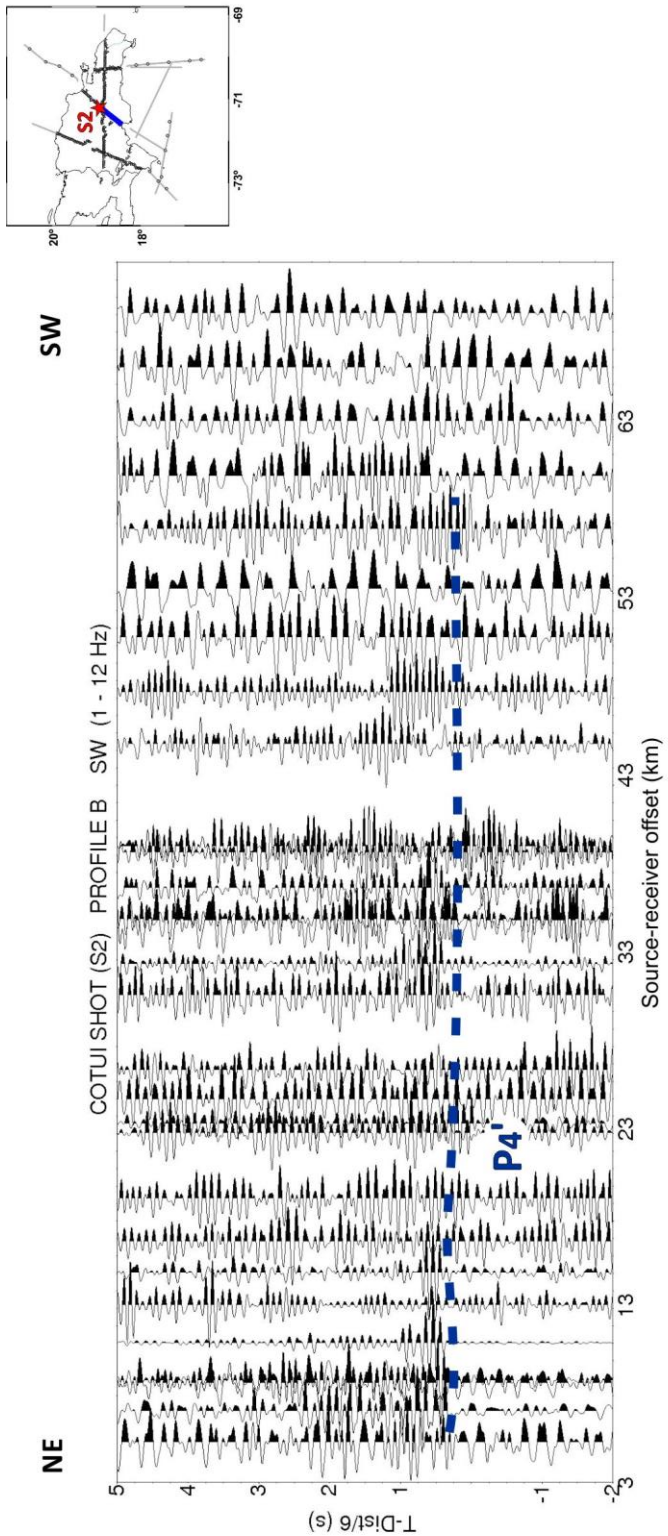

Fig. 5.4.1.8. Seismic record section of Shot 2 (Cotuí, DR) registered by land seismic portable stations of Profile B installed from the shot to SW. Vertical component, amplitude-trace normalized and band-pass filtering of 1 – 12 Hz. Colored lines point out reflected/refracted P-wave trains. On the top, shot point in red and blue line shows the stations that record this shot.

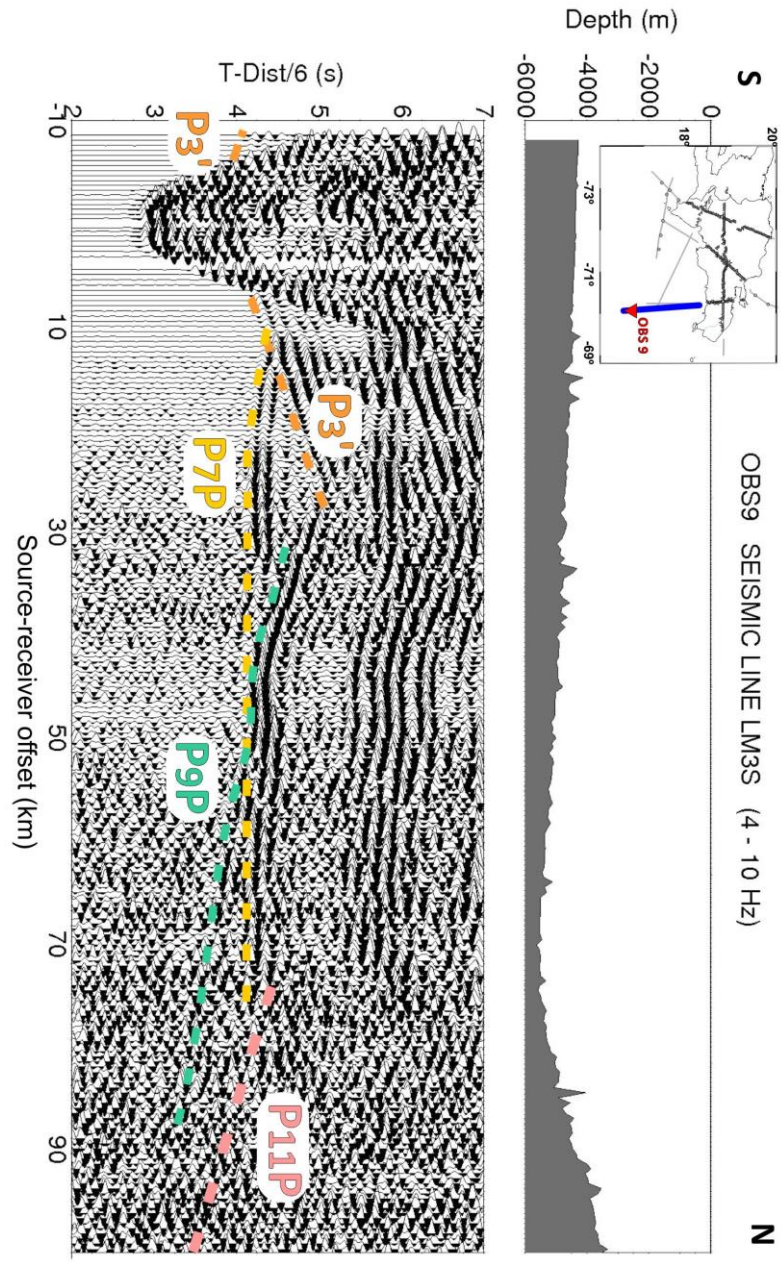

Fig. 5.4.1.9. Seismic record section corresponding to OBS 9 registering seismic line LM3S. Colored lines point out reflected/refracted P-wave trains. In this figure vertical component and bathymetry along this line over this section are shown. In the upper left corner red triangle shows location of registration point and blue line the marine seismic line. Reduction velocity is 6 km/s, band-pass filtering of 4 – 10 Hz and amplitudes-trace normalized.

Located at the Llanura Costera del Caribe (Fig. 5.3.1), land station L8D registered the marine seismic line L8 obtained during GEOPRICO-DO project. This station is located 44 km from the northernmost point of the line. The figure 5.4.1.10 shows the seismic record section corresponding to this station. The first P-wave phase identified in the figure is P_3' from an offset range between 44 and 59 km and the a.a.v. is 4.1 km/s. This phase is followed by a reflected phase over seventh discontinuity, P_7P, interpreted from 62 to 84 km. Next phases are P_8P and P_9P, which can be correlated from 83 km to 96 km and from 98 km to 125 km offset. The deepest phase shown in this seismic record section is $P_{10}P$ whose offset interval is 124-171 km.

Land station C21 (Fig. 5.4.1.11) was set up close to the location that land station L8H (Fig. 5.4.1.12) had during GEOPRICO-DO project to calibrate the observations made and improve the data quality due to the improvement in the shooting power. The separation between both stations was 1.5 km. C21 land station is located 57 km from first shot of marine shooting line LM3S. The phase interpretation in both seismic record sections has reported the same observed P-phases, as might be expected. As example, C21 seismic record section is shown in figure 5.4.1.11, where it is possible to correlate the first phase between 57 km and 82 km of source-receiver offset and interpret as a head wave that travels through Moho discontinuity, P_n, with an a.a.v of 4.8 km/s. From 80 km to 105 km offset range, P_7P is followed while P_8P is determined between 102 km and 124 km. The deepest phases observed in this figure correspond to $P_{10}P$ and $P_{11}P$. The offset interval of both phases is 114-134 km and 129-195 km, respectively.

Last seismic station set up in the profile H was L8H. The distance from first shot of marine line L8 is 75 km. The seismic record section of L8H (Fig. 5.4.1.12) shows similar phases being the first one corresponding to P_n phase whose offset interval is 77-90 km and a.a.v of 5.1 km/s. Following phase is interpreted as P_7P between 91 km and 111 km as it is shown in Fig. 5.4.1.12, while P_8P is observed from 112 km to 125 km. $P_{11}P$ is the deepest phase determined in this seismic record section. The arrivals of this phase are found between 131 km to 172 km of distance.

In Samaná Peninsula, some land stations were deployed during CARIBE NORTE project. Most of them did not report useful information due to high noise/signal ratio but the seismic record section of C37 shows some correlations. This seismic record section is presented in figure 5.4.1.13, where all observed arrivals correspond to reflected phases over discontinuities of eighth, ninth and eleventh layers (P_8P, P_9P and $P_{11}P$, respectively). The offset intervals for these P-wave phases are: 104-112 km for P_8P, 122-144 km for P_9P and 164-206 km for $P_{11}P$.

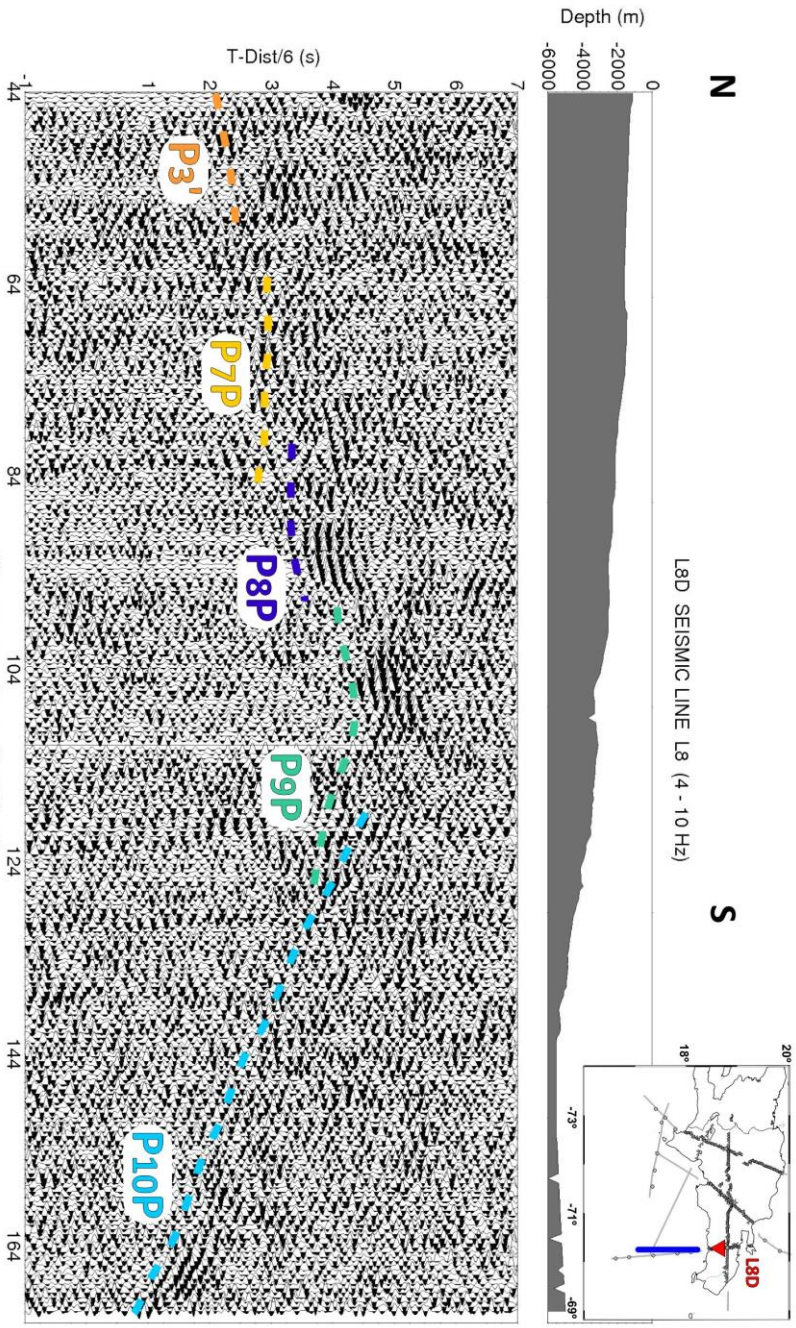

Fig. 5.4.1.10. L8 seismic transect record, station D. Vertical component, velocity reduction is 6 km/s, amplitude-trace normalized and band-pass filtering of 4 – 10 Hz. Colored lines point out reflected/refracted P-wave trains. On the top, bathymetry along this line and registering point location map where red triangle shows the station situation and blue line the marine shooting line.

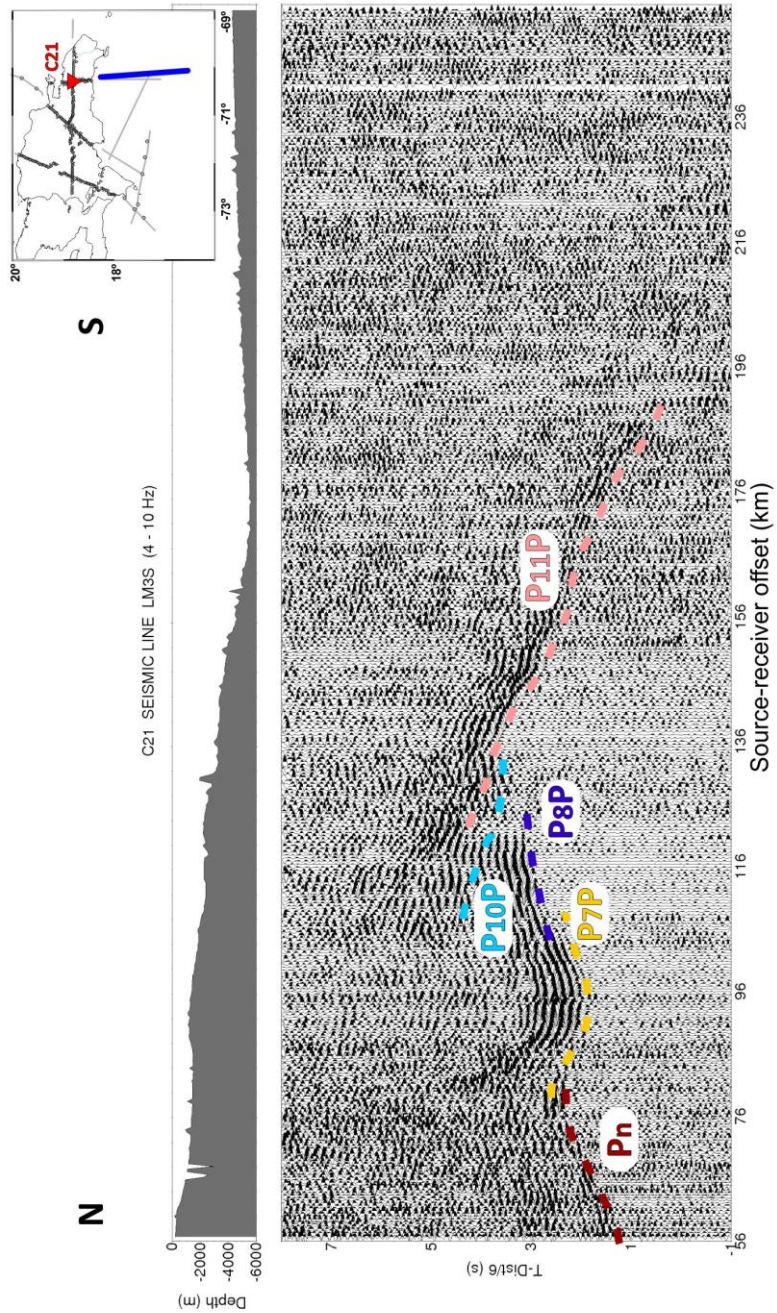

Fig. 5.4.1.11. Seismic record section corresponding to station C21 registering seismic line LM3S. Colored lines point out reflected/refracted P-wave trains. In this figure vertical component and bathymetry along this lines over this section are shown. In the upper left corner red triangle shows location of registration point and blue line the marine seismic line. Reduction velocity is 6 km/s, band-pass filtering of 4 – 10 Hz and amplitudes-trace normalized.

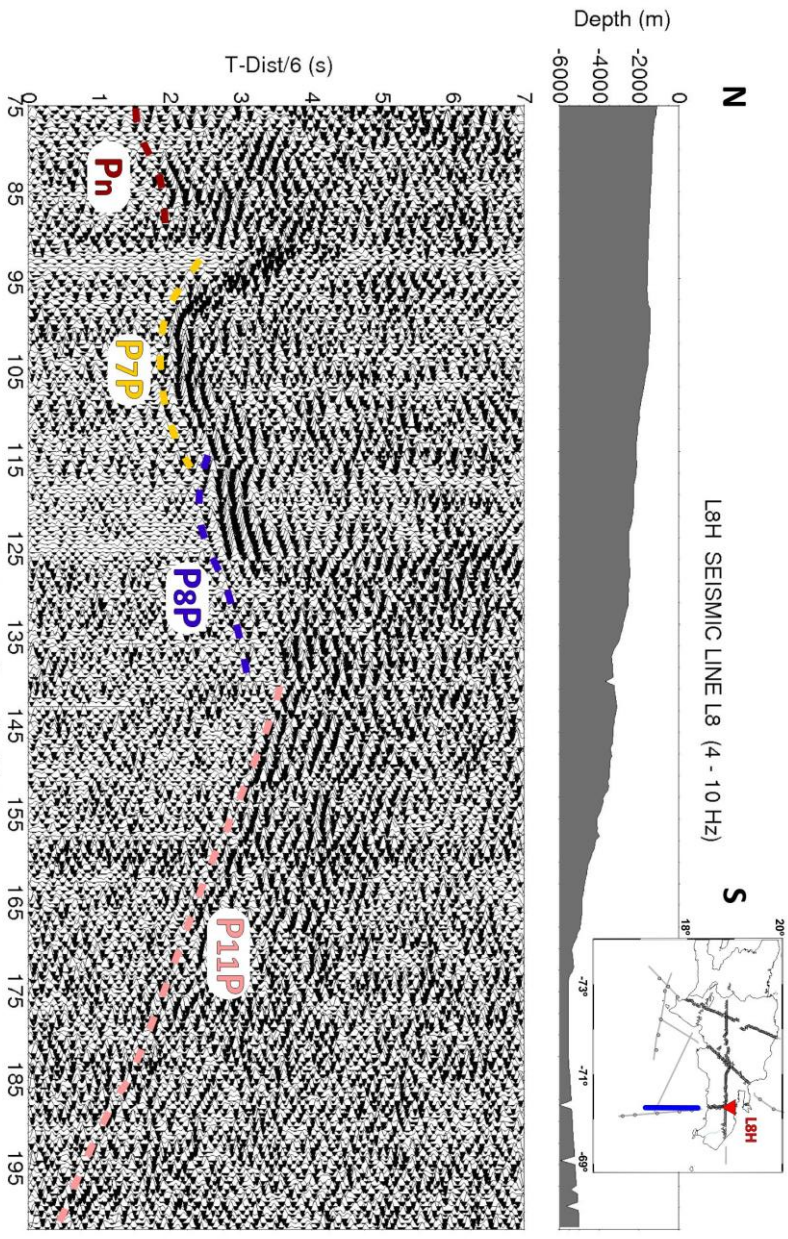

Fig. 5.4.1.12. L8 seismic transect record, station H. Vertical component, velocity reduction is 6 km/s, amplitude-trace normalized and band-pass filtering of 4 – 10 Hz. Colored lines point out reflected/refracted P-wave trains. On the top, bathymetry along this line and registering point location map where red triangle shows the station situation and blue line the marine shooting line.

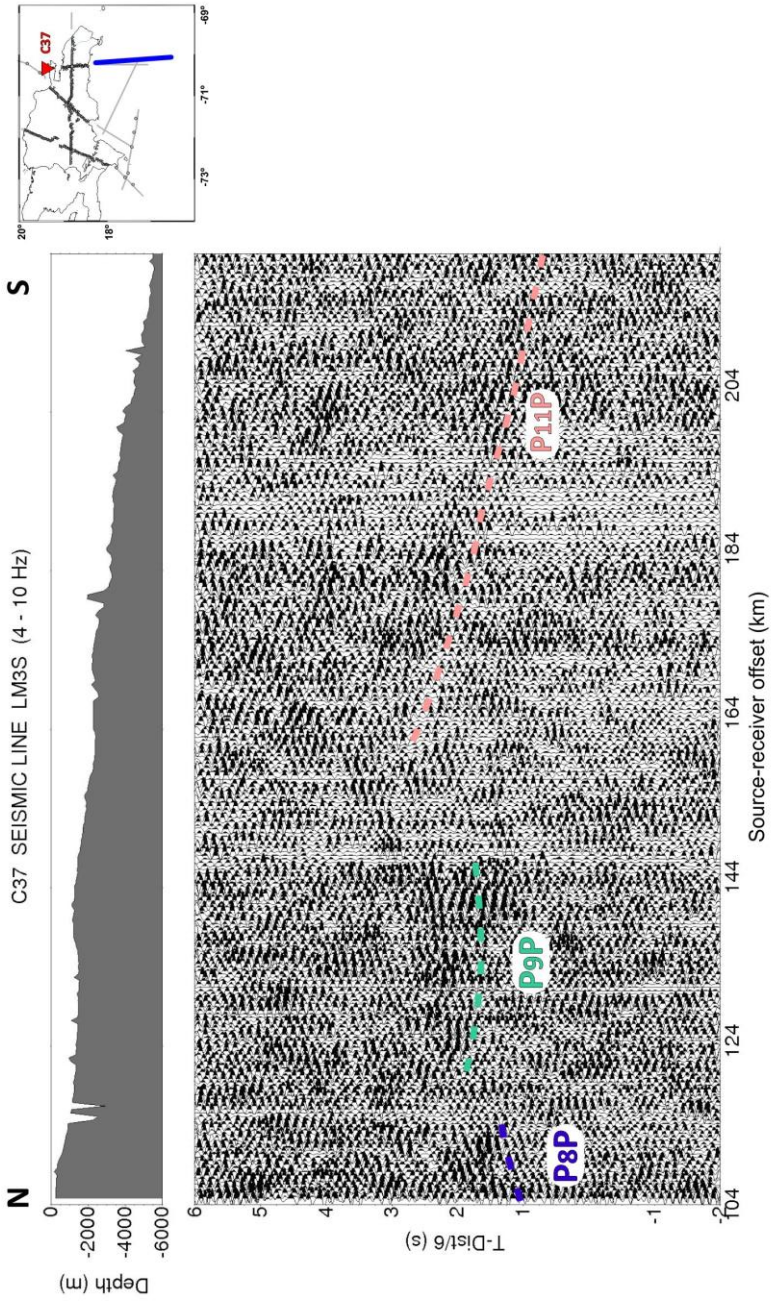

Fig. 5.4.1.13. Seismic record section corresponding to station C37 registering seismic line LM3S. Colored lines point out reflected/refracted P-wave trains. In this figure vertical component and bathymetry along this lines over this section are shown. In the upper left corner red triangle shows location of registration point and blue line the marine seismic line. Reduction velocity is 6 km/s, band-pass filtering of 4 – 10 Hz and amplitudes-trace normalized.

Single shot registered by land station profile

To obtain a crustal velocity model for Profile C (Fig. 5.3.1), different seismic sources have been incorporated in this chapter. In the previous part of this section, it has been examined different seismic record section related to marine seismic lines LM3S and L8. Then, land shot S1 and one of the three marine shots extracted from marine line LM3N will be analyzed.

Figure 5.4.1.14 shows the seismic record section corresponding to shot 151 from LM3N marine seismic line registered by Profile C land stations. In this figure, reflected phases have been interpreted starting with the reflected phase on sixth layer, P_6P. This phase is correlated from offset ranges of 68 km to 132 km. Following phase corresponds to P_9P interpreted between 43 km to 132 km while $P_{10}P$ is followed from 75 km to 132 km of distance. The deepest phase observed in this seismic record section is $P_{11}P$ whose offset interval is 68-132 km.

Borehole explosion S1 (Fig. 5.3.1) was located near Hato Mayor. Figures 2.2.2.9 and 2.2.2.10 of Chapter 2 show a scheme of a borehole and the preparation to detonate the charges carried out during CARIBE NORTE experiment. Now, the figure 5.4.1.15 shows the seismic record section of shot S1 registered by the seismic stations of Profile C from Hato Mayor to San Pedro de Macorís in the south. In this seismic record section three first arrival phases are identified and, also, it is possible to identify S-phases and S – P conversion phases (Fig. 5.4.1.15), which have not been used to obtain the crustal velocity model in this study. First phase is interpreted as P_3' and is characterized by change in amplitude that decreases with distance. The apparent velocity is 5.4 km/s with offset range between 1 km and 14 km. Second phase is characterized by rapid amplitude decay from 15 to 35 km and no more seismic energy beyond 35 km. This phase is interpreted as P_4' with an a.a.v of 6.0 km/s. Last P-wave phase observed in this seismic record section corresponds to P_n phase whose picks have higher uncertainties than previous phases due to an increase in the noise level. This phase is followed from 24 km to 32 km.

The seismic record section corresponding to shot S1 registered by the seismic stations of Profile C from Hato Mayor to the north in Samaná Peninsula is shown in figure 5.4.1.16. First phase observed, P_3', is characterized by an offset interval for of 1-9 km while the apparent velocity in average is 5.0 km/s. Next phase, interpreted as P_4', can be followed from 10 km to 26 km. The a.a.v is 6.0 km. The deepest phase is P_n whose a.a.v is 7.1 km/s and is interpreted between 46 km and 51 km in the area of Samaná Peninsula.

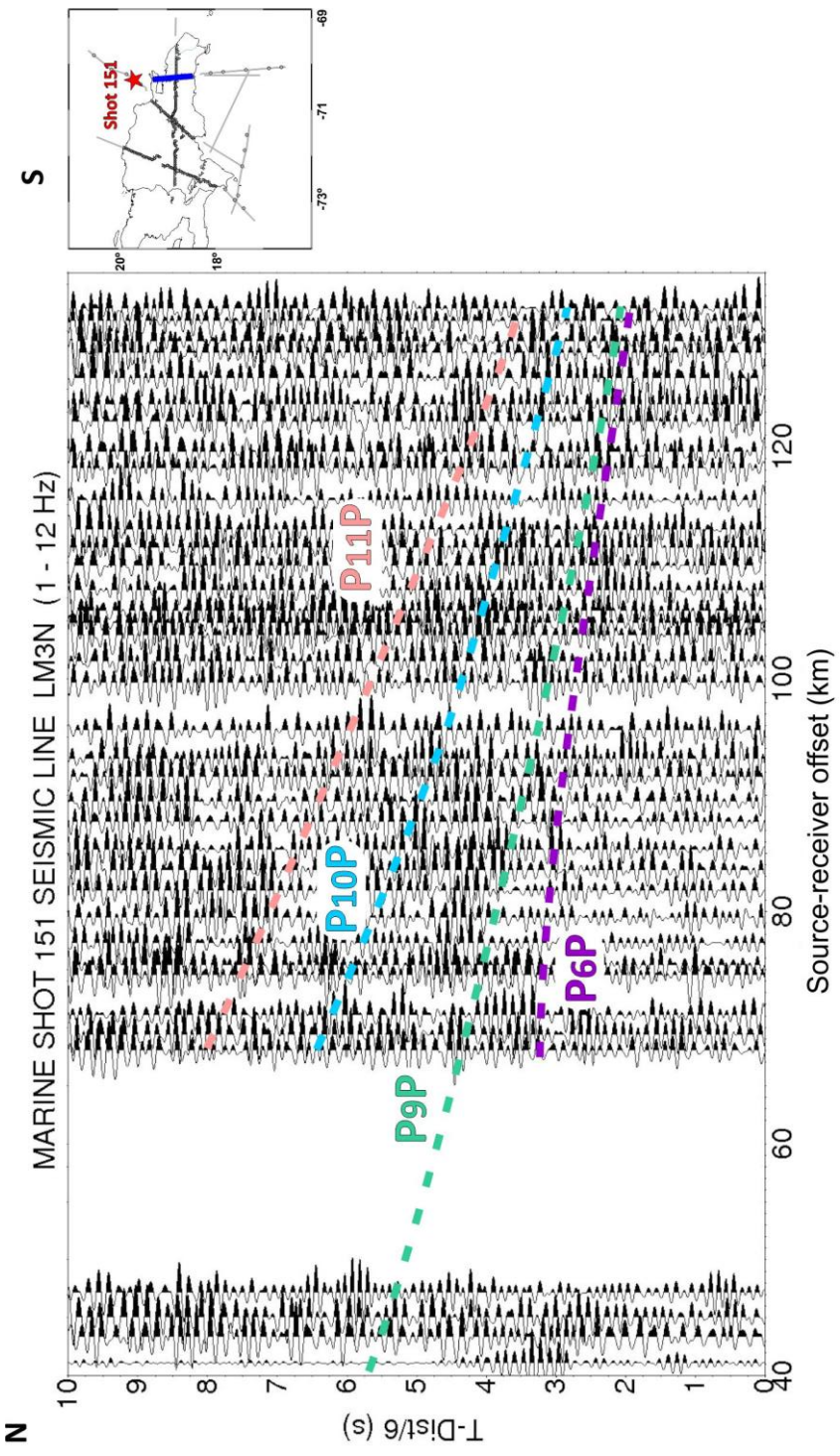

Fig. 5.4.1.14. Seismic record section corresponding to marine shot number 151 recorded by Profile C stations with correlated phases. Vertical component, amplitude-trace normalized and band-pass filtering of 1 – 12 Hz. Colored lines point out reflected/refracted P-wave trains. On the top, shot point in red and blue line shows the stations that record this shot.

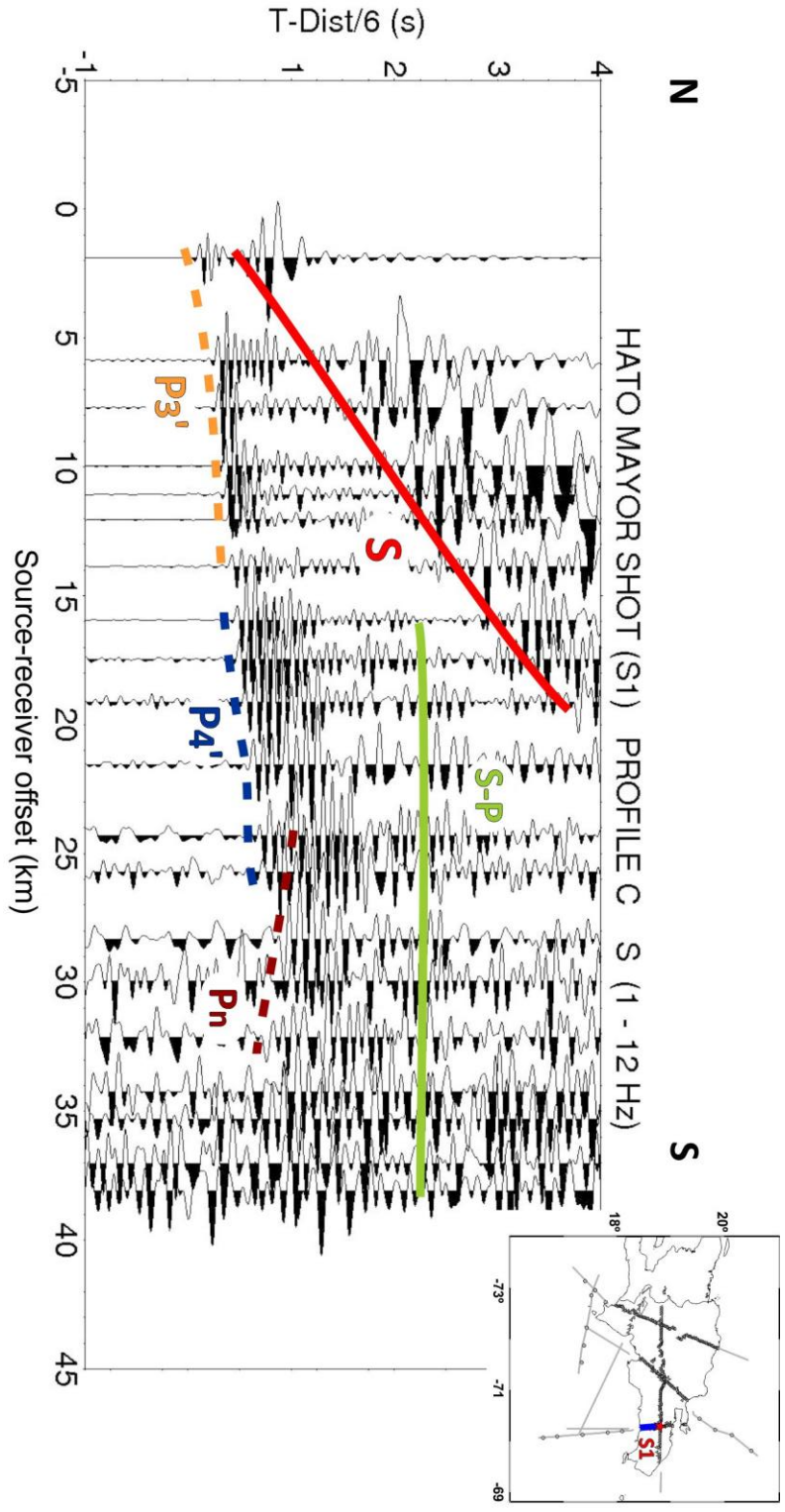

Fig. 5.4.1.15. Seismic record section of Shot 1 (Hato Mayor, DR) registered by land seismic portable stations of Profile C installed from the shot to the south. Vertical component, amplitude-trace normalized and band-pass filtering of 1 – 12 Hz. Colored lines point out reflected/refracted P-wave trains. On the top, shot point in red and blue line shows the stations that record this shot.

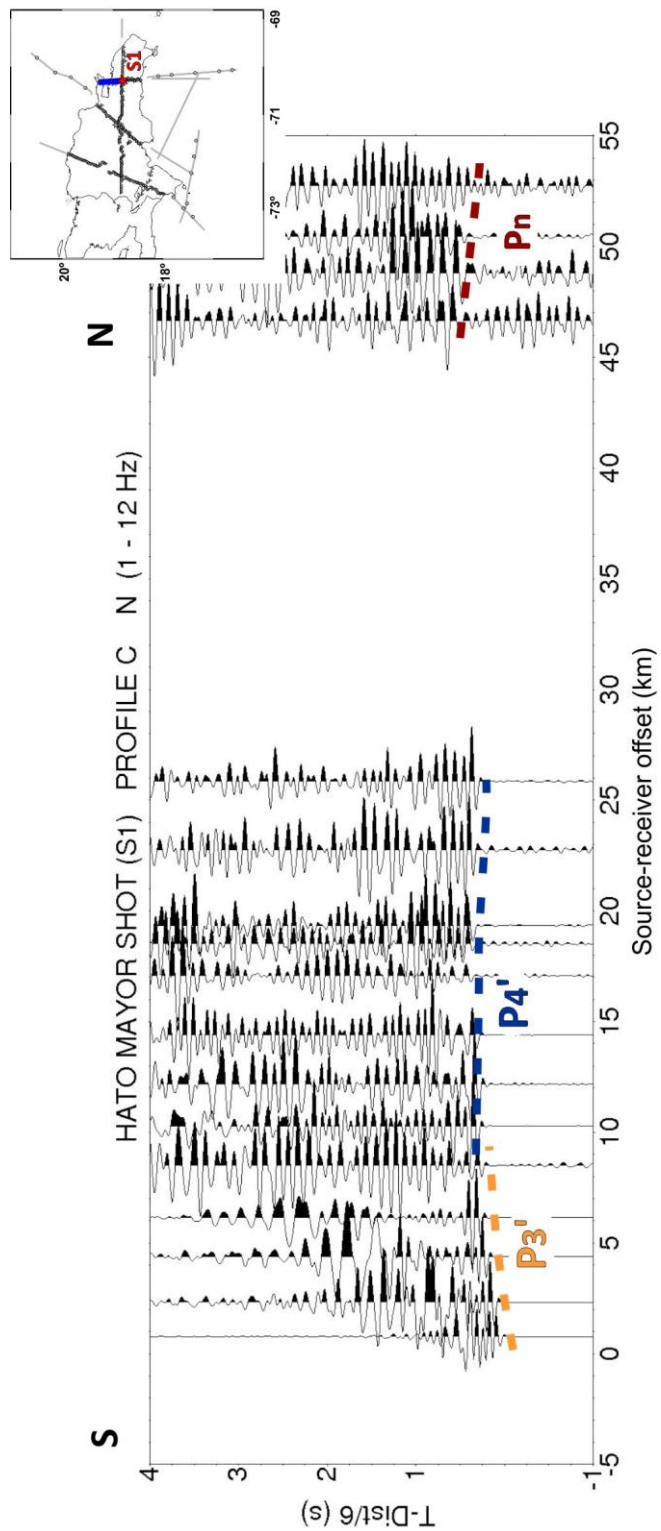

Fig. 5.4.1.16. Seismic record section of Shot 1 (Hato Mayor, DR) registered by land seismic portable stations of Profile C installed from the shot to the north. Vertical component, amplitude-trace normalized and band-pass filtering of 1 – 12 Hz. Colored lines point out reflected/refracted P-wave trains. On the top, shot point in red and blue line shows the stations that record this shot.

5.4.2 Modeling

Seismic wide-angle data have been interpreted using forward modeling techniques [Zelt & Smith, 1992]. Water-depth/elevation from the airgun-shots/land stations was taken from the navigation data.

Joint modeling of deployed stations along profiles B and C (Fig.5.3.1) allows to obtain a global velocity model for both profiles which represent the data features and its interpretation from north to south in the central and eastern part of Dominican Republic from the Bahamas Platform to the north of the Muertos Trough.

Wide-angle seismic data used for building the crustal velocity model for Profile B come from four OBS deployed in the northern coast of DR and Bahamas Platform (Fig. 5.2.1), eight one-component land stations from CARIBE NORTE project and four from GEOPRICO-DO project (Fig. 5.3.1). The Profile B network also registered the shot S2 (Fig. 5.3.1). For Profile C, it has been used data from five OBS, thirteen one-component land stations from CARIBE NORTE project and three from GEOPRICO-DO project (Fig. 5.3.1). All seismic stations deployed along Profile C also registered one land shot, S1, and three marine shots from marine transect LM3N.

Profile B

As it is exposed before, the study of Profile B (Fig. 5.3.1) has been carried out combining two marine shooting lines, one in the north from CARIBE NORTE experiment and another one in the south from GEOPRICO-DO project (*see Section 1.3.2 and 1.3.1, Chapter 1, respectively*). The velocity model of this profile is 450 km length and 100 km depth with twelve layers whose discontinuities are displayed in figure 5.4.2.1. This model presents three differentiated regions with different seismological properties. First region corresponds to the northern offshore part of the profile where water layer is 3.5-4.8 km thick and P-wave velocity of 1.5 km/s. In this part, a thin sedimentary layer is found with a maximum thickness of 2 km and a V_P of 3.3 ± 0.1 km/s. Figure 5.4.2.2 shows shallow model part.

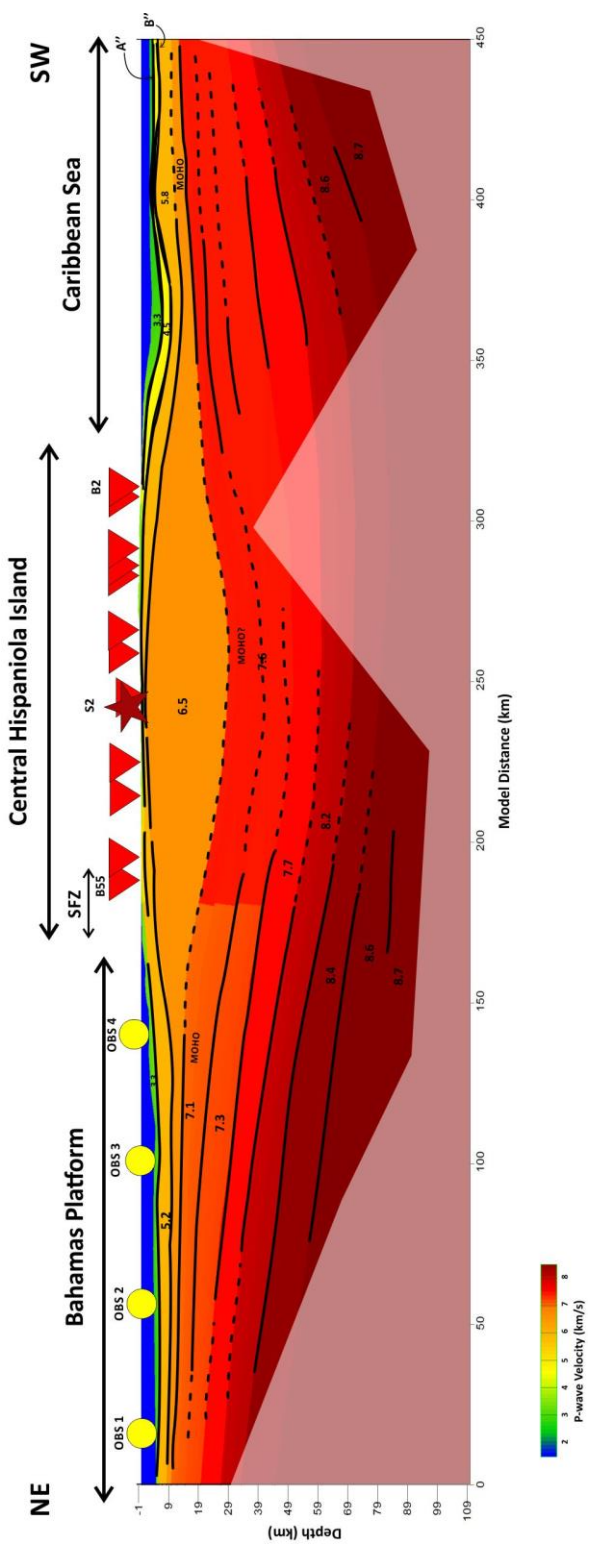

Fig. 5.4.2.1 P-wave velocity model corresponding to Profile B studied in this work where inverted red triangles denote land stations and yellow circles correspond to OBS. The black lines show the discontinuities where P-waves have been reflected and refracted. The shaded regions show areas not illuminated by the ray beams. Figure is scaled according depth and distance. Color scale denotes P-wave velocity in km/s.

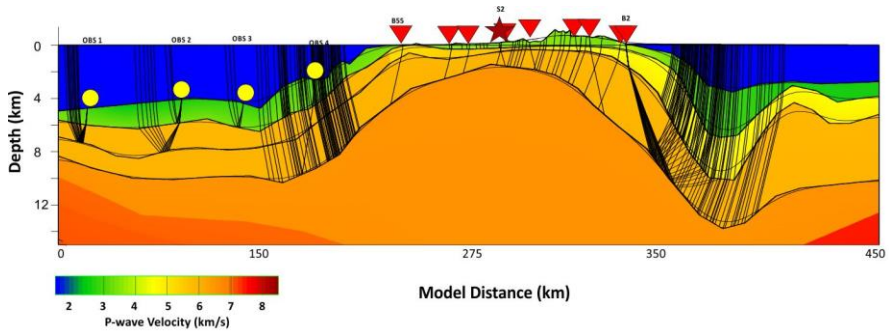

Fig. 5.4.2.2. Ray tracing and P-wave velocity model corresponding to shallow structure in Profile B. Red inverted triangles represent land stations, yellow circles OBS and garnet star land shot S2.

Below this layer, basement is situated at 8 km depth formed by two layers with V_P of 5.1-5.2 ± 0.1 km/s. In this area, middle crust is thin, getting more relevance the layers immediately below where Moho discontinuity is located at 10 ± 1 km deep and increasing with model distance up to reach the coast where depth is 17 ± 1 km. Figure 5.4.2.3 shows ray tracing corresponding to OBS 1 (Fig. 5.3.1) that represents these features and figure 5.4.2.4 shows the synthetic seismogram section of this station where relative amplitudes are comparable with amplitudes showed in seismic record section. First layers of upper mantle have been determined in this study reaching maximum depth of 85 ± 4 km. The P-wave velocity increases between 7.7 km/s to 8.7 ± 0.3 km/s. The deepest layers slopes provide a dip angle with values between 8º and 9º.

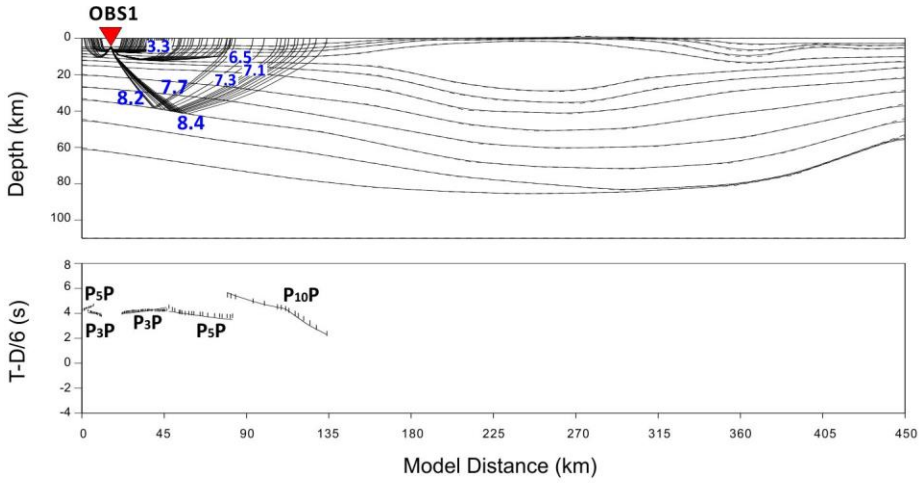

Fig. 5.4.2.3 *Top*: Ray tracing corresponding to OBS 1 and velocity model (km/s). *Bottom*: Comparison between calculated (lines) and observed (vertical bars) travel times. Distances refer to the origin of the velocity model.

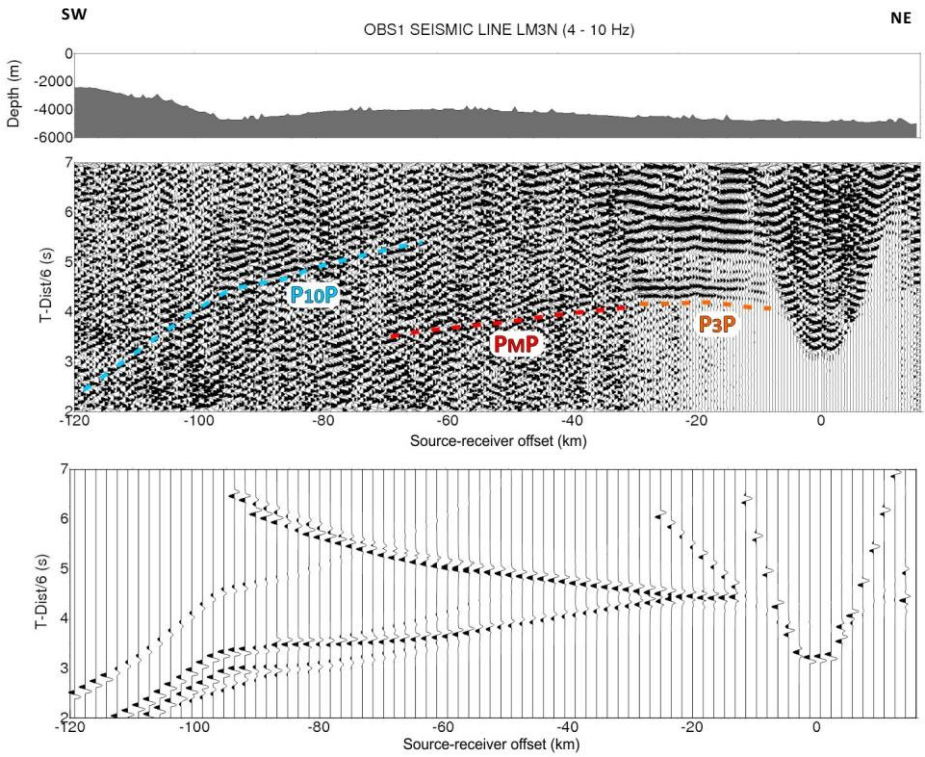

Fig. 5.4.2.4. *Top*: Seismic record section with correlated phases. Vertical component and Amplitude-trace normalized. *Bottom*: Synthetic seismogram corresponding to OBS 1 recording marine shots of line LM3N (CARIBE NORTE Project). Amplitude-trace normalized.

Second region determined in this velocity model corresponds to section of Hispaniola Island crossed by the profile (Fig. 5.3.1). In this region, the sedimentary cover is very thin, except in the south where reaches thicknesses between 0.6 and 1 km with a resolution less than 1 km and V_P of 3.3 ± 0.1 km/s. Basement is 4.2 km deep in the northern of the model section, decreasing towards the interior of the island, being quite superficial, with minimum depth value of 1.6 km. In southern coast, its depth increases up to 7 km. In figure 5.4.2.5, it is observed that the lower crust is thick and whose discontinuity with the upper mantle, Moho, is reached at 19 ± 2 km in the north and 21 ±2 km in the south being its maximum depth 29 ± 2 km. The P-wave velocities change from 6.5 ± 0.2 km/s to 7.6 ± 0.2 km/s and present a lateral variation for first upper mantle layers whose value is 7.0-7.6 ± 0.2 km/s. This fact could be due to the presence of SFZ in this area. In this part of the model, lithospheric mantle has an average thickness of 55 ± 3 km.

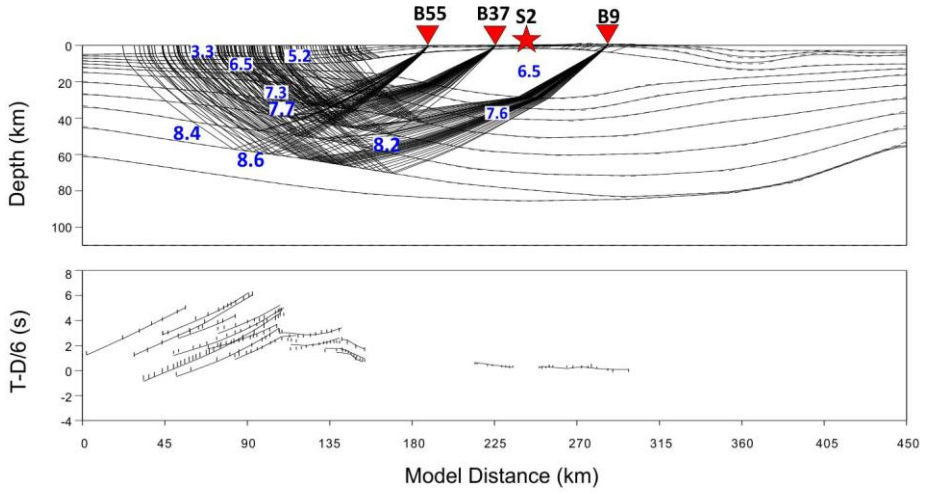

Fig. 5.4.2.5. *Top*: Ray tracing corresponding to land stations B55, B37, B9 and land shot S2. Velocity model in km/s. *Bottom*: Comparison between calculated (lines) and observed (vertical bars) travel times. Distances refer to the origin of the velocity model.

Last region corresponds to southern coast of Hispaniola Island where Beata Ridge collides with the island and Muertos Trough. This fact is reflected in the velocity model as thickening in sedimentary cover and basement nearest to the coast. After that, basement disappears where could be the contact between Beata Ridge and Muertos Trough. Sedimentary layer velocity decreases from 3.3 ± 0.1 km/s to 2.2 ± 0.1 km/s. Figure 5.4.2.6 shows the comparison between phases identified in seismic record section and phases interpreted in synthetic seismogram calculated. Moho depth descends from 19 km to 12 km southward where crustal total thickness is 10 km, with 1 km of depth uncertainty. Ray tracing of complete profile (Fig. 5.4.2.7) shows that P-wave velocity in upper mantle increases from 7.6 ± 0.2 km/s to 8.6 ± 0.3 km/s in depth. Figure 5.4.2.7 shows the deepest layers that present high dip angles, whose values vary between 12º and 18º.

Estimates of arrival-time fit quality for each phase and for all phases are given in Table 5.4.I. Our final model produces a normalized χ^2 of ~ 4 with most of no individual phase over-fit ($\chi^2 > 1$ for all phases). According to Zelt and Smith (1992), final values of χ^2 much greater than 1 generally indicates that the data is sampling small-scale heterogeneities that they cannot resolve. The observed arrival-times are adequately fit by the predicted ones. Our model is able to predict most of the observed arrival-times (NC and NR are similar) but deep travel-time misfits are not really similar to the pick uncertainty.

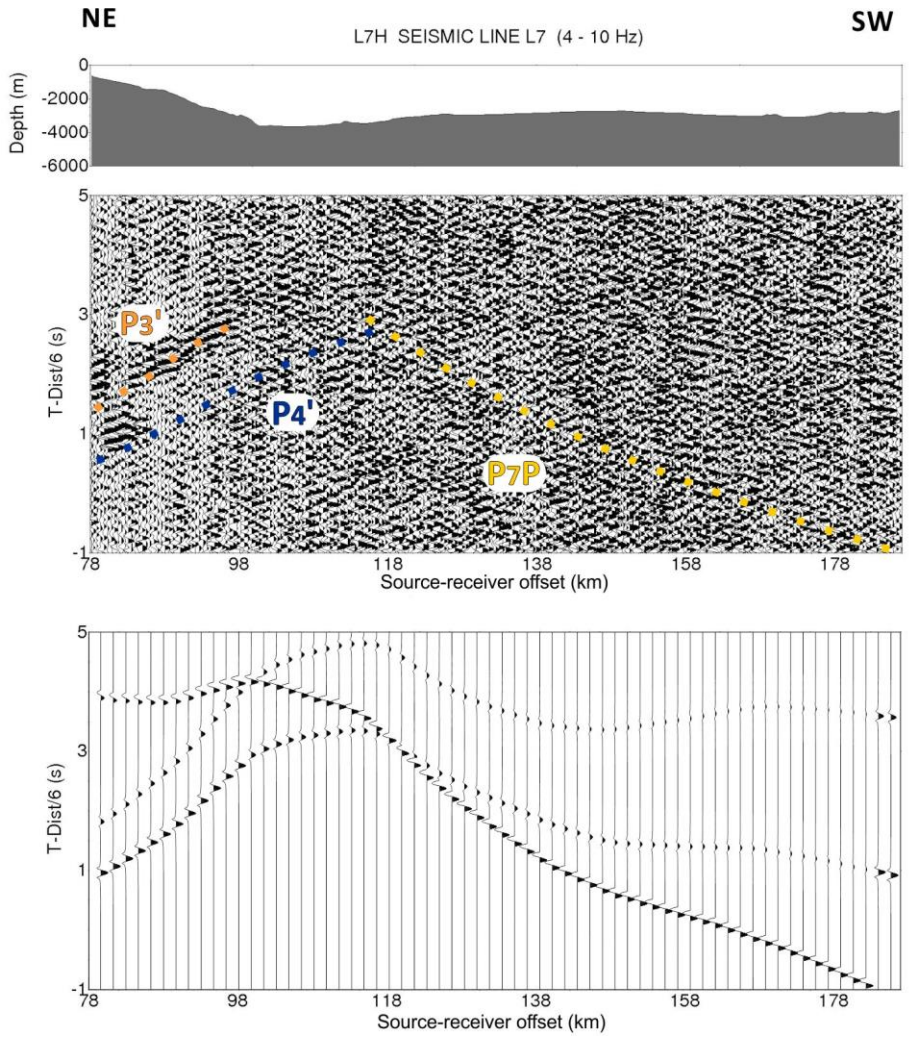

Fig. 5.4.2.6. *Top*: Seismic record section with correlated phases. Vertical component and Amplitude-trace normalized. *Bottom*: Synthetic seismogram corresponding to land station L7H recording marine shots of line L7 (GEOPRICO-DO Project). Amplitude-trace normalized.

Phase	NC	SIGMA (s)	NR	Trms (s)	χ^2
$P_2/P_2P/P_2'$	36	0.110	33	0.225	4.249
P_3P/P_3'	118	0.107	118	0.188	2.884
P_4P/P_4'	169	0.143	168	0.247	3.488
P_MP	75	0.186	75	0.220	1.411
P_n	16	0.145	16	0.193	1.895
Under Moho: $P_7P/P_8P/P_9P$	312	0.141	311	0.287	4.795
Deepest: $P_{10}P/P_{11}P/P_{12}P$	218	0.168	213	0.286	4.325
FIT	944	0.146	934	0.258	3.871

Table 5.4.I Travel-time fit for each phase: NC = number of picks; SIGMA = mean pick uncertainty; NR = number of traced rays; Trms = travel time root mean square misfit; χ^2 = normalized chi square.

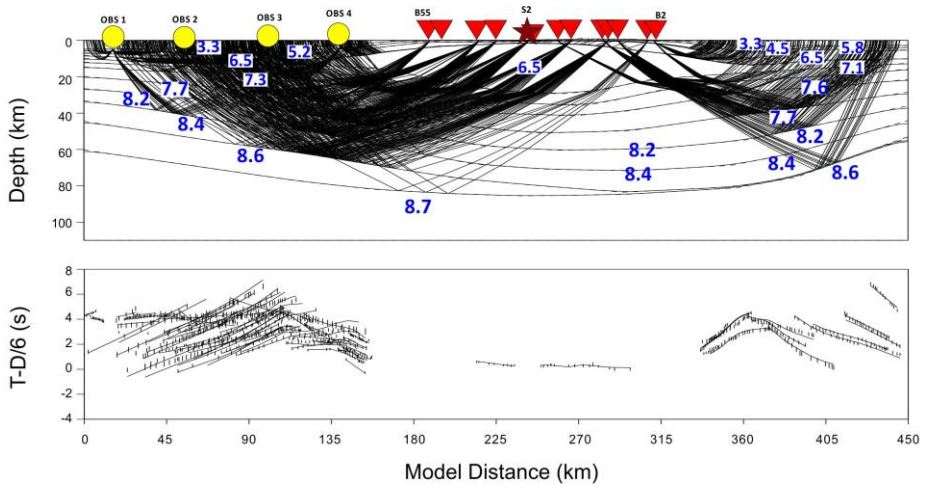

Fig. 5.4.2.7. *Top*: Ray tracing corresponding to Profile B (Fig. 5.3.1) where yellow inverted triangles represent the OBS and red ones land stations deployed. The position of land shot S2 is marked as a red star. Velocities in model in km/s. *Bottom*: Comparison between calculated (lines) and observed (vertical bars) travel times. Distances refer to the origin of the velocity model.

Profile C

Crustal velocity model obtained for Profile C (Fig. 5.3.1) is the result of two marine shooting lines analysis in the area of Caribbean Sea (LM3S and L8), three marine shots from seismic line LM3N and one land shot, S1, that were registered by seismic station deployed during two different experiments. The velocity model is 350 km length and 80 km depth with eleven seismic discontinuities (Fig. 5.6.2.8).

This model shows the deepest area of Caribbean Sea studied in this work that reaches just over 5 km. In this area, the sedimentary layer is 1.2 km thick with V_P of 2.1 ± 0.1 km/s comparable with the velocities obtained for this layer in Profile B (Fig. 5.4.2.1). OBS 9 ray tracing shows this features in figure 5.4.2.9 and figure 5.4.2.10 displays synthetic seismogram corresponding to this station where correspondence between amplitude observed and calculated is established, indicating correct calculations about P-wave velocities. At 80 km model distance, a second sedimentary layer appears with 3.1-3.3 ± 0.1 km/s of P-wave velocity. This area corresponds to San Pedro Basin. The layer is alternated with the previous one, obtaining maximum thicknesses of 3.5 km that decrease as they approach the coast.

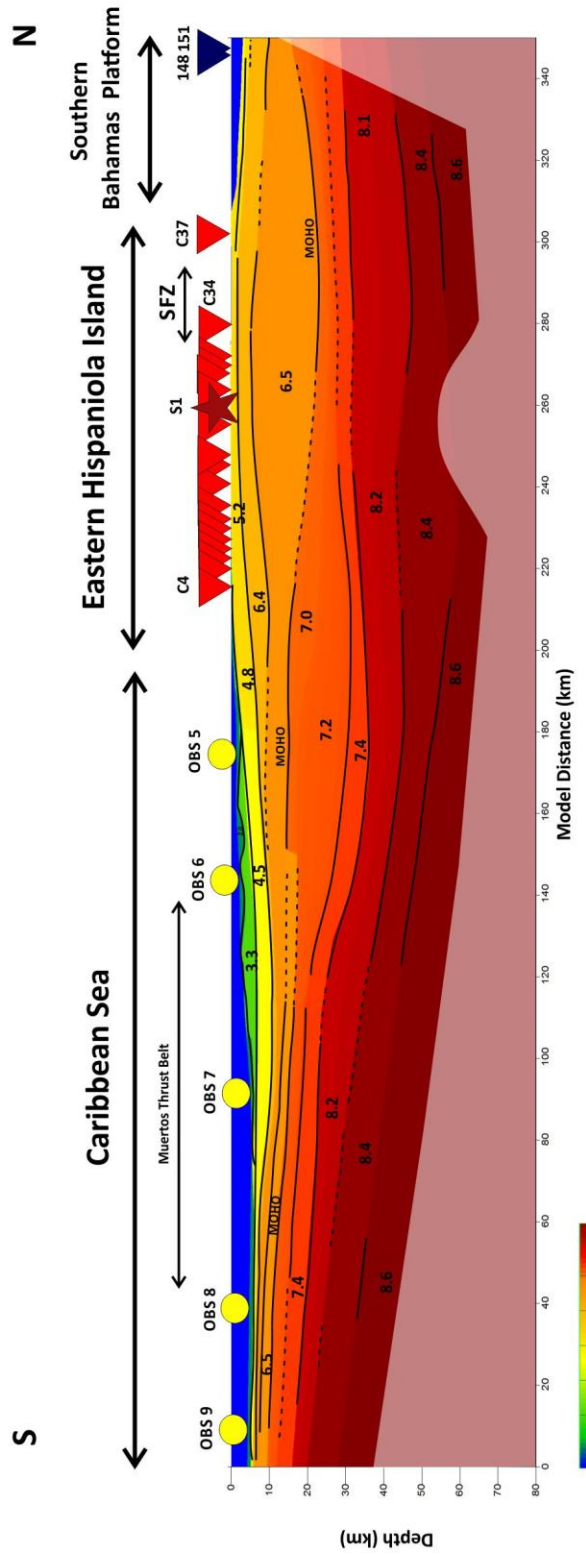

Fig. 5.4.2.8. P-Wave velocity model of CARIBE NORTE seismic profile C across Caribbean Sea, eastern Hispaniola Island and southern Bahamas Platform. Shadow zone denotes the areas not illuminated by ray beams. Yellow circles show OBS, red inverted triangles the land stations used in this study, red star corresponds to shot S1 and blue stars the marine shots. The black lines show the discontinuities where P-waves have been reflected and refracted. Figure is scaled according depth and distance. Color scale denotes P-wave velocity in km/s.

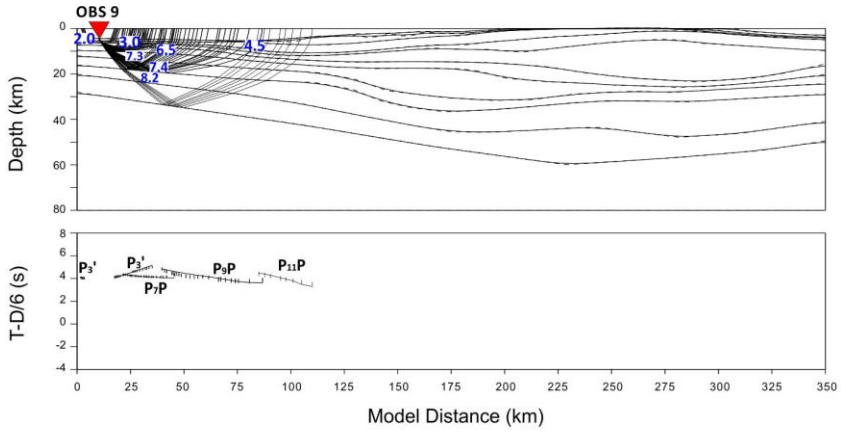

Fig. 5.4.2.9 *Top*: Ray tracing corresponding to OBS 9 and velocity model (km/s). *Bottom*: Comparison between calculated (lines) and observed (vertical bars) travel times. Distances refer to the origin of the velocity model.

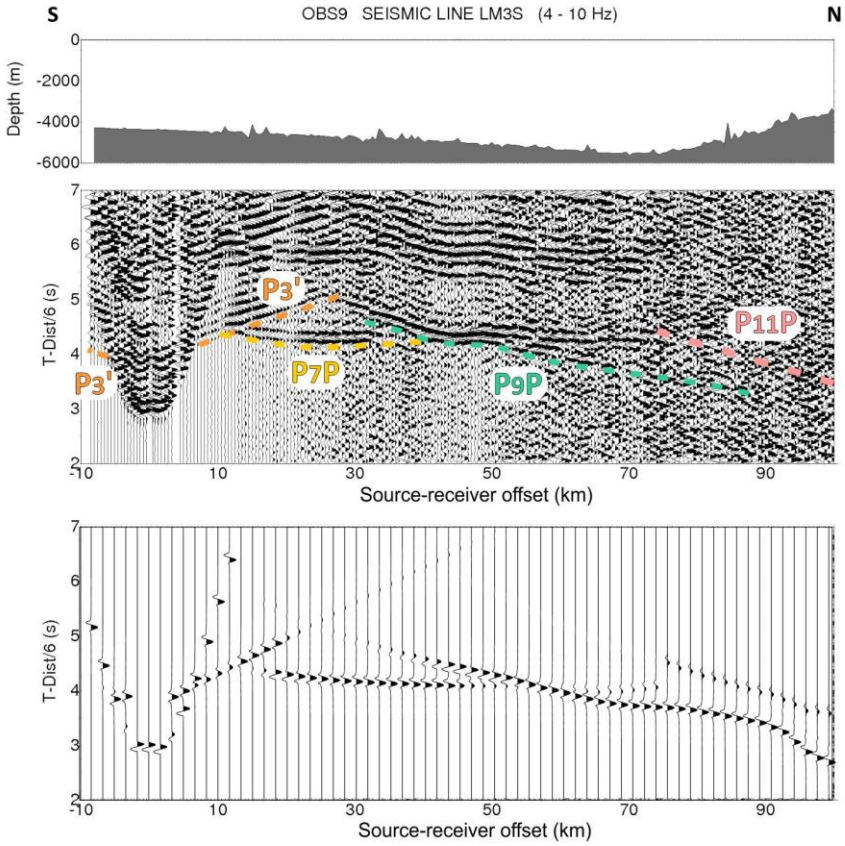

Fig. 5.4.2.10. *Top*: Seismic record section with correlated phases. Vertical component and amplitude-trace normalized. *Bottom*: Synthetic seismogram corresponding to OBS 9 recording marine shots of line LM3S (CARIBE NORTE Project). Amplitude-trace normalized.

Basement is shallow in the initial part of the model and increases in depth in San Pedro Basin up to 7 km, whose thickness remains constant up to reach the coast. The V_P changes from 4.8 km/s to 5.8 km/s, with 0.1 km/s of V_P uncertainty. Depth uncertainty is less than 1 km in the shallow part of the model.

In this area, Moho discontinuity is reached at 10 ± 1 km deep whose value grows up to 17 km at 140 km model distance with a velocity contrast of 6.5-7.1 ± 0.2 km/s. Regarding upper mantle, it is possible to observe that is bending toward the island with a dip angle for deepest layers between 7° and 8° with the highest velocity (8.6 ± 0.3 km/s). Near San Pedro Basin, upper mantle is deformed producing a thickening for first layers that disappears below the island. This effect could be due to the collision of Muertos Trough with the southern coast of Hispaniola.

At 200 km, the southern coast of Hispaniola Island is reached. In this area, sedimentary layer is thinner than southern offshore area but thickness is 1.2 km with P-wave velocity interval of 2.3-3.4 ± 0.1 km/s and basement reaches 5.5 km deep with V_P of 5.2 ± 0.1 km/s. These features are characteristic of Llanura Costera del Caribe (Fig. 5.2.2). In the central part of the island, sedimentary cover is thin and basement is shallow with depth of 1.6 km (Fig. 5.4.2.11).

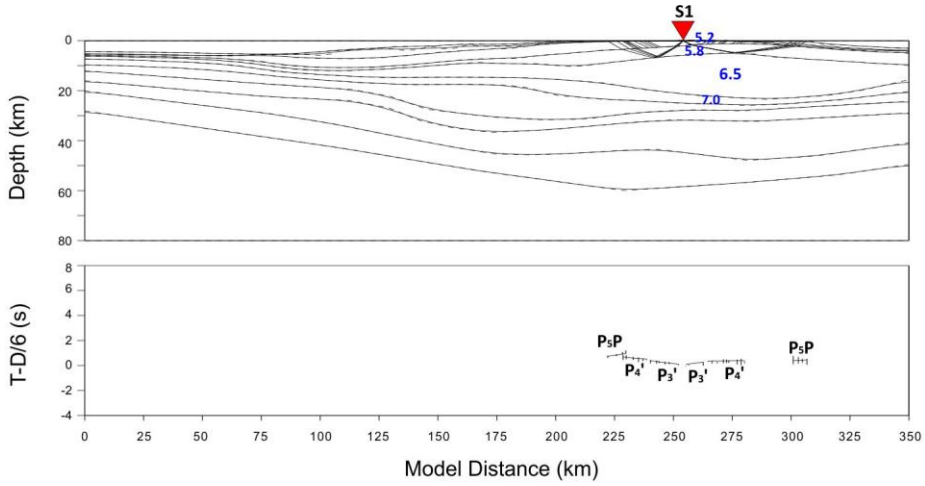

Fig. 5.4.2.11 *Top*: Ray tracing corresponding to land shot S1 registered by land stations of Profile C (Fig. 5.3.1) and velocity model (km/s). *Bottom*: Comparison between calculated (lines) and observed (vertical bars) travel times. Distances refer to the origin of the velocity model.

Total crustal thickness is 24 ± 2 km and upper mantle depth observed is 57 ± 3 km with P-wave velocities that increase from 7.3 ± 0.2 km/s to 8.6 ± 0.3 km/s. Figure 5.4.2.12 shows ray tracing corresponding to land station L8H (Fig. 5.4.1.4), deployed during GEOPRICO-DO experiment (*see Section 1.3.1, Chapter 1*) and registered marine shooting line L8 (Fig. 5.3.1).

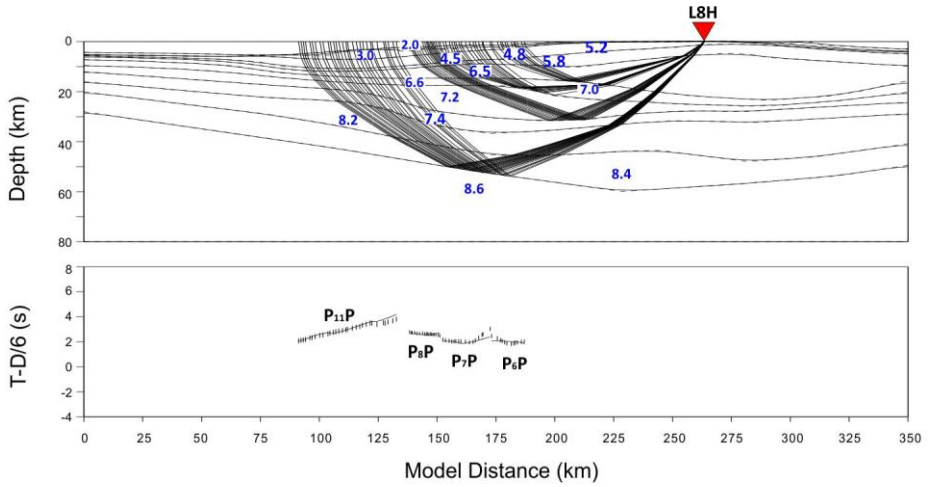

Fig. 5.4.2.12 *Top*: Ray tracing corresponding to land station L8H (Fig. 5.4.1.4) and velocity model (km/s). *Bottom*: Comparison between calculated (lines) and observed (vertical bars) travel times. Distances refer to the origin of the velocity model.

Between 280 km and 290 km, approximately, upper part of the model (Fig. 5.4.2.8) shows that the first layers are closely spaced and the P-wave velocity changes from values of 4 km/s to 5 km/s, with 0.1 km/s of uncertainty. This area corresponds with Samaná Bay where SFZ is located whose effect appears as a thinning of the uppermost layers and a lateral variation in the velocity. In the Chapter 4, crustal velocity model does not present a significant structural change when SFZ is crossed by the profile.

Southern Bahamas Platform structure(Fig. 5.2.1) is obtained from the analysis of three marine shots (blue stars in Fig. 5.4.2.8). Figure 5.4.2.13 shows synthetic seismogram corresponding to marine shot number 151 where amplitude relation between observed and calculated is analyzed. In this area, the uppermost layers are from 3.3 to 5.2 km/s (± 0.1 km/s) with total thickness of 2 km. These values are in correspondence with values obtained in profiles A and B models. Moho depth is raising from 22 km to 15 km (± 2 km). The deepest layers of upper mantle show a dip angle of 6^{o} and are characterized by V_P of 8.4 ± 0.3 km/s and 8.6 ± 0.3 km/s, respectively. In figure 5.4.2.14, ray tracing of all data used for Profile C velocity model is observed.

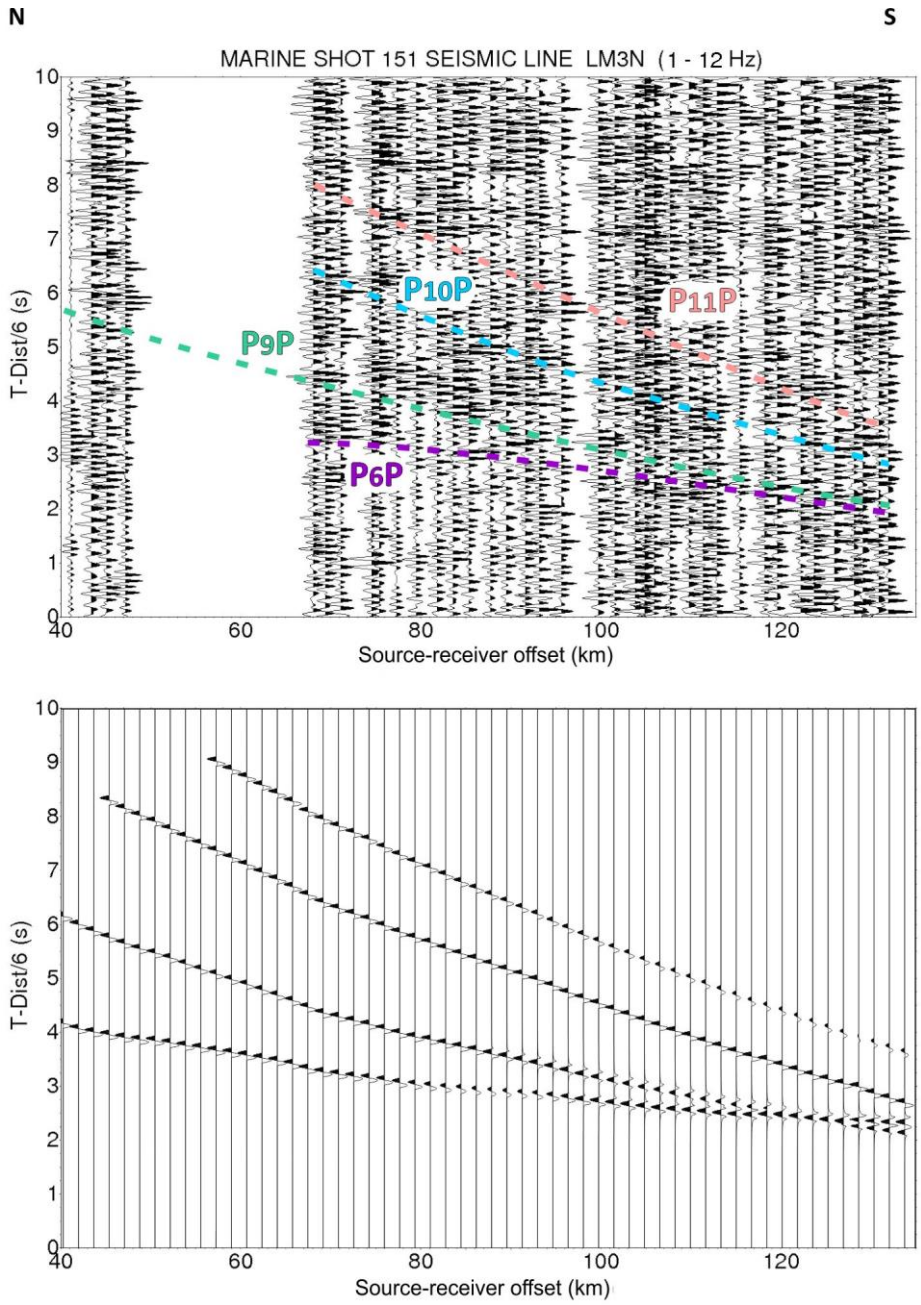

Fig. 5.4.2.13. *Top*: Seismic record section with correlated phases. Vertical component and Amplitude-trace normalized. *Bottom*: Synthetic seismogram corresponding to marine shot 151 of line LM3N (Fig. 5.3.1) recorded by land stations of Profile C (CARIBE NORTE Project). Amplitude-trace normalized.

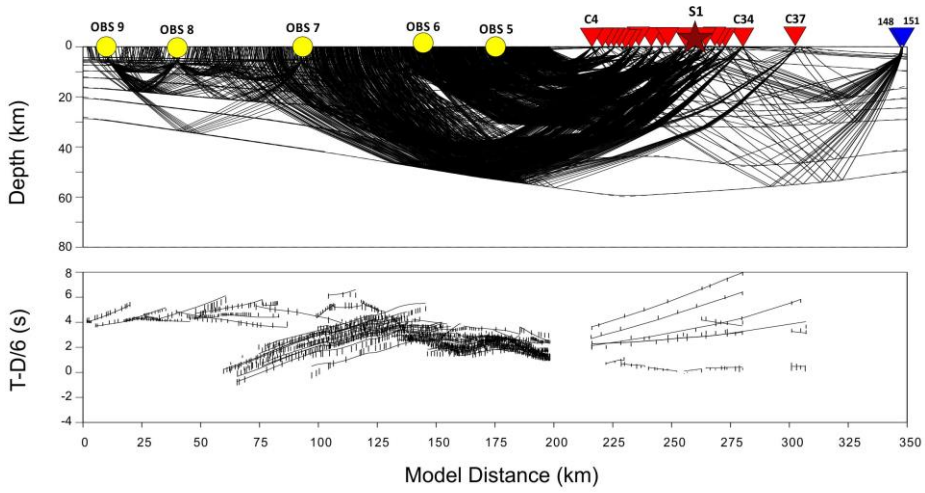

Fig. 5.4.2.14. *Top*: Ray tracing corresponding to Profile C (Fig. 5.3.1) where yellow inverted triangles represent the OBS and red ones the land stations deployed. The position of land shot S1 is marked as a red star and marine shots as blue inverted triangles. Velocities in model in km/s. *Bottom*: Comparison between calculated (lines) and observed (vertical bars) travel times. Distances refer to the origin of the velocity model.

Estimates of arrival-time fit quality for each phase and for all phases are given in Table 5.4.II. Our final model produces a normalized χ^2 of ~ 2 with most of no individual phase over-fit ($\chi^2 > 1$ for all phases). The observed arrival-times are adequately fit by the predicted ones. Our model is able to predict most of the observed arrival-times (NC and NR are similar) but deep travel-time misfits are not really similar to the pick uncertainty.

Phase	NC	SIGMA (s)	NR	Trms (s)	χ^2
P_2'	64	0.112	64	0.138	1.411
$P_3/P_3P/P_3'$	123	0.119	122	0.190	3.832
P_4P/P_4'	120	0.141	119	0.131	0.953
P_MP	184	0.150	184	0.250	3.309
P_n	194	0.153	193	0.156	1.093
P_7P	298	0.149	282	0.201	1.887
Under Moho: P_8P/P_9P	329	0.176	327	0.333	3.508
Deepest: $P_{10}P/P_{11}P$	453	0.197	442	0.282	2.237
FIT	1765	0.163	1733	0.248	2.391

Table 5.4.II Travel-time fit for each phase: NC = number of picks; SIGMA = mean pick uncertainty; NR = number of traced rays; Trms = travel time root mean square misfit; χ^2 = normalized chi square.

5.5 RESULTS AND CONCLUSIONS

Main tectonic processes that are altering the central and eastern Hispaniola Island come from north and south. The south-central part is being penetrating by Beata Ridge that is hitting with Muertos Trough while the southeast is impacted by Muertos Trough. In the north, Bahamas Platform is colliding with the island and the strike-slip movement of SFZ is affecting the northern part, separating Samaná Peninsula from Hispaniola Island. In this section, a summary of the main results obtained of central and eastern Hispaniola Island seismic study is shown.

Main features of the Profile B velocity model

Profile B crustal velocity model (Fig. 5.4.2.1) consists of twelve layers of 450 km length that is well differenced into three tectonic regions from NNE to SSW.

South Bahamas Platform and northern coast of Hispaniola Island (Fig. 5.3.1) is characterized by a thin sedimentary layer followed by a basement that reaches 8 km deep with velocities between 5.2 km/s and 5.8 km/s ($\Delta V_P = 0.1$ km/s). In this area, Moho discontinuity is shallow and its depth is determined between 10 km and 15 ± 1 km from northeastern velocity model up to approach the coast. These values are comparable with Moho depth obtained in the previous chapter for northern part of Profile A velocity model. The first upper mantle velocities are 7.0-7.6 ± 0.2 km/s and increase in depth up to reach 8.7 ± 0.3 km/s. It is noteworthy that dip angles between 8º and 9º are been obtained from deepest layers of upper mantle. The maximum depth from reflected phase data is 85 ± 3 km.

Northern onshore part of the model is characterized by the presence of Río San Juan Complex and SFZ. The effect of both structures is observed in the velocity model and corresponds with a lateral variation in P-wave velocity from offshore to onshore regions increasing towards the island. This change reaches the first layers of upper mantle and it is not observed in Cordillera Septentrional region of Profile A.

Central Hispaniola Island is characterized by a thin sedimentary cover and a shallow basement whose depth decreases from 4.2 km in the north and 1.6 km in the interior of the island increasing towards the south up to 7 km. In this part of the island, crust is thicked reaching depth about 29 ± 2 km where Moho discontinuity is reached. Moho topography changes from 19 ± 2 km, in northern coast, to 21 ± 2 km in southern coast. Central part of upper mantle is not well resolved because of the absence of ray beams in the area.

In the southernmost part of the model, Beata Ridge is colliding with the island and Muertos Trough. This fact is noticeable by thickening in sedimentary cover and basement near the coast. Previous MCS studies [Mauffret and Leroy, 1997] have allowed to determine the Horizons A'' and B'' in the area that are comparable with

sedimentary layers of 3.3 ± 0.1 km/s and 4.5-4.8 ± 0.1 km/s obtained in this study and crustal velocity model of Profile E [Núñez, et al., submitted in PAGEOPH]. The Caribbean Sea part of the model reveals that Moho discontinuity rises from 21 ± 2 km in southern coast to 10 ± 1 km. Upper mantle layers show a strong slope with dip angles between 12º and 18º.

Main features of Profile C velocity model

Crustal velocity model of Profile C (Fig. 5.4.2.8) goes across 350 km with eleven seismic layers in 80 km deep from northern flank of Muertos Trough to Navidad and Silver Banks in Bahamas Platform.

Southern Bahamas Platform is characterized by sedimentary cover with P-wave velocities from 3.3 km/s to 5.2 km/s ($\Delta V_P = 0.1\ km/s$) in correspondence with velocity model of Profiles A and B. In this area, Moho discontinuity is going down from 15 km to 22 km deep (± 2 km) in the north towards to Samaná Peninsula coast. The deepest layers of upper mantle show dip angle of 6º with a V_P of 8.4 km/s and 8.6 km/s ($\Delta V_P = 0.3\ km/s$). Samaná Bay is crossed from west to east by SFZ. The effect produced for this fault zone in our velocity model consists of thickness reduction of uppermost layers and also presents a lateral velocity variation from 5 km/s to 4 km/s, with 0.1 km/s of uncertainty.

In the interior of the island, both sedimentary layer and basement are thinned due to the presence of Cordillera Oriental. Moho depth is thickened reaching maximum values of 24 ± 2 km and upper mantle presents a total thickness of 33 ± 2 km with V_P between 7.3 ± 0.2 km/s and 8.6 ± 0.3 km/s. Going southward, sedimentary cover is increased obtaining values of 1.2 km with 2.3-3.4 ± 0.1 km/s while basement reaches 5.5 km depth in the area of Llanura Costera del Caribe. Moho discontinuity is reached at 17 ± 2 km in southern coast of Hispaniola.

Southern onshore Hispaniola, San Pedro Basin (Fig. 5.2.1) appears in the model as two sedimentary layers with thickness increasing as the profile moves into the Caribbean Sea reaching 3.5 km with P-wave velocities of 2.1 ± 0.1 km/s and 3.1-3.3 ± 0.1 km/s, respectively, over a layer of 5.0 ± 0.1 km/s that could represent the Horizons A'' and B'' [Mauffret and Leroy, 1997], but there is not seismic information about that. This area is characterized by the deformation of the crust and upper mantle due to the presence of Muertos Thrust Belt and Muertos Trough producing a thickening in the first layers of upper mantle and subsequent a thinning further to the south. The southernmost part of the model shows a thin sedimentary cover and basement. Moho discontinuity and upper mantle also are relatively shallow at 10-12 ± 1 km deep being the last layer between 28 ± 2 km and 48 ± 3 km. The deepest layers of upper mantle determined in this study present a dip of 7º-8º.

Comparison with other studies

The central and eastern seismic velocity models, presented in this chapter, show some differences from eastern to western Hispaniola Island. In this region, previous studies using different geophysical and geological data also indicate those differences. Cotilla et al., (2007 and 2010) establish the existence of two large gravimetric zones or macroblocks, western and eastern, from a neotectonic point of view, that are limited by a zone of transversal – diagonal lineaments in the direction of Beata Ridge and coincides with the Profile B direction (Fig. 5.3.1) exposed in this chapter. Moreover, our study has determined that Beata Ridge is dipping 18º into the island in agreement those authors. The crustal velocity model of Profile B (Fig. 5.4.2.1), exposed in this chapter, complete this study from a seismic point of view determining the deep structure along this first order lineament that is transversely articulated with EPGFZ and SFZ active faults and could explain the divergence of rivers and basins in opposite directions, indicated by Cotilla et al., (2007).

In order to compare the results of wide-angle seismic in the area of Muertos Trough (Fig. 5.4.2.8) with gravity model of Granja-Bruña et al., (2010), our P-wave velocity model has been transformed in densities. To do this, the empirical law based on Nafe-Draka curve [Ludwig et al., 1970] has been applied. It provides a good average fitting between ρ and V_P in the range of $1.5 < V_P < 8.5$ km/s, which is suitable to our study region:

$$\rho = 1.6612V_P - 0.4721V_P^2 + 0.0671V_P^3 - 0.0043V_P^4 + 0.000106V_P^5 \qquad (5.1)$$

Figure 5.5.1 shows the density model obtained from this equation. This model has been compared with density models obtained by Granja-Bruña, et al., (2010) (density values shown in italics), specifically, with their *g* and *h* models. These models show that the obtained values in Venezuela Basin region (plateau) with a crustal thickness of 9-10 km and Moho located at 13-15 km of depth, are in agreement with our velocity model and seismic data shown by Mauffret and Leroy, (1997) or Diebold et al., (1999). However, our density model provides information about depths both Caribbean Plateau and island arc due to the starting P-wave velocity model establishes seismically those depths. Furthermore, our density model has more detail in the areas of upper arc crust and deformed wedge, whose calculated density values are 2.4-2.7 g/cm^3 and 2.3 g/cm^3, respectively.

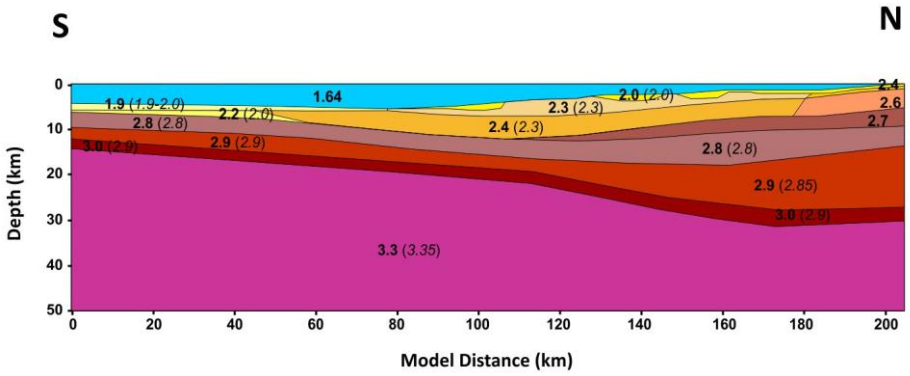

Fig. 5.5.1 Gravity model for Profile C (Fig. 5.4.2.8). Numbers represent densities given in g/cm^3. Bold numbers correspond to data obtained from velocity model Profile C, while italic numbers are from Granja-Bruña, et al., 2010.

The uncertainties determined for velocity model (Section 5.4.2) allows to define, from error propagation in equation 5.1, uncertainties in the densities of 0.2, 0.3 and 0.5 g/cm^3 for V_P uncertainties of 0.1, 0.2 and 0.3 km/s, determined in our velocity model. Those values allow to establish that the velocity model (Fig. 5.4.2.8) is in agreement with density model of Granja-Bruña et al., (2010).

Conclusions

As a synthesis, final conclusions of the study on the crustal structure from southern Bahamas Platform to northern Beata Ridge and Muertos Trough crossing the central and eastern Dominican Republic are enumerated.

- It has been obtained two crustal velocity models from different seismic sources (CSS and wide-angle seismic data) obtained during GEOPRICO-DO and CARIBE NORTE projects.
- From a seismic point of view, velocity model for Profile B is made of 12 layers in a NNE-SSW direction along 450 km revealing the differences between northern and southern offshore areas of the study. Northern area is characterized by a thin sedimentary layer and thin middle crust that increases considerably toward the interior of the island. The Caribbean Sea area of study is characterized by a thickening of sedimentary cover and southernmost a thinning associated to the presence of the Beata Ridge and Muertos Trough. The deep structure of the model is characterized by Moho discontinuity at 10 ± 1 km deep, in the north, that increasing at 29 ± 2 km in the central Hispaniola and 12 ± 1 km in the southern part of the model.
- The crustal velocity model obtained in this study for Profile C is composed by 11 seismic layers across a N-S transect of 350 km length showing the

deformation produced by Muertos Trough and Muertos Thrust Belt over San Pedro Basin and eastern Hispaniola Island. From north to south, Moho discontinuity varies between 15 ± 1 km, 24 ± 2 km in the central part of island and 10 ± 2 km in the northern flank of Muertos Trough.

- The analysis of the wide-angle seismic data reveals the presence of Septentrional Fault Zone in both profiles. For Profile B, a velocity lateral variation is found near northern Hispaniola coast, both subsurface and upper mantle that could be related with Río San Juan Complex and Septentrional Fault Zone. The effect observed in Profile C in the area of Samaná Bay is a thinning of the uppermost layers of the model and also a velocity lateral variation.
- This study have provided the knowledge of deep structure corresponding to southern part of first-order alignment in the Profile B direction, showing a thickening in the deepest layers, which dip 12^{o}-18^{o} northwards. This alignment explains the divergence of rivers and basins in opposite directions.
- The sedimentary cover determined in the area of Caribbean Sea could be correlated with the Horizons A'' and B'' obtained from MCS studies in the interior of Caribbean Plate.
- Northern part of Profile B and C reports a structure dipping between 8^{o}-9^{o} and 6^{o}-7^{o}, respectively. While, in the south of Profile B it is dipping with 12^{o}-18^{o} due to the collision between Beata Ridge over Muertos Trough and Hispaniola. Gravity studies in the area of Muertos Trough reports dip angles values similar to values obtained for Profile C.
- One density model has been calculated from V_P values in the area of Muertos Trough. The comparison with other density models from gravity data shows similar values but our model improves the information about depths in the Caribbean Plateau and island arc.

CHAPTER 6

LITHOSPHERE STRUCTURE BENEATH DOMINICAN REPUBLIC FROM CORDILLERA CENTRAL TO CORDILLERA ORIENTAL BASED ON CSS, WIDE ANGLE SEISMIC AND SEISMICITY DATA

Manuscript in preparation (to be submitted)

6.1 INTRODUCTION

Located on the northern margin of the Caribbean Plate, the Island of Hispaniola is a tectonic collage produced by the oblique convergence to final collision of the Caribbean island-arc/back arc system with the North American Plate, which began in the Lower Cretaceous [Draper et al., 1994]. Hispaniola holds the second largest island with 77.914 km^2 and has the highest elevations (Pico Duarte, 3098 m). Its topography contains imprints from several stages of its development, although features of the neotectonic stage prevail.

Hispaniola has been divided into different tectonostratigraphic terrains based on their different geological history [Mann et al., 1991], tectonically placed together by post-Eocene/Oligocene strike-slip, WNW-ESE fault zones (Fig. 6.1.1). Central Hispaniola is a composite of oceanic derived units bound by the left-lateral strike-slip Hispaniola and Bonao-La Guácara fault zones. The structure of Central Hispaniola is characterized by the presence of folds, thrust, and left-lateral subvertical faults and shear zones. In south central Hispaniola, convergence reactivated Upper Cretaceous structures and lead to the formation of the Upper Eocene-Oligocene SW-vergent Peralta Fold-and thrust belt, the associated San Juan foreland basin the Neogene thrust bound ramp or push-down Azúa basin [Hernáiz-Huerta and Pérez-Estaún, 2002].

In this chapter, the results of lithosphere structure from western to eastern Dominican Republic using wide-angle seismic (marine and land sources) and seismicity data are described.

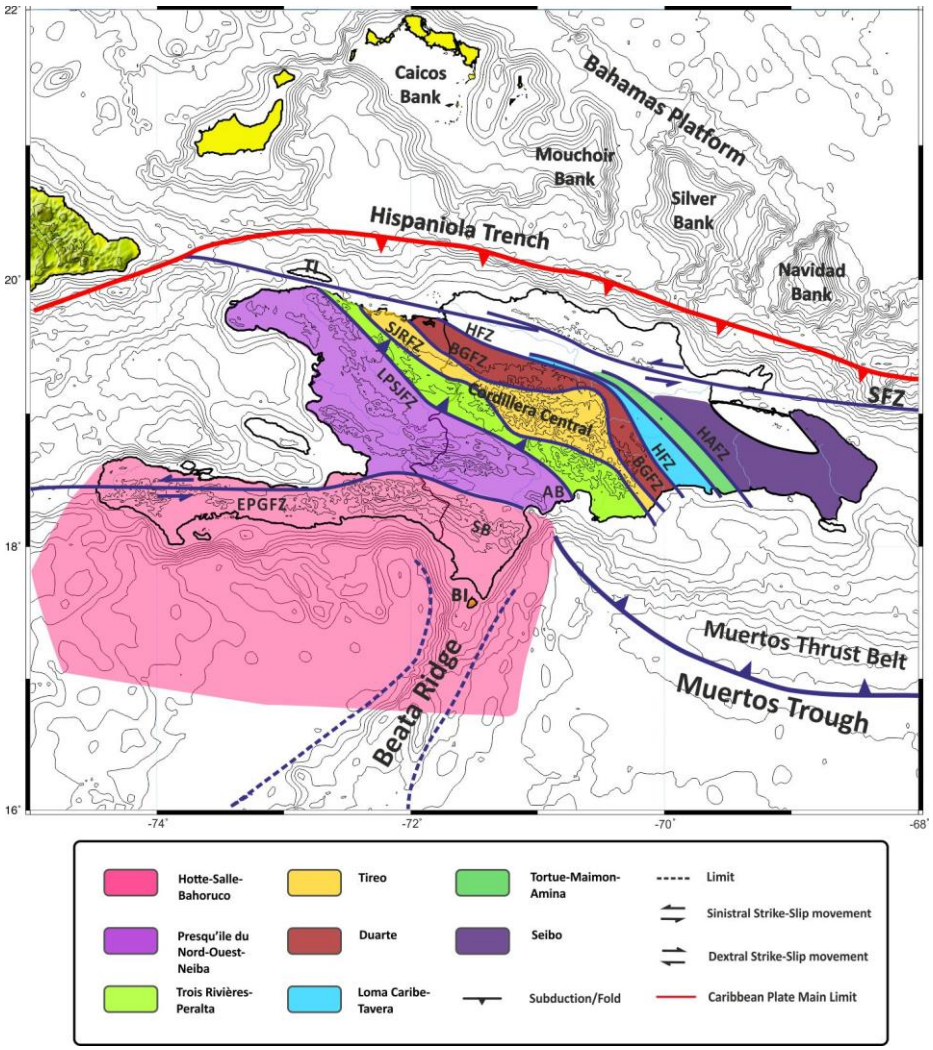

Fig. 6.1.1 Schematic tectonic frame of Hispaniola Island with main tectonic and geologic features in studied area (modified of Mann et al., 1991). AB = Azúa Basin; BI = Beata Island; TI = Tortue Island; SB = Sierra de Bahoruco; SFZ = Septentrional Fault Zone; EPGFZ = Enriquillo-Plantain Garden Fault Zone; LPSJFZ = Los Pozos – San Juan Fault Zone; SJRFZ = San José – Restauración Fault Zone; BGFZ = Bonao – La Guacara Fault Zone; HFZ = Hispaniola Fault Zone; HAFZ = Hatillo Fault Zone.

6.2 GEOLOGY AND TECTONIC SETTING

West-central part of the Hispaniola Island consists of high topography bounded by dominantly reverse and oblique-slip faults along the edges of the uplifted mountain ranges. The eastern part of the island is much lower in elevation than the rest of the island and is not extensively affected by active faulting. Escarpments and lineaments forming west-north-west and north-west-striking boundaries of morphotectonic zones in the central part of the island closely follow island arc terrain boundaries and suggest that Cretaceous to Eocene island-arc structures were reactivated by early Miocene to Recent collisional and transpressional tectonics.

Regional Setting

Several NNW-SSW to WNW-ESE trending fault zone that bound different crustal domains or tectonic blocks characterize the area studied in this chapter (Fig. 6.1.1). In the western area of Dominican Republic, the Pesquile du Nord – Ouest – Neiba tectonic terrain is delimited by San Juan – Los Pozos Fault Zone (SJLPFZ) followed by Trois Rivières – Peralta area that is separated from Tireo Fm. by left-lateral strike-slip San José – Restauración Fault Zone (SJRFZ). Eastern to Tireo block, the Bonao – La Guacara Fault Zone (BGFZ) and Hispaniola Fault Zone (HFZ) border Duarte terrain. The last tectonic domains towards east region of Dominican Republic are Loma Caribe – Tavera and Tortue – Maimón – Amina separated from El Seibo terrain by Hatillo Fault Zone (HAFZ) (Fig. 6.2.1).

The Sierra de Neiba is a small area of mainly Eocene volcanic and volcaniclastic rocks with 2500 m of basalts overlain by 1 km of deep water limestone [Mann et al., 1991]. The contact between Sierra de Neiba and Enriquillo basin is a sequence of folds with high angles associated to tears. The SJLPFZ (Fig. 6.1.1) separates previous terrain from Peralta Belt (Fig. 6.2.1) (part of Trois Rivières – Peralta block in DR) and has evidence of late Cenozoic motion, but with no preset-day displacement [Calais et al., 2002].

Between Trois – Rivières – Peralta domain and Tireo Fm (*see section 5.2*), the NW-SE trending SJRFZ is found. This fault system is 1 km wide and has numerous subparallel features characteristic of subvertical faults [Stein et al., 2004].

The Tireo domain is a complex unit of volcano-sedimentary origin that is related to the development of the island arc during the Upper Cretaceous. This formation constitutes mainly Central Cordillera topography. These outcrops cross Hispaniola Island in NW-SE direction and thrust to SW over Trois Rivieres-Peralta terrain through SJRFZ (Fig. 6.1.1).

The Bonao – La Guacara Fault Zone (Fig. 6.1.1) runs in direction WNW-ESE in the lower northern flank of the central mountainous range. It is considered a sinistral

transcurrent fault with a high dip angle. Field evidence indicates a high degree of tectonics in adjacent rocks, as well as trapezoidal in the slopes, suggesting the potential of it being active. The southern part of this fault traces a concave curve towards the east, going from the central mountain range to the Cibao valley, in the proximities of Bonao. It is considered an inverse fault because the disposition of its geological units on both of its sides (Duarte Complex and Tireo Fm). From GPS measurements, this fault is either non-active or slipping at very slow rates [Calais et al. 2002].

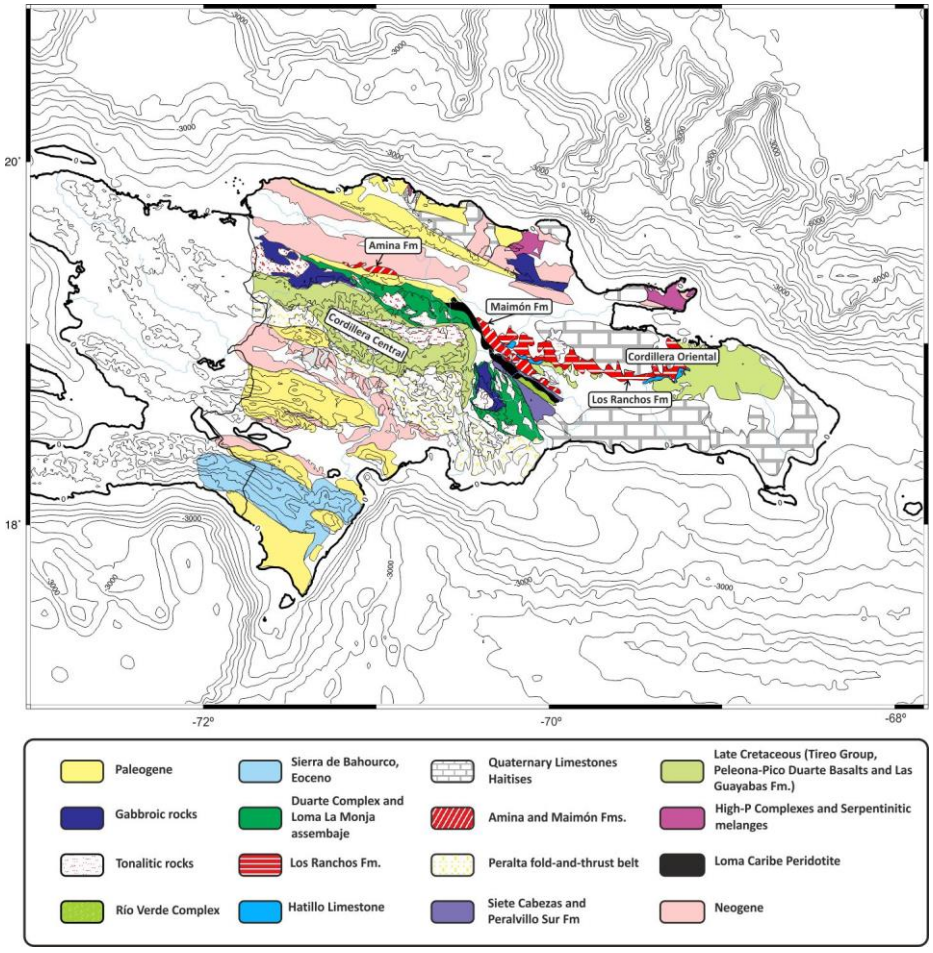

Fig. 6.2.1 Schematic geological map of the studied area in Central Hispaniola (based on Escuder-Viruete et al., 2006; Escuder-Viruete et al., 2011 and Braga et al., 2012).

The Duarte terrain (Fig. 6.1.1) crops out along the northern flank of the Cordillera Central and consists of mainly schistose volcanic rocks [Draper and Lewis, 1991] divided in two lithology units: a lower unit of mainly mafic and an upper unit of thin

flows, pillow basalts, and intrusive diabases [Lewis and Jiménez, 1991]. The association of Duarte terrain with these lithology units suggests that the Duarte terrain formed as a part of an Early Cretaceous ocean island or seamount that was later modified by Late Cretaceous-Eocene island-arc magmatism [Lewis et al. 1991].

Loma Caribe – Tavera (Fig. 6.1.1) disrupted terrain consists of two main rocks occupying a 150 km long and between 5 and 15 km wide of fault-bounded belt (HFZ) crossing diagonally central Hispaniola from NW to SE. The contacts of this terrain with Duarte to the south and Amina – Maimón – Tortue to the north are a high-angle fault onlapped by Oligocene limestone in the first and late Miocene conglomerate in the second [Mann et al., 1991; Palmer, 1979].

Tortue – Amina – Maimón (Fig. 6.1.1) is a long (300 km), narrow (5-15 km), discontinuous outcrop of metamorphic rocks extending diagonally across central Hispaniola from NW to SE. This terrain can be divided into three areas based on the largest continuous outcrops: Tortue Island off of the north coast of Haiti, the Amina Fm on the northern flank of the Cordillera Central and the Maimón Fm (Fig. 6.2.1) of the Cordillera Oriental (Fig. 6.2.1). This terrain is mainly constituted by metaigneous and metasedimentary rocks varying in degree of deformation and metamorphism. To the NE of the HFZ, a NW-trending belt of mafic and felsic Amina schists occur under the Neogene sediments of the Cibao Basin [Escuder-Viruete et al., 2010].

The HFZ (Fig. 6.1.1) is the longest tectonic feature affecting whole Hispaniola and place together the Amina-Maimón schist belt against the units of the Cordillera Central [Draper and Lewis, 1991]. This fault zone may combine strike-slip and thrust motion, as suggested by earthquake focal mechanisms [Dolan and Wald, 1998]. It runs in direction WNW-ESE in the lower northern flank of the central mountainous range and is considered a sinistral transcurrent fault with a high dip angle.

The last tectonic terrain involved in the study area is the Seibo terrain (Fig. 6.1.1). This stratigraphic terrain is a fragment of the volcano-plutonic part of island arc [Mann et al., 1991]. This area can be divided in two areas: the western part of the Cordillera Oriental (Los Ranchos Formation (LRFm) (*See section 5.2*)) and the eastern part of the Cordillera Oriental (Fig. 6.2.1). The Seibo terrane is separated from the Tortue-Amina-Maimón terrane to the southwest by the Hatillo fault zone (Fig. 6.1.1), which is a thrust fault dipping about 45^{o} to the southwest.

6.3 DATA

In the area of Dominican Republic, different studies have been carried out, mainly geologic studies in the onshore area. Most of them were made from Programa de Cartografía Geotemática de la República Dominicana (2002-2004) [Escuder-Viruete et al., 2006, 2010; Lewis et al., 2002]. Others use GPS measurements, stratigraphic, geological and gravity data [Mann et al., 1991; Dolan et al., 1991; Calais et al., 2002; Cotilla and Córdoba, 2010; among others] but any of them have combined control source seismology, wide-angle seismic data and data from events recorded by land stations deployed along seismic line. The Caribe Norte project (*see Section 1.3.2, Chapter 1*) encompasses these data and whose analysis is expounded on this chapter.

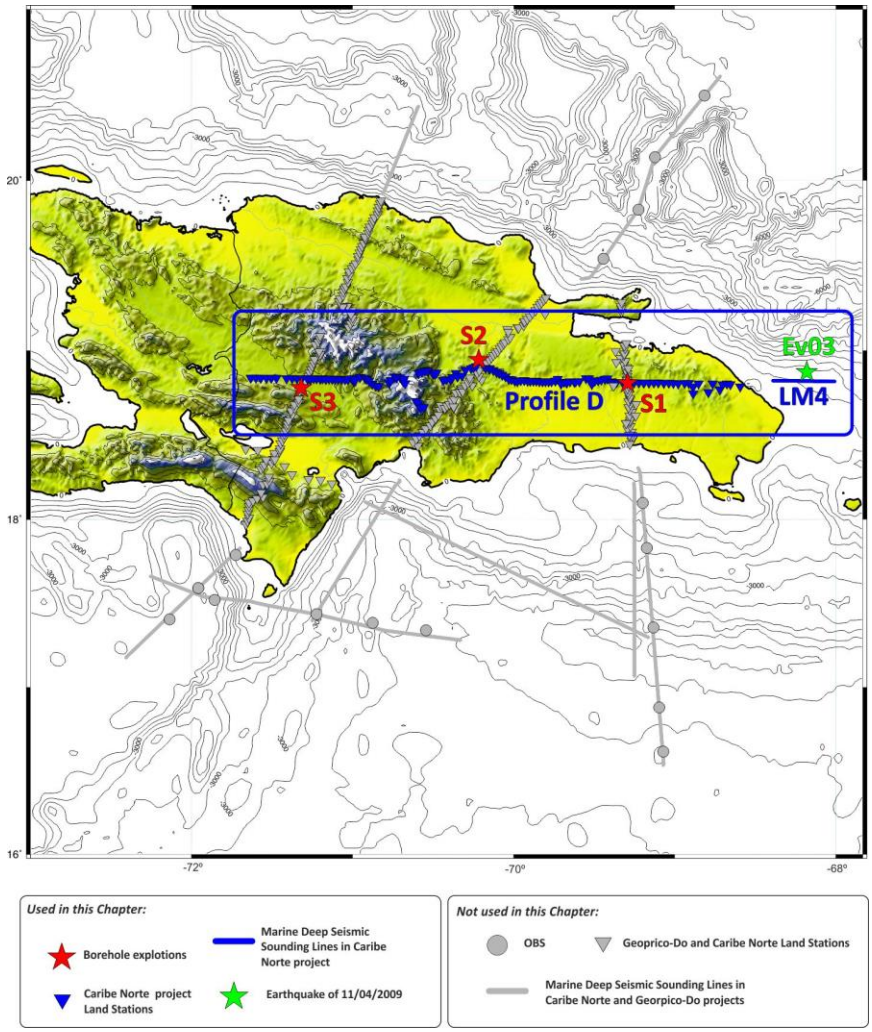

Fig. 6.3.1 Deployment map with stations and seismic sources used in this chapter and all stations deployed during Caribe Norte and Geoprico-Do projects (grey symbols). Blue rectangle represents the study area.

The seismic data studied for that purpose correspond to Profile D of Caribe Norte project (Fig. 6.3.1). This profile is W – E oriented in a length of 450 km. The deployment was made of 140 land seismic stations of one vertical component and one land station of three components located near Hato Mayor. These stations were recording from 11th to 17th of April 2009.

The seismic sources used in this line have been three land borehole explosions 1 Ton (S1, S2 and S3), one marine shooting line (LM4) and one earthquake occurred while seismic stations were recording the Profile D. The LM4 marine shooting line had a total length of 40 km. The total number of shots for this line was 165. The propagation of seismic energy across the crust and Upper Mantle was registered for a maximum distance of 250 km while the event seismic energy was registered 365 km far from the epicenter.

Earthquake relocation

During Caribe Norte project experiment, 6 earthquakes around and inside Hispaniola Island have occurred and land seismic stations registered them, but just one of them was located along Profile D. In this chapter, this earthquake occurred on April 11, 2009 off the east coast of the Dominican Republic is analyzed. The data obtained from the International Seismological Centre (ISC) about this earthquake are:

AUTHOR	RSPR (Red Sísmica de Puerto Rico)
DATE	2009-04-11
TIME	17:42:15.86
LATITUDE	18.8255º
LONGITUDE	-68.2027º
DEPTH	94.7 km
MAGNITUDE	MD 2.9

Table 6.3.I Seismological data information of earthquake from ISC.

From this information, it has been obtained the corresponding seismic record section whose analysis has shown inconsistencies about the estimated depth. This fact is due to first P-wave arrival time of nearest stations is close to origin time of the

event indicating that the depth is shallower than 94.7 km. Some proofs suggest this inconsistency:

- Direct wave has been calculated with an apparent velocity of 7.2 km/s. So, if the 95 km depth were correct, the slope of this direct wave would be much higher than 7.2 km/s.
- This depth cannot be superficial because it would appear head waves that are not observed in the seismic record section.

These reasons show the need to relocate this event. To this purpose, program HYPO71 has been used [Lee and Lahr, 1972]. The input data needed are P and S waves arrival times, seismic station deployed around epicentral location and 1D velocity model that represents the area of study. The seismic stations used to relocate this event belong to different seismic networks (Fig. 6.3.2):

- Caribbean Network (USGS) (**CU**).
- Puerto Rico Seismic Network (PRSN) & Puerto Rico Strong Motion Program (PRSMP) (**PR**).
- Instituto Sismológico Universitario (Universidad Autónoma de Santo Domingo) (ISU-UASD) (**DR**).
- Caribe Norte experiment seismic stations deployed along Profile C and D.

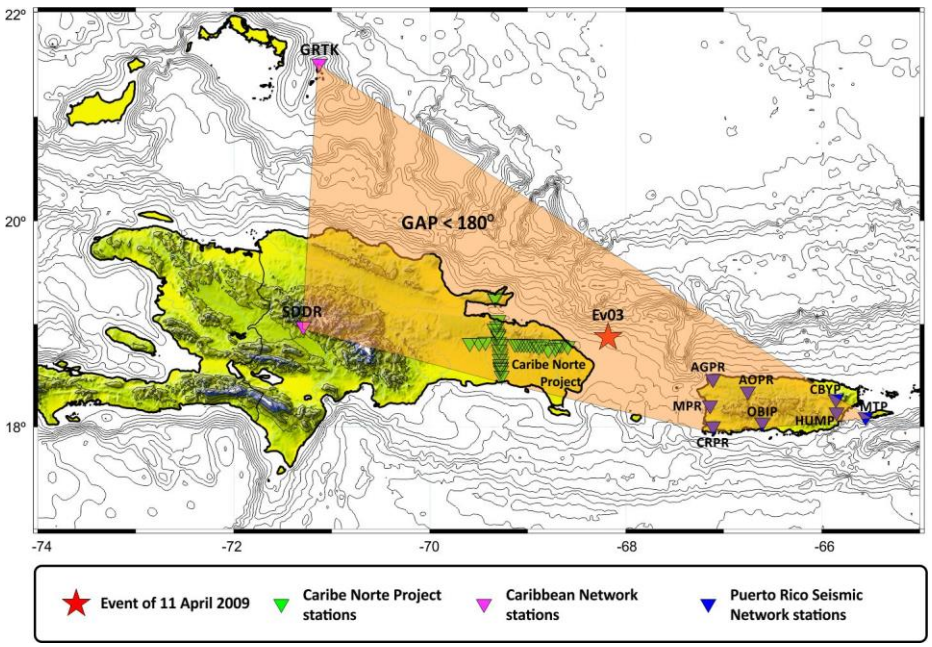

Fig. 6.3.2. Map showing event and stations used to relocate the 2009-04-11 earthquake MD 2.9 inside GAP < 180º.

Different 1D velocity models have been used to check the parameters obtained after relocation. These models have been provided by Instituto Sismológico Universitario (DR) and Puerto Rico Seismic Network (PR). Moreover, Profile D velocity model, described in this chapter, has been used to check the accuracy of the model respect to models used by networks that operate in the area. The results obtained after running the relocation program are summarized in the following table.

VELOCITY MODEL	DR	PR	PROFILE D
TIME	17:42:17.80	17:42:17.00	17:42:17.02
LATITUDE	18.849º	18.856º	18.873º
LONGITUDE	-68.187º	-68.181º	-68.180º
DEPTH (km)	16	17	23
RMS	0.21	0.20	0.19
ERH	2.1	1.9	1.9
ERZ	0.9	1.9	2.1

Table 6.3.II Relocation data summary of earthquake of 11 April 2009.

Checking the results showed in the table, it is possible to observe that the results are very similar between them and different with ISC data. Comparing the previous results with seismic record section data, it is possible to extract that the best result that corresponds with the best RMS is the velocity model of Profile D.

6.4 INTERPRETATION

Data processing allowed obtaining seismic record sections whose interpretation has provided the travel times and distances important to elaborate Profile D velocity model. This interpretation consisted of determining the P-wave phases observed in each seismic record section and their corresponding apparent velocities. Subsequently, ray tracing models and synthetic seismograms have been made to finally obtain the velocity models corresponding to this profile.

6.4.1 Seismic record sections and Correlation Data

In seismic record sections obtained for this task, it was possible to identify time correlations corresponding to P-wave refractions and reflections in crustal and upper mantle discontinuities. Each phase is assigned a color and a code with subscripts, which represent the layer relative position respects to subsurface (*see Table 2.5.I, Section 2.5, Chapter 2*).

Profile D (Fig. 6.3.1) is 385 km length from Haiti border region to offshore area of eastern Dominican Republic. This profile is characterized by different tectonic features (*see section 6.2 of this chapter*) and has been interpreted using different seismic sources as the marine shooting line LM4, three marine shots extracted from line LM4, three borehole explosions located in the Cordillera Central, central part of the island and Cordillera Oriental (S1, S2 and S3) and one earthquake occurred while Caribe Norte project land stations were deployed in the seismic line of Profile D.

Land sources

In western area of the profile, land shot S3 is located (Fig. 6.4.1.1). This seismic record section provides seismic information in the western area of this profile and shows deep P-wave phases towards east while west part is characterized by reflected wave of the third layer from 6 to 35 km source-receiver offset. The first phase observed on the eastern part is P_2P correlated from 6 to 12 followed by P_3P between 6 and 15 km and the head wave that travels through layer 3 with 6.2 km/s a.a.v. From 39 to 93 km offset range is interpreted the reflected phase over layer 4 (P_4P) and. Following phase determines the discontinuity between the crust and upper mantle (Moho discontinuity, P_MP) and is followed from 100 to 240 km. In figure 6.4.1.1, the deepest phase interpreted is P_8P from 160 to 250 km of distance.

The reverse seismic record section of land shot S3 corresponds to land shot S1 (Fig. 6.4.1.2). The borehole is located 248 km distance from westernmost land station in Cordillera Oriental. To the east of S1, it is interpreted two head waves phases that travel through discontinuity of layer 3 and 4 and 4 and 5. The first one, P_3', is correlated up to 20 km and P_4' between 20 km to 70 km source-receiver offset range. The average apparent velocities of both phases are 5.1 km/s and 6.0 km/s. To the west, the seismic record section is 250 km length. In this side, P_3' is interpreted up to 11 km with a.a.v of 5.4 km/s followed by P_4' between 13 km to 64 km offset with 6.1 km/s of a.a.v. The following phase corresponds to refracted wave in the layer 5 that can be followed from 70 km to 80. From this phase, reflected phases are interpreted. P_6P is estimated from 80 to 135 km offset followed by P_7P between 88 km to 190 km of long-offset. Deep phases interpreted in figure 6.4.1.2 are $P_{11}P$ and $P_{12}P$ followed from 151 to 200 km and 165 km to 237 km offset, respectively.

Marine Sources

In the central area, land seismic station D62 (Fig. 6.4.1.3) is located. This station is situated over a gabbroic rocks area 137 km distance from westernmost land station and is the farthest station that records the marine seismic line LM4 (Fig.6.3.1). The phases interpreted in this seismic record section come from below Moho discontinuity being the first one the reflected phase on the bottom of seventh layer correlated from 206 km to 239 km epicentral distance with a.a.v 6.4 km/s. Between

206 to 246 km are followed P_9P and $P_{10}P$ reflected phases with average apparent velocities of 7.4 km/s and 9.3 km/s, respectively. The reduced observed time for $P_{10}P$ indicated this phase is deep.

In the area of Duarte terrain (Fig. 6.2.1), D76 is placed at 166 km distance from westernmost land station (Fig. 6.4.1.4). The first phase interpreted corresponds to P_7P and it is possible to follow it from 177 km to 203 km with low amplitude and a.a.v. 70 km/s.

The phase P_9P is correlated between 177 km to 212 km of source-receiver offset. The near average apparent velocity is estimated in 7.6 km/s. The deepest phase observed is $P_{10}P$. The amplitude is relatively higher than previous phases and it is possible to follow it from 177 to 218 km and 9.1 km/s of approximate a.a.v.

In Cordillera Oriental area (Fig. 6.2.1), the three components station HATO MAYOR is located 248 km distance from westernmost land station. This station records the marine seismic line LM4 and the perpendicular profile (Profile C) registering LM3N and LM3S seismic lines (*see Chapter 5*). Figure 6.4.1.5 shows the P-wave phases observed in the vertical component. Between 104 km to 139 km offset is correlated the head wave that travels through the discontinuity between layer 4 and 5 (P_4') with a.a.v. of 6.7 km/s. The reflected wave on 6^{th} layer is followed from 133 km to 144 km offset range. The estimated average apparent velocity for this phase is 8.1 km/s. In figure 6.4.1.5, the reverberations with similar amplitudes could indicate a possible lamination in the eastern area of the profile shown.

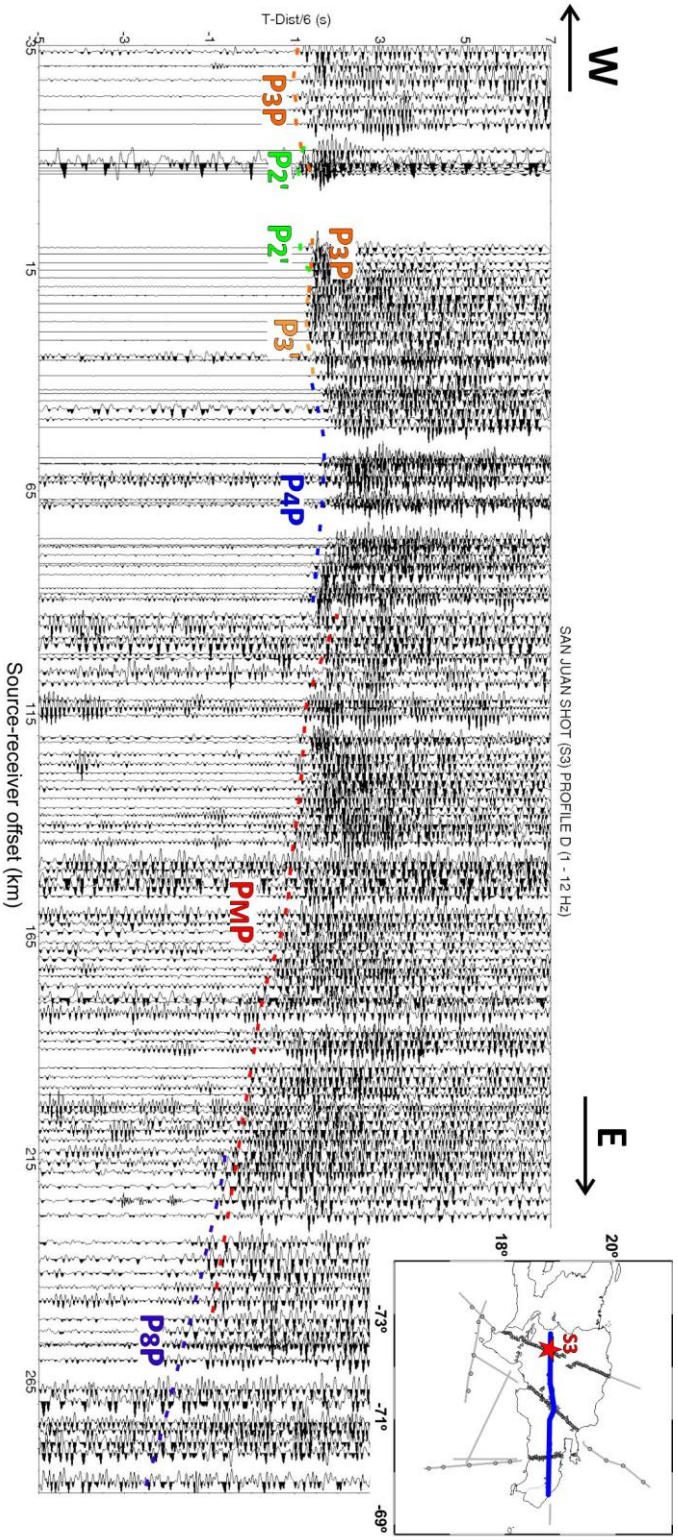

Fig. 6.4.1.1. Seismic record section corresponding to land shot S3 registered by seismic station of Profile D. Colored lines point out reflected/refracted P-wave trains. In this figure vertical component is shown. In the upper right corner, red star shows location of registration point and blue line the recording seismic line. Reduction velocity is 6 km/s, band-pass filtering of 1 – 12 Hz and amplitudes-trace normalized.

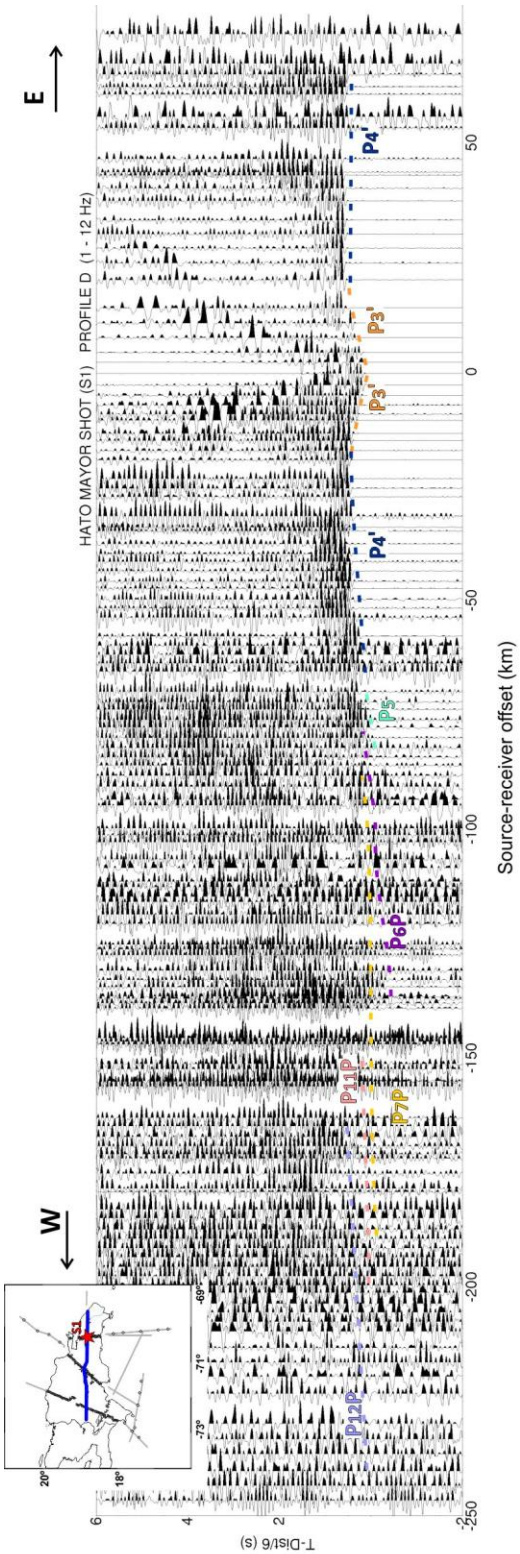

Fig. 6.4.1.2. Seismic record section corresponding to land shot S1 registered by seismic station of Profile D. Colored lines point out reflected/refracted P-wave trains. In this figure vertical component is shown. In the upper left corner, red star shows location of registration point and blue line the recording seismic line. Reduction velocity is 6 km/s, band-pass filtering of 1 – 12 Hz and amplitudes-trace normalized.

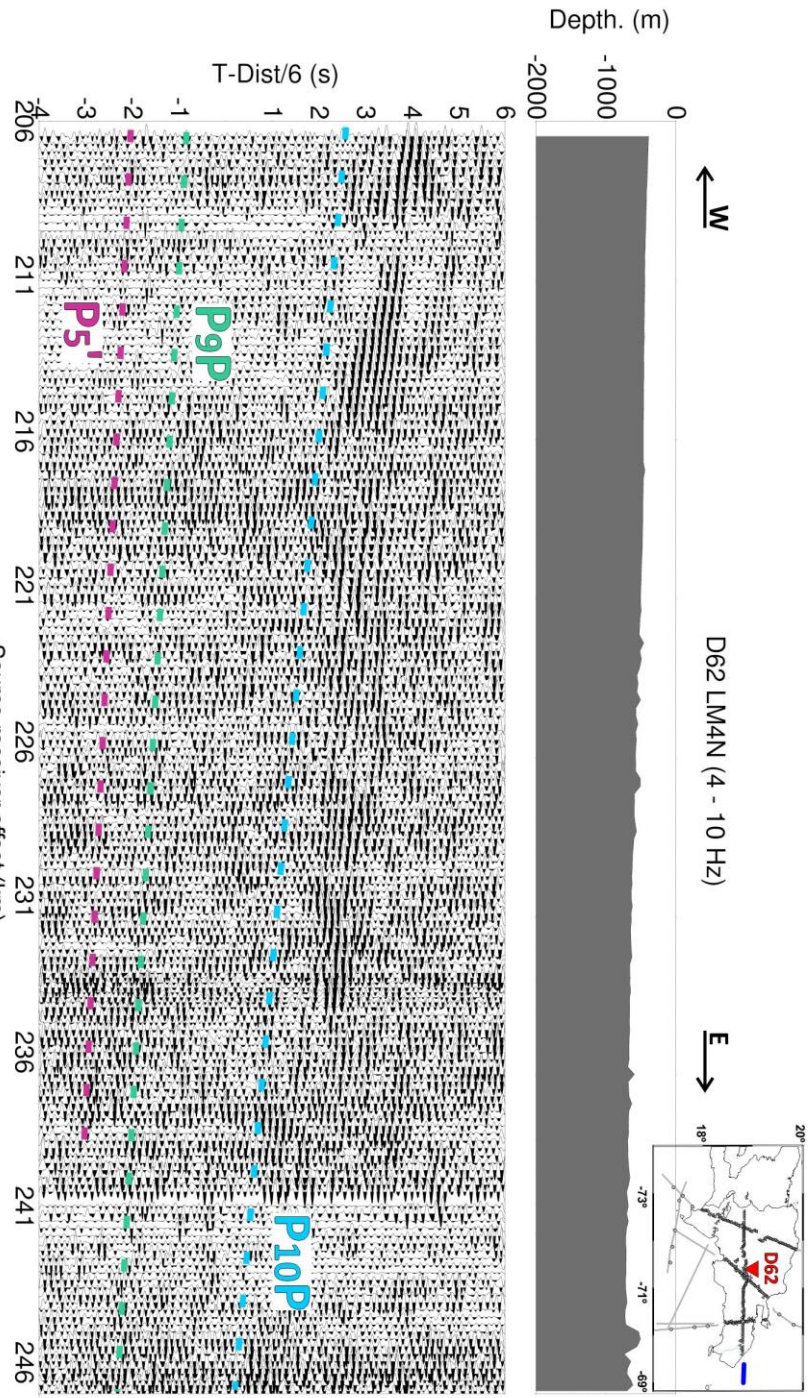

Fig. 6.4.1.3. LM4 seismic transect record, station D62. Vertical component, amplitude-trace normalized and band-pass filtering of 4 – 10 Hz. Colored lines point out reflected/refracted P-wave trains. On the top, bathymetry along this line. In the upper right corner, red triangle shows location of registration point and blue line the marine seismic line.

D137 seismic station is located close to the eastern coast of Dominican Republic at 312 km distance from westernmost land station. Figure 6.4.1.6 shows the seismic record section corresponding to this station. In this figure, it is possible to interpreted two diving waves traveling through discontinuities between third and fourth layers and fourth and fifth layers, respectively. P_3' is correlated from 30 to 36 km offsets while P_4' from 36 to 71 km. Both phases provide estimated apparent velocities of 5.4 km/s and 6.0 km/s.

Earthquake

The seismic record section corresponding to earthquake happened on 11 April 2009 is shown in figure 6.4.1.7. In this section, it is possible to observe some features and deep P-wave phases that reach layer number 12. In the Section 6.3, the parameters of this earthquake have been recalculated and the comparison between different velocity models has estimated a depth of 22.8 km. The direct wave interpreted corresponds to direct wave of fifth layer from 45 km to 105 km offset to the west with a.a.v of 7.3 km/s. After this phase, it is found P_6P from 41 to 146 km offset range with a similar apparent velocity, 7.4 km/s. Between source-receiver offset ranges 91 km to 122 km, P_7P is interpreted. The apparent velocity of this phase is slightly higher than previous with a value of 7.6 km/s. Then, it is correlated P_8P from 91 km to 180 km and a.a.v of 8.2 km/s. Next three phases are P_9P, P_{10}P and P_{11}P are followed between 140 to 300 km, 110 to 345 km and 200 to 330 km offsets with similar a.a.v with values 7.6 km/s, 7.3 km/s and 7.8 km/s, respectively. The previous phases show apparent velocities very close, which can mean the existence of lamination in the Upper Mantle. The deepest phase observed in the seismic record section of the event is P_{12}P. The average apparent velocity corresponding to this phase is 8.2 km/s followed from 280 km to 360 km offset.

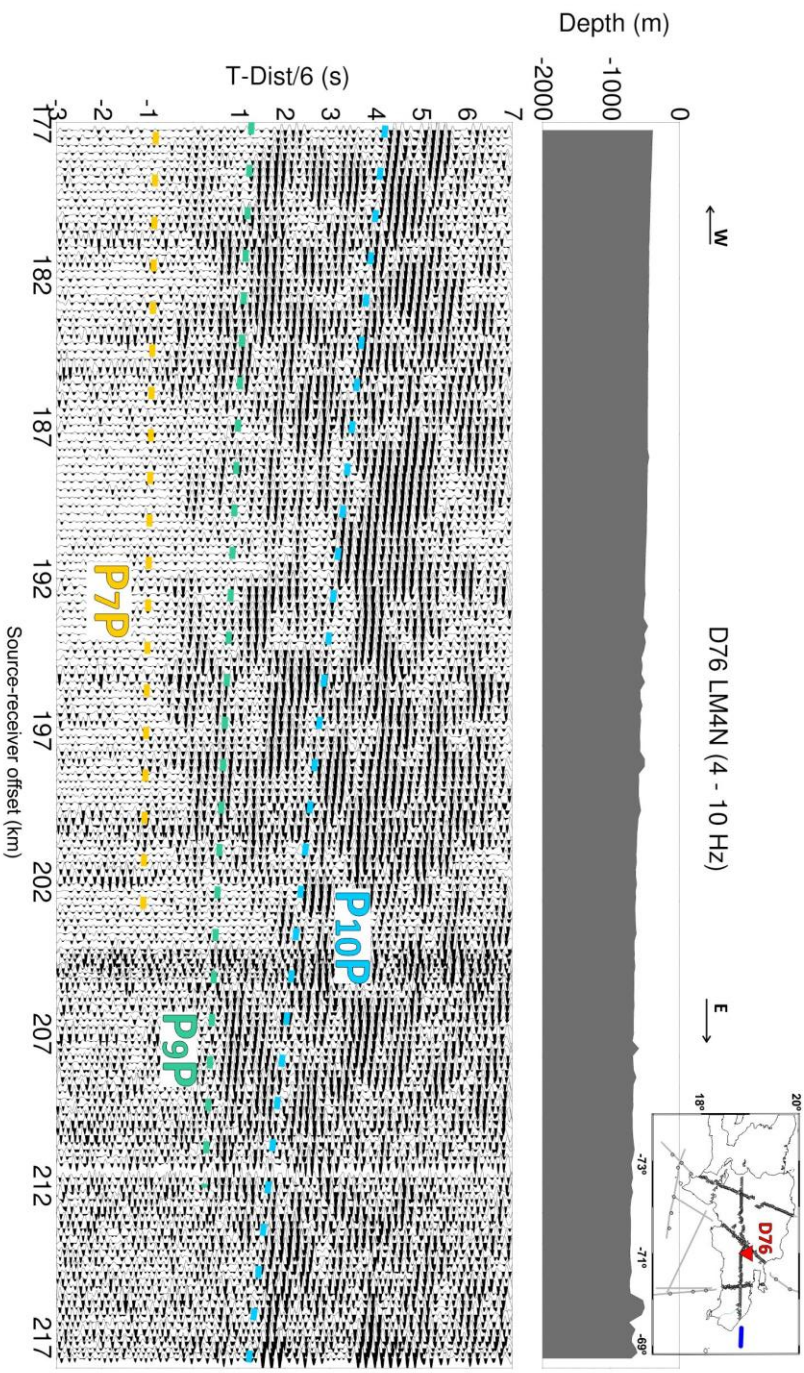

Fig. 6.4.1.4. LM4 seismic transect record, station D76. Vertical component, amplitude-trace normalized and band-pass filtering of 4 – 10 Hz. Colored lines point out reflected/refracted P-wave trains. On the top, bathymetry along this line. In the upper right corner, red triangle shows location of registration point and blue line the marine seismic line.

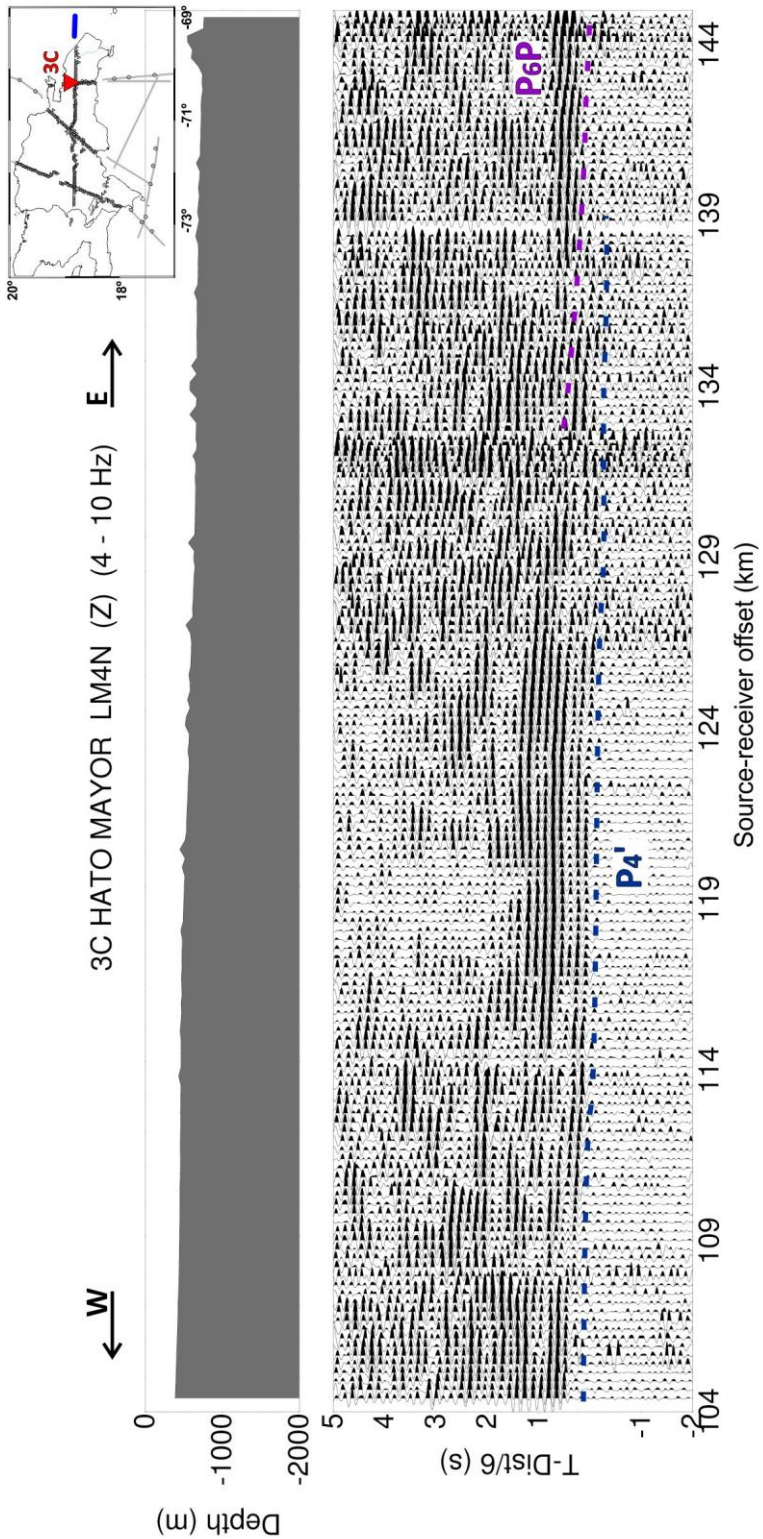

Fig. 6.4.1.5. Seismic record section corresponding to HATO MAYOR station registering seismic line LM4. Colored lines point out reflected/refracted P-wave trains. In this figure vertical component and bathymetry along this line are shown. In the upper right corner, red triangle shows location of registration point. Reduction velocity is 6 km/s, band-pass filtering of 4 – 10 Hz and amplitudes-trace normalized.

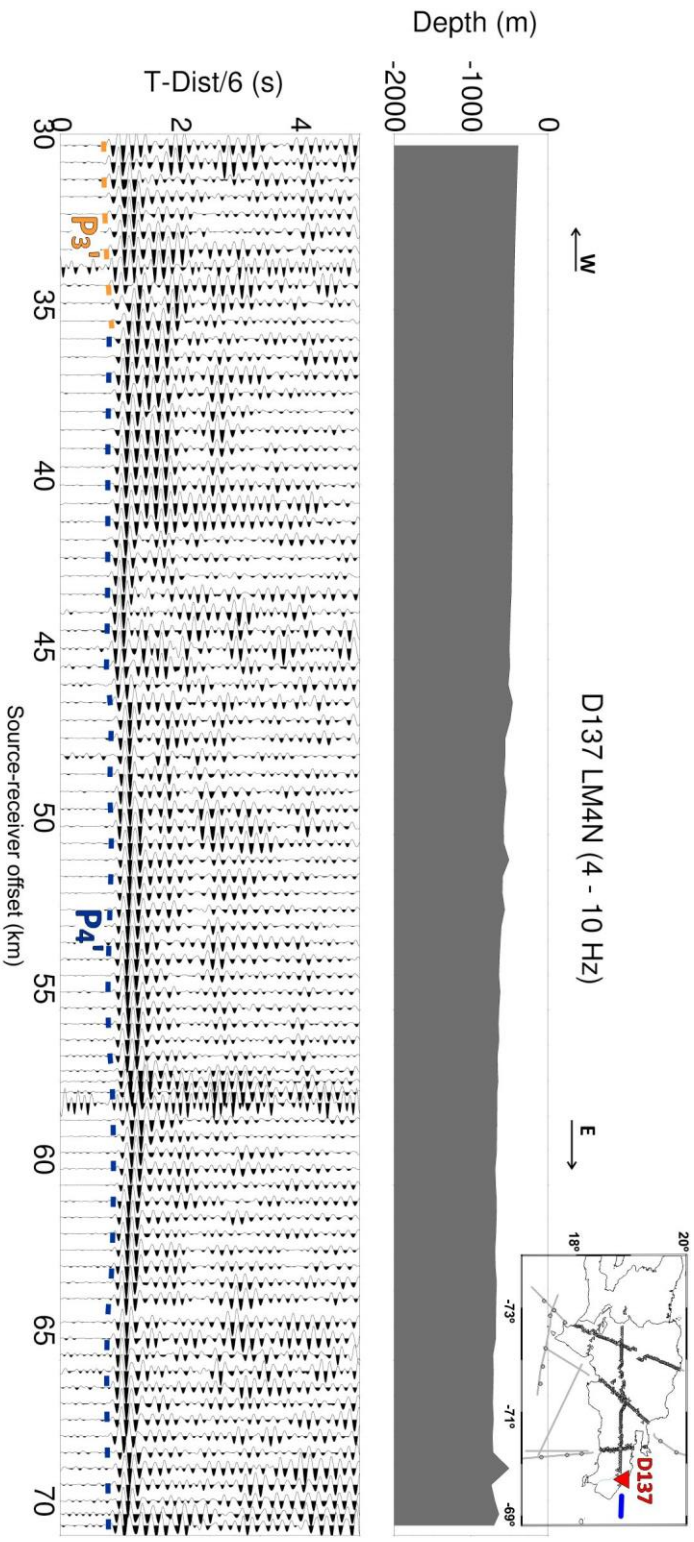

Fig. 6.4.1.6. Seismic record section corresponding to land station D137 recording marine shooting line LM4. Vertical component, amplitude-trace normalized and band-pass filtering of 4 – 10 Hz. Colored lines point out reflected/refracted P-wave trains. On the top, bathymetry along this line registering point location map where red triangle shows the station situation and blue line the marine shooting line.

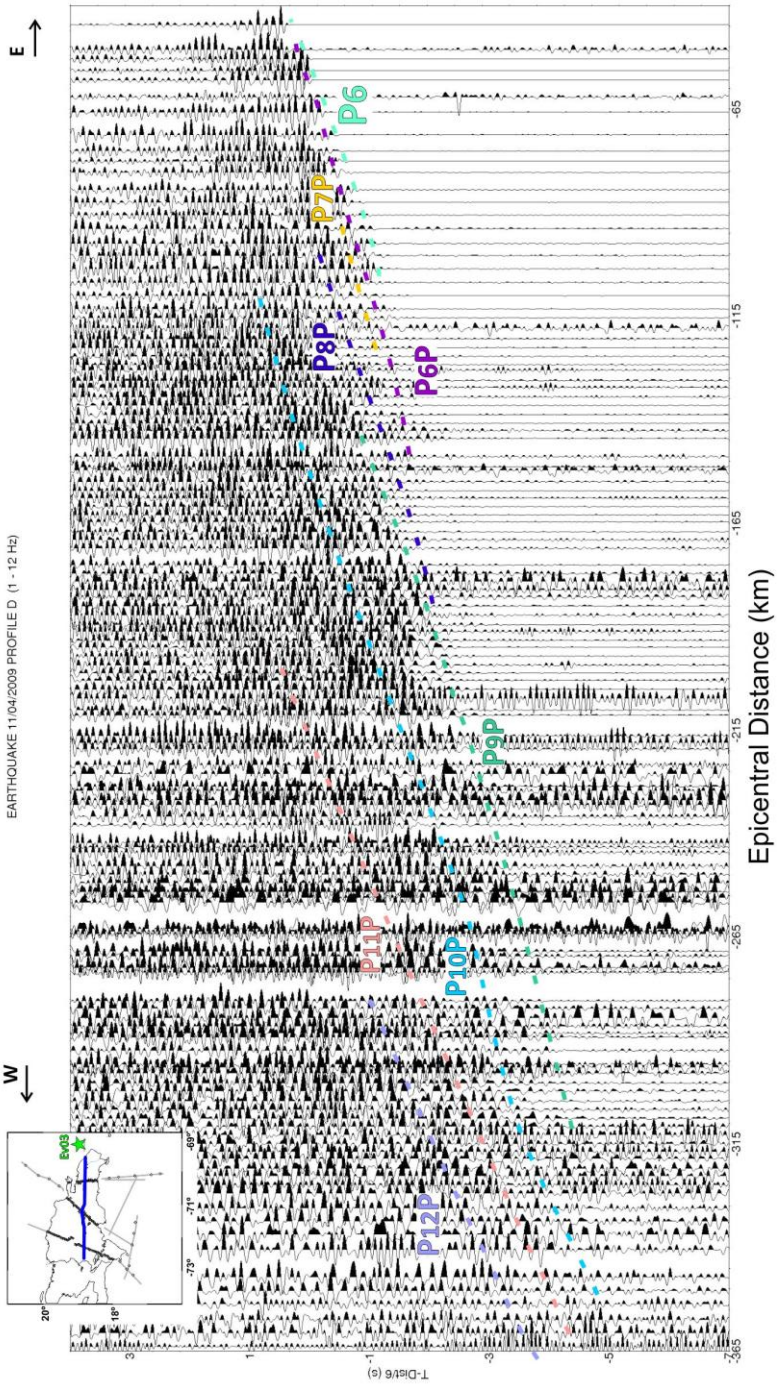

Fig. 6.4.1.7. Seismic record section corresponding to earthquake occurred on 11 April 2009 and registered by seismic station of Profile D. Colored lines point out reflected/refracted P-wave trains. In this figure vertical component is shown. In the upper left corner, red star shows location of registration point and blue line the recording seismic line. Reduction velocity is 6 km/s, band-pass filtering of 1 – 12 Hz and amplitudes-trace normalized.

6.4.2 Modeling

Seismic wide-angle data have been interpreted using forward modeling techniques [Zelt & Smith, 1992]. Water-depth/elevation from the airgun-shots/land stations was taken from the navigation data.

The joint modeling of deployed stations along Profile D allows obtaining a velocity model that represents tectonic and geological features and its interpretation from west to east of Dominican Republic.

In western area of the model (Fig. 6.4.2.1), a thin sedimentary layer with 3.3 ± 0.1 km/s and 2.7 km of maximum thickness in southeastern flank of San Juan Basin (Fig. 6.2.1) is determined. Between 95 km to 115 km, this sedimentary layer disappears to provide high relevance the layer immediately below with a V_P of 5.2 ± 0.1 km/s. This effect is due to the presence of the Peralta Belt in southern flank of Cordillera Central. Basement is reached at 2.4 km with a velocity of 5.2 ± 0.1 km/s over a layer with 5.8 ± 0.2 km/s on western area. In this zone, Moho discontinuity is reached at 39 ± 2 km decreasing eastward up to 15 ± 1 km depth below Bonao zone. The velocity change in the discontinuity is 6.5 ± 0.2 km/s over 7.7 ± 0.2 km/s. Upper mantle is divided in different layer with an increasing velocity in depth with values between 7.7 ± 0.2 km/s to 8.6 ± 0.3 km/s reaching a depth of 120 ± 5 km. Figure 6.4.2.2 shows the comparison between seismic record section and synthetic seismogram of land shot S3 (Fig. 6.3.1) where it is possible to corroborate the velocities and amplitudes obtained in the modeling process.

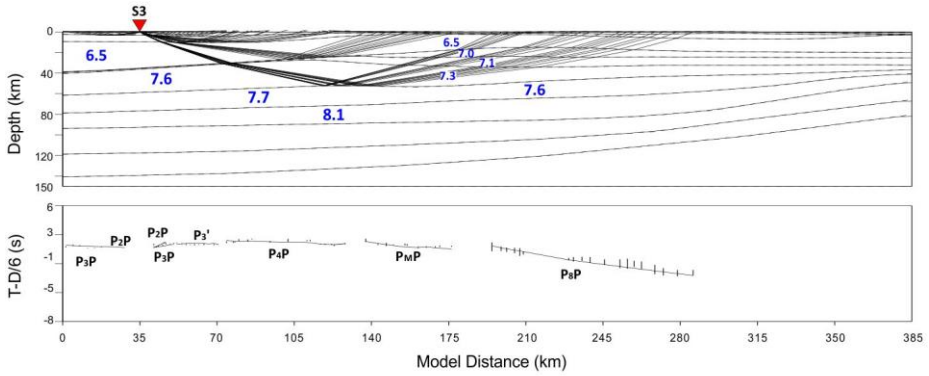

Fig. 6.4.2.1. Top: Ray tracing corresponding to shot S3 and velocity model (km/s). Bottom: Comparison between calculated (lines) and observed (vertical bars) travel times. Distances refer to the origin of the velocity model.

Eastward, the V_P of sedimentary layer is lower with a value of 2.7 ± 0.1 km/s in an extension of 60 km. Below it, basement and lower layers practically disappear having more relevance the fifth layer with a thickness between 12 and 18 km and average velocity of 6.4 ± 0.2 km/s. This area shows a lateral variation in the structure of

velocity model showed in the seismic record sections corresponding to land stations D77 to D89 and, also, this area is layered in Bonao zone. Lateral velocity variation in the sixth, seventh and eighth layers are 7.6 km/s to 7.0, 7.1 and 7.3 km/s, with 0.2 km/s of V_P uncertainty. The following layers maintain this lateral variation but are less obvious than previous ones with values of 7.7 and 8.1 ± 0.2 km/s compared to 7.6 and 7.9 ± 0.2 km/s, respectively. These layers remain almost constant and parallel until the end of the model with thicknesses of 8 km, 10 km and 14 km.

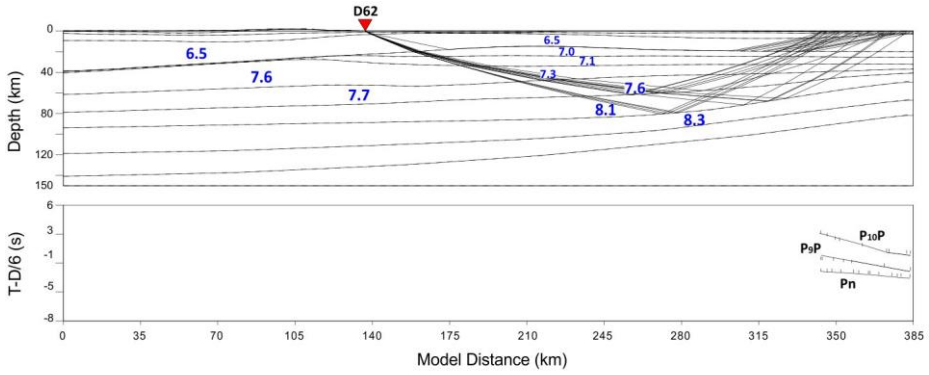

Fig. 6.4.2.3. Top: Ray tracing corresponding to land station D62 registering marine shooting line LM4 and velocity model (km/s). Bottom: Comparison between calculated (lines) and observed (vertical bars) travel times. Distances refer to the origin of the velocity model.

Between 225 and 310 km model distance corresponding to Seibo terrain (Fig. 6.1.1 and 6.2.1), the sedimentary layer disappears being basement the main layer observed (Fig. 6.4.2.4). This layer has a depth of 2 km and a velocity of 5.2 ± 0.1 km/s.

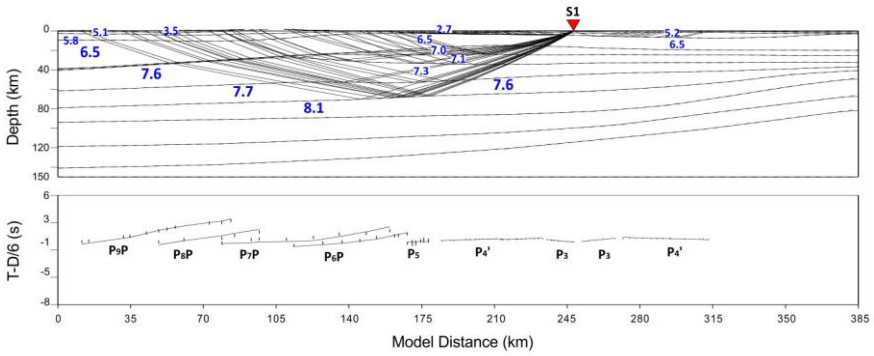

Fig. 6.4.2.4. Top: Ray tracing corresponding to shot S1 and velocity model (km/s). Bottom: Comparison between calculated (lines) and observed (vertical bars) travel times. Distances refer to the origin of the velocity model.

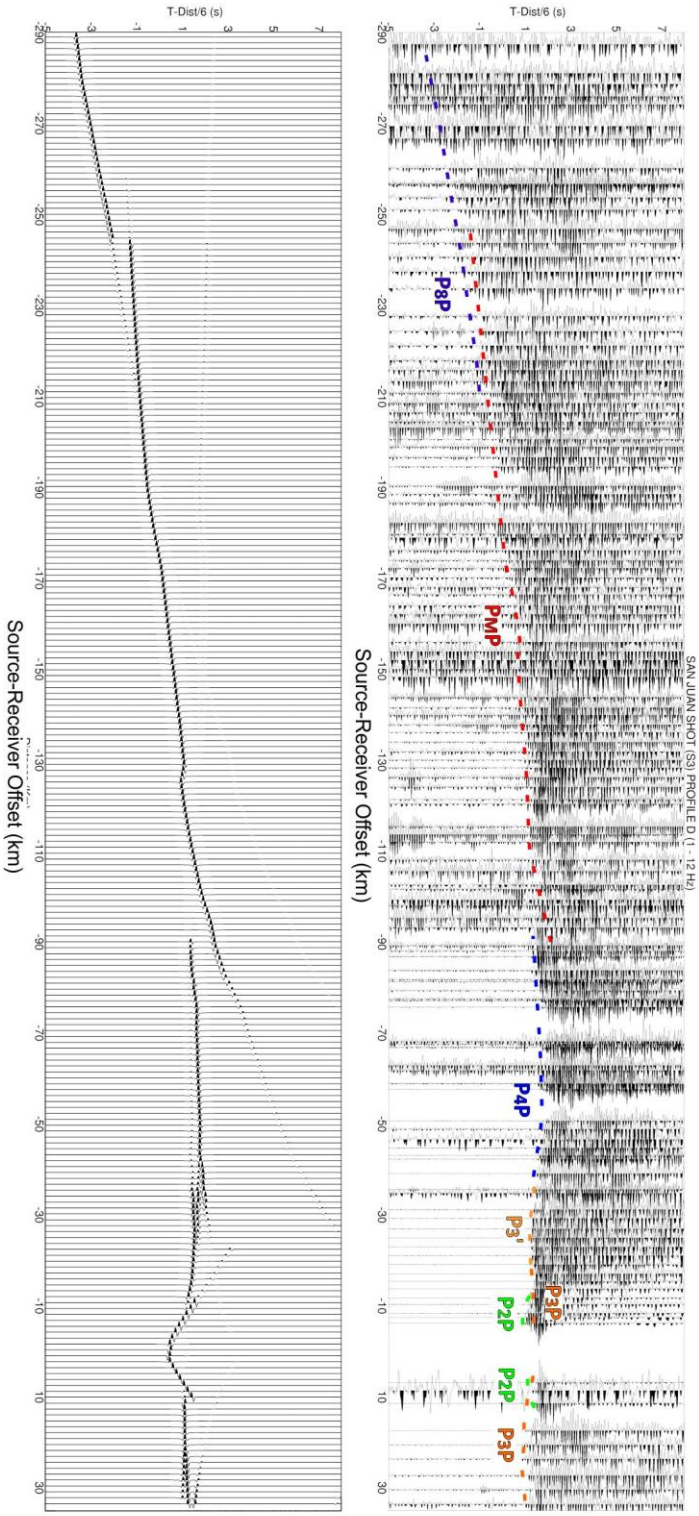

Fig. 6.4.2.2 Top: Seismic record section with correlated phases. Vertical component and Amplitude-trace normalized. Bottom: Synthetic seismogram corresponding to land shot S3 recorded by stations deployed along Profile D. Amplitude-trace normalized.

Following layer is 1.6 km thick but thickened to the east reaching a maximum value of 5.5 km.

When offshore area is reached (Fig. 6.4.2.5 – 6.4.2.7), a sedimentary layer appears, being 1.6 km thick. In this area, basement and following layer disappear showing a thick layer of 17 km with 6.5 ± 0.2 km/s. Lower layers have a dip of approximately 18º. The P-wave velocities determined for these layers are 8.2, 8.4 and 8.6 ± 0.3 km/s, respectively. In ray tracing corresponding to event Ev03 (Fig. 6.4.2.5) shows the correlation between observed and calculated travel time whose velocities observed are corroborated by the synthetic seismogram (Fig. 6.4.2.6). This synthetic seismogram shows a possible lamination where the energy appears dispersed and lateral variation of the velocity will provide an increasing in noise level.

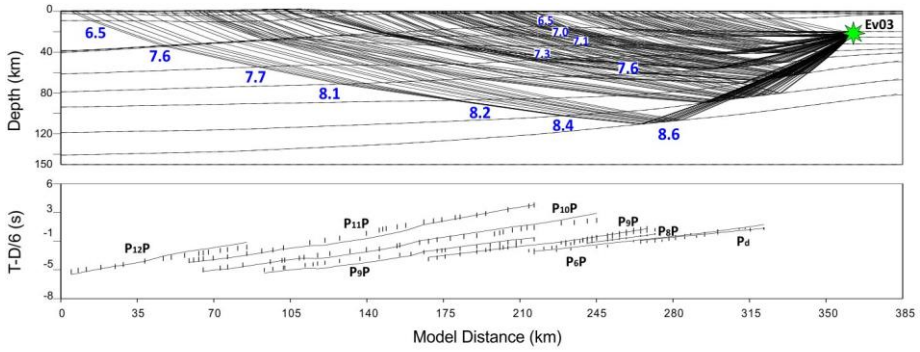

Fig. 6.4.2.5. Top: Ray tracing corresponding to event Ev03 and velocity model (km/s). Bottom: Comparison between calculated (lines) and observed (vertical bars) travel times. Distances refer to the origin of the velocity model.

Figure 6.4.2.7 displays the ray tracing of complete Profile D studied in this chapter showing the comparison between calculated and observed travel times.

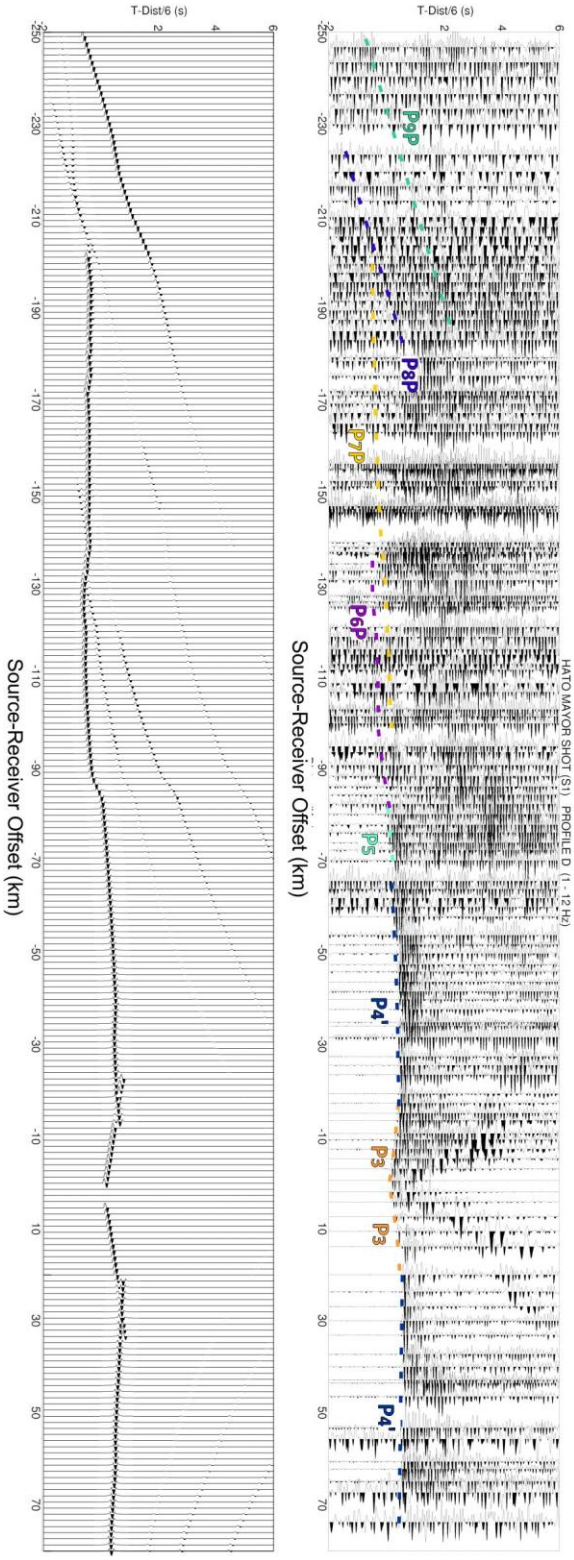

Fig. 6.4.2.6 Top: Seismic record section with correlated phases. Vertical component and Amplitude-trace normalized. Bottom: Synthetic seismogram corresponding to earthquake of 11 April 2009 recorded by stations deployed along Profile D. Amplitude-trace normalized.

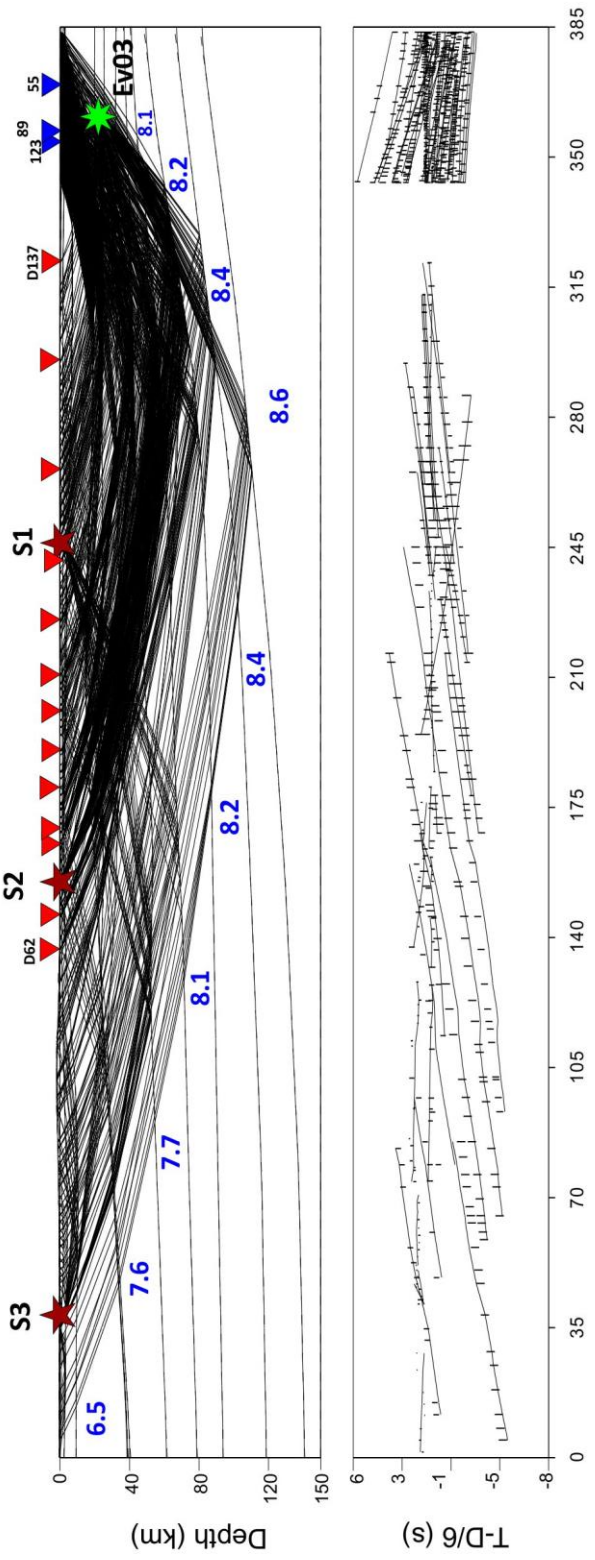

Fig. 6.4.2.7. Top: Ray tracing corresponding to all land stations of Profile D to obtain velocity model (km/s). Bottom: Comparison between calculated (lines) and observed (vertical bars) travel times. Distances refer to the origin of the velocity model. Blue triangles represent marine shots that are registered by all land stations. Red triangles show land stations used for this study and red stars are shots S1, S2 and S3 while green star represent the location of event Ev03 at the Caribbean Sea.

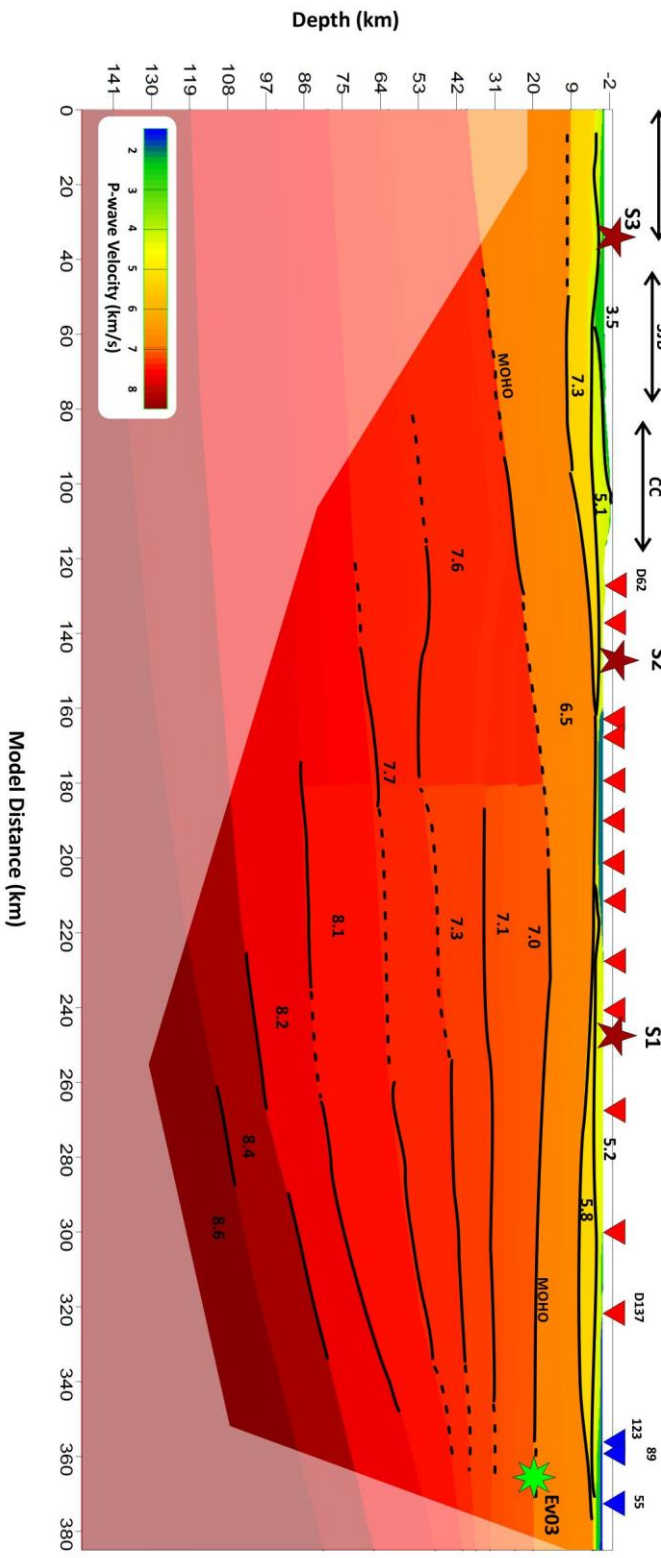

Fig. 6.4.2.8. P-wave velocity model corresponding to Profile D studied in this work where inverted red triangles denote land stations and black star corresponds to land shots S1, S2 and S3. The dashed lines show the discontinuities where P-waves have been reflected and refracted. The shaded regions show areas not illuminated by the ray beams. SN = Sierra de Neiba; SJB = San Juan Basin; CC = Cordillera Central. In grey, different tectonic terrains along the profile. All figures are scaled according depth and distance. Color scale and numbers denote P-wave velocity in km/s.

Estimates of arrival-time fit quality for each phase and for all phases are given in Table 6.4.I. Our final model produces a normalized χ^2 of ~ 3 with most of no individual phase over-fit ($\chi^2 > 1$ for all phases). The observed arrival-times are adequately fit by the predicted ones. Our model is able to predict most of the observed arrival-times (NC and NR are similar) but deep travel-time misfits are not really similar to the pick uncertainty.

Phase	NC	SIGMA (s)	NR	Trms (s)	χ^2
P_4P/P_4'	281	0.102	279	0.150	2.557
P_MP	26	0.153	26	0.242	6.028
P_n	186	0.170	184	0.241	1.924
P_{6d}	12	0.150	12	0.201	1.950
P_6P	98	0.161	88	0.202	2.072
Under Moho: P_7P /P_8P /P_9P	250	0.219	249	0.365	3.033
Deepest: $P_{10}P/P_{11}P/P_{12}P$	194	0.252	185	0.457	4.122
FIT	1047	0.178	1012	0.322	3.239

Table 6.4.I Travel-time fit for each phase: NC = number of picks; SIGMA = mean pick uncertainty; NR = number of traced rays; Trms = travel time root mean square misfit; χ^2 = normalized chi square.

6.5 RESULTS AND CONCLUSIONS

The different tectonostratigraphic terrains that Hispaniola Island is divided are crossed by Profile D of Caribe Norte project. Folds, thrust and left-lateral faults and shear zones characterize the central area of this island being the main tectonic elements Peralta Belt, Tireo Fm and Duarte terrain limited by San Juan – Los Pozos, San José – Restauración, Bonao – La Guácara and Hispaniola Fault Zones. The seismic investigation carried out in Caribe Norte project reveals the aspects shown in this section.

Main features of the Profile D model

Crustal velocity model is conformed by 12 layers in a total length of 385 km determined from different seismic sources registered by one and three components land stations providing knowledge about the crust that varies in thickness from west to east.

Sedimentary and basement layers define the upper part of the crust. In the western area, the sedimentary layer varies between 1 and 3 km thick and 3.5 ± 0.1 km/s to disappear nearby Peralta Belt while the basement is 2 km depth having more relevance in the Cordillera Central to be thinner after this tectonic element. In the central area of the model, the sedimentary layer appears with V_P of 2.7 ± 0.1 km/s where different formations are merged as Los Ranchos Fm, Amina and Maimón Fm, Loma Caribe Peridotite and Siete Cabezas and Peralvillo Sur Fm (Fig. 6.2.1). In this area, the basement and lower layer disappear showing more importance the layers immediately below. Eastward, sedimentary layer disappears corresponding to

volcano-plutonic part of the island arc of Seibo terrain up to it reaches the eastern offshore part of the model with a value practically constant of 1.6 km. In the eastern part of the model, the basement and the lower layer acquire greater relevance compared to the sediment layer with maximum value of 5.5 km depth. In the offshore area, both layers disappear being more important the layers immediately below. This part of the model is characterized by depth uncertainties less than 1 km.

The lower crust is limited by Mohorovicic discontinuity whose effect is more evident in the western area up to Peralta Belt vicinity where appears laminated with a lateral velocity contrast. This fact is due to the presence of the San José – Restauración and Bonao – La Guácara Fault Zones that are near each other in this region as it is shown in the Figure 6.1.1. Moho depth at the beginning of the model is 39 ± 2 km with V_P change of 6.5 ± 0.2 km/s to 7.6 ± 0.2 km/s, decreasing to the east up to 15 ± 2 km in the transition area where velocity increases gradually in a thickness of 20 ± 2 km approximately. These layers are slightly thinner at the end of the velocity model.

The lowest layers of the velocity model in the Upper Mantle (Fig. 6.4.2.8) are better determined in the eastern area due to the high number of rays reflected in these layers (Fig. 6.4.2.7) with V_P values of 8.2, 8.4 and 8.6 km/s (± 0.3 km/s). The calculated dip of these layers is 18^o reaching a maximum depth of 120 ± 5 km estimated from event EV03 seismic record section interpretation.

Comparison with any other studies and data of some areas that cross the profiles

The velocity model proposed in this work is in agreement with different studies, mainly in shallow region. In Mann et al. (1991) is provided a global idea about the tectono-stratigraphic structure of the whole Hispaniola Island. In particular, the authors analyze the structure of the shallow crust in four cross sections across central and eastern Hispaniola in NE – SW direction. It is possible to compare some parts of these sections with cross section obtained in this chapter. First, Mann et al. (1991) propose that high-level thrust and reverse faults of the Presqu'ile du Nord – Ouest – Neiba and Trois Rivières – Peralta terrains root in the detachment at depth of 10 to 15 km. From wide-angle seismic data, it has been determined for this area a depth between 9 and 11 km that is in correspondence with Mann et al. (1991) showed in Fig. 6.4.2.8.

The structure and topography of eastern Hispaniola contrasts markedly with that of western and central Hispaniola. Easter Hispaniola exhibits much less topographic relief and less extensive evidence for recent faulting. Deep seismic zones beneath eastern Hispaniola are attributed to southward subduction of Atlantic Ocean crust beneath eastern Hispaniola [McCann and Sykes, 1984] and simultaneous northward subduction of Caribbean crust beneath eastern Hispaniola [Byrne et al., 1985]. Lower topography and less Neogene deformation of eastern Hispaniola suggests that

subduction, and not crustal shortening, is the dominant tectonic process affecting eastern Hispaniola [Ladd et al., 1981]. The model proposed in this chapter establishes a dip of 17º in the eastern area that could be result of oblique subduction of NAP.

Conclusions

As a synthesis, final conclusions about the study of the crust and Upper Mantle in a west to east seismic transect in Dominican Republic from different seismic sources are enumerated.

- It has been established a crustal velocity model for study area through controlled source seismology, seismicity and wide-angle seismic data obtained during Caribe Norte project.
- From a seismic point of view, the crustal velocity model for Profile D consists of 12 layers in a W – E direction with a transition zone that reveals the different structure between west and east regions of Dominican Republic.
  - Upper Crust is characterized by a thin sedimentary layer with different V_P along transect and a basement. In western area, sedimentary layer is 3 km thick due to the profile crosses southern San Juan Basin area. Then, this layer disappears to reappear with V_P lower in a mixed area formed by Los Ranchos Fm, Amina and Maimón Fm, Loma Caribe Peridotite and Siete Cabezas and Peralvillo Sur Fm. In the offshore part of the model, this layer is 2 km thick.
  - The Lower Crust is a homogeneous layer along the profile whose thickness is higher in the west than in the east with no lateral velocity variations.
- Mohorovicic discontinuity depth has been established. The study has revealed that San José – Restauración Fault Zone reaches this layer implying the appearance of lateral velocity variation and lamination of the layer with increasing velocity in depth.
- The eastern part of the model reports a structure dipping 18º and reaches 120 ± 5 km depth that could be associated to oblique subduction of NAP. But, there is not enough information about this structure from western part to define a possible subduction or its behavior in that area.
- The earthquake of 11th April 2009 has been relocated from 3 different 1D velocity models and the best solution has been provided by the P-wave velocity model of wide-angle seismic refraction model obtained in this study. This fact implies a good validation for our model.

CHAPTER 7

REFERENCE 1D P-WAVE VELOCITY MODEL FOR NORTHEASTERN PART OF CARIBBEAN PLATE

7.1 INTRODUCTION

The refraction models presented in the previous chapters provide detailed insight in the tectonic structure below the Dominican Republic along different lines, as a first part of the results of this thesis. The second part is related to the high seismicity level in the region (*see Section 1.1.4, Chapter 1*). This fact offers for the opportunity to derive a regional seismic velocity model by implementation of Local Earthquake Tomography (LET) technique using the seismicity registered in the area.

- Seismic Networks in the NE Caribbean

Studies of seismic tomography at regional and local scales often require merging of phase picks from several networks. This fact implies the appearance of inconsistencies due to each network follows different ways of recording and treating the data, uses different velocity models for routine earthquake locations [Quintero & Kissling, 2001]. Furthermore, the differences in the picking behavior of network analysts in terms of absolute timing, timing uncertainties and phase interpretations can be another point of inconsistencies, but a potential phase misidentification can be detected from calculation of residuals between reference hand picks and routine picks [Diehl et al, 2009]. Misinterpretations in station codes and station coordinates directly affect to the hypocenter determination. To avoid these problems, it is necessary to compile a master station list based on Solarino et al., (1997) procedure.

The number of seismic networks operating in the Caribbean has been a steady increase in recent years as well as an extension and update on the instrumentation of such networks mainly due to the earthquake in Haiti in 2010. The combination of

these networks will allow us to establish a regional station network selected for our study area by building a Master Station List.

The operating networks in this zone (Fig. 7.1.3) and their owners are:

- Caribbean Network (USGS) (**CU**).
- Puerto Rico Seismic Network (PRSN) & Puerto Rico Strong Motion Program (PRSMP) (**PR**).
- Instituto Sismológico Universitario (Universidad Autónoma de Santo Domingo) (ISU-UASD) (**DR**)
- Canadian National Seismograph Networks (**CN**)
- US Geological Survey Networks (**GS**)

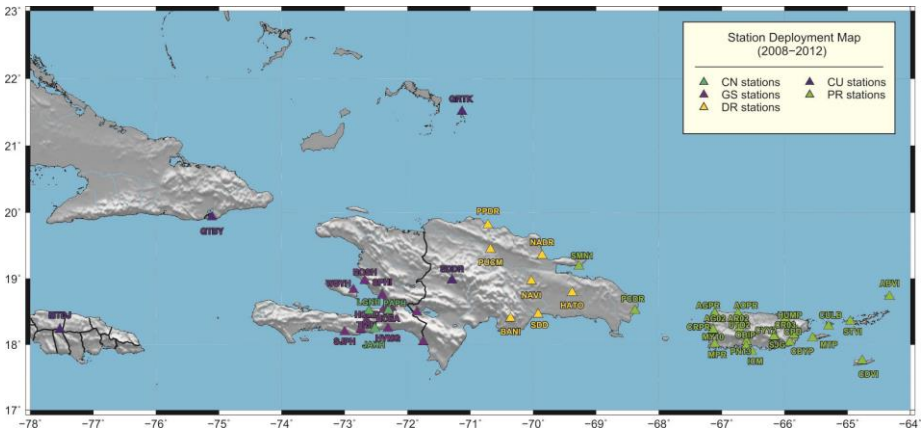

Fig. 7.1.3. Operative Seismic Networks and stations in the Caribbean region. Triangles denote seismic stations and colors indicate the corresponding network affiliation. Legend: 1) Green triangle: stations of Canadian National Seismograph Network (CN); 2) orange triangle: stations of Caribbean Network (USGS) (CU); 3) pink triangle: stations of US Geological Survey Networks (GS); 4) blue triangle: stations of Puerto Rico Seismic Network (PRSN) & Puerto Rico Strong Motion Program (PRSMP) (PR); 5) yellow triangle: stations of Instituto Sismologico Universitario (ISU-UASD) (DR).

A master station list [Solarino et al., 1997] is a complete list of all stations where the owner is known of all permanent and temporary stations operative during a period of time in a region. In our case, we compile a master station list since the year 2000 to present in the area of Dominican Republic and its surroundings (Annex II). After known the owner of each station, we cross-check the coordinates and names of these stations with each seismological services. Then, we correlate the station names reported by the owners and used by seismological services for stations outside their own network published in various catalogues. The catalogues used are:

- International Seismological Centre (ISC).
- Incorporated Research Institutions for Seismology (IRIS).

- Puerto Rico Seismic Network (PRSN)
- US Geological Survey (USGS)

From these stations we are able to define the appropriated region to seismic tomography studies with GAP < 180º (Fig. 7.1.4) characterized by high density of ray coverage traced between earthquakes and stations. This area limits the earthquake selection for our study.

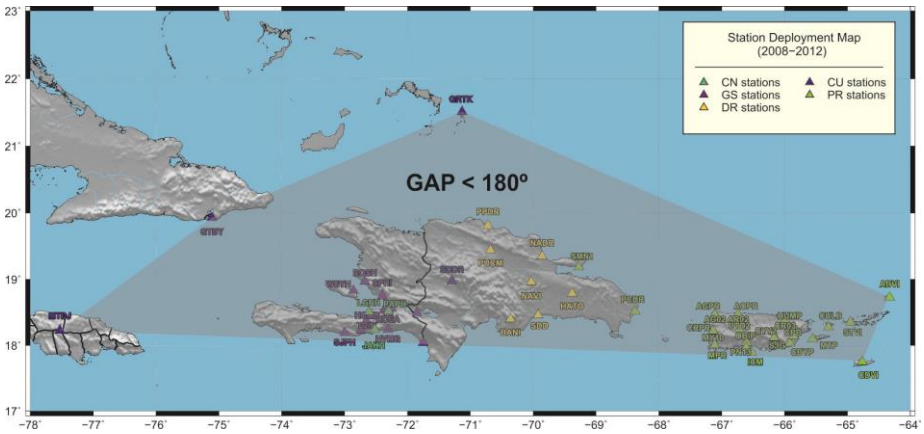

Fig. 7.1.4. Delimited area for seismic tomography study of Dominican Republic where the earthquakes with GAP<180º are selected.

Since the period in which these stations are operative is not the same, we selected two periods according to the increment of seismic stations number in the area after Earthquake of Haiti in 2010.

7.2 EVENT DATA SET COMPILATION AND HAND PICKING

The events selected for this study have been obtained from different event catalog provided mainly by IRIS, ISC and USGS. According to the number of stations, we have divided data from 1st January 2008 to 31st January 2010 (Period I) and from 1st February 2010 to 15th October 2012 (Period II). Figures 6.2.1 and 6.2.2 show events for Periods I and II, respectively, with stations that were operative in each period. Data obtained from IRIS catalog that merges data from catalogs:

- **NEIC PDE**: The 'NEIC PDE' catalog is populated from the USGS ENS (Earthquake Notification Service) and the USGS ftp site serving PDE Bulletins.
- **ISC**: The 'ISC' catalog is populated from the International Seismological Centre's ftp site.

- **ANF**: The 'ANF' catalog is populated from origin information from US Array Transportable Array sources.

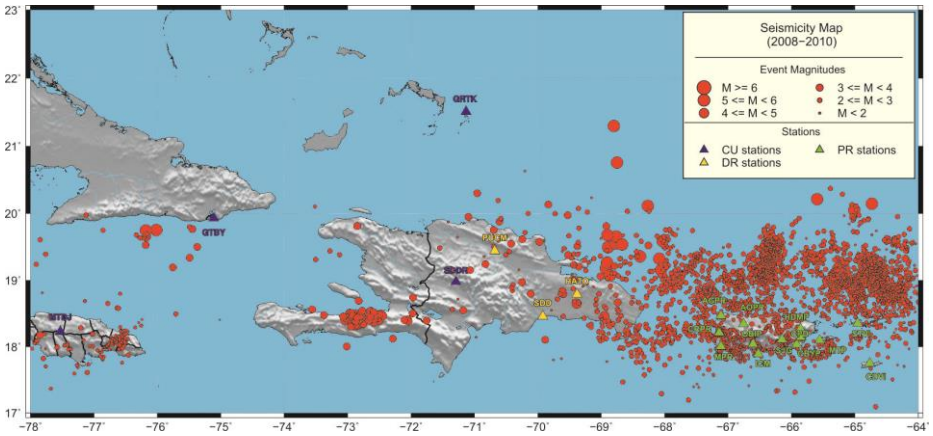

Fig. 7.2.1 Map showing the seismicity during PERIOD I for this study (from USGS, ISC and IRIS data bases). Legend: 1) Red circles: events scaled by magnitudes; 2) blue triangles: stations of Caribbean Network (USGS) (CU); 3) yellow triangle: stations of Instituto Sismologico Universitario (ISU-UASD) (DR); 4) light green triangle: stations of Puerto Rico Seismic Network (PRSN) & Puerto Rico Strong Motion Program (PRSMP) (PR).

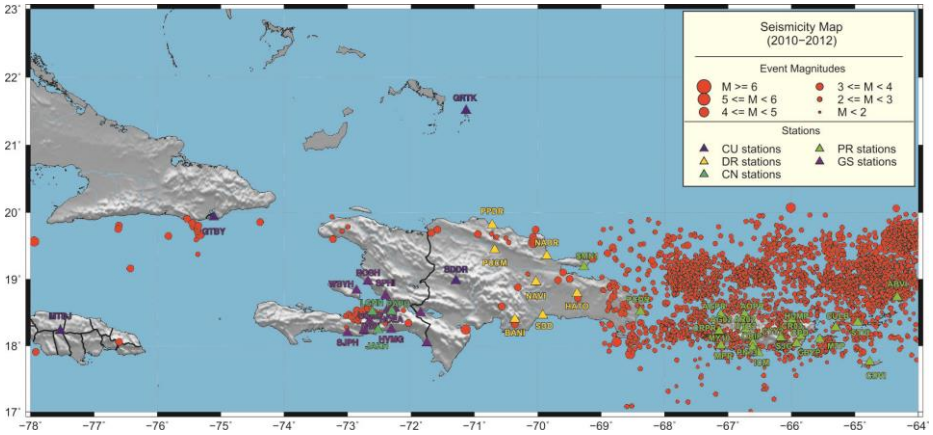

Fig. 7.2.2 Map showing the seismicity in the study area for PERIOD II (from USGS, ISC and IRIS data bases). Legend: 1) Red circles: events scaled by magnitudes; 2) blue triangles: stations of Caribbean Network (USGS) (CU); 3) yellow triangle: stations of Instituto Sismologico Universitario (ISU-UASD) (DR); 4) light green triangle: stations of Puerto Rico Seismic Network (PRSN) & Puerto Rico Strong Motion Program (PRSMP) (PR); 5) Green triangle: stations of Canadian National Seismograph Network (CN); 6) purple triangle: stations of US Geological Survey Networks (GS).

After observing these maps, we select events inside the area established in Fig. 7.1.4. The selection for Period I has been done in different steps (Fig. 7.2.3). In the first step, we selected events with M > 4.5 in longitudes between -78° and -72°. From -72° to -69.5°, all events have been extracted. Finally, we have chosen events with M > 4 between -69.5° to -64°. This selection is due to the station deployment during Period

I is concentrated principally in Puerto Rico and eastern part of Dominican Republic regions and we must assure the greatest possible number of events recorded by all stations to get the maximum number of observations.

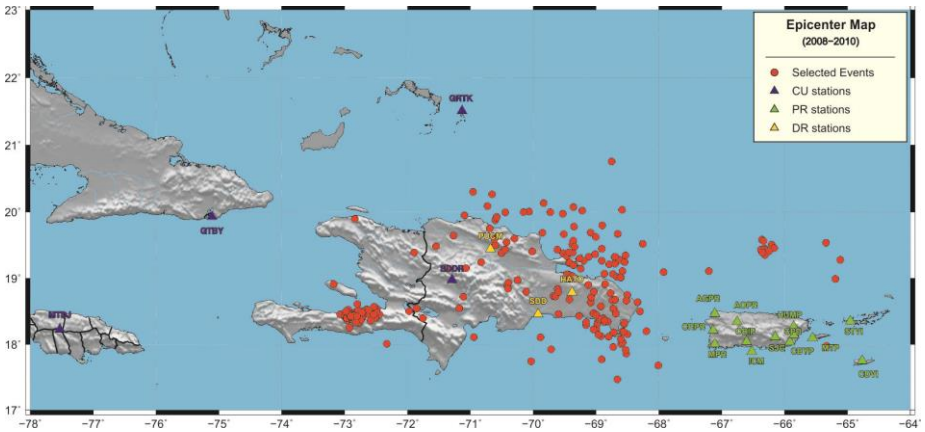

Fig. 7.2.3. Selected events map for Period I (relocated events). Legend: 1) Red circles: events selected; 2) blue triangles: stations of Caribbean Network (USGS) (CU); 3) light green triangle: stations of Puerto Rico Seismic Network (PRSN) & Puerto Rico Strong Motion Program (PRSMP) (PR); 4) yellow triangle: stations of Instituto Sismologico Universitario (ISU-UASD) (DR).

The events for Period II (Fig. 7.2.4) have been selected principally according to new distribution of stations after Haiti Earthquake (January 12, 2010). This new deployment allows us find earthquakes around Hispaniola Island, which will provide us good coverage of rays.

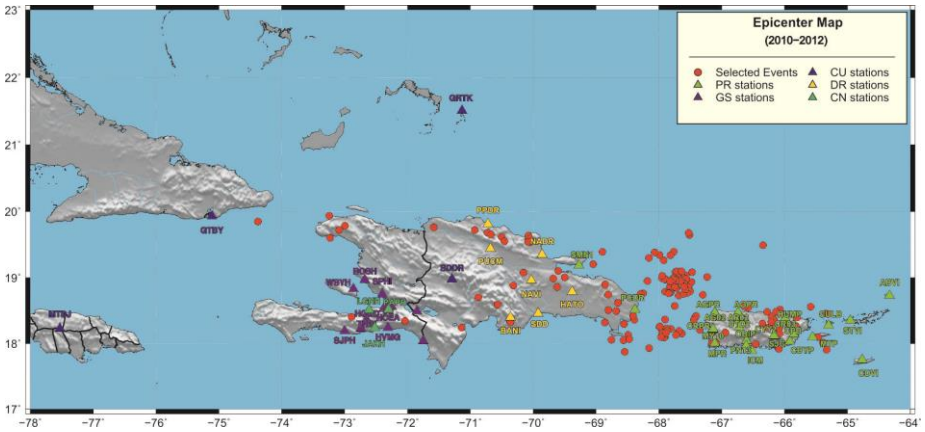

Fig. 7.2.4. Map of selected events for Period II (relocated events). Legend: 1) Red circles: events selected for this period; 2) blue triangles: stations of Caribbean Network (USGS) (CU); 3) yellow triangle: stations of Instituto Sismologico Universitario (ISU-UASD) (DR); 4) light green triangle: stations of Puerto Rico Seismic Network (PRSN) & Puerto Rico Strong Motion Program (PRSMP) (PR); 5) Green triangle: stations of Canadian National Seismograph Network (CN); 6) purple triangle: stations of US Geological Survey Networks (GS).

The master event list obtained from both periods is shown in Annex III.

After obtaining master station and event lists, we have combined both to get all the events recorded by each station. We have used online options (JWEED v3.2 and Vase2.9.1) and archived data (BREQ_FAST) provided by IRIS to get waveforms.

JWEEDv3.2 and Vase2.9.1 are JAVA programs to obtain waveforms from any institution which has implemented DHI servers. The basic steps to obtain data from JWEED are:

- Select some servers grouped by organization (IRIS, GSC, ISC, BERKELEY, CALTECH, IPGP,…) and type (Seismogram, Network, Event)
- Select some events defining Start/End time, Magnitude/Depth parameters, Catalogs or defining a region in "Map" screen. All events fetched from DHI event server within the time range specified are mapped in "Map" screen.
- Select some stations within given criteria such as location or distance from events which are mapped in "Map" screen
- Create a request file based on these events and stations.
- Download the waveform data based on the request file from Online or Archival Systems. The waveforms can be saved in SAC or miniseed formats. Moreover, it is possible to watch seismograms in one screen per event.

The process of obtaining waveforms from Vase2.9.1 is slightly different from the one by JWEED. The main points are:

- Select some servers in the same way as JWEED.
- Select an area of interest drawing a box in Map/Find stations panel.
- Select a Start/End time and query the available stations for this period with online data.
- In Stations panel appears all obtained stations grouped by network.
- Display seismograms in View panel selecting one or more stations. In this screen, it is possible to save the waveforms in SAC or miniSEED formats.

These two retrieving programs, however, are insufficient to complete our data base since not all waveforms corresponding to the selected events are available online. For this reason, we have requested the archived data in IRIS Data Management Center archive by electronically mailing a specially formatted file (BREQ_FAST file) or filling in the form in http://www.iris.edu/SeismiQuery/breq_fast.phtml. The process involves filling in a form with required parameters (Network, Station, data start and end times, personal data such as name, email, address and label for the file) and selecting the appropriated data format (full SEED, dataless SEED, miniSEED, sync file or RESP file). Then, an email will be sent to the DMC and the DMC will return the data with previous selected formats in a period of time, which will depend on when

the request form was sent. This process requires sending an email per event and station. In Annex III is shown the master event list including stations that recorded every event ordered by year.

After downloading data from ftp://ftp.iris.washington.edu/pub/userdata, we can check their quality viewing them with SeisGram2K (http://alomax.free.fr/seisgram/SeisGram2K.html). SeisGram2K Seismogram Viewer is a Java software package for interactive visualization and analysis of earthquake seismograms. This program displays one or more sets of single trace or 3-component seismograms and can read data in SAC binary and ASCII, PEPP, GSE2.1, mini-SEED (preliminary), SEED (preliminary), TITAN (preliminary) and other formats with multiple analysis tools.

Finally, we compiled an Event Data Base composed by 475 earthquakes with their corresponding waveforms per seismic component and station.

- Principles of picking

In the following section, we present the procedure followed to pick manually every seismogram with a consistent quality assessment for timing uncertainty and phase interpretation exposed in Chapter 2 and according to Diehl et al. (2009). For this purpose, we used the program PILOT.

PILOT is a MATLAB based program to determine ("picking") P- and S-phase onsets and to estimate magnitudes of local and regional earthquakes. For localization, the FORTRAN based software package HYPOINVERS and HYPOSAT can be used. PILOT has been developed at the Ruhr Universität-Bochum by the seismology working group. PILOT is able to process ASCII, SAC and GSE2 data.

The process to convert SEED data, obtained directly from IRIS for each event, into SAC file appropriated for PILOT, requires a set of previous steps. During this process, we have to be careful given that a seismological format may not contain all the relevant information for other formats. In http://www.orfeus-eu.org/Software/conversion.html, we can find different softwares for conversion in different seismic formats. In our case, the first step is to convert SEED file into SAC file with RDSEEDv5.1 program. This program is provided by IRIS filling a small request (http://www.iris.edu/forms/rdseed_request.htm). After this conversion, we do not get one single SAC file, but we get as many files as stations we have multiplied by 3 component per station. In addition, we have to add the fact of we can get more files if the station stops recording during the requested time.

An appropriated file for PILOT must have some features like same origin and end times and size. For this purpose, we use SAC (Seismic Analysis Code,

http://www.iris.edu/software/sac/manual.html) to visualize, synchronize and cut the waveform files. Originally, SAC files are in Little-endian and we have to convert to Big-endian with program sacswapbyte (https://sites.google.com/site/foo4funreborn/software/sacswapbyte). Moreover, SAC file name must have the following format: XXXXyymmdd_hhmmss_i.sac (ex. SDDR100112_215310_z.sac), where

- XXXX: Station name
- yy: year
- mm: month
- dd: day
- hh: hour
- mm: minute
- ss: second
- i: East, North or Vertical component (e, n, z)

All SAC files for the same event must be in a folder named as exxxx.ddd.yy (ex. e0001.012.10), where

- xxxx: event number
- ddd: julian day
- yy: year

As well, PILOT needs as input files events.loclist and info.dat. In events.loclist, it is possible to find all data related with events like name, origin time, latitude, longitude and depth and info.dat contains data about station location.

After this process, we are able to run PILOT. In the initial screen, we define the event for picking and its path. And then, we visualize the seismograms of every station that registered the selected event ordered by epicentral distance (Fig. 7.2.5).

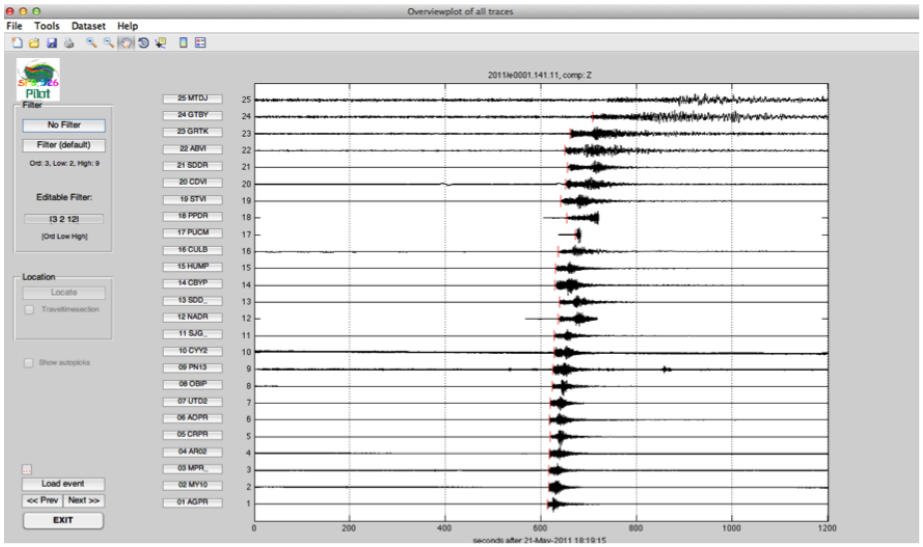

Fig. 7.2.5. Example of event registered by 25 stations where red vertical line shows first arrival pick for event e0001.141.11 (vertical component).

After choosing one station, PILOT opens a new window where all components are plotted (Fig. 7.2.6).

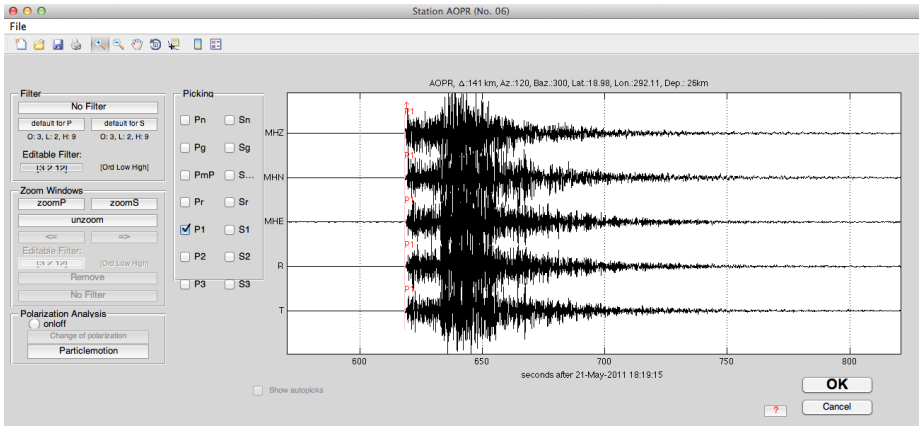

Fig. 7.2.6. Seismic record example corresponding to AOPR station event e0001.141.11.

As we are working with first arrivals of P waves, we zoom in to the vertical component locating this onset. The figure 7.2.7 shows where first arrival has been picked (red vertical line) with earliest and latest times (light red vertical lines) according Diehl et al. (2009).

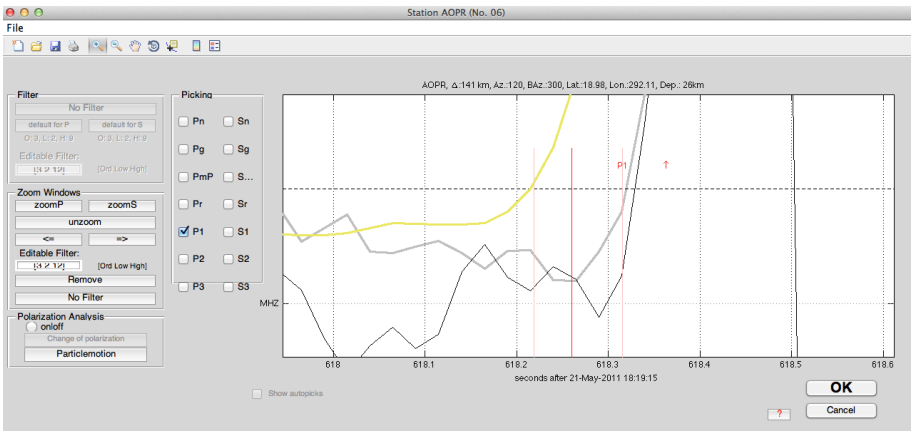

Fig. 7.2.7. P wave first arrival pick represented by red vertical line (AOPR station). Earliest and latest times represented by light red lines. Black line shows filtered signal and grey line shows signal without any filter.

The simultaneous inversion of arrival time data for seismic velocities and hypocenter locations requires hypocenter locations are well located to resolve the coupling between seismic velocities and hypocenter locations problem. The quality of the inversion depends strongly on data selection. For this reason, we need a minimum of 8 P-wave observations (and/or 8 S-wave observations) and an azimuthal gap between stations of GAP < 180^{o} per event [Kissling, 1988]. Nevertheless, we must establish another important feature related with uncertainties, the observational weights. These weights are obtained from grouping the given uncertainties in picking arrival time. The Table I shows the weights assignment followed in the present work including the number of observations per class. It is remarkable that values over 0.32 have not been selected.

Weights (Quality Class)	Uncertainty Interval (s)	# Obs per class
0	± 0.04	1954
1	± 0.08	368
2	± 0.16	549
3	± 0.32	324
4	> 0.32	0
TOTAL		3195

Table 7.2.I. Observational weights and associated uncertainty interval with number of observations per class used in this study.

The average overall observation error is estimated for this data set as follow:

$$\frac{\sum(Uncertainty\ interval * \#obs.\ per\ class)}{Total\ obs} \qquad (7.1)$$

From this calculation, it has been obtained a value of 0.094 s.

7.3 MINIMUM 1D MODEL

- Calculation

The concept of Minimum 1D model, introduced by Kissling (1988), represents a solution to the coupled hypocenter-velocity problem represented by a 1D velocity model with appropriate station delays and well-located hypocenters. Subsequently, the minimum 1D velocity model corresponding to the local earthquake data set may serve as initial reference model for 3D tomography and in combination with the station delays it may be used for routine uniform high precision hypocenter locations even in regions of complex tectonics and significantly laterally varying seismic velocities [Kissling et al. 1994]. The computation of minimum 1D model is a trial-and-error procedure with each trial containing a simultaneous inversion of arrival time data from local earthquakes for hypocenter locations, seismic velocities, and station delays. Each such inversion represents a full solution to the coupled hypocenter-velocity problem solved iteratively by the FORTRAN routine VELEST [Kissling et al., 1994]. Since in a 1D model inversion the number of unknowns is significantly smaller than for a 3D inversion, a smaller set of earthquakes (>100 earthquakes) is usually sufficient to compute a minimum 1D model. This allows only the high-quality data to be selected for the computation of a minimum 1D model, thus improving the reliability of the obtained model [Husen et al., 2011].

VELEST program may be operated in two modes: simultaneous mode and single-event-mode. The single-event-mode (LOCVEL) solves the location problem for local earthquakes, blasts, and shots and is used to analyze individual earthquakes. While the simultaneous mode (SIMVEL) solves the coupled hypocenter-velocity model problem for a large number of local earthquakes, quarry blasts, and shots simultaneously. Hence, in simultaneous mode, VELEST performs the Joint-Hypocenter-Determination (JHD) fixing velocity model and station corrections.

Within an area of 1500 km by 500 km (lat. 17-22N, long. 78-64W) more than 3000 earthquakes have been located during the period 2008-2012. Using a preliminary selection of events due to the station distribution (mainly requirements of a gap less than 180^{o}, i.e., epicenter to lie within station network) and by trying to assure a large number of stations recording the events, we selected 475 events. Picking arrival times by hand for these events, our final data set consists of 354 events with at least 8 P-phase observations registered in different periods of time by 55 seismic stations.

During the process of calculating the Minimum 1D model a few problems with events and stations were detected thus further reducing the data set to 252 events with a total of 3195 P observations. The following figure shows the ray distribution between events and stations used in this work (Fig. 7.3.2).

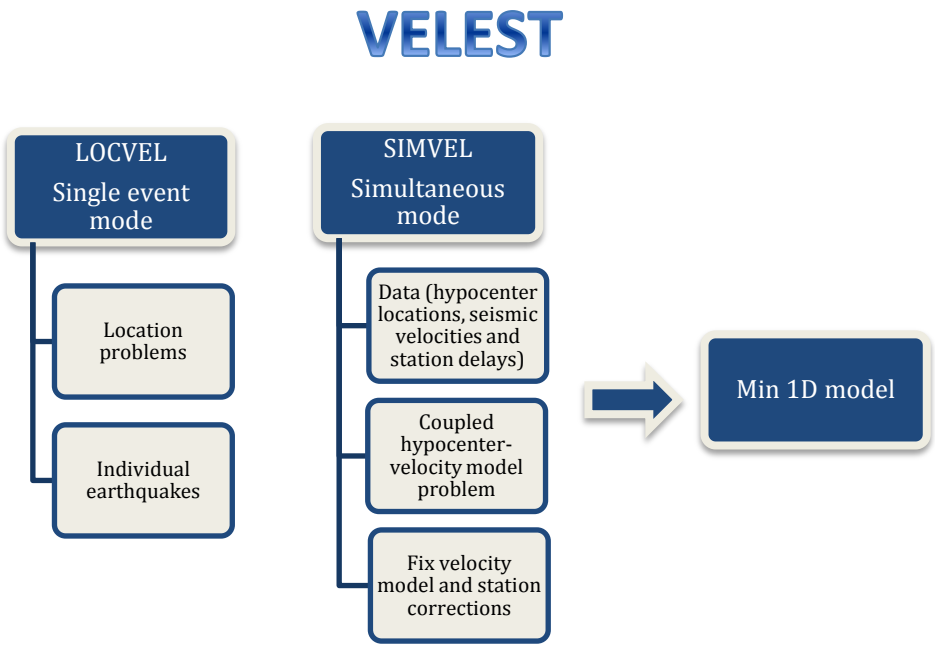

Fig. 7.3.1 Schematic flowchart of VELEST.

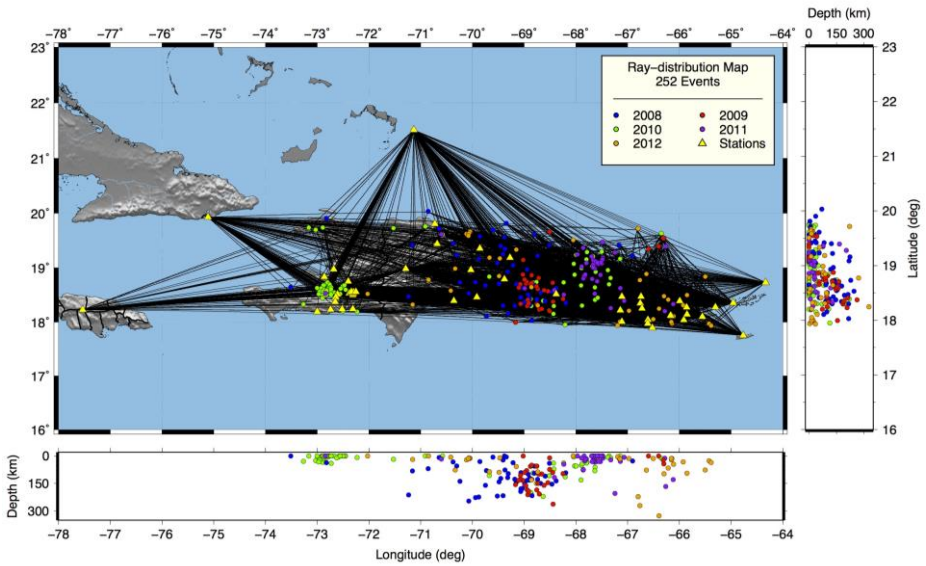

Fig. 7.3.2 Hypocenter locations of 252 relocated earthquakes differenced by 2008 (blue circles), 2009 (red circles), 2010 (green circles), 2011 (purple circles) and 2012 (orange circles) years. Black lines show ray path between epicenters and stations. Stations are marked by yellow triangles.

The RMS value decreases from initial velocity model (A1) 6.67887 to 0.92 with almost no changes in the velocities and only minor station delay adjustments for last velocity model (E1). Then, we establish E1 model as the minimum 1D model (Fig. 7.3.3) according our data set and previous calculations.

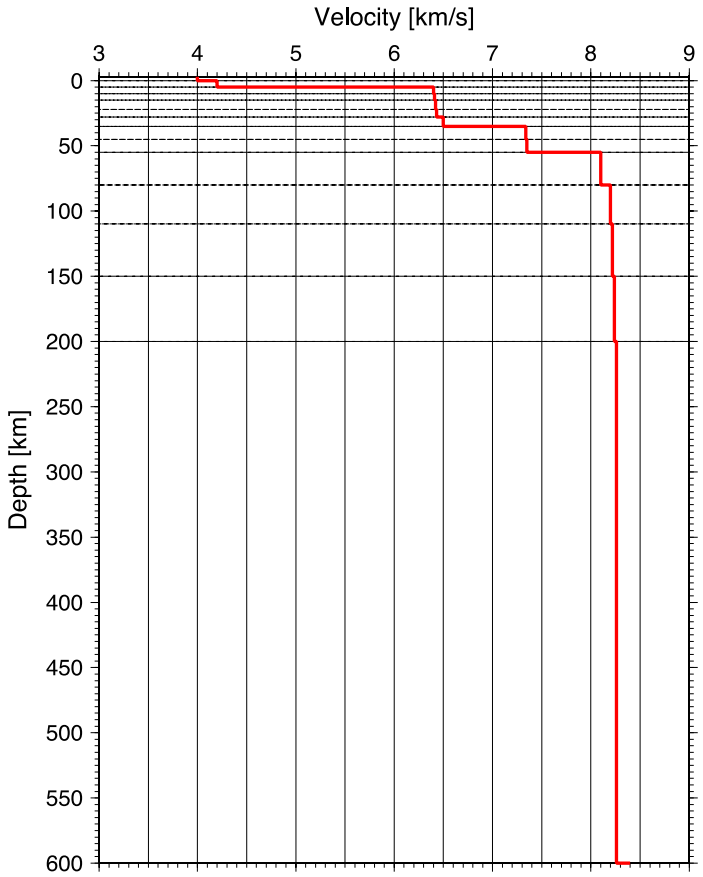

Fig. 7.3.3. Velocity-Depth function of a priori Minimum 1D model.

In the Minimum 1D model represented in the previous figure, we observe at 28 km depth a variation in the velocity from 6.5 km/s to 7.4 km/s that we can attribute to Moho depth but at 55 km, we find a similar increment in the velocity.

Many ray paths transect the upper crust because of abundant shallow seismicity in the area (Fig. 7.3.2). This fact provides us important information about the sedimentary and granitic layers, which discontinuity is located at 5 km depth with a change in velocity of 4.2-6.4 km/s.

- Testing Minimum 1D model

As the process of computing a minimum 1D model can lead to ambiguous results, the final models need to be verified with independent geological information. The stability of a minimum 1D model need to be tested, including randomly and systematically shifted hypocenter locations as initial hypocenter locations and so-called high-low tests (Husen et al., 1999; Kissling et al., 1994). If the minimum 1D model represents a stable minimum in the solution space, final models from these tests will converge to the same minimum 1D model for layers that are well resolved by the data (Husen et al., 2011). In this case, it has been used four tests that shift hypocenters ±10 km in latitude, longitude and depth direction in the following way:

Test 1: event 1 x shift to +10km, event 2 x shift to -10km, event 3 x shift to +10km, event 4 x shift to -10km and so on …

Test 2: event 1 y shift to +10km, event 2 y shift to -10km, event 3 y shift to +10km, event 4 y shift to -10km and so on…

Test 3: event 1 x shift to +10km, event 2 x shift to -10km, event 3 y shift to +10km, event 4 y shift to -10km and so on …

Test 4: event 1 x shift to +10km, event 2 y shift to +10km, event 3 z shift to +10km, event 4 x shift to +10km, event 5 y shift to +10km and so on …

The resulting velocity models are shown in the following figure (Fig. 7.3.4), where it is possible to observe that velocity models obtained for tests converge to Min1Dmodel.

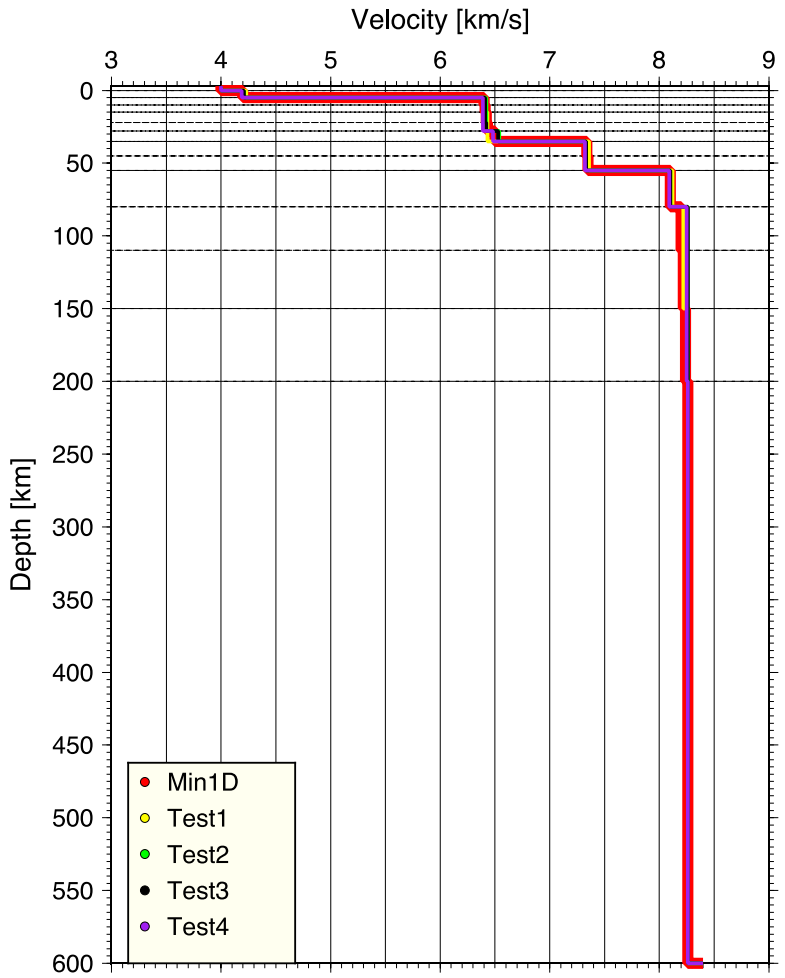

Fig. 7.3.4. Velocity-depth functions of 1D models obtained after testing Minimum 1D model.

Most of the events recover their original hypocenter locations after three iterations. The inversion results are displayed in the following figures (Fig. 7.3.5 a, b and c) for x and y coordinates and depth.

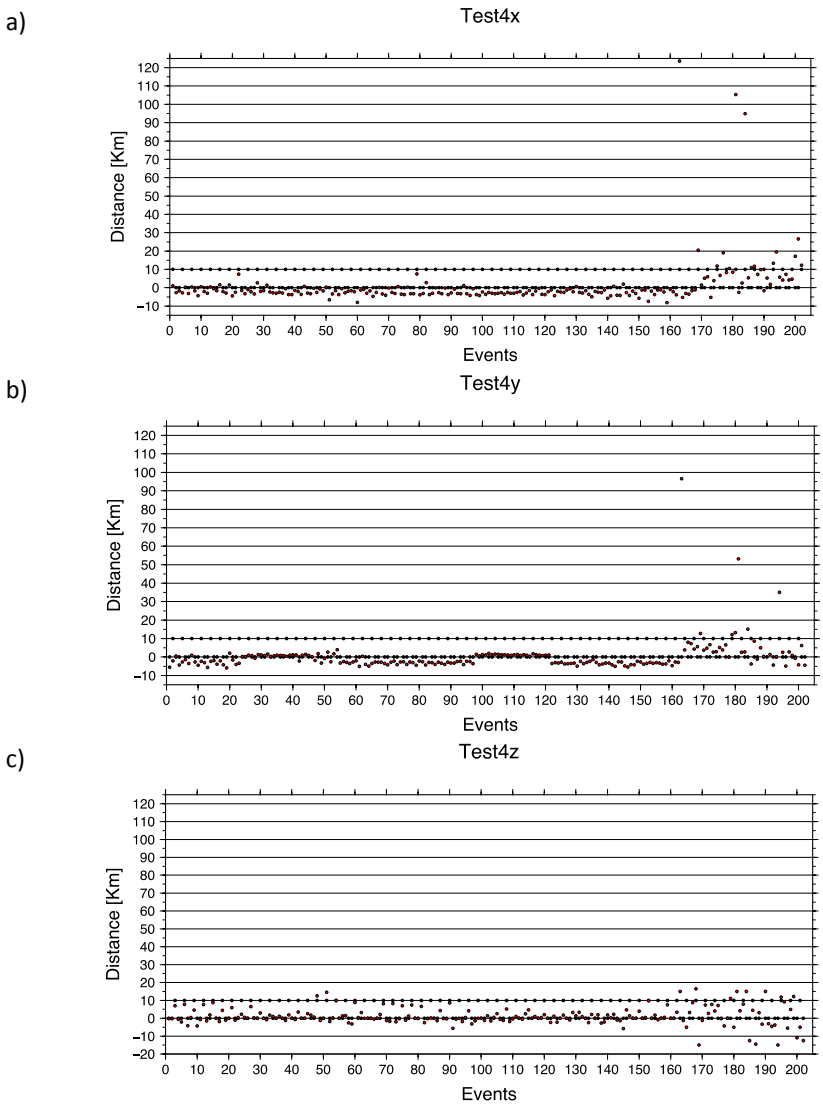

Fig. 7.3.5 Example of inversion results for x, y and z coordinates (a, b and c, respectively) in Test 4, where the original hypocenter coordinate is defined as zero, the initial shift is shown in black dots and the final recovered coordinate in red dots.

- Comparison between Min1D model and routine velocity used in NE Caribbean

The min1D model obtained in this work is compared with the velocity models provided by Dominican Republic and Puerto Rico Seismic Networks. This fact is shown in the following figure (Fig. 7.3.6).

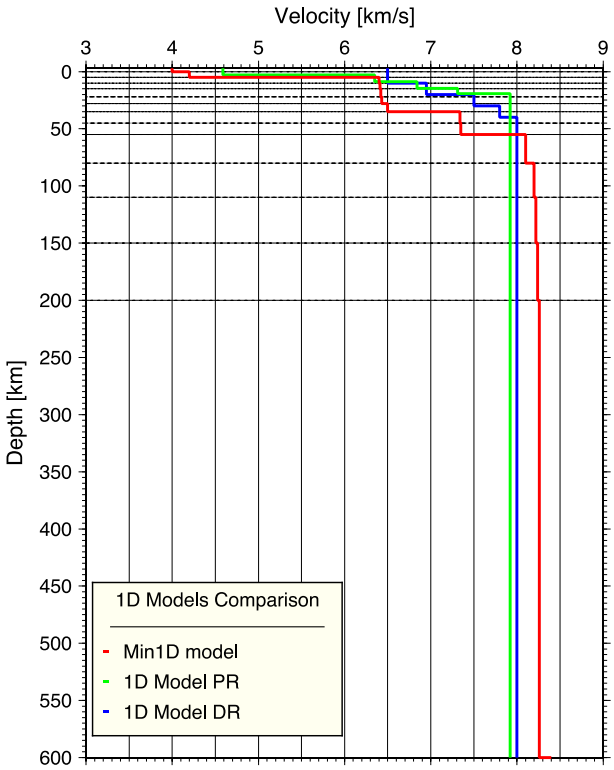

Fig. 7.3.6. Comparison between Puerto Rico, Dominican Republic and obtained in this work minimum 1D models.

In this figure, we can observe our Min1D model improves significantly the knowledge of first crustal layers respect to other velocity models, mainly due to inclusion of shallow seismicity data which provided average velocities relating to sedimentary layers that, for example, DR network model ignores. This fact will improve the location of numerous shallow earthquakes that occur each year in this area.

Between 5 km and 50 km, we find that average velocities are higher in DR and PR models than in our model, reaching Moho depth at 14 km and 20 km for PR and DR models, respectively. Moho depth used by PR Seismic Network may be adequate for this island because geological and structurally both islands are different due to the strong presence of NAP subduction. In layers deeper than 50 km, we observe our model improves the velocities used in other models providing layers with calculated values higher than 8.0 km/s.

Difference between models is mainly due to fact that Min1D model is the expression of best average velocity structure sampled by all rays in data set, while routine models are best a priori estimates with possible local attributes.

- Discussion

Combining minimum 1D model and stations delays should provide a correlation with local geology for stations with good azimuthal coverage of the observations. They should be dominated by large scale deviations in crustal structure from the modeled 1D structure for stations with limited azimuthal coverage of the observations. The magnitude of station delays usually increases with the distance of a station from the center of the network as the difference between modeled and unmodeled structure accumulates with longer ray paths [Husen et al., 2011]. Figure 7.3.6 shows this effect.

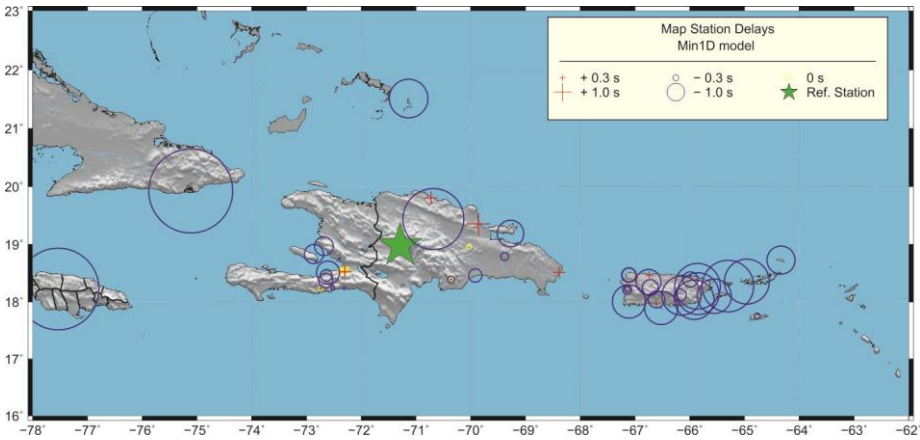

Fig. 7.3.7. Station delays of minimum 1D model for NE Caribbean. Red crosses and blue open circles denote station delays relative to the reference station SDDR marked by green star.

Due to mostly long ray paths and limited azimuthal ray coverage, station corrections in the outer regions of the network contain velocity information of the shallow subsurface and linear effects of the deep structure [Haslinger et al., 1999]. In our minimum 1D model, most of stations are situated near the coast on islands around Hispaniola with negative station delays.

In the regional settings of previous chapters have been explained the main geological and tectonic features of Dominican Republic. The figure 6.2.1 shows a schematic geology map of the Dominican Republic. The reference station is located close to the Jicomé block. This block is composed of a > 3 km thick sequence of arc- and Caribbean large igneous province related volcanic, subvolcanic and volcano-sedimentary rocks of the Tireo Group and the overlying Peña Blanca and Pelona-Pico Duarte Fms. [Escuder Viruete et al., 2011]. The Tireo Group includes two main volcanic sequences with different geochemical characteristics [Escuder Viruete et al., 2007]. Figure 7.3.7 represents a schematic lithostratigraphic column corresponding to Jicomé block.

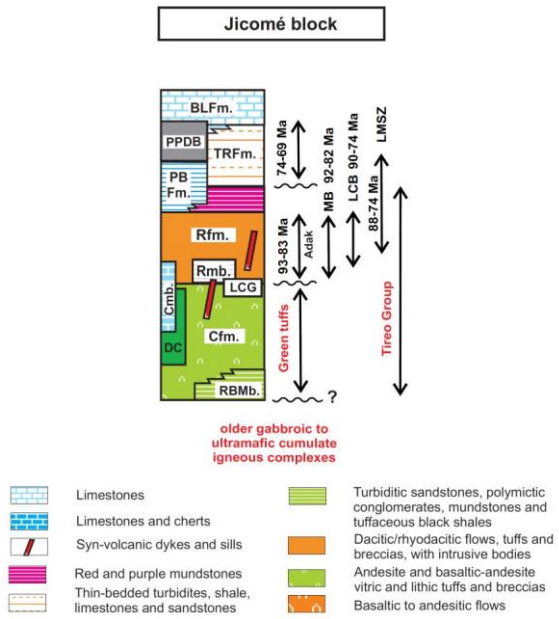

Fig. 7.3.8 Schematic lithostratigraphic column of Jicomé block. BLFm. = Bois de Lawrence Fm.; PPDB = Pelona – Pico Duarte basalts; TRFm. = Trois Rivières Fm.; PBFm. = Peña Blanca Fm.; RFm. = Restauración Fm.; RBMb = Río Blanco Member; CFm. = Constanza Fm.; DC = Dejabón Chert; CMb = Constanza Member.

1D velocity model obtained from velocity models of refraction lines close to reference station (*see Chapter 4, A58 seismic land station position)* show the first 5 km are divided into two layers whose velocities are 3.3 km/s and 5.2 km/s. Between 5 and 30 km, it is observed one layer with 6.3 km/s followed by 17 km thick layer with 7.5 km/s of P-wave velocity. At 55 km deep, a velocity of 8.3 km/s is reached (Fig. 7.3.9). Comparing the values obtained from refractions modeling with those provided by Min1D model, we can extract that there are important similarities between them, being the values of first layers of Min1D model average of the values obtained from refraction seismology, while the differences could be related to the fact that rays from earthquakes image a larger region than rays from active sources. The figure 7.3.9 shows these features and, also, it is plotted as two dash black lines the velocity and depth error estimation determined for CARIBE NORTE seismic velocity model (*see Section 2.7, Chapter 2*).

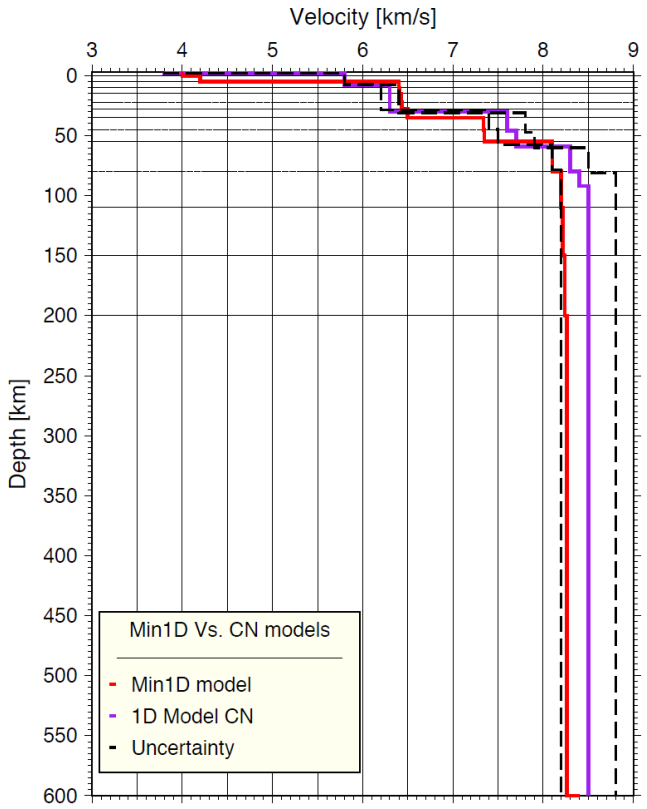

Fig. 7.3.9. Comparison between Min1D model and 1D model obtained from refraction seismology during this work.

For a geologically meaningful Min1D model, station delays should correlate with local geology for station with good azimuthal coverage of the observations. The magnitude of station delays usually increases with the distance of a station from the center of the network as the difference between modeled and unmodelled structure accumulates with longer ray paths [Husen et al., 1999]. In our case, the reference station is located in the central part of the island while most stations are located on the coast or nearby islands, which is significantly lower cortical thickness.

7.4 CONCLUSIONS AND OUTLOOK

Main results obtained during this study are summarized as follow:

- Min1D model improves the quality in hypocentral locations and 3D tomography but we need more observations. Our data set will be used as reference for automatic picking MPX to calibrate the new data. The value obtained of average overall observation error (0.094 s) compared with final RMS of Min1D model that there remains a significant effect of 3D-velocity structure in the data to be resolved. However, in order for the resulting 3D model to be reliable, there must be enough data to resolve a significant volume of study well and this demands some more data.
- The station delays obtained with the minimum 1D P-velocity model indicate the change structural in the crust respect to the reference station showing the thickening in the central part of the Hispaniola Island. In general, the station delays correlate well with surface geology. Thus, the station delays demonstrate the need for using a minimum 1D model for high-precision earthquake location [Kissling et al., 1994] but also document the potential and the need for seismic tomography applications.
- After that, STATISVEL selects from the relocated 252 events all those events with GAP less than 180^{o}. The result is 196 events. STATISVEL calculates histograms of RMS and residual values for events located with VELEST. The input control data contains the borders of the classes used in the histograms, being Class-Type 1 the RMS value and Class-Type 2 the residual of each reading, treated separately for each reading weight (0, 1, 2, 3, 4) (Table 7.2.I). These events are the input for SIMULPS.
- Preliminary data obtained from SIMULPS show the need to increase the number of events to obtain good seismic tomography models.
- The need for a consistent relocation of seismicity in the study region is demonstrated by relocation analysis of the earthquake used in modeling profile D (Chapter 6). Moreover, relocated hypocenter location will give important insights in the orientation and depth extent of the subducting slabs in the study region.
- Comparison with P-wave velocity model obtained from wide-angle seismic data corroborates the presence of thickened crust in the interior of island and, also, V_P obtained in Moho discontinuity applying two different methodologies and two different data sets.

CHAPTER 8

DISCUSSION AND CONCLUDING REMARKS

The North America-Caribbean plate boundary is a complex area of mainly left-lateral strike-slip deformation. In our study area, the Hispaniola Island is being impacted by collision with the Bahamas Platform in the north and in the south, Beata Ridge is penetrating into the island and hitting with Muertos Trough. These processes alter the central and eastern parts of Hispaniola Island dividing it into different tectonostratigraphic terrains characterized by folds, thrust and left-lateral faults and shear zones.

In this chapter, it is summarized the main results and conclusions of this thesis and its contribution for lithospheric structure knowledge of NE border of Caribbean Plate, and, particularly, in the area of Dominican Republic, which will be structured from N to S and where will be commented the results for every important tectonic structure of the zone, providing an overall view both onshore and offshore Dominican Republic. Moreover, a schematic interpretation of these results are shown in figure 8.1.

North American – Caribbean Plates boundary (Northern Dominican Republic)

In the northwestern Dominican Republic, the southern Bahamas Platform (Mouchoir Bank) (Fig. 4.2.1) is characterized by shallow water depth with thin sedimentary cover (less than 1 km) and basement increasing through the coast where reaches 6.1 km in the area of Puerto Plata Basement Complex (Fig. 4.2.1), while in the area of Samaná Complex (Fig. 5.2.2) this depth is 8 km with P-wave velocities of 3.3 ± 0.1 km/s for sediments and for the basement ranges between 5.2 km/s and 5.8 km/s, both with ± 0.1 km/s. The presence of the Silver and Navidad Banks is reflected in the sedimentary layer with an increase respect to the west, reaching 2 km deep. These areas also are characterized by shallow Moho discontinuity that it has been possible to determine at 10 ± 1 km in the west and 10-15 ± 1 km in the eastern study area. Then, it is possible to establish that the effect of Bahamas Platform over northern Hispaniola Island.

The deep structure of the crust and upper mantle in the northern region presents dipping layers penetrating into the island with different dip angles reducing its value towards to the east. From W to E, these angles are 12º, 9º and 6º but it is noteworthy that the orientation of profiles, where these angles have been obtained, is not parallel between them (Figs. 4.3.1 and 5.3.1). Then, the NAP is subducting beneath CP with NNE-SSW direction in our study area and the subducting angle corresponds to 12º. Also, in this thesis it has been possible to determine V_P of the first seismic layers in the upper mantle with maximum values of 8.6 ± 0.3 km/s reaching depths up to 85 ± 4 km.

The northern onshore part is characterized by the presence of Puerto Plata Basement Complex, Cordillera Septentrional and Samaná Peninsula separated from Cibao Basin and Samaná Bay by Septentrional Fault Zone. In the western part of this area, sedimentary layer increases in depth up to 2 km while in the east area is thinner. The basement is 6 km and 8 km deep from W to E. The northern cortical thickness of Dominican Republic becomes progressively thicker toward the center of the island, starting from values of 15 ± 1 km in the area of Samaná Peninsula, between 10 ± 1 km and 15 ± 1 km in the middle (Fig. 5.2.1), while in the westernmost part is shallower.

Hispaniola Island

West-central part of the Hispaniola Island consists of high topography bounded by dominantly reverse and oblique-slip faults along the edges of the uplifted mountain ranges alternated by sedimentary basins. The eastern part is much lower in elevation and is practically not affected by active faulting.

Our study has characterized seismically these basins and mountain ranges in the shallow crustal structure. The results have corroborated previous data and have provided slight changes respect to the previous studies in the area. Thus, we have obtained the following characterization of the main sedimentary basins: 1) *Cibao Valley* consists in different stratigraphic sequences that reach a maximum thickness of 4 km; 2) *San Juan Basin* is not as deep as previous studies indicated in this area (7 km), reaching a sedimentary depth of 5 km, while in the southeastern area of this basin is 2.7 km; 3) *Enriquillo Basin* (Angostura and Mella blocks), defined by being under sea level and filled by alluvium deposits, is 5.7 km of basin thickness; 4) *Llanura Costera del Caribe* defined by thin sedimentary layer with V_P of 2.3-3.4 ± 0.1 km/s and 1.2 km deep and a basement of 5.5 km. Main effects observed in the crustal velocity model of the mountain range areas are the absence of sedimentary cover and the rise of basement to the subsurface. These effects appear in Cordillera Central and its southern flank with Peralta Belt, Cordillera Oriental and Sierra de Bahoruco excepting Sierra de Neiba (Fig. 4.2.1), whose basement is deeper than other mountain ranges, providing better knowledge about the volcano-sedimentary

rocks velocities that is made of. Moreover, the stage of the seismic profiles through the western flank of Cordillera Septentrional does not provide enough information to define its structure.

Deep structure in the area of Dominican Republic is featured by a crustal thickening that in this study has been characterized in three seismic transect with N-S direction and one oriented from W to E. Through these data, it has been possible to establish the marked differences between N and S and from W to E. Particularly, Moho discontinuity increases towards the interior of the island from Bahamas Platform to the interior of the island but gets different maximum depth values being roughly 30 ± 2 km deep in the western and central, while rises up to 24 ± 2 km deep, in the eastern area. Moreover, in the Peralta Belt vicinity appears laminated and showing a lateral velocity contrast due to the presence of the San José - Restauración and Bonao – La Guácara Fault Zones. This fact is observable in the crustal velocity model showed in figure 6.4.2.8. Going toward southern coast, Moho depth decreases being shallower in the west (19 ± 2 km) and east (16 ± 2 km), and deeper in Bahía de Ocoa area (21 ± 2 km). In this area, Beata Ridge is colliding and penetrating into the island [Cotilla et al., 2007], whose effect is reflected in the P-wave velocity model as the existence of thickening of the crust.

It is noteworthy that the comparison between P-wave velocity and layer depths obtained from two different data and methodologies (refraction seismology data and seismicity applied to LET), provides similar values of these magnitudes. Being 7.6 ± 0.2 km/s from refraction data and 7.5 km/s from LET, average values of P-wave velocity. While average values of Moho depth under Hispaniola Island are close to 30 ± 2 km.

Eastern offshore Hispaniola

The different crustal structure, topography and deep seismicity in the eastern offshore and onshore area of Hispaniola make more pronounced the difference between the west and the east. Previous studies attribute this fact to the oblique subduction of North American Plate, establishing this process as dominant [Ladd et al., 1991; McCann and Sykes, 1984]. In the present study, a structure dipping towards eastern interior of the island has been obtained with a dip angle of 18^{o} reaching depths of 120 ± 5 km. The relocation and P-wave phases analysis of one earthquake registered by CARIBE NORTE land seismic deployment have allowed obtaining these values. This structure could explain deep seismicity in the area. Furthermore, it has been shown that the earthquake relocation based on 1D models obtained from the wide-angle and local earthquake tomography data, greatly improve the event parameters derived from those used by the seismic networks operating in the region.

Beata Ridge and Muertos Trough Contact (Southern Dominican Republic)

The Beata Ridge is a NE-SW trending structure located in the interior of the Caribbean Plate, between the extended Colombian and Venezuelan basins. The northern part of the ridge is colliding with Hispaniola Island and this contact is observed along a transverse NE alignment that constitutes a morphostructural limit producing the interruption of the Cibao Valley and the divergence of the rivers and basins in opposite directions [Cotilla et al., 2007]. Nevertheless, Muertos Trough is a EW-trending depression with northward curvature, which is extended from Beata Ridge to the Aves Ridge along 650 km. Muertos Thrust Belt forms the southern margin of Hispaniola and Puerto Rico.

The study carried out in this thesis provides values of the crust beneath the Beata Ridge that are not as deep as expected being thickened beneath Beata Island whose differences could be due to the existence of contemporary set of active faults. Moreover, some tectonic differences from west to east zones separated by Beata Island in the shallow structure have been determined. Westward, the Haiti Basin is characterized by two sedimentary layers with V_P of 3.3 ± 0.1 km/s and 4.5-4.8 ± 0.1 km/s, respectively, and a maximum total thickness of 4.4 km. While eastward, these layers remain constant at 8 km depth due to the presence of Venezuela Basin. In the area of southern Hispaniola, where Beata Ridge collides with the island and Muertos Trough, the sedimentary cover and basement appear thickened and then, disappear in the junction with Muertos Trough. To the east, San Pedro Basin consists of two alternated sedimentary layers over a 5.0 ± 0.1 km/s layer that could represent the Horizons A'' and B'' in the Caribbean region.

Moho depth under Beata Island is thickened with a maximum value of 24 ± 2 km confirming the crust of Caribbean Plateau is unusually thick. Then, it rises up to 13 ± 2 km in the area of seamount located further east and is constant at 15 ± 2 km in Venezuela Basin area. The deepest layers follow the topography established by Moho with increasing V_P in depth, reaching values of 8.5 ± 0.3 km/s. Eastward, this area is characterized by crustal and upper mantle deformation due to the presence of Muertos Thrust Belt and Muertos Trough, producing a thickening of the first layers of upper mantle and subsequent a thinning further to the south. In this area, Moho discontinuity and upper mantle are relatively shallow (10-12 ± 1 km deep) presenting a dip angle of 7º-8º northwards. Furthermore, it has been obtained one density model in this area, which is in agreement with previous gravity models [Granja Bruña et al., 2009; 2010] and, also, report similar dip angle values. These results would be more consistent with the hypothesis of double subduction (*Section 1.2*), considering that the Caribbean plate penetrates only a few km under the island

and the slab seems not to have continuity. Strictly, CP is thrusting under Hispaniola Island.

The extension towards Hispaniola of NE direction of the Beata Ridge structure, as morphotectonic alignment, is transversely articulated with EPGFZ and SFZ active fault zones. This alignment has been identified as a first-order limit between mountain and plain morphostructures [Cotilla et al., 2007] explaining the divergence of rivers and basins in opposite directions. Seismic deep structure along this lineament have been determined in this study, obtaining a thickening in the upper mantle dipping into the island 12º-18º in a SN direction and reaching depths of up to 80 ± 4 km.

Septentrional and Enriquillo – Plantain Garden Fault Zones

The left-lateral Septentrional strike-slip fault and the south-dipping thrust faults of the North Hispaniola deformed belt accommodate deformation in North, while, in the South, the deformation is accommodated along the left-lateral Enriquillo-Plantain Garden Fault and north-dipping thrust faults of the Los Muertos deformed belt.

Along northern Dominican Republic, Septentrional Fault Zone is responsible for the uplift of the Cordillera Septentrional and faulting in Cibao Valley area. Our study reveals that the presence of Septentrional Fault in the westernmost area appears as loss of seismic energy in the seismic record sections, while in the central and eastern parts, it is possible to establish an effect of this structure in the velocity models. In the area of Río San Juan Complex, this effect is characterized as a lateral variation in V_P from offshore to onshore regions, increasing its value towards the island and reaching the first layers of upper mantle. In the area of Samaná Bay, Septentrional Fault Zone indicates a thinning of the uppermost layers and a lateral velocity variation. The seismicity in the region shows a concentration of events north of Cordillera Septentrional whose shallow seismicity could be associated Septentrional Fault but the deepest is tied to Hispaniola Trench.

The region of Enriquillo Basin is mainly traversed by Enriquillo-Plantain Garden Fault Zone that is formed as response to oblique subduction of the Bahamas Platform due to the thicker-than-average crust subduction of the Bahamas Platform resisted the eastward motion of the central and northern parts of Hispaniola. Our study has obtained an anomalous zone with a lateral velocity variation observed in two consecutive layers. The shallowest layer decreases from 7.6 ± 0.2 km/s to 7.0 ± 0.2 km/s, while the deepest one changes from 8.0 ± 0.2 km/s to 7.5 ± 0.2 km/s in WE (Fig. 8.1. A). The structure corresponding to this change reaches the first layers of upper mantle up to 60 ± 3 km deep.

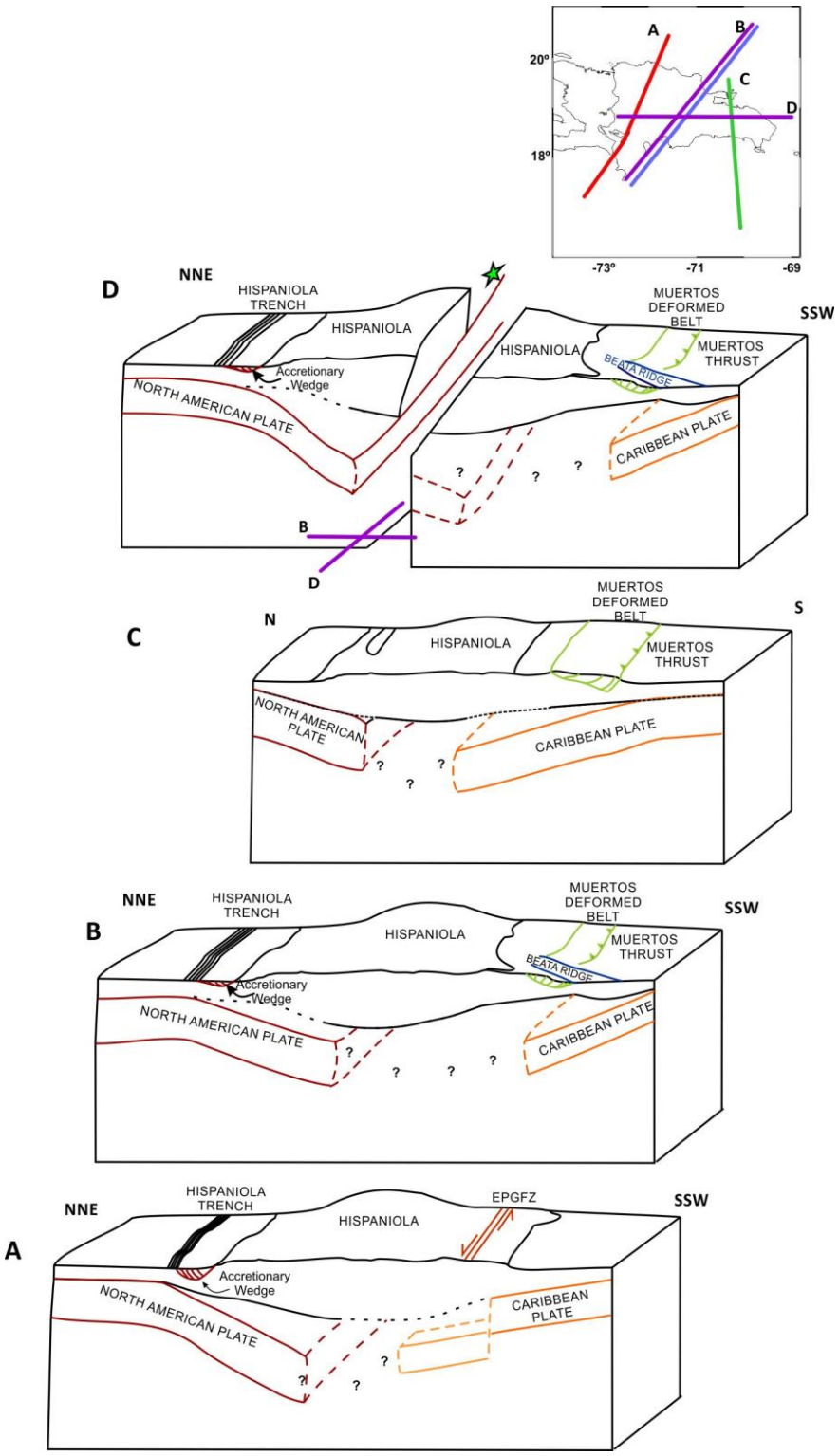
A
B
C
D
20°
18°
-73°
-71
-69
D
NNE
HISPANIOLA TRENCH
HISPANIOLA
Accretionary Wedge
NORTH AMERICAN PLATE
MUERTOS DEFORMED BELT
SSW
HISPANIOLA
MUERTOS THRUST
BEATA RIDGE
CARIBBEAN PLATE
B
D
C
N
S
HISPANIOLA
MUERTOS DEFORMED BELT
MUERTOS THRUST
NORTH AMERICAN PLATE
CARIBBEAN PLATE
B
NNE
HISPANIOLA TRENCH
HISPANIOLA
MUERTOS DEFORMED BELT
SSW
MUERTOS THRUST
BEATA RIDGE
Accretionary Wedge
NORTH AMERICAN PLATE
CARIBBEAN PLATE
A
NNE
HISPANIOLA TRENCH
HISPANIOLA
EPGFZ
SSW
Accretionary Wedge
NORTH AMERICAN PLATE
CARIBBEAN PLATE

Fig. 8.1 Schematic representation of main structures analyzed in this manuscript, whose profiles are oriented following the map situated above. Section D is oriented in NNE-SSW direction and cutted across E-W direction showing the oblique subduction of NAP.

This structure has been interpreted as Enriquillo – Plantain Garden Fault Zone. The seismicity associated to this region reveals that events in the southeastern part are deeper than those of the southwest and some of them reach depths of 90-100 km indicating that this structure reaches large depths. Moreover, it is also possible to correlate the bottom of this area as a detached slab, as it was proposed by Mann et al., (2002). However, our results could indicate that this detached slab comes from CP while these authors establish that it comes from NAP.

To conclude, this work provides a better knowledge about the lithospheric structure in NE Caribbean Plate and a better understanding of the tectonic conditions that could explain the high seismicity in the area, according main and specific objectives proposed for our study (*Section 1.4*). Furthermore, the results show that NAP is subducting into Hispaniola while CP is thrusting under the island.

Main Conclusions and Contributions of this Thesis

After the study that is carried out during the elaboration of this thesis, it is possible to emphasize in the following aspects:

i. This study combines seismic wide-angle data from two geophysical experiments where eight seismic transects have been processed and interpreted. Moreover, controlled-source seismology and seismicity data complete the data set.
ii. It is the first time that a method for uncertainty estimation developed for earthquake phase picking has been applied to wide-angle seismic data, allowing to obtaining phase correlation uncertainties used to determine error estimations in layer depth and seismic velocities.
iii. All data from GEOPRICO-DO and CARIBE NORTE seismic experiments have been processed and more than 120 seismic record sections have been interpreted to obtain six P-wave velocity models with more than 7800 rays traced, providing information onshore and offshore Dominican Republic in NS and EW directions checked by ray tracing and synthetic seismogram calculations.
iv. Lithosphere structure under Dominican Republic has been obtained, showing for first time a perspective more elaborated, characterizing shallow and deep parts including Moho and upper mantle. The results show differences between northern and southern and also, western and eastern parts of the Dominican Republic and adjacent marine regions.

v. The contact between Bahamas Platform – North American Plate and Hispaniola Island in northern and eastern areas has been determined. This contact corresponds to an oblique subduction in a NNE-SSW direction with dip angles of 12º to the north and 12º-18º to the east.

vi. Beata Ridge, Muertos Trough and Muertos Thrust Belt have been described seismically, as well as the contact between these structures with southern coast of the island.

vii. Main active fault zones (Septentrional and Enriquillo-Plantain Garden Fault Zones) in the island have been seismically defined obtaining P-wave velocities and depths.

viii. It has been obtained a minimum 1D velocity model computed by simultaneous inversion of arrival time data for seismic velocities and hypocenter locations (Local Earthquake Tomography technique), which improves the 1D velocity models used in regional seismic networks and it is the starting point to generate a 3D structure model. Also, obtained P-wave velocities below Moho and upper mantle from this technique corroborate that values obtained with refraction seismology and observed in the literature.

Future Investigation Lines

The velocity models presented in this manuscript are the starting point to get lithospheric and sublithospheric model in the area of Hispaniola Island. The main investigation line that it is possible to follow for improving the crustal velocity models is applied new methodologies based on tomographic codes and full waveform analysis. Moreover, we are going to include new wide-angle data processing, as applying multichannel seismic reflection techniques to refraction data and having into account that it is possible to consider a seismic station line as a streamer. Also, the study of S-waves observed in land shot seismic record sections will complete the obtained P-wave velocity models and Poisson ratio calculation will be calculated to obtain the elastic properties of the crust or mantle in our study area.

Another important investigation line is including much more earthquakes in the database for Local Earthquake Tomography and applying an automatic program to increase the number of observables. After that, it will be possible to obtain reliable 3D seismic tomography models comparable with the models obtained from refraction seismology.

CHAPTER 9

REFERENCES

A

Ali, S. T., Freed, A.M., Calais, E., Manaker, D.M., and McCann, W.R., 2008. Coulomb stress evolution in Northeastern Caribbean over the past 250 years due to coseismic, postseismic and interseismic deformation. *Geophys. J. Int*., **174**, 904-918.

Arnaiz Rodríguez, M.S., and Garzón, Y., 2012. Nuevos mapas de anomalías gravimétricas del Caribe. *Intercencia*, vol. 37, num. 3, pp. 176-182.

B

Bowin, C., 1975. The Geology of Hispaniola. *The Ocean Basins and Margins*, vol. 3. Edited by A.E.M. Nairn and F. G. Stehli. Chapter 12, pp. 501-552.

Bowin, C., 1976. Caribbean Gravity Field and Plate Tectonics. *GSA Special Papers*, v. 169, p. 1-82. doi: 10.1130/SPE169-p1

Bunce, E.T., and Fahlquist, D.A., 1962. Geophysical investigations of the Puerto Rico Trench and Outer Ridge. *Journal of Geophysical Research*, vol. 67, pp. 3955-3972

Bracey, D.R. and Vogt, P.R., 1970. Plate tectonics in the Hispaniola area. *Geol. Soc. Am. Bull.,* 81:2855-2860.

Braga, J.C., Díaz de Neira, A., Lasseur, E., Mediato, J., Aguirre, J., Abad, M., Hernaiz-Huerta P.P., Monthel, J., Pérez-Valera, F., Lopera, E., 2012. Pliocene-Lower Pleistocene shallow-water mixed siliciclastics and carbonates (Yanigua and Los Haitises formations) in eastern Hispaniola (Dominican Republic). *Sedimentary Geology*, 265-266, 182-194

Brocher T.M., 2005. Empirical relations between elastic wavespeeds and density in the earth's crust. *Bull Seismol Soc. Am* 95(6): 2081–2092.

Burke, K., Fox, P., and Sengör, A.M.C., 1982, Buoyant ocean floor and the

evolution of the Caribbean*, J. Geophys*. Res., 83, 3949-3954.

Burke, K., 1988. Tectonic evolution of the Caribbean. *Annual Rev. Earth and Planetary Science Letter*, 16, pp. 201-230.

Byrne, D.B., Suarez, G., and McCann, W.R., 1985. Muertos Trough subduction-microplate tectonics in the northern Caribbean*? Nature*, vol. 317, pp 420-421.

C

Calais, E., Béthoux, N., Mercier de Lépinay, B., 1992. From transcurrent faulting to frontal subduction: a seismotectonic study of the northern Caribbean plate boundary from Cuba to Puerto Rico, *Tectonics*, vol. 11, No.1, pp. 114-123.

Calais, E., Mazabraud, Y., Mercier de Lépinay, B., Mann, P., Mattioli, G., Jansma, P., 2002. Strain partitioning and fault slip rates in the northeastern Caribbean from GPS measurements, *Geophysical Research Letters*, Vol. 29, p. 3-1-3-4. DOI: 10.1029/2002GL015397.

Calais, E., A. Freed, G. Mattioli, F. Amelung, S. Jonsson, P. Jansma, S.H. Hong, T. Dixon, C. Prepetit, and R. Moplaisir. 2010. Transpressional rupture of an unmapped fault during the 2010 Haiti earthquake, *Nature Geoscience*, vol. 3, pp. 794-799.

Carbó, A., Córdoba, D., Martín Dávila, J., ten Brink, U., Herranz, P., Von Hilldebrandt, C., Payero, J., Muñoz Martín, A., Pazos, A., Catalán, M., Granja, J.L., Gómez, M., GEOPRICO-DO Working Group, 2005. New marine geophysical survey explores active tectonics at northe-eastern Caribbean Plate Boundary. *EOS, Trans. Amer. Geophys. U.*, 86 (51): 537,540.20Dec2005.

Carbó, A., Córdoba, D., Martín-Dávila, J., Granja-Bruña, J.L., Llanes, P., Muñoz-Martín, A., and Ten Brink, U., 2010, Exploring active tectonics in the Dominican Republic*, EOS*, vol. 91, no. 30, 261-268.

Case, J.E., and Holcombe, T.L., 1980. Geologic-tectonic map of the Caribbean region: Reston, Virginia, USA, *U.S Geological Survey Miscellaneous Investigations Series Map I-1100, scale: 1:2500000*.

Case, J.E., MacDonal, W.D., Fox, P.J., 1990, Caribbean crustal provinces; seismic and gravity evidence. In: Dengo, G., Case, J.E., (Eds.), The Geology of North America, Volume H, The Caribbean Region. *Geological Society of America*, Boulder, Colorado, pp. 15-36.

Catalán, M., and Martín-Dávila, J., 2013. Lithospheric magnetic mapping of the northern Caribbean region. *Geologica Acta*, Vol. 11, n. 3, pp. 311-320. DOI: 10.1344/105.000001872.

Cerveny, V., Molotkov, I., and Psencik, I., 1977. Ray Method in Seismology. Prague, Czechoslovakia: University of Karlova.

Córdoba, D., Pazos, A., Carbó, A., Martín Dávila, J., **Núñez, D.,** Payero, J., Fort, M., López, O., and Granja, J.L., 2009. Estudios sísmicos mar-tierra en el borde NE de la Placa Caribe. Proyectos GEOPRICO y CARIBE NORTE. Oral presentation in Reunión Annual 2009 de la Unión Geofísica Mexicana (Puerto Vallarta (Mexico)).

Christensen N.I., Mooney, W.D., 1995. Seismic velocity structure and composition of the continental crust: a global view. *J. Geophys. Res*. 100: 9761–9788.

Córdoba, D., **Núñez, D.,** Pazos, A., Martín Dávila, J., Carbó-Gorosabel, A., Granja-Bruña, J.L., Llanes-Estrada, M.P., Polanco-Rivera, E., Muñoz, S., Calzadilla, M., Payero, J., Fort, M., Cotilla, M.O., and CARIBE NORTE Working Group, 2010. Seismic images of the crust across the North-Eastern border of the Caribbean Plate (Southern Hispaniola Island) from wide-angle profiles. Poster communication in 2010 The Meeting of the Americas (Foz Do Iguazzu (Brasil)).

Cotilla, M.O., Díaz, L., González, D., Fundadora, M., and Pachecho M., 1997. Estudio morfoestructural de La Española. Revista Minería y Geología, vol XIV, 3: 73-88 (in Spanish)

Cotilla, M.O., Córdoba, D., and Calzadilla. M., 2007. Morphotectonic study of the Hispaniola. Geotectonics, 41 (5): 38-62.

Cotilla Rodríguez, M.O., and Córdoba Barba, D., 2010. Determination of Lineaments in Hispaniola. Revista Geográfica, n. 147, pp. 133-154.

Cotilla Rodríguez, M. O., 2011. ¿Tsunamis en Cuba? Física de la Tierra, Vol. 23, 173-197.

Cotilla Rodríguez, M. O., and Córdoba Barba, D., 2011. Comments About Tsunami Occurrences in the Northern Caribbean, Tsunami – A Growing Disaster, Prof. Mohammad Mokhtari (Ed.), ISBN: 978-953-307-431-3, InTech, Available from: http://www.intechopen.com/books/tsunami-agrowing-disaster/comments-about-tsunami-occurrences-in-the-northern-caribbean

Cotilla Rodríguez, M.O., Córdoba Barba, D., and **Núñez Escribano, D.,** 2013a. Alternative Interpretation for the Cuban Active Zones. (accepted in *GEOTECTONICS*)

Cotilla Rodríguez, M.O., Córdoba Barba, D., and **Núñez Escribano, D., 2013b**. The Guane Fault, Western Cuba. *IZVESTIYA, PHYSICS OF THE SOLID EARTH FIZIKA ZEMLI* (accepted)

Cotilla Rodríguez, M.O., and **Núñez Escribano, D.,** 2013**.** Historia sobre la Sismología del Caribe Septentrional, *Revista Historia de América,* n. 143, Julio-diciembre 2013.

D

DeMets., C., Gordon,R.G., and Argus, D.F., 2010. Geologically current plate motions. Geophys. J. Int., 181, 1-80.

Diebold, J.B., Stoffa, E, Buhl, E, Truchan, M., 1981. Venezuela Basin crustal structure. *J. Geophys. Res*. 86, 7901-7923.

Diebold, J.B., Driscoll, N.W., EW9501 Team, 1999. New insights on the formation of the Caribbean basalt province revealed by multichannel seismic images of volcanic structures in the Venezuelan Basin, in: Hsü, K.J., (Series Ed.) *Sedimentary Basins of the World, 4. Caribbean Basins*. Mann, P. (Ed), Elsevier Science, N.Y. 561-589.

Diehl, T., Kissling, E., 2008, Users Guide for Consistent Phase Picking at Local to Regional Scales, Appendix 'C' of Ph.D. thesis of T. Diehl.

Diehl, T., Kissling, E., Husen, S., Aldersons, F., 2009. Consistent phase picking for regional tomography models: application to the greater Alpine region*, Geophys. J. Int.*, vol. 176, pp. 542-554.

Dillon, W.P., Austin Jr., J.A., Scanlon, K.M., Edgar, N.T. and Parson, L.M., 1992. Accretionary margin of north-western Hispaniola: Morphology, structure, and development of the northern Caribbean plate boundary. *Mar. Pet. Geol*., 9: 70-88.

Dillon, W.P., Edgar, N.T., Scanlon K.M., Coleman D.F., 1996. A review of the tectonic problems or the strike-slip northern Boundary of the Caribbean plate and examination by GLORIA. In: Gardner, J.V., Field. M.E., Twichel D.C. (eds.) *Geology of the United States Seafloor: the view from GLORIA*, vol. 9. Cambridge University Press, United Kingdom, pp. 135-164.

Dolan, J., Mann, P., Monechi, S., De Zoeten, R., Heubeck, C., and Shiroma, J., 1991. Sedimentologic, Stratigraphic, and Tectonic Synthesis of Eocene-Miocene Sedimentary Basins, Hispaniola and Puerto Rico. In: Tectonic Development of the North America-Caribbean Plate Boundary Zone in Hispaniola, *GSA Special paper 262* (eds. P. Mann, G. Draper, and J. Lewis)

Dolan, J.F., and Wald, D.J., 1998. The 1943-1953 north-central Caribbean earthquakes: Active tectonic setting, seismic hazards and implications for Caribbean-North America plate motions. En J.F. Dolan, P. Mann (eds.), Active Strike-Slip and Collisional Tectonics of the Northern Caribbean Plate Boundary Zone. *Geological Society of America Special Paper 326*, 143-169.

Dolan, J.F., and Mann, P. (Eds.) 1998. Active Strike-Slip and Collisional Tectonics of the Northern Caribbean Plate Boundary Zone. *Geological Society of America. Special Paper, 326*, pp. 1-17.

Dolan, J.F., Mullins H.T., Wald D.J., 1998. Active tectonics of north-central Caribbean: oblique collision,

strain partitioning, and opposing subducted slabs, in Active Strike-slip and Collisional Tectonics of the Northern Caribbean Plate Boundary Zone, Vol. 326, pp. 1–62, eds Dolan, J.F. & Mann, P., *Geol. Soc. Am. Spec. Paper*.

Dolan, J.F., & Bowman, D.D., 2004. Tectonic and seismologic setting of the 22 September 2003, Puerto Plata, Dominican Republic earthquake: implications for earthquake hazards in northern Hispaniola*, Seism. Res. Lett*. **75**, 587-597.

Donnelly T. W., 1973. Late Cretaceous basalts from the Caribbean, a possible flood basalt province of vast size. *EOS* 54, 1004.

Draper, G., and Lewis, J.F., 1991. Metamorphic belts in central Hispaniola. En P. Mann, G. Draper, J.F. Lewis (eds.). Geologic and tectonic development of the North America-Caribbean plate boundary in Hispaniola. *Geological Society of America, Special Paper 262*, 29-15.

Draper, G., Mann, P., Lewis, J.F., 1994. Hispaniola. In: Donovan, S.K., Jackson, T.A. (Eds.), Caribbean Geology: An Introduction. *University of the West Indies Publishers Association*, Kingston, Jamaica, pp. 129-150.

Driscoll, N. W., and J. B. Diebold, Deformation of the Caribbean region: One plate or two?, *Geology*, 26, 1043 – 1046, 1998.

E

Edgar, N.T., Ewing, J.I., and Hennion, J., 1971. Seismic refraction and reflection in the Caribbean Sea. *Am. Assoc. Petrol. Geol*. 55, 833-870.

Eldholm O. and Coffin M. F., 2000. Large igneous provinces and plate tectonics. *AGU Monograph* 121, 309–326

Erikson, J.P., Pindell, J.L., Karner, G.D., Sonder, L.J., Fuller, E., and Dent, Logan., 1998. Neogene Sedimentation and Tectonics in the Cibao Basin and Northern Hispaniola: An Example of Basin Evolution near a Strike-Slip-Dominated Plate Boundary*, The Journal of Geology*, Vol. 106, No. 4 (July 1998), pp. 473-494.

Escuder-Viruete, J., Hernaiz-Huerta, P.P., Draper, G., Gutiérrez, G., Lewis, J.F., Pérez-Estaún, A., 2002. Metamorfismo y estructura de la Formación Maimón y los Complejos Duarte y Río Verde, Cordillera Central Dominicana: implicaciones en la estructura y la evolución del primitivo Arco Isla Caribeño. In: Pérez-Estaún, A., Tavares, I., García Cortés, A., Hernaiz, P.P. (Eds.), Evolución geológica del margen norte de la Placa del Caribe, República Dominicana: *Acta Geologica Hispanica*, 37, pp. 123-162.

Escuder-Viruete, J., Díaz de Neira, A., Hernáiz Huerta, P.P., Monthel, J., García Senz, J., Joubert, M., Lopera, E., Ullrich, T., Friedman, R., Mortensen, J., Pérez-Estaún, A., 2006,

Magmatic relationships and ages of Caribbean Island arc tholeiites, boninites and related felsic rocks, Dominican Republic*, Lithos* 90 161-186.

Escuder-Viruete, J., Pérez-Estaún, A., Contreras, F., Joubert, M., Weis, D., Ullrich, T.D., Spadea, P., 2007. Plume mantle source heterogeneity through time: Insights from the Duarte Complex, Hispaniola, northeastern Caribbean, *JGR*, vol 112, B04203, doi: 10.1029/2006JB004323.

Escuder-Viruete, J., Pérez-Estaún, A., Weis, D., and Friedman, R., 2010. Geochemical characteristics of the Río Verde Complex, Central Hispaniola: Implications for the paleotectonic reconstruction of the Lower Cretaceous Caribbean island-arc, *Lithos*, 114, 168-185.

Escuder-Viruete, J., Pérez-Estaún, A., Booth-Rea, G., Valverde-Vaquero, P., 2011. Tectonometamorphic evolution of the Samaná complex, northern Hispaniola: Implications for the burial and exhumation of high-pressure rocks in a collisional accretionary wedge, *Lithos*, 125, pp. 190-210.

Escuder-Viruete, J., Valverde-Vaquero, P., Rojas-Agramonte, J.G., Castillo-Carrión, M., and Pérez-Estaún, A., 2013. Timing of deformational events in the Río San Juan complex: implications for the tectonic controls on the exhumation of high-P rocks in the northern Caribbean subduction-accretionary prism, *Lithos*, DOI: 10.1016/j.lithos.2013.07.006

Ewing, J.I., Officer, C. B., Johnson, H.R., and Edwards, R.S., 1957. Geophysical investigations in the eastern Caribbean: Trinidad Shelf, Tobago Trough, Barbados Ridge, Atlantic Ocean. *Geological Society of America Bulletin*, vol. 68, n. 7, pp. 897-912.

Ewing, J., Antoine, J., and Ewing, M., 1960. Geophysical measurements in the Western Caribbean Sea and in the Gulf of Mexico. *J. Geophys. Res*. 65, 4087-4125.

Ewing, J., Antoine, J., and Ewing, M., 1960 a. Geophysical investigations in the Eastern Caribbean: Trinidad Shelf, Tobago Trough, Barbados Ridge, Atlantic Ocean*. Geol. Soc. Am. Bull*., 68: 897-912.

F

Fox, P.J., Ruddiman, W.F., Ryan, W.B.F., and Heezen, B.C., 1970. The Geology of the Caribbean Crust, I: Beata Ridge. *Tectonophysics*, 10, 495-513.

G

Gardner G.H.F., Gardner L.W., Gregory A.R., 1974. Formation velocity and density: the diagnostic basics for stratigraphic traps. *Geophysics* 39:770–780

Ghosh, N., Hall, S., and Casey, J., 1984. Sea floor spreading magnetic anomalies in the Venezuelan Basin:

the Caribbean-South American Plate Boundary. *Geol Soc Am Mem* 162:65–80

Girard, D., Beck, C., Stephan, J.F., Blanchet, R. y Maury, R., 1982. Pétrologie géochimie et signification géodynamique de quelques formations volcaniques crétacées péri-caraibes. *Bulletin de la Société Géologique de France*, 24, 535-544.

Giunta, G., Beccaluva, L., Siena, F., 2006. Caribbean Plate margin evolution: constraints and current problems, *Geologica Acta*, Vol. 4, Nº 1-2, pp. 265-277.

Granja Bruña, J.L., ten Brink, U., Carbó-Gorosabel A., Muñoz-Martín, A., Gómez, M., 2009. Morphotectonics of Central Muertos thrust belt and Muertos Trough (north-eastern Caribbean). *Mar. Geol.* 263: 7-33, doi: 10.1016/j.margeo.2009.03.010

Granja Bruña, J.L., Muñoz-Martin, A., ten Brink, U.S., Carbó-Gorosabel, A., Llanes Estrada, P., Martín-Dávila, J., Córdoba-Barba, D., Catalán Morollon, M., 2010. Gravity modeling of the Muertos Trough and tectonic implications (north-eastern Caribbean), *Mar. Geophys. Res*. 31: 263-283

Granja Bruña, J.L., Carbó-Gorosabel, A., Llanes Estrada, P., Muñoz-Martín, A., ten Brink, U.S., Gómez Ballesteros, M., Druet, M., and Pazos, A., 2014. Morphostructure at the junction between the Beata ridge and the Greater Antilles island arc (offshore Hispaniola southern slope), *Tectonophysics*, 618, 138-163.

H

Haslinger, F., Kissling, E., Ansorge, J., Hatzfeld, D., Papadimitriou, E., Karakoastas, E., Makropoulus, K., Kahle, H.G., and Peter, Y., 1999. 3D crustal structure from local earthquake tomography around the Gulf of Arta (Ionian region, NW Greece). *Tectonophysics*, 304, 201-218.

Hauff F., Hoernle K., Tilton G., GrahamD. W., and Kerr A. C., 2000. Large volume recycling of oceanic lithosphere over short time scales: geochemical constraints from the Caribbean Large Igneous Province. *Earth Planet. Sci. Lett*. 174, 247–263

Hernáiz-Huerta, P.P., and Pérez-Estaún, A., 2002. Estructura del cinturón de pliegues y cabalgamientos de Peralta, República Dominicana. *Acta Geológica Hispánica*, v.37, nº 2-3, p. 183-205.

Hernaiz Huerta, P.P., Pérez-Valera, F., Abad. M., Monthel, J., and Diaz de Neira, A., 2011. Mélanges and olistostromes in the Puerto Plata area (northern Dominican Republic) as a record of subduction and collisional processes between the Caribbean and North-American plates, *Tectonophysics*, doi:10.1016/j.tecto.2011.10.020.

Houtz, R.Z., Ludwig, W.J., 1977. Structure of the Colombia Basin, Caribbean Sea, from profiler sonobuoy measurements. *J. Geophys. Res*. 82, 4861-4867.

Husen, S., Kissling, E., Flueh, E., & Asch, G. (1999). Accurate hypocentre determination in the seismogenic zone of the subducting Nazca Plate in northern Chile using a combined on-/offshore network. *Geophysical Journal International*, 138, 687-701.

Husen, S., Kissling, E., and J. F. Clinton, 2011. Local and regional minimum 1D models for earthquake location and data quality assessment in complex tectonic regions: application to Switzerland*, Swiss J. Geosci.*, DOI 10.1007/s00015-011-0071-3.

J

James, K.H., 2007, The Caribbean Ocean Plateau – an overview, and a different understanding (http://kjgeology.com/wp-content/uploads/2014/01/2007-the-CaribbeanPlateau.pdf)

Jansma, P. E., A. Lopez, G. S. Mattioli, C. DeMets, T. H. Dixon, P. Mann, and E. Calais, 2000. Neotectonics of Puerto Rico and the Virgin Islands, northeastern Caribbean, from GPS geodesy, *Tectonics*, 9, 1021 – 1037.

K

Kerr, A.C., Marriner, G.F., Tarney, J., Nivia, A., Saunders, A.D., Thirlwall, M.F., and Sinton, C.W., 1997 a. Cretaceous basaltic terranes in western Colombia: elemental, chronological and Sr-Nd constraints on petrogenesis*. J. Petrol*. 38, pp. 677-702.

Kerr A. C., Tarney J., Marriner G. F., Nivia A., and Saunders A. D., 1997 b. The Caribbean–Colombian Cretaceous igneous province: the internal anatomy of an oceanic plateau. In Large Igneous Provinces; Continental, Oceanic and Planetary Flood Volcanism, *American Geophysical Union Monograph* 100 (eds. J. J. Mahoney and M. Coffin), pp. 45–93

Kerr, A.C., Iturralde-Vinent, M.A., Saunders, A.D., Babbs, T.L., and Tarney, J., 1999. A new plate tectonic model of the Caribbean: implications from a geochemical reconnaissance of Cuban Mesozoic volcanic rocks. *Geol. Soc. Am. Bull*. 111, 1581-1599.

Kerr, A.C., 2003. Oceanic plateaus, Treatise on Geochemistry, Volume 3. Editor: Roberta L. Rudnick. Executive Editors: Heinrich D. Holland and Karl K. Turekian. pp. 659. ISBN 0-08-043751-6. Elsevier, p.537-565.

Kerr, A.C., Mahoney, J.J., 2007. Oceanic Plateaus: Problematic plumes, potential paradigms, *Chemical Geology*, 241, pp. 332-353.

Kissling, E., 1988. Geotomography with local earthquake data*, Rev. of Geophysics*, Vol. 26, No. 4, Pages 659-698.

Kissling, E., Ellsworth, W.L., Eberhar-Phillips, D., and U. Kradolfer, 1994. Initial reference models in local earthquake tomography, *J. Geophys. Res*., 99, 19635-19646.

Kissling, E., Solarino, S., and Cattaneo, M. (1995). Improved seismic velocity reference model from local earthquake data in Northwestern Italy. *Terranova*, 7, 528-534.

Krebs, M., Maresch, W.V., Schertl, H.P., Baumann, A., Draper, G., Idleman, B., Münker, C., Trapp, E., 2008. The dynamics of intra-oceanic subduction zones: a direct compar-ison between fossil petrological evidence (Rio San Juan Complex, Dominican Re- public) and numerical simulation. *Lithos* 103, 106–137.

Kroenke L. W., 1974. Origin of continents through development and coalescence of oceanic flood basalt plateaus. *EOS* 55, 443.

L

Ladd, W.J., Worzel, J.L., Watkins, J.S., 1977. Multifold seismic reflections records from the northern Venezuela basin and the north slope of Muertos Trench. *Marine Science Institute*. University of Texas, pp. 41-56.

Ladd, J., Shih, T., and Tsai, C., 1981. Cenozoic tectonics of central Hispaniola and adjacent Caribbean Sea*, American Association of Petroleum Geologists Bulletin*, v. 64, p. 466-489.

Lee, W. H. K. and Lahr, J.C., 1972. HYP071: A computer program for determining hypocenter, magnitude, and first motion pattern of local earthquakes, Open File Report, *U. S. Geological Survey*, 100 pp.

Leroy, S., 1995. Structure et origine de la plaque Caribe. Implications geodynamiques. (These) de l'Universite Paris 6.

Lewis, J.F., and Jiménez, J.G., 1991. Duarte Complex in the La Vega-Jarabacoa-Janico area, central Hispaniola: Geologic and geochemical features of the sea floor during the early stages of arc evolution. In P. Mann, G. Draper, J.F. Lewis (eds.). Geologic and tectonic development of the North America-Caribbean plate boundary in Hispaniola. *Geological Society of America, Special Paper 262*, 115-141.

Lewis, F.L., Amarante, A., Bloise, G., Jiménez, J.G., and Domínguez, H.D., 1991. Lithology and stratigraphy of upper Cretaceous volcanic and volcaniclastic rocks of the Tireo Group, Dominican Republic and correlations with the Massif du Nord in Haiti. In P. Mann, G. Draper, J.F. Lewis (eds.). Geologic and tectonic development of the North America-Caribbean plate boundary in Hispaniola. *Geological Society of America, Special Paper 262*, 143-164.

Lewis, J.F., Escuder Viruete, J., Hernaiz Huerta, P.P., Gutiérrez, G., Draper, G., Pérez Estaún, A., 2002. Subdivisión geoquímica del Arco Isla

Circum-Caribeño, Cordillera Central Dominicana: implicaciones para la formación, acreción y crecimiento cortical en un ambiente intraoceánico. *Acta Geologica Hispanica* 37, 81–122.

Ludwig, W.J., Nafe J.E., and C. L. Drake, 1970. Seismic refraction, in *The Sea*, A. E. Maxwell (Editor), Vol. 4, Wiley-Interscience, New York, 53–84.

Ludwig, W.J., Houtz, R.E., Ewing, J.I., 1975. Profiler sonobuoy measurements in Colombia and Venezuela Basins, Caribbean Sea. *Am. Assoc. Pet. Geol. Bull*. 59, 115-123.

M

Manaker, D.M., Calais, E., Freed, A.M., Ali, S.T., Przybylski, P., Mattioli, G., Jansma, P., Prépetit, C., de Chabalier, J.B., 2008. Interseismic Plate coupling and strain partitioning in the Northeastern Caribbean. *Geophysical Journal International* 174, 889-903. doi:10.1111/j.1365-246X.2008.03819.x.

Mann, P., and Burke, K., 1984. Neotectonics of the Caribbean, *Reviews of Geophysics and Space Physics*, Vol. 22, NO. 4, p. 309-362.

Mann, P., Burke, K., and Matumoto, T., 1984. Neotectonics of Hispaniola: Plate motion, sedimentation, and seismology at a restraining bend. *Earth Planet Sci. Lett.*, 70:311-324.

Mann, P., Schubert, C., and Burke, K., 1990, Review of Caribbean neotectonics, in Dengo, G., and Case, J.E., eds., The Caribbean Region: Boulder, Colorado, *Geological Society of America, The Geology of North America*, v. H, p. 307-338.

Mann, P., and Lawrence, S.R., 1991: Petroleum Potential of Southern Hispaniola, *Journal of Petroleum Geology*, vol. 14 (3), July 1991, pp. 291-308.

Mann, P., Draper, G., and Lewis, J.F., 1991. An overview of the geologic and tectonic development of Española. En P. Mann, G. Draper, J.F. Lewis (eds.). Geologic and tectonic development of the North America-Caribbean plate boundary in Hispaniola. *Geological Society of America Special Paper 262*, 1-28.

Mann, P., Taylor, F.W., Laurence Edwards, R., The-Lung Ku, 1995. Actively evolving microplate formation by oblique collision and sideways motion along strike-slip faults: An example for the northeastern Caribbean plate margin, *Tectonophysics* 246, pp. 1-69.

Mann, P., Prentice, C. S., Burr, G., Peña, L. R., and Taylor, F. W., 1998. Tectonic geomorphology and paleoseismology of the Septentrional fault system, Dominican Republic, in Dolan, J. F., and Mann, P., eds., Active Strike-Slip and Collisional Tectonics of the Northern Caribbean Plate Boundary Zone: Boulder, Colorado, *Geological Society of America Special Paper 326*

Mann, P., McLaughlin, P.P., Van Den Bold, W.A., Lawrence, S.R., and Lamar, M.E., 1999. Tectonic and Eustatic Controls on Neogene Evaporitic and Siliciclastic Deposition in the Enriquillo Basin, Dominican Republic, *Caribbean Basins. Sedimentary Basins of the World, 4* edited by P. Mann (Series Editor: K.J. Hsü), pp. 287-342. Elsevier Science B. V.

Mann, P., E. Calais, J.C. Ruegg, C. DeMets, P. E. Jansma, and G. S. Mattioli, 2002. Oblique collision in the northeastern Caribbean from GPS measurements and geological observations, *Tectonics*, 21(6), 1057, doi: 10.1029/2001TC001304, 2002.

Mann, P., Calais, E., Demets, C., Prentice, C.S., and Wiggins-Grandison, M., 2008. Enriquillo-Plantain Garden Strike-Slip Fault Zone: A major seismic hazard affecting Dominican Republic, Haiti and Jamaica, *18th Caribbean Geological Conference*, Santo Domingo, Dominican Republic, March 24-28.

Masson, D.G., and Scanlon, K.M., 1991. The neotectonic setting of Puerto Rico. *Geological Society of America Bulletin*, v. 103, pp. 144-154, DOI: 10.1130/0016-7606(1991)1032.3.CO:2.

Mauffret, A., and Leroy, S., 1997. Seismic stratigraphy and structure of the Caribbean igneous province. *Tectonophysics* 283, pp. 61-104.

Mauffret, A., and S. Leroy, 1999. Neogene intraplate deformation of the Caribbean plate at the Beata Ridge, in *Sedimentary Basins of the World*, vol. 4, *Caribbean Basins*, edited by P. Mann, pp. 627-669, Elsevier Sci., New York.

Maurrasse, F., Husler, J., Georges, G., Schmitt, R. Y Damond, P. 1979. Upraised Caribbean Sea floor below acoustic reflector B" in the Southern Peninsula of Haiti, *Geologie* en Mijnbuow, 58, 71-83.

McCann, W. R., and L. R. Sykes 1984. Subduction of aseismic ridges beneath the Caribbean plate: Implications for the tectonics and seismic potential of the northeastern Caribbean, *J. Geophys. Res*., 89, 4493 – 4519.

McCann, W.R. 2007. The Muertos Trough as a major earthquake and tsunami hazard for Puerto Rico. *EOS Trans AGU* 88 (23): Jt Assemby Suppl Abs S52A-03.

Meltzer, A.S., Levander, A.R. and Mooney, W.D., 1987, Upper crustal structure, Livermore Valley and vicinity, California Coast Ranges. *Bull. Seis. Soc. Am*. 77, 1655-1673.

Mercier de Lepinay, B., Mauffret, A., Jany, I., Bouysee, P., Mascle, A., Renard, V., Stephan, J.F. and Hernandez, E., 1988, Une collision oblique sur de la bodure nord-caraïbe à la junction entre la ride de Beata et la fosse de Muertos. C.R. Acad. Sci, Paris, 307:1289-1296.

Mereu, R.F., Wang, D., Kuhn, O., Forsyth, D.A., Green, A.G., Morel, P., Buchbinder, G.G.R., Crossley, D., Schwarz, E., duBerger, R., Brooks, C., and Clowes, R., 1986, The 1982 COCRUST seismic experiment across the Ottawa-Bonnechere graben and Grenville Front in Ontario and Quebec, *Geophys. J. Roy. Astr. Soc*. 84, 491-514.

Molnar, P., Sykes, L.R., 1969. Tectonics of the Caribbean and Middle America Regions from Focal Mechanisms and Seismicity, *GSA Bulletin*, v 80, p. 1639-1684.

Moore, G.T., and Fahlquist, D.A., 1976. Seismic profile tying Caribbean DSDP Sites 153, 151, and 152, *Geological Society of America Bulletin*, v. 87, p. 1609-1614.

Mullins, H.T., Breen, N., Dolan, J., Wllner, R.W., Petruccione, J.L., Gaylord, M., Anderse, B., Melillo, A.J., Jurgens, A.D. and Orange, D., 1992. Carbonate platforms along the southeast Bahamas-Hispaniola collision zone. *Mar. Geol*., 105:169-209.

N

Núñez, D., Córdoba, D., Pazos, A., Martín-Dávila, J., Carbó, A., Granja-Bruña, J.L. Payero, J., and Cotilla, M.O., 2010. Seismic images of the crust across the northern Beata Ridge (NE Caribbean). Poster communication in *EGU General Assembly* 2010 (Vienna (Austria)).

Núñez, D., Kissling, E., Córdoba, D., and Pazos, A., 2011 a. Consistency in CSS phase correlation: Application to CARIBE NORTE data set. Poster communication in *EGU General Assembly* 2011 (Vienna (Austria)).

Núñez, D., Córdoba, D., and Pazos, A., 2011 b. Estructura de la corteza y manto superior a través de La Española: desde la Cresta de Beata a la Plataforma de las Bahamas (Proyecto CARIBE NORTE). Oral communication *in Reunión Annual 2011 de la Unión Geofísica Mexicana* (Puerto Vallarta (Mexico)).

Núñez, D., Córdoba, D., Cotilla, M.O., and Pazos, A., submitted in *PAGEOPH*, Modeling the crust and upper mantle in northern Beata Ridge (CARIBE NORTE project) **

O

Officer, C.J., Ewing, J., Edwards, R., Johnson, H., 1957. Geophysical investigations in the eastern Caribbean: Venezuela Basin, Antilles Island arc, and Puerto Rico trench. *Geol. Soc. Am. Bull*. 68, 359-378.

Orihuela Guevara, N., García, A., and Arnaiz, M. 2012. Magnetic anomalies in the Eastern Caribbean. *Int J Earth Sci* (Geol Rundsch) DOI 10.1007/s00531-012-0828-6

P

Palmer, H.C., 1979. Geology of the Monción-Jarabacoa area, Dominican

Republic, Hispaniola. In Lidz, B., and Nagle, F., eds., Hispaniola: Tectonic focal point of the northern Caribbean; Three geologic studies in the Dominican Republic: Miami, Florida, *Miami Geological Society*, p. 29-68.

Pindell, J.L., and Barrett, S.F., 1990. Geological Evolution of the Caribbean Region; A plate tectonic perspective. The Geology of North America. Vol. H, The Caribbean Region. Chapter 16, *The Geological Society of America*.

Pindell, J., 1991. Geologic rationale for hydrocarbon exploration in the Caribbean and adjacent regions, *Journal of Petroleum Geology,* vol. 14 (3), pp. 237-257.

Prentice, C., Mann, P., Pena, L., and Burr, G., 2003. Slip rate and earthquake recurrence along the central Septentrional fault, North American–Caribbean plate boundary, Dominican Republic*: Journal of Geophysical Research*, v. 108, no. B3, p. 2149, doi: 10.1029/2001JB000442, 2003.

Prentice, C.S., Mann, P., Crone, A.J., Gold, R.D., Hudnut, K.W., Briggs, R.W., Koehler, R.D., and P. Jean, 2010. Seismic hazard of the Enriquillo-Plantain Garden fault in Haiti inferred from palaeosesmology, *Nature Geoescience*, vol. 3, DOI:10.1038/NGEO991

Pubellier, M., Mauffret, A., Leroy, S., Vila, J.M., and Amilcar, H., 2000. Plate boundary readjustment in oblique convergence: Example of the Neogene of Hispaniola, Greater Antilles*, Tectonics*, Vol. 19, No. 4, pp 630-648, August 2000.

Q

Quintero, R., Kissling, E., 2001. An improved P-wave Velocity reference model for Costa Rica*, Geofisica Internacional*, Vol. 40, Num. 1, pp. 3-19.

R

Révillon, S., Hallot, E., Arndt, N.T., Chauvel, C., and Duncan R. A., 2000. A Complex History for the Caribbean Plateau: Petrology, Geochemistry, and Geochronology of the Beata Ridge, South Hispaniola. *The Journal of Geology*, vol. 108, p. 641-661.

Russo, R.M., and A. Villaseñor, The 1946 Hispaniola earthquakes and the tectonics of the North America-Caribbean plate boundary zone, northeastern Hispaniola, *J. Geophys. Res.,* vol. 100, no. B4, pp. 6265-6280, 1995.

S

Sen, G. R., Hickey-Vargas, Waggoner, G., Marausse F. 1988. Geochemistry of basalts from the Dumisseau Formation, southern Haiti; Implications for the origin of the Caribbean crust. *Earth and Planetary Science Letters*, 87, 423-437.

Sinton, C.W., Duncan, R.A., Storey M., Lewis, J., and Estrada, J.J., 1998. An oceanic flood basalt province within

the Caribbean plate. *Earth Planet. Sci. Lett*., 155, pp. 221-235.

Solarino, S., Kissling, E., Sellami, Souad, Smriglio, G., Thouvenot, F., Granet, F., Bonjer, K. P., and Sleijko, D., 1997, Compilation of a recent seismicity data base of the greather Alpine region from several seismological networks and preliminary 3D tomographic results, *Annali di Geophysica*, Vol. XL, N. 1, January 1997.

Spence, G.D., Clowes, R.M., and Ellis, R.M., 1985, Seismic structure across the active subduction zone of western Canada*. J. Gephy. Res*. 90, 6754-6772.

Stein, G., Ardévolli., Bourdillon, Ch., Bonnemaison, M., Escuder Viruete, J., Le Goff, E., Escuer, J., Lopera, E., Antón Pacheco, C., García Lobón, J.L., Mortensen, J.K., Ullrich, T., Friedman, R., 2004. Mapa Geológico de la República Dominicana a E. 1:50.000, Restauración (5873-I). Dirección General de Minería, Santo Domingo, 168 pp

Sykes, L.R., McCann, W.R., and Kafka, A.L., 1982, Motion of Caribbean plate during last 7 million years and implications for earlier Cenozoic movements*. J. Geophys. Res.*, 87:10656-10676. DOI: 10.1029/JB087iB13p10656

T

Taber, S., 1922. The seismic belt in the Greater Antilles. *Bulletin of the Seismological Society of America*, v. 12, no. 4, 199-219.

Talwani, M., Windisch, C.C., Stoffa, P.L., Buhl, P., Houtz, R.E., 1977. Multichannel seismic study in the Venezuelan Basin and Curaçao Ridge. In: Talwani, M., Pitman, W.C.I. (Eds.), Islands Arcs, Deep Sea Trenches, and Back-Arc Basins. *Am. Geophys. Union*, Maurice Ewing Ser. 1, 83-98.

ten Brink, U. and Lin, J., 2004. Stress interaction between subduction earthquakes and forearc strike-slip faults: modeling and application to the northern Caribbean plate boundary, *J. geophys. Res*., 109, 12 310–12 324, doi: 10.1029/2004JB003031.

ten Brink, U., Marshak, S., and Granja-Bruña, J.L., 2009. Bivergent thrust wedges surrounding oceanic island arcs: Insight from observations and sandbox models of the northeastern Caribbean plate, *GSA Bulletin*, v. 121; no. 11/12; p. 1522-1536; doi: 10.1130/B26512.1

ten Brink, U.S., Bakun, W.H., and Flores, C.H., 2011. Historical perspective on seismic hazard to Hispaniola and the northeast Caribbean region. *JGR*, Vol., 116, B12318, doi: 10.1029/2011JB008497

W

White, R.S., McKenzie, D., 1995. Mantle plumes and flood basalts. *J. Geophys. Res*. 100, 17543-17585.

Z

Zelt, C.A., and Ellis, R.M., 1988. Practical and efficient ray tracing in two-dimensional media for rapid traveltime and amplitude forward modeling. *Canadian Journal of Exploration Geophysics*, Vol. 24, NO. 1, pp. 16-31.

Zelt, C.A., and Smith, R.B., 1992. Seismic traveltime inversion for 2-D crustal velocity structure, *Geophys. J. Int*., 108, 16-34.

Zelt, C.A., and Forsyth, D.A., 1994. Modelling wide-angle seismic data for crustal structure - Southeastern Grenville Province., *J. Geophys. Res.*, *Solid Earth*, 99 (B6), 11687-11704

Zelt, C.A., 1999. Modelling wide-angle traveltime data. *Geophys. J. Int*. 139, 183-204.

Web pages consulted:

International Seismological Centre, *On-line Bulletin*, http://www.isc.ac.uk, Internatl. Seis. Cent., Thatcham, United Kingdom, 2001.

IRIS - Incorporated Research institutions for Seismology, http://www.iris.edu

JWEED manual: http://www.iris.edu/manuals/jweed/

Vase manual: http://www.iris.edu/manuals/vase/

BREQ_FAST Request manual: http://www.iris.edu/manuals/breq_fast.htm

RDSEED manual: http://www.iris.edu/manuals/rdseed.htm

SAC manual: http://www.iris.edu/software/sac/manual.html

SacSwapByte: https://sites.google.com/site/foo4funreborn/software/sacswapbyte

Seis Wide: http://seismic.ocean.dal.ca/utilities/seiswide/index.php

http://www.bolt-technology.com/index.htm

http://www.utm.csic.es/hesperides.asp

http://www.nanometrics.ca/products/taurus

http://www.reftek.com/products/seismic-recorders-125A-02.htm

ANNEX I

Publications

Cotilla Rodríguez, M.O., and **Núñez Escribano, D.,** 2013**.** Historia sobre la Sismología del Caribe Septentrional, *Revista Historia de América,* n. 143, Julio-diciembre 2013.

Cotilla Rodríguez, M.O., Córdoba Barba, D., and **Núñez Escribano, D.,** 2013a. Alternative Interpretation for the Cuban Active Zones. (accepted in *GEOTECTONICS*)

Cotilla Rodríguez, M.O., Córdoba Barba, D., and **Núñez Escribano, D., 2013b**. The Guane Fault, Western Cuba. *IZVESTIYA, PHYSICS OF THE SOLID EARTH FIZIKA ZEMLI* (accepted)

Núñez, D., Córdoba, D., Cotilla, M.O., and Pazos, A., submitted in *PAGEOPH*, Modeling the crust and upper mantle in northern Beata Ridge (CARIBE NORTE project) **

Núñez, D., Córdoba, D., Seismic images of the crust in western Dominican Republic from wide-angle data (CARIBE NORTE & GEOPRICO-DO Projects) (*In preparation to be submitted to GRL*)

Núñez, D., Córdoba, D., Seismic transect across Bahamas Carbonate Platform-Dominican Republic-Muertos Thrust (NE Caribbean Plate) (*In preparation*)

Núñez, D., Córdoba, D., Lithosphere structure beneath Dominican Republic based on CSS, wide-angle data and seismicity data (*In preparation*)

International Conferences

Núñez, D., Córdoba, D., Pazos, A., Martín-Dávila, J., Carbó, A., Granja-Bruña, J.L. Payero, J., and Cotilla, M.O., 2010. Seismic images of the crust across the northern Beata Ridge (NE Caribbean). Poster communication in *EGU General Assembly* 2010 (Vienna (Austria)).

Núñez, D., Kissling, E., Córdoba, D., and Pazos, A., 2011 a. Consistency in CSS phase correlation: Application to CARIBE NORTE data set. Poster communication in *EGU General Assembly* 2011 (Vienna (Austria)).

Núñez, D., Córdoba, D., and Pazos, A., 2011 b. Estructura de la corteza y manto superior a través de La Española: desde la Cresta de Beata a la Plataforma de las

Bahamas (Proyecto CARIBE NORTE). Oral communication *in Reunión Annual 2011 de la Unión Geofísica Mexicana* (Puerto Vallarta (Mexico)).

Córdoba, D., Pazos, A., Carbó, A., Martín Dávila, J., **Núñez, D.,** Payero, J., Fort, M., López, O., and Granja, J.L., 2009. Estudios sísmicos mar-tierra en el borde NE de la Placa Caribe. Proyectos GEOPRICO y CARIBE NORTE. Oral presentation in Reunión Annual 2009 de la Unión Geofísica Mexicana (Puerto Vallarta (Mexico)).

Córdoba, D., **Núñez, D.,** Pazos, A., Martín Dávila, J., Carbó-Gorosabel, A., Granja-Bruña, J.L., Llanes-Estrada, M.P., Polanco-Rivera, E., Muñoz, S., Calzadilla, M., Payero, J., Fort, M., Cotilla, M.O., and CARIBE NORTE Working Group, 2010. Seismic images of the crust across the North-Eastern border of the Caribbean Plate (Southern Hispaniola Island) from wide-angle profiles. Poster communication in 2010 The Meeting of the Americas (Foz Do Iguazzu (Brasil)).

Pazos, A**., Núñez Escribano, D**., Córdoba Barba, D., Martín Dávila, J., 2012. Método de corrección de OBS's fuera de línea en perfiles de sísmica activa/A correction method for OBS 's out of the active seismic profile line. Oral presentation in 7ª ASAMBLEA HISPANO PORTUGUESA DE GEODESIA Y GEOFISICA (San Sebastián, Spain).

Núñez Escribano, D., Córdoba Barba, D., Bartolomé, R. 2010. Seismic Crustal Structure in the Southern Segment of the Gulf of California (Mexico) from Geophysical Data Modelling. Poster presentation in AGU THE MEETING OF AMERICAS 2010 (FOZ DO IGUAZZU, Brazil).

Núñez Escribano, D., Córdoba Barba, D., Bartolomé, R., Dañobeitia, J.J. 2009. SEISMIC CRUSTAL STRUCTURE IN SOUTHERN GULF OF CALIFORNIA. Oral presentation in EGU GENERAL ASSEMBLY 2010 (Viena, Austria)

Núñez Escribano, D., Córdoba Barba, D., Bartolomé, R., Dañobeitia, J.J. 2009. ESTRUCTURA DE LA CORTEZA EN LA ZONA MERIDIONAL DEL GOLFO DE CALIFORNIA, MEXICO. Oral presentation in REUNION ANUAL UNION GEOFISICA MEXICANA 2009 (PUERTO VALLARTA, Mexico)

Córdoba Barba, D., Pazos, A., Carbó Gorosabel, A., Martín Dávila, J**., Núñez Escribano, D**., Payero, J., Fort, M., López, O., Granja Bruña, J.L., 2009. ESTUDIOS SÍSMICOS MAR-TIERRA EN EL BORDE NE DE LA PLACA CARIBE. PROYECTOS GEOPRICO Y CARIBE NORTE. Oral presentation in REUNION ANUAL UNION GEOFISICA MEXICANA 2009 (PUERTO VALLARTA, Mexico).

Núñez Escribano, D., Córdoba Barba, D. 2009. SEISMIC IMAGES OF THE CRUST AT THE SOUTHERN PART OF THE GULF OF CALIFORNA (MEXICO). Oral presentation in

1st SPAIN-CHINA SYMPOSIUM ON GEOPHYSICAL & GEOCHEMICAL GEOSYSTEMS (SG3) (ZARAGOZA, Spain)

Córdoba Barba, D., Pazos, A., Carbó, A., Martín Dávila, J., **Núñez Escribano, D.,** Fort, M., López, O., Granja Bruña, J.L.. 2009. THE CARIBE NORTE SEISMIC ONSHORE-OFFSHORE PROJECT: A DEEP SEISMIC SURVEY OF THE CRUSTAL STRUCTURE IN THE NORTHERN CARRIBEAN PLATE. Poster presentation in 1st SPAIN-CHINA SYMPOSIUM ON GEOPHYSICAL & GEOCHEMICAL GEOSYSTEMS (SG3) (ZARAGOZA, Spain)

Participation in R&D&I projects funded in competitive calls by public or private bodies

1 Proyect: Caracterización del peligro sísmico y tsunamigénico asociado con la estructura cortical del contacto Placa de Rivera-Bloque de Jalisco (TSUJAL).
Responsible Institution: Universidad Complutense de Madrid (Spain)
Head researcher: DIEGO CORDOBA BARBA
Funding institution: Ministerio de Economía y Hacienda
Start date: 01/12/2012 End date: 31/12/2014
Total amount: 200.000

2 Project: TOPO-IBERIA
Responsible Institution: Instituto de Ciencias de la Tierra Jaume Almera (Spain)
Head researcher: JOSEP GALLART MUSET
Funding institution: Ministerio de Educación y Ciencia
Start date: 01/12/2006 End date: 2013
Total amount: 4.500.000

3 Project: PLAN OCEANOGRÁFICO-HIDOGRÁFICO DE LA ZONA ECONÓMICA EXCLUSIVA ESPAÑOLA. CARTOGRAFÍA SISTEMÁTICA Y ESTUDIO DE LAS ZONAS DE AMPLIACIÓN SEGÚN LA CONVENCIÓN DEL DERECHO DEL MAR DE NACIONES UNIDAS
Responsible Institution: InstitutoEspañol de Oceanografía (Spain)
Head researcher: PEDRO HERRANZ CANO
Start date: 01/2008 End date: 12/2012

4 Project: MODELO CORTICAL DE LA TRANSICIÓN ENTRE LAS COORDILLERAS CENTRAL Y ORIENTAL DE LA REPÚBLICA DOMINICANA: MANATÍ
Responsible Institution: Universidad Complutense de Madrid (Spain)
Head researcher: DIEGO CORDOBA BARBA
Funding institution: Ministerio de Ciencia e Innovación.
Start date: 01/02/2009 End date: 31/01/2010
Total amount: 35.000

5 Project: ANÁLISIS DEL CONTACTO ENTRE LAS PLACAS CARIBE Y NORTEAMERICANA: DESDE LA CRESTA DE BEATA (R. DOMINICANA) HASTA EL PASAJE DE ANEGADA (ANTILLAS MENORES). CARIBENORTE
Responsible Institution: Universidad Complutense de Madrid (Spain)
Head researcher: DIEGO CORDOBA BARBA
Funding institution: MINISTERIO DE EDUCACION Y CIENCIA
Start date: 2006 End date: 2010
Total amount: 99.000

6 Project: INTEGRATED OBSERVATIONS FROM NEAR SHORE SOURCES OF TSUNAMIS: TOWARDS AN EARLY WARNING SYSTEM (NEAREST)
Head researcher: NEVIO ZITELLINI
Funding institution: EUROPEAN UNION, VI FRAMEWROK PROGRAM, STREP (SPECIFIC TARGETED RESEARCH)
Start date: 01/10/2006 End date: 01/10/2009
Total amount: 2.850.000

Stays in public or private R&D&I centres

1 Institution: ETHZ
Faculty, institute or centre: Institute for Geophysics
City: Zurich, Switzerland
Start date: 26/11/2012, 13 days End date: 08/12/2012
Aims of the stay: Doctorate
Provable tasks: Seismic Tomography

2 Institution: Oklahoma State University
Faculty, institute or centre: Boone Pickens School of Geology
City: Stillwater (OK), United States of America
Start date: 31/05/2012, 90 days End date: 28/08/2012
Aims of the stay: Doctorate
Provable tasks: Seismic Tomography

3 Institution: ETHZ
Faculty, institute or centre: Institute for Geophysics
City: Zurich, Switzerland
Start date: 09/05/2012, 10 days End date: 18/05/2012
Aims of the stay: Doctorate
Provable tasks: Seismic Tomography

4 Institution: ETHZ
Faculty, institute or centre: Institute for Geophysics
City: Zurich, Switzerland

Start date: 05/02/2012, 13 days End date: 17/02/2012
Aims of the stay: Doctorate
Provable tasks: Seismic Tomography

5 Institution: ETHZ
Faculty, institute or centre: Institute for Geophysics
City: Zurich, Switzerland
Start date: 10/10/2011, 75 days End date: 23/12/2011
Aims of the stay: Doctorate
Provable tasks: Seismic Tomography

6 Institution: ETHZ
Faculty, institute or centre: Institute for Geophysics
City: Zurich, Switzerland
Start date: 13/09/2010, 92 days End date: 13/12/2010
Aims of the stay: Doctorate
Provable tasks: Seismic Tomography

Grants and scholarships obtained

Name of the grant: Formación de Personal Investigador
Aims: Pre-doctoral
Conferring institution: Ministerio de Ciencia e Innovación. Investigación
Conferral date: 22/08/2008 Duration of the grant: 48 months
End date: 31/08/2012
Name of institution: Universidad Complutense de Madrid
Faculty, institute or centre: Facultad de Ciencias Físicas

Field Works and Maritime Course

2008. Potential fields data recovery fieldtrip onboard R/V HESPÉRIDES offshore Galicia (Spain).

2008. Seismic data recovery fieldtrip onshore southern Portugal.

2009. Seismic data recovery fieldtrip onshore Dominican Republic.

2014. STCW 95 Basic Safety and Security Training (80 hours) and getting the Seaman's Book.

2014. MCS and wide-angle data recovery fieldtrip onboard RRS JAMES COOK offshore western coast of Mexico.

Participation in research, development or innovation groups/teams

Name of the group: MODELIZACIÓN LITOSFÉRICA: ESTRUCTURA Y DINÁMICA
Aims of the group: Investigación de la estructura litosférica a partir de datos de sísmica de reflexión y gran ángulo, gravimetría y magnetismo y modelización numérica.

Type of collaboration: Co-authorship of projects and their development
Institution: University Complutense de Madrid
Start date: 01/09/2008, 5 years - 5 months

Teaching activity

1 Name of subject/course: Laboratorio de Física
Qualification: Doble Grado en Matemáticas y Física
Start date: 11/02/2012 End date: 31/05/2012
Date of the last time: 2012
Institution: Universidad Complutense de Madrid
Faculty, institute or centre: Facultad de Ciencias Físicas

2 Name of subject/course: Laboratorio de Física
Qualification: Grado en Fisica
Start date: 11/02/2012 End date: 31/05/2012
Date of the last time: 2012
Institution: Universidad Complutense de Madrid Type of institution: University
Faculty, institute or centre: Facultad de Ciencias Físicas

Experience organising R&D&I activities

1 Title: SEMINARIOS DE GEOFISICA
Type of activity: ORGANIZACION DEL SEMINARIO Area of the activity: Regional
Convening institution: Universidad Complutense de Madrid
City: MADRID, Community of Madrid, Spain
Start date: 01/03/2010, 3 years - 11 months End date: 31/01/2014

2 Title: TALLER PRACTICO SOBRE LA GENERACION DE TSUNAMIS
Type of activity: ORGANIZACION E IMPARTICION DEL TALLER
Area of the activity: Regional
Convening institution: Universidad Complutense de Madrid
Type of institution: University
City: MADRID, Community of Madrid, Spain
Start date: 24/03/2011, 1 day End date: 24/03/2011

3 Title: TERREMOTOS Y TSUNAMIS
Type of activity: ORGANIZACION E IMPARTICION DEL TALLER
Area of the activity: Regional
Convening institution: Universidad Complutense de Madrid
Type of institution: University
City: MADRID, Community of Madrid, Spain
Start date: 11/2009, 1 day End date: 11/2009

ANNEX II MASTER STATION LIST

STAT	NET	SITE	LAT	LONG	ELEV	START	FINISH	STATUS	SOURCE
BANI	DR	BANI, DR	18.3923	-70.3582	1038			Open	ISC
			18.4	-70.36	1038	01/01/2010	31/12/2599		IRIS
JIDR	GS	Jimani, DR	18.491	-71.8507	13			Open	ISC
			18.49	-71.85	13	16/03/2010	31/12/2999		IRIS
NADR	DR	Centro Regional Nagua (Curna), DR	19.3541	-69.8561	4			Open	ISC
			19.35	-69.86	4	30/01/2010	31/12/2599		IRIS
PCDR	PR	Punta Cana DR, DR	18.5139	-68.3814	7			Open	ISC
			18.51446	-68.3809	0				PRSN
PPDR	DR	Centro Regional Atlantico (CURA), UASD,Puerto Plata, DR	19.8053	-70.7243	4			Open	ISC
			19.81	-70.72	4	30/01/2010	31/12/2599	Open	IRIS
PUCM	DR	Universidad PUCCM,Santiago, DR	19.4403	-70.6814	177			Open	ISC
			19.44	-70.68	177	01/01/2007	31/12/2599		IRIS
SDD	DR	Estación Central Sismológica, Santo Domingo, DR	18.4579	-69.9134	10				ISC
			18.46	-69.92	34	01/01/2004	31/12/2599		
SMN1	PR	Samana DR, DR	19.1878	-69.2733	521			Open	ISC
			19.19	-69.27	50	08/03/2007	31/12/2599		IRIS
			19.18778	-69.2733	50				PRSN
HATO	DR	El Peon, Hato Mayor, Dominican Republic	18.79	-69.38	438	01/01/2005	31/12/2599		IRIS
NAVI	DR	Loma La Naviza, Cotui, DR	18.96	-70.03	680	01/01/2010	31/12/2599		IRIS
JAKH	CN	Jacmel, Haiti	18.23767	-72.5180	47				ISC
			18.24	-72.52	47	16/02/2010	31/12/2599		IRIS
LGNH	CN	Leogane, Haiti	18.51097	-72.6058	62				ISC
			18.51	-72.61	62	14/02/2010	31/12/2599		IRIS
PAPH	CN	Port-au-Prince, Haiti	18.52253	-72.2993	218				ISC
			18.52	-72.3	218	11/02/2010	31/12/2599		IRIS

PEDR	GS	Pedernales, Dominican Republic	18.03622	-71.7461	0				ISC
			18.04	-71.75	27	12/03/2010	31/12/2999		IRIS
WSYH	GS	Wesleyan Hospital on Ile de La Gonave, Haiti	18.83297	-72.8627	29				ISC
			18.83	-72.86	29	10/03/2010	31/12/2999		IRIS
DBAD	GS	Dispensory Bahott MRP USAID north of Bainet, Haiti	18.23	-72.74	534	15/03/2010	25/06/2010		IRIS
HBME	GS	Bureau of Mines, Port au Prince, Haiti	18.56	-72.3	85	09/03/2010	31/12/2999		IRIS
HCEA	GS	Ceant home, La Boule	18.5	-72.31	746	09/03/2010	31/12/2999		IRIS
HCMD	GS	Health Care Medical Center in Dufort, Haiti	18.46	-72.64	74	13/03/2010	25/06/2010		IRIS
HHMT	GS	Hotel Montana, Gros Morne	18.53	-72.3	335	10/03/2010	31/12/2999		IRIS
HPKH	GS	Killick Coast Guard, Port au Prince	18.53	-72.38	5	28/01/2010	31/12/2999		IRIS
HPLZ	GS	Plaza Hotel, Port au Prince	18.54	-72.33	34	03/05/2010	31/12/2999		IRIS
HVCV	GS	Voila NOC, Canape Vert	18.53	-72.31	267	11/03/2010	31/12/2999		IRIS
HVGZ	GS	Voila, St. Louis Gonzagua School, Port au Prince	18.55	-72.3	86	12/03/2010	31/12/2999		IRIS
HVMG	GS	Voila Cell tower above Marigot, Haiti	18.24	-72.31	145	16/03/2010	24/06/2010		IRIS
HVPR	GS	Voila, Pont Rouge, Port au Prince	18.56	-72.34	6	11/03/2010	31/12/2999		IRIS
JIDR	GS	Jimani, Dominican Republic	18.49	-71.85	13	16/03/2010	31/12/2999		IRIS
ROSH	GS	Rosseau Hospital near Montrouis, Haiti	18.97	-72.68	139	09/03/2010	22/06/2010		IRIS
SJPH	GS	Saint Joseph Clinic in Cotes de Fers, Haiti	18.19	-73	22	16/03/2010	24/06/2010		IRIS
SPHI	GS	Satelite Telecommunications facility for Haiti National TV,	18.75	-72.4	101	11/03/2010	22/06/2010		IRIS
TRIN	GS	Catholic Churh in Tourin, Haiti	18.37	-72.65	334	17/03/2010	25/06/2010		IRIS
USEM	GS	US Embassy, Tabarre	18.56	-72.25	65	27/01/2010	31/12/2999		IRIS

ANWB	CU	Willy Bob, Antigua and Barbuda	17.66853	-61.7855	39				ISC
			17.67	-61.79	39	07/09/2007	31/12/2599		IRIS
			17.669	-61.786	39	2,007,250			USGS
BBGH	CU	Gun Hill, Barbados	13.14336	-59.5587	180				ISC
			13.14	-59.56	180	06/09/2006	31/12/2599		IRIS
			13.143	-59.559	180	2,006,249			USGS
BCIP	CU	Isla Barro Colorado, Panama	9.166477	-79.8373	61				ISC
			9.17	-79.84	61	02/12/2006	31/12/2599		IRIS
			9.166	-79.837	61	2,006,336			USGS
GRGR	CU	Grenville, Grenada	12.13239	-61.6540	195				ISC
			12.13	-61.65	195	12/12/2006	31/12/2599		IRIS
			12.132	-61.654	195	2,006,346			USGS
GRTK	CU	Grand Turk, Turks and Caicos Islands	21.5115	-71.1326	12				ISC
			21.51	-71.13	12	18/12/2007	31/12/2599		IRIS
			21.511	-71.133	12	2,007,352			USGS
GTBY	CU	Guantanamo Bay, Cuba	19.92681	-75.1108	79.2				ISC
			19.93	-75.11	79	27/08/2007	31/12/2599		IRIS
			19.927	-75.111	79	2,007,239			USGS
MTDJ	CU	Mount Denham, Jamaica	18.22606	-77.5345	925				ISC
			18.23	-77.53	925	08/12/2007	31/12/2599		IRIS
			18.226	-77.535	925	2,007,342			USGS
SDDR	CU	Presa de Sabenta, Dominican Republic	18.98211	-71.2878	589				ISC
			18.98	-71.29	589	30/08/2006	31/12/2599		IRIS
			18.982	-71.288	589	2,006,242			USGS
BBJ	JSN	Bamboo Saint Ann, Jamaica	18.383	-77.267	641			open	ISC
			18.38	-77.26	760				JSN
BEV		Beverley, Jamaica	18.4517	-77.3	123				ISC
BNJ	JSN	Bonny Gate, Jamaica							ISC
			18.32	-76.95	490				JSN
CMJ	JSN	Castle Mountains, Jamaica	18.13581	-76.3726	333				ISC
			18.14	-76.36	390				JSN
CVJ	JSN	Coleyville, Jamaica	18.22619	-77.5348	985.6				ISC
			18.23	-77.53	990				JSN

GWJ	JSN	Greenwich, Jamaica	18.074	-76.728	1200				ISC
			18.07	-76.73	1170				JSN
HOJ	JSN	Hope, Jamaica	18.00453	-76.7493	179.7			open	ISC
			18.00453	-76.7493	179.7				JSN
STH	JSN	Stony Hill, Jamaica	18.07672	-76.8094	418.5			open	ISC
			18.08	-76.81	500			open	JSN
YHJ	JSN	Yallahs, Jamaica	17.892	-76.493	600				ISC
			17.89	-76.49	600				JSN
ABVI	PR	Anegada Island, Puerto Rico	18.72967	-64.3325	8				ISC
			18.73	-64.33	8	25/04/2007	31/12/2599		IRIS
			18.72967	-64.3325	7.97				PRSN
AGPR	PR	Aguadilla, Puerto Rico	18.4675	-67.1112	119			open	ISC
			18.47	-67.11	119.9	01/02/2004	31/12/2599		IRIS
			18.46749	-67.1111	119.874				PRSN
AOPR	PR	Arecibo Observatory, Puerto Rico	18.3466	-66.7539	355				ISC
			18.35	-66.75	355.1	31/03/2003	31/12/2599		IRIS
			18.34665	-66.7539	355.146				PRSN
APR	PR	Arecibo, Puerto Rico	18.44222	-66.7247	50				ISC
			18.44397	-66.7256	33.45				PRSN
CBYP	PR	Canovanas, Puerto Rico	18.27161	-65.8566	606				ISC
			18.27	-65.86	606.9	08/02/2001	31/12/2599		IRIS
			18.27167	-65.8566	606.903				PRSN
CDPB	PR	Cerro de Punta, Puerto Rico	18.17	-66.59	1300			closed	ISC
			18.17316	-66.5909	1284.89			closed	PRSN
CELP	PR	Cerrillos, Puerto Rico	18.07489	-66.5791	195				ISC
			18.07485	66.5791	195.65				PRSN
CPD	PR	Cerro la Pandura, Puerto Rico	18.03681	-65.9151	385			open	ISC
			18.03678	-65.9151	385.67				PRSN
CRPR	PR	Cabo Rojo, Puerto Rico	18.00639	-67.1096	6			open	ISC
			18.01	-67.11	64.8	07/03/2005	31/12/2599		IRIS
			18.0064	-67.1096	64.88				PRSN
CSB	PR	Colonia Sabana, Puerto Rico	18.2897	-66.1567	470			open	ISC
			18.28951	-66.1576	447.106				PRSN

CULB	PR	Culebra, Puerto Rico	18.326	-65.301	161.2				ISC
			18.33	-65.3	580	19/10/2000	31/12/2599		IRIS
			18.27561	-65.3007	161.25				PRSN
GBPR	PR	Guanica, Bosque Seco, Puerto Rico	17.9751	-66.8792	16			open	ISC
			17.9751	-66.8792	162				PRSN
HUMP	PR	Col San Antonio, Puerto Rico	18.14211	-65.8498	79				ISC
			18.14	-65.85	79.1	30/08/2002	31/12/2599		IRIS
			18.14207	-65.8488	79.095				PRSN
ICM	PR	Isla Caja Muertos, Puerto Rico	17.89339	-66.521	7			closed	ISC
			17.89	-66.52	77.2	25/01/2001	31/12/2599		IRIS
			17.89336	-66.5209	77.242				PRSN
IDE	PR	Isla Desecho, Puerto Rico	18.38639	-67.4741	203			open	ISC
			18.38444	-67.4791	203.073				PRSN
IMO	PR	Isla Mona, Puerto Rico	18.1095	-67.9081	3			open	ISC
			18.11	-67.91	90.9	20/12/2000	31/12/2599		IRIS
			18.10947	-67.9080	90.941				PRSN
IMPR	PR	Mona Island, Puerto Rico	18.077	-67.9311	10			open	ISC
			18.075675	-67.93111	1.45				PRSN
LRS	PR	Lares, Puerto Rico	18.29139	-66.8446	455			open	ISC
			18.29139	-66.8445	455.976				PRSN
LSP	PR	Las Mesas, Puerto Rico	18.17569	-67.0858	389			Open	ISC
			18.17574	-67.0858	389.847				PRSN
MGP	PR	Maguayo, Puerto Rico	18.00761	-67.0891	60			Open	ISC
			18.01	-67.09	35.2	09/03/2001	31/01/2005		IRIS
			18.00762	-67.0891	35.161				PRSN
MPR	PR	Mayaguez, Puerto Rico	18.21169	-67.1398	22			Open	ISC
			18.21	-67.14	22.4	19/02/2004	31/12/2599		IRIS
			18.21169	-67.1397	22.409				PRSN
MTP	PR	Monte Pirata, Puerto Rico	18.09719	-65.5525	120			Open	ISC
			18.1	-65.55	35.2	24/05/2000	31/12/2599		IRIS
			18.09722	-65.5525	191.886				PRSN
OBIP	PR	Obispado Ponce, Puerto Rico	18.04281	-66.60619	102				ISC
			18.04	-66.61	102.6	18/12/2002	31/12/2599		IRIS
			18.0428	-66.6062	102.621				PRSN

PORP	PR	Portuguez, Puerto Rico	18.06289	-66.6363	199.9			Open	ISC
			18.06298	-66.6363	199.87				PRSN
SJG	CU/ PR	San Juan, Puerto Rico	18.11167	-66.15	45			Open	ISC
			18.10906	-65.1501	456.879				PRSN
			18.109	-66.15	420				USGS
AG02	PR	UPR Aguadilla	18.47	-67.11	119.9	25/05/2006	31/12/2599		IRIS
AR02	PR	UPR Arecibo	18.47	-66.74	100	25/05/2006	31/12/2599		IRIS
BFI1	PR	Airport Beef Islands	18.44	-64.54	100	05/01/2006	31/12/2599		IRIS
CR03	PR		18.39	-65.99	50	13/08/2006	31/12/2599		IRIS
CTN1	PR	Cataño Defensa Civil	18.44	-67.13	10	27/01/2004	31/12/2599		IRIS
MY10	PR	UPR Mayaguez	18.22	-67.14	22.4	05/03/2003	31/12/2599		IRIS
PN13	PR	UPR Ponce	17.97	-66.61	100	05/03/2003	31/12/2599		IRIS
SJ07	PR	UPR Ciencias Médicas, San Juan	18.4	-66.07	100	02/12/2003	31/12/2599		IRIS
UTD2	PR	UPR Utuado	18.25	-66.72	200	02/12/2003	31/12/2599		IRIS
CDVI	PR	Country Days School, St. Croix, USVI	17.75175	-64.7661	31.14				PRSN
STVI	PR	UVI, St. Thomas, USVI	18.35244	-64.9566	383.05				PRSN
TBVI	PR	DDM Office Tortola, British VI	18.41497	-64.6186	35.867				PRSN

ANNEX III MASTER EVENT LIST

EVENTS FOR PERIOD I

2008	CATALOG	CONTRIB.	DATE	TIME	LAT/LON	DEPTH	MAGN
1	ISCCD	ISC	01/01/08	18:12:47	17.8593/-68.5197	63	MD/3.43
2	ISCCD	ISC	12/01/08	04:52:11	19.9717/-69.5272	50.9	MD/4.11
3	WHDF	NEIC	14/01/08	14:31:11	17.801/-63.269	29	MB/4.1 MD/3.9
4	ISCCD	ISC	14/01/08	14:31:11	17.801/-63.2689	29	MB/4.1
5	FINGER	NEIC	16/01/08	04:11:54	17.68/-68.01	23.1	M/4.3
6	ISCCD	ISC	16/01/08	04:11:56	17.5652/-68.0861	65.6	ML/4.5
7	ISCCD	ISC	18/01/08	20:53:40	19.3262/-69.1146	39.7	MD/3.86
8	ISCCD	ISC	19/01/08	02:54:30	18.911/-68.8537	96.6	MD/3.73
9	WHDF	NEIC	26/01/08	03:04:02	19.751/-70.693	72.5	MD/4.6
10	ISCCD	ISC	26/01/08	03:04:02	19.7515/-70.6932	72.5	MD/4.51
11	WHDF	NEIC	27/01/08	04:18:37	17.678/-63.311	5.9	MD/4.0
12	WHDF	NEIC	27/01/08	23:11:13	19.521/-68.254	158.7	MD/4.0
13	ISCCD	ISC	27/01/08	23:11:13	19.5212/-68.2542	158.7	MD/4.04
14	ISCCD	ISC	29/01/08	08:06:44	19.8/-68.8999	8	MS/4.7 MS7/4.5
15	WHDF	NEIC	29/01/08	08:06:46	19.812/-68.919	8	MD/4.3
16	WHDF	NEIC	01/02/08	07:46:41	19.179/-63.214	36.2	MB/3.9
17	ISCCD	ISC	01/02/08	07:46:41	19.013/-63.3309	34.5	MD/4.2
18	ISCCD	ISC	04/02/08	07:43:46	19.0959/-67.9262	10	MB/5.5 MS/4.6
19	ISCCD	ISC	04/02/08	07:43:53	19.109/-66.9509	19	MS/4.8 MB/5.4
20	NEICALRT	NEIC	04/02/08	07:43:55	18.9736/-66.9382	26.9	MB/5.2
21	ISCCD	ISC	04/02/08	07:43:56	19.0/-66.8699	16	MW/5.52
22	ISCCD	ISC	04/02/08	07:44:08	20.868/-66.1759	33	MS/4.9 MB/5.4
23	WHDF	NEIC	04/02/08	17:02:24	18.198/-68.579	127.5	MD/3.7
24	ISCCD	ISC	04/02/08	17:02:24	18.1978/-68.5787	127.5	MD/3.74
25	WHDF	NEIC	07/02/08	14:49:51	19.266/-68.906	126.4	MD/4.3
26	WHDF	NEIC	10/02/08	17:07:43	17.467/-68.661	85.1	MD/3.6
27	ISCCD	ISC	10/02/08	17:07:43	17.4673/-68.6611	85.1	MD/3.57
28	WHDF	NEIC	15/02/08	01:46:28	20.072/-69.361	13	MD/3.9
29	ISCCD	ISC	17/02/08	23:23:50	17.493/-63.1326	182.2	MD/4.22

30	ISCCD	ISC	25/02/08	18:36:21	19.1547/-71.0681	117.8	MD/4.71
31	ISCCD	ISC	03/03/08	06:27:47	19.6/-70.2999	10	MS/4.8 MS7/4.8
32	WHDF	NEIC	03/03/08	20:30:25	18.668/-68.742	170.2	MD/4.0
33	ISCCD	ISC	03/03/08	20:30:25	18.6678/-68.7422	170.2	MD/4.02
34	WHDF	NEIC	09/03/08	18:45:14	18.395/-68.884	124.4	MD/3.8
35	ISCCD	ISC	09/03/08	18:45:14	18.3945/-68.8841	124.4	MD/3.75
36	WHDF	NEIC	09/03/08	20:02:30	18.126/-68.92	140.9	MD/3.7
37	ISCCD	ISC	09/03/08	20:02:30	18.1263/-68.9199	140.9	MD/3.72
38	WHDF	NEIC	14/03/08	18:41:36	18.542/-68.722	168	MD/3.8
39	ISCCD	ISC	14/03/08	18:41:36	18.5417/-68.7221	168	MD/3.76
40	WHDF	NEIC	15/03/08	22:01:43	18.777/-68.771	113.6	MD/3.6
41	ISCCD	ISC	15/03/08	22:01:43	18.7767/-68.7704	113.6	MD/3.59
42	WHDF	NEIC	16/03/08	01:54:06	19.379/-69.521	61.8	MD/4.2
43	ISCCD	ISC	16/03/08	01:54:06	19.3787/-69.5207	61.8	MD/4.15
44	WHDF	NEIC	25/03/08	09:59:46	18.029/-68.572	86.9	MD/3.5
45	ISCCD	ISC	25/03/08	09:59:46	18.0292/-68.5719	86.9	MD/3.45
46	WHDF	NEIC	29/03/08	18:25:38	19.433/-69.615	63.5	MD/3.7
47	WHDF	NEIC	30/03/08	02:26:16	19.78/-69.351	100.8	MD/3.9
48	ISCCD	ISC	30/03/08	02:26:16	19.78/-69.3504	100.8	MD/3.87
49	QED	NEIC	30/03/08	09:08:28	18.306/-68.98	116	MD/3.7
50	ISCCD	ISC	30/03/08	09:08:28	18.3065/-68.9801	115.8	MD/3.73
51	WHDF	NEIC	31/03/08	01:27:28	20.021/-69.22	19.4	MD/4.0
52	ISCCD	ISC	31/03/08	01:27:28	20.0205/-69.2201	19.4	MD/3.91
53	WHDF	NEIC	01/04/08	20:28:37	18.903/-69.122	125.8	MD/3.8
54	WHDF	NEIC	03/04/08	07:23:17	18.972/-70.249	104.9	MD/4.0
55	ISCCD	ISC	03/04/08	07:23:17	18.9717/-70.2489	104.9	MD/4.04
56	WHDF	NEIC	06/04/08	03:57:40	18.84/-69.608	98.9	MD/4.0
57	ISCCD	ISC	06/04/08	03:57:40	18.8395/-69.6076	99	MD/4.03
58	WHDF	NEIC	11/04/08	17:34:09	20.133/-69.834	189.5	MD/4.3
59	ISCCD	ISC	11/04/08	19:39:10	19.3188/-68.7067	92.4	MD/3.38
60	WHDF	NEIC	16/04/08	12:16:44	18.75/-68.503	20.9	MD/2.9
61	ISCCD	ISC	16/04/08	12:16:44	18.7503/-68.5031	20.9	MD/2.85
62	ISCCD	ISC	17/04/08	02:22:49	19.2787/-65.1154	0	ML/4.1 MS/3.4
63	ISCCD	ISC	17/04/08	02:22:52	19.2026/-65.2116	14	MS/3.29 MB/4.04

64	WHDF	NEIC	17/04/08	02:22:54	19.141/-65.16	6.1	MD/4.1
65	WHDF	NEIC	17/04/08	02:49:18	18.683/-69.423	28.4	MD/3.7
66	ISCCD	ISC	17/04/08	02:49:18	18.6827/-69.4227	28.4	MD/3.66
67	ISCCD	ISC	23/04/08	07:12:19	19.1108/-67.2026	54.8	ML/4.0
68	WHDF	NEIC	23/04/08	13:46:57	19.335/-69.467	149.2	MD/3.9
69	ISCCD	ISC	23/04/08	13:46:57	19.335/-69.4672	149.3	MD/3.87
70	WHDF	NEIC	23/04/08	16:06:19	19.625/-69.003	176.4	MD/4.1
71	WHDF	NEIC	23/04/08	21:53:43	19.232/-69.431	152.1	MD/4.1
72	ISCCD	ISC	23/04/08	21:53:43	19.2315/-69.4312	152.1	MD/4.06
73	ISCCD	ISC	24/04/08	22:20:51	19.9743/-64.989	0	ML/6.5 MS/3.4
74	WHDF	NEIC	24/04/08	22:20:56	20.051/-65.009	45.7	MB/4.4
75	ISCCD	ISC	24/04/08	22:20:56	20.051/-65.0089	45.7	MB/4.4
76	ISCCD	ISC	25/04/08	21:18:25	18.6385/-69.0852	84.6	MD/3.58
77	WHDF	NEIC	01/05/08	04:40:57	18.395/-71.755	16.1	MD/4.3
78	ISCCD	ISC	01/05/08	04:40:57	18.3945/-71.7546	16.1	MD/4.21
79	WHDF	NEIC	01/05/08	20:57:28	19.895/-72.837	22.7	MB/4.6
80	ISCCD	ISC	03/05/08	06:36:36	19.3933/-64.3503	10	MB/4.6
81	ISCCD	ISC	03/05/08	06:36:41	19.455/-64.1669	49.1	MD/4.7
82	FINGER	NEIC	03/05/08	06:36:44	19.36/-64.17	49.5	M/4.3
83	ISCCD	ISC	03/05/08	06:36:44	19.364/-64.1669	49.5	MB/4.5
84	WHDF	NEIC	03/05/08	19:54:49	19.205/-69.353	130.8	MD/4.0
85	ISCCD	ISC	03/05/08	19:54:49	19.2047/-69.3526	130.8	MD/3.96
86	ISCCD	ISC	04/05/08	11:15:47	20.019/-65.0289	34.5	MD/4.7
87	WHDF	NEIC	04/05/08	11:15:49	20.061/-65.039	35.4	MB/4.5
88	ISCCD	ISC	04/05/08	11:15:50	19.849/-64.9945	40.2	ML/4.4
89	WHDF	NEIC	04/05/08	11:24:24	19.213/-68.791	149.9	MD/4.0
90	ISCCD	ISC	04/05/08	11:24:24	19.2132/-68.7906	149.9	MD/3.99
91	ISCCD	ISC	05/05/08	01:47:20	18.731/-69.6785	134.6	MB/3.55
92	WHDF	NEIC	05/05/08	01:47:22	18.826/-69.618	129.6	MB/3.8
93	WHDF	NEIC	09/05/08	17:11:42	18.663/-68.518	164.8	MD/3.6
94	ISCCD	ISC	09/05/08	17:11:42	18.663/-68.5174	164.8	MD/3.59
95	WHDF	NEIC	11/05/08	16:24:49	18.379/-68.945	134.8	MD/3.5
96	ISCCD	ISC	11/05/08	16:24:49	18.379/-68.9452	134.8	MD/3.47
97	ISCCD	ISC	13/05/08	02:30:44	18.7255/-69.6485	115.2	MB/3.41

98	WHDF	NEIC	13/05/08	02:30:44	18.822/-69.699	93.9	MD/3.8
99	WHDF	NEIC	20/05/08	13:15:18	19.061/-69.461	95.9	MD/3.1
100	WHDF	NEIC	21/05/08	06:21:35	19.242/-70.826	134.5	MD/4.5
101	ISCCD	ISC	21/05/08	06:21:35	19.2418/-70.8259	134.5	MD/4.49
102	WHDF	NEIC	23/05/08	14:33:50	18.792/-69.6	107.5	MD/4.0
103	ISCCD	ISC	23/05/08	14:33:50	18.7925/-69.6002	107.5	MD/3.95
104	WHDF	NEIC	31/05/08	10:22:03	18.799/-70.11	142.1	MD/4.0
105	ISCCD	ISC	31/05/08	10:22:03	18.799/-70.1097	142.1	MD/4.04
106	WHDF	NEIC	05/06/08	00:42:16	19.064/-68.733	162.4	MD/3.7
107	ISCCD	ISC	05/06/08	00:42:16	19.0637/-68.7329	162.4	MD/3.68
108	ISCCD	ISC	07/06/08	16:56:02	17.976/-65.3349	33	MS/4.3 MB/4.9
109	ISCCD	ISC	07/06/08	16:56:07	19.3225/-64.5042	10	MB/4.9 MS/3.9
110	WHDF	NEIC	07/06/08	16:56:09	19.758/-64.209	30.2	MB/4.9
111	NEICALRT	NEIC	07/06/08	16:56:14	19.3626/-64.4379	35	MB/4.8
112	WHDF	NEIC	11/06/08	10:39:39	18.154/-68.501	82.6	MD/3.5
113	ISCCD	ISC	11/06/08	10:39:39	18.1538/-68.5004	82.6	MD/3.47
114	WHDF	NEIC	12/06/08	00:41:34	18.884/-70.413	79.6	MD/3.6
115	ISCCD	ISC	12/06/08	00:41:34	18.8837/-70.4134	79.6	MD/3.56
116	WHDF	NEIC	14/06/08	07:56:46	18.931/-70.392	97.6	MD/3.8
117	ISCCD	ISC	14/06/08	07:56:46	18.9307/-70.3914	97.6	MD/3.81
118	QED	NEIC	16/06/08	07:43:10	19.431/-64.401	10	MB/4.4
119	ISCCD	ISC	16/06/08	07:43:12	19.3994/-64.3787	39.6	MS/3.65
120	WHDF	NEIC	18/06/08	12:20:25	18.469/-68.685	126.6	MD/3.4
121	ISCCD	ISC	18/06/08	12:20:25	18.4687/-68.6846	126.6	MD/3.42
122	WHDF	NEIC	27/06/08	15:06:09	19.389/-69.37	70.4	MD/3.4
123	ISCCD	ISC	27/06/08	15:06:09	19.3892/-69.3697	70.4	MD/3.36
124	WHDF	NEIC	28/06/08	14:16:35	19.394/-69.431	77.4	MD/3.5
125	ISCCD	ISC	28/06/08	14:16:35	19.3938/-69.4312	77.4	MD/3.51
126	WHDF	NEIC	28/06/08	22:53:05	18.549/-71.174	78.2	MD/4.0
127	ISCCD	ISC	28/06/08	22:53:05	18.5492/-71.1744	78.2	MD/3.97
128	WHDF	NEIC	04/07/08	18:02:00	19.146/-69.243	150	MD/3.8
129	ISCCD	ISC	04/07/08	18:02:00	19.1463/-69.2427	150	MD/3.79
130	ISCCD	ISC	08/07/08	09:43:34	19.483/-71.5449	52.9	MD/3.33
131	WHDF	NEIC	09/07/08	20:42:52	18.43/-69.269	92.4	MD/3.6

132	ISCCD	ISC	09/07/08	20:42:52	18.43/-69.2689	92.4	MD/3.56
133	NEICALRT	NEIC	10/07/08	01:41:12	19.535/-65.343	5.6	MD/4.8
134	ISCCD	ISC	10/07/08	01:41:13	19.5347/-65.3431	5.6	MD/4.83
135	ISCCD	ISC	10/07/08	01:41:23	19.4/-65.2999	97	MB/4.7
136	ISCCD	ISC	11/07/08	07:42:51	18.4578/-69.5984	10.6	MD/3.34
137	WHDF	NEIC	14/07/08	06:19:58	18.991/-69.413	56.6	MD/3.7
138	ISCCD	ISC	14/07/08	06:19:58	18.9907/-69.4131	56.6	MD/3.66
139	ISCCD	ISC	14/07/08	16:18:34	19.6869/-69.8523	10.4	MS/3.01
140	WHDF	NEIC	14/07/08	16:18:35	19.583/-69.871	5.9	MD/4.2
141	ISCCD	ISC	14/07/08	16:18:38	19.6272/-69.8622	5	MD/4.18
142	ISCCD	ISC	15/07/08	23:24:49	18.8452/-70.4024	110.5	MD/3.34
143	ISCCD	ISC	17/07/08	05:20:01	22.7092/-67.4006	25	MD/4.24
144	ISCCD	ISC	18/07/08	01:23:14	17.9157/-68.5307	80.5	MD/3.52
145	ISCCD	ISC	18/07/08	10:55:56	18.2/-68.1999	78	MS/4.5
146	WHDF	NEIC	18/07/08	10:55:59	18.217/-68.232	78.4	MD/4.1
147	ISCCD	ISC	20/07/08	07:07:13	20.0307/-68.5854	40.1	MD/3.47
148	WHDF	NEIC	22/07/08	13:29:28	18.64/-68.339	127.3	MD/4.1
149	ISCCD	ISC	22/07/08	13:29:28	18.6397/-68.3386	127.3	MD/4.1
150	WHDF	NEIC	26/07/08	07:34:02	19.511/-69.378	125	MD/4.1
151	WHDF	NEIC	01/08/08	00:29:59	19.671/-68.655	15.3	MD/2.7
152	WHDF	NEIC	01/08/08	10:41:24	19.218/-68.698	124.7	MD/3.7
153	ISCCD	ISC	01/08/08	10:41:24	19.2182/-68.6976	124.7	MD/3.72
154	WHDF	NEIC	02/08/08	06:15:41	19.363/-69.012	23	MD/3.2
155	ISCCD	ISC	02/08/08	06:15:41	19.363/-69.0119	23	MD/3.18
156	WHDF	NEIC	02/08/08	19:55:26	19.997/-69.727	114.1	MD/3.5
157	WHDF	NEIC	04/08/08	15:03:08	19.266/-69.193	115	MD/2.9
158	WHDF	NEIC	05/08/08	09:34:39	18.119/-68.797	118.3	MD/3.7
159	ISCCD	ISC	05/08/08	09:34:39	18.1188/-68.7969	118.3	MD/3.66
160	ISCCD	ISC	05/08/08	09:49:11	18.913/-73.1739	0.1	MD/5.1
161	WHDF	NEIC	05/08/08	10:42:45	18.291/-69.156	96.8	MD/3.3
162	ISCCD	ISC	05/08/08	10:42:45	18.2912/-69.1556	96.8	MD/3.26
163	WHDF	NEIC	06/08/08	00:56:07	19.448/-68.908	111.1	MD/3.8
164	ISCCD	ISC	06/08/08	06:25:50	18.4737/-69.0411	101.5	MD/3.69
165	WHDF	NEIC	06/08/08	18:30:22	18.577/-68.923	110.4	MD/3.9

166	ISCCD	ISC	06/08/08	18:30:22	18.5773/-68.9229	110.4	MD/3.87
167	WHDF	NEIC	07/08/08	11:20:44	18.714/-69.077	145.9	MD/3.8
168	ISCCD	ISC	07/08/08	11:20:44	18.7143/-69.0767	146	MD/3.8
169	WHDF	NEIC	07/08/08	19:43:04	19.568/-69.364	66.3	MD/3.7
170	ISCCD	ISC	07/08/08	19:43:04	19.5678/-69.3641	66.3	MD/3.69
171	ISCCD	ISC	08/08/08	21:50:50	19.9925/-70.4456	113.3	MD/3.5
172	ISCCD	ISC	10/08/08	13:50:40	17.7425/-70.0321	67.8	MD/3.4
173	WHDF	NEIC	13/08/08	04:53:12	18.325/-68.549	117.5	MD/3.4
174	ISCCD	ISC	13/08/08	04:53:12	18.3247/-68.5492	117.5	MD/3.44
175	WHDF	NEIC	13/08/08	15:49:44	19.345/-68.529	87.5	MD/3.2
176	ISCCD	ISC	13/08/08	15:49:44	19.3453/-68.5291	87.5	MD/3.18
177	ISCCD	ISC	13/08/08	23:03:07	19.4063/-70.0153	0	ML/2.8 MS/3.6
178	NEICALRT	NEIC	13/08/08	23:03:09	19.5703/-69.9401	5.2	MB/4.6
179	ISCCD	ISC	13/08/08	23:03:14	19.5453/-69.9499	5.1	MD/4.1
180	ISCCD	ISC	15/08/08	10:06:12	18.545/-71.8559	0	MD/4.0 ML/3.3
181	WHDF	NEIC	15/08/08	10:06:17	18.74/-71.966	25	MD/4.3
182	ISCCD	ISC	15/08/08	10:06:17	18.7398/-71.9661	25	MD/4.26
183	WHDF	NEIC	17/08/08	13:23:29	19.24/-69.42	106.1	MD/2.5
184	ISCCD	ISC	18/08/08	14:49:56	20.2652/-70.6547	53.4	MD/3.97
185	WHDF	NEIC	18/08/08	20:49:59	19.925/-70.583	97.9	MD/3.8
186	WHDF	NEIC	19/08/08	10:04:03	18.448/-69.001	73.9	MD/3.4
187	ISCCD	ISC	19/08/08	10:04:03	18.4477/-69.0004	73.9	MD/3.4
188	WHDF	NEIC	26/08/08	03:09:06	19.877/-70.604	96.5	MD/4.0
189	ISCCD	ISC	26/08/08	03:09:06	19.8773/-70.6041	96.5	MD/3.96
190	WHDF	NEIC	26/08/08	17:35:23	18.798/-69.036	136.3	MD/3.7
191	ISCCD	ISC	26/08/08	17:35:23	18.7982/-69.0359	136.3	MD/3.74
192	WHDF	NEIC	26/08/08	22:57:52	19.916/-70.582	98.6	MD/3.7
193	ISCCD	ISC	26/08/08	22:57:52	19.9162/-70.5822	98.6	MD/3.74
194	WHDF	NEIC	29/08/08	19:05:30	19.382/-70.505	83.3	MD/3.5
195	ISCCD	ISC	29/08/08	19:05:30	19.3818/-70.5044	83.4	MD/3.51
196	ISCCD	ISC	01/09/08	18:11:45	18.3363/-68.8713	121.4	MB/3.5
197	WHDF	NEIC	01/09/08	18:11:48	18.708/-68.673	137.6	MD/4.1
198	WHDF	NEIC	02/09/08	04:52:57	19.644/-71.267	35	LG/2.9
199	ISCCD	ISC	02/09/08	04:52:57	19.644/-71.2669	35	MN/2.9

200	WHDF	NEIC	03/09/08	23:17:01	19.11/-68.579	164.7	MD/3.8
201	ISCCD	ISC	03/09/08	23:17:01	19.1095/-68.5787	164.7	MD/3.75
202	WHDF	NEIC	07/09/08	00:36:52	19.546/-70.422	110.1	MD/4.2
203	ISCCD	ISC	07/09/08	00:36:52	19.5465/-70.4214	110.1	MD/4.12
204	WHDF	NEIC	08/09/08	00:54:23	18.222/-68.995	117.2	MD/3.5
205	ISCCD	ISC	08/09/08	00:54:23	18.222/-68.9947	117.2	MD/3.47
206	WHDF	NEIC	10/09/08	23:42:43	18.383/-68.915	129.2	MD/3.7
207	ISCCD	ISC	10/09/08	23:42:43	18.383/-68.9154	129.2	MD/3.68
208	ISCCD	ISC	14/09/08	19:39:23	20.0868/-70.7251	39.9	MS/3.63
209	WHDF	NEIC	14/09/08	19:39:25	20.151/-70.711	36.2	MB/4.0
210	WHDF	NEIC	14/09/08	20:15:22	18.336/-69.156	97.2	MD/3.6
211	ISCCD	ISC	14/09/08	20:15:22	18.3357/-69.1561	97.2	MD/3.58
212	QED	NEIC	22/09/08	02:46:19	17.774/-68.911	89	MD/3.5
213	ISCCD	ISC	23/09/08	20:34:56	18.1485/-68.9629	96.6	MD/3.23
214	WHDF	NEIC	25/09/08	08:36:45	19.477/-69.342	10	MD/3.7
215	WHDF	NEIC	25/09/08	16:35:57	19.666/-69.511	37.2	MD/3.6
216	ISCCD	ISC	25/09/08	16:35:57	19.666/-69.5106	37.2	MD/3.63
217	WHDF	NEIC	27/09/08	02:04:14	19.023/-68.67	165.4	MD/3.6
218	ISCCD	ISC	27/09/08	02:04:14	19.0232/-68.6702	165.4	MD/3.59
219	WHDF	NEIC	29/09/08	03:29:23	19.012/-68.606	182	MD/3.9
220	ISCCD	ISC	29/09/08	03:29:23	19.012/-68.6057	182	MD/3.85
221	ISCCD	ISC	11/10/08	10:40:09	19.1947/-65.0146	10	MB/6.0 MS/5.5
222	ISCCD	ISC	11/10/08	10:40:12	19.149/-64.7999	24	MS/5.8 MB/6.1
223	QED	NEIC	11/10/08	10:40:14	19.16/-64.786	23	MB/6.2
224	ISCCD	ISC	11/10/08	10:40:16	19.29/-64.3999	21	MB/6.1
225	ISCCD	ISC	11/10/08	10:40:35	21.959/-63.3029	23	MB/5.8
226	WHDF	NEIC	12/10/08	02:46:12	19.203/-64.84	47.5	MB/4.2
227	ISCCD	ISC	12/10/08	02:46:12	19.203/-64.8399	47.5	MB/4.2
228	ISCCD	ISC	12/10/08	11:40:12	18.7213/-71.1085	0	ML/2.9 MS/3.0
229	QED	NEIC	12/10/08	11:40:15	18.623/-71.388	10	MD/4.4
230	ISCCD	ISC	12/10/08	11:40:17	18.6958/-71.2754	5	MD/4.35
231	WHDF	NEIC	14/10/08	12:32:36	17.924/-69.714	118.7	MD/3.9
232	ISCCD	ISC	14/10/08	12:32:36	17.9235/-69.7134	118.7	MD/3.87
233	ISCCD	ISC	21/10/08	16:55:11	19.1565/-71.3741	165.7	MD/4.55

234	ISCCD	ISC	23/10/08	20:53:53	19.9483/-71.0937	110.7	MD/4.56
235	QED	NEIC	25/10/08	05:14:03	19.3/-69.264	60	MD/3.6
236	WHDF	NEIC	29/10/08	04:35:10	18.19/-68.561	141.9	MD/3.8
237	ISCCD	ISC	29/10/08	04:35:10	18.1898/-68.5607	141.9	MD/3.77
238	WHDF	NEIC	02/11/08	04:07:20	19.004/-69.417	138.2	MD/4.0
239	ISCCD	ISC	02/11/08	04:07:20	19.004/-69.4172	138.3	MD/4.0
240	ISCCD	ISC	02/11/08	20:42:32	19.5833/-66.3633	10	MB/5.3 MS/4.9
241	ISCCD	ISC	02/11/08	20:42:36	19.413/-66.3769	33	MS/5.1 MB/5.3
242	FINGER	NEIC	02/11/08	20:42:37	19.43/-66.38	10	M/5.5
243	ISCCD	ISC	02/11/08	21:00:59	19.5656/-66.3374	10.2	MB/4.48
244	WHDF	NEIC	02/11/08	21:01:02	19.65/-66.282	21.1	MB/4.8
245	ISCCD	ISC	02/11/08	21:02:32	19.3995/-66.2447	0	MB/3.8 MB1/4.2
246	ISCCD	ISC	02/11/08	21:05:17	19.5099/-66.2063	0	MB/3.9 MB1/4.2
247	ISCCD	ISC	04/11/08	08:53:08	19.124/-64.8599	27.1	MD/4.0
248	WHDF	NEIC	06/11/08	05:59:15	18.11/-70.943	80.3	MD/4.2
249	ISCCD	ISC	06/11/08	05:59:15	18.1095/-70.9432	80.3	MD/4.22
250	WHDF	NEIC	08/11/08	05:12:00	18.106/-69.885	133.5	MD/4.0
251	ISCCD	ISC	08/11/08	05:12:00	18.1058/-69.8846	133.5	MD/4.01
252	ISCCD	ISC	08/11/08	13:57:43	19.4516/-66.3217	0	MB/3.8 MB1/4.2
253	FINGER	NEIC	08/11/08	13:57:46	19.41/-66.29	19.9	M/4.3
254	ISCCD	ISC	08/11/08	13:57:48	19.3789/-66.3357	42.5	MB/4.09
255	WHDF	NEIC	08/11/08	18:40:08	19.277/-68.621	70	MD/3.6
256	ISCCD	ISC	08/11/08	18:40:08	19.277/-68.6209	70	MD/3.55
257	ISCCD	ISC	09/11/08	02:19:52	19.4566/-66.1642	0	MB/3.6 MB1/4.0
258	WHDF	NEIC	10/11/08	22:52:54	20.754/-68.752	24.6	MD/3.5
259	WHDF	NEIC	11/11/08	04:07:34	17.96/-68.725	42.4	MD/2.9
260	WHDF	NEIC	11/11/08	09:39:24	19.072/-68.866	7.2	MD/3.9
261	WHDF	NEIC	11/11/08	17:45:20	19.245/-68.546	65.8	MD/3.2
262	ISCCD	ISC	11/11/08	17:45:20	19.2453/-68.5462	65.8	MD/3.15
263	ISCCD	ISC	13/11/08	14:52:58	19.4328/-66.3112	19.7	MS/3.82
264	WHDF	NEIC	13/11/08	14:53:01	19.479/-66.354	15.3	MB/4.6
265	ISCCD	ISC	15/11/08	11:58:29	18.5/-68.2999	158	MB/5.0
266	ISCCD	ISC	15/11/08	11:58:31	18.1208/-68.5212	143.9	MB/3.5
267	NEICALRT	NEIC	15/11/08	11:58:31	18.546/-68.342	157.5	MD/4.2

268	ISCCD	ISC	23/11/08	09:05:16	19.3518/-66.3116	0	ML/2.7 MS/4.3
269	NEICALRT	NEIC	23/11/08	09:05:18	19.3554/-66.2789	10	MB/5.1
270	ISCCD	ISC	23/11/08	09:05:20	19.5/-66.2999	47	MS/5.6 MS7/5.3
271	QED	NEIC	23/11/08	10:21:58	19.013/-68.614	60	MD/3.3
272	ISCCD	ISC	23/11/08	10:21:58	19.0132/-68.6141	59.8	MD/3.29
273	WHDF	NEIC	26/11/08	09:47:06	18.348/-68.813	125	MD/3.7
274	ISCCD	ISC	26/11/08	09:47:06	18.348/-68.8129	125	MD/3.73
275	ISCCD	ISC	27/11/08	10:15:31	18.226/-69.0384	130.6	MD/3.72
276	QED	NEIC	27/11/08	22:29:25	19.198/-69.358	125	MD/4.1
277	ISCCD	ISC	27/11/08	22:29:25	18.9146/-69.4287	117.9	MB/3.45
278	ISCCD	ISC	29/11/08	01:44:20	18.1807/-68.7184	166.7	MD/3.73
279	ISCCD	ISC	02/12/08	00:33:12	19.4332/-66.3769	21.9	MS/3.38
280	WHDF	NEIC	02/12/08	00:33:14	19.5/-66.357	35	MB/4.6 MD/4.0
281	WHDF	NEIC	05/12/08	19:10:04	19.392/-66.355	10	MB/4.1 MD/3.7
282	ISCCD	ISC	05/12/08	19:10:04	19.392/-66.3549	10	MB/4.1
283	ISCCD	ISC	07/12/08	21:35:43	19.4116/-66.2473	0	MS/4.1 MS1/4.1
284	ISCCD	ISC	11/12/08	20:01:26	19.4308/-70.4489	23.9	MD/3.49
285	ISCCD	ISC	14/12/08	03:12:05	18.0797/-68.6064	46.4	MD/2.32
286	WHDF	NEIC	14/12/08	17:23:10	18.61/-64.239	39.9	MB/4.0
287	ISCCD	ISC	14/12/08	17:23:10	18.61/-64.2389	39.9	MB/4.0
288	WHDF	NEIC	17/12/08	19:55:54	18.991/-65.192	28.9	MB/4.6
289	ISCCD	ISC	17/12/08	19:55:54	18.991/-65.1919	28.9	MB/4.6
290	ISCCD	ISC	18/12/08	17:13:46	19.033/-69.3752	131.8	MD/5.17
291	FINGER	NEIC	18/12/08	17:13:47	18.64/-69.38	104.6	M/5.2
292	ISCCD	ISC	18/12/08	17:13:52	18.128/-67.8279	104.9	MB/5.3
293	ISCCD	ISC	25/12/08	00:56:18	19.5908/-70.6184	105.2	MD/2.93
294	ISCCD	ISC	28/12/08	23:34:44	20.2995/-70.9574	64.8	MD/4.19

2009	CATALOG	CONTRIB.	DATE	TIME	LAT/LON	DEPTH	MAGN
1	ISCCD	ISC	06/01/09	21:13:57	19.9977/-70.1521	17.1	MD/2.96
2	WHDF	NEIC	07/01/09	02:13:42	19.477/-69.585	79	MD/3.9
3	ISCCD	ISC	07/01/09	02:13:42	19.4767/-69.5846	79	MD/3.88
4	WHDF	NEIC	08/01/09	02:01:08	18.499/-68.747	2.1	MD/3.8
5	WHDF	NEIC	12/01/09	08:14:18	19.029/-68.901	143.1	MD/3.5

6	ISCCD	ISC	12/01/09	08:14:18	19.0293/-68.9014	143.1	MD/3.54
7	WHDF	NEIC	12/01/09	20:59:44	18.568/-68.983	117.1	MD/3.8
8	ISCCD	ISC	12/01/09	20:59:44	18.5678/-68.9832	117.1	MD/3.82
9	ISCCD	ISC	14/01/09	01:23:10	18.69/-70.1649	50	MD/4.3 ML/4.0
10	WHDF	NEIC	14/01/09	01:23:12	19.741/-70.237	10	MB/3.9
11	WHDF	NEIC	19/01/09	19:00:54	18.409/-68.727	143.3	MD/3.1
12	ISCCD	ISC	19/01/09	19:00:54	18.409/-68.7269	143.3	MD/3.11
13	QED	NEIC	24/01/09	00:50:09	18.044/-68.54	104	MD/3.3
14	ISCCD	ISC	24/01/09	00:50:09	18.0438/-68.5397	104.1	MD/3.26
15	ISCCD	ISC	24/01/09	11:30:26	18.0892/-69.0099	114.9	MD/3.47
16	WHDF	NEIC	28/01/09	08:27:56	18.387/-68.733	92.1	MD/2.7
17	ISCCD	ISC	28/01/09	08:27:56	18.387/-68.7332	92.1	MD/2.74
18	QED	NEIC	03/02/09	01:31:46	18.2/-68.883	45	MD/2.8
19	WHDF	NEIC	13/02/09	04:24:41	19.634/-66.3	35.2	MB/4.5
20	NEICALRT	NEIC	13/02/09	04:39:29	19.3924/-66.1186	3.3	MB/4.9
21	WHDF	NEIC	13/02/09	04:39:33	19.469/-66.358	6.4	MB/4.8
22	QED	NEIC	13/02/09	22:45:05	17.986/-68.699	49	MD/3.4
23	NEICALRT	NEIC	14/02/09	07:48:38	18.5092/-68.9531	117.5	MB/5.1
24	WHDF	NEIC	19/02/09	09:36:40	18.608/-68.95	119.6	MD/3.6
25	WHDF	NEIC	20/02/09	01:17:43	17.979/-68.655	81.5	MD/3.8
26	WHDF	NEIC	04/03/09	22:30:26	18.286/-68.563	163.1	MB/5.0
27	WHDF	NEIC	05/03/09	19:43:01	18.204/-68.97	83.6	MD/3.6
28	QED	NEIC	06/03/09	00:09:28	19.107/-68.787	81	MD/3.8
29	WHDF	NEIC	07/03/09	13:10:05	18.172/-68.609	149.2	MD/3.1
30	WHDF	NEIC	09/03/09	23:20:16	18.375/-68.611	126.8	MD/3.7
31	NEICALRT	NEIC	12/03/09	02:05:36	19.0539/-66.4576	23.7	MB/4.9
32	WHDF	NEIC	14/03/09	11:22:27	19.106/-68.832	66.7	MD/3.5
33	WHDF	NEIC	16/03/09	12:47:43	18.132/-68.75	149.2	MD/3.4
34	QED	NEIC	18/03/09	03:23:57	19.264/-68.628	35	MD/3.7
35	WHDF	NEIC	22/03/09	18:12:40	18.133/-69.039	116.4	MD/3.9
36	WHDF	NEIC	02/04/09	12:20:43	19.655/-70.485	10	MB/4.2
37	WHDF	NEIC	04/04/09	21:42:06	18.952/-68.726	104.1	MD/3.8
38	WHDF	NEIC	05/04/09	17:37:57	19.327/-65.104	30	MB/4.4 MD/4.5
39	WHDF	NEIC	13/04/09	06:31:27	17.893/-68.847	35.9	MD/3.1
40	WHDF	NEIC	14/04/09	04:02:51	18.496/-68.544	87.7	MD/3.3
41	WHDF	NEIC	14/04/09	21:43:42	19.355/-65.066	56.2	MD/4.0
42	QED	NEIC	22/04/09	01:36:55	18.211/-68.546	147	MD/3.7
43	QED	NEIC	24/04/09	02:08:15	17.923/-68.561	61	MD/3.4
44	FINGER	NEIC	25/04/09	06:59:27	17.93/-68.57	55.6	M/3.2
45	QED	NEIC	28/04/09	05:23:28	18.414/-68.639	137	MD/3.7
46	QED	NEIC	01/05/09	21:18:43	18.576/-69.052	105	MD/4.1

47	FINGER	NEIC	06/05/09	21:28:37	19.3/-70.22	10	M/4.2
48	WHDF	NEIC	09/05/09	18:25:14	18.131/-68.919	146.5	MD/3.4
49	WHDF	NEIC	12/05/09	11:53:48	18.477/-68.709	112.5	MD/2.9
50	WHDF	NEIC	13/05/09	16:55:07	18.441/-68.582	159.9	MD/3.5
51	FINGER	NEIC	20/05/09	03:36:05	19.0/-65.55	11	M/4.6
52	QED	NEIC	20/05/09	03:36:09	19.002/-65.497	19	MB/4.6
53	QED	NEIC	01/06/09	04:33:53	19.452/-63.45	36	MB/4.5
54	FINGER	NEIC	01/06/09	04:35:09	19.58/-63.42	40.5	M/4.7
55	NEICALRT	NEIC	01/06/09	04:35:13	19.1387/-63.5092	43.3	MB/4.8
56	FINGER	NEIC	02/06/09	22:17:43	19.08/-68.57	115.3	M/2.9
57	WHDF	NEIC	09/06/09	20:24:11	17.569/-68.611	54.7	MD/3.1
58	WHDF	NEIC	13/06/09	16:12:32	19.184/-66.587	8.8	MB/5.0
59	NEICALRT	NEIC	22/06/09	02:10:43	19.206/-64.351	24.9	MD/4.0
60	FINGER	NEIC	22/06/09	22:13:17	19.31/-70.62	9.2	M/3.2
61	FINGER	NEIC	03/07/09	21:42:45	18.44/-68.83	197.9	M/3.7
62	QED	NEIC	20/07/09	23:23:14	19.059/-68.503	73	MD/3.8
63	QED	NEIC	21/07/09	00:33:39	18.429/-70.954	51	MD/3.4
64	WHDF	NEIC	21/07/09	19:00:22	19.116/-64.803	30.8	MB/4.7
65	QED	NEIC	31/07/09	21:00:55	18.556/-70.944	10	MB/4.7
66	WHDF	NEIC	12/08/09	18:39:48	19.518/-65.275	112.9	MB/4.4
67	FINGER	NEIC	13/08/09	14:48:37	19.31/-65.81	5.7	M/4.9
68	QED	NEIC	13/08/09	14:48:41	19.215/-65.835	53	MB/4.9
69	WHDF	NEIC	13/08/09	18:31:52	19.224/-65.694	87.8	MB/4.2
70	WHDF	NEIC	14/08/09	09:48:16	19.288/-65.716	93.4	MB/4.5
71	WHDF	NEIC	14/08/09	09:50:24	19.258/-65.723	46.9	MB/4.9
72	NEICALRT	NEIC	14/08/09	09:50:31	19.1771/-65.7635	119.2	MB/4.9
73	WHDF	NEIC	18/08/09	11:43:32	18.168/-68.291	78.8	MB/4.4
74	NEICALRT	NEIC	23/08/09	03:00:29	18.6747/-69.2618	98.1	MB/4.6
75	FINGER	NEIC	23/08/09	12:02:57	18.89/-68.91	77.2	M/4.0
76	QED	NEIC	27/08/09	21:10:04	18.039/-68.558	70	MD/3.3
77	WHDF	NEIC	04/09/09	09:45:14	19.872/-71.412	35	MB/4.4
78	QED	NEIC	29/09/09	01:47:59	19.991/-64.617	46	MD/4.0
79	QED	NEIC	22/10/09	23:01:26	19.352/-65.547	61	MD/4.1
80	FINGER	NEIC	23/10/09	03:14:32	19.41/-65.51	35	M/4.0
81	FINGER	NEIC	27/10/09	19:18:19	18.98/-69.13	10	M/4.5
82	WHDF	NEIC	27/11/09	13:17:25	19.492/-66.243	51.1	MB/4.3
83	QED	NEIC	05/12/09	04:48:20	18.601/-68.791	121	MD/3.7
84	FINGER	NEIC	06/12/09	07:09:18	18.86/-68.92	112.4	M/3.8
85	QED	NEIC	26/12/09	14:56:34	18.58/-69.068	99	MB/3.7

2010	CATALOG	CONTRIB.	DATE	TIME	LAT/LON	DEPTH	MAGN
1	NEICALRT	NEIC	04/01/10	01:08:48	18.3619/-68.8634	166.2	MB/4.5
2	NEICALRT	NEIC	12/01/10	21:53:10	18.4514/-72.4452	10	MW/7.0
3	QED	NEIC	12/01/10	22:00:42	18.369/-72.823	10	MB/5.9
4	WHDF	NEIC	12/01/10	22:07:02	18.463/-72.626	10	MB/5.0
5	QED	NEIC	12/01/10	22:12:05	18.478/-72.514	10	MB/5.5
6	WHDF	NEIC	12/01/10	22:52:51	18.437/-72.848	10	MB/4.7
7	QED	NEIC	12/01/10	23:07:03	18.496/-72.629	10	MB/4.6
8	WHDF	NEIC	12/01/10	23:12:04	18.402/-72.513	10	MB/5.3
9	NEICALRT	NEIC	12/01/10	23:27:37	18.4818/-72.8102	10	MB/4.8
10	WHDF	NEIC	12/01/10	23:35:39	18.382/-72.868	10	MB/4.6
11	QED	NEIC	12/01/10	23:47:38	18.479/-72.846	10	MB/4.5
12	WHDF	NEIC	13/01/10	00:23:13	18.499/-72.792	10	MB/4.5
13	NEICALRT	NEIC	13/01/10	00:23:56	18.4096/-72.7159	10	MB/4.8
14	NEICALRT	NEIC	13/01/10	00:43:28	18.541/-72.4855	10	MB/5.0
15	WHDF	NEIC	13/01/10	00:59:05	18.354/-72.807	10	MB/5.2
16	WHDF	NEIC	13/01/10	01:00:26	18.455/-73.069	10	MB/4.7
17	QED	NEIC	13/01/10	01:05:49	18.533/-72.649	10	MB/4.6
18	WHDF	NEIC	13/01/10	01:16:51	18.425/-72.814	10	MB/5.1
19	QED	NEIC	13/01/10	01:24:32	18.462/-72.835	10	MB/4.6
20	QED	NEIC	13/01/10	01:32:44	18.378/-72.942	10	MB/5.3
21	FINGER	NEIC	13/01/10	01:36:31	18.36/-72.83	10	M/5.5
22	NEICALRT	NEIC	13/01/10	01:55:17	18.3968/-72.8242	10	MB/5.0
23	QED	NEIC	13/01/10	01:57:35	18.412/-72.903	10	MB/5.4
24	QED	NEIC	13/01/10	02:11:31	18.422/-73.002	10	MB/5.0
25	QED	NEIC	13/01/10	02:17:56	18.526/-72.941	10	MB/4.6
26	QED	NEIC	13/01/10	02:26:34	18.464/-72.822	10	MB/4.7
27	NEICALRT	NEIC	13/01/10	02:43:48	18.4838/-72.9841	10	MB/4.7
28	NEICALRT	NEIC	13/01/10	02:54:20	18.3932/-72.9742	10	MB/4.6
29	WHDF	NEIC	13/01/10	03:17:11	18.414/-72.958	10	MB/4.6
30	NEICALRT	NEIC	13/01/10	03:31:57	18.2541/-72.9219	10	MB/4.7
31	WHDF	NEIC	13/01/10	04:29:49	18.446/-72.941	10	MB/4.5
32	WHDF	NEIC	13/01/10	04:37:51	18.465/-72.777	10	MB/4.5
33	FINGER	NEIC	13/01/10	05:02:57	18.37/-72.96	10	M/5.8
34	NEICALRT	NEIC	13/01/10	05:18:03	18.3859/-72.9052	10	MB/5.2
35	NEICALRT	NEIC	13/01/10	05:24:02	18.5045/-72.7265	11.7	MB/4.9
36	WHDF	NEIC	13/01/10	05:49:23	18.4/-72.966	10	MB/4.6
37	WHDF	NEIC	13/01/10	06:24:16	18.373/-72.875	10	MB/4.6
38	NEICALRT	NEIC	13/01/10	06:48:03	18.3794/-72.8759	10	MB/4.5
39	WHDF	NEIC	13/01/10	06:58:26	18.417/-72.904	10	MB/4.6
40	WHDF	NEIC	13/01/10	07:23:04	18.381/-72.836	10	MB/4.9

41	WHDF	NEIC	13/01/10	12:28:25	18.407/-72.806	10	MB/4.5
42	NEICALRT	NEIC	13/01/10	12:41:45	18.4114/-72.8142	10	MB/4.7
43	FINGER	NEIC	13/01/10	14:43:44	18.45/-72.92	10	M/5.3
44	NEICALRT	NEIC	13/01/10	18:54:17	18.4471/-72.6072	10	MB/4.6
45	WHDF	NEIC	13/01/10	21:26:16	18.492/-72.495	10	MB/4.9
46	WHDF	NEIC	13/01/10	22:21:13	18.363/-72.581	10	MB/4.9
47	NEICALRT	NEIC	14/01/10	08:15:42	18.3297/-72.7654	10	MB/4.7
48	WHDF	NEIC	14/01/10	10:32:29	18.434/-72.771	10	MB/4.5
49	WHDF	NEIC	14/01/10	12:39:03	18.376/-72.737	10	MB/4.8
50	WHDF	NEIC	15/01/10	08:56:05	18.411/-72.817	10	MB/4.6
51	WHDF	NEIC	15/01/10	13:41:42	18.338/-72.818	10	MB/4.6
52	NEICALRT	NEIC	15/01/10	20:04:12	18.4386/-72.8564	10	MB/4.6
53	FINGER	NEIC	15/01/10	21:04:46	18.01/-72.33	10	M/4.7
54	NEICALRT	NEIC	15/01/10	21:04:50	18.0712/-72.2879	33.8	MB/4.5
55	NEICALRT	NEIC	16/01/10	15:59:56	18.4552/-72.5388	10	MB/4.5
56	NEICALRT	NEIC	17/01/10	17:51:09	18.5713/-72.5321	10	MB/4.7
57	NEICALRT	NEIC	17/01/10	18:19:20	18.5186/-72.783	10	MB/4.6
58	WHDF	NEIC	18/01/10	17:22:41	19.326/-68.694	68.9	MD/3.7
59	FINGER	NEIC	20/01/10	11:03:43	18.43/-72.8	10	M/5.9
60	NEICALRT	NEIC	21/01/10	16:45:19	18.6091/-72.7982	10	MB/4.9
61	QED	NEIC	21/01/10	16:54:09	18.489/-72.718	10	MB/4.8
62	WHDF	NEIC	23/01/10	02:29:20	18.504/-71.975	10	MB/4.2
63	NEICALRT	NEIC	24/01/10	21:51:54	18.5206/-72.6175	4.1	MB/4.7
64	QED	NEIC	25/01/10	18:40:28	18.489/-72.949	10	MB/4.8
65	WHDF	NEIC	26/01/10	11:16:58	18.502/-72.977	10	MB/4.5
66	WHDF	NEIC	27/01/10	00:57:25	18.427/-72.902	10	MB/4.9
67	QED	NEIC	31/01/10	03:45:31	18.678/-68.699	186	MD/3.6

EVENTS FOR PERIOD II

2010	CATALOG	CONTRIBUTOR	DATE	LAT/LON	DEPTH	MAGN
1	FINGER	NEIC	12/02/2010 12:09:14.000	19.85/-74.38	10	M/5.4
2	QED	NEIC	12/02/2010 12:09:14.500	19.833/-74.376	10	MB/5.4
3	NEICALRT	NEIC	12/02/2010 12:09:14.700	19.8493/-74.3755	10	MB/5.4
4	MHDF	NEIC	12/02/2010 12:09:14.870	19.855/-74.378	10	MB/5.3 MS/4.6
5	WHDF	NEIC	12/02/2010 12:09:14.870	19.855/-74.378	10	MB/5.3 MS/4.6
6	FINGER	NEIC	11/03/2010 6:20:31.000	19.76/-71.58	10	M/4.1
7	QED	NEIC	11/03/2010 6:20:31.200	19.744/-71.585	10	MB/4.1
8	WHDF	NEIC	15/03/2010 17:25:46.330	18.989/-69.68	118	MB/4.8

9	FINGER	NEIC	22/03/2010 2:53:49.000	19.72/-70.93	10	M/4.6
10	NEICALRT	NEIC	22/03/2010 2:53:49.200	19.7195/-70.9289	10	MB/4.6
11	QED	NEIC	22/03/2010 2:53:50.500	19.741/-70.958	15	MB/4.6
12	WHDF	NEIC	22/03/2010 2:53:53.000	19.678/-70.944	38.2	MB/4.6
13	WHDF	NEIC	22/03/2010 8:52:40.300	18.573/-67.746	93.1	MD/3.0
14	WHDF	NEIC	23/03/2010 1:59:13.000	19.076/-70.154	73.4	MD/3.2
15	WHDF	NEIC	26/03/2010 16:21:17.620	19.934/-73.246	10	ML/3.2
16	FINGER	NEIC	18/04/2010 20:16:39.000	18.13/-68.49	86.2	M/5.1
17	WHDF	NEIC	18/04/2010 20:16:39.400	18.136/-68.515	84.5	MB/5.1
18	NEICALRT	NEIC	18/04/2010 20:16:39.600	18.1311/-68.4853	86.2	MB/5.1
19	QED	NEIC	18/04/2010 20:16:39.600	18.131/-68.485	86	MB/5.1
20	WHDF	NEIC	17/05/2010 14:34:18.590	19.615/-70.501	10	ML/3.3
21	QED	NEIC	31/05/2010 10:24:11.500	19.784/-72.992	10	ML/3.8
22	WHDF	NEIC	31/05/2010 10:24:11.570	19.784/-72.992	10	ML/3.8
23	FINGER	NEIC	05/06/2010 18:26:33.000	18.79/-67.9	70	M/4.2
24	QED	NEIC	05/06/2010 18:26:33.400	18.798/-67.878	69	MB/4.1
25	WHDF	NEIC	02/07/2010 4:44:47.060	18.318/-68.861	172.1	MB/4.4
26	WHDF	NEIC	02/07/2010 15:15:04.060	18.151/-67.636	70.3	MD/3.0
27	WHDF	NEIC	08/07/2010 8:22:43.040	19.722/-73.087	10	MB/3.7
28	FINGER	NEIC	12/07/2010 9:09:19.000	18.88/-68.69	195.2	M/4.1
29	WHDF	NEIC	16/07/2010 3:09:31.720	18.091/-67.911	130.8	MD/3.1
30	WHDF	NEIC	17/07/2010 7:01:36.500	19.601/-73.232	10	MB/4.2
31	FINGER	NEIC	17/07/2010 7:01:44.000	19.35/-72.93	37.9	M/4.3
32	QED	NEIC	17/07/2010 7:01:44.600	19.317/-72.94	39	MB/4.2
33	WHDF	NEIC	22/07/2010 18:30:28.350	18.183/-67.688	108.6	MD/3.0
34	WHDF	NEIC	28/07/2010 2:40:45.630	18.836/-67.821	80.5	MD/3.1
35	QED	NEIC	30/07/2010 7:04:07.600	18.401/-67.424	11	MD/3.4
36	WHDF	NEIC	30/07/2010 7:04:07.620	18.401/-67.424	10.8	MD/3.4
37	QED	NEIC	30/07/2010 7:33:55.600	18.765/-68.248	59	MD/3.3
38	QED	NEIC	01/08/2010 9:49:39.500	18.959/-67.644	7	MD/3.4
39	WHDF	NEIC	01/08/2010 9:49:39.580	18.959/-67.644	7.2	MD/3.4
40	WHDF	NEIC	03/08/2010 17:42:45.590	19.086/-67.739	14.5	MD/3.0
41	WHDF	NEIC	13/08/2010 1:00:16.590	18.78/-67.812	3.1	MD/3.1
42	WHDF	NEIC	14/08/2010 1:47:07.020	18.774/-67.832	46.6	MD/3.2

43	WHDF	NEIC	14/08/2010 21:15:28.420	18.848/-67.781	7.1	MD/3.1
44	WHDF	NEIC	16/08/2010 4:52:39.040	19.082/-67.684	81.4	MD/3.3
45	WHDF	NEIC	18/08/2010 23:58:57.430	18.421/-67.407	18	MD/3.3
46	QED	NEIC	20/08/2010 5:58:30.800	18.359/-67.445	8	MD/3.3
47	WHDF	NEIC	20/08/2010 5:58:30.820	18.359/-67.445	8.1	MD/3.3
48	QED	NEIC	29/08/2010 10:03:51.600	18.509/-68.804	128	MD/3.4
49	WHDF	NEIC	01/09/2010 5:41:37.660	18.493/-68.68	157.1	MD/4.2
50	QED	NEIC	11/09/2010 8:37:11.700	18.191/-67.679	13	MD/3.3
51	WHDF	NEIC	11/09/2010 8:37:11.760	18.191/-67.679	12.5	MD/3.3
52	WHDF	NEIC	20/09/2010 23:57:58.140	18.208/-67.351	72.9	MD/3.0
53	WHDF	NEIC	23/09/2010 7:25:31.580	19.011/-67.233	9.2	MD/3.2
54	QED	NEIC	26/09/2010 2:36:01.600	18.179/-67.95	94	MD/3.0
55	WHDF	NEIC	26/09/2010 2:36:01.610	18.179/-67.95	94.2	MD/3.0
56	WHDF	NEIC	04/10/2010 17:59:26.460	18.049/-68.563	88.6	MD/4.0
57	WHDF	NEIC	10/10/2010 22:36:18.950	19.644/-67.513	15	MD/3.0
58	WHDF	NEIC	10/10/2010 22:37:52.390	19.678/-67.526	12.8	MD/3.0
59	WHDF	NEIC	13/10/2010 6:13:55.460	18.728/-67.684	86.9	MD/3.3
60	WHDF	NEIC	17/10/2010 14:50:50.460	18.84/-67.715	30	MD/3.0
61	FINGER	NEIC	19/10/2010 3:56:56.000	19.3/-68.16	22	M/4.0
62	QED	NEIC	19/10/2010 3:56:56.100	19.292/-68.16	24	MD/4.0
63	WHDF	NEIC	19/10/2010 3:56:57.540	19.281/-68.202	35	MB/4.2 MD/4.1
64	WHDF	NEIC	19/10/2010 5:22:18.610	18.224/-67.81	138	MD/3.3
65	WHDF	NEIC	29/10/2010 16:56:18.130	18.131/-67.729	50.8	MB/4.3
66	WHDF	NEIC	29/10/2010 19:14:26.760	19.681/-70.726	10	ML/3.4
67	WHDF	NEIC	10/11/2010 7:45:29.990	19.263/-67.924	68.3	MD/3.1
68	WHDF	NEIC	13/11/2010 4:35:39.470	17.874/-68.541	94.6	MB/5.6
69	QED	NEIC	13/11/2010 4:35:39.500	17.879/-68.53	95	MB/5.6
70	FINGER	NEIC	13/11/2010 4:35:40.000	17.92/-68.57	96.6	M/5.6
71	NEICALRT	NEIC	13/11/2010 4:35:40.000	17.9235/-68.5707	96.6	MB/5.6
72	WHDF	NEIC	16/11/2010 3:15:41.000	18.253/-67.989	113	MD/3.1
73	WHDF	NEIC	18/11/2010 20:46:00.400	18.948/-68.184	15	ML/3.1
74	WHDF	NEIC	24/11/2010 1:18:25.860	18.068/-68.472	62.1	MB/4.0
75	QED	NEIC	26/11/2010 7:43:51.300	19.393/-67.763	40	MD/3.1
76	WHDF	NEIC	26/11/2010 7:43:51.380	19.393/-67.763	40.4	MD/3.1

77	WHDF	NEIC	26/11/2010 16:15:53.520	19.34/-67.816	60	MD/3.1
78	WHDF	NEIC	02/12/2010 14:21:35.450	19.342/-67.989	73.1	MD/3.2
79	WHDF	NEIC	09/12/2010 11:23:52.390	18.23/-67.877	7.8	MD/3.0
80	WHDF	NEIC	18/12/2010 4:19:39.240	18.794/-67.505	9.4	MD/3.0
81	WHDF	NEIC	29/12/2010 1:16:46.030	18.197/-67.865	53.1	MD/3.1

2011	CATALOG	CONTRIB	DATE	LAT/LON	DEPTH	MAGN
1	WHDF	NEIC	25/01/2011 17:24:56.190	18.166/-67.936	117.1	MD/3.0
2	WHDF	NEIC	30/01/2011 1:09:54.030	18.921/-67.783	7.4	MD/3.1
3	WHDF	NEIC	11/03/2011 0:25:28.810	18.897/-68.855	166.1	MD/4.0
4	FINGER	NEIC	16/03/2011 13:42:32.000	18.99/-67.95	33.7	M/5.0
5	QED	NEIC	16/03/2011 13:42:33.500	19.033/-67.918	56	MD/5.4
6	WHDF	NEIC	16/03/2011 13:42:33.590	19.033/-67.918	56	MB/5.0 MW/5.0
7	WHDF	NEIC	16/03/2011 13:42:33.590	19.033/-67.918	56	MB/5.0 MW/5.0
8	WHDF	NEIC	11/04/2011 5:05:53.590	18.259/-67.984	103.2	MD/3.3
9	FINGER	NEIC	03/05/2011 21:44:25.000	19.65/-70.67	1	M/3.9
10	WHDF	NEIC	03/05/2011 21:44:25.880	19.64/-70.649	10	MB/4.5 MD/3.9
11	QED	NEIC	03/05/2011 21:44:27.000	19.606/-70.663	20	MD/3.9
12	WHDF	NEIC	07/05/2011 1:40:58.860	18.366/-67.899	93.3	MD/3.1
13	FINGER	NEIC	07/05/2011 17:01:24.000	18.36/-68.39	60.8	M/2.8
14	WHDF	NEIC	13/05/2011 1:19:19.970	19.552/-70.456	22.9	MB/3.8
15	QED	NEIC	13/05/2011 1:19:20.000	19.587/-70.447	21	MB/4.0
16	FINGER	NEIC	13/05/2011 1:19:21.000	19.54/-70.42	35.8	M/4.0
17	QED	NEIC	21/05/2011 18:29:14.700	18.975/-67.888	26	ML/4.8
18	WHDF	NEIC	21/05/2011 18:29:14.790	18.975/-67.888	25.5	MB/4.7
19	FINGER	NEIC	21/05/2011 18:29:16.000	18.88/-67.57	21.6	M/4.6
20	WHDF	NEIC	21/05/2011 18:42:08.110	18.875/-67.82	24.2	MD/3.1
21	WHDF	NEIC	21/05/2011 18:43:05.290	18.914/-67.737	20	MD/3.4
22	WHDF	NEIC	21/05/2011 19:33:51.700	19.038/-67.576	11.4	MD/3.1
23	WHDF	NEIC	21/05/2011 19:47:07.090	18.976/-67.731	18.3	MD/3.5
24	WHDF	NEIC	21/05/2011 22:12:51.250	19.017/-67.641	24.8	MD/3.0
25	WHDF	NEIC	22/05/2011 0:13:19.940	18.881/-67.743	18.8	MD/3.1
26	WHDF	NEIC	22/05/2011 2:02:05.060	19.07/-67.642	25.6	MD/3.2
27	WHDF	NEIC	22/05/2011 2:06:44.260	18.933/-67.482	56.1	MD/3.9
28	WHDF	NEIC	22/05/2011 3:12:55.020	18.912/-67.731	32.2	MD/3.1
29	WHDF	NEIC	22/05/2011 3:20:37.290	19.077/-67.688	24.8	MD/3.3
30	WHDF	NEIC	22/05/2011 5:35:46.620	18.74/-67.3	14.7	MD/3.2
31	WHDF	NEIC	22/05/2011 9:25:37.660	19.046/-67.712	15.6	MD/3.1

32	WHDF	NEIC	22/05/2011 14:18:47.050	18.845/-67.579	8	MD/3.2
33	WHDF	NEIC	22/05/2011 23:48:42.070	18.981/-67.564	6.3	MD/3.0
34	WHDF	NEIC	23/05/2011 6:04:39.920	19.083/-67.471	7	MD/3.1
35	WHDF	NEIC	23/05/2011 18:19:44.860	18.97/-67.903	13.8	MD/3.1
36	QED	NEIC	01/06/2011 3:46:43.600	19.392/-68.898	95	MD/4.0
37	WHDF	NEIC	01/06/2011 3:46:43.650	19.392/-68.898	95.3	MD/4.0
38	QED	NEIC	28/07/2011 2:22:50.900	18.996/-67.773	25	MD/3.4
39	QED	NEIC	29/07/2011 7:25:40.900	19.03/-67.946	25	MD/3.3
40	QED	NEIC	30/07/2011 7:11:00.300	18.763/-67.844	89	MD/3.2
41	QED	NEIC	04/08/2011 2:59:11.500	18.921/-67.62	20	MD/3.0
42	QED	NEIC	04/08/2011 4:17:47.000	18.978/-67.701	16	MD/3.1
43	QED	NEIC	05/08/2011 7:51:43.500	18.971/-67.719	24	MD/3.2
44	QED	NEIC	05/08/2011 8:33:24.500	18.985/-67.713	25	MD/3.1
45	QED	NEIC	06/08/2011 4:30:58.600	18.42/-68.408	117	MB/4.3
46	FINGER	NEIC	06/08/2011 4:30:59.000	18.38/-68.37	125	M/4.3
47	QED	NEIC	06/08/2011 7:12:00.400	18.769/-67.551	127	MD/3.1
48	QED	NEIC	11/08/2011 3:47:38.100	18.989/-67.714	23	MD/3.0
49	QED	NEIC	12/08/2011 5:43:38.100	18.757/-67.606	41	MD/3.0
50	QED	NEIC	12/08/2011 23:30:31.700	18.888/-67.732	76	MD/3.5
51	QED	NEIC	13/08/2011 0:26:49.100	19.008/-67.703	46	MD/3.2
52	QED	NEIC	14/08/2011 12:17:33.400			
53	QED	NEIC	14/08/2011 16:18:08.600	18.945/-67.723	24	MD/3.0
54	QED	NEIC	15/08/2011 2:48:17.100	18.903/-67.594	6	MD/3.2
55	QED	NEIC	16/08/2011 3:25:46.200	18.857/-67.529	8	MD/3.0
56	QED	NEIC	16/08/2011 4:46:40.200	18.823/-67.579	6	MD/3.2
57	QED	NEIC	16/08/2011 5:02:57.170	18.864/-67.601	38.5	MD/3.3
58	QED	NEIC	18/08/2011 17:50:20.140	18.745/-68.806	117	MD/4.2
59	QED	NEIC	21/08/2011 3:01:23.400	18.974/-67.729	17	MD/3.0
60	QED	NEIC	21/08/2011 3:33:28.400	18.859/-67.748	38	MD/3.1
61	QED	NEIC	27/08/2011 23:16:37.500	18.947/-67.658	70	MD/3.2
62	QED	NEIC	27/08/2011 23:21:55.300	19.097/-67.716	46	MD/3.0
63	QED	NEIC	04/09/2011 22:20:24.420	19.097/-67.641	48.4	MD/3.0
64	FINGER	NEIC	06/09/2011 20:01:35.000	18.96/-67.73	18	M/3.2
65	QED	NEIC	12/09/2011 8:52:22.570	18.161/-67.891	101.2	MD/3.2
66	QED	NEIC	12/09/2011 8:52:22.570	18.161/-67.891	101.2	MD/3.2
67	QED	NEIC	19/09/2011 10:07:05.870	17.932/-68.156	105.8	MD/3.0
68	FINGER	NEIC	22/09/2011 16:33:10.000	18.62/-68.65	156.5	M/4.0
69	QED	NEIC	22/09/2011 16:33:11.000	18.617/-68.652	156.6	MD/4.0
70	QED	NEIC	27/09/2011 17:05:00.150	18.98/-67.773	27.2	MD/3.0
71	QED	NEIC	28/09/2011 8:25:54.470	18.1/-67.964	74.9	MD/3.2
72	QED	NEIC	14/10/2011 1:37:26.540	18.944/-67.818	69.6	MD/3.1

73	QED	NEIC	22/10/2011 22:04:36.000	18.757/-68.289	96.4	MD/3.1
74	NEIC_PDE/NEIC_ALERT		2011/10/20 19:35:22.5000	19.479/-68.816	139.8	MD/4.1
75	NEIC_PDE/NEIC_ALERT		2011/07/28 14:20:27.5000	18.937/-68.804	103	MD/4
76	NEIC_PDE/NEIC_PDE-Q		2011/01/07 18:23:53.4300	18.545/-68.765	144.9	MD/3.4
77	NEIC_PDE/NEIC_ALERT		2011/07/06 12:58:25.1000	18.534/-68.655	164.9	MD/4.1
78	NEIC_PDE/NEIC_PDE-Q		2011/08/27 18:26:45.1300	18.578/-68.356	120	MD/3.1
79	NEIC_PDE/NEIC_PDE-Q		2011/05/14 00:23:09.9600	17.653/-68.383	16.7	MD/3.3
80	NEIC_PDE/NEIC_PDE-Q		2011/03/29 17:45:13.5900	18.733/-68.377	124	MD/3.2
81	NEIC_PDE/NEIC_PDE-Q		2011/02/17 00:55:41.9000	18.244/-68.3	89.7	MD/3.2
82	NEIC_PDE/NEIC_PDE-Q		2011/05/12 06:00:44.3600	18.191/-68.297	105	MD/3.2
83	NEIC_PDE/NEIC_PDE-Q		2011/09/17 20:06:00.1400	18.804/-68.142	55.8	MD/3.1
84	NEIC_PDE/NEIC_PDE-Q		2011/03/09 08:37:30.2300	18.066/-68.122	84.2	MD/3.3
85	NEIC_PDE/NEIC_PDE-Q		2011/04/09 10:46:17.7800	18.23/-68.045	131.4	MD/3.1
86	NEIC_PDE/NEIC_PDE-Q		2011/03/15 13:07:51.3400	18.284/-68.046	105.5	MD/3
87	NEIC_PDE/NEIC_PDE-Q		2011/02/16 21:19:09.5600	18.166/-68.064	88.8	MD/3.2
88	NEIC_PDE/NEIC_PDE-Q		2011/07/29 19:28:53.5000	19.041/-67.973	45	MD/3
89	NEIC_PDE/NEIC_PDE-Q		2011/07/28 20:34:40.4000	19.025/-67.927	10.5	MD/4.6
90	NEIC_PDE/NEIC_PDE-Q		2011/08/11 18:48:08.5700	18.97/-67.876	72.6	MD/3.6
91	NEIC_PDE/NEIC_PDE-Q		2011/08/05 19:01:12.9000	18.956/-67.842	20	MD/3.1
92	NEIC_PDE/NEIC_PDE-Q		2011/07/18 21:36:49.8700	18.911/-67.841	24.2	MD/3.2
93	NEIC_PDE/NEIC_PDE-Q		2011/07/10 02:35:03.2200	18.086/-67.837	55.5	MD/3
94	NEIC_PDE/NEIC_PDE-Q		2011/06/03 22:40:19.4000	18.469/-67.844	106.9	MD/3.3
95	NEIC_PDE/NEIC_PDE-Q		2011/09/16 06:56:46.6100	18.937/-67.734	24.4	MD/3
96	NEIC_PDE/NEIC_PDE-Q		2011/08/29 04:15:11.1500	18.891/-67.713	8.5	MD/3
97	NEIC_PDE/NEIC_PDE-Q		2011/08/06 18:54:09.0900	18.987/-67.716	24	MD/3.3
98	NEIC_PDE/NEIC_PDE-Q		2011/08/06 16:20:11.6000	18.976/-67.727	24.3	MD/3.3
99	NEIC_PDE/NEIC_PDE-Q		2011/08/05 17:49:39.7900	18.942/-67.702	10	MD/3.2
100	NEIC_PDE/NEIC_PDE-Q		2011/07/31 17:10:34.3900	18.949/-67.714	21.6	MD/3.3
101	NEIC_PDE/NEIC_PDE-Q		2011/07/30 16:21:25.5500	18.961/-67.715	24.5	MD/3.1
102	NEIC_PDE/NEIC_PDE-W		2011/12/17 06:11:03.7400	18.17/-67.165	41.1	MD3.2
103	NEIC_PDE/NEIC_PDE-W		2011/12/12 15:20:55.4200	18.566/-66.644	103	MD3.1
104	NEIC_PDE/NEIC_PDE-W		2011/11/28 06:42:22.8600	18.242/-66.259	7.9	MD3.2
105	NEIC_PDE/NEIC_PDE-W		2011/11/13 15:38:44.4500	18.233/-66.086	125	MD3.2
106	NEIC_PDE/NEIC_PDE-W		2011/11/12 10:32:36.1300	18.098/-65.467	15.3	MD3.1
107	NEIC_PDE/NEIC_PDE-W		2011/11/10 17:50:36.7900	18.56/-65.585	93	MD3.3
108	NEIC_PDE/NEIC_PDE-W		2011/10/27 01:26:20.5800	18.486/-66.137	104.8	MD3.0
109	NEIC_PDE/NEIC_PDE-W		2011/11/14 11:53:37.9500	18.404/-72.886,	37.6	MB4.4

2012	CATALOG	CONTRIB	DATE	LAT/LON	DEPTH	MAGN
1	NEIC_PDE/NEIC_PDE-Q		2012/10/17 03:30:47.0400	18.707/-70.873	12.7	MB4.7

2	NEIC_PDE/NEIC_PDE-Q	2012/10/15 02:46:41.8100	19.203/-69.044	61.3	MB4.4
3	NEIC_PDE/NEIC_PDE-Q	2012/08/09 23:45:58.7500	19.005/-69.496	40.6	MB4.1
4	NEIC_PDE/NEIC_PDE-Q	2012/08/05 21:51:24.9300	19.104/-69.599	85	MB4.4
5	NEIC_PDE/NEIC_PDE-Q	2012/08/04 06:40:42.3300	18.885/-70.314	84	MB4.3
6	NEIC_PDE/NEIC_PDE-Q	2012/07/11 09:11:18.5300	18.859/-69.617	50.2	MB4.5
7	NEIC_PDE/NEIC_PDE-Q	2012/07/07 20:32:38.2300	18.243/-71.136	26.7	MB5.1
8	NEIC_PDE/NEIC_PDE-W	2012/03/13 04:15:06.9900	19.381/-68.068	30.6	MB4.5
9	NEIC_PDE/NEIC_PDE-W	2012/03/08 02:51:32.4000	18.346/-72.038	6.6	MB4.7
10	NEIC_PDE/NEIC_PDE-W	2012/03/05 22:52:53.8300	18.296/-68.555	179.9	MB4.3
11	NEIC_PDE/NEIC_PDE-W	2012/01/27 01:25:33.7500	19.57/-70.08	14.7	MB4.1
12	NEIC_PDE/NEIC_PDE-W	2012/01/24 22:15:25.0300	19.635/-70.078	10	MB4.2
13	NEIC_PDE/NEIC_PDE-W	2012/01/24 21:45:25.6900	19.54/-70.052	29.8	MB4.6
14	NEIC_PDE/NEIC_PDE-W	2012/01/24 14:33:30.7600	19.589/-70.055	13.8	MB4.5
15	NEIC_PDE/NEIC_PDE-W	2012/01/23 20:50:14.5000	19.542/-70.077	8.8	MW5.2
16	NEIC_PDE/NEIC_PDE-W	2012/01/19 06:28:19.0900	18.058/-68.755	102.9	MW5.0
17	NEIC_PDE/NEIC_PDE-W	2012/01/05 22:02:39.6800	18.595/-70.567	35	MB4.6
18	NEIC_PDE/NEIC_PDE-W	2012/01/05 09:35:32.1000	18.325/-70.361	39.8	MW5.5
19	NEIC_PDE/NEIC_PDE-Q	2012/10/05 19:45:32.7000	18.518/-66.071	119	MD3.2
20	NEIC_PDE/NEIC_PDE-Q	2012/09/28 01:35:46.9300	18.019/-65.392	24.8	MD3.1
21	NEIC_PDE/NEIC_PDE-Q	2012/09/02 19:07:54.2100	18.001/-67.158	14	MD3.0
22	NEIC_PDE/NEIC_PDE-Q	2012/08/26 07:21:32.3100	18.417/-66.209	113	MD3.0
23	NEIC_PDE/NEIC_PDE-Q	2012/07/30 12:30:07.1300	18.303/-66.352	131.1	MD3.0
24	NEIC_PDE/NEIC_PDE-Q	2012/07/24 07:19:02.3500	17.998/-67.097	6.8	MD3.4
25	NEIC_PDE/NEIC_PDE-Q	2012/07/24 05:11:38.9400	18.007/-67.088	7.3	MD3.7
26	NEIC_PDE/NEIC_PDE-Q	2012/07/22 12:10:22.6600	17.907/-65.33	18.6	MD3.0
27	NEIC_PDE/NEIC_PDE-Q	2012/07/19 06:27:39.0000	18.459/-65.339	114	MB4.1
28	NEIC_PDE/NEIC_PDE-Q	2012/07/19 00:52:23.6200	17.939/-66.103	12.4	MD3.0
29	NEIC_PDE/NEIC_PDE-Q	2012/07/18 20:33:19.6800	17.932/-66.101	12.2	MD3.1
30	NEIC_PDE/NEIC_PDE-Q	2012/07/18 20:26:07.7100	17.919/-66.09	6.6	MD3.1
31	NEIC_PDE/NEIC_PDE-Q	2012/07/18 04:41:29.2200	18.275/-66.169	129.7	MD3.2
32	NEIC_PDE/NEIC_PDE-Q	2012/07/11 06:37:52.9400	18.156/-66.079	39.2	MD3.0
33	NEIC_PDE/NEIC_PDE-W	2012/06/10 08:44:24.7400	18.168/-66.942	12	MD3.0
34	NEIC_PDE/NEIC_PDE-W	2012/05/27 11:29:03.1700	18.483/-66.277	108	MD3.0
35	NEIC_PDE/NEIC_PDE-W	2012/05/27 05:00:53.5400	18.397/-65.804	84	MD3.1
36	NEIC_PDE/NEIC_PDE-W	2012/05/24 02:31:57.3300	17.992/-66.459	12.9	MD3.0
37	NEIC_PDE/NEIC_PDE-W	2012/05/14 04:26:58.0800	18.546/-66.579	100.4	MD3.1
38	NEIC_PDE/NEIC_PDE-W	2012/02/25 03:36:34.0600	18.36/-66.172	127.5	MD3.2
39	NEIC_PDE/NEIC_PDE-W	2012/02/04 08:53:07.1800	18.469/-66.089	113.2	MD3.1
40	NEIC_PDE/NEIC_PDE-W	2012/01/28 21:41:28.2200	18.332/-66.213	69.7	MD3.2

The North America-Caribbean plate boundary is a complex area of mainly left-lateral strike-slip deformation. Hispaniola Island is being impacted by collision with the Bahamas Platform in the north and in the south, Beata Ridge is penetrating into the island and hitting with Muertos Trough. These processes alter the central and eastern parts of Hispaniola Island dividing it into different tectonostratigraphic terrains characterized by folds, thrust and left-lateral faults and shear zones.

This PhD Thesis presents the main results and its contribution for lithospheric structure knowledge of NE border of Caribbean Plate, and, particularly, in the area of Dominican Republic. This study combines wide-angle, controlled-source seismology and seismicity data of two geophysical experiments (GEOPRICO-DO and CARIBE NORTE Projects), which have been processed and interpreted along eight seismic transects providing important results about this complex region.

ISBN 978-84-697-0331-1